THE DISTRIBUTION OF VOLCANISM ON VENUS AND GLOBAL TECTONIC IMPLICATIONS

M. W. Airey, T. A. Mather, and D. M. Pyle, *Department of Earth Sciences, University of Oxford, South Parks Road, Oxford, OX1 3AN, UK. (martin.airey@earth.ox.ac.uk)*

Introduction:

The expression of volcanic features and their distribution on a planet's surface offer clues as to the global tectonic processes occurring in the interior. This study describes an analysis of distribution patterns of volcanic features on Venus around the Beta-Atla-Themis (BAT) region, and the surrounding vicinity, and their relationships to each other and related zones of geological rifting. Geospatial analysis is used to quantify these relationships in order to answer the following questions: 1) how do certain volcanic features occur relative to others of their own kind, 2) how do they occur relative to features of other kinds, and 3) how do they occur relative to rifts?

On Earth, the lithosphere is being continuously recycled via the process of plate tectonics. On Venus however, it is proposed that a single global plate constitutes the lithosphere in what is known as a stagnant lid regime. This regime inhibits plate motion and requires conduction to be the dominant heat loss mechanism, supplemented by periodic global volcanic resurfacing events [1]. There is, however, abundant evidence for tectonic processes in the form of extensional (rifts/faults), and compressional (mountain formation/wrinkle ridges) features [2]. This apparent paradox is investigated further in this study using GIS analysis of volcanic and tectonic features and the implications for the global tectonic regime is explored.

Methods:

The geospatial analysis was performed in ArcGIS, and the spatial relationships between volcanic features and rifts on Venus were analysed and applied to planetary evolutionary concepts. The rifts and volcanic features evident on Venus were mapped from existing databases; the maps were then combined and modified to form a new hybrid database for the most intensely rifted region on Venus (the Beta-Atla-Themis region). Firstly, the nearest neighbour index (NNI) was calculated for each type of volcanic feature. This quantity determines the ratio of the observed mean distance between points to the expected mean distance between points in a random distribution and gives an indication of clustering. The mean random NNI of corresponding sample sizes was calculated for comparison with the real populations. To determine the features' relationship with the rift axes, the distance of each feature point on the map from the nearest rift was measured in order to identify any preferred distance from, or affinity for occurring near, rifts. These distances were also measured with only the distance to the young rifts [3] considered. Population distribution histograms were produced for all these data as well as the corresponding results recorded using the previously selected random datasets for comparison. In order to display on the map where any clustering may be concentrated, feature kernel density maps were also produced.

Results:

The analyses of these data defined new evidence supporting aspects of the directional model of Venus' evolution [4]. This shift from the globally dispersed, relatively small-scale, volcanism spread randomly across the planetary surface towards the gradually more rift-focused distribution is indicative of a corresponding shift in global tectonic regime. The model stages suggested here (Figure 1) are that of a stagnant lid scenario, with widely dispersed, discrete zones of small plume-fed activity, followed by a transition via gradual conductive cooling to that of a subcrustal spreading regime similar to that outlined in [5]. These findings describe a scenario where ongoing localised volcanism may occur against the background of the sequence of global volcano-tectonic epochs described in the directional model.

References

[1] Turcotte, D.L. (1993) *Journal of Geophysical Research: Planets*, *98*, E9, 17061-17068 [2] Ivanov, M.A. and Head, J.W. (2011) *Planetary and Space Science*, *59*, 13, 1559-1600 [3] Krassilnikov, A.S., et al. (2012) *Planetary and Space Science*, *68*, 1, 56-75 [4] Basilevsky, A.T. and Head, J.W. (2000) *Planetary and Space Science*, *48*, 1, 75-111 [5] Ghail, R.C. (2015) *Planetary and Space Science*, *113*, 2-9

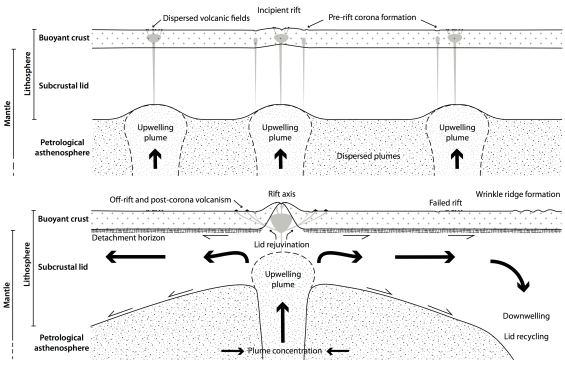

Figure 1. Cartoons to illustrate a proposed Venusian global tectonic regime (a) before and (b) after the onset of subcrustal spreading.

VOLCANIC LIGHTNING ON VENUS AND EARLY EARTH

M. W. Airey, *Department of Earth Sciences, University of Oxford, South Parks Road, Oxford, OX1 3AN, UK. (martin.airey@earth.ox.ac.uk),* **K. L. Aplin**, *Department of Physics, University of Oxford, Denys Wilkinson Building, Keble Road, Oxford, OX1 3RH, UK.*

Introduction:

Lightning may have been crucial in the development of life as it enables key chemical reactions to occur as famously demonstrated in the Miller and Urey experiments [1]. In addition to lightning generated in thunderclouds, volcanic activity also generates electrical discharges within ash plumes and it has been postulated that this kind of lightning may actually be more important for prebiotic chemistry due to the richer variety of, and higher concentrations of, synthesised organic molecules generated around volcanic vents [2]. We cannot directly observe early Earth's hot, CO_2-rich, atmosphere; however, we can find similar conditions today on Venus.

Magnetic signals characteristic of lightning have been previously detected at Venus by orbiting spacecraft [3]. However, lightning flashes have not been optically detected despite the fact that any within-cloud lightning is expected to be detectable in this manner by orbiting spacecraft [4], as it is at Earth. This suggests that lightning could be occurring below the cloud layer. Recent observations made by ESA's Venus Express satellite have provided evidence for active volcanism [5-7], as well as evidence for lightning discharges [e.g. 8], which may be volcanic in origin.

This work will use laboratory experiments to simulate volcanic ash generation and electrical charging of ash under typical atmospheric conditions for Venus and the early Earth (specifically the Hadean eon, up to 4 billion years ago, and the Archean eon, from 4 billion to 2.5 billion years ago); both planets share common origins as CO_2-dominated environments characterised by high pressures (~9 MPa) and temperatures (~700 K). The work will address the following questions: (a) is volcanic activity a feasible mechanism for lightning generation on Venus and early Earth, (b) how would these extreme environmental conditions affect lightning, (c) can the similarities in atmospheric conditions inform us of planetary evolutionary concepts, (d) could volcanic lightning have been important in the emergence of life on Earth, and (e) what are the wider implications for the likelihood of the emergence of life on other planets?

Electrostatic fields within volcanic plumes are formed when different sized particles with opposite charges settle at differing rates. The relative contributions of different charging mechanisms in volcanic plumes are still poorly understood, although the predominant processes are thought to be triboelectrification (frictional charging of particles) [9] and fractoemission (charges generated as a result of particle fragmentation processes, particularly important when magma fragments during explosive volcanism) [10]. This project provides a unique research opportunity to understand how atmospheric conditions affect fractoemission.

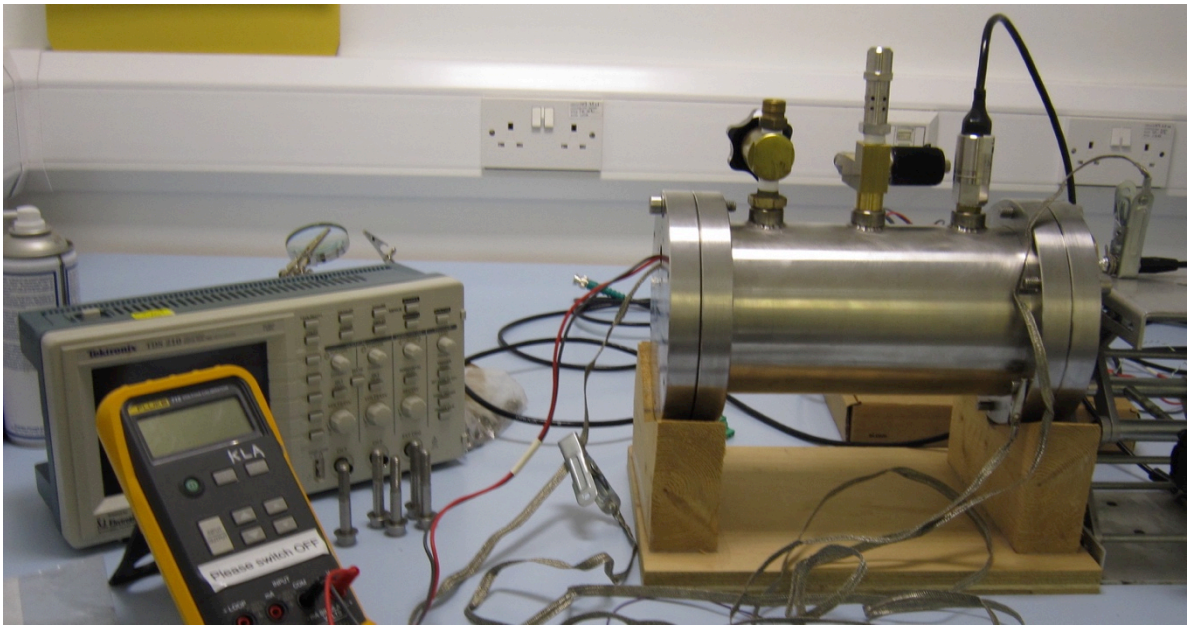

Figure 1. Planetary atmosphere simulation tank setup.

Methods:

The study will utilise a 1-litre atmospheric simulation chamber (Figure 1). This facility can simulate a close approximation of the high-pressure, high-temperature, CO_2-dominated atmospheres of the surface of early Earth, and Venus at ~10 km altitude (~5 MPa, 650 K). A key finding of my previous work [11] is that ash plume-forming eruptions (capable of potentially producing electric fields and lightning within the ash column) are much more likely to occur at higher altitudes such as these on Venus. The chamber contains temperature/pressure monitoring and logging equipment, a rock collision apparatus to generate the charged rock fragments, and charge measurement electrodes connected to a high-precision electrometer. The rock fragmentation mechanism within the chamber is based on the proven method of [12] which has been shown to effectively generate charged rock fragments through fractoemission.

A systematic programme of experiments will be designed to measure the effects of varying temperature, pressure, atmospheric, and sample composition. This programme will explore the relative effects of the investigated variables under a range of conditions appropriate to Venus and early Earth. Comparative work with present day Earth conditions will be undertaken in order to explore the independent effects of each variable on fractoemission charging in these environments.

The study will be applied to palaeo-planetary atmospheres. By comparing the effects on atmospheric electrical phenomena due to the transition from palaeo to current atmospheric conditions, the occurrence of volcanic lightning may be placed in the context of planetary evolution. Very recent work [13] has identified isotopically light, likely to be biogenic, carbon in zircon crystals dated to ~4.1 Ga, suggesting that biological carbon fixation may have been occurring as long ago as the late Hadean (zircon is a mineral used to radiometrically date rocks using the decay of uranium). This work will help to understand atmospheric electrical behaviour during this time and may even inform us of whether favourable conditions for life may have been present on other planets.

In addition to the experimental investigations, this project will include a remote sensing aspect utilising new data acquired by the Japan Aerospace Exploration Agency's (JAXA) Lightning and Airglow Camera (LAC) onboard the Venus Climate Orbiter (aka Akatsuki). Following JAXA's triumphant efforts to recover the probe after the initial failed orbital insertion in 2005, Akatsuki achieved successful Venus Orbit Insertion on 7 December 2015. The LAC instrument will observe lightning in Venus' atmosphere over at least the following two years. Whether or not any detections are volcanic in origin, may be inferred in conjunction with results obtained from one of the infrared cameras (IR1) on the spacecraft [14]. There have, for a long time, been reported observations of lightning on Venus using indirect methods as described above. Akatsuki will, for the first time, be capable of conclusively confirming this atmospheric phenomenon using high-speed optical detection at 777.4 nm [14], the wavelength associated with the excitation of atomic oxygen found to be a strong emitter of lightning discharges under Venus atmospheric conditions in laboratory simulations [15]. This will greatly increase the reliability of the conclusions of the radar study and any inferences drawn from the comparisons with the experimental work.

References

[1] Miller, S.L. and Urey, H.C. (1959) *Science*, *130*, 3370, 245-251

[2] Hill, R.D. (1992) *Origins of Life and Evolution of the Biosphere*, *22*, 5, 277-285

[3] Russell, C.T., et al. (2007) *Nature*, *450*, 7170, 661-662

[4] Yair, Y. (2012) *Advances in Space Research*, *50*, 3, 293-310

[5] Marcq, E., et al. (2012) *Nature Geoscience*, 1-4

[6] Shalygin, E.V., et al. (2015) *Geophys. Res. Lett.*, *42*

[7] Smrekar, S.E., et al. (2010) *Science*, *328*, 5978, 605-608

[8] Russell, C.T., et al. (2008) *Journal of Geophysical Research-Planets*, *113*

[9] Houghton, I.M.P., et al. (2013) *Phys. Rev. Lett.*, *111*, 11, 5

[10] James, M.R., et al. (2008) *Space Sci. Rev.*, *137*, 1-4, 399-418

[11] Airey, M.W., et al. (2015) *Planetary and Space Science*, *113-114*, 33-48

[12] James, M.R., et al. (2000) *Journal of Geophysical Research-Solid Earth*, *105*, B7, 16641-16649

[13] Bell, E.A., et al. (2015) *Proceedings of the National Academy of Sciences*

[14] Takahashi, Y., et al. (2008) *Space Sci. Rev.*, *137*, 1-4, 317-334

[15] Borucki, W.J., et al. (1996) *Icarus*, *123*, 2, 336-344

THE DAVINCI VENUS PROBE DESCENT MODULE AND ENGINEERING DEVELOPMENT UNIT.

Michael J. Amato[1], J. Generie[1], L. Glaze[1], D. Robinson[1], et al. [1]NASA Goddard Space Flight Center (GSFC), Greenbelt MD.

Introduction:

Venus is our nearest neighbor and the closest in size to our home planet. Yet it remains largely unexplored, its runaway greenhouse atmosphere remains unexplained and it's geologic past unknown. The deep atmosphere of Venus remains largely unexplored and key details of its trace gas chemistry remain unmeasured. The history of key volatile reservoirs and surface-atmosphere-interior exchange processes is poorly established and based on limited data. Noble gases within the bulk Venus atmosphere, as well as isotopes of hydrogen, oxygen, and sulfur, are essentially unmeasured to the degree required to address fundamental questions about the evolution of the planet. The planet that is the most capable of teaching us about our own planet must not remain so mysterious. The gaps in deep atmosphere and surface ground truth must be closed. The value of past and future remote sensing at Venus is threatened by our lack of in-situ data and unanswered fundamental questions about the atmosphere and surface. Planetary probes capable of in-situ chemistry measurements within the atmosphere of Venus enable critical science measurements that are needed to answer unresolved science questions. There is critical science data that is not measureable from orbit or from other remote sensing approaches. Much of the needed constituent, chemical and dynamic information requires in situ measurements. Models for solar system formation and the evolution of atmospheres depend on measurements probes can deliver, as do comparisons between the Earth and planets like Venus.

DAVINCI Probe:

The Deep Atmosphere Venus Investigation of Noble gases, Chemistry, and Imaging (Davinci) Venus mission was recently selected for Phase A in the Discovery competition. It fills the fundamental voids that exist in critical Venus in situ knowledge that are crucial to understanding Venus, Earth and future Venus orbital remote measurements. Davinci employs a well instrumented deep atmosphere probe to fill these voids. Davinci's in situ probe allows the mission to address most of the key Decadal Survey New Frontiers "Venus In Situ Explorer" (VISE) science objectives. This includes atmosphere composition, noble gases, nitrogen isotopes, hydrologic cycles and many physical properties of the atmosphere, all crucial to origin and evolution objectives. Davinci's probe also enables resolving key surface atmosphere interaction and pursues radiative balance and surface physics and chemistry goals.

The Davinci probe is designed to enter the atmosphere and carry its instruments through the atmosphere as they carry out their measurements, to the surface where pressures and temperatures are challenging. Science objectives require state-of-the-art neutral mass spectrometer capabilities to achieve seminal measurements of noble gas isotopes while also allowing for high mass resolution and time rate sampling of trace gases. Instruments developed at NASA's Goddard Space flight Center, the world's most experienced space flight mass spectrometer instrument organization, are designed to achieve these pivotal observations. The mass spectrometer is linked to tunable laser spectrometer instrumentation, similar in capability to that which is part of SAM instrument on NASA's Mars Science Laboratory (MSL). The physical context for the atmospheric chemistry measurements is an essential part of the scientific measurement strategy and Davinci takes advantage of current state-of-the-art approaches in atmospheric structure instrumentation for pressure, temperature, and accelerations. The photometry of the atmosphere beneath the cloud deck, as well as imaging of surfaces in regions not explored by the many decades old Soviet Venera landers is enabled by a very capable descent imaging system. The design enables observations that were not possible during the decades old first era of *in situ* Venus reconnaissance (i.e., *PV, Venera*), and which go well beyond what orbital or flyby remote sensing can achieve.

These scientific measurement instruments have been combined into Davinci's optimized "descent sphere" within a probe flight system that includes an aero-entry capsule with a thermal protection system and parachutes. The instruments and thermal solutions lend themselves to probe descent module of reasonable size and power using proven approaches that are combined with updated approaches. The basic Davinci probe descent sphere is shown in Figure 1. Figure 2 shows the descent module in the heat shield.

Figure 1 - Davinci probe descent module layout.

Figure 2 – Davinci Probe descent module and entry and descent system.

The Davinci concept is based upon Pioneer Venus designs and approaches, combined with over six years of NASA Goddard Space Flight Center investments, prototypes, engineering test units and tests. The instrument packaging and science requirements, combined with the high temperature and high pressure conditions near the surface, drive many design elements. Packaging, thermal control, seals, materials trades, aerodynamics, communication links, reliability, testing approaches and heat shield materials challenges drive design options and are also linked to higher level mission flight dymincs decisions. The analysis and prototype work being done by the team has rapidly advanced the design maturity to a level allowing low risk probe missions. The test work has also allowed us to solve, prove, hone, practice and test the key steps of designing building, and testing the Davinci probe. This includes Davinci probe manufacturing, Venus surface environment test procedures, integration and test, and thermal design implementations. NASA GSFC has built Davinci probe engineering development and test units (EDU) and tested them through multiple full Venus descent test conditions. Figure 3 shows one of the EDUs just after a full Venus surface conditions test.

Figure 3 – Davinci Probe descent module EDU just after one of the Venus surface environment tests.

We believe the Davinci probe design approach is the lowest risk and most cost-effective approach to resolving key scientific issues for Venus within the context of competed mission programs at NASA.

The author would like to acknowledge the many team members involved in the probe design, build and test work.

On Venusian polar vortex: numerical experiments and radio occultation measurements

H. Ando[1] *(hando@ac.jaxa.jp)*, **N. Sugimoto**[2], **M. Takagi**[3], **T. Imamura**[1], **H. Kashimura**[4], **Y. Matsuda**[5], **S. Tellmann**[6], **M. Pätzold**[6] **and B. Häusler**[7]

1. ISAS/JAXA, 2. Keio University, 3. Kyoto Sangyo University, 4. JAMSTEC, 5. Tokyo Gakugei University, 6. Universität zu Köln, 7. Universität der Bundeswehr München

Introduction: Unlike the polar vortices observed in the Earth, Mars and Titan atmospheres, the observed Venus polar vortex is warmer than the midlatitudes at cloud-top levels (~65 km). This warm polar vortex is zonally surrounded by a cold latitude band located at ~60° latitude, which is a unique feature called 'cold collar' in the Venus atmosphere [e.g. Taylor et al. 1980; Piccioni et al. 2007]. Although these structures have been observed in numerous previous observations, the formation mechanism is still unknown. In addition, an axi-asymmetric feature is always seen in the warm polar vortex. It changes temporally and sometimes shows a hot polar dipole or S-shaped structure as shown by a lot of infrared measurements [e.g. Garate-Lopez et al. 2013; 2015]. However, its vertical structure has not been investigated. To solve these problems, we performed numerical simulations of the Venus atmospheric circulation using a general circulation model named AFES for Venus [Sugimoto et al. 2014] and reproduced these puzzling features. Moreover, we used temperature profiles retrieved by radio occultation measurement to investigate the vertical structure of the axi-asymmetric feature seen in the polar vortex. And then, the vertical structure clarified by radio occultation measurement was compared with that seen in the polar vortex reproduced by AFES.

Method: Venus atmospheric dynamics has been studied numerically using GCMs. However, there were no numerical studies which succeeded in reproducing a unique structure of the Venus polar atmosphere in realistic model settings. Thermal tides are planetary scale waves excited by the solar heating. In the Venus atmosphere, they are strongly excited at the cloud levels because a large part of the solar flux is absorbed there [Takagi et al. 2005]. However, their effects on the atmospheric structure in the polar region have not yet been examined. In this study, we investigate the structure of the Venus upper polar atmosphere using a GCM named AFES for Venus. To examine the dynamical effects of thermal tides, we perform two numerical experiments with observation-based distributions of solar heating: one with the diurnal components (Case A) and one without them (Case B). The thermal tides are excited only in Case A. See Sugimoto et al. [2014] for the details of the settings.

To investigate the vertical structure of the axi-asymmetric feature is always seen in the Venusian polar vortex, the temperature profiles retrieved by radio occultation measurement, which was performed almost consecutively from 13 to 25 January 2008, were used. We obtained the vertical structure of the amplitude and phase of the temperature perturbation associated with this feature from these profiles. See Häusler et al. [2006] for the details of the measurement.

Result and Discussion: Fig. 1 shows the time evolution of the horizontal temperature distribution at ~68 km obtained in Case A. The cold collar surrounds the warmer polar region at ~60°N. The maximum temperature difference between 60°N and the pole is ~20 K.

Figs. 2a and 2b show latitude–height distributions of zonal- and temporal-mean zonal wind and temperature above the cloud top level averaged over two Venusian solar days (~234 Earth days) obtained in Cases A and B. The axis of the midlatitude jet in Case A is located at a lower latitude and altitude than in Case B. This might be due to the momentum transport by thermal tides. In Case A, the temperature decreases with latitude in association with the positive vertical shear of the mean zonal wind in the equator-side of 60°N with height below 70 km; whereas the temperature increase with latitude in the pole-side of 70°N with height above 67 km. A remarkable cold collar is observed at 67–70 km levels at 60°–70° latitudes along with the polar warm region indicated by red color near the north pole. In Case B, on the other hand, there is no local minimum of the temperature, which corresponds to cold collar.

Figs. 2c and 2d show temporally averaged residual mean meridional circulation by arrows and mass stream function by contours, in Cases A and B, respectively. In Case A, the residual mean meridional circulation above the cloud-top level (~70 km) reaches the polar region and remarkable downward motion occurs, which warms the atmosphere through adiabatic heating and forms the polar warm region. Also in Case B, the downward motion of the residual mean meridional circulation is observed in the polar region. However, it is three times slower than that in Case A, and the adiabatic heating rate associated with the downward flow in the polar region in Case B is much lower than that in Case A.

Fig. 3 shows the vertical distributions of the mean static stability in this observation period, the amplitude and the phase of the perturbation for the 3

days-period component. The static stability is almost zero below 57 km altitude and increases rapidly above this altitude. The amplitude has a local minimum around 57 km altitude, where the static stability rapidly increases with height, and the phase has a gap around this altitude and little varies above and below that altitude. These features are also seen in the temporal development of the vertical distributions of the temperature fluctuation amplitude calculated in AFES (see Fig. 4). The necessary condition for barotropic instability is satisfied in the polar region in our model, and there is little poleward heat flux near the pole. These results suggest that the axi-asymmetric feature, which is often observed by infrared measurements and creates the morphology in the Venusian polar vortex, might be caused by barotropic instability generated in the polar region.

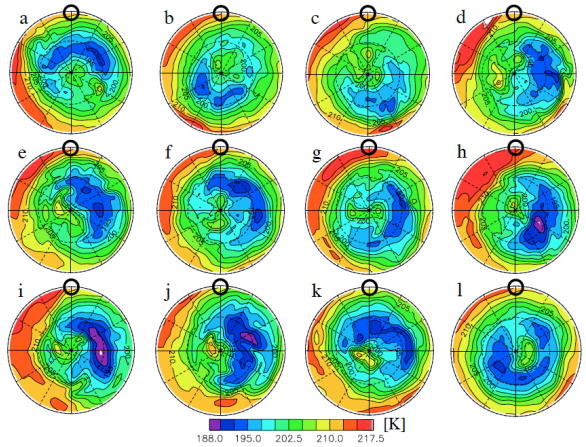

Fig. 1: Time evolution of temperatures (K) in the polar plot at the altitude of ~68 km (the pressure level of 4×10^3 Pa) in Case A. The black circle represents the local solar noon. The time interval of respective figures is one day.

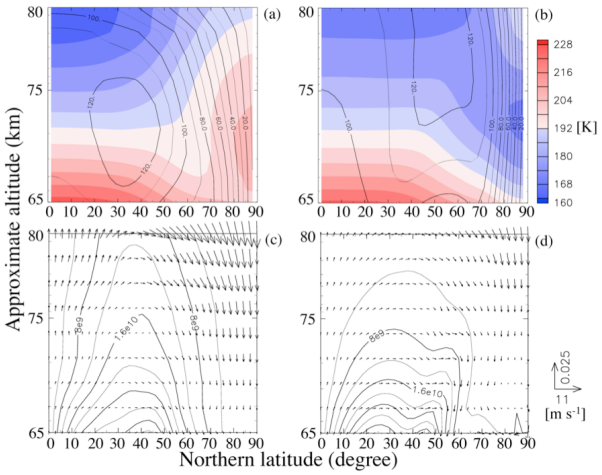

Fig. 2: (Top) Meridional cross sections of the zonal- and temporal-mean zonal wind (solid line) and (colour shade); and (Bottom) the residual mean meridional circulation (vector) and mass stream function (contour). Left (a and c) and right (b and d) figures are for Cases A and B, respectively.

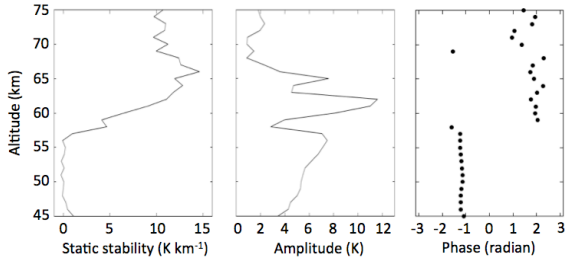

Fig. 3 Vertical distributions of (a) the background static stability, (b) the temperature amplitude, and (c) the phase of the perturbation for the spectral component having the period of ~3 days.

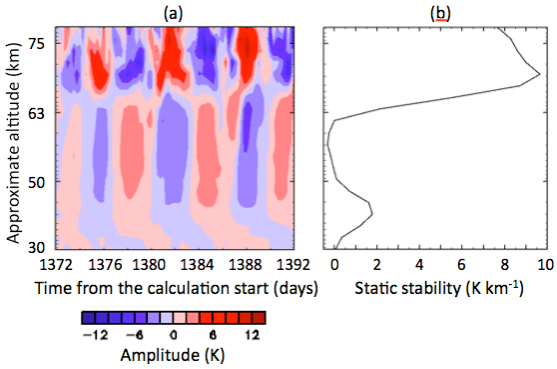

Fig. 4: (a) Temporal development of the vertical distributions of the temperature fluctuation amplitude and (b) mean vertical distribution of the atmospheric stability at 80°N calculated in AFES.

References:

Garate-Lopez, I. et al. A chaotic long-lived vortex at the southern pole of Venus. *Nat. Geosci.* **6**, 254-257 (2013).

Garate-Lopez, I. et al. Instantaneous three-dimensional thermal structure of the southern polar vortex of Venus. *Icarus* **245**, 16-31 (2015).

Häusler, B. et al. Radio science investigations by VeRa onboard the Venus Express spacecraft. *Planetary and Space Sci*. **54**, 1315-1335 (2006).

Piccioni, G. et al. South-polar features on Venus similar to those near the north pole. *Nature* **450**, 637-640 (2007).

Sugimoto, N. et al. Waves in a Venus general circulation model. *Geophys. Res. Lett.* **41**, 7461-7467 (2014).

Takagi, M. et al. Sensitivity of thermal tides in the Venus atmosphere to basic zonal flow and Newtonian cooling. *Geophys. Res. Lett.* 32, doi:10.1029/2004GL022060, (2005).

Taylor, F. W. et al. Structure and meteorology of the middle atmosphere of Venus: infrared remote sensing from the Pioneer Orbiter. *J. Geophys. Res.* **85**, 7963-8006 (1980).

GLOBAL AERIAL EXPLORATION OF OUR SISTER WORLD VIA THE VENUS ATMOSPHERIC MANEUVERABLE PLATFORM (VAMP): SCIENCE OBJECTIVES AND POTENTIAL INSTRUMENTATION.

K. H. Baines, S. S. Limaye, *Space Science and Engineering Center, University of Wisconsin-Madison, Madison, WI, USA* (*blueskies4321@yahoo.com),* **R. Polidan, G. Lee, B. Sen**, *Northrop Grumman Aerospace Systems, Redondo Beach, CA, USA.*

Introduction: VAMP, the Venus Atmospheric Maneuverable Platform, under development by Northrop Grumman, is a versatile twin-engine buoyant aircraft capable of sustained (> months) exploration of Venus. Utilizing both dynamic and buoyant lift, the flying-wing-shaped aerial rover is capable of exploring a wide range of altitudes from its 50-km free-floating "safe-haven" level to over 65 km in altitude. Its solar-powered twin electric engines not only provide power for vertical ascents, but also the power for unprecedented mobility, enabling the aircraft to cruise up to ~ 30 knots airspeed, and thus allowing poleward/equatorward aerial excursions extending over 1400 km (over 12 degrees of latitude) per terrestrial day. Over 4-5 days, the planet's ~180 knot zonal wind enables the craft to circle the planet exploring all longitudes and times-of-day.

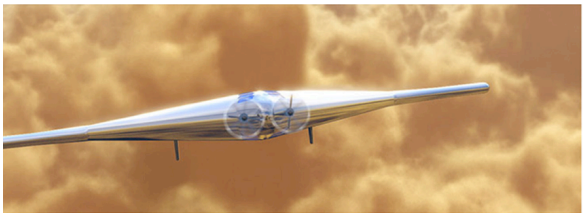

Fig.1 : The VAMP hybrid aerial rover exploring the skies of Venus, powered by twin solar-powered motors

As currently envisioned, VAMP provides unprecedented large amounts of payload mass, power, and volume for an *in-situ* Venus explorer. While still under assessment, it is clear that VAMP will provide more than 20 kg for science instrumentation with electrical power exceeding several kilowatts during daylight hours and perhaps a kilowatt during nighttime conditions. The relatively large size of the aircraft – with its wings spanning more than 15 meters – provides opportunities for instrumentation requiring relatively large volumes and/or space for an array of apertures (e.g., various forms of radar or electromagnetic detectors).

Atmospheric Science with VAMP: Objectives and Techniques: VAMP thus provides an unusually versatile platform for the *in-situ* aerial exploration of Venus, conducting an array of novel measurements that promise to provide crucial insights into virtually all aspects of Venus atmospheric science, including (1) the planet's origin and evolution, (2) its active and varying chemistry, driven by latitudinally, time-of-day, and vertically varying photochemical/thermodynamical processes, and (3) its global circulation, dynamics, and meteorology. Via mass spectrometry (MS), new insights into the origin and evolution of Venus can be provided through accurate measurements of the D/H ratio and the noble gases and their isotopes over both altitude and time-of-day, to correct for fractionation effects. Via tunable laser spectrometry (TLS), the isotopes of other light elements (e.g., nitrogen, carbon, and oxygen) can be measured as well, providing additional insights into Venus' origin and evolution.

VAMP provides *in-situ* sampling of key reactive gas species such as H_2O, CO, OCS, and SO_2 , and can do so regularly over altitude, latitude, and time-of-day via the MS, TLS and/or a near-infrared spectrometer operating in the 1-2.7-μm range. Using a nephelometer that includes a high-resolution optical microscope for aerosol imaging, the size, shape, and chemical composition of aerosols can be accurately determined, which, together with the reactive gas abundance data, promises to provide additional valuable insights into chemical cycles within Venus' dynamic clouds.

VAMP's mobility promises to be extremely effective at measuring crucial aspects of the planet's dynamics and circulation, including local meteorological effects. The aerial rover's ability to travel across nearly the entire globe over several weeks (likely limited by diminishing solar power poleward of ~ 70^o latitude) enables it to measure key aspects of any Hadley cells as well as the characteristics of planetary and gravity waves over nearly the entire planet. Using Doppler radar, it can measure its ground speed both day and night and thus accurately measure both the meridional and zonal winds from 50 to ~ 65 km altitude. Its pressure (P) and temperature (T) sensors will continually sample the atmosphere. Vertical traverses (typically both ascents during the day, and descents from high altitudes during the night), will allow the temperature gradient (dT/dz) to be assessed, from which the stability of the atmosphere, as a function of altitude, can be determined. A key parameter for understanding the planet's thermal structure and stability at lower altitudes is the vertical variability of the N_2 abundance. While commonly considered to be constant at 3.5%, previous probes strongly suggest

some 40% variability from ~ 22 km to ~52 km altitude. VAMP is well-suited to repeatedly measure N_2 and its vertical variability above 50 km as observed over day/night conditions and latitude. Any confirmed variability would have strong implications on the planet's lapse rate, thermal structure, stability, and flux of material, temperature, and momentum from near the surface to the cloud level, potentially providing significant new insights into mechanisms driving the planet's circulation, including its not-well-understood super-rotation. Within the clouds, the vertical component of the wind can be measured from an on-board vertical wind sensor combined with the pressure (P) data, from which, when combined with the dT/dz information, the relative roles of convection and vertical waves (e.g., gravity waves) can be assessed over various terrains as well as latitudes and time-of-day. Investigations of vertical dynamics combined with measurements of lightning from an onboard lightning detector will provide new insights into the role lightning and convective storms play in Venus's meteorology and chemistry, particularly in the production of lightning-generated species (e.g., NO).

Additional information over altitude comes from two other aspects of a likely mission. First, during atmospheric entry, VAMP's low-density design enables it to slow to "observing speed" above ~ 90 km altitude, enabling the aircraft to make *in-situ* measurements from well above the unexplored UV aerosol layer down to ~ 50 km level. Second, the relatively large payload capability allows the possibility for both drop-sondes and balloon-borne "rise sondes" to be deployed, sampling both lower and higher altitudes than the 50-~65 km altitude regularly sampled by VAMP.

Surface/Geologic Science with VAMP: Objectives and Techniques: Beyond aerial exploration for atmospheric science, VAMP also provides a valuable platform for discovering new insights into the planet's surface geology and interior. RADAR maps and nighttime near-IR images can be used to characterize the surface topography, surface texture, and crude chemical make-up (e.g., igneous vs basaltic rocks), from which geological insights (e.g., the extent and relative age of surface volcanism) can be made. As well, an array of aural seismic detectors can be deployed which listen for the deep rumble of seismic events. As well, a large (multi-meter-wide) electromagnetic array carried aboard VAMP could possibly sound more than 10 km below the planet's surface, to map the depth of the lithosphere.

Conclusion: VAMP thus provides a particularly versatile aerial platform for the exploration of nearly the entire planet, with particular emphasis on sampling highly diagnostic gases, aerosols, winds, temperatures, pressures and lightning characteristics, as well as for mapping key characteristics of surface geology. As such, it is an ideal platform around which to base an internationally collaborative mission.

Synthesis of Venera Lander Results and Future Problems.

A. T. Basilevsky, **M. A. Ivanov**, *Vernadsky Institute of Geochemistry and Analytical Chemistry, RAN, Moscow, Russia (atbas@geokhi.ru)*, **J. W. Head**, *Department of Earth, Environmental and Planetary Sciences, Brown University, Providence, Rhode Island 02912 USA.*

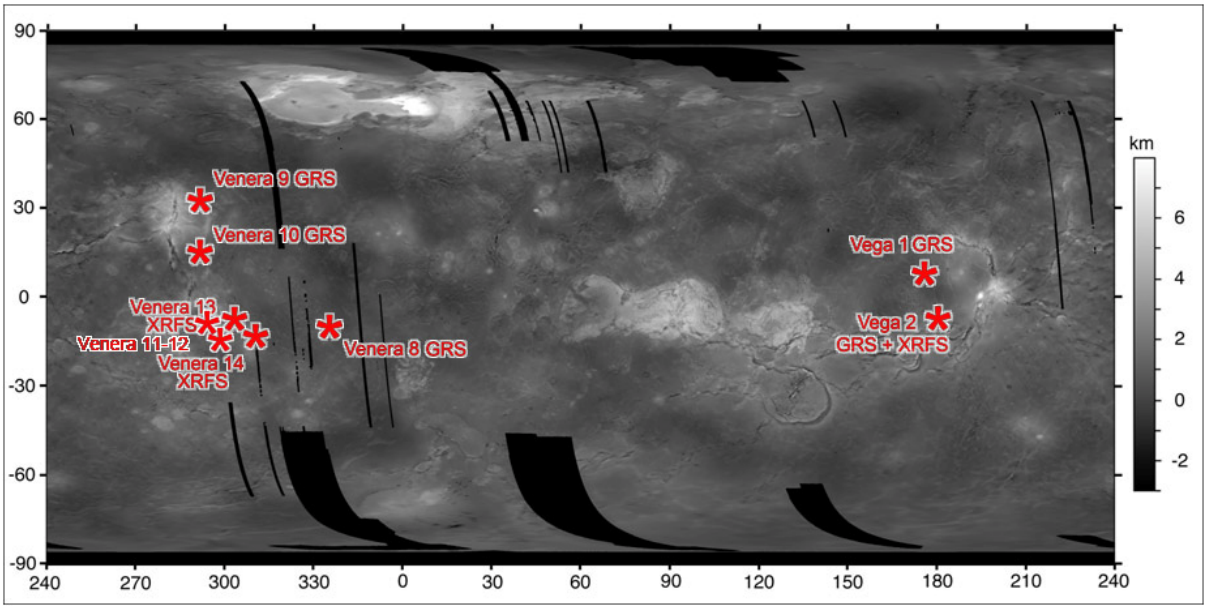

Introduction: There were nine essentially successful landing missions on Venus which showed close up images of the surface, measured its chemical composition and provided information on the near-surface environment.

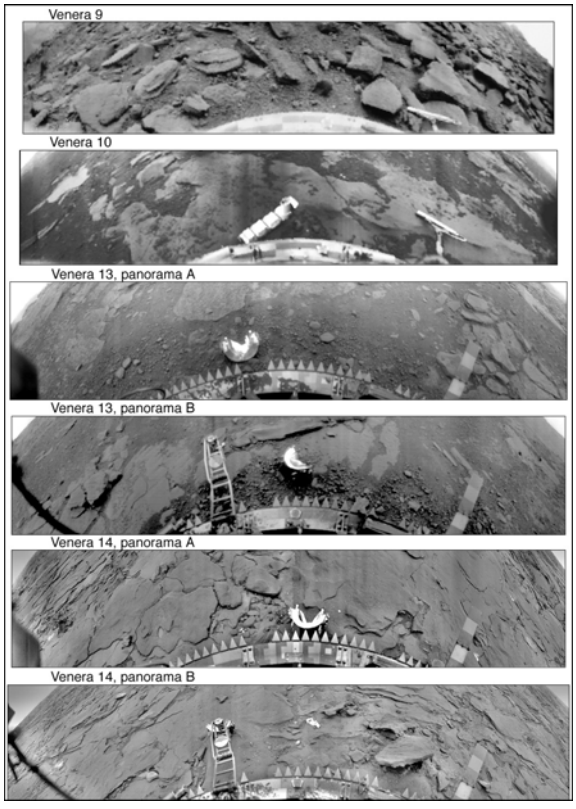

Mission description: ***Venera 8*** was a Venus atmospheric probe and lander that landed on July 22, 1972 at 10.70°S 335.25°E. Its instrumentation included temperature and pressure sensors, accelerometer, photometers, ammonia analyser, gamma ray spectrometer, and a radar altimeter.

Venera 9 was a Venus atmospheric probe/lander and orbiter that landed on October 22, 1975 at 31.01°N 291.64°E, The lander instrumentation included: temperature and pressure sensors, accelerometer, Visible/IR photometer, nephelometers, mass spectrometer, panoramic telephotometers, anemometer, gamma ray spectrometer, gamma ray densitometer

Venera 10 was a Venus atmospheric probe/lander and orbiter – twin mission to Venera 9, that landed on October 25, 1975 at 15.42°N 291.51°E.

Venera 11 was a Venus atmospheric probe and lander that landed on December 25 at 14°S 299°E. The lander instrumentation included: backscatter nephelometer, mass spectrometer, gas chromatograph, X-ray fluorospectrometer, 360° scanning photometer, spectrometer (430–1170 nm), microphone/anemometer, 4 thermometers, 3 barometers, accelerometer, penetrometer, soil analysis device, and 2 color cameras on which the windows did not open.

Venera 12 was a Venus atmospheric probe and lander – twin mission to Venera 11 that landed on December 25 at 7°S 294°E.

Venera 13 was a Venus atmospheric probe and lander that landed on March 1, 1982, at 7.5°S 303°E.

The lander instrumentation included: accelerometer - impact analysis, thermometers, barometers, spectrometer/directional photometer, ultraviolet photometer, mass spectrometer, penetrometer / soil ohmmeter, chemical redox indicator, 2 color telephotometer cameras, gas chromatograph, radio/seismometer, nephelometer, hydrometer, X-ray fluorescence spectrometer (aerosol), X-ray fluorescence spectrometer (soil), soil drilling apparatus.

Venera 14 was a Venus atmospheric probe and lander – twin mission to Venera 13 that landed on March 5, 1982, at 13.25°S 310°E.

Vega 1 was a Venus atmospheric probe/lander and balloon; the flyby part travelled to Halley's comet. The lander instrumentation included: accelerometer, temperature and pressure measuring sensors, UV spectrometer, hygrometer, aerosol analyzer, spectrometer/nephelometer, gas-phase chromatograph, X-ray spectrometer, mass spectrograph, drilling device, gamma ray spectrometer and X-ray fluorescence spectrometer. Vega 1 landed on June 11, 1985, at 7.2°N 177.8°E.

Vega 2 was a Venus atmospheric probe and lander – twin mission to Vega 1 that landed on June 15, 1985, at 7.14°S 177.67°E.

Surface analysis results: Based on measurements of the instruments mentioned above a lot of key information on the surface and atmosphere characteristics of Venus was acquired. The GRS and XRFS measurements showed that surface material at the Venera-9, 10, 13, 14 and Vega 1,2 sites is of basaltic composition [1]. At the Venera 11/12 sites analyses of this sort were not done. The measured basaltic surface composition agrees well with the results of photogeological analysis of the Magellan images of the planet [2-4]. Only areas of tessera terrain [3,4] and some steep-sided domes probably are not basaltic but rather felsic [5-8]. Centimeter-scale platy surface seen at the Venera-9, 10, 13, 14 panoramas is probably composed of air-fall deposits resulted from fine ejecta of impact craters located upwind [9]. Normally the near-surface winds are slow but the high density of the atmosphere makes sculpturing of the surface possible [10]. At zero altitude level, the surface temperature on Venus is 470C and the atmospheric pressure is 93 bar [11]. The major constituents of the Venus atmosphere are CO_2 (96.5 mol %) and N_2 (3.5%) [12]. The geochemically important H_2O vapor content is ~45 ppm, and the SO_2 content normally is ~100 ppm [12]. But in 1980 the SO_2 content was as high as ~400 ppm and then for several years gradually decreased [13]. This peak content could be a result of massive volcanic eruption but purely meteorological causes are also not excluded. The D/H ratio of the Venus atmosphere is more than factor 100 higher than that in the Earth's ocean, suggesting that in its early history Venus could have had an ocean [14]. Recent observations of the surface "hot spots" in the Ganiki rift zone suggest that this planet is still volcanically active [15], but this conclusion needs to be confirmed in other areas of the planet.

Problems to be resolved in future studies: On the basis of our experience, key outstanding problems include:

• What was happening on Venus between its accretion and the formation of tessera terrain?
• Did Venus once have an ocean?
• Did plate tectonics ever occur on Venus?
• Is tessera terrain composed of thickened basaltic crust or of a different low-density material?
• What was the mechanism of tessera formation (deformation resulted from upwelling or downwelling) and how long was the tessera-forming phase?
• How did the folded mountain ranges surrounding Lakshmi Planum form?
• Is Venus still volcanically and tectonically active?
• Are coronae manifestations of mantle plumes or negative diapirs? Are some of them still active?
• What is the origin of layered rocks seen in the Venera panoramas?

References: [1] Surkov, Y.A., *Exploration of Terrestrial Planets from Spacecraft: Instrumentation, Investigation, Interpretation*, 2nd ed., 446 pp. John Wiley, Hoboken, N. J., 1997. [2] Head J. W. et al. (1992) *JGR*. V. 97(E8), 13153-13197. [3] Basilevsky A.T. & Head J.W. (1995), *Earth, Moon, Planets*, *66*(3), 285–336. [4] Ivanov, M.A., and J.W. Head (2011) *Planet. Space Sci.*, *59*(13), 1559–1600. [5] Helbert J. et al. (2008) *Geophys. Res. Lett.* V. 35, L11201. [6] Mueller N. et al. (2008) *J. Geophys. Res.* 113, E00B17. [7] Gilmore M.S. et al. (2011) *Lunar Planet. Sci*., 2053. [8] Basilevsky A.T. et al. (2012) *Icarus* 217 (2012) 434–450. [9] Basilevsky et al. (2004) JGR, V. 109, E12003. [10] Florensky et al. (1983) *Science*. V. 221. 57-59. [11] Moroz V. I. *Space Science Reviews*. V. 29, no. 1, 1981, 3-127. [12] Hunten D.M. (1999) *Encyclopedia of the Solar System.* Academic Press. 147-160. [13] Esposito L. et al. (1997) In: *Venus II*, 415-458. [14] Grinspoon D.H. (1993) *Nature*. V. 363. 428-431. [15] Shalygin et al. (2015) *Geophys. Res. Lett.* V. 42. 4762-4769.

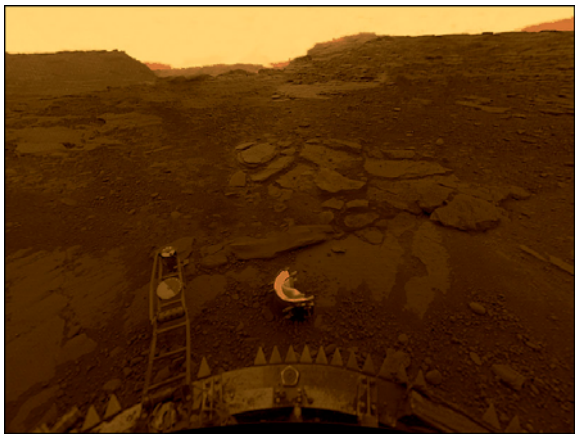

Venera 13 : Mosaicing and art by Don Mitchell

Distribution of SO_2 content at the night side of Venus' upper mesosphere

D. A. Belyaev , *IKI RAS, Moscow, Russia (bdenya.iki@gmail.com)*, **D. Evdokimova,** *IKI RAS,* **F. Montmessin**, *LATMOS-UVSQ/CNRS/IPSL, Guyancourt, France,* **E. Marcq**, *LATMOS,* **A. Fedorova**, *IKI RAS*, **O. Korablev**, *IKI RAS*, **J.-L. Bertaux**, *LATMOS.*

Introduction:

Venus has a dense CO_2 atmosphere with a thick cloud layer (50-70 km) consisting of sulfuric acid (H_2SO_4) aerosols. Sulfur oxides (SO_x) are directly associated with those aerosols and plays an important role in chemistry of the atmosphere. Any change of its content within or above the clouds has an influence on photochemical processes in the mesosphere (70-100 km). Recent ground-based observations [1-4] and continuous monitoring from the Venus Express orbiter [5-7] have shown high temporal and spatial variability of SO_2 abundance mostly on the day side: from 20 to 500 ppbv above the clouds. There is a lack in the detailed analysis at the nighttime mesosphere where photo dissociation of sulfur dioxide is replaced by interaction with the global subsolar/antisolar circulation and chemical reactions with atoms of Cl, OH, O etc.

In this paper we present vertical distribution of SO_2 content at the night side of Venus upper mesosphere that resulted from stellar occultations made by the SPICAV UV spectroscopy. This mode of occultation occurred for the entire VEx mission, and it gave us possibility to observe yearly variations for period 2006-2014 at altitudes 85-100 km. In parallel, we have reprocessed the terminator dataset from the UV solar occultations at the same altitude range [5] up to 2014. Like this, we have got whole the nighttime coverage of SO_2 distribution from the sunset to the sunrise twilights of the upper mesosphere.

Experiment:

SPICAV UV channel operated in the spectral range 118-320 nm with a resolution 1-2 nm at nadir or stellar/solar occultation modes [8]. Here we deal with measurements of SO_2 atmospheric absorption in stellar and solar occultation modes. In the case of stellar occultation the instrument observes night-side mesosphere while in solar occultation it probes evening/morning twilights at altitude range 85-100 km. SPICAV can register SO_2 absorption bands at 190-220 and 270-300 nm and CO_2 bands at 120-210 nm.

In the occultation mode an instrument registers the solar (or a stellar) flux out of planetary atmosphere and a flux, having passed through different levels of the atmosphere. The ratio of the second flux to the first one determines the atmospheric transmission at a fixed tangent altitude. This transmission (a relative quantity) is interpreted as due to the extinction from aerosols and gases that can be identified by their spectral signature, and their quantity along the line of sight (LOS) of the instrument (Fig. 1).

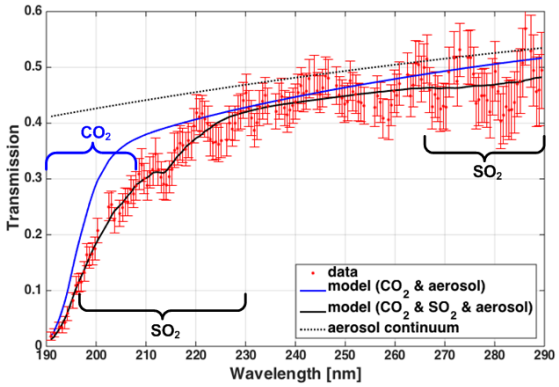

Fig. 1. An example of measured transmission spectrum (red dots with error bars) from a stellar occultation at altitude 90 km (orbit 1073, LT 2:00am, Lat 37.81°N). Molecular absorptions of CO_2 (in blue) and SO_2 (in black) are detected together with aerosol continuum (black dashed): $N_{CO2}=3\cdot10^{23}$ cm^{-2}; $N_{SO2}=8\cdot10^{16}$ cm^{-2}.

Solar occultation. In the solar occultation mode the vertical FOV varied from 0.5 to 15 km, depending on the instrument's CCD recording algorithm and on a distance to the planet's limb. For our study we selected orbits with an altitude FOV less than one scale height of the atmospheric density (i.e. <4 km). It reduced the importance of the stray light, which comes from different parts of the atmosphere in the case of a wide FOV. At present, we have processed 330 sessions of solar occultation occurring from 2007 to 2014, in the latitude range 30°S-90°N, and in conditions of sunrise (06:00am of Venus local time) or sunset (06:00pm). Most of the observations took place close to the Northern pole with a short distance to the planet's limb (< 2000 km), due to peculiarities of the VEX's polar orbit.

Stellar occultation. The stellar occultation technique is similar to the solar one with the difference that a star is observed as a respectively weak point source and the night side of the atmosphere is probed. The instrument's FOV is directed to an UV star with maxima of radiance at wavelengths 100-300 nm. During the VEX mission stellar occultation mode occurred regularly with ~60 different target stars, covering latitudes from 70°S to 70°N and local time on Venus from 07:00pm to 05:00am. In order to avoid detection of the Sun brightening from the dayside atmosphere we selected observations with a solar-zenith angle more than 100°. Thus, we have collected statistics with 210 sessions of stellar occultations from June 2006 to May 2014.

Results:

Figure 1 (see above) demonstrates a clear detection of SO_2 absorption on a background of CO_2 and aerosol abundances. This is a case of a rather large mixing ratio of sulphur dioxide at altitude 90 km: 270 ppb. Nevertheless, in some observations we retrieved rather low values – down to 10 ppb. It shows a high variability of SO_2 content in Venus' upper mesosphere either from solar occultation or from stellar one. On average, the volume mixing ratio increases with altitude from 10-30 ppbv at 85 km to 100-300 ppbv at 100 km (Fig. 2).

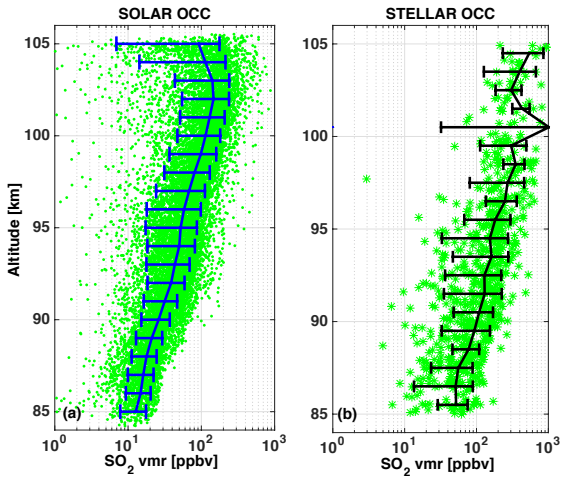

Fig. 2. Altitude distribution of SO_2 mixing ratio from SPICAV UV solar (a) and stellar (b) occultations. Solid lines are weighted mean values with standard deviations. Error bars of individual dots (not shown) are less than the dispersion of the data.

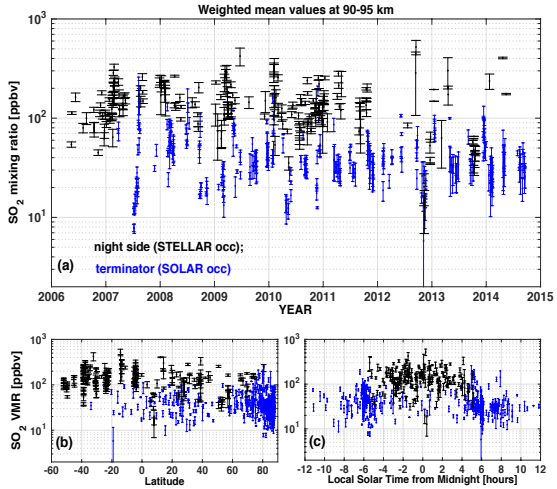

Fig. 3. Time (a), latitude (b) and Local time (c) diagrams of SO_2 variations at altitude level 90-95 km (blue – solar occultations, black – stellar occultations).

Time variations of SO_2 show a few peaks with values >100 ppb from both regimes of occultation (Fig. 3a). These events are local in time and they are not revealed on the latitude diagram (Fig. 3b). We can also look on the Local time diagram where average SO_2 content around midnight are 2-4 times higher than at the evening/morning twilights (Fig. 3c). Additional analysis is going on together with properties of aerosol particles [9], in order to establish correlations between SO_2 peaks and particles sizes and densities.

Acknowledgements

Venus Express is an ESA mission. D. Belyaev and D. Evdokimova acknowledge support from the RFFI grant № 16-02-00633a in 2016. F. Montmessin, E. Marcq, and J.-L. Bertaux acknowledge support from the CNES and from the CNRS. We also thank to the support provided by ISSI, through the organization of the International Team meeting "Sulphur dioxide variability in the Venus Atmosphere" in 2013-2015. (http://www.issibern.ch/teams/venusso2/).

References:

[1] Encrenaz T. et al., 2012. HDO and SO_2 thermal mapping on Venus: evidence for strong SO_2 variability. A&A 543, A153.

[2] Krasnopolsky V.A., 2010. Spatially-resolved high-resolution spectroscopy of Venus. 2. Variations of HDO, OCS, and SO_2 at the cloud tops. Icarus 209, 314-322.

[3] Sandor B.J. et al., 2010. Sulfur chemistry in the Venus mesosphere from SO_2 and SO microwave spectra. Icarus 208, 49–60.

[4] Jessup et al., 2015. Coordinated Hubble Space Telescope and Venus Express observations of Venus' upper cloud deck. Icarus. http://dx.doi.org/10.1016/j.icarus.2015.05.027.

[5] Belyaev D. et al., 2012. Vertical profiling of SO_2 and SO above Venus' clouds by SPICAV/SOIR solar occultations. Icarus 217, 740–751.

[6] Marcq E. et al., 2013. Variations of sulphur dioxide at the cloud top of Venus's dynamic atmosphere. Nature Geoscience, vol. 6, 25-28. DOI: 10.1038/NGEO1650.

[7] Mahieux A. et al., 2015. Venus mesospheric sulfur dioxide measurement retrieved from SOIR on board Venus Express. Planet. Space Sci. v.113-114, p.193–204.

[8] Bertaux J.-L. et al., 2007. SPICAV on Venus Express: three spectrometers to study the global structure and composition of Venus atmosphere. Planet. Space Sci. 55, 1673–1700.

[9] Luginin M. et al., 2016. Venus' upper haze aerosol properties from SPICAV IR data. This issue.

INFLUENCE OF VENUS TOPOGRAPHY ON THE ZONAL WIND AND ALBEDO AT CLOUD TOP LEVEL: THE ROLE OF STATIONARY GRAVITY WAVES.

J.L. Bertaux, **E.Marcq,** *LATMOS/CNRS/UVSQ Guyancourt France (jean-loup.bertaux@latmos.ipsl.fr),* **I.V. Khatunstsev,** *Space Research Institute RAS Moscow, Russia,* **W.J. Markiewicz** *MPS Solar System Research, Göttingen, Germany,***A. Hauchecorne,** *LATMOS/CNRS/UVSQ Guyancourt France* **S. Lebonnois,** *LMD/CNRS/UPMC Paris France,* **M. Patsaeva, A. Turin, A. Fedorova,** *Space Research Institute RAS Moscow, Russia.*

Introduction:

Based on the analysis of UV images (at 365 nm) of Venus cloud top (altitude 67±2 km) collected with VMC (Venus Monitoring Camera) on board Venus Express (VEX), it is found that the zonal wind speed south of the equator (from 5°S to 15°s) shows a conspicuous variation (from -101 to -83 m/s) with geographic longitude of Venus, correlated with the underlying relief of Aphrodite Terra. We interpret this pattern [1] as the result of stationary gravity waves produced at ground level by the up lift of air when the horizontal wind encounters a mountain slope. These waves can propagate up to cloud top level, break there and transfer their momentum to the zonal flow.

Comparison of wind data with topography:

Zonal wind just below equator (average of 6,312 measurements) plotted with longitude correlate quite well with topography, when the wind is shifted by +30°.

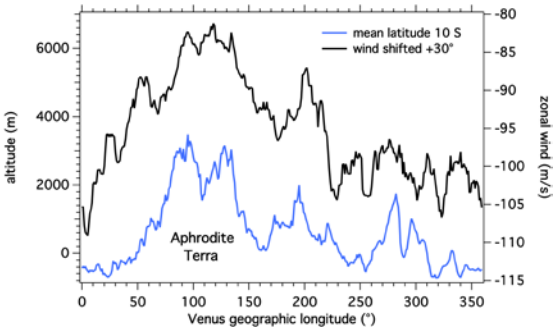

Figure 1. Longitude distributions of the relief altitude and of the zonal wind in the latitude-selected region (from 5°S to 15 °S). Blue curve: altitude in m, left scale. Black curve: zonal wind (m/s), right scale. The longitude for the zonal wind was displaced by +30° from the altitude one, to emphasize the correlation between the zonal wind and the relief, ~65 km below.

We also compare a geographic longitude-latitude map of Venus topography (from 5°S to 45°S, figure 2a, 2b) to a map of the zonal wind in the same latitude range (figure 3), well covered by VMC and containing conspicuous mountains named Aphrodite Terra and Atla Regio. The zonal wind map shows a region of greatly decreased zonal wind, a fact that was totally unexpected and ignored up to now.

There is an obvious correlation between the two maps (topography and wind speed), with the region of minimum wind (absolute speed) being displaced by ~30° downstream. The minimum zonal wind at -82 m/s (in absolute value) is found 30° downstream of Aphrodite Terra, a high altitude region (3,000 m) extending from 40° to 160° in longitude.

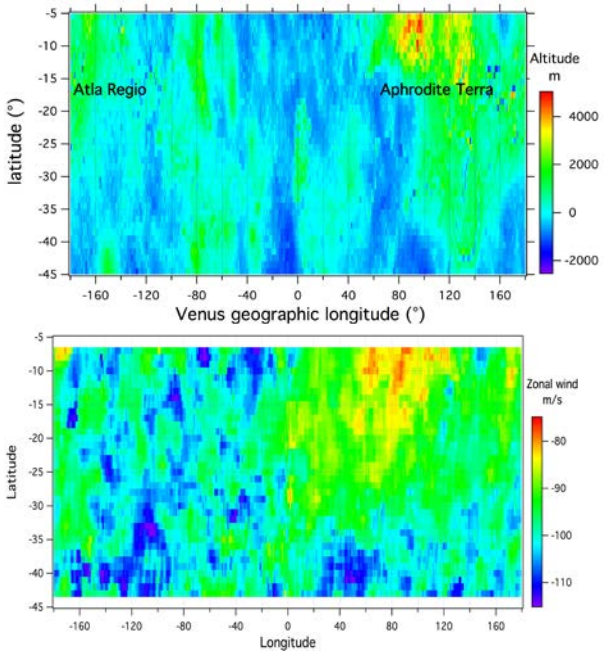

Figure 2a (top). Partial topographic map of Venus. Altitude is color coded. The latitude coverage of the map is limited from 5° S to 45° S to match the map of zonal wind. The zonal wind is blowing right to left from East to West, toward decreasing longitudes. Figure 2b (bottom). Map of the zonal wind speed in m/s (color coded).

We propose that stationary gravity waves (Fig.3) are generated by the horizontal wind flowing over a relief; then they propagate upward up to the altitude where they break and transfer their momentum to the general circulation. Since they are stationary, they decelerate the zonal flow.

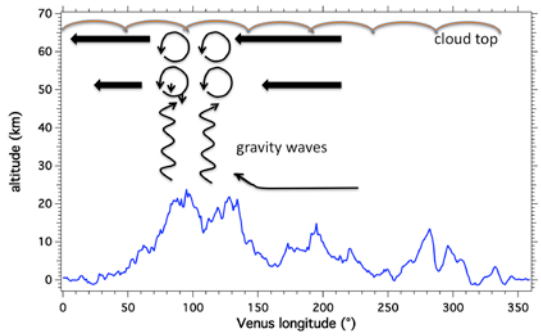

Figure 3. Sketch of gravity waves generated by interaction of the zonal wind on the mountains, propagating upward, breaking in the altitude region 50-60 km and decelerating

the zonal wind at this altitude and higher. The altitudes of the relief is exaggerated by a factor 7 for better clarity.

Mapping of UV albedo and H_2O at cloud top:

The UV albedo measured by VMC at 365 nm shows also a longitude variation correlated with the wind (figure 4).

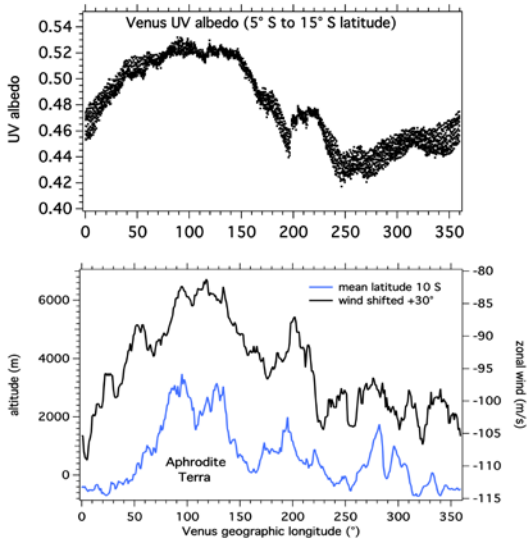

Figure 4. Latitude averages between 5 ° S and 15 °s of altimetry, zonal wind, and UV albedo. The curve of zonal wind is shifted 30° to the right to emphasize the correlation with the relief. The albedo points are representing averages within 1x1° latitude-longitude bins.

On figure 5a is displayed a geographic map of the UV albedo at 365 nm measured by VMC. It is an average of 1442 images obtained over 7.5 years from VEX orbit 30 (May 2006) to orbit 2714 in September 2013 (more than 12 Venus years). While the UV albedo poleward of 40°S is pretty uniform and higher than near the equator, a well known fact [2] there are totally unexpected structures at other places nearer the equator, both in longitude and latitude.

At the same time, a map of H_2O at cloud top level was recently obtained [3] from the near-infrared spectral feature at 1.38 µm detected in the solar back-scattered radiation (from SPICAV IR instrument on Venus Express). It reveals (fig.5b) There is more H_2O poleward of 60° of latitude than elsewhere in both hemispheres, which is due to the decrease of H_2O mixing ratio with altitude and lower cloud altitude by ~6 km at high latitudes.

In the low latitude regions from -30 to +30° of latitude, the H_2O mixing ratio is pretty uniform at 5.5- 6 ppmv, except for a conspicuous region, centered slightly below the equator and reaching 7 to 7.5 ppmv. This region extends from -130° to + 30° of longitude. This H_2O feature is statistically solid, and it demonstrates an increased upwelling of air in this particular region. The geographic maps of H_2O and UV albedo show a striking similarity in the low latitude regions, at least up to 40° of latitude. The region of low UV albedo coincides with the region of increased water vapor both in longitude and latitude, as shown by the iso-contours at 6.5 ppmv. We conclude that the UV absorber is present in upwelling regions, and therefore it must be produced below the cloud top level.

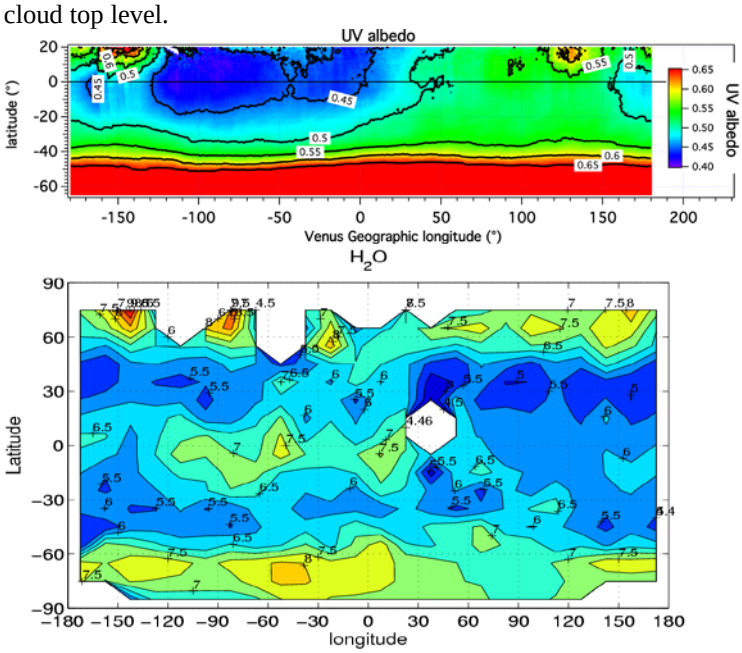

Figure 5a top. Venus geographic map of the UV albedo. The number of points per bin ranges from ~1000 to 5000. Iso-contours of UV albedo are drawn.

Figure 5b bottom. Geographic distribution at cloud top altitude of H_2O mixing ratio (reproduced from Fedorova et al. [2016]). Iso-contours are indicated in ppmv.

A plausible scenario:

Conservation of matter indicates that, since the divergence of the horizontal wind field at cloud top is different from 0, it requires a convergence of the vertical motion of air to compensate. There is upwelling in the longitude range of wind acceleration (from +60 to -30° after proper re-shift of the wind longitude profile) as revealed by H_2O map. This upwelling motion brings water vapor and the UV absorber from below, which is then transported horizontally in the general flow, as a plume of a minor constituent. Further downstream, a sign reversal of the zonal flow longitude derivative is encountered, around 190° longitude (or -170°), where the upwelling ceases, the UV albedo increases and water vapor decreases along downstream.

Acknowledgements. Venus Express is an ESA mission.

References:

[1] Bertaux et al., Influence of Venus topography on the zonal wind and albedo at cloud top level: the role of stationary gravity waves, *J. Geophys Res., in revision*, 2016

[2] Limaye and Suomi, A normalized view of Venus, *J. Atmos. Sci.*, **34**, 205– 215, 1977

[3] Fedorova, A., E. Marcq, M. Luginin, O. Korablev, J.-L. Bertaux, and F. Montmessin, Variations of the water vapor and the cloud haze in the Venus' mesosphere from SPICAV/VEx observations, *Icarus*, 2016.

RADIO OCCULTATION EXPERIMENTS WITH VENUS EXPRESS USING THE PLANETARY RADIO INTERFEROMETRY AND DOPPLER EXPERIMENT (PRIDE) TECHNIQUE.

T.M. Bocanegra-Bahamón, *Department of Astrodynamics and Space Missions, Delft University of Technology, The Netherlands (t.m.bocanegrabahamon@tudelft.nl)*, *Joint Institute for VLBI in Europe, The Netherlands*, *Shanghai Astronomical Observatory, China*, **L.I. Gurvits, G. Cimò, S.V. Pogrebenko,** *Joint Institute for VLBI in Europe, The Netherlands*, **G. Molera-Calvés,** *Aalto University, Finland*, **D.A. Duev,** *California Institute of Technology*.

The Planetary Radio Interferometry and Doppler Experiment (PRIDE) is a technique that can provide a multi-disciplinary enhancement of the science return of planetary missions. By performing precise Doppler tracking of a spacecraft carrier radio signal, at Earth-based radio telescopes, and VLBI-style processing of these signals in phase-referencing mode, the technique allows the determination of the radial velocity and lateral coordinates of the spacecraft with very high accuracy [1].

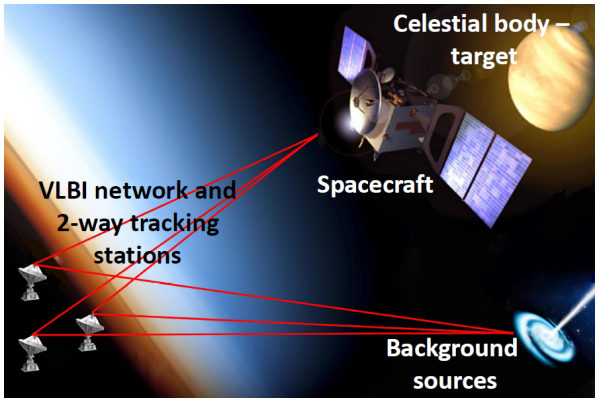

Figure 1: Generic PRIDE configuration.

Because of the accurate examination of the changes in phase and amplitude of the radio signal propagating from the spacecraft to the multiple stations on Earth, the PRIDE technique can be used for several fields of planetary research. The application of this technique for atmospheric studies has been assessed by observing ESA's Venus Express (VEX) during Venus occultation events in 2012 and 2014. During the two sessions of radio occultation experiments in April 2012 and March 2014, VEX was tracked with several telescopes from the European VLBI Network (EVN) at X-band. From these experiments, radio occultation profiles of neutral density and electron density of the atmosphere and ionosphere of Venus were obtained from ingress and egress occultation tracking, using a software developed for this specific purpose (see Fig. 2).

The first part of the software, which comprises the SWSpec, SCTracker, PLL and SFXC correlation software [1, 2], (yellow blocks) is used for every standard PRIDE experiment. This first processing steps bring the data from raw to level 2 data. The second part of the software was developed for the sole purpose of processing radio occultation experiments. It consists of three main modules, the frequency residuals derivation module, the geometrical optics module and the Abelian integral inversion module, from which vertical density profiles, and subsequently, temperature and pressure profiles of the target's atmosphere can be derived.

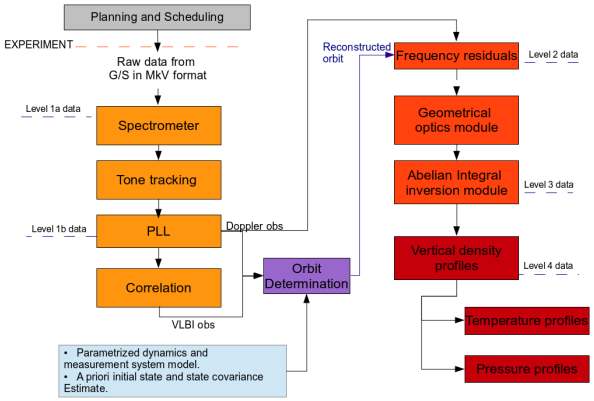

Figure 2: Data processing pipeline.

The highly accurate Doppler detections achieved by PRIDE are used to obtain the Doppler residuals, and the VLBI mode of the experiment is used to derive precise estimates of the spacecraft state vectors. The technique is particularly suitable for radio occultation experiments, due to its sensitivity to signal path deviations perpendicular to the line of sight of the antenna pointing.

These activities serve as demonstration of the applicability of the PRIDE technique for radio occultation studies, and provides a benchmark against the traditional Doppler tracking, for the same purposes.

Acknowledgements

The PRIDE-team activities are partially supported by funding from the European Community's Seventh Framework Program (FP7/2007-2013) under Grant Agreement No. 263466 for the ESPaCE project. T.M.Bocanegra Bahamon acknowledges the NWO-ShAO agreement.

The EVN is a joint facility of European, Chinese, South African and other radio astronomy institutes funded by their national research councils.

References

[1] Duev, D.A., Molera Calvés, G., and Pogrebenko, S.V., Gurvits, L.I., Cimo, G. and Bocanegra Bahamon, T.M.: Spacecraft VLBI and Doppler tracking: algorithms and implementation, Astronomy & Astrophysics, Vol. 541, 2012.

[2] Keimpema, A., Kettenis, M.M., Pogrebenko, S.V., Campbell, R.M., Cim, G., Duev, D.A., Eldering, B., Kruithof, N., van Langevelde, H.J., Marchal, D. and Molera-Calvés, M., 2015. The SFXC software correlator for very long baseline interferometry: algorithms and implementation. Experimental Astronomy, pp.1-21.

UPPER ATMOSPHERE TEMPERATURE AND CO VMR STRUCTURE AT THE VENUSIAN TERMINATORS: A COMPARISON OF RECENT SOIR MODELS AND VTGCM SIMULATIONS

S. W. Bougher, C. D. Parkinson, D. J. Shields, *CLaSP Department, U. of Michigan, Ann Arbor, MI USA (bougher@umich.edu),* **B. Sandor,** SSI, Boulder, CO USA, **A. S. Brecht,** BAERI, NASA ARC, Moffett Field, CA USA, **A. C. Vandaele, A. Mahieux, V. Wilquet,** IASB/BIRA, Brussels, Belgium.

Introduction and Motivation:

One of the major goals of the Venus Express (VEx) mission has focused upon increasing our understanding of the highly variable global circulation and wave processes impacting the Venus mesosphere-thermosphere (~80 – 200 km). Several VEx instruments (e.g. SOIR, SPICAV and VIRTIS) and ground based observations have provided measurements that characterize the upper atmosphere structure and underlying variable dynamics during the solar minimum-to-moderate period of the solar cycle when VEx measurements were obtained (2006-2014). In particular, SOIR profiles of terminator temperatures (T) and CO volume mixing ratios (vmr) have been obtained and analyzed. We utilize these datasets to establish a statistically averaged mean state and characterize the variability of the upper mesosphere and thermosphere structure. The goal is to determine the spatial and temporal variability about the mean, thereby providing boundaries for planetary and tidal wave experiments that are planned for making use of the VTGCM code.

We review these key SOIR measurements that provide constraints on these changing global circulation patterns and wave processes. We also provide initial data-VTGCM comparisons of terminator T and CO vmr profiles as a function of latitude (~80-150 km). Implications for variable SS-AS (subsolar-to-antisolar) and RSZ (retrograde super-rotating zonal) winds are discussed. Overall temporal variability in T and CO vmr profiles is quantified.

SOIR Temperature-CO Datasets and Models:

The spectral range covered by SOIR allows the observation of several key species of the Venus atmosphere, such as CO_2, CO, HCl, HF, H_2O and its isotopologue HDO, as well as SO_2. The retrieval technique to derive CO_2 densities and trace gas densities is the same and has been described in detail (1, 2). CO_2 has been observed in almost all occultations, except at the beginning of the mission. Knowing the CO_2 density allows one to derive volume mixing ratios of all trace gases.

Previously, Solar Occultation at Infrared (SOIR) terminator profiles of CO_2 densities and temperatures were organized and presented for up to 132-selected orbits obtained between 2006-2013 (1, 3, 4). The SOIR instrument measured CO_2 absorption across a broad spectral window. The observed atmospheric transmittance spectra are subsequently inverted to obtain vertical density (and inferred temperature) profiles. This compilation provided a global view of the atmospheric characteristics at the Venusian terminators over ~70 to 160 km. These initial measurements showed a striking permanent temperature minimum (at ~125 km) and a weaker temperature maximum (over ~100-115 km). These features are reflected in the corresponding CO_2 density profiles, and provide detailed constraints for global circulation models of the upper atmosphere of Venus (3, 4, 5).

Recently, CO profile measurements were collected into 4-latitude bins (see **Table 1**), with corresponding temperatures, yielding a new model of self-consistent CO vmr and T profiles (6). These SOIR bin averaged profiles are used for comparison to VTGCM simulated profiles.

Latitude bins	Number of observations AM Terminator (MT)	Number of observations PM terminator (ET)
0°-30°	25	24
30°-60°	21	19
60°-80°	31	29
80°-90°	32	29
Total	109	101

Table 1: Statistics of the CO observations for the different latitude bins and on each side of the terminator considering hemispherical symmetry.

VTGCM Model Basics:

The Venus Thermospheric General Circulation Model (VTGCM) is a 3-D finite difference hydrodynamic model of Venus' upper atmosphere (7) which is based on the National Center for Atmospheric Research (NCAR) terrestrial Thermospheric General Circulation Model (TGCM). The VTGCM has been documented in detail as revisions and improvements have been made over more than two decades (e.g. 7, 8, 9, 10, 11, 12, 13, 14).

The VTGCM solves the time-dependent primitive equations for the neutral upper atmosphere. The diagnostic equations (hydrostatic and continuity) provide geopotential and vertical motion fields. Additionally, the prognostic equations are typically solved for steady-state solutions for the temperature, zonal and meridional velocities, and the mass mixing ratios of specific species. The VTGCM composition includes major (CO_2, CO, O, N_2) and minor species (O_2, $N(^4S)$, $N(^2D)$, NO, SO, SO_2), plus dayside photochemical ions (CO_2^+, O_2^+, O^+, N_2^+, NO^+). The VTGCM model domain covers a 5° by 5° latitude-longitude grid, with 69 evenly spaced log-pressure levels in the vertical, extending from ~70 to 300 km (~70 to 200 km) at local noon (midnight). This altitude range insures that all dynamical influences contributing to the nightglow layers (e.g. O_2 IR (1.27-μm), NO UV (δ band 190-290 nm and γ band 225-270 nm emissions) can be captured, and wave propagation (i.e. tidal plus planetary waves and gravity waves) above the cloud tops can be accommodated. The VTGCM lower boundary conditions near ~70 km are taken from a lower atmosphere GCM, thereby providing a self-consistency among the temperature, height, and zonal wind fields (as a function of latitude) at this bottom pressure level.

The VTGCM can capture the full range of EUV-UV flux conditions. For this study, solar minimum and moderate fluxes (F10.7 = 70 and 130, at Earth) were specified for conducting VTGCM simulations, yielding appropriate terminator T and CO vmr profiles for comparison to SOIR datasets.

Approach to data-VTGCM comparisons:

The motivation for studying self-consistent T and CO vmr profiles together is found in spatially resolved disk maps of T and CO distributions obtained from ground-based measurements (15). These distributions were found to be typically correlated, such that enhancements in the CO vmr are usually associated with warmer temperatures. The interpretation thusfar is that T and CO fields are best correlated with time-average wind patterns (i.e. where the timescale may be a few months, but is not well known). An example of spatially resolved and correlated T and CO distributions from a specific ground-based observation is given in **Figure 1**. The enhancements of CO vmr and corresponding warmer temperatures are seen after midnight, consistent with a modest RSZ wind component at ~105 km. ET versus MT asymmetries in T and CO vmr profiles may also be observable in SOIR datasets consistent with the changing SS-AS and RSZ wind system as a function of altitude. Hence, data-VTGCM comparisons are used to interpret the changing RSZ wind patterns as a function of altitude and time.

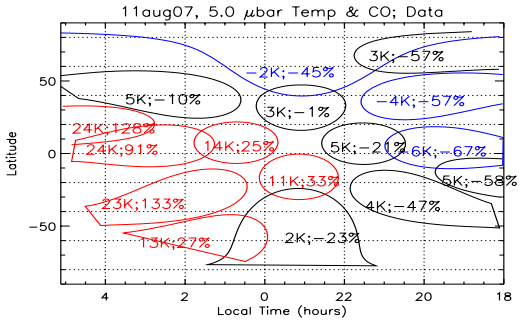

Fig. 1. Latitude vs. LT map of correlated T and CO volume mixing ratio variations at 105 km across the nightside of Venus for ground-based observations obtained on 11 August 2007 (adapted from Clancy et al. 2012). Red regions correspond to warmer temperatures (K) and enhanced CO volume mixing ratios (percent) with respect to midnight. Blue regions correspond to cooler temperatures (K) and depleted CO mixing ratios. Black regions constitute a mixture of responses.

Key References :

(1) Mahieux, A., et al. (2010). *JGR*, **115**, E12014, 2010. (2) Vandaele, A. C., et al., (2008), *JGR*, **113.** (3) Mahieux, A., et al. (2012)., *JGR.*, **117**, E07001. (4) Mahieux, A., et al. (2015). *PSS*, **113-114**, 310-321. (5) Bougher, S. W., et al. (2015). *PSS*, **113-114**, 336-346 (6) Vandaele, A. C., et al., (2015), Contribution from SOIR/VEx to the Updated Venus Int'l Reference Atmosphere (VIRA), *Journal*, Submitted. (7) Bougher, S. W., et al. (1988). *Icarus*, ***73***, 545-573. (8) Bougher, S. W., et al., (1990). *JGR*, ***95,*** 6271-6285. (9) Bougher, S. W., et al. (1997). *Venus II*, pp. 259-292, U. of Arizona Press. (10) Bougher, S. W., et al. (1999). *JGR.*, ***104***, 16591-16611. (11) Bougher, S. W., et al. (2008). *SSR*, ***139***, 107-141. (12) Brecht, A. S., et al. (2011). *JGR.*, ***116***, E08004. (13) Brecht, A. S., et al. (2012). *Icarus*, ***217(2)***, 759-766. (14) Brecht, A. S. and S. W. Bougher (2012), *JGR*, **117**, E08002. (15) Clancy, R.T., et al., (2012). *Icarus*, 779-793.

ON THE PROBLEM OF A DRY VENUSIAN CRUST.

D. Breuer, DLR, *Institute of Planetary Research, Berlin, Germany (doris.breuer@dlr.de),* **N. Tosi,** *Technische Universität Berlin, Germany and* DLR, *Institute of Planetary Research, Berlin, Germany* **A-C Plesa**, DLR, *Institute of Planetary Research, Berlin, Germany*

Introduction:

The interior of the terrestrial planets and the Moon is expected to be more volatile-rich than previously assumed as suggested by recent analysis of lunar samples and Martian meteorites. This assumption is supported by accretion models showing that some of the planet forming material might be water-rich [e.g., 1]. It is thus reasonable to assume that also Venus contained or still contains water in its interior as also indicated at Venus surface with lavas showing a wide range of viscosities [2].

Water strongly influences the mantle dynamics as it reduces even in small amounts of a few tens of ppm the mechanical strength of rocks during deformation and –for a larger amount > 100 ppm – also the melting temperature of mantle material. During melting, these volatiles are preferentially enriched in the liquid phase. This partial melt rises toward the surface and redistributes the volatiles: Typically, erupting material will release essentially most dissolved volatiles into the atmosphere as the solubility of volatiles in magmas at surface pressure is low. However, in the case of Venus with its dense atmosphere much more water on the order of 1 wt.% can be solved in the magma. (The situation is different for CO_2 with its much lower solubility at these pressures and most of the carbon contained in surface melts can be outgassed.) [3]. In addition, volatiles in intrusive material will mostly remain in the crust. As a consequence, depending on the initial amount of water in the mantle, the enrichment and the efficiency of outgassing, a significant amount of water can be stored in the crust, which then may have a weak rheology. However, the topography on Venus [e.g., 4,5,6] suggest an apparent stiffness of the Venusian crust and has been used to argue for dry crustal conditions resulting in high viscosity [7]. It has been suggested that this dryness may be created by 'baking' under the high surface temperatures of the planet [8]. However, this is mainly effective for hydrous minerals but not for water stored in anhydrous minerals in the form of hydroxyl, OH^-.

In the present study, we model the thermal history of the mantle, the outgassing evolution of H_2O and CO_2, and the resulting volatile distribution in Venus. It will be shown that a water-rich crust suggesting a weak mechanical strength can be formed even for an initial water concentration of 100 ppm.

Model:

We employ a 1-D model of parameterized stagnant-lid convection to simulate the evolution of melt generation, crust production, and volatile extraction over a time span of 4.5 Gyr, focusing on the effects of three key mantle parameters: the initial temperature, which controls the overall volume of partial melt produced; the initial water content, which affects the mantle rheology and solidus temperature; and the oxygen fugacity, which is employed in a model of redox melting to determine the amount of carbon stored in partial melts. The enrichment of water and radioactive elements into the melt is obtained by assuming fractional melting, considering that the amount of water is not limited by the saturation concentration of water in the melt at the depth of melt generation. Within the frameworks of fractional melting, the partioning coefficient, melt fraction, and bulk content of water determine the concentration in the melt. The partition coefficient of water is close to 0.01. We further assume that the planet lost its primordial atmosphere and use the H_2O and CO_2 outgassed from the interior to build up a secondary atmosphere over time. We calculate the concentration of H_2O and CO_2 in mantle and crust as well as the atmospheric pressure based on the solubility of in basaltic magmas at the evolving pressure conditions of the surface.

Results:

The interior evolution is characterized by a large initial production of partial melt accompanied by the formation of crust that rapidly grows until its thickness matches that of the stagnant lid so that the convecting sublithospheric mantle prevents further crustal growth. Lower crustal material including its volatiles is continuously recycled into the interior. The enrichment of water into melt varies with time and depends strongly on the initial water content and the melt fraction. Figure 1 shows the concentration of water in the melt and the solubility of water which can be stored in the melt as a function with time. In the case that the water concentrations in the surface melt is higher that the solubility of water, water can be degassed. For lower values, water remains in the melt and the crystallizing crust. Even for high water concentrations in excess of thousands of ppm, the high solubility of water in surface magmas limits the maximal partial pressure of atmospheric H_2O to a few tens of bars, which places de facto an upper bound on the amount of water that can be delivered to the surface and atmosphere from the interior. As a consequence, the crust is water-rich with values up a few thousand ppm. Interestingly, water may degas in

the late evolution (Fig. 1a) when the degree of partial melting becomes small resulting in a high water concentration in the melt. It should be noted though that the presented models do not reproduce the present atmospheric pressure of Venus as we only consider the atmospheric pressure due to secondary volcanism – lower pressure values are obtained and thus degassing of water into the atmosphere is even overestimated.

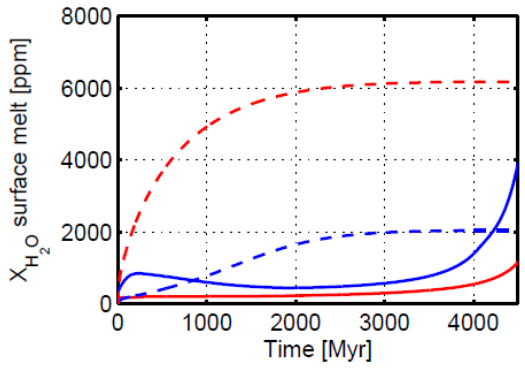

a

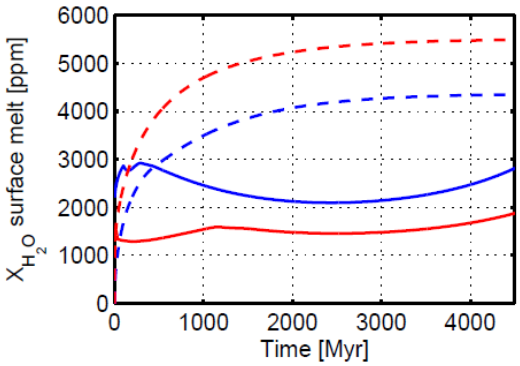

b

Fig. 1 Concentration of water in surface melt as a function of time (solid lines) for an initial mantle temperature of 1600 K (blue lines) and 1900 K. (red lines). Dashed lines represent the solubility of water depending on atmospheric pressure. a) for an initial water concentration in the mantle of 100 ppm and b) for an initial water concentration of 1000 ppm.

Conclusions:

Assuming that the interior of Venus contained some amount of water, a crust formed with time that is likely enriched in water which did not degas due to the high water solubility in melt at thigh atmospheric pressure. These water concentrations suggest that the mechanical strength of the crust is weakened and not stiff as suggested by the Venusian topography [4,5,6,7]. This may argue for a primordial dry Venusian interior but is at odds with the recent findings of more water-rich planetary interiors. Alternatively, remelting of a water-rich crust may 'dry' out the lower crust but redistributes the water-rich material toward the surface. On the other hand, a weak mechanical crust is supported by a recent study [9] arguing that a large strength contrast at the crust-mantle interface results in rheological decoupling and impedes the surface motion of the Venusian crust and, as such, may explain the absence of plate tectonics on Venus. If this is a likely scenario, one may reconsider the assumption of a dry crust from topography and gravity. A higher resolution is necessary to permit admittance and coherence methods for better estimating elastic thickness, which is currently limited to regions with the highest resolution. An improved gravity model will be generated by the proposed VERITAS mission [10].

l

References

[1] Rubie et al. 2014 Icarus, 248 [2] Elkins-Tanton et al. 2007 JGR, 112, [3] Newman and Lowenstern, 2002, Computer and Geosciences, 28 [4] Grimm and Solomon, 1988 JGR, 93 [5] Bindschadler and Parmentier, 1990 JGR 95 [6] Kiefer and Hager, 1991 JGR, 96 [7] Smrekar and Solomon, 1992 JGR 97 [8] Mackwell et al., 1998 JGR 103 [9] Azuma et al. 2014, Science Reports,4 [10] Smrekar et al 2016, this meeting

A RADAR SOUNDER INSTRUMENT FOR THE ANALYSIS OF THE VENUS SUB-SURFACE

L. Bruzzone, **L. Carrer**, **A. Tamponi**, *Dept. of Information Engineering and Computer Science, University of Trento, Trento, Italy (lorenzo.bruzzone@unitn.it*), **E. Pettinelli**, **S.E. Lauro**, *Dept. Mathematics and Physics, Roma Tre University, Rome, Italy*, **R. Oresei**, *INAF/IRA, Bologna, Italy*, **F. Bovolo**, *Fondazione Bruno Kessler, Trento, Italy.*

Introduction and Background:

This paper addresses the definition and the development of a radar sounder instrument for the analysis of the Venus sub-surface. Radar sounders have been successfully used for the study of the subsurface geology and geophysics of Mars with the Mars Advanced Radar for Subsurface and Ionosphere Sounding (MARSIS) on Mars EXpress (MEX) [2] and the SHAllow RADar (SHARAD) on Mars Reconnaissance Orbiter (MRO) [2]. Moreover, the Radar for Icy Moon Exploration (RIME) is currently under development in the JUpiter ICy moons Explorer (JUICE) mission for the study of the icy moons Ganymede, Europa and Callisto [3],[4].

The ESA M-class EnVision mission proposal [5] presents a Venus orbiter aimed at investigating the surface and the atmospheric activity apparent in Venus Express data. Many open science questions are related to the characterization of the surface and the subsurface of Venus. Given the atmospheric conditions and the properties of the surface, some of the key science questions and the related science goals can be effectively addressed only by using properly designed radar instruments. Currently, the use of a SAR system with interferometric capabilities is considered a crucial payload. This is aimed to address science goals related to the measurements of the topography and of the surface displacements according to differential interferometric techniques. However, this system can only study the surface structure and movement and cannot provide any direct measure on the subsurface, leaving unsolved many open questions related to the internal structure of Venus. Accordingly, in this paper we propose and discuss a complementary radar instrument which is a low-frequency radar sounder.

Proposed Radar Sounder: Science

The use of a low frequency nadir looking radar sounder can provide the ideal complementary information to both the Synthetic Aperture Radar (SAR) data obtained by Magellan and the information acquired by an interferometric SAR (InSAR). This would result in a full and detailed investigation of the surface and subsurface geology of Venus. A radar sounder, which can operate at HF, VHF or UHF frequencies, can acquire fundamental information on subsurface geology, which cannot be achieved with the InSAR system. In particular, it can focus on mapping the vertical structure of geologic units by exploring the subsurface properties of tessera, plains, lava flows and impact debris. The sounder could analyze the shallow subsurface of Venus to detect and map geological structures and to identify mechanical and dielectric interfaces. This kind of instruments also provides information on the surface in terms of roughness, composition and dielectric properties at wavelengths completely different from those of SAR, thus allowing a better understanding of the surface properties. Moreover, a fusion of the InSAR data (both intensity, topography and displacement variables) with the sounder data would result in an exceptional capability to understand the link between the surface and subsurface processes on Venus. Note that depending on the design of the system, the sounder could also acquire measurements for characterizing the ionosphere.

Proposed Radar Sounder: Instrument

The radar sounder can be designed to achieve relative high penetration depth and moderate vertical resolution or shallow penetration and very high vertical resolution. This choice can emphasize different geological science goals. The capability of penetration of the electromagnetic waves strongly depends on the choice of the central frequency of the radar sounder, on the design of the systems in terms of overall budget and on the characteristic of the surface (roughness) and subsurface. The radar signal attenuation is affected by the physical properties of Venus subsurface. In fact, the dielectric properties of rocks and, in particular the loss tangent which is the parameter controlling the attenuation, depend on polarization and conduction phenomena. The polarization term is only slightly affected by temperature, whereas conductivity is strongly affected by such parameter. However, in the MHz range (i.e., the operating range of radar sounders) the latter term is not predominant. Based on the dielectric measurements performed on both Moon samples and terrestrial basaltic rocks, in this paper we will show that at the temperature of Venus surface, the attenuation

would not prevent a subsurface penetration of the radar signals.

The pros and cons of considering a radar sounder will be addressed in the presentation and its complementarities with the InSAR system will be discussed in detail.

References

[1] G. Picardi, et al. “Radar Soundings of the Subsurface of Mars,” Science, Vol. 310, pp. 1925-1928, 2005.

[2] R. Seu, et al., “SHARAD sounding radar on the Mars Reconnaissance Orbiter,” Journal of Geophysical Research (Planets), Vol. 112, No. 5 2007.

[3] L. Bruzzone, et al., “Jupiter Icy Moon Explorer (JUICE): Advances in the Design of the Radar for Icy Moons,” IEEE 2015 Int. Geoscience and Remote Sensing Symposium, (IGARSS '15), Milan, Italy, 26-31 July 2015.

[4] L. Bruzzone, et al., “Sub-Surface Radar Sounding of the Jovian Moon Ganymede,” *Proceedings of the IEEE*, Vol. 99, No.5, pp. 837-857, 2011.

[5] http://www.envisionm4.net

SIMILARITIES IN LARGE-SCALE TECTONIC DEFORMATION ON VENUS AND EARTH

Paul K. Byrne, *Department of Marine, Earth, and Atmospheric Sciences, North Carolina State University, Raleigh, NC 27695, USA* (paul.byrne@ncsu.edu), **Christian Klimczak**, *Department of Geology, University of Georgia, Athens, GA 30602, USA*, **A. M. Celâl Şengör**, *Department of Geology, Faculty of Mines and the Eurasia Institute of Earth Sciences, Istanbul Technical University, 34469 Maslak, Istanbul, Turkey*, and **Sean C. Solomon**, *Lamont-Doherty Earth Observatory, Columbia University, Palisades, NY 10964, USA*.

Introduction: On Earth, large-scale tectonic deformation is driven by plate motion, and is primarily manifest as narrow zones of concentrated extensional, shortening, or strike-slip strain at the boundaries of these torsionally rigid plates [e.g., 1]. Yet the plates themselves are also subject to deformation, particularly in continental interiors, but in a much more spatially distributed manner such as that seen throughout eastern Asia [2]. That displacements from distributed strains are individually so small, and are dispersed across areas hundreds or thousands of kilometres in breadth [3], means that the contribution to large-scale tectonic deformation other than from plate boundaries can be overlooked on other planetary bodies.

Venus, for example, shows no evidence for plate-driven tectonics, but the planet nonetheless boasts abundant evidence for substantial tectonic deformation [e.g., 4]. This deformation generally occurs as long belts consisting of some combination of normal faults, graben, thrust faults, and folds. In this contribution, we review several zones of distributed extension, shortening, and strike-slip deformation on Earth that bear strong structural similarities to heavily deformed regions on Venus.

Large-scale Tectonics: The Basin-and-Range Province in western North America is the result of distributed transtensional strain that has yielded heavily deformed terrain. The strong north–south fabric here is composed of normal-fault-bounded blocks that disrupt an area formerly shortened in which thrust faults and folds subparallel to the currently active normal faults once dominated. This region resembles, and so may provide an analogue to, wide zones of extension on Venus, including the five major chasmata [5] and Lavinia Planitia [6].

The tectonics of southern China include the vast foreland shortening structures of the Qin-Ling (in the north) and the Xiangganzhe (southeast and centre) fold and thrust belts. The curvilinear tectonic fabric of these systems reflects shortening of at least 1,000 km atop décollement horizons of thin sedimentary sheets that eventually root into crystalline thrusts to the north and southeast. These and other fold belts, including the Appalachian Valley and Ridge Province (USA) and the Verkhoyansk system (Russia) (**Figure 1**), bear a strong structural similarity to Venus' ridge belts, such as those in Atalanta and Vinmara Planitiae [5] (**Figure 2**).

Many fold belts on Earth also show substantial transpression. The lineated terrain along the Middle and Saharan Atlas mountain chains consists of rocks folded by transpression, albeit much eroded and in places buried under desert sand. Even so, these belts are likely analogues to areas of transpression on Venus, including the region separating the eastern Ovda and northwestern Thetis Regiones [7].

Outlook: Distributed intraplate deformation on Earth, often characterised by prominent curvilinear fabrics, may provide a framework with which to more fully understand large-scale tectonics on Venus. We suggest that future work should consider Venus' ridge and fracture belts [e.g., 3–5] in this light, and frame questions addressible with observations by future spacecraft missions.

Bibliography: [1] Wilson J. T. (1965) Nature, 207, 343–347; [2] Molnar P. & Tapponnier P. (1975) *Science*, *189*, 419–426; [3] Burke K. et al. (1980) *J. Geol.*, *88*, 375–386; [4] Solomon S. C. et al. (1991) *Science*, *252*, 297–312; [5] McGill G. E. et al. (2010) *in* Watters T. R. & Schultz R. A. (eds.) *Planetary Tectonics*, Cambridge, pp. 81–120; [6] Koenig E. & Aydin A. (1998) *Geology*, *26*, 551–554; [7] Kumar P. S. (2005) *JGR*, *110*, doi:10.1029/2004JE002387; [8] Rosenberg E. & McGill G. E. (2001) *Geologic Map of the Pandrosos Dorsa Quadrangle* (V–5), Venus: U.S.G.S. Geologic Invest. Ser. I–2721.

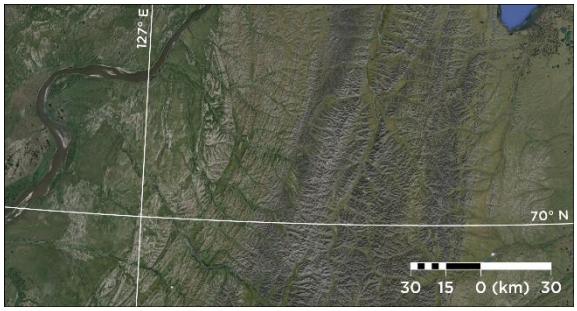

Figure 1. A portion of the Verkhoyansk Range in northeastern Siberia (from Google Earth).

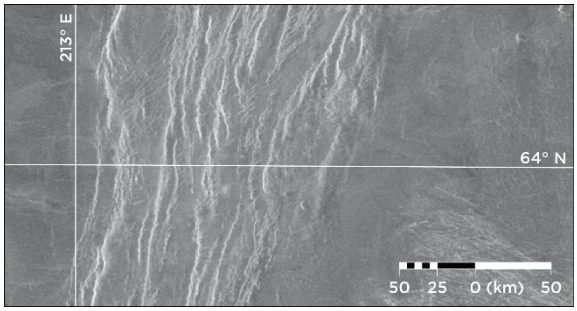

Figure 2. A portion of the Pandrosos Dorsa ridge belt to the east of Vinmara Planitia [after 8].

VENUS SCIENTIFIC AND PLATFORM DATA CORRELATION

Octavio Camino, *European Space Agency, Fermi Avenue OX11OFD Oxfordshire UK (octavio.camino@esa.int),* **Jose Antonio Martinez Heras** *Black Hat S.L.- Córdoba – 14002 Spain,* **Alessandro Donati**, *European Space Agency - Darmstadt, 64293, Germany,* **David Heather** *- Villanueva de la Cañada 28692 Spain.*

Introduction:

Venus Express scientific operations have been subject of improvement along the years of the mission. In particular the concepts developed for Mission Planning, Automation and Data Processing are considered a reference for next future missions. This paper deals with the implementation of web-based tools that permitted fast and intuitive data correlation between different types of spacecraft platform data and others used for planning, in particular flight dynamics and mission planning data. The result provided a simple mechanism to correlate different types of data in graphical form.

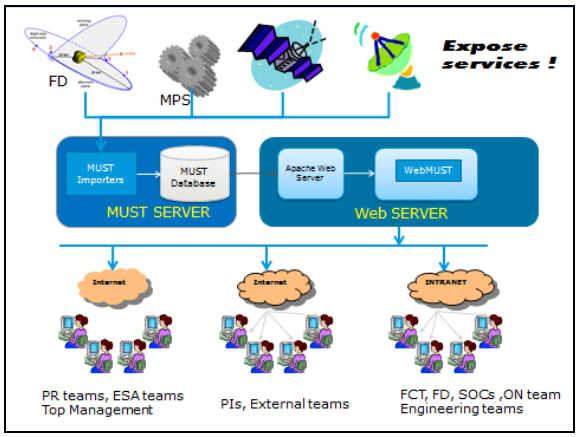

Furthermore the Advanced Mission Concepts Office at ESA/ESOC has developed complementary plug-ins functions that permitted the search and identification of patterns and novelty detection mechanisms to anticipate to aging or failures.

WebMUST:

The core tool used for the data analysis and data correlation at ESOC is called “Web MUST”.

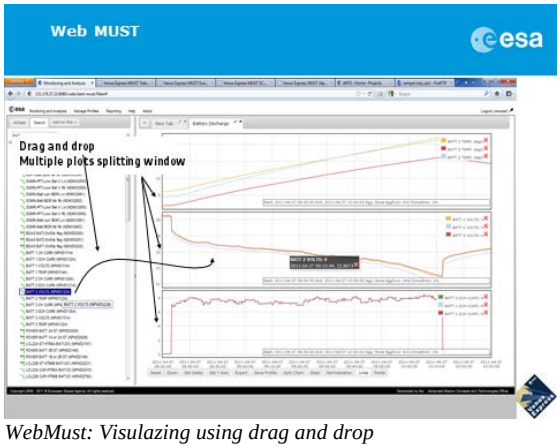

WebMust: Visulazing using drag and drop

Any data format is imported into a common database by means of the so called “MUST Importers”.

They are instances of an application that imports the data into the database having the time as the main key reference.

The data can be of any type except graphical data at the moment. In the case of Venus Express these were: Flight Dynamics data, Mission Planning Data, Spacecraft data and Ground Station data. In principle nothing prevents the current tool to add new sets of data and this explains the main intention of this paper.

Once all different types of data are in the repository the users have several options: Visualization of the data in text or graphical form, search for specific patterns and activate intelligent algorithms for anomaly detection.

The VEX operations engineers and the scientists could only access payload housekeeping data since it is the only one decoded at the operations centre.

In order to be able to efficiently visualize data with different sampling rates, the tool uses “Fractal Resampling”. This technique allows high sampling on the source while sending much fewer samples that carry almost the same information.

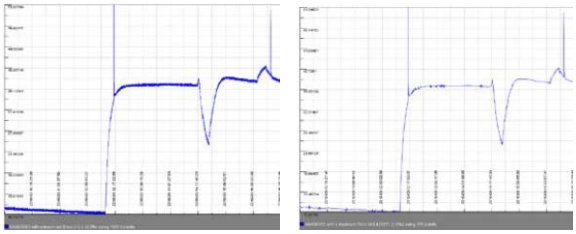

Fractal Resampling: Venus Express Thrusters’ Temperature. Left: original time series with 10003 samples; right: fractal resampled version allowing 1% error with 356 samples.

This separation between data and information allows gaining on-board observability while reducing bandwidth requirements. Fractal Resampling works by accepting a small configurable error. The resulting resampled time series guarantees that the error made is not bigger than the configured one at any given sample.

DrMUST:

Another functionality added to the MUST tool is the so called “DrMUST”. This function which is also protected by an ESA patent allows performing pattern matching & correlation analysis between different data sets which may be the cause for a particular behavior like an event or an anomaly. DrMUST can be used not only for anomaly investigation but also

to perform characterizations.

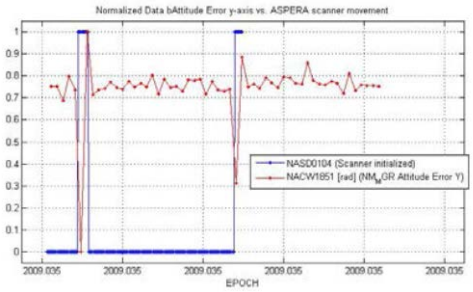

Dr. MUST discover ASPERA as the cause of VEX attitude errors

Novelty Detection:

Novelty Detection allows detecting new behaviors in all parameters. It automates the process of having engineers looking every day to 20,000 parameters and noticing new behaviors. It needs very little configuration and can run unattended. It makes the assumption that an unusual behavior is often a signature of an anomaly in the way to develop.

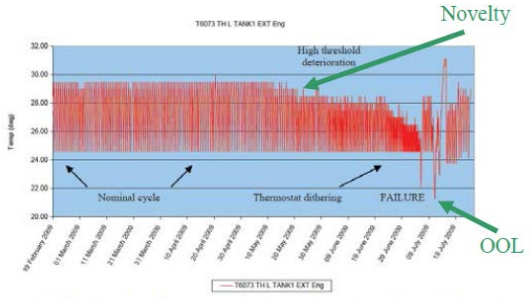

Novelty Detection find the Anomaly 2 months before de Out-Of-Limits

The Planetary Science Archive team at ESAC in Spain has been having access to the some of these services for limited analysis/evaluation of the science data. Information from MUST has been critical to better understand the calibrations applied to the data and the limitations that should be placed on interpretation of the data resulting from instrument and/or spacecraft performance. Overall MUST has provided an aid to the processing of the science data before going into the archive, and has helped to validate the quality of the data before being archived.

Data from MUST were also used for the interpretation of the Aero Drag Experiment (ADE), when the spacecraft skimmed the Venusian atmosphere and experienced a drag effect. Similarly, MUST data have been used to interpret the data from the dedicated aerobraking phase when, towards the end of the mission, Venus Express pushed a little deeper into the atmosphere for more extended periods. In both cases, the MUST data were and are being used for preparation of the data sets that will be placed in the Planetary Science Archive.

This paper proposes to extend the methodology and the implementation to payload operations with the inclusion of other data types (especially images and video) that will serve future scientific experimenters and those involved with future robotics exploration to easily visualize their data.

VENUS'S ULTRAVIOLET ABSORBER: CYCLO-OCTAL (S_8) AND POLYMERIC SULFUR (S_x) AND THEIR LATITUDINAL BEHAVIOR.

R. W. Carlson, *Jet Propulsion Laboratory, California Institute of Technology, Pasadena, California USA (Robert.W.Carlson@jpl.nasa.gov),* **G. Piccioni, G. Filacchione**, *Istituto di Astrofisica e Planetologia Spaziali, Roma, Italy*, **Y. Yung, P. Gao**, *California Institute of Technology, Pasadena, California USA.*

Introduction

The identity of the ultraviolet absorber in Venus's atmosphere has not yet been established. Among the many possibilities, two candidates are currently preferred: ferric chloride ($FeCl_3$) and elemental sulfur. It is possible to distinguish between these and other choices by using spatially resolved spectra as obtained by the ultraviolet (UV) and visible channel of the VIRTIS-M spectrometer on *Venus Express* (VEx). However these data must first be corrected for scattered light and interfering diffraction orders. A correction method has been developed (see poster by Carlson, Piccioni, and Filacchione, this conference) and applied to VIRTIS data cubes. Determining the spatial variations of the spectral shape is conveniently performed using reference (ratio) spectra relative to a non-absorbing "white" spectrum as found from the nearly pure sulfuric acid clouds of Venus's polar regions.

Spectra from a north-south swath

Ratio spectra obtained as VIRTIS scans Venus in latitude are shown in Fig. 1, along with a stretched image of the observation using VIRTIS's 380-400 nm bands. The spectra correspond to the left-most vertical line of image pixels and cover the latitude range from approximately -45° to -75°. The signature of the UV absorber is apparent in all except those near the southern pole and show variations in strength and shape. Those at mid-latitudes are consistent with relatively sharp absorption edge of cyclo-octal sulfur, S_8 (and possibly $FeCl_3$). At high southern latitudes the absorption extends to longer wavelengths, indicative of the presence of both polymeric sulfur (S_x) and S_8. It is reasonable to assume that the mid- and high-latitudes regions are both due to sulfur aerosols and that their molecular form depends on their formation and evolution.

An Initial interpretation

It is thought that Venus's hot lower atmosphere contains small sulfur molecule, S_2 and S_3, from surface sublimation of pyrite and sulfur and from chemical reactions and photolysis of COS (Fegley Jr. et al., 1997; Krasnopolsky, 2007; Lyons, 2008; Yung et al., 2009). As these molecules diffuse to cooler altitudes they combine to form the stable S_8 molecule that then condense to form S_8 aerosols at somewhat higher altitudes. Turbulence in mid-latitudes introduces these fresh aerosols into the cloud region. As these upper atmosphere aerosols move poleward in the upper branch of the Hadley cell, solar ultraviolet radiation striking the sulfur grains produces polymeric sulfur that has absorption extending to longer wavelengths (Hapke and Nelson, 1975) and is clearly seen in the high southern latitude spectra.

References

Fegley Jr., B., et al. 1997. *Icarus* **125,** 416-439. Hapke, B., Nelson, R., 1975. *J. Atmos. Sci*. **32,** 1212-1218. Krasnopolsky, V. A., 2007. *Icarus* **191,** 25-37. Lyons, J. R., 2008. *J. Sulfur Chem.* **29,** 269-279. Yung, Y. L., et al., 2009. *J. Geophys. Res*. **114,** E00B34.

Figure 1. Spectra from VIRTIS-M observation VV0459_03 The image height is 216 pixels and covers approximately the 45° to 75° south latitude range. The spectra are for the column of pixels on the left edge and corresponds to the center sample of the spectrometer entrance slit, for which we have obtained a Vega-based calibration. Each spectrum is an average of 4 vertical pixels. The image location of each spectrum is approximately at the level of the value at 640 nm and indicated for four spectra. All of these ratio spectra were normalized to unity at 700 nm and a 0-1 scale is shown at the left. The reference "white" spectrum was obtained at a latitude between the bottom two spectra. Small artifacts from the correction procedure are evident. In the image, darker indicates more UV absorption.

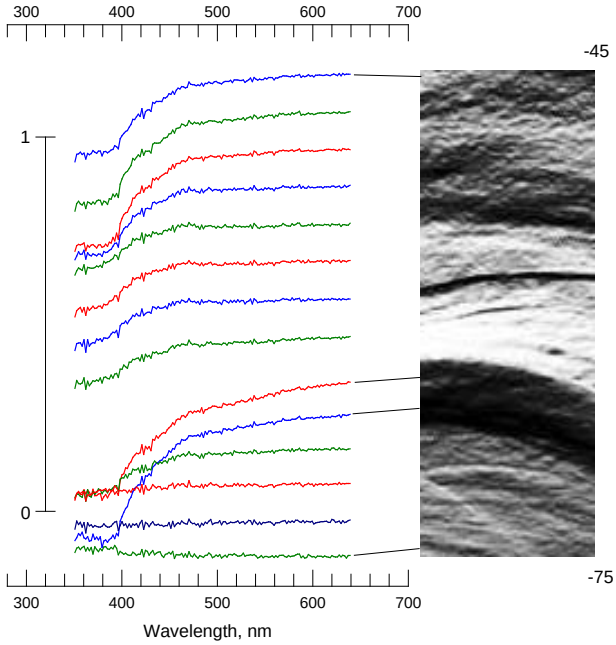

VENUS EXPRESS VIRTIS-M VISIBLE-CHANNEL: DIFFRACTED AND SCATTERED LIGHT CORRECTIONS.

R. W. Carlson, *Jet Propulsion Laboratory, California Institute of Technology, Pasadena, California USA (Robert.W.Carlson@jpl.nasa.gov),* **G. Piccioni, G. Filacchione**, *Istituto di Astrofisica e Planetologia Spaziali, Roma, Italy.*

Introduction

The VIRTIS-M imaging spectrometer is a dispersive instrument using a bipartite diffraction grating to obtain spectra from approximately 300 nm in the ultraviolet (UV) region to 5200 nm in the infrared (IR). The visible channel of the VIRTIS-M spectrometer shares the grating with the infrared channel, using the central portion of the grating with a ruling density that is five times greater than the IR portion. The infrared portion is blazed to send most of the radiation striking it to the infrared array detector, which is on the opposite side of the central image than the visible array. While most of the IR radiation is sent to the IR detector, there is some energy in the negative orders that is diffracted in the opposite direction and can be a source of false signal, especially in the UV where the true signal is low.

In addition, grating spectrometers in general suffer from scattered light due to grating and mirror imperfections and imperfect suppression of scattered light from the central image.

These diffraction and scattered light effects hinder quantitative spectroscopy by *Venus Express'* (VEx) VIRTIS in the UV, where signatures from Venus's absorber occur. A wealth of UV and visible data can be employed if a large part of the unwanted contribution can be estimated and removed. We have developed such a method and briefly describe it here.

Removal of diffraction orders

An important set of measurements were performed by G. Filacchione and co-workers (*Rev. Sci. Instrum*. **77**, 103106, 2006) on the *Rosetta* version of VIRTIS-M, which is nearly identical to the VEx spectrometer. They illuminated VIRTIS's telescope with collimated light from a monochromator and recorded the dispersed radiation from the various orders of the grating (1st order from the visible portion, the 2nd through the 8th negative orders from the IR portion). The incident radiation was varied in steps over the range of visible channel, enabling us to model the diffracted spectrum for a given incident spectrum. The source was too weak in the region below 400 nm so we used computed grating efficiencies for those wavelengths and normalized them to the experimental data.

Estimating the diffracted light from a target such as Venus must be performed iteratively, resulting in a unique spectrum and its corresponding diffraction component. However one must also consider scattered light as described below.

Removal of scattered light

Instrumentally scattered light occurs throughout the spectrum, but most of its contribution is from the green and red portion where the solar spectrum is most intense and CCD detectors are highly sensitive. Consequently, the scattered light's spectral dependence is roughly constant in shape, and the generic scattered light spectrum only needs to be normalized to give an adequate estimate. We use the strong Fraunhofer structure in the 370 to 390-nm region in our solar reference spectrum (Thullier et al.'s spectrum convolved to VIRTIS resolution × the instrument sensitivity) to estimate how much scattered light must be removed to match the Fraunhofer structure. This removal must be done by iteration, and each of these iterations uses the iterative grating corrections. Results for a typical Venus spectrum are shown below.

Continuing work

Pipeline processing software is being developed for application to the VIRTIS VEx data and the same techniques described here are being applied to *Rosetta* data of comet 67/P. Preliminary Vega-based calibrations have been determined for VEx and *Rosetta*.

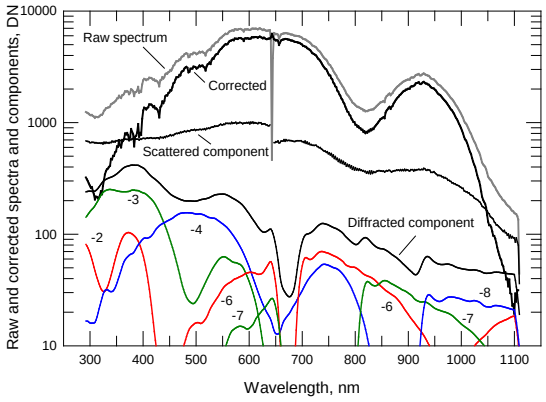

Figure 1. Raw and corrected DN (data number) spectra and the total scattered and negative-order diffraction components. The individual orders are also shown. The -5 order has the same dispersion as the first order of the visible grating portion and considered part of the true signal. Note that the scattered light component is larger than the scattered light component.

SULFURIC ACID OPTICAL CONSTANTS IN VENUS'S INFRARED-WINDOWS REGION.

R. W. Carlson, *Jet Propulsion Laboratory, California Institute of Technology, Pasadena, California USA (Robert.W.Carlson@jpl.nasa.gov),* **M. S. Anderson**, *Jet Propulsion Laboratory, California Institute of Technology, Pasadena, California USA.*

Introduction:

Venus's clouds, deep atmosphere, and surface can be studied using infrared spectral windows, regions of relative transparency between gaseous molecular absorption bands. Thermal emission emanating from the surface and lower atmosphere and transmitted through the clouds has been observed by ground based telescopes, flyby spacecraft, and extensively by VIRTIS on the orbiting Venus Express spacecraft. Radiation in these windows, particularly the 2.3-μm window, is absorbed by sulfuric acid, with the absorption varying with wavelength, acid concentration, and temperature. Accurate determinations of the optical properties of sulfuric acid are necessary for interpretation of remote cloud observations but there are few measurements of sulfuric acid absorption at concentrations relevant to Venus, and there are regions where there are no measurements.

Measurements:

We have measured the imaginary index from 1.7 to > 2.6 μm for concentrations of 68, 72, 76, 84, 88, 92, and 96 weight-% at 295 K. Since sulfuric acid is extremely hydrophilic, care was taken to ensure against water contamination. We used a transmission cell of known thickness (52 μm) and accurately determined optical properties. The near infrared measurements were made with a Cary 5000 spectrometer. The background is collected on the cell holder aperture (no cell). The quartz cells were made from 2 quartz plates with a Teflon gasket strips. The thickness of the empty cell was measured using the interference fringe technique. The sulfuric acid solution was made from a 95-98% reagent grade sulfuric acid (Sigma Aldrich). The sulfuric acid and water solutions were accurately measured using a Dionex ICS 3000 Ion Chromatograph (Sunnyvale CA). To avoid water uptake, a drop of sulfuric acid is placed on the quartz slide and rapidly sandwiched together under a blanket of dry nitrogen. The spectra are then immediately acquired.

Results:

The imaginary indices determined at ~ 4% accuracy and are in good agreement with Gosse et al.'s measurement of 72% sulfuric acid and Palmer and Williams 95.6% solution, but are ~ 5% greater than for their 75 and 84.5% solutions (see Fig.s 1 and 2). These data are available from Carlson who can be reached at the e-mail address above.

References:

Gosse, S. F., Wang, M., Labrie, D., and Chylek, P.: Imaginary part of the refractive index of sulfates and nitrates in the 0.7-2.6 μm spectral region, *Appl. Optics* **36**, 3622-3634, 1997.

Palmer, K. F. and Williams, D.: Optical constants of sulfuric acid: Application to the clouds of Venus?, *Appl. Optics* **14**, 208-219, 1975.

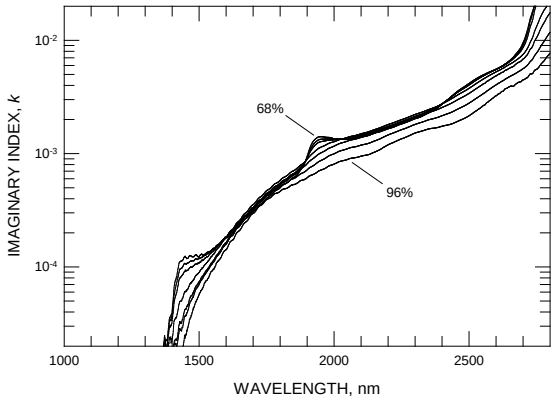

Figure 1:Measured imaginary index for 68, 72, 76, 84, 88, 82, and 96% solutions.

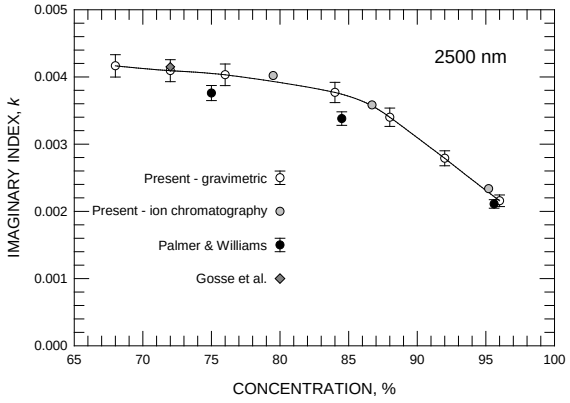

Figure 2. Comparison to prior measurements at 2.5 μm.

PRELIMINARY EXPERIMENTAL RESULTS ON ATMOSPHERE-SURFACE INTERACTION UNDER VENUS CONDITIONS

A. Cathala, **G. Berger,** *Institut de Recherche en Astrophysique et Planétologie (IRAP), Université Paul Sabatier, CNRS, 14 avenue E. Belin, 31400 Toulouse, France.*

Introduction:

Chemical interaction between the deep atmosphere and the surface of Venus is important for the comprehension of both atmosphere chemistry and surface mineralogy. The composition of its subcloud atmosphere is dominated by CO_2 with small amounts of sulfured species and H_2O in trace. The reactivity of the basaltic material prevailing at the Venus surface raises questions on the thermodynamics and kinetics of fluid-rock interactions when the fluid is a non-polar supercritical fluid.

Given the paucity of remote or in-situ analyses of Venus surface, the best way to address these questions is a theoretical and experimental approach.

The general aims of our work address both the atmosphere chemistry and the surface mineralogy: 1) what is the potential of a Venus-like gas to transport elements as a function of its chemistry, 2) how the surface mineralogy is affected during a volcanic wet outgassing such as discussed in [1, 2] and 3) how long survive early hydrous minerals in the present-day dry Venus atmosphere.

Previous Work:

Few studies on the weathering of typical Venus rocks have been done and most of them concerned the mineral transformation. When conducted with pure CO_2, the analyzed rocks show mass changes implying gas transport and chemical reactions at the surface, for instance the formation of iron oxide [3]. Other experiments with SO_2 in the gas also show a global sulfurization of the surface [4,5].

But the most important changes occur with H_2O-CO_2 mixtures we experimented few years ago. We observed the fast and widespread alteration of olivine and the recrystallization of vitreous samples (Figure 1, [6]).

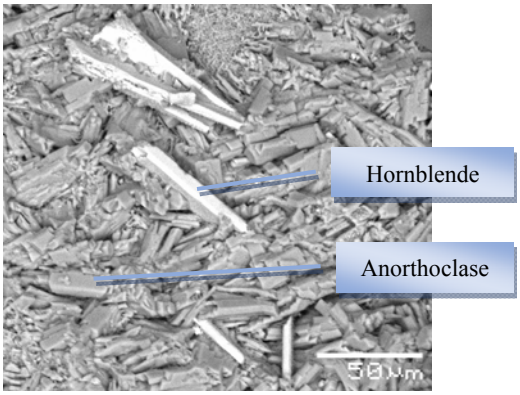

Figure 1: Recrystallized obsidian after one week in a H_2O-CO_2 fluid at 470°C and 235bar

Experimental Details:

We developed a Venus chamber dedicated to the fluid-rock reaction in the continuation of [6]. This chamber works up to 500°C and 400 bars for an internal volume of 300 ml and is made of a steel alloy called hastelloy C-276 that minimizes any corrosion process. A gas sampler device completes the reactor in order to analyze the gas composition during the run.

The mineral transformations of the investigated rock samples were observed *post-mortem* by SEM and XRD. The mass transfer between the rocks and the fluid was evaluated by sampling during the run the supercritical fluid in a KOH solution under the P and T of the experiment, and analyzing the solution by ICP-MS for their content in a wide range of cations. SO_2, H_2S and CO were monitored in the fluid phase by a gas detector.

Three kinds of silicate material were investigated for one week in each kind of "atmosphere" described further: a picritic basalt, a clay-rich altered basalt and an obsidian. The previous tested fluid compositions (pure CO_2 fluid, CO_2-H_2O mixture) were completed by a dry S-bearing fluid. It was composed of 130 ppm SO_2, 15 ppm H_2S, 15 ppm CO, 3.5% N_2 in a CO_2 basis. A wet version of this gas is also planned.

Results:

The results in dry S-bearing fluids show no evidence of alteration as previously observed in pure CO_2 after one week run. However, several rock forming elements are transferred in the gas phase, in particular Si, but also Al, Ca, Mg and some metals like Ni, Sn, Mo and Cr as showed on figure 2. This correlates the observation of Si spherules on the colder part of the reactor (Figure 3, [6]).

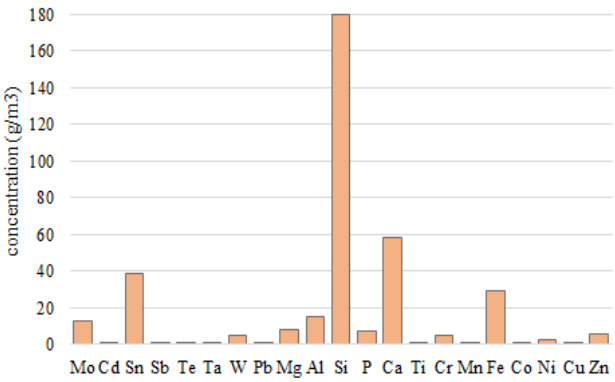

Figure 2: Element concentration (g/m3) in the S-bearing

gas after one week at 470°C and 90bar

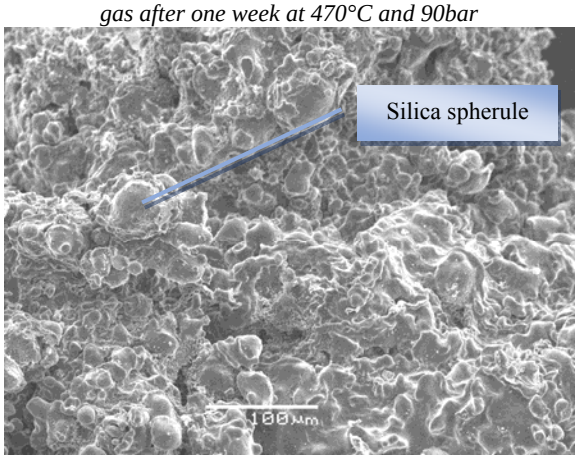

Figure 3: Silica spherule deposit in the colder part of the reactor / scale bar: 100µm

Another important result is the depletion of almost all H_2S and all SO_2 from the fluid after one week run. This observation is discussed below.

Discussion and concluding remarks:

The absence of mineral reaction in dry fluids, by contrast with previous observations in wet fluid, can easily be understood by considering the difficulty of a non-polar fluid to breakdown covalent bounds. The question of the short duration of the runs is obviously a limitation of this conclusion. However, the previous experimental attempts to alter silicate materials with Venus-like fluid reported only the sulfurization of the surface even after several years of reaction [5]. On the other hand, the question of the (meta) stability of previously formed hydrous phases in a dry Venusian atmosphere is still an open question [6,7].

Experimentation with a complex gas points at the difficulty of maintaining the concentration of SO_2 and H_2S in the chamber. The H_2S loss can be explained by the formation of carbonyl sulfide (COS) that is thermodynamically stable under Venusian conditions [8]. Another explanation should not be excluded as H_2S and/or SO_2 can react with the reactor itself (hastelloy) [9]. The observed gas enrichment in Cr, Ni and Mo can be related to hastelloy corrosion. The relative contribution of each process is under investigations.

Despite the sulfur gas depletion, the transport of usual components of basalt (Si, Ca, Al, Mg…) even in dry fluid and the observation of silicic spherules in colder part of the reactor open new perspectives for how considering mass transfer through the atmosphere between the lower (hot) and upper (colder) part of the surface.

The flexibility of our equipment will be used to test mass transfer under thermal gradients. Further experiments will also focus on the effect of H_2O in the gas and the stability of hydrous phase when the Venus atmosphere changes from wet to dry conditions.

References:

[1] Smrekar, S. E. & Sotin, C. Constraints on mantle plumes on Venus: Implications for volatile history. *Icarus* **217,** 510–523 (2012).

[2] Airey, M. W. *et al.* Explosive volcanic activity on Venus: The roles of volatile contribution, degassing, and external environment. *Planet. Space Sci.* **113-114,** 33–48 (2015).

[3] Treiman, A. H. & Allen, C. C. Chemical weathering on Venus: Preliminary results on the interaction of basalt with carbon dioxide. in *Lunar and Planetary Science Conference* **25,** 1415 (1994).

[4] Fegley Jr, B. Thermochemical kinetics of SO2 reactions with possible Venus crustal minerals: First data for calcite. in *Lunar and Planetary Science Conference* **19,** 315 (1988).

[5] Aveline, D. C. *et al.* Rock and mineral weathering experiments under model Venus conditions. in *Lunar and Planetary Science Conference* **42,** 2165 (2011).

[6] Berger, G. & Aigouy, T. Experimental rocks alteration under Venus-like conditions. in (2011).

[7] Johnson, N. M. & Fegley, B. Tremolite decomposition on Venus II. Products, kinetics, and mechanism. *Icarus* **164,** 317–333 (2003).

[8] Svoronos, P. D. N. & Bruno, T. J. Carbonyl Sulfide: A Review of Its Chemistry and Properties. *Ind. Eng. Chem. Res.* **41,** 5321–5336 (2002).

[9] Rong Tu, T. G. Corrosion Behavior of Hastelloy-XR Alloy in O2 and SO2 Atmosphere. *Mater. Trans.* **46,** 1882–1889 (2005).

An Induced Global Magnetic Field Looping Around the Magnetotail of Venus

L. H. Chai, **Y. Wei, W. X. Wan, Z. J. Rong, H. Zhang,** *Institute of Geology and Geophysics, CAS, Beijing, China. (chailihui@mail.iggcas.ac.cn),* **T. L. Zhang,** *Space Research Institute, Austrian Academy of Sciences, Graz, Austria.* **M. Fraenz, E. Dubinin,** *Max-Planck-Institute for solar system research, Goettingen, Germany.* **S. Barabash**, *Swedish Institute of Space Physics, Kiruna, Sweden.*

Introduction:

Venus serves as the prototype of solar wind interaction with unmagnetized planetary bodies with atmospheres. It has no intrinsic dipole or crustal magnetic field, the only magnetic field is believed to be formed by the draped interplanetary magnetic field (IMF). However, the large-scale magnetic field observed over the north polar region of Venus has a bias in the dawnward direction and seemingly unresponsive to the IMF's direction. Although broad attention has been paid to these dawnward magnetic fields and several mechanisms have been suggested in the past few years the source of these dawnward fields remains a mystery.

Results:

Based on the long-term observations of VEX and PVO, and a joint observations of VEX and Messenger, we show that the induced magnetosphere contains a second type of global magnetic field, whose morphology decouples from the IMF's orientation and the dawnward field is only a part of it. This global field, referring to as “looping field” has a shape of a cylindrical shell around the magnetotail and a direction of counterclockwise looking from the tail toward the planet (the red circles in Figure 1).

To confine the looping field in a shell-shaped region, theoretically, it needs two currents flowing in and out of the planet along the Sun-planet line at the outer and inner shells, respectively. It also needs two currents crossing the draped field in the dayside and nightside of the planet, so that the current circuit is closed. We suggest that the dayside inward current is inside the deep ionosphere and the nightside outward current distributes in the region where the draped fields become weak (the green arrows in Figure 1).

The statistic results of MGS observation on Mars and the case studies of Voyager 1 and Cassini observations on Titan also suggest that the looping field is most likely a universal phenomenon for unmagnetized planetary bodies with atmospheres.

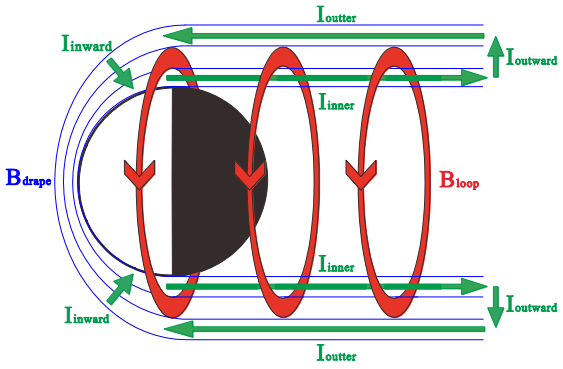

Figure 1: Schematic illustration of the looping magnetic field (red cycles) and its associated current system (green arrows) at Venus.

Reference:

Chai et al., 2016, JGR, doi:10.1002/2015JA021904

LOCAL TIME VARIATIONS OF THE HYDROGEN CORONA OBSERVED BY SPICAV-UV/VEX.

J-Y. Chaufray, J-L. Bertaux, E. Quémerais, and F. Leblanc , *LATMOS-IPSL, CNRS, UVSQ, UPMC, Guyancourt, France (chaufray@latmos.ipsl.fr)*

Introduction:

As all the terrestrial planets, Venus is surrounded by an hydrogen corona coming from the photodissociation of the water vapor followed by its vertical transport at very high altitudes. From the UV observations of the resonant scattering Lyman-alpha emission, two components have been observed in this corona. A cold component corresponding to hydrogen population at equilibrium with the global atmosphere dominant below ~ 2000 km. A suprathermal component, produced by collisions between energetic protons with the cold component in the upper atmosphere. Due to its large energy, this hot population is able to reach very high altitudes, and escape and becomes dominant above ~4000 km (e.g. Bertaux et al. 1982).

Observations:

The hydrogen corona of Venus has been observed systematically from the UV spectrometer SPICAV aboard Venus Express (Bertaux et al. 2007). It has been observed at dayside, confirming most of the results obtained by past studies, and for the first time at the nightside. As shown in Fig. 1, the two components corona is seen through the two scale heights profile obtained at limb above the dayside (LT = 12H). The nightside profiles are very different due to the low illumination of the shadow by multiple scattering.

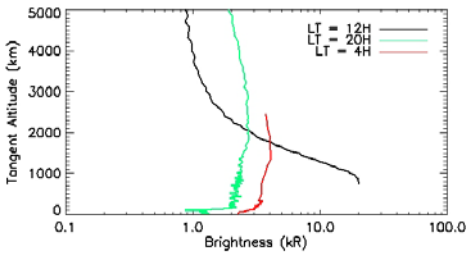

Fig. 1 Altitude profile of the Lyman-α brightness at different local times.

Results:

Chaufray et al. (2012) have analyzed the first profiles obtained at the dayside and derive a cold hydrogen density of ~1-2x10^5 cm^{-3} and an exospheric temperature ~ 250-300 K at 250 km. A larger brightness was observed at the morning terminator (LT = 6h) compared to the evening terminator (LT=18h), confirming an asymmetry observed from the mass spectrometer aboard Pioneer Venus Orbiter (PVO), but the hydrogen density needed to reproduce the profile at the morning terminator was lower than the hydrogen density derived by this instrument.

At higher altitudes, the brightness was dominated by the interplanetary emission making difficult an accurate retrieval of the hot hydrogen density. The hydrogen density derived was better constrained at the middle of the observed altitude range (~ 5000 km) and the hot hydrogen density estimated to ~50 cm^{-3}.

More recently, Chaufray et al. (2015) reproduce the first brightness profiles at the nightside evening terminator (LT = 20H), using a radiative transfer model including both cold and hot hydrogen populations as well as the interplanetary emission partly scattered by the Venusian hydrogen corona.

The cold hydrogen density and temperature of the cold hydrogen population derived at the exobase was 4x10^6 cm^{-3} and temperature between 175-225 K, confirming a cooler and denser nightside corona compared to the dayside corona. The hot hydrogen density derived at 5000 km was ~ 100 – 200 cm^{-3} larger than the derived hot hydrogen density at the dayside and presenting a very short variability of a factor 2 in only few days. This variabilty could be driven by a variation of the dayside ionosphere.

In this presentation, we will summarize these recent results and present other observations obtained at the nightside morning side (LT = 4H) (Fig; 1), confirming the large variability of the hydrogen density with local time at the nightside.

.

Bibliography:

Bertaux, J-L., V.M. Lepine, V.G. Kurt, and A.S. Smirnov, 1982, Icarus, 52, 221-224

Bertaux, J-L. et al., 2007, Planet. Space Sci., 55, 1673-1700

Chaufray, J-Y., J-L. Bertaux, E. Quémerais, E. Villard, and F. Leblanc, 2012, Icarus, 217, 767-778

Chaufray, J-Y., J-L. Bertaux, E. Quémerais, F. Leblanc, and S. Sulis, 2015, Icarus, 262, 1-8

TITLE: A new view on exoplanet transits: Transit of Venus described using three-dimensional solar atmosphere Stagger-grid simulations

A. Chiavassa (andrea.chiavassa@oca.eu), **C. Pere, P. Tanga** (Laboratoire Lagrange, Observatoire de la Cote d'Azur, Nice, France)

Abstract:
The transit of Venus in 2004 is an important benchmark for current observational techniques and theoretical modeling of exoplanet atmospheres and, eventually, it is useful to characterize stellar activity (in particular, convection-related surface structures) that potentially cause fluctuations affecting the transit light curves. In this context, we simulate the transit of Venus in 2004, which was observed by the satellite ACRIMSAT, using the realistic three-dimensional (3D) radiative hydrodynamical (RHD) simulation of the Sun from the Stagger-grid and synthetic images computed with the radiative transfer code Optim3D. We explain ACRIMSAT observations and show that the granulation pattern causes fluctuations in the transit light curve. Moreover, we show that the granulation pattern can partially explain the observed discrepancies between the limb darkening models used so fare and the data. Being able to consistently explain the data of 2004 is a new step forward for 3D RHD simulations, which are becoming important for detecting and characterizing exoplanets. They show that granulation has to be considered as an intrinsic uncertainty (as a result of stellar variability) on precise measurements of exoplanet transits of, most likely, planets with small diameters. In this context, it is very important to obtain a comprehensive knowledge of the host star, including a detailed study of the stellar surface convection.
REFERENCE: Chiavassa et al. 2015, A&A, Vol 576, id. A13

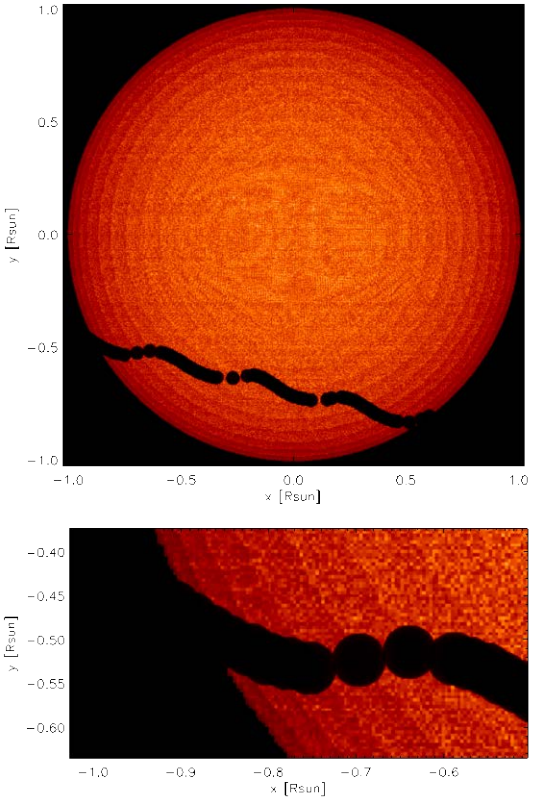

Figure: Synthetic transit of Venus of 2004 (as seen by ACRIMSAT) with the solar disk image computed with the radiative hydrodynamical simulation of the Sun (figure from Chiavassa et al. 2015, A&A, Vol 576, id. A13). i

HIGHLAND TARGETS FOR AN ORBITAL INSAR MISSION TO VENUS.

C. G. Cochrane, *Department of Earth Science and Engineering, Imperial College London, London, SW15 3HA, UK, (c.cochrane@imperial.ac.uk),* **R. C. Ghail**, *Department of Civil and Environmental Engineering, Imperial College London, London, SW15 3HA, UK, (r.ghail@imperial.ac.uk).*

Introduction:

Venus is the most Earth-like planet known yet extremely inhospitable; understanding this paradox is a key aim for future exploration of Venus. Its current rate of geological activity is a major uncertainty, with hypotheses ranging between a currently inactive planet to one almost as active as Earth. Recent Earth Observation missions have shown that, if an orbit is adjusted to repeat its trajectories to an accuracy of < 100 m, then surface movements of a few mm can be detected by repeated InSAR observations [1]. However, the data volume for global InSAR coverage of Venus is very large [2]. Fortuitously, Venus hypsography shows that more than 90% of the surface can be explained by one mechanism: lithospheric thinning. Hence, mapping only a subset of this area, and the remaining ~10%, is sufficient to characterise resurfacing mechanisms and rates.

Hypsography:

Magellan altimetry data have a unipolar profile, unlike the bipolar profile for Earth but their upper tails are similar. The major part of the hypsographic profile of Venus conforms to a Poisson distribution of discrete probabilities, implying that its topography is due to many independent events, well-separated in time. These events effectively reset the lithospheric lid thickness to zero, at an elevation that corresponds with that of hot, uncompressed mantle. On Earth, this elevation is approximately equal to the crest elevation of the mid-ocean ridges, 2800 ± 400 m below sea level [3], and is equal to the elevation at the top of the Poisson distribution for the oceans excluding the continental shelves, which cause the broad shoulder to the peak. On Venus, this elevation likewise corresponds to the top of the Poisson distribution, at 1900 m above the Mean Planetary Radius (MPR, equal to 6051.8 km radius).

Resurfacing models cover a spectrum between two end members: a global resurfacing event followed by negligible activity [4], [5], and forms of equilibrium resurfacing [6], [7], [8], which InSAR mapping should be able to distinguish between. The origin of the lowlands of Venus may be explained by time-random volcanic processes, whether or not spatially organised [9], but not the highlands.

The Venus highlands are less strongly separated in elevation from the lowlands than Earth's, perhaps reflecting a smaller density contrast, and they cover a smaller area: 5~10% of Venus compared with 40~45% of Earth. However, they may record a longer history and wider range of processes than the lowlands [10], and may represent the sum of several, perhaps many, non-random processes and are therefore of greatest interest for further study.

Target Area Selection:

The selected highland target areas are identified below in descending order of area, with a description of their principal geological features.

a. *Aphrodite Terra, 60˚– 148˚E; 10˚N – 29˚S.* Includes Ovda and Thetis Regios, on the flanks of which are canyons almost as deep as those in Dali, and none of which may be isostatically compensated. To the south of Thetis, perhaps on its flank, a deep canyon separates most of Artemis from Aphrodite, as it curves to define the northern, eastern and southern boundaries of the Corona.

b. *Ishtar Terra, 300˚ – 69˚E; 52˚ – 79˚N.* Includes Lakshmi Planum, Fortuna Tessera and Maxwell Montes. Maxwell peaks at 11 km above MPR, with escarpments that may not be isostatically compensated. Lakshmi Planum is circular, not unlike a corona but maybe of different origin [11]; Colette and Sacajawea, at more than 2 km above MPR and ringed by mountains with steep escarpments [12], indicate the region may be dynamically supported.

c. *Beta Regio, 274˚– 295˚E; 13˚– 39˚N.* Consists of two large volcanoes, Rhea and Theia Mons. Beta might also form a contiguous unit with Asteria Regio and Hundla Regio, and be linked to Pheobe Regio via Devana Chasma.

d. *Atla Regio 183˚– 208˚E; 25˚N – 10˚S.* Dominated by Maat, Ozza and Sapas Mons. Ozza may be a volcano topped by a caldera but Maat Mons (8.87 km above MPR) is the highest, rising steeply (gradient of ~ 1:14) from a canyon floor, 0.5 km below MPR. This canyon leads southwest, divides into several lines around both sides of Zemina Corona, which coalesce further west into Dali Chasma. This volcanic region may be more similar to the Yellowstone caldera than the Hawaiin or other oceanic hotspots [13] and may show the presence of continental crust on Venus. Other canyons extend north, north east and south east of Atla Regio, descend to more than 1 km below MPR, and contain many sharp peaks, some rising ~7 km at a gradient of 1:2. Recently, Parga Chasma, running south east from Atla Regio, may be the most active region on Venus [14].

e. *Pheobe Regio 278˚– 291˚E; 3˚N – 20˚S.* A highland ridge running south from Devana Chasma

to the east, Pheobe has several highland peaks, tesserae, and two coronae. Further east, on the edge of Navka Planitia, are the landing sites of the Pioneer Venus North Probe, and Venera 13 and 14, both of which found evidence for sedimentary deposits [15].

f. *Lada Plateau 4˚ – 13˚E; 64˚ – 70˚S*. A largely featureless highland in western Lada Terra with a curved, radar-bright perimeter that rises, in the main, to just under 2 km above MPR. There is a small (~350 km^2) prominence at the eastern end of the radar-bright feature. This plateau is the only area higher than 2 km above MPR south of 30˚ S latitude, and Lada Terra is certainly a continental-sized unit with features indicative of long-lived and recent volcanic activity [16]. InSAR therefore should help explain the processes responsible for the uplift (or perhaps subsequent subsidence) of Lada Terra.

g. *Dali Plateau 166˚ – 174˚E; 15˚ – 24˚S*. Located immediately south of Dali Chasma, with a mirror-image canyon curving around the plateau on its southern side. Both Chasma and canyon have steep sides and mountainous ridges on the inside of their curve, i.e. the plateau is ringed by a rim of mountains not unlike that around a corona or a crater. Around Dali a series of canyons, incuding Diana and Dali Chasmas, curve around coronae and extend into the foothills of adjacent highland units: Ovda, Thetis, and Atla. To the north of Diana Chasma is Scathach Fluctus, a recently identified large pyroclastic flow deposit [17], and unusually low emissivity plains, which together may indicate unusual geochemistry that may be important in the origin of the highlands.

Geological Assessment of these Target Areas:

A review of these 7 target areas suggests that the highlands comprise 4 geological features:

***Continents*.** Venus Express data suggests Earth-like, relatively low density, continental crust is probable [18], [19], e.g.: Ishtar Terra, Ovda Regio and Thetis Regio. Several mechanisms are proposed: down-welling and contraction [20], up-welling and extension [21], and continental-like accretion [22]. They may record a long and complex history predating any global resurfacing event [10].

***Large Volcanoes*.** Two targets are major volcanic centres that probably overly large, stable mantle plumes [23]. Atla Regio lies at the intersection of Dali, Hecate and Parga rifts; and Beta Regio lies at the intersection of Hecate and Devana rifts. Atla Regio includes Ozza Mons, with both a volcanic plateau and a caldera, and Maat Mons - taller and steeper-sided than Ozza. Emissivity on Maat's summit implies recent volcanic activity [24]. Arecibo radar data may indicate activity at Theia Mons in Beta Regio [25].

Rift Valleys. A steep-sided canyon runs approximately north-south through Atla Regio. The floor of this canyon is densely packed with steeply-sided cones, many several km tall. Arguably, Maat Mons is the tallest of these and so large that it obliterates the canyon. Devana Chasma is a similar canyon oriented approximately north-south through Beta and Pheobe Regios [26], containing many steep escarpments unlikely to be in isostatic equilibrium. The preponderance of steep cones in the canyons is reminiscent of the seamounts associated with Earth's mid-ocean ridges and indeed some are analogous to very slow spreading centres [13].

High-altitude Plateaus. The tilting of Cleopatra crater, gravity data indicating dynamic support, and its close association with Lakshmi Planum, all imply that Maxwell Montes are actively uplifting. Like Lakshmi Planum, the plateau in western Lada Terra and the plateau partly bounded by Dali Chasma are all noticeably circular, featureless and relatively flat.

Summary:

We propose a mapping strategy that covers a sufficient area of lowlands (~10% of the surface) to characterise their common origin through time-random volcanism, and which targets all areas >1900 m above MPR (also ~10%). The higher data rates achievable close to inferior conjunction will make high-resolution InSAR coverage of > 20% of the surface of Venus feasible, and sufficient to clarify many significant unknowns about Earth's twin."

References:

[1] Ferretti et al., *Geosci. and Remote Sensing, IEEE Trans. 45*, 1142-1153 (2007). [2] Meyer & Sandwell, *Planet. Space Sci.* 73, 130-144 (2012). [3] Korenaga and Korenaga, *Earth and Planet. Sci. Ltrs 268*, 41-51 (2008). [4] Romeo, *Planet. & Space Sci. 87, 157-172,* (2013). [5] Turcotte, *JGR: Planets 98, 17061-17068* (1993). [6] Guest and Stofan, *Icarus 139, 55-66* (1999); [7] Hansen and Young, *GSA Sp. Papers 419, 255-273* (2007); [8] Hauck et al., *JGR: Planets 103, 13635-13642* (1998). [9] Rosenblatt et al., *GR Ltrs 21, 465-468* (1994). [10] Romeo et al., *Icarus 175, 320-334* (2005). [11] Roberts and Head, *Earth Moon Planet 50-51, 193-249* (1990). [12] Smrekar and Solomon, *JGR: Planets 97, 16121-16148* (1992). [13] Stoddard and Jurdy, *Icarus 217, 524-533* (2012). [14] Jurdy and Stefanick, *Icarus 139, 93-99* (1999). [15] Florensky et al., *Science 221, 57-59* (1983). [16] Ivanov and Head, *Planet. & Space Sci. 58, 1880-1894* (2010). [17] Ghail and Wilson, *Geo Soc, London, Sp Pubs 401* (2013). [18] Hashimoto et al., *JGR 113* (2008). [19] Mueller et al., *JGR 113* (2008). [20] Gilmore et al., *JGR: Planets 103, 16813-16840* (1998). [21] Ghent and Hansen, *Icarus 139, 116-136* (1999). [22] Ghail, *JGR 107, 5060* (2002). [23] Vezolainen, *JGR 109* (2004). [24] Campbell et al., *JGR: Planets 104, 1897-1916* (1999). [25] Carter et al., *JGR 111* (2006). [26] Kiefer and Swafford, (2006)

THE ELECTRIC WIND OF VENUS

Authors: G. A. Collinson[1,2,3 *], R. A. Frahm[4], A. Glocer[1], A. J. Coates[2], J. Grebowsky[1], S. Barabash[5], A. Fedorov[6,7], Y. Futaana[5], L. K. Gilbert[2], G. Khazanov[1], T. A. Nordheim[8,2], D. Mitchell[9], T. E. Moore[1], W. K. Peterson[10], J. D. Winningham[4], and T. L. Zhang[11]

Affiliations:

[1] NASA Goddard Space Flight Center, Greenbelt, Maryland, USA
[2] Mullard Space Science Laboratory, University College London, Surrey, UK
[3] Institute for Astrophysics and Computational Sciences, The Catholic University of America, Washington, District of Columbia, USA
[4] Southwest Research Institute, San Antonio, Texas, USA
[5] Institutet för rymdfysik, Swedish Institute of Space Physics, Kiruna, Sweden
[6] CNRS, L'Institut de Recherche en Astrophysique et Planétologie, Toulouse, France
[7] University Paul Sabatier, Toulouse, France
[8] Jet Propulsion Laboratory, California Institute of Technology, Pasadena, California, USA
[9] Space Sciences Laboratory, University of California, Berkeley, USA
[10] Laboratory for Atmospheric and Space Physics, Boulder, Colorado, USA
[11] Space Research Institute, Austrian Academy of Sciences, Graz, Austria

*Correspondence to: Glyn Collinson, Heliophysics Science Division, NASA Goddard Space Flight Center, Greenbelt, MD, USA (glyn.a.collinson@nasa.gov)

Abstract:

Venus lost the bulk of its water to space early in its history. At Earth, an important mechanism for atmospheric escape is a weak electric field above the polar caps that helps ionospheric ions overcome gravity. Although such a field is predicted at any planet with an atmosphere, its measurement is exceptionally challenging and to date even in Earth's ionosphere we only have upper limits on its magnitude. We report the discovery of an unexpectedly strong electric potential in the topside ionosphere of Venus, finding it to be a persistent, global feature. Contrary to expectations it is five times stronger than has been measured in Earth's similar ionosphere, despite comparable gravity, and unlike Earth is sufficient to directly accelerate water group ions to escape velocities.

The Ionospheric Fossil Fields of Venus: Simultaneous multipoint observations by Venus Express and MESSENGER

Authors: G. A. Collinson[1*], Yingjuan Ma[2], Lynn B. Wilson III[1], J. Grebowsky[1], D. Sibeck[1], E. Zesta[1], Y. Futaana[3], and T. L. Zhang[4]

Affiliations:

[1] NASA Goddard Space Flight Center, Greenbelt, Maryland, USA
[2] Institute of Geophysics and Planetary Physics, University of California, Los Angeles, California, USA

[3] Space Research Institute, Austrian Academy of Sciences, Graz, Austria

[4] Institutet för rymdfysik, Swedish Institute of Space Physics, Kiruna, Sweden

*Correspondence to: Glyn Collinson, Heliophysics Science Division, NASA Goddard Space Flight Center, Greenbelt, MD, USA (glyn.a.collinson@nasa.gov)

Abstract:

The induced magnetosphere of Venus freely rotates and restructures with the orientation of the interplanetary magnetic Field (IMF). However, with this orientation must usually be inferred from earlier or later at times when the same vessel was outside the planetary bow shock, and the timescales on which magnetospheric reconfiguration occurs is unknown. On June 5th 2007 the NASA MErcury Surface, Space ENvironment, GEochemistry, and Ranging (MESSENGER) spacecraft was ~90 Venus Radii sunward of Venus as it approached for a gravitational assist maneuver, providing exceptionally rare IMF observations usptream from Venus. We present ESA Venus Express electron and magnetic observations from this day, finding the magnetic configuration

of the ionosphere was not consistent with that expected from conditions measured upstream, indicating that the ionosphere responds very slowly to changes in IMF orientation (>1hr). By contrast, a large and sudden rotation of the field in the ionosheath co-incident with a solar wind discontinuity indicates that (consistent with previous studies) the magnetosphere above the ionopause responds very rapidly to changes in upstream conditions (~ minutes). This results in two long-lived magnetic regimes with high shear separated by a current sheet, wherein conditions are ideal for particle acceleration and heating through magnetic reconnection, jxB forces, and waves. Given the frequent occurence of solar wind discontinuities at Venus, we hypothesize this to be a commonly occurring phenomenon.

VENUS: EXPLORING ITS INTERIOR WITH SEISMIC AND INFRASONIC TECHNIQUES[1]

J. A. Cutts , M. Pauken, *Jet Propulsion Laboratory, California Institute of Technology, Pasadena, CA U.S.A, J.M. Jackson, Division of Geological and Planetary Sciences, California Institute of Technology, Pasadena, California, U.S,A., David Mimoun Institut Supérieur de l'Aéronautique et de l'Espace, Toulouse, France and Members of the Keck Institute for Space Studies (KISS) Venus Interior Study and Development Teams*

Introduction:

The formation, evolution and structure of Venus remain a puzzle more than fifty years after the first visit by a robotic spacecraft. Radar images have revealed a surface that is much younger than those of the Moon, Mercury and Mars as well as a variety of enigmatic volcanic and tectonic features quite unlike those generated by plate tectonics on Earth. To understand how Venus works as a planet it is necessary to probe the interior of Venus. This paper describes the application and adaptation of seismic and infrasonic techniques to exploit and cope with the unique environment of Venus in order to probe its interior and characterize its seismicity.

Background

Conventional seismology uses sensors in contact with the planetary surface but for Venus with current technology, this approach is impractical because of the Venus environment (460ºC and 90 bars). However, the dense atmosphere of Venus, which efficiently couples seismic energy into the atmosphere as infrasonic waves, enables an alternative: detection of infrasonic waves in the upper atmosphere using either high altitude balloons or orbiting spacecraft. In June 2014, the Keck Institute for Space Studies (KISS) at the California Institute of Technology sponsored a one week workshop with 30 specialists in the key techniques and technologies relevant to investigating Venus's interior structure. The report of that study (Cutts, Mimoun, & Stevenson, 2015) identifies the most promising approaches for developing seismic sensors tolerant of the high temperatures as well as means of observing the infrasonic signal.

High Temperature Seismic Sensors

The surface of Venus, with temperatures near 460ºC is a very hostile environment for instruments. Conventional electronics are out of the question as there are currently, nor are there in prospect, techniques for protecting components from the environment for more than a few hours. Technologies for tolerating the environment involving vacuum electronics and high temperature semiconductors require many years of development (Cutts, Mimoun, & Stevenson, 2015). Work must continue on these technologies but alternative techniques are needed for near term missions and that is the focus of this paper.

Infrasonic Techniques

Infrasonic techniques for probing the Venus interior can be implemented without exposing sensors to the severe environment of the Venus surface. This approach takes advantage of the fact that approximately 60X the energy from a seismic event on Venus is coupled into the atmosphere on Venus as would occur for a comparable event on Earth. (Lognonne, Geophysics of the Terrestrial Planets, 2010). The KISS report (Cutts, Mimoun, & Stevenson, 2015) evaluates the possibility of detecting seismic events on Venus as infrasonic waves from balloon platforms floating at altitudes where conventional electronics and sensor components can be used and from orbital spacecraft by observing an optical signal produced by the infrasonic wave. Both a direct or epicentral wave can be detected where infrasonic energy is generated right above the event by the piston motion produced by the quake and an indirect wave produced at distance where seismic energy propagates through the crust and interior of the planet and vertical motions at the surface atmosphere interface then excite the vertically moving infrasonic wave. Only the indirect wave probes the interior of the planet. However, the epicentral wave can be a sensitive detector of seismicity across the planet which is itself a subject of considerable interest.

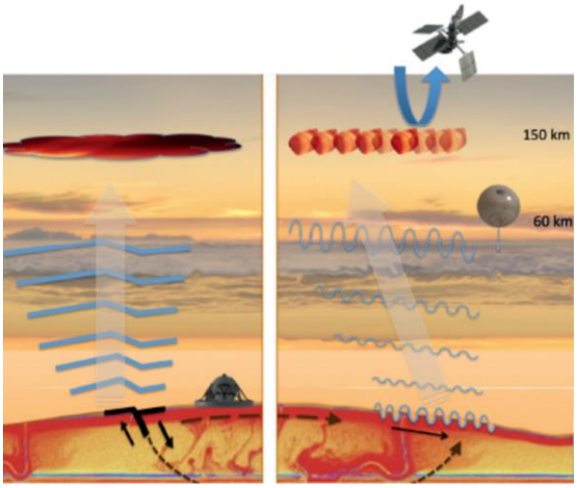

Figure 1 Generation of infrasonic waves by a seismic event on Venus. The direct or epicentral wave (left) propagates vertically above the event. The indirect wave (right) propagates through the planet as a Rayleigh wave and then couples to an infrasonic wave.

[1] This research was carried out at the California Institute of Technology Jet Propulsion Laboratory under a contract from NASA.

Balloon Infrasonic Detection – Sensitivity

Despite the much larger losses at the ground-atmosphere interface on Earth quite small earthquakes can be detected. For example, (Arrowsmith, et al., 2011) report the detection of a magnitude 4.7 quake in Utah across a statewide network of ground based infrasonic stations.

In addition to the fact that more seismic energy will be communicated into the atmosphere on Venus, the balloon station is moving with the medium which will substantially reduce the wind noise which generally determined the threshold of detection for quakes on Earth. This sensitivity advantage of a balloon platform was recently established by comparison of infrasonic measurements from a stratospheric balloon on earth with nearby ground stations (Bowman & Lees, 2016).

The instrumental limits for detection of seismic events on Venus are likely to be well below the Earth and may be determined by the background for other types of infrasonic source. While no inventions are needed at the component level, developments of experimental techniques are needed and these should involve terrestrial flights on both tropospheric and stratospheric balloons. In particular, we need to know more about how to identify and discriminate quake signatures from volcanic events, lighting and other storm activity and meteor impacts.

Seismic and Infrasonic Sources on Venus

Most researchers contend that the level of seismic activity on Venus is somewhere between that on Mars and Earth. Although there is abundant evidence of tectonic activity on Venus, questions remain as to whether the planet is still active and whether energy releases are seismic or aseismic. The lack of observable water suggests brittle release; the high temperatures more plastic behavior. However, another quake source mechanism is a metastable mineral phase change, and we have begun an investigation of the possibility of this occurring.

Quakes are not the only source of seismic energy. In recent years, seismologists have developed techniques for probing crustal and interior structure in parts of the Earth such as Australia where there are very few quakes. We have begun an effort to determine if this is possible for Venus also. Just as seismic energy propagates more efficiently upward across the surface atmosphere interface, equally acoustic energy originating in the atmosphere will propagate downwards more effectively. Potentially, these two can be used to probe the interior. The stratospheric balloon measurements of (Bowman & Lees, 2016) include signatures in the spectral range of the ocean microbarom, which is an important source in terrestrial ambient noise seismology. Measurements from a balloon platform at Venus could assess the nature and spectral content of such sources.

Relevance to Future Missions:

The great advantage of the infrasonic approach to studying the Venus interior is that the basic technology is ready today. While independent balloon and orbital missions could contribute valuable information, the real strength of this technique will involve the synergies between them. The balloon technique provides a synoptic view but there is less energy particularly at the higher frequencies that propagates to the top of the Venus atmosphere and will be visible from space.

Opportunities for a mission with multiple platforms are currently being considered for Russia's Venera D but the baseline mission does not currently include balloons. The U.S. National Research Council's Planetary Science Decadal Survey of 2011 advocated a Venus Climate Mission which did feature a synoptic orbiter and balloon platforms but focused exclusively on atmospheric objects. The same flight elements could be employed to extend the capabilities of that mission as a Venus Climate and Interior Mission. As NASA prepares for its next decadal survey this option should be considered.

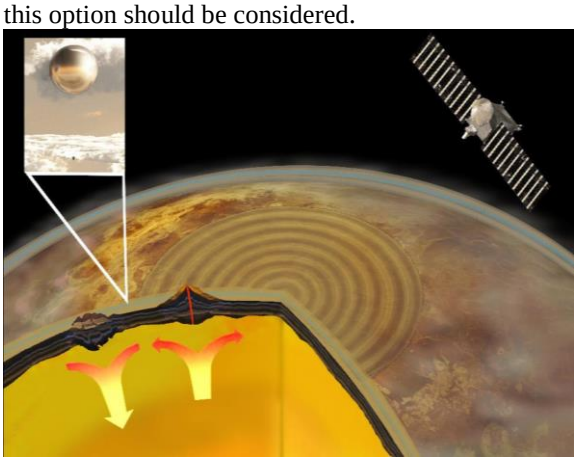

Figure 2 Coordinated observations of the infrasonic signatures from an orbital spacecraft and a balloon platform could provide confirmation of seismic event detections and complementary information

References

Arrowsmith, S. J., Burlacu, R., Pankow, K., Stump, B., Stead, R., Whitaker, R., & Haywood, C. (2011). A seismoacoustic study of the 1011 jan 3 Circleville Earthquake. *Geophysicis Journal International*.

Bowman, D., & Lees, J. (2016). Infrasound in the middle strateosphere measured with a free flying acoustic array. *Geophysical Research Letters*, in press.

Cutts, J. A., Mimoun, D., & Stevenson, D. (2015). *Probing the Interior Structure of Venus.* Keck Insitute of Space Studies, Final Report http://kiss.caltech.edu.

Lognonne, P. (2010). *Geophysics of the Terrestrial Planets.* Keck Institute for Space Studies Report.

Lognonne, P. (2015). Seismic measurements at the Telluric Planets. *Amercan Geophysical Union.* San Francisco: American Geophysical Union.

Geodynamical modeling of Venus in the laboratory: plume-induced coronae, subduction and microplates.

A. Davaille , *Laboratoire FAST, CNRS / Univ. Paris-Sud, Orsay, FRANCE (davaille@fast.u-psud.fr),* **S. Smrekar**, *NASA Jet Propulsion Laboratory, Pasadena, USA.*

Introduction:

The possible role of plate tectonics in creating habitable zones and the conditions required to start plate tectonics are currently hotly debated due to the discovery of many Earth-sized exoplanets. The initiation of subduction is the gateway to plate tectonics but modeling the details of plate failure, gravitational instability, and sinking in the mantle, is very challenging due to the complexity of plate rheology. However, the development of new visualization techniques and the use of complex-rheology fluids in the laboratory open a new area for planetary geodynamic modeling, as observations of surface patterns (i.e. faults, folds, ridges, trenches) can be related to convective instabilities inside the laboratory mantle analog. Here, we report a new convective regime whereby plumes are able to trigger subduction. This process therefore closely associates large coronae with subduction, and even microplates formation. The gravity and topography data in Venus regions such as Lada Terra could be compatible with this interpretation.

Laboratory set up: See fig.1.

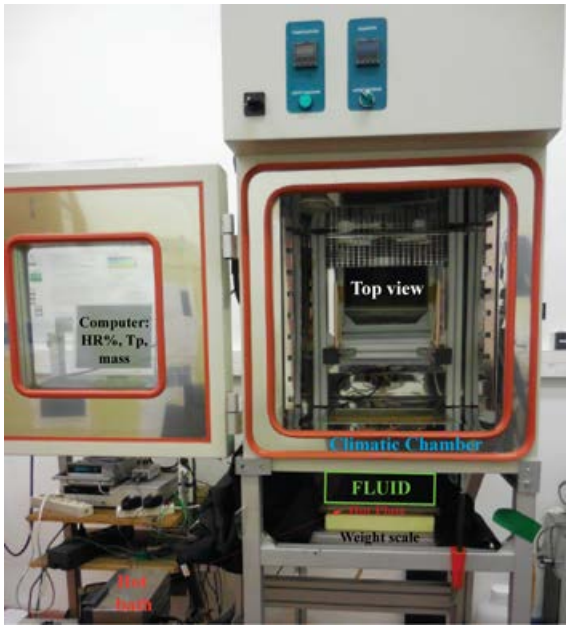

Fig.1: Experimental set up. The surface of the experimental tank is regulated in temperature and humidity with a climatic chamber. A thermostated hot fluid is circulated through the bottom heat exchanger.

As an analog fluid, we use colloidal aqueous dispersions of silica nanoparticles. Their rheology depends strongly on the solid particle fraction, φ_p, deforming in the Newtonian regime at low φ_p, and transitioning to strain-rate weakening, plasticity, elasticity, and brittle properties as φ_p increases [1]. So, as the system is dried from above, a dense skin grows on the surface, akin to a planetary lithosphere. When it is also heated from below, hot plumes develop [2].

Laboratory observations:

When a hot plume impinges under the skin, it triggers a new mode of subduction: as the upwelling plume material breaks the lithosphere and flows above the denser skin, it forces it to sink.

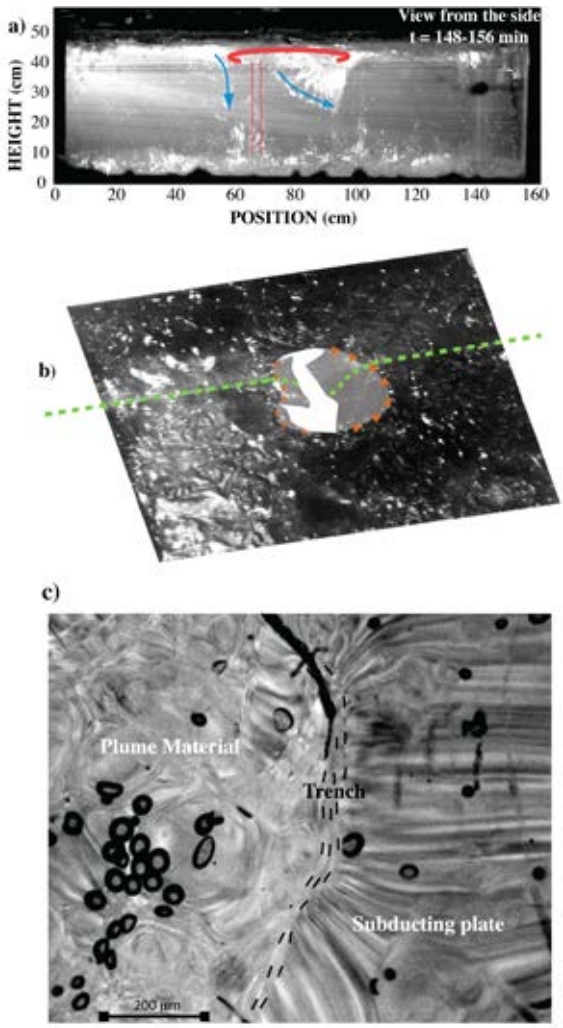

Fig.2: Plume-induced subduction in the laboratory. a) side view. 10 images have been superimposed to show the slab roll-back as the plume spreads. b) 3D view from

above where the plume material has been removed. c) close up (1 cm across) on the boundary between plume material and subducting plate. Darker areas are thicker. The outer bulge close to the trench presents cracks and stripes. The trench (black dashed lines) shows faults parallel to it. The small black ovoids are spurious bubbles.

The experiments further suggest that a weaker lithosphere than that present on Earth today is required for such a convective regime.

Subduction: The subduction trenches are localized along the rim of the plumes and strong roll-back is observed (fig.2a). Subduction always occurs along partial circles (fig.2b), a situation very different from the purely viscous case. This is due to the brittle character of the upper part of the experimental lithosphere: it cannot deform viscously to accommodate roll-back and sinking motions. Instead, the plate tears, as a sheet of paper would do upon intrusion (fig.2b). The trench zone presents a succession of faults/cracks parallel to it, and the outer bulge shows extensional features such as stripes and cracks (fig.2c). As a plume is a transient phenomenon, the subduction eventually stops and most of the time, a slab stays dangling for a while until necking and foundering occur.

Microplate: Two types are observed. First, the upwelling plume material creates a set of new plates inwards the different trenches, and these new plates are expanding through time but are not subducting. In a few cases, we observe also additional microplates outwards of the trenches. This happens when the subducting plate already contained fabric heterogeneities (e.g. fractures) and when the subducted slab is long enough for slab pull to become efficient.

Coronae: If we define coronae by their circular morphology, we observe in the laboratory two populations. The first one is created by plume impacts (typically a few cm across), and is therefore closely associated with subduction events. But we can see on fig.2c that small circular features (~ 2 mm diameter) are also present. They are due to the gravitational destabilization of the bottom of the skin.

Plume-induced coronae, subduction and microplates on Venus ?

These experimental observations strongly resemble a number of features observed on Venus, including the association of large coronae with trenches that had been proposed as subduction zones based on their similar morphology compared to Earth's [3,4].

For exemple, *Lada Terra* is a ~1000 km diameter topographic rise centered near 65°S, 10°E. The 800 km diameter Quetzelpetlatl Corona (QC) defines the western margin (fig.3a). The western edge of QC is defined by a trench and outer rise (fig.3b). The latter presents also graben and fractures similar to the extensional features seen in the laboratory (fig.3c).

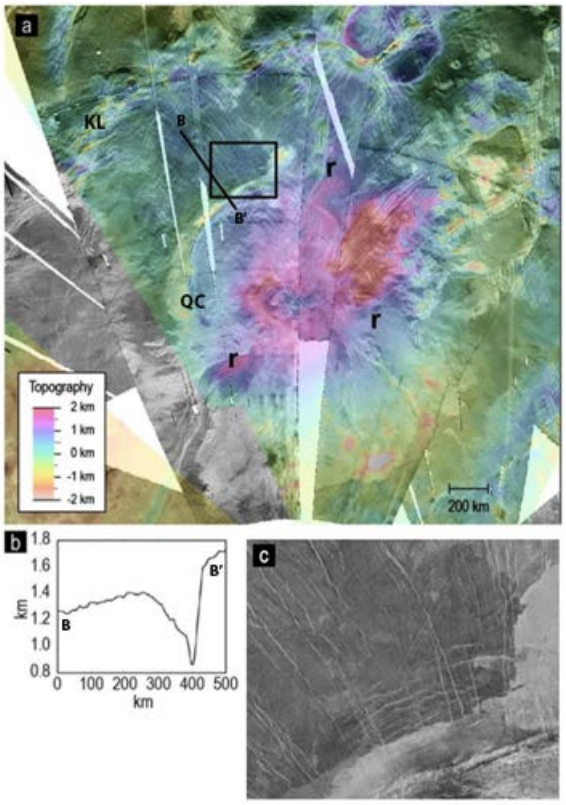

Fig.3: Lada Terra region. a) Radar (gray scale) and topography (colour) image. Quetzelpetlatl Coronae includes a ~180° arc ("QC"). North of it is Kalaipahoa Linea ("KL"). b) Topography across the outer bulge and trench along the black profile BB' in a). c) Zoom on the trench and outer bulge (black square in a)) showing graben and fractures.

The subsurface density variations inferred from modeling the gravity and topography data at QC are compatible with the existence of a slab at depth [5]. Moreover, the presence of an extension zone to the North (Kalaipahoa Linea) could mark the Northern edge of a microplate currently subducting at QC.

Besides, evidence for geologically recent volcanism at Quetzelpetlatl [6] suggests that subduction may be currently active on Venus. Hence Lada Terra could be an interesting target for high resolution imagery and altimetry, as well as interferometry and spectroscopy, in a future mission such as VERITAS [7].

Bibliography:

[1] Di Giuseppe E. et al. (2012) *Rheol. Acta* 51(5), 451-465.
[2] Davaille A., et al. (2011) EPSC-DPS abst, p.694
[3] Sandwell D.T. and G. Schubert (1992) *Science, 257*, 766-770.
[4] Schubert G and D. T. Sandwell, (1995) *Icarus 117*, 173-196.
[5] Smrekar S., A. Davaille & S. Tomlinson (2016) subm.
[6] Helbert J. *et al.* (2008) *GRL* **35**, doi:10.1029/ 2008GL033609.
[7] Smrekar S. et al. (2016) this meeting.

DISTRIBUTION AND DYNAMIC OF PLASMA IN THE MAGNETOSPHERES OF VENUS AND MARS.

E. Dubinin, *Max-Planck-Institute for Solar System Research (dubinin@mps.mpg.de),* **M. Fraenz,** *Max-Planck-Institute for Solar System Research,* **R. Modolo**, *LATMOS, Université Versailles Saint Quentin, Guyancourt, France*

General features of plasma characteristics in different regions of the induced magnetospheres of Venus and Mars observed by Venus Express, Mars Express and MAVEN are discussed. There are several important plasma reservoirs with different mechanisms of plasma filling and plasma energization. Among them are the ionosphere, boundary layer at the interface between the ionosphere and solar wind, plasma sheet, lobes, ion plume. Dynamics of ions in these regions is strongly controlled by the solar wind and the IMF parameters. Multi-ion origin of plasma introduces additional important features which are important for ion dynamics and filling of plasma reservoirs. The existence of crustal magnetic field on Mars modifies not only the ionosphere but also influences a filling of more remote plasma reservoirs.

TIDAL CONSTRAINTS ON THE INTERIOR OF VENUS.

C. Dumoulin, *Université de Nantes, UMR6112, Laboratoire de Planétologie et Géodynamique, Nantes, France (caroline.dumoulin@univ-nantes.fr)*, **G. Tobie,** *CNRS UMR6112, Laboratoire de Planétologie et Géodynamique, Nantes, France*, **O. Verhoeven,** *Université de Nantes, UMR6112, Laboratoire de Planétologie et Géodynamique, Nantes, France*, **P. Rosenblatt,** *Observatoire Royal de Bruxelles, Belgique*, **N. Rambaux,** *Université Pierre et Marie Curie, UPMC Paris 06, Institut de Mécanique Céleste et Calcul des Ephémérides, Paris, France*.

As a prospective study for a future exploration of Venus, we propose to systematically investigate the signature of the internal structure in the gravity field and the rotation state of Venus, through the determination of the moment of inertia and the tidal Love number.

Introduction

Although Venus is very similar in size and mass to the Earth (and therefore often referred to as its twin sister), their internal structures might differ in several ways. Indeed, the lack of plate tectonics as means to expel heat probably leads to a hotter interior for Venus. As a consequence, Venus's core should be at least partially, and maybe entirely, molten. The determination of the tidal Love number k_2 from Magellan data by [1] seems indeed to confirm the presence of a fluid core. However, there is few data to constrain the core mass : Cosmochemical models ([2]) suggest core mass fractions between 23.6 and 32.0% implying a mantle mass similar to or greater than Earth's. The Venera landers returned a number of K, U and Th measurements that imply bulk ratios, and hence internal radiogenic heating rates, comparable with Earth. As the moment of inertia of the planet is not known, the first order internal structure depicted for Venus is often just a scaled version of the Earth's one. In addition, the Venus Express Mission measured a variation in the venusian length-of-day [3] that could bring information on the interior. However, the rotational models were not able to explain this large variations [4].

Mantle composition and core state

We test various mantle compositions, core size and density as well as temperature profiles representative of different scenarios for formation and evolution of Venus. The mantle density ρ and seismic v_P and v_S wavespeeds are computed in a consistent manner from given temperature and composition using the Perple_X program [5]. This method computes phase equilibria and uses the thermodynamics of mantle minerals developped by [6].

Computation of tidal deformation

The viscoelastic deformation of the planet interior under the action of periodic tidal forces are computed following the method of [7]. The Poisson equation and the equation of motions are solved for small perturbations in the frequency domain using a compressible viscoelastic rheology. The Love number k_2 and the dissipation function, Q^{-1} are computed by integrating the radial functions associated with the radial and tangential displacements, the radial and tangential stresses, and the gravitational potential, as defined by [8]. The deformation of the liquid core is assumed to be static, and the simplified formulation of [9] is thus employed.

Love number and moment of inertia

For a variety of interior models of Venus, the Love number, k_2, and moment of inertia factor, I/MR^2, are computed following the method described above. The objective is to determine the sensitivity of these synthetic results to the internal structure. These synthetic data are then used to infer the measurement accuracies required on the time-varying gravitational field and the rotation state (precession rate, nutation and length of day variations) to provide useful constraints on the internal structure.

We show that a better determination of k2, together with an estimation of the moment of inertia, the radial displacement, and of the phase shift, if possible, will refine our knowledge on the present-day interior of Venus (size of the core, mantle temperature, composition and viscosity). Inferring these quantities from a future exploration mission will provide essential constraints on the formation and evolution scenarios of Venus.

References

[1] Konopliv, A.S. and Yoder, C.F. : Venusian k2 tidal Love number from Magellan and PVO tracking data, Geophys. Res. Lett., 23, 1857–1860, 1996.

[2] Fegley, B. Jr. : Venus. In *Treatise on Geochemistry, Vol. 1, Meteorites, Comets and Planets*, edited by A. M. Davis, Elsevier, Amsterdam, 487-507, 2005.

REFERENCES

[3] Mueller, N. T., Helbertb, J., Erard, S., Piccionid, G. and Drossart P. : Rotation period of Venus estimated from Venus Express VIRTIS images and Magellan altimetry, Icarus, 217, 474-483, 2012.

[4] Cotterreau L., Rambaux N., Lebonnois S, and Souchay J. : The various contributions in Venus rotation rate and LOD, Astronomy and Astrophysics, vol. 531, A45, 2011.

[5] Connolly, J. A. D. : Computation of phase equilibria by linear programming: A tool for geodynamic modeling and its application to subduction zone decarbonation. Earth and Planetary Science Letters, 236:524-541, 2005.

[6] Stixrude, L. and Lithgow- Bertelloni, C. : Thermodynamics of mantle minerals - II. Phase equilibria. Geophysical Journal International, 184:1180-1213, 2011.

[7] Tobie, G., Mocquet, A., and Sotin, C.: Tidal dissipation within large icy satellites: Applications to Europa and Titan, Icarus 177, 534, 2005.

[8] Takeushi, H. and Saito, M.: Methods in computational Physics, in B. A. Bolt (ed.), Vol. 1, pp 217-295, Academic Press, New York, N. Y., 1972.

[9] Saito, M. : Some problems of static deformation of the Earth, J. Phys. Earth 22, 123, 1974.

VARIABILITY OF SO_2 AND HDO AND THERMAL STRUCTURE IN THE LOWER MESOSPHERE OF VENUS FROM INFRARED SPECTROSCOPY

T. Encrenaz, *LESIA, Paris Observatory, France (therese.encrenaz@obspm.fr),* **T. K. Greathouse,** *SwRI, San Antonio, TX, USA,* **M.J. Richter & C. DeWitt** *(University of California Davis, CA, USA),* **T. Widemann, B. Bézard & T. Fouchet,** *LESIA, Paris Observatory, France*), **S. K. Atreya**, *U. of Michigan, Ann Arbor, MI, USA,* **H. Sagawa,** *Kyoto Sangyo Univ., Japan.*

Introduction:

Since January 2012, we have mapped the SO_2 and HDO mixing ratios at the cloudtop of Venus in the thermal regime, using the Texas Echelon Cross Echelle Spectrograph (TEXES) at the Infrared Telescope Facility (IRTF). The HDO maps appear homogeneous over the Venus disk. In contrast, the SO_2 maps show strong variations over the disk and on a time scale as short as two hours. Both molecules show long-term variations, but without any apparent correlation between them. In addition, thermal structure in the lower mesosphere is retrieved from the analysis of different CO_2 bands.

Observations:

Five observing runs have been obtained (Jan. & Oct. 2012, Feb. & July 2014, March 2015). We selected the 1343-1353 cm^{-1} (7.4 μm) range, where weak transitions of CO_2, SO_2 and HDO are present. At this wavelength, the radiation probes the cloud top at an altitude of about 63 km. We mapped the SO_2 and HDO mixing ratios by making the ratio of these molecules relative to the CO_2 line depth [1]. The maps were achieved by orienting the 8-arcsec slit along the north-south celestial axis, offsetting to the west off the planet, and then stepping it by half slit-width steps east across Venus to the other side. The diameter of Venus ranged from 12 arcsec (July 2014) to 33 arcsec (February 2014), so that several scans taken at different north/south positions were required to map the whole planet. The resolving power was 8×10^4 [1-4].

Results:

HDO & SO_2 variability:

Figure 1 shows maps of HDO recorded between October 2012 and March 2015. The maps are globally uniform, with a drop of intensity by about a factor of 2 in July 2014, observed during two consecutive days. The mean H_2O mixing ratio, assuming a D/H value of 200 SMOW (Standard Mean Ocean Water) [5] is about 1.0 +/- 0.5 ppmv, in agreement with previous ground-based and space measurements [5-8] Figure 2 shows maps of SO_2 recorded in July 2014 and March 2015. In contrast with HDO, both sets of maps show strong spatial variations (as already observed in 2012 [1, 2]). Temporal variations (also observed in 2012) are noticeable on a time scale of two hours.

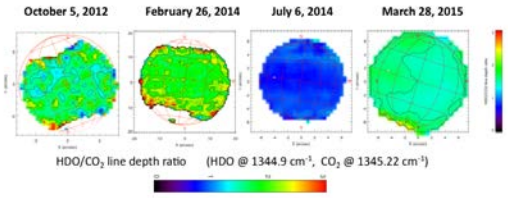

Figure 1: Maps of the HDO/CO_2 line depth ratio at the cloudtop of Venus between October 2012 and March 2015. A HDO/CO_2 line depth ratio of 1.5 corresponds to a H_2O mixing ratio of about 1 ppmv [2, 3]. A drop of the water content by a factor 2 is visible in the February 2014 dataset.

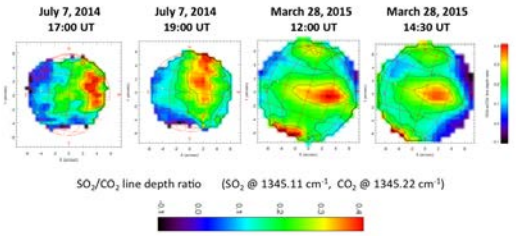

Figure 2: Maps of the SO_2/CO_2 line depth ratio at the cloudtop of Venus in Jul. 2014 and Mar. 2015. A SO_2/CO_2 line depth ratio of 0.2 corresponds to a SO_2 mixing ratio of about 120 ppbv at the cloudtop [2].

The SO_2 mixing ratios are in overall agreement with other past and recent measurements in the same altitude range [7, 9 – 11]. All studies illustrate the high spatial and temporal variability of SO_2.

Figure 3 shows the long-term variations of the SO_2 and H_2O (inferred from HDO) mixing ratios at the cloudtop, between January 2012 and March 2015. The HDO curve shows a clear depletion (by a factor

of about 2) in July 2014. The SO_2 curve is constant over time, except for a drop by a factor 3 (significantly outside the noise level) in February 2014. It is interesting to note that there is no correlation between the SO_2 and H_2O curves. In the same way, the absence of spatial and short-term variations in the HDO maps illustrate that different processes are at work in the behaviors of the two species at the cloudtop. In the case of SO_2, its short photochemical lifetime of one day could be somewhat responsible for its high spatial and short-term variability, but dynamical and thermodynamical effects probably contribute in a major way.

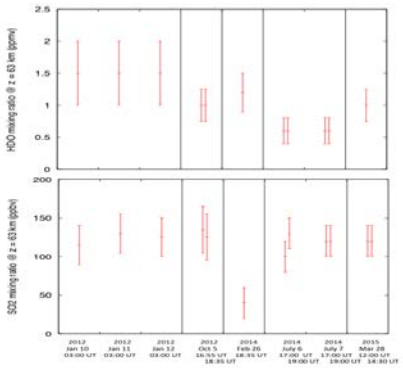

Figure 3: Temporal variations of the disk-integrated SO_2 and HDO mixing ratios at the cloudtop of Venus between January 2012 and March 2015. Note that the time scale in abscissa is not linear.

Thermal structure:

Measuring CO_2 transitions of various intensities in different bands at 7, 10.5, 12.5 and 19 μm allows us to retrieve information about the thermal structure above the clouds as a function of latitude and local hour. At high latitudes (around 70 N and S), our data show the isothermal or inversion layer just above the cloud associated with the polar collar. This effect is clearly stronger around the morning terminator (Oct. 2012, Feb. & July 2014) than at the evening terminator (Jan. 2012, March 2015). In addition, data recorded in the CO_2 hot band at 10.5 μm show at the limb a non-thermal emission on the dayside, consistent with previous heterodyne spectroscopy observations at the same wavelength [12]. Figure 4 shows a map of the temperature at an altitude of 15 km above the cloudtop, as a function of latitude and local hour, recorded from the flux measured in the center of a strong CO_2 band at 956.2 cm^{-1} (removing the non-LTE emission at the dayside limb of the planet).

Acknowledgements:

TE, TKG and CDW were visiting astronomers at the InfraRed Telescope Facility, which is operated by the University of Hawaii under Cooperative Agreement no. NNX-08AE38A with National Aeronautics and Space Administration, Science Mission Doctorate, Planetary Astronomy Program. We thank the IRTF staff for the support of TEXES observations. TE, TW, BB and TF acknowledge support from CNRS and Programme National de Planétologie INSU/CNRS. TKG acknowledges support of NASA grant NNX14AG34G. TF acknowledges support from UPMC. TW acknowledges support from the University Versailles-Saint-Quentin.

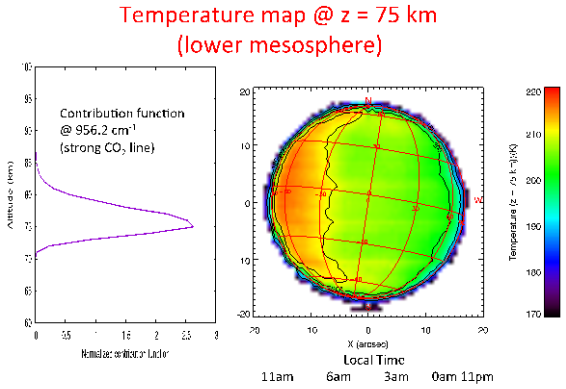

Figure 4: Left: The weighting function of the Venus radiance at 956.2 cm^{-1}, in the core of a strong CO_2 band. Right: Map of the temperature at an altitude of 15 km above the cloud top.

References:

[1] Encrenaz, T. et al., HDO and SO_2 thermal mapping on Venus: Evidence for strong SO_2 variability. Astron. Astrophys. 534, A153, 2012.

[2] Encrenaz, T. et al., HDO and SO_2 thermal mapping on Venus. II: The SO_2 spatial distribution above and within the clouds. Astron. Astrophys. 559, A65, 2013.

[3] Encrenaz, T. et al., Imaging spectroscopy of Venus in the infrared. EPSC, Cascais, September 2014.

[4] Encrenaz, T. et al., Variability of SO_2 and HDO at the cloudtop of Venus from high-resolution infrared spectroscopy. EPSC, Nantes, September-October 2015.

[5] Fedorova, A. et al. HDO and H_2O vertical distributions and isotopic ratio in the Venus mesosphere by Solar Occultation at Infrared spectrometer on board Venus Express. J. Geophys. Res. 113, CiteID E00B22, 2008.

[6] Cottini, V. et al. Water vapor near the cloud tops of Venus from Venus Express/VIRTIS dayside data. Icarus 217, 561-569. 2012.

[7] Krasnopolsky, V. A. Spatially-resolved high-resolution spectroscopy of Venus. 2. Variations of HDO, OCS, and SO_2 at the cloud tops. Icarus 209, 314-322, 2010.

[8] Matsui, H. et al. Latitudinal distribution of HDO abundance above Venus' clouds by ground-based 2.3 μm spectroscopy. Icarus 217, 610-614, 2012.

[9] Zasova, L. V. et al. SO_2 in the middle atmosphere of Venus: IR Measurements from Venera-15 and comparison to UV Data. Icarus 105, 92-109, 1993.

[10] Marcq, E. et al. An investigation of the SO_2 content of the venusian mesosphere using SPICAV-UV in nadir mode. Icarus 211, 58-69, 2011.

[11] Beyaev, D. A. et al. Vertical profiling of SO_2 and SO above Venus' clouds by SPICAV/SOIR solar occultations. Icarus 217, 740-751, 2012.

[12] Sornig, M. et al. Venus' upper atmospheric dynamical structure from ground-based observations shortly before and after Venus' inferior conjunction 2009. Icarus 225,

828-839.

Review of ASPERA-4 results on Venus–solar wind interaction: After 8 years operation at Venus

Y. Futaana[1] *(futaana@irf.se)*, **S. Barabash**[1], **and ASPERA-4 team**.
[1] *Swedish Institute of Space Physics, Kiruna, Sweden*

Abstract:

Venus Express (VEX) was launched on 9 November 2005, and inserted into a highly elliptic polar orbit of Venus on 11 April 2006. The main focus of the Venus Express mission is global, long-term and comprehensive investigations of the surface, atmosphere and plasma environment of Venus by means of remote sensing and in situ measurement. Until its fuel outage happened on 28 November 2014, VEX had provided a large amount of valuable data of Venus.

Analyser of Space Plasma and EneRgetic Atoms (ASPERA-4) is one of the scientific instruments onboard VEX. ASPERA-4 measured the plasma and energetic neutral atom (ENA) in the near-Venus space [Barabash et al., 2007]. It was operated almost continuously near the pericenter of the VEX orbit. It covers the solar wind, the magnetosheath, the induced magnetosphere, the ionosphere, and their bondaries. In addition, the solar wind close to Venus (~0.7 AU) had been monitored, which can be utilized to the space environment study of the inner solar system.

ASPERA-4 was composed of four sensors measuring ions, electrons, and ENAs. Ion Mass Analyzer, IMA, measured the 3-D ion distribution functions (10 eV–36 keV) with modest mass separation. Electron Spectrometer, ELS, measured electrons (10 eV–15 keV) with a time resolution of 4 s. With the scanner, ELS could measure the 3D electron velocity distribution functions with 32 s. Neutral Particle Imager (NPI) and Neutral Particle Detector (NPD) were for measuring ENAs. NPI had high angular resolution (~4.6x11.5˚) within a 360˚ plane, while NPD had the energy resolution using the time-of-flight system. All the sensors functioned throughout the mission without serious problems.

In this presentation, we will overview the scientific outcome obtained from ASPERA-4 after the eight-year operations. The original scientific goals of ASPERA-4 [Barabash et al., 2007] are in particular emphasized:

• How is the Venus atmosphere coupled with the solar wind?
• How is mass added to and removed from the atmosphere?
• What is the structure of the interaction region?
• Could the solar wind interaction have contributed to the water escape? Is the process the same as for that from Mars?
• What is the mass composition of the escaping plasma? To what degree are the outflow processes mass dependent, and can this explain the Venus loss of water and greenhouse effect?
• What is the neutral–plasma interaction on Venus? How does the presence of the neutral gas affect plasma dynamics?
• What are similarities and differences in the solar wind interaction with the other terrestrial planets, Earth and Mars?

In addition, the extended scientific objectives regarding the solar wind-Venus interaction will be reviewed as well:

• How does the solar wind interaction depend on the solar activity?
• How does the Venusian system response to abrupt phenomena in the solar wind, such as coronal mass ejection or corotating interaction region?

References:

Barabash, S, et al., The Analyser of Space Plasmas and Energetic Atoms (ASPERA-4) for the Venus Express mission, Planet. Space Sci., 55(12), 1772–1792, doi:10.1016/j.pss.2007.01.014, 2007.

TITLE: INFRASOUNDS FROM VENUS QUAKES: NUMERICAL MODELING AND BALLOON OBSERVATION PROJECT

R. F. Garcia, D. Mimoun, Q. Brissaud, *Institut Supérieur de l'Aéronautique et de l'Espace (ISAE-SUPAERO), Toulouse, France (raphael.garcia@isae.fr),* **S. Lebonnois**, Laboratoire de Météorologie Dynamique (LMD), Paris France.

Introduction:

The solid/atmosphere coupling on Venus is enhanced, compared to Earth case, by the strong air density at Venus surface. Previous investigations suggest that 15% of quake energy is lost in Venus atmosphere (Lognonné et al., 2010), and that quakes of magnitude larger than 6.0 may be detected in the upper atmosphere (Garcia et al., 2005). A Recent report by the Keck Institute for Space Studies investigated various ways of performing atmospheric seismology on Venus (Cutts et al., 2015). This study continue these investigations in two complementary directions: simulations of wind shear effects on infrasonic wave propagation, and preliminary study of a balloon payload.

Numerical simulations of infrasound wave propagation in a windy Venus atmosphere:

The numerical modeling of infrasonic waves is performed with Finite Differences. The tool is able to simulate the propagation of acoustic and gravity waves in the same run for a bottom forcing by surface displacements induced by seismic surface waves. The effects of 3D variations of static parameters (sound speed, density, pressure Brunt-Vaissala frequency …) and vertical variations of horizontal winds are taken into account. The attenuation of acoustic and gravity waves in CO2 atmospheres are also modeled properly by taking into account relaxation modes of CO2 molecules. Our study focus mainly on the effects of attenuation and wind shear on acoustic wavefronts in realistic atmosphere models. Acoustic wave propagations are simulated in different regions of Venus atmosphere up to thermosphere layers.

Preliminary design of a balloon payload:

Atmospheric dynamics will impose limitations in the ability to detect Venus quakes on the surface, from a balloon or from orbit. Although it might be difficult to estimate the turbulence level in the Venus atmosphere, key contributors of the noise budget, such as gravity waves, have to be estimated. Ambient noise establishes both a limit on the size of Venus quakes that can be detected from both a surface platform and an atmospheric platform and a potential opportunity for probing the subsurface in the absence of quakes using the methods of ambient noise tomography.

In order to understand constraints, put by the ambient seismic noise on Venus and provide key inputs to the design of an infrasonic experiment using a balloon platform, we have designed a breadboard of a microbarometer payload, similar to what we intend to fly on Venus, and that we plan to test on a balloon in a terrestrial flight, in environmental conditions similar to the upper atmosphere of Venus (over the clouds, at about 60 km). This experiment includes two barometers separated by about 100 m of altitude. This configuration will help us discriminate seismo-acoustic waves generated by the ground and propagating upwards from the barometric waves (altitude …) and other waves due to the atmosphere turbulence.

Conclusion:

Our simulations demonstrate, for realistic Venus atmosphere models, that the attenuation of infrasounds has a limited impact for periods larger than 20s. The wind shear has a strong influence on the propagation of infrasonic waves. However, the infrasonic waves created by seismic surface waves have an almost vertical propagation. So, this effect is limited due to a shearing almolst parallel to acoustic wavefronts. Consequently, the waves observed by various markers in the upper atmosphere should not be strongly deformed by horizontal wind shear at a given altitude. The noise budget of a infrasonic measurement in the Venus atmosphere and the balloon infrasound sensor project are presented.

References:

Cutts, J. A., Mimoun, D., & Stevenson, D. (2015). *Probing the Interior Structure of Venus.* Keck Insitute of Space Studies, Final Report http://kiss.caltech.edu.

Garcia, R., Lognonné, P., & Bonnin, X. (2005). Detecting atmospheric perturbations produced by Venus quakes. *Geophysical research letters*, *32*(16).

Lognonné, P., et al., (2010). 3 Planetary Seismology. *Planets and Moons: Treatise on Geophysics*, *10*, 69.

Structures in the O_2 and NO Venus night airglow: observations and two-dimensional simulations.

J.-C. Gérard (jc.gerard@ulg.ac.be), **L. Soret, A. Collet,** *Laboratoire de Physique Atmosphérique et Planétaire, Université de Liège, Liège, Belgium.*

Introduction:

Limb images constructed from VIRTIS-M observations in the Venus northern hemisphere show that the $O_2(^1\Delta_g)$ nightside airglow at 1.27 μm frequently shows localized regions of enhanced emission between ~95 and 100 km (Figure 1). These structures are quite different from the global picture obtained after averaging all nadir observations of the VIRTIS dataset. These bright spots have been described based on ground-based [Allen et al., 1992; Crisp et al., 1996] and VIRTIS-M observations [Gérard et al., 2014; Soret et al., 2014]. They are characterized by a horizontal size on the order of 500-1000 km, and their lifetime is typically one Earth day or less. Similarly, the NO delta and gamma bands, produced by radiative recombination of O and N atoms, show latitudinal structures with multiple peaks observed along the orbital track [Stiepen et al., 2013].

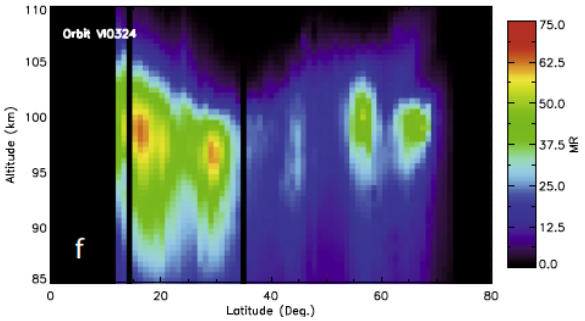

Figure 1: Limb distribution of the $O_2(^1\Delta_g)$ nightglow observed at the limb with the VIRTIS-M instrument on board Venus Express. Multiple bright spots are frequently observed and show morphology variations over 24-hour periods.

Another unexpected feature of the Venus nightglow is the difference in latitudinal distribution of the UV nitric oxide emission near 115 km and the $O_2(^1\Delta_g)$ airglow measured during concurrent nadir observations of the two emissions [Gérard et al., 2013]. The two emissions appear geographically separated, probably a consequence of the different altitudes of the two emissions.

Time dependent model simulations:

In this work, we compare these observations with the predictions of a two-dimensional model combining simplified odd oxygen and nitrogen chemistry with vertical and horizontal transport. It was described by Collet et al. [2010]. The horizontal wind speed is assumed to be constant with altitude. Vertical transport is parameterized by an altitude dependent eddy diffusion coefficient. The coupled nonlinear system of the partial differential equations describing the spatio-temporal variations of the minor species is solved using a finite volume method with a forward Euler method for the time integration scheme. Numerical time dependent simulations confirm that the observed airglow brightening may result from a confined increase of the downward flux of O and N atoms. In the simulation, the vertical fluxes of the two constituents are locally increased to simulate a change in the supply of atoms from the dayside. The two emissions reach their peak intensity at a different time and location, which generates delocalization of the two emissions. This behavior may be explained by the different altitudes of the emission peak between NO resulting from two-body O+N recombination, while $O_2(^1\Delta_g)$ production is a three-body process occurring at lower altitude. The lifetime of these enhancements depends on the O number density, which in turn varies with the altitude of the emission peaks controlled by the magnitude of the downward flux of O atoms.

Repeated localized increases of the flux of atomic oxygen through the upper boundary create structures in the O density and the airglow distribution that are very reminiscent of the bright spots observed by VIRTIS (Figure 2). The spots are also predicted, but are not identical, in the NO airglow distribution, as in the case for a continuous localized flux increase.

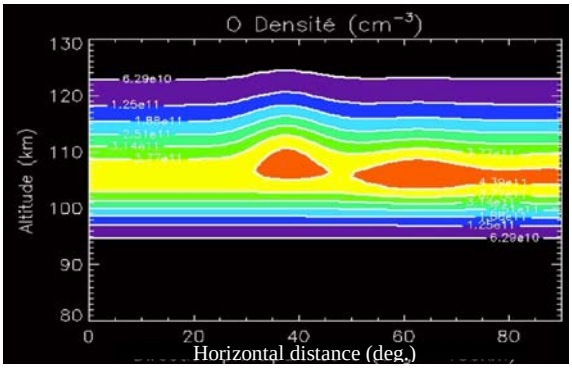

Figure 2: Calculated two-dimensional distribution of the O density following injection of three blobs of oxygen atoms centered on x=20 and temporally separated by 28 hours through the model upper boundary. A constant horizontal wind is assumed to blow from left to right at a constant speed of 25 m s^{-1}.

Conclusions:

Regions of enhanced airglow intensity has been consistently observed from the ground and further documented by the space observations made with the VIRTIS-M spectral imager. The 2-D model simulations are able to reproduce the lack of spatial correlation observed between the NO and the O_2 airglow bright spots. Both emissions are enhanced downwind from the region of atom injection, but their peak brightening are separated by several degrees, depending on the wind speed. This spatial and temporal separation is a consequence of the largely different chemical lifetimes of the O and N atoms. A time modulation of the supply of atoms produces a series of bright airglow spots resembling the structure observed by Venus Express at the limb.

References:

Allen, D. A., D. Crisp, & V. S. Meadows, Variable oxygen airglow on Venus as a probe of atmospheric dynamics, Nature, 1992, 359, 516-518.

Collet, A. and Cox, C. & Gérard, J.-C., Two-dimensional time-dependent model of the transport of minor species in the Venus night side upper atmosphere, Planet. Space Sci., 2010, 58, 1857-1867.

Crisp, D., et al., Ground-based near-infrared observations of the Venus nightside: 1.27-μm $O_2(a\ ^1\Delta_g)$ airglow from the upper atmosphere, J. Geophys. Res., 1996, 101(E2), 4577–4593.

Gérard, J.-C. et al., Latitudinal structure of the Venus O_2 infrared airglow: A signature of small-scale dynamical processes in the upper atmosphere, Icarus, 2014, 236, 92-103.

Gérard, J.-C et al., Concurrent observations of the ultraviolet nitric oxide and infrared $O_2(a^1\Delta)$ nightglow emissions with Venus Express, J. Geophys. Res., 2009, 114, E00B44.

Soret, L. et al., Time variations of $O_2(a^1\Delta)$ nightglow spots on the Venus nightside and dynamics of the upper mesosphere, Icarus, 2014, 237, 306-314.

Stiepen, A. et al., Venus nitric oxide nightglow mapping from SPICAV nadir observations, Icarus, 2013, 226, 428-436.

FAREWELL FANTASTIC VENUS: A NEW UNDERSTANDING OF OUR CLOSEST SIBLING

R. C. Ghail, *Department of Civil and Environmental Engineering, Imperial College London, London, SW7 2AZ, UK. (r.ghail@imperial.ac.uk)*

Introduction:

Farewell Fantastic Venus, a science fiction anthology edited by Brian Aldiss and Harry Harrison, was published in 1968 to lament the loss of the primordial steamy world of the imagination with the harsh reality discovered in the early space age. After Magellan, Venus again became a world of the imagination with competing ideas about resurfacing at a global scale, disconnected from the constraints of surface geology by the apparently random distribution of impact craters. However, recent observations by Venus Express and a re-evaluation of Magellan data are leading to a more nuanced understanding of our most Earth-like neighbour: a geologically complex, diverse and active planet, but in its own unique way.

Background:

NASA Magellan data show a near random distribution of ~940 impact craters, implying a globally uniform surface age of ~750 million years [1–3]. Episodic global resurfacing [4–8] and a proposed global stratigraphic sequence [9,10] postulate an early rapid resurfacing followed by a long period of quiescence. The absence of an asthenosphere in a dry mantle implies a stagnant lid regime [11–14] in which the lithospheric lid is coupled to a high viscosity mantle that convects slowly enough for conductive cooling to be the dominant heat transport mechanism. Some authors regard this regime as either complementary to episodic global resurfacing [4,15] or as a change in the convective regime following the last global resurfacing event [13].

However, this self-consistent view does not explain the observed geological complexity. Geological observations from Magellan data imply a variety of age relationships and long-term activity [16,17], with at least some activity into the recent past [18–20]. There is a non-random distribution of topography (e.g., the highs form semi-linear features) and an association between geological features and elevation, such that the uplands are consistently more deformed than the lowlands. The distribution of impact craters is not strictly random either [19,21,22], with recent observations about the degree of crater alteration [23] permitting a wider range of possible recent geological activity [21,24–28].

The distribution of volcanoes is also far from random, with a concentration more than twice the global average in the so-called "BAT" region between Beta, Atla and Themis. Recent and perhaps continuing volcanic activity may have been observed in both Venus Express [20,29,30] and Magellan [31] data.

Maintenance of the clouds requires a constant input of H_2O and SO_2 [32] which, assuming a saturated magma source, equates to a modest $0{\cdot}5$ km^3 a^{-1}. However, only one volatile-rich pyroclastic deposit has been detected to date [33], partly because of the difficulty in distinguishing pyroclastic deposits from other surface materials, but the morphology of most of the larger volcanoes implies that low volatile eruptions are the norm. The actual magmatic rate on Venus may therefore be far higher, perhaps ~10 km^3 a^{-1}, about one third of Earth's [34].

The slow moving dense lower atmosphere of Venus creates a sedimentary environment similar to the deep oceans on Earth so that dunes and other aeolian features are rarely large enough to be visible in Magellan images. However, even at Magellan resolution landslides are common on steep slopes, such as rift systems. The Venera landers imaged partially eroded lithified clastic sediments [35], sometimes with what appear to be ripples. In places these are fractured into plates and cobbles with accumulations of fine grained sediment [36] in the lows between. Active aeolian transport may be common [37] and is demonstrated by the removal of fine sand sized sediment from the lander ring of Venera 13 over a period of about an hour [38].

Almost nothing is known about the internal properties of Venus: it is less dense than an Earth of the same mass, but its moment of inertia is unknown. Cosmochemical models [39] predict a core mass fractions between $23{\cdot}6$ and $32{\cdot}0$%—hence its mantle might actually be thicker than Earth's—and its k_2 Love number implies that it is at least partly liquid [40].

A Complex System:

Even the plains of Venus host a variety of geological features at all scales, a complexity that is in stark contrast to the uniform surface age inferred from the distribution of impact craters. Simple end-member models of catastrophic versus equilibrium resurfacing may be helpful at a global scale but are incapable of predicting the observed complexity. The highland plateaux have long been recognised as a distinctive unit, perhaps equivalent to continental crust, but the Venus crust and lithosphere appear to be globally heterogeneous. Subcrustal lid rejuvenation [41] goes part-way to explaining why subduction occurs in some places [42,43] but inversion in others [44], and elsewhere obduction [18], by noting that a weak lower crust detachment will form under temperature gradients of more than ~20 mW m^{-2}, leading to significant

changes in the rate and scale of geological activity with temperature and hence, location. While an improvement on simpler models, it does not predict the range and variety of small-scale features observed, or the observed distribution of impact craters.

That the lowlands also appear more similar to terrestrial continents than to ocean basins, in terms of their geological structures, need not be surprising. In both cases, the crust is buoyant, weak and heterogeneous [45], leading to smaller structural block sizes, wider deformation belts, and a greater sensitivity to geological history. Stresses are transmitted along fractures rather than through intact crust, leading to a structural block regime controlled by strike-slip movements [16,46–48] driving diffuse collisional or extensional crumple zones between adjacent blocks.

The scale of structural blocks, ~1000 km across, with 100−200 km wide deformation boundary zones, is intriguingly similar to the average crater spacing of ~800 km. Craters impacting onto the active boundary crumple zone will be unrecognisable in a relatively short time compared with craters impacting onto the interior of a structural block, where craters are infilled and erased only relatively slowly [23]. Hence both the distribution of impact craters and the number of modified craters is explicable if the impact rate is similar to the rate of burial in block interiors.

Geochemical Cycles:

The rate of crater floor infilling and the obscuration of lava flow boundaries constrains the block interior resurfacing rate to between 0·1 and 1·0 mm a^{-1}, based on a mean surface age of 750 Ma. This brackets the global marine sedimentation rate but is $>10^5$ higher than previous estimates and surprising given the paucity of sedimentary features in Magellan images. Rapid lithification can reconcile these contrasting observations: reprocessed Magellan data indicate that sedimentary rocks (i.e. lithified sediments) cover almost half the Venus surface, primarily in the plains. The main sediment sources appear to be upland erosion and the mass wasting of steep slopes, from which sand-sized granular material may be transported globally and deposited across the plains, to be lithified into thinly layered clastic rocks. It may be helpful to consider the supercritical fluid Venus lower atmosphere as an oceanic system in which sedimentary processes play an important part in geochemical cycles, particularly in acting as a sink for volcanogenic SO_2.

Conclusions:

Venus is the most Earth-like planet in the solar system, yet its geology has rarely been a constraining factor in understanding the planet, which has been dominated by the apparently random distribution of impact craters. That perception is changing and Venus is becoming recognised as being far more complex than our ideas have been to date. However, understanding that complexity, and why Venus evolved so differently to Earth, requires new observations at high resolution and over an extended period of time to constrain geological relationships and rates of activity. EnVision, a proposed ESA M-class mission, is designed to obtain these measurements and transform our understanding of our nearest neighbour.

References:

[1] McKinnon W.B. et al.: Bougher SW, Hunten DM, Phillips RJ, editors. *Venus II*. Tucson, Arizona: University of Arizona Press 1997. p. 969–1014. [2] Phillips R.J. et al. *JGR*. 1992 97:15923–48. [3] Strom R.G. et al. *JGR*. 1994 99:10899–926. [4] Fowler A.C. et al. *JGR*. 1996 101:4755–63. [5] Noack L. et al. *Icarus*. 2012 217:484–98. [6] Papuc A.M. et al. *Icarus*. 2012 217:499–509. [7] Turcotte D.L. *JGR*. 1993 98:17061–8. [8] Turcotte D.L. et al. *Icarus*. 1999 139:49–54. [9] Basilevsky A.T. et al. *JGR*. 1998 103:8531–44. [10] Ivanov M.A. et al. *PSS*. 2011 59:1559–600. [11] Armann M. et al. *JGR*. 2012 117. [12] Reese C.C. et al. *JGR*. 1998 103:13643–57. [13] Reese C.C. et al. *Icarus*. 1999 139:67–80. [14] Solomatov V.S. et al. *JGR*. 1996 101:4737–53. [15] Sleep N.H. *JGR*. 2000 105:17563–78. [16] Chetty T.R.K. et al. *PSS*. 2010 58:1286–97. [17] DeShon H.R. et al. *JGR*. 2000 105:6983–95. [18] Ghail R.C. *JGR*. AGU 2002 107:5060. [19] Price M.H. et al. *JGR*. 1996 101:4657–71. [20] Smrekar S.E. et al. *Science (80-.)*. 2010 328:605–8. [21] Campbell B.A. *JGR*. 1999 104:21951–5. [22] Hauck S.A. et al. *JGR*. 1998 103:13635–42. [23] Herrick R.R. et al. *JGR*. 2011 116. [24] Guest J.E. et al. *Icarus*. 1999 139:55–66. [25] Hansen V.L. et al. *GSA Spec. Pap*. 2007 419:255–73. [26] Johnson C.L. *JGR*. 2003 108. [27] Stofan E.R. et al. *Icarus*. 2005 173:312–21. [28] Stofan E.R. et al. *GRL*. 2001 28:4267–70. [29] Marcq E. et al. *Nat. Geosci*. Nature Publishing Group 2013 6:25–8. [30] Shalygin E. V et al. *LPSC*. 2014 45. [31] Bondarenko N. V et al. *GRL*. 2010 37. [32] Bullock M.A. et al. *Icarus*. 2001 150:19–37. [33] Ghail R.C. et al. *GSL Spec. Publ*. 2013 401. [34] Grimm R.E. et al. *Venus II*. 1997. p. 1205. [35] Florensky C.P. et al. *Science (80-.)*. 1983 221:57–9. [36] Surkov Y.A. et al. *Adv. Sp. Res*. 1985 5:17–29. [37] Lorenz R.D. *Icarus*. 2015 264:311–5. [38] Selivanov A.S. et al. *Pis'ma v Astron. Zhurnal*. 1982 8:433–6. [39] BVSP, Pergamon Press 1981. [40] Konopliv A.S. et al. *GRL*. AGU 1996 23:1857–60. [41] Ghail R.C. *PSS*. 2015 113:2–9. [42] McKenzie D.P. et al. *JGR*. 1992 97:13533–44. [43] Sandwell D.T. et al. *JGR*. 1992 97:16069–83. [44] Bilotti F. et al. *Icarus*. 1999 139:137–57. [45] Burov E.B. *Mar. Pet. Geol*. 2011 28:1402–43. [46] Koenig E. et al. *Geology*. 1998 26:551–4. [47] Tuckwell G.W. et al. *EPSL* 2003 211:45–55. [48] Harris L.B. et al. *GSL Spec. Publ*. 2014 401.

ENVISION M5 VENUS ORBITER PROPOSAL: OPPORTUNITIES AND CHALLENGES.

R. C. Ghail, *Department of Civil and Environmental Engineering, Imperial College London, London, SW15 3HA, UK, (r.ghail@imperial.ac.uk),* **C. F. Wilson**, *Department of Atmospheric, Oceanic and Planetary Physics, Oxford University, Oxford, OX1 3PU, UK, (Colin.Wilson@physics.ox.ac.uk),* **T. Widemann**, *Observatoire de Paris – LESIA UMR CNRS 8109, 92190 Meudon, France, and Université Versailles St-Quentin - DYPAC EA 2449, France, (thomas.widemann@obspm.fr)*

Introduction:

In geological terms, Venus is the most Earth-like planet in the Solar System. Mars may have had a past environment favourable for life but at one tenth the mass, it was unable to sustain its early benign environment. Being so similar to Earth, Venus may also have had a habitable past, possibly even sustaining a living biosphere. Why has it not turned out more like Earth? The key question for Venus surface science is how active is the planet? The next stage of exploration must therefore focus on its geology and geochemical cycles, seeking evidence for present and past activity. With its unparalleled radar, IR and UV instruments based on a long European heritage in change detection and monitoring, EnVision will revolutionise our understanding of Venus and enable us to understand why our closest neighbour is so different.

Background:

ESA's M5 call, expected in April 2016, is a more conventional Medium-class mission call than M4. Cost-at-Completion is expected to be more restrictive than either Euclid (M2) or Plato (M3) but higher than M4. A nominal 2029/2030 launch date on Ariane 6.2 removes the mass/volume constraints of Soyuz, resulting in truly cost-limited design. The Envision proposal being developed for M5 is therefore different in several key aspects compared to that proposed for M4, while addressing the same science themes. Here we explore the implications of these constraints and opportunities for EnVision at M5.

Science Observations:

What lessons can be learned from Venus about the life story of terrestrial planets in general, in this era of discovery of Earth-like exoplanets? Were the radically different evolutionary paths of Earth and Venus driven solely by distance from the Sun, or do internal dynamics, geological activity, volcanic outgassing and weathering also play an important part? ESA's Venus Express answered many questions about our nearest planetary neighbour and discovered tantalising hints of current volcanic activity including a tenfold change in mesospheric SO_2, anomalously dark lava surrounding volcanoes, and surface temperature changes that all point towards activity which had not been expected from NASA's Magellan mission of the early 1990s. That mission showed that Venus has abundant volcanic and tectonic features but did not have the resolution or technology necessary to detect geological activity. The core goal of EnVision is to detect activity and measure rates of change on Venus, including geological and geochemical cycles involving the interior, surface and atmosphere. Many natural phenomena follow the Pareto relationship [1]; recently [2] showed that the rate of volcanic activity can be very well constrained by observations at one in ten volcanoes on Venus. Hence rather than aiming for global coverage, the mission will repeatedly observe specific targets with the widest possible range of measurements to fully characterise these areas, in effect trading quantity for quality to maximize the science return. EnVision will observe >20% of the surface with all instruments, exceeding the Pareto threshold, and will obtain gravity and emissivity data globally. Core science measurements are:

Surface change: $< \pm 1$ cm a^{-1} at <35 m spatial
Geomorphology: multipolar images at <35 m spatial
topography at <35 m vertical, <350 m spatial
High-resolution mapping: <10 m spatial
Spotlight (50 km² areas): ~1 m spatial
Subsurface: 50 m vertical, <1 km spatial
0.8-1.2 μm thermal emission: s/n >100, 50 km spatial
SO_2: ±1% at <300 km spatial and 30–40 km altitude
H_2O: $< \pm 10\%$ at <300 km spatial and <15 altitude
D/H: $< \pm 10\%$ at <300 km spatial and <15 altitude
Gravity: Spherical harmonic degree and order >90
Spin rate: $< \pm 10^{-8}$ (1 minute in one Venus day)
Spin axis: $< \pm 0{\cdot}001°$ in RA and Dec
Spin axis: $< \pm 0{\cdot}001°$ in RA and Dec

Instruments:

The instrument suite for M5 is under review but will likely comprise the same three instruments as at M4: VenSAR, VEM and SRS.

VenSAR. The largest payload instrument is a phased array S-band radar, developed from the UK's low-cost NovaSAR-S instrument, with ERS, ENVISAT and Sentinel-1 heritage, optimized for Venus, and essentially unchanged from the instrument proposed at M4. Use of spacecraft pointing for side-looking, instead of a fixed slant, simplifies the observation strategy (Fig 1) to three pairs of ~9 minutes/orbit (~36° latitude, ~3800 km) pass-to-pass In-SAR swaths (or opposite-look swaths after Cycle 1), two ~9 minutes/orbit multipolar (HH-HV-VV) swath at

lower incidence angle for stereo mapping, two ~3 minutes/orbit (~12° latitude, ~1300 km) high resolution swath and either one or two S-band emissivity swaths per day.

InSAR swaths are contiguous to meet the repeat-pass requirement while gaps in the StereoPolSAR, HiRes and emissivity are filled in during later passes, providing a full suite of data for specific targets totaling ~25% of the surface. ~1 m resolution sliding spotlight images, each ~50 km^2 in area, will also be obtained at the Venera landing sites and other loca-tions identified during the mission. In addition, InSAR will be acquired along a narrow equatorial strip and across the North Pole to measure variability in the spin rate and axis.

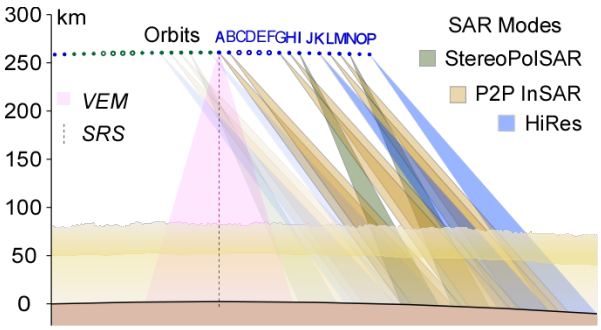

Fig. 1 Example 24-hour observation strategy. Orbits AB, GH, and LM: InSARs; orbits I, N: StereoPolSAR; orbits K, P: HiRes; and orbits J, O: S-band emissivity. VEM and SRS are obtained in each of these orbits. Orbits CDEF have the HGA pointed to Earth for the 6-hour communications link, during which no science operations are planned.

VEM. The Venus Emissivity Mapper suite comprises two UV and IR spectrometer channels in addition to the VEM-M IR mapping. VEM-M global IR-mapper [3] incorporates lessons learned from VEx/VIRTIS: band-center and width-scatter are ~5 × more stable, with decreased scattered light and improved sensitivity; a filter array provides wavelength stability and maximizes signal to the focal plane array (FPA). VEM-H is high-resolution, nadir-pointing, infrared spectrometer, the ideal instrument to enable characterization of volcanic plumes released from the surface of Venus by observing SO_2, H2O and HDO through the 1 µm, 1.7 µm, and 2-2.3 µm atmospheric windows. Specifically, VEM-H is a redesign of the LNO (Limb, Nadir and Occultation) channel of NOMAD, retaining much heritage from the original with minor modifications to meet the science objectives of the M5 EnVision mission. The third channel, VEM-UV is an upper-atmosphere UV spectrometer dedicated to global SO_2 & sulfur cycles.

SRS. The Subsurface Radar Sounder will image faults, stratigraphy and weathering in the upper ~100 m of the areas mapped by VenSAR, to identify structural relationships and geological history.

Operations:

EnVision M5 has a simplified mechanical design to one with a fixed SAR and HGA, with an AOCS capable of several changes in space-craft pointing during each 90-minute orbit. These principally allow for radiator, power generation, communications, and the 15-minute science operation modes. Daily Earth-pointing communications occur in 6 hour blocks, occupying 4 of the 15½ orbits in every 24 hours, during which science operations are suspended.

The 3-m body-fixed HGA achieves a link rate sufficient for continuous InSAR and for StereoPolSAR and HiRes during closest approach (Fig 2) across ~25% of the surface, for a total of 336 Tbits in the nominal mission.

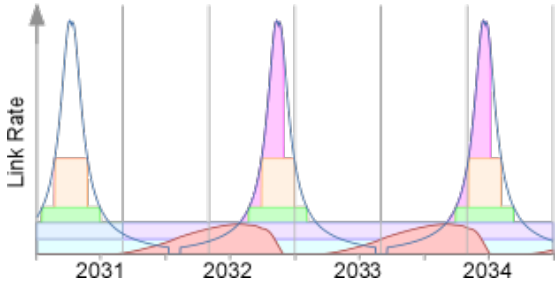

Fig. 2 Graph illustrating possible science observations and data return. Blue shades are InSAR; green is multipolar stereo SAR; orange is high resolution mapping. Data storage is in red and return in pink. Blue line is the achievable data rate (inversely proportional to Earth-Venus distance), vertical grey lines are Venus rotational cycles.

Summary:

EnVision achieves its science goals within the M5 constraints by focusing on ~25% of the surface with a comprehensive suite of observations, sufficient to identify types and rates of geological activity and characterise its geochemical cycles. The opportunity for the science community is to help de-fine these areas and maximize the value of the science data return.

References:

[1] Newman, M. *Contemp. Phys.* 46, 323–351 (2005). [2] Lorenz, R. D. *Planet. Space Sci.* 117, 356–361 (2015). [3] Helbert, J. et al. *LPSC* 47, 1913 (2016).

IMPACT OF A NON-OROGRAPHIC GRAVITY WAVES PARAMETERIZATION IN THE VENUS UPPER ATMOSPHERE BY THE LMD-VGCM.

G. Gilli, S. Lebonnois, F. Lott, *Laboratoire de Meteorologie Dynamique, CNRS, Paris, France (ggilmd@lmd.jussieu.fr)*, **F. Lefevre,** *Laboratoire Atmospheres, Milieux, Observations Spatiales, IPSL, Paris, France*.

Introduction

An improved version of the Venus GCM developed at *Laboratoire de Meteorologie Dynamique* (LMD) is currently operational from the surface up to 150 km [1]. The LMD-VGCM has been used to study the role of thermal tides and other waves in the superrotation of Venus atmosphere and to interpret recent temperature and winds measurements by Venus Express (VEx) up to 100 km [2, 3],[see also *Lebonnois et al.* this issue]. The latest improvements in [1] take into account physical processes relevant to the upper mesosphere/lower thermosphere of Venus, following the work done for the Martian GCM [4]. In addition, this version is fully coupled with the photochemical model developed at *Laboratoire Atmospheres, Milieux, Observations Spatiales* (LATMOS) [5] for the first time up to the thermosphere. This ground-to-thermosphere model provides self-consistently 3D fields of temperature, wind and composition and contribute to a better understanding of atmospheric layers above 100 km.

Results in [1] focused on the thermal structure and show a qualitative good agreement with recent measurements by VEx. However, zonal winds are too strong and produce intense equatorial jets and vertical transport from the low to the upper mesosphere, particularly before the morning terminator, causing data-model discrepancies. In order to reduce those instabilities and improve the comparison, a preliminary gravity waves (GW) parametrization was implemented in the LMD-VGCM [1], following the formalism developed for the Earth GCM described in [6]. The source of GWs is still unknown and their main features poorly constrained, although the presence of GWs in the atmosphere of Venus has been confirmed by several measurements.

The goal of this work is twofold: first to improve the GW parameterization in the VGCM by analyzing the impact of the parameters' uncertainties in the model results, secondly to help interpreting the large variability observed in the upper atmosphere of Venus.

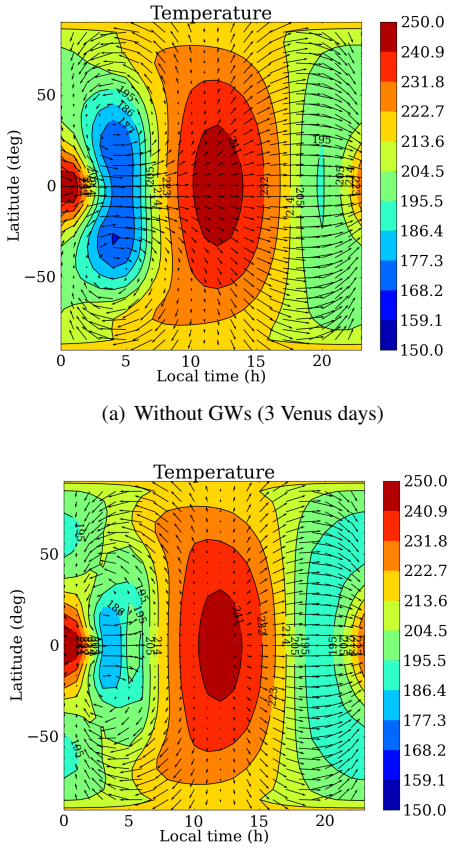

(a) Without GWs (3 Venus days)

(b) With GWs (10 Venus days)

Figure 1: Latitude-local time cross section of temperature average fields, after 3 Vd (a) and 10 Vd (b), corresponding to runs without and with the GW parameterization, respectively. Pressure level is 1 Pa (105 km approximately).Wind vectors (in m/s) are over-plotted.

Non-orographic GW parameterization in the LMD-VGCM

Gravity waves are believed to play a major role in Venus upper atmosphere dynamics and commonly invoked in the literature to explain density, temperature and cloud structure variations. Supposed to be generated above the thick convective layer, in the middle cloud region (50-60 km), GWs propagate upwards and break in the thermosphere, providing a significant source of momentum and energy. Several general circulation models investigated the effect of gravity waves on the variation of winds velocity in the Venusian lower thermosphere. [7] assumed Rayleigh friction and suggested that wave drag would decelerate the subsolar-to-antisolar (SS-AS) winds in the thermosphere. In [8], the authors suggested that gravity waves did not propagate above an altitude of about 115 km at the terminator, because of total internal reflection. In this work we follow the formalism described in [6] based on a stochastic approach, where a large ensemble of monochromatic GW is generated just above the convective layer by launching a few waves at each time step, and by adding the effect of these waves to that of the waves launched before. The source of the GW is here chosen uniform, without latitudinal variation, and fixed at roughly 55 km, near the top of the modelled convective layer. The frequency, horizontal wave numbers and the relative phase velocity amplitude of each wave are chosen randomly, with an arbitrarily fixed probability distribution.

Impact on temperature and general circulation

Two examples of the effect of the implementation of the GW parametrization in the VGCM are shown in Figures 1 and 2. Maps of simulated temperatures after 3 Venus days (Vd) and 10 Vd in Figure 1 correspond to simulations without and with GWs, respectively. Strong equatorial jets and upward flux produce colder temperatures between 2-5 LT but they are noticeably reduced by the GWs propagation in the upper atmosphere. In other words, GWs drag on the zonal winds in the equatorial region and delay the formation of a complex dynamical structure, that is probably linked to the angular momentum transport by the thermal tides, or planetary-scale waves propagation from the lower to the upper mesosphere.

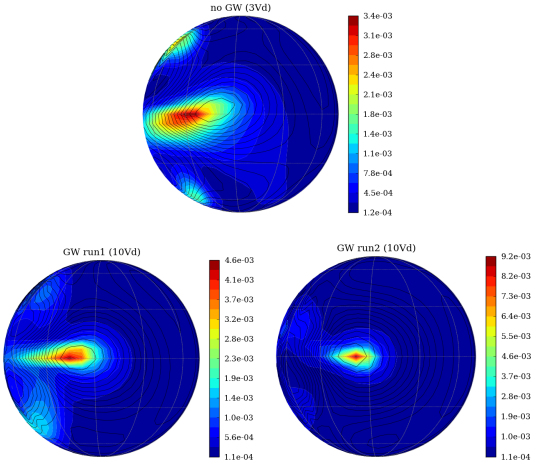

Figure 2: Night-time atomic Oxygen vmr maps at 1 Pa (approx. 105 km) by the VGCM. Top panel: without GWs (after 3 Vd). Bottom panels: with GWs (after 10 Vd) using different wave phase velocity values (see text). Temperature fields contours are shown in black.The centre of each map is approximately the anti-solar point.

Figure 2 shows the variation of atomic oxygen distribution (in vmr) at nighttime predicted by the model, tuning the GWs parameters. The pressure level of the maps is 1 Pa (about 105 km), near the observed intensity peak of O. The simulation on the top obtained without GWs (after 3 Vd), is compared with two runs (after 10 Vd) performed including the GWs parameterization scheme. In *Run1* (bottom left) the maximum value of the relative phase velocity is fixed to 60 m/s, in *Run2* (bottom right) it is 110 m/s.
As shown in Figure 2, after the GWs implementation, the O density bulge is closer to the anti-solar point, as expected by a dominant SS-AS circulation. At the same time, our model shows O abundance spots at middle-high latitudes, as also observed by VEx [11], but not yet predicted by current 3D thermospheric models [10].

Does the LMD-VGCM reproduce the observed variability?

The large variability of the zonal winds, in the region between 90 and 120 km is usually attributed to the changing nature of the GW breaking. A proper fine-tuning of unconstrained GW features is essential to reproduce the observed values. This work indicates that our GCM is potentially able to reproduce latitudinal and time variations produced by small-scale dynamical process, as observed in the upper atmosphere of Venus by VEx [9, 11], but not yet explained by current GCMs.

Future work is ongoing at LMD to develop a mesoscale model for the VGCM (see *Lefevre et al.* this issue), based on the same physics as the GCM. This will also allow a better constraint of the GW parameterization and to take into account the variation of the distribution, amplitude and intensity of the gravity waves.

References

[1] Gilli G. et al. (2016): Thermal structure of Venus upper atmosphere by a self-consistent ground-to-thermosphere GCM, *Icarus*, submitted.

[2] Lebonnois S. et al. (2010) *JGR*, 115, E06006

[3] Lebonnois S. et al. (2016): Wave analysis in the atmosphere of Venus below 100-km altitude, simulated by the LMD Venus GCM, *Icarus*, submitted

[4] Gonzalez-Galindo F. et al. (2009) *JGR* (Planets) 114, E04001

[5] Stolzenbach A. et al. (2014): Three-dimensional modelling of Venus photochemistry, in EGU General Assembly 2014.

[6] Lott F. et al. (2012) *GRL*, 39, L06807

[7] Bougher S. et al. (1988) *Icarus*, 73, 545-573

[8] Zalucha A. M. et al. (2013) *JGR* (Planets), 118, 147-160

[9] Soret L. et al. (2012) *Icarus*, 217, 849-855

[10] Brecht A. et al. (2012), *Icarus*, 217, 759-766

[11] Gerard J.C. et al. (2014), *Icarus*, 236, 92-103

[12] Lefevre M. et al. (this issue): Three-Dimensional mesoscale modeling of the Venusian cloud layer and associated gravity waves.

LARGE IMPACTS ON VENUS: EFFECTS ON LONG TERM EVOLUTION.

C. Gillmann, *Royal Observatory of Belgium, Brussels, Belgium* (cedric.gillmann@observatoire.be), **G. Golabek**, *University of Bayreuth, Germany*, **P. Tackley**, *ETH Zürich, Switzerland*.

Introduction:

Recently, perception of the importance of interactions between interior and exterior has led to better understanding of the evolution of planets [1, 2, 3]. Our main interest is to understand how different parts of a terrestrial planet interact and how different mechanisms contribute to changes in long term evolution. Here, in particular, we investigate how the coupled evolution of Venus' atmosphere and mantle is modified by large impacts. Due to its characteristics and dense atmosphere, Venus is a perfect place to test models. Additionally, its solid part could still be active [4, 5]. We focus on volatile fluxes in and out of the atmosphere: atmospheric escape and degassing. We link those processes into a coupled model of mantle convection and atmospheric evolution. Feedback of the atmosphere on the mantle is included via surface temperature. As large impacts are capable of contributing to atmospheric escape, volatile replenishment and energy transfer, we estimate their effects on the evolution of Venus.

Model:

The model can be separated into four different parts.

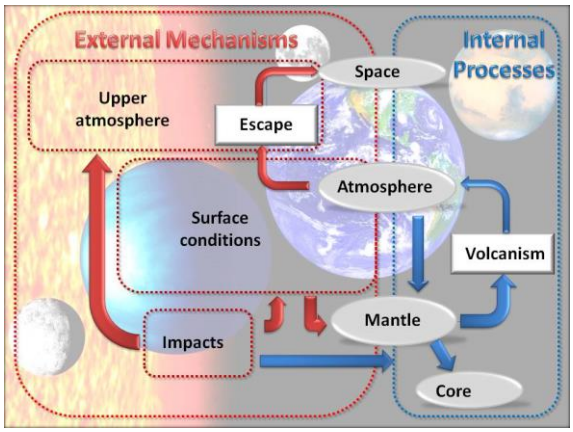

Figure 1: basic layout of the model.

(i) Internal processes are dependent on mantle dynamics. We use a variation of the StagYY code designed for Venus [6]. Physical are depth-dependent. The phase transitions in the olivine system and in the pyroxene-garnet system are included. The assumed rheology is Newtonian diffusion creep plus plastic yielding. Degassing is calculated when melting occurs and we use a wide range of possible lava compositions (10-300 ppm for water, 5-5000ppm for CO2).

(ii) Atmospheric escape modeling involves two different aspects: hydrodynamic escape (0-500 Myr) and non-thermal escape mechanisms (dominant post 4 Ga). Hydrodynamic escape is the massive outflow of light volatiles into space occurring when the solar energy input (Extreme UV and solar wind) is strong. Post 4 Ga escape from non-thermal processes is comparatively low. It is also powered mainly by EUV. Mechanisms include sputtering, ion pick-up, plasma clouds and dissociative recombination. Constraints include present-day measurements by the ASPERA instrument and recent numerical simulations.

(iii) Surface conditions are calculated from the greenhouse effect of main gases from the atmosphere: water and CO2. We use a one-dimensional radiative-convective grey atmosphere model modified from [1]. Surface temperature is thus calculated and used in the mantle convection model as a boundary condition.

(iv) Impacts can bring volatiles and erode the atmosphere. Mantle dynamics are modified by the large amount of energy brought to the mantle. A thermal anomaly created by the impact is used and can lead to melting. Volatile evolution due to impacts is heavily debated so we test a broad range of impactor parameters (size, velocity, timing) and test different impact erosion factors.

Results:

General evolution: We are able to produce models leading to present-day-like conditions through episodic volcanic activity consistent with Venus observations (eruption rates, present-day state, possible resurfacing events).

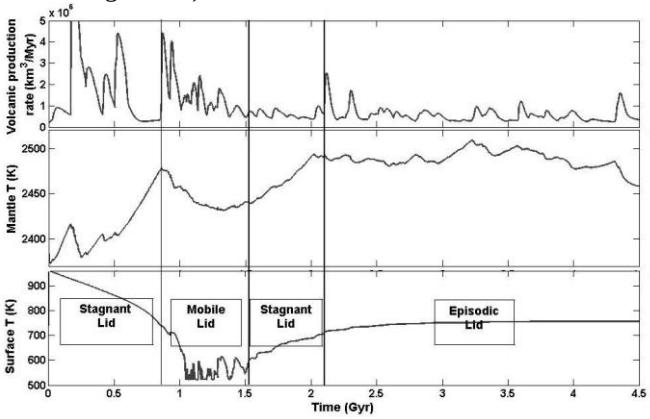

Figure 2: Evolution of the coupled model and evidence of feedbacks between mantle and atmosphere.

Changes in water vapor partial pressure lead to variations in surface temperatures of up to 200 K during, which have been identified to have an effect on volcanic activity. We note a clear correlation between low temperature and mobile lid regime.

Impacts: Small (0-50 km) meteorites have a negligible effect on the global scale: they only affect the impact point and do not have lasting consequences on surface conditions or the mantle of Venus. Medium ones (50-150 km) have strong short term influence through volatile degassing due to the melting of the solid parts of the bodies. Only larger impactors (300+ km) have lasting effects on the planet, though. In all cases, however, atmospheric erosion appears to be mitigated by volatiles brought by the collision.

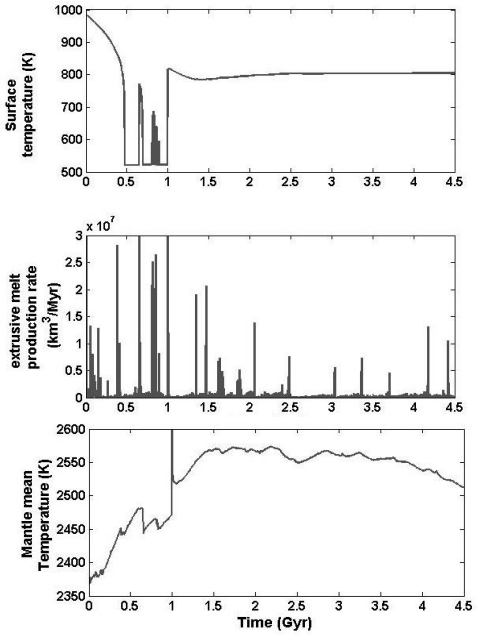

Figure 3: Long term evolution of Venus with a 400 km impact 3.5 Ga ago.

The main consequences of impacts are directly linked to the melting they generate, and their action on volatiles. Indeed, large impacts inject enough energy into the system to allow massive immediate degassing. This can lead to an increase in surface temperature in the order of 200 K before factoring the volatiles brought by the impactor (between 0.1 and 10 times the volcanic degassing from the planet, depending on the parameters used).

Additionally, the disrupting effect of the impact has numerous other consequences on the mantle convection regime. It removes pre-existing crust and can lead to the emplacement of new crust in specific locations (near the impact location). It also induces a lateral motion of the upper mantle away from the impact due to the physics of the thermal anomaly that is positively buoyant in the mantle, generating high strain in that region. The global dynamics can be affected with the creation of a short term mantle plume under the impact point and a large downwelling at the antipodal position.

We also identified that a key-factor for the long term evolution was the timing of the impact.

Early impacts can deplete much of the initial volatile content of the mantle due to the massive early melting they cause. This allows primordial volatiles to be lost to space during the intense early escape phase, removing them from the system. It also leads to low later degassing if the mantle is not replenished (subduction) and to a dryer planet with a somewhat thinner atmosphere.

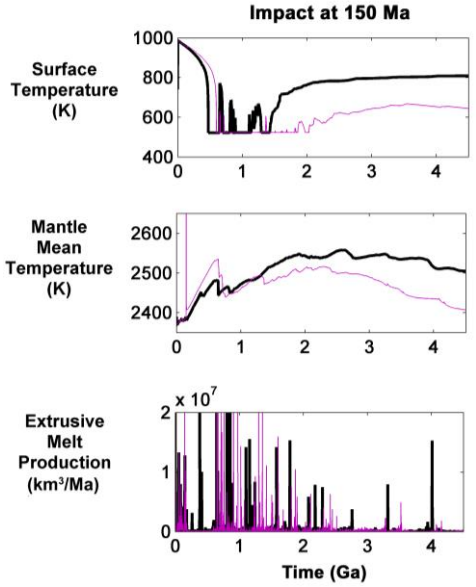

Figure 4: Degassing and volatile depletion consequences for an early impact.

On the other hand, later impacts, when they occur during an era when the atmospheric escape is less intense, can counteract the effect of atmospheric loss by releasing volatile into the atmosphere at a larger rate than volcanism in a single event. The resulting high surface temperatures affect directly mantle convection pattern and can prevent mobile lid regime from initiating, with profound consequences for volatile exchanges and mantle evolution.

Bibliography:

[1] Phillips, R.J., et al. Climate and interior coupled evolution on Venus. Geophys. Res. Lett. 28, 2001. **[2]** Gillmann, C. and Tackley, P., Atmosphere/mantle coupling and feedbacks on Venus, JGR Planets, 2014. **[3]** Noack, L., et al., Coupling the Atmosphere with Interior Dynamics: Implications for the Resurfacing of Venus, Icarus 2012. **[4]** Bullock, M.A., Grinspoon, D.H., The recent evolution of climate on Venus. Icarus 150, 2001. **[5]** Smrekar, S. E., et al., Recent Hotspot Volcanism on Venus from VIRTIS Emissivity Data. Science 328, 2010. **[6]** Armann, M., and P. J. Tackley, Simulating the thermochemical magmatic and tectonic evolution of Venus's mantle and lithosphere: Two-dimensional models, J. Geophys. Res., 2012.

THE SEARCH FOR UNADULTERATED VENUS TESSERA TERRAIN

M. S. Gilmore , *Dept. of Earth and Environmental Sciences, Wesleyan University, Middletown CT 06459, USA (mgilmore@wesleyan.edu).*

Introduction: Tessera terrain consistently appears locally and perhaps even globally [1] as the stratigraphically oldest material on Venus which has an average surface crater age of ~300 [2] to ~800 Ma [3]. The composition, detailed morphology and geologic history of tessera terrain are currently unknown [e.g., 2, 5]; improved measurements of these parameters would critically constrain Venus geochemistry, geodynamics and the history of water on the planet.

Because of our ignorance, the Venus community tends to discuss the 35 million km^2 [1] of tessera terrain as if it is all the same material with the same age. However, multiple morphological and compositional terrains and contacts are suggested by the analyses of Magellan data [1, 4, 20] and VIRTIS data [5]. Missions proposed as part of the Discovery [e.g., Smrekar et al. and Glaze et al., submitted to LPSC 2016] and New Frontiers Programs offer the opportunity to make new measurements about tessera terrain at higher resolution, forcing us to consider how to find the rocks that are most likely to represent original tessera materials. The identification of such pristine tessera targets is key to the interpretation of any improved 1 micron emissivity, radar or altimetry data collected of the surface as well as for the interpretation of optical imagery collected from probes or balloons. Better knowledge of tessera provenance also enables geochemical and mineralogical measurements of tessera composition from surface landers.

Which material should we avoid to measure pristine tesserae terrain?

High Reflectivity Mountaintops. Materials at elevations >~6054 km have high radar reflectivity values, interpreted to result from an increase in the dielectric constant of the rocks [e.g., 6]. Most models agree that the materials are formed via a surface-atmosphere chemical reaction at the lower temperatures at these elevations [e.g., 7, 8]. The chemistry and extent of these reactions are poorly constrained. I would argue that these materials should be avoided if we want to directly measure primary tessera compositions, although tessera composition may be inferable if the near-surface atmosphere is well constrained.

Crater Parabolas. Campbell et al. [9] recognized parabolic deposits associated with some craters and interpreted to be crater ejecta entrained and redeposited westward by the upper level winds. For plains craters, this ejecta is nominally basaltic and may distribute cm-thick deposits of materials 100s - 1000 km away from the crater [9]. Observations of some parabolas in multipolarized Arecibo data show that the parabola deposites may extend further than what is visible in Magellan data and may persist in topographic hollows [10]. There are ~60 craters with parabolas recognized in Magellan [9, 11]. Observations of multiple parabola degradation states and the youthful appearance of parabola craters support the idea that the parabolas are young and ephemeral features, meaning that all craters above a certain diameter likely generated parabola deposits [e.g., 9, 12]. Certainly tesserae have received such aeolian deposits over the course of their lifetime. However, it is not clear that these deposits prohibit access to tessera rocks. Large (~10 km scale) mass movements are observed to occur on steep slopes along Venus chasmata [13] and we would expect the mass movements occur on steep slopes within tesserae as well. As on Earth, fresh extensional fault scarps are predicted to lie at 60-70° slopes, however, processes of mechanical weathering will serve to reduce these slopes to the angle of repose (~35°) on both planets. Measurements of 170 faults across Venus using radargrammetry yield an average slope of 36±2° [14] consistent with mass wasting along these faults. As weathering on Venus is largely limited to mass wasting, tessera surfaces similar to scree slopes in arid regions on Earth are expected, where submeter scale rocks form talus deposits of tessera rocks at the angle of repose. If the talus formation rate > the aeolian deposition rate, tesserae rocks should be readily available and widely distributed at the surface below these faults. In this case, one might target tessera regions with pervasive fractures and graben (e.g., Fortuna tessera) – a typical region in central Ovda Regio shows graben slopes comprise only 1% of the area. SAR radargrammetry data (~2 km spatial resolution) [15], show average kilometer scale slopes in a typical region in central Ovda Regio tessera terrain are ~5-10° and areas with slopes >10° are limited (0-5% of the region). High resolution image data are necessary to help constrain the nature of tessera weathering and deformation style.

Obducted and assembled materials. There are several examples of tessera boundaries where there is clear evidence that plains materials are being deformed, uplifted and incorporated onto older regions of tesserae. Prominent examples are W. Alpha Re-

gio [4], SW Tellus Regio [16], and N. Ovda Regio [17]. Tellus and Ovda Regio also show evidence of assembly of regions of tessera with distinct structural fabrics [16, 18, 19]. These pieces can be placed in stratigraphic context, for example central Tellus Regio is deformed by and thus predates SW Tellus. There is also recognition of contacts within tessera terrain between materials with different structural fabrics and between older fabrics and plains materials that are subsequently deformed [e.g., 20, 21]. With higher resolution imagery and compositional data, such regions may provide a stratigraphic framework for geomorphic and material units.

Plains materials and flooding. North-central Tellus lies at very low elevations and is thoroughly flooded by plains. Several coronae intersect Ovda Regio. The structural fabric of Phoebe tessera is unlike all other major tessera occurrences in that is dominated by extensional structures [1] and may not be representative of the general characteristics of the terrain. These areas should be avoided.

Which rocks should we target to measure pristine tesserae terrain?

Tessera Craters. Gilmore et al. [22] conservatively recognized 80 craters on tessera terrain. Tessera craters of course will excavate and redistribute tessera materials from depth over large regions. We may identify the freshest of these craters via bright floors and preserved impact melt. Such candidates include crater Khatun in E. Tellus.

Summary. The qualitative analysis presented here suggests that the most unadulterated tessera surfaces can be found in W-Central Alpha, Tellus, central W. Ovda, eastern Fortuna, Meshkenet and N. of Thetis (Figure 1).

References: [1] Ivanov and Head (1996) JGR 101, 14861. [2] Strom et al. (1994) JGR 99, 10899. [3] McKinnon et al. (1997) in Venus II, 969. [4] Gilmore and Head (2000) Meteor. Plan. Sci. 35, 667. [5] Gilmore et al., (2015) Icarus 254, 350. [6] Pettengill et al. (1992) JGR 97, 13091. [7] Brackett et al. (1995) JGR 100, 1553. [8] Pettengill et al. (1996) Science 272, 1628. [9] Campbell and Campbell (1992) JGR 97, 16293. [10] Campbell et al. (2015) 250, 123. [11] [14] Herrick et al. Venus Magellan Impact Crater Database http://astrogeology.usgs.gov/geology/venus-magellancrater- database. [12] Arvidson et al., (1992) JGR 97, 13303. [13] Malin et al. (1992) JGR 97, 16337. [14] Connors and Suppe (2001) JGR 106, 3237. [15] Herrick et al. (2010) LPSC 41, #1622. [16] Straley and Gilmore (2007) LPSC 38, 1657. [17] Parker and Saunders (1994) LPSC 25, #1528. [18] Chadwick and Shaber (1994) LPSC 25, #1115. [19] Ghent and Hansen (1999) Icarus 139, 116. [20] Ivanov (2001) Solar Sys. Res. 35, 3. [21] Romeo and Capote (2011) Plan. Space Sci. 59, 1428. [22] Gilmore et al. (1997) JGR 102, 13357. [23] Basilevsky et al. (2004) JGR 109, E12003.

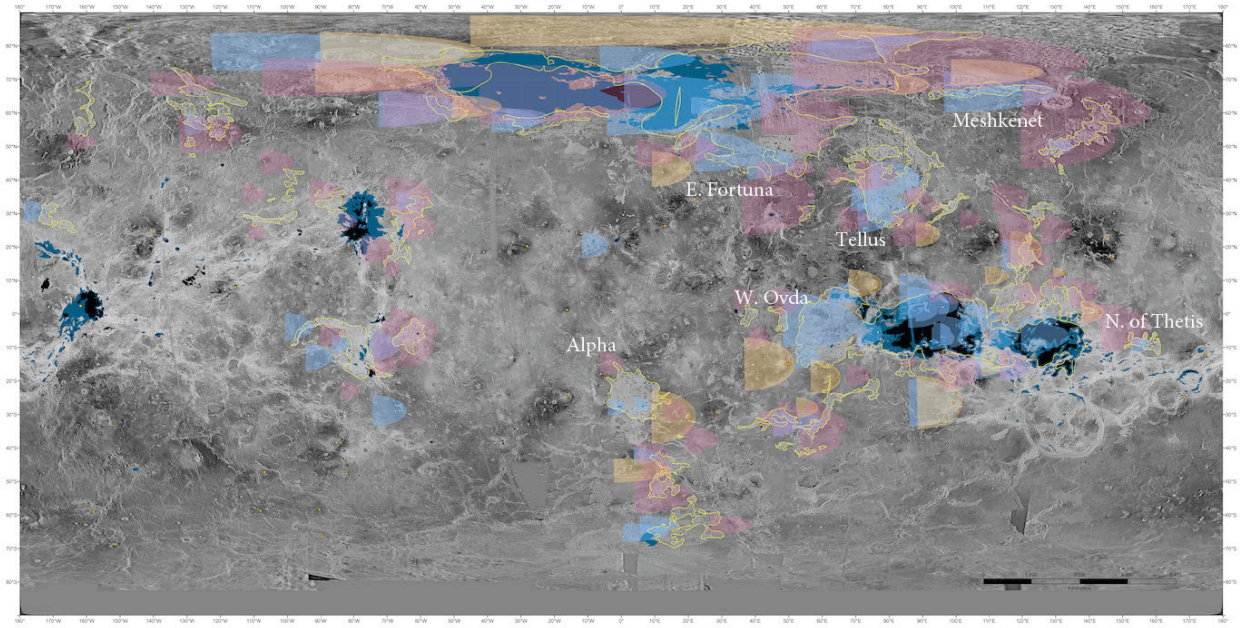

Fig. 1. Map of Venus, tesserae outlined in yellow. Black: Magellan reflectivity >0.7; Dark Blue: Elevations >6054 km; Orange: visible crater parabolas [9, 14] from craters on plains that intersect tesserae; Pink: Modeled crater parabolas that intersect tesserae [23] assuming all craters >11km once had a parabola (conservative model); Bright Blue: Tessera craters [22] may excavate fresh tessera materials. Relatively pristine tesserae materials may be found in regions that avoid parabolas and high reflectivity/elevation and coincide with tessera craters and include regions in Alpha, Tellus, W. Ovda, W. Fortuna, Meshkenet and N. of Thetis

DAVINCI: DEEP ATMOSPHERE VENUS INVESTIGATION OF NOBLE GASES, CHEMISTRY, AND IMAGING.

L. S. Glaze, **J. B. Garvin, N. M. Johnson,** *NASA Goddard Space Flight Center (GSFC), Greenbelt, MD, USA (Lori.S.Glaze@nasa.gov)*, **D. Atkinson,** *Jet Propulsion Laboratory (JPL), Pasadena, CA, USA,* **S. Atreya,** *U. Michigan,* **J. Blacksberg,** *JPL,* **W. Brinckerhoff,** *NASA GSFC,* **B. Campbell,** *Smithsonian Institution,* **D. Crisp,** *JPL,* **F. Forget,** *Laboratoire de Météorologie Dynamique, Paris, France,* **M. Gilmore,** *Wesleyan U.,* **D. Grinspoon,** *Planetary Science Institute,* **N. Izenberg,** *Johns Hopkins University Applied Physics Laboratory (JHU APL),* **P. R. Mahaffy,** *NASA GSFC,* **W. Kiefer,** *Lunar and Planetary Institute,* **R. Lorenz,** *JHU APL,* **A. A. Pavlov,** *NASA GSFC,* **M. Ravine,** *Malin Space Science Systems,* **M. G. Trainer,** *NASA GSFC,* **C. Webster,** *JPL,* **K. Zahnle,** *NASA Ames Research Center,* **M. Zolotov,** *Arizona State U.*

Introduction: Venus formed in the same part of our solar system, apparently from similar materials, as Earth. Although both planets are about the same size, their differences are profound. Venus and Earth experienced vastly different evolutionary pathways resulting in unexplained differences in atmospheric composition and dynamics, as well as in geophysical processes of the planetary surfaces and interiors. Understanding when and why the evolutionary pathways of Venus and Earth diverged is key to understanding how terrestrial planets form and how their atmospheres and surfaces evolve. The proposed Deep Atmosphere Venus Investigation of Noble gases, Chemistry, and Imaging (DAVINCI) mission will provide these missing puzzle pieces needed to understand terrestrial planet formation and evolution in the solar system and beyond.

Mission Concept: DAVINCI is one of five Discovery-class missions selected by NASA for Phase A studies. Launching in November 2021 and arriving at Venus in June of 2023, DAVINCI would be the first U.S. entry probe to target Venus' atmosphere in 45 years. DAVINCI is designed to study the chemical and isotopic composition of Venus' atmosphere at a level of detail that has not been possible on earlier missions and to image the surface at optical wavelengths and process-relevant scales. The three major DAVINCI science objectives are:

- Atmospheric origin and evolution: Understand the origin of the Venus atmosphere, how it has evolved, and how and why it is different from the atmospheres of Earth and Mars.
- Atmospheric composition and surface interaction: Understand the history of water on Venus and the chemical processes at work in the lower atmosphere.
- Surface properties: Provide insights into tectonic, volcanic, and weathering history of a typical tessera terrain.

The DAVINCI probe will make *in situ* measurements during a one-hour descent through the Venus atmosphere. The mission is tightly focused on answering fundamental questions that have been ranked as high priority by the last two National Research Council (NRC) Planetary Decadal Surveys [1-3] as well as by the Venus Exploration Analysis Group (VEXAG) since the time of its inception in 2005 [4]. For example, DAVINCI will make measurements of the heaviest noble gases, including dramatic improvements in quantifying krypton abundance and the first ever measurements of xenon, as well as precise isotopic measurements [5]. These definitive measurements, which will be made well below the homopause to avoid any uncertainties, are sufficient to answer questions as framed by the NRC Planetary Decadal Survey and VEXAG, without the need to repeat them in New Frontiers or other future missions. The relative abundances of these inert gases, together with high precision measurements of the isotopes of argon, nitrogen, sulfur and carbon provide critical insight into the origin of Venus' atmosphere as well as clues regarding the role of large impacts in its atmospheric evolution.

DAVINCI will make definitive measurements of hydrogen isotopes that can be used to constrain when and at what rates Venus lost its putative early water oceans. DAVINCI will also make the first-ever *in situ* trace gas composition measurements within 12 km of the surface (the altitude at which commercial airlines cruise on Earth) where 2/3 of the Venus atmospheric mass resides. These observations will be very useful to future orbiting missions that need to characterize the deep atmosphere in order to quantitatively interpret infrared emissivity observations. The measured composition of chemically active gases will provide information about chemical processes in the sub-cloud atmosphere, the oxidation state of the atmosphere, and the degree of equilibration among gases in the vicinity of the surface. This never before obtained information regarding the composition of the near-surface Venus atmosphere will lead to new evaluations of stability of minerals and improved understanding of pathways for chemical weathering of the surface.

Finally, DAVINCI will return the first-ever high spatial resolution optical images of the enigmatic highland regions known as tessera terrain that may be analogous to remnant continents. Existing Magellan radar and topography, combined with Venus Express emissivity results are more than adequate for identifying an appropriate DAVINCI descent location. The carrier spacecraft receives all data during descent and relays those data back to Earth without requiring the presence of additional Venus-orbiting spacecraft.

Payload: DAVINCI builds on the tremendous success of the Mars Science Laboratory Sample Analysis at Mars (MSL/SAM) suite carried on the Curiosity rover [6-13], by pairing the Venus Mass Spectrometer (VMS) led by NASA's Goddard Space Flight Center with the Venus Tunable Laser Spectrometer (VTLS) led by the Jet Propulsion Laboratory. Combined, these two instruments provide the first comprehensive measurements of noble and trace gas species, as well as key elemental isotopes.

These two state-of-the art instruments are complemented by the Venus Atmospheric Structure Investigation (VASI), which provides measurements of the structure and dynamics of the Venus atmosphere during entry and descent as context for the chemistry measurements, and enables reconstruction of the descent profile.

High-contrast descent imaging of the tessera terrain is enabled by the Venus Descent Imager (VenDI), provided by Malin Space Science Systems based on a design that leverages experience with the Curiosity Rover's Mastcam and MARDI descent video imaging systems.

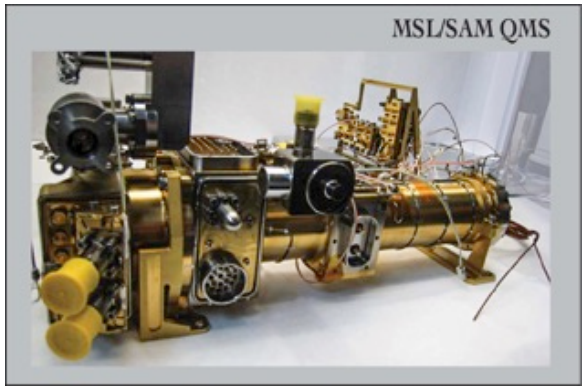

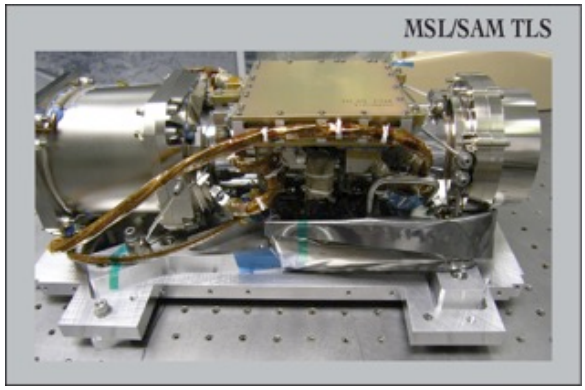

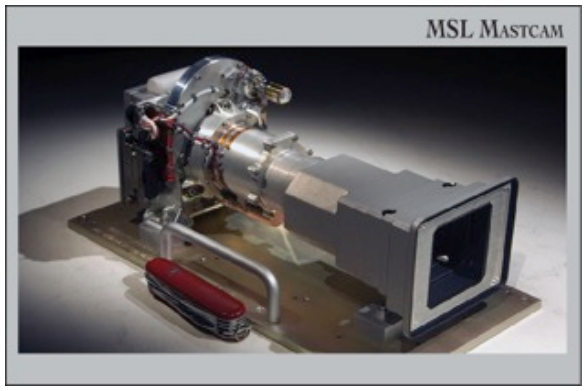

Bibliography: [1] Crisp, D., *et al.* (2002) *ASP conference Series, 272*, Ed. MV Sykes, 5-34. [2] New Frontiers in the Solar System (2003) National Research Council of the National Academies, National Academies Press. [3] Visions and Voyages (2011) National Research Council of the National Academies, National Academies Press. [4] VEXAG (2014) http://www.lpi.usra.edu/vexag/reports/GOI-140625.pdf. [5] Trainer *et al.* (2016) Abstract, this meeting. [6] Mahaffy *et al.* (2015) *Science, 347*, 412-414. [7] Webster *et al.* (2015) *Science, 347*, 415-417. [8] Atreya *et al.* (2013) *GRL, 40*, 5605-5609. [9] Mahaffy *et al.* (2013) *Science, 341*, 263-266. [10] Webster *et al.* (2013) *Science, 341*, 260-263. [11] Wong *et al.* (2013) *GRL, 40*, 6033-6037. [12] Conrad *et al.* (2014) *LPSC XLV*, Abstract #2366. [13] Webster *et al.* (2016) Abstract, this meeting.

OXYGEN NIGHTSIDE AIRGLOW ON VENUS IN RELATION TO ATMOSPHERIC DYNAMICS BASED ON VIRTIS-M OBSERVATIONS

D. Gorinov , **L.Zasova**, *Space Research Institute (IKI), Moscow, Russia* (gorinov-dmitry@yandex.ru*)*

Introduction:

Atmospheric oxygen $O_2(a^1\Delta_g)$ on Venus forms on the dayside in high altitudes and emits on the 1.27 um wavelength on the nightside, thus being an important indicator of the day-night circulation of the atmosphere.

This work studies the distribution of the O_2 nightside airglow using both nadir (southern hemisphere) and limb (northern hemisphere) measurements made by the M-channel of VIRTIS instrument on-board of Venus Express spacecraft.

Data analysis:

After processing 718 data cubes the following analyses were made:

- Comparison between northern and southern hemispheres
- Variability of the airglow with time
- Comparison with the underlying topography of the planet
- Comparison with the wind velocities
- Appearances of the double peaks in the vertical intensity profiles

Implication:

The global map of the O_2 nightglow distribution, based on data from 718 data cubes, indicates a complex character of the circulation in this transition region. Appearance of maximum intensity before midnight (from equator up to high latitudes) cannot be explained in terms of known modes of circulation: superposition of zonal retrograde and sub-solar – anti-solar modes of circulation of the Venus atmosphere. No influence on the O_2 night airglow horizontal distribution of the zonal retrograde superrotation in the global map for Southern hemisphere was found: the averaged intensity of the O_2 nightglow emission before midnight (0.43 MR) exceeds the averaged intensity after midnight (0.26 MR), the opposite of how it would be in the case of the presence of the zonal superrotation. Wave activity may affect the observed O_2 nightglow distribution.

Bibliography:

1. Gérard, J.-C., Saglam, A., Piccioni, G., Drossart, P., Cox, C., Erard, S., Hueso, R., and Sánchez-Lavega, A., 2008 Distribution of the O_2 infrared nightglow observed with VIRTIS on board Venus Express. Geophys. Res. Lett. V35. L02207. doi:10.1029/2007GL032021

2. Hueso, R., Sánchez-Lavega, A.,G. Piccioni, Drossart, P., Gérard, J. C., Khatuntsev, I., Zasova, L., Migliorini, A., 2008. Morphology and dynamics of Venus oxygen airglow from Venus Express/Visible and Infrared Thermal Imaging Spectrometer observations, J. Geophys. Res., 113, E00B02, doi:10.1029/2008JE003081.

3. Piccioni, G., Zasova, L., Migliorini, A., Drossart, P., Shakun, A., García Muñoz, A., Mills F. P., Cardesin-Moinelo, A., 2009. Near-IR oxygen nightglow observed by VIRTIS in the Venus upper atmosphere. J. Geophys. Res., 114, E00B38, doi:10.1029/2008JE003133.

4.Shakun, A. V., Zasova, L. V., Piccioni, G., Dro ssart, P., Migliorini, A., 2010. Investigation of oxygen $O_2(a^1\Delta_g)$ emission on the nightside of Venus: Nadir data of the VIRTIS-M experiment of the Venus Express mission. Cos. Res., Volume 48, Issue 3, pp.232-239, doi: 10.1134/S0010952510030044

EFFECTS OF SOLAR STORMS ON THE VENUSIAN IONOSPHERE.

C. Gray, *New Mexico State University, Las Cruces, NM, USA (candaceg@nmsu.edu)*, **N. Chanover, T. Slanger, K Molaverdikhani, K. Peter, B. Häusler, S. Tellman, O. Witasse, P.-L. Blelly, G. Collinson.**

Introduction

Observations of nightglow (upper atmospheric emission from atoms and molecules on the nightside of planets) allow for a multifaceted study of planetary atmospheres including interactions between the upper atmosphere of a planet and the solar wind. One of the brightest nightglow features on Earth is the OI (^{1}S - ^{1}D) 5577 Å line (the oxygen green line) generated in the mesosphere due primarily through dissociative recombination (Barth & Hildebrandt, 1961) and in the ionosphere as aurora, which is highly dependent on the conditions of the solar wind. Closely connected to the green line is the OI (^{1}D - ^{3}P) oxygen red line doublet at 6300.3 and 6363.8 Å. While it is more energetically favorable than the ^{1}S state, it has a longer radiative lifetime (116 sec compared to 0.82 sec Froese Fischer & Tachiev (2004)) and is collisionally quenched in the mesosphere, thus providing altitude information on emission processes.

The oxygen green line is a highly temporally variable emission line on Venus (Slanger et al., 2001, 2006, 2012; Gray et al., 2014; Gray et al., 2016). Emission was observed to increase after solar flares (outbursts of EUV emission and charged particles), coronal mass ejections (CMEs, large ejections of solar plasma), and co-rotating interaction regions (dense solar wind streams). Based on increases in green line emission after solar storms, particularly after large CMEs, Gray et al. (2014) concludes that the green line is auroral in nature.

The oxygen red line has never been detected on Venus. If the green line is the result of electron precipitation, it would likely occur high in the atmosphere where intensities of the red line should be greater than the green line (e.g. Slanger et al., 2012; Fox, 2011). The fact that the red line is not detected indicates that this emission is occurring lower in the atmosphere (i.e., below 150 km Slanger et al. (2012)).

To determine if higher energy solar wind electrons are penetrating to low altitudes in the Venusian nightside ionosphere, we compare electron energy spectra and electron density profiles observed by Venus Express (VEX) before and after solar storms. These data are used to model the Venusian nightglow to constrain the main chemical reactions responsible for emission.

Ground-Based Observations and Results

We observed Venus on 20 different dates between December 2010 to April 2015 on the Astrophysical Research Consortium (ARC) 3.5-m telescope at Apache Point Observatory (APO) using the ARC Echelle Spectrograph (ARCES, R $\sim$ 31,500). As solar storms are unpredictable events that occur over very short time scales (minutes to hours), we required Target of Opportunity observations, allowing us to observe an unpredictable event by overriding a scheduled observer. We detected the green line on 9 separate observations, always after solar storms.

We calculate a Matthews correlation coefficient (M, or phi coefficient) for binary data (where 1 is perfect correlation, -1 is perfect anti-correlation, and 0 is no correlation) in order to determine the statistical significance of electrons from CMEs and CIRs. We do not consider charged particles from solar flares in this calculation because we cannot properly distinguish which flares will contribute and which flares will not. Using all observations from 1999 to 2014, consisting of 29 data points, we find a green line emission and charged particles correlation of 0.86, a statistically significant value.

Space-Based Observations and Results

VEX is equipped with the Analyser of Space Plasmas and Energetic Atoms-4 (ASPERA-4) instrument package that includes the Electron Spectrometer (ELS). The ELS is used to measure electron energy and density as VEX sweeps through the Venusian ionosphere. We compare peak electron energy and flux values taken at similar altitudes and solar zenith angles (SZA) before an after an isolated solar flare and CME. After a solar flare, there is an increase in electron flux on the nightside of Venus but not an increase in electron energy. After a CME, there is an increase in electron flux and energy. We interpret this as electrons precipitating directly into the nightside atmosphere.

In order to determine how CMEs affect the low altitude nightside ionosphere of Venus, we use the VEX Venus Radio Science Experiment (VeRa), to compared variations in the Venusian nightside electron density profile before and after CME impacts. The Venusian V1 and V2 electron layers peak at 125 km and 150 km, respectively. The V2 layer is typically the dominant layer but the nightside ionosphere is known to be highly variable due to the solar wind and the peaks have been observed to disappear during solar minimum (Kliore & Luhmann, 1991). After each set of observed storms, the V2 and V1 layer were observed to change in density with the V1 layer increasing in electron density and the V2 layer decreasing in density. For the most extreme case, the V2 layer decreases by a factor of four, becoming nearly undetectable, we detected green line emission from APO.

Modeling of the Green Line

In order to determine the importance of electron flux versus energy on the Venusian green line, we model the nightside Venusian ionosphere using TRANSCAR, a 1-D magnetohydrodynamic (MHD) model (Witasse et al., 2008), by applying precipitating electron spectra observed by VEX. All ions are generated via electron impact with neutrals. Dayside transport of ions and photoelectrons are not considered. Production of N_2^+, O_2^+, O^+, H^+, N^+, CO_2^+, CO^+, O^+, C^+, CO_2^{++} are generated from electron impact as well as secondary electrons. Additional ions are generated from chemical reactions.

We consider five reactions to produce the O^1S and O^1D state. Preliminary results indicate that during normal solar wind conditions, the electron impact of O and O_2^+ are the primary contributers to green line emission. After a CME impact, we find electron impact of O + e to be the dominate source for O^1S production. On Earth, the dominate reaction for auroral green line emission is O_2^+ + e.

Discussion and Conclusions

Based on ground-based and space-based observations as well as modeling results, we conclude that the the leading cause for emission is due to O + e which increases as increased energy and flux of precipitating electrons enter directly into the Venusian nightside atmosphere. While we were able to use the TRANSCAR model to reproduce increases in green line intensity, we were unable to model the behavior of the V1 and V2 electron density changes after CMEs. This is likely due to two reasons: we did not consider increases in magnetic fields at the top of the atmosphere or the transport of O^+ ions from the dayside.

We propose that the decrease in the V2 electron density is due to the increase dynamic pressure generated by the passage of a CME. The nightside ionosphere and the V2 of Venus is maintained due to large amounts of O^+ (1.5×10^8 cm s^{-1}, Brannon & Fox (1994)) being transported above the exobase from the dayside to the nightside, diffusing downward, reacting with CO_2 and generating O_2^+ V2 peak (Taylor et al., 1979). However, observations from PVO show that the Venusian nightside ionosphere 'disappears' during times of high solar dynamic pressure (Cravens et al., 1982; Lazarus & McNutt, 1990). Cravens et al. (1982) showed that the P_{sw} for the disappearing ionosphere was on a average over 10.4 nPa. We find that for large CMEs the P_{sw} can increase to 70 nPa. Similar ionospheric behavior was observed on Mars for th M1 and M2 layers after solar storms (Withers et al., 2012; Gray et al., 2016).

In addition to similar electron density variations, Mars and Venus both exhibit auroral emission after solar storms. Recent results from Mars Atmosphere and Volatile Evolution (MAVEN) mission (Schneider et al., 2015) show that diffuse aurora is present on Mars after solar storms. This aurora was found to be deep in the atmosphere (60 km) and located away from the crustal magnetic fields. Like Venus, the Martian aurora is seen across the nightside of the planet. Given the complementary auroral and ionospheric observations of Venus and Mars, we conclude that this behavior is typical of non-magnetic planets with CO_2 atmospheres.

References

Barth, C. A., & Hildebrandt, A. F. 1961, , 66, 985

Brannon, J. J., & Fox, J. L. 1994, , 112, 396

Cravens, T. E., et al. 1982, , 51, 271

Fox, J. L. 2011, Icarus, 216, 625

Froese Fischer, C., & Tachiev, G. 2004, Atomic Data and Nuclear Data Tables, 87, 1

Gray, C. L., Chanover, N. J., Slanger, T., & Park, M. 2016, Planetary and Space Science, submitted

Gray, C. L., Chanover, N. J., Slanger, T. G., & Molaverdikhani, K. 2014, , 233, 342

Kliore, A. J., & Luhmann, J. G. 1991, , 96, 21281

Lazarus, A. J., & McNutt, Jr., R. L. 1990, in Physics of the Outer Heliosphere, ed. S. Grzedzielski & D. E. Page, 229–234

Schneider, N. M., et al. 2015, Science, 350, 0313

Slanger, T., Huestis, D., Cosby, P., Chanover, N., & Bida, T. 2006, Icarus, 182, 1

Slanger, T. G., Chanover, N. J., Sharpee, B. D., & Bida, T. a. 2012, Icarus, 217, 845

Slanger, T. G., Cosby, P. C., Huestis, D. L., & Bida, T. a. 2001, Science (New York, N.Y.), 291, 463

Taylor, H. A., Brinton, H. C., Bauer, S. J., Hartle, R. E., Cloutier, P. A., Daniell, R. E., & Donahue, T. M. 1979, Science, 205, 96

Witasse, O. G., Helou, M., Blelly, P., Paetzold, M., Tellmann, S., & Hausler, B. 2008, AGU Fall Meeting Abstracts, A1432

Withers, P., et al. 2012, Journal of Geophysical Research (Space Physics), 117, 12307

HEAT LOSS AND GEOLOGY OF A YOUNG VENUS.

R.E. Grimm, Planetary Science Directorate, Southwest Research Institute, Boulder, CO, USA. *(grimm@boulder.swri.edu).*

Programmatic Information:

This is a placeholder abstract: per email with Colin Wilson, I will submit "actual" abstract after I get past a proposal due on the 22nd. I appreciate a little more time.

Introduction:

The impact-crater population and morphology of Venus have been interpreted as indicating "global resurfacing" at ~750 Ma, with sharply reduced geological activity since. However, this has been challenged both in observations of the geological sequence and the modification state of craters. Furthermore, Bottke et al [DPS, 2015 and LPSC, 2016] have determined a crater-retention age 150-200 Ma for Venus based on a direct mapping of the NEO population to crater SFDs. This has profound implications for the geodynamics of Venus:

(1) unique "catastrophic" resurfacing in the last few percent of the planet's history is implausible; the young age instead must be a manifestation of continuous "equilibrium" processes, or patchy resurfacing that looks like a continuum.

(2) the topography, gravity, and heat-flow are consistent with a "steady-state" Venus in which the average age of the thermal lithosphere is 150-200 Ma. Magmatism comprises several percent of the heat budget, which can account for the resurfacing rate and suggestions of recent or active volcanism. The original "hot-spot" model of Venus geodynamics may be valid.

NEW USER INTERFACE FOR ACCESSING ARCHIVED EUROPEAN SPACE AGENCY PLANETARY SCIENCE DATA

E. Grotheer, **C. Arviset**, **I. Barbarisi**, **M. Barthelemey**, **S. Besse**, *European Space Astronomy Centre (ESAC), Villanueva de la Cañada, Spain (emmanuel.grotheer@esa.int)*, **G. DeMarchi,** *European Space Research and Technology Centre (ESTEC), Noordwijk, Netherlands,* **R. Docasal**, **D. Fraga**, **J. Gonzalez**, **D. Heather**, **T. Lim**, **A. Macfarlane**, **C. Rios**, *European Space Astronomy Centre (ESAC), Villanueva de la Cañada, Spain.*

Introduction:

All Venus Express (VEX) instruments delivered their data products according to the Planetary Data System version 3 (PDS3) standard. The European Space Agency's (ESA) Planetary Science Archive (PSA), which can be accessed at www.rssd.esa.int/PSA, is being upgraded to make PDS4 data available from upcoming missions such as ExoMars and BepiColombo. Thus, the PSA development has been working to ensure that the legacy PDS3 data will be accessible via the new interface as well.

We will preview some of the new methods of accessing legacy VEX data via the new interface. This includes accessing the data using Geographic Information Systems (GIS) and our plans for making this and other data sets compatible with the Virtual European Solar and Planetary Access (VESPA) project for creating a virtual observatory.

The PSA team is greatly interested in receiving feedback from the scientific community about new functionality that could be included in the PSA to improve its applicability to current and future research endeavors.

Comparison of sectional and modal cloud microphysics representations for Venus: VenLA vs. MAD-VenLA

S. Guilbon, A. Määttänen, F. Montmessin, *Université Versailles St-Quentin; Sorbonne Universités, UPMC Univ. Paris 06; CNRS/INSU, LATMOS-IPSL, Guyancourt, France*, **J. Burgalat**, *GSMA UMR CNRS 7331, Université de Reims Champagne-Ardenne, Reims, France,* **S. Bekki**, *Université Versailles St-Quentin; Sorbonne Universités, UPMC Univ. Paris 06; CNRS/INSU, LATMOS-IPSL, Guyancourt, France.*

Introduction:

The mesospheric Venusian clouds are similar to the stratospheric aerosol layer that is composed of sulfuric acid-water solution droplets. Like clouds on Earth, the Venus clouds play a crucial role on the climate of the planet. That is why we are interested in the formation and the time evolution of the cloud particles.

The goal is to develop a microphysical representation to complete the 3D IPSL Venus-GCM (Global Climate Model) [6]. To this end, we are developing a sectional model VenLA based on PSC model [5] and the modal representation MAD-VenLA. In this work, we compare these two models in a 0D setting.

Model description:

Sectional representation. The Venus Liquid Aerosol (VenLA) cloud model is a sectional representation of microphysical processes developed at LATMOS [7]. The term 'sectional' means that the particle size distribution is divided into several radius intervals, called bins. At high radius resolution, VenLA is computationally too demanding to be integrated in the IPSL Venus Global Climate Model. Often in GCMs another representation is used: the moment method.

Modal representation. The Modal Aerosol Dynamics of Venusian Liquid Aerosol cloud model (MAD-VenLA) uses moment scheme to describe the size distribution and the microphysical processes.
Instead of bins, the particle size distribution is described by two or three global parameters: total particle number, mean radius and/or the variance [9]. Moreover, with this representation, the form of the size distribution is fixed. Analytical equations of microphysics are derived to express the changes in the parameters (moments) of the distribution.
In theory, the moment method is computationally more efficient than a sectional representation [1].

Comparison of VenLA and MAD-VenLA:

Modeling approach. We will compare, in 0D, the precision of each model and their computational efficiency. For VenLA, we can change the resolution with the number of bins: high (100 bins for example) to low resolution (<10 bins). However, the MAD-VenLA model describes the size distribution with two or three global parameters chosen during the model development. These parameters are the mean radius, the total particle number and the variance of the size distribution function. To make this comparison, we defined a lognormal particle size distribution function and we consider modes 1 and 2 of Venus cloud droplets [4,10] defined in [3]. The liquid droplets are composed of sulfuric acid-water solution.

First results

First, we focus on homogeneous nucleation, condensation and the thermodynamical equilibrium of the droplet in the atmosphere like in [3]. The model using modal scheme of the processes will be tested and compared with bibliography. The comparison between the two models (VenLA and MAD-VenLA) on these microphysical processes will be presented.

Then, a status report on the coagulation in VenLA and MAD-VenLA will be presented.

Summary and Conclusions

Here we present a status report on the development of the modal representation MAD-VenLA and we compare it with the sectional model VenLA at different resolutions. We will then compare these models to baseline high-resolution models present in the literature [2].

Perspective

The moment method is already used in the IPSL Titan GCM to describe the cloud and aerosol microphysics. Therefore, it is interesting to use it also in the IPSL Venus GCM.

The goal of our work is to choose the best representation - It will be the balance between precision and computational efficiency - to complete the IPSL 3D Venus-GCM and understand the cloud formation and the climate evolution of the Earth's evil twin.

Acknowledgements: This work has been supported by the French Planetology program (Programme National de Planétologie, ATMARVEN project).

References:

[1] Burgalat , J., Rannou, P., Cours, T. and Rivière, E. Modeling cloud microphysics using a two-moments hybrid bulk/bin scheme for use in Titan climate models: Application to the annual and diurnal cycles. Icarus, Vol.231, pp.310-322, 2014.

[2] Jacobson, M.Z. Analysis of aerosol interactions with numerical techniques for solving coagulation, nucleation, condensation, dissolution, and reversible chemistry among

multiple size distribution. Journal of Geophysical Research, Vol.107, 2002.

[3] James and al., E.P., Toon, O.B. and Shubert, G. A Numerical Microphysical Model of the Condensational Venus Cloud. Icarus, vol.129, pp.147-171, 1997 1997.

[4] Knollenberg, R. G. and Hunten, D. M. The microphysics of the clouds of Venus - Results of the Pioneer Venus particle size spectrometer experiment. Journal of Geophysical Research, Vol.85, pp.8039-8058, 1980.

[5] Larsen, N. Polar Stratospheric Clouds Microphysical and optical models. Danish Meteorological Institute, Ministry of transport, Lyngbyvej 100, DK-2100 Copenhagen, Denmark, 2000.

[6] Lebonnois, S., Hourdin, F., Eymet, V., Crespin, A., Fournier, R. and Forget, F. Superrotation of Venus atmosphere analyzed with a full general circulation model. J. Geophysical Research, Vol.115, 2010.

[7] Määttänen, A., Guilbon, S., Stoltzenbach, A., Bekki, S., Montmessin, F. The LATMOS Venus Cloud Model VenLA: Status Report. Venus Conference, 4–8 April 2016. Oxford, U.K., 2016.

[8] Pruppacher, H. R. and Klett, J. D. Microphysics of Clouds and Precipitation - Second Edition, Vol.18, Springer, 2010.

[9] Seigneur, C., Belle Hudischewskyj, A., Seinfield, J.H., Whitby, K.T., Whitby, E.R., Brock, J.R. and Barnes, H.M. Simulation of Aerosol Dynamics: A Comparative Review of Mathematical Models. Aerosol Science and Technology, 5:2, pp.205-222, 1986.

[10] Toon, O. B. , Ragent, B., Colburn, D., Blamont, J. and Cot, C., Large, solid particles in the clouds of Venus: Do they exist? Icarus, Vol.160, pp.57-143, 1984.

[11] Whitby, E., Stratmann, F., Wilck, M. Merging and remapping modes in modal aerosol dynamics models: a “Dynamic Mode Manager”. Journal of Aerosol Science, vol.33, pp623-645, 2002.

THE EVOLUTION OF VENUS, A GLOBAL PERSPECTIVE—FROM EXOGENIC TO ENDOGENIC OVER TIME.

V. L. Hansen, *Dept. Earth & Environ. Sci., University of Minnesota, Duluth MN, USA, (vhansen@d.umn.edu)*, **I. López**, *Área de Geología. Universidad Rey Juan Carlos, Mostoles Madrid, Spain (ivan.lopez@urjc.es)*.

Introduction: NASA's Magellan mission of two decades ago revealed that Venus lacks plate tectonics, yet Venus' surface evolution and operating geodynamic system has remained elusive. Geologic mapping and surface modeling studies lead to the emergence of a comprehensive model of Venus' global evolution. The picture that emerges is one of early exogenic-instigated events and global thin lithosphere, followed by an evolution to thicker lithosphere and largely endogenic-driven processes that became regionally more focused with time. Observations and implications are briefly noted below, followed by a proposed geodynamic evolution.

What can impact craters tell us?: Observations: Venus has ~1000 well-preserved craters that are distributed in a near random pattern across its surface; craters range in diameter from 1-270 km, with 30-km average; early SAR analysis indicated that ~175 craters show signs of modification [1-4]. Global crater density results in an average model surface age (AMSA) for the planet [5], however, AMSA does not constrain the extent of recorded geohistory [5,6]. Craters also show evidence of progressive degradation providing relative-age constraints [7,8], which together with crater density define three distinct AMSA provinces [6,9]. The young-AMSA province corresponds to the Beta-Atla-Themis (BAT) and Lada regions, which host high concentrations of young volcanic flows [10,11] and clear partially buried craters [9]. Complete crater burial requires ≥1 km-thick flows [12,13]. Analysis of crater DEMs [12,14] indicates that >>175 craters show modification by volcanic processes, not originally recognized, and that many craters *do not* lie at the top of local stratigraphy, as required by catastrophic resurfacing and global stratigraphy hypotheses [15-20]. Postulated relative ages of craters and wrinkle ridges are non-unique, posing no temporal constraints [24]. Venus lacks craters >290 km dia., indicating that large craters failed to form or, if formed, they were destroyed or escape recognition.

What can ribbon-tessera terrain tell us?: Ribbon-tessera terrain (rtt) forms a unique tectonic fabric of ribbons, folds and graben that characterizes crustal plateaus [22,23], and occur as lowland inliers–remnants of 'collapsed crustal plateaus' [24-26,27]. Although rtt formation is debated all mechanism consider that: 1) ribbon and fold formation overlapped in time, 2) graben formed relatively late, and 3) local volcanism accompanied rtt formation [22,23,28-32]. Thermal modeling indicates that ribbons require very high geothermal gradient [30,35]. Crustal plateau formation is debated, however, all hypotheses include the following conditions [22,23,26,29-32,36]: 1) plateaus formed on thin (global) lithosphere; 2) rtt formation resulted in destruction of earlier formed local impact craters; 3) individual plateaus formed spatially separate, and 4) at different times (i.e., time-transgressively).

Global-scale rtt patterns provide additional conditions based on the following observations [37]: 1) rtt inliers occur within all volcanic rises, except Imdr and Themis; 2) rtt occurs within most lowland basins, and 3) rtt occurs independent of basin topography (i.e. it can occur at the deepest level); 4) groups of rtt inliers describe regional-scale linear to arcuate patterns, and 5) these patterns may show no obvious correlation with long-wavelength topography–that is, rtt patterns track across basins and rises; 6) few, if any, large ($>7\times10^6$ km^2) rtt-poor regions exist; an inverse statement is that rtt occurs in a widely distributed fashion across Venus' surface. Collectively these observations are *inconsistent* with global-scale flooding of low regions across Venus, as required in the context of both catastrophic resurfacing and global stratigraphy hypotheses.

What can Artemis tell us?: Artemis [38] is much larger than initially recognized, including a: wide outer trough (>5000 km dia.), radial dike swarm (>12000 km dia.), and concentric wrinkle ridge suite (>13000 km dia.) [39]. The wrinkle ridge suite previously described as 'circum-western Aphrodite' and attributed to topographic loading of western Aphrodite Terra [40,41] do not match the circum-western Aphrodite model predictions, and is better described as circum-Artemis. Temporal relations indicate that Artemis formed after crustal plateaus and rrt inliers. Greater Artemis' evolution included formation of its interior and chasma, accompanied by lateral propagation of its huge radial dike/fracture suite; escape of magma to the surface formed local cover deposits that buried some host radial fractures; cover deposits were cut, in turn, by wrinkle ridges marking Artemis deflation and defining the huge Artemis-concentric suite. The outer wide trough formed late relative to radial fractures, cover deposits and wrinkle ridges, possibly accompanying deflation and wrinkle ridge formation. For these geologic relations to be preserved, greater-Artemis would have to form *after* postulated global catastrophic resurfacing, yet Artemis represents a major tectonomagmatic feature [39]; thus its formation would violate postulated quiescence required by catastrophic resurfacing. Artemis represents the sig-

nature of superplume during an era marked by relatively thin lithosphere. Ishtar Terra, proposed to have formed by ponding of mantle-melt residuum by a large regional downwelling [42], could have resulted from a near antipodal position from the global-scale upwelling associated with the Artemis superplume.

What can wrinkle ridges tell us?: In addition to the Artemis-concentric suite, wrinkle ridges also form relatively small concentric suites centered on highland features including: Themis, Lada Terra, Gula Mons, Sappho Patera, Pavlova Corona, and Bell Regio [39,40,43]; formation of these suites is inconsistent with stresses induced in the lithosphere due to high surface-T induced stress superposed on gravitational stresses associated with topography and lithospheric structure [44,45], given they occur at high elevation and/or positive geoid values [41]. Wrinkle ridges did not form during a single time in Venus' history, rather they represent tectonic suites associated with individual host geomorphic features [39,43,46]. In the Niobe and Aphrodite 1:10M map areas some wrinkle ridges represent inversions structures (47-49). All of these studies call into question temporal assumptions required by models in which wrinkle ridges result from postulated high surface-T due to catastrophic volcanism [50].

Constraints from volcanic deposits: Venus' extensive lowlands record a rich volcanic history. Geologic mapping of large tracts of the surface indicates a wide range of volcanic units occur throughout local stratigraphic stacks inconsistent predictions of global stratigraphy [13]; a majority of lowland volcanic units in individual planitiae source from local volcanoes or coronae [48,49,51]. Recent emissivity data provides evidence for contemporary volcanic activity [52,53]. Thin shield deposits occur across large spatial regions (~22% of the surface), and formed time-transgressively, occurring at different stratigraphic levels in different areas, rather than a single restricted time period [13,54-57]. It is notable that for these deposits to be preserved at the surface, they would all have to post-date postulated catastrophic resurfacing. Several large regional map areas record 'non-directional' geologic histories [13,58] contrary to the sequence of events proposed within the context of proposed global stratigraphy hypotheses.

What can Monte Carlo modeling tell us?: Modeling indicates what is possible, not necessarily what happened; models do not impose constraints, rather they test specific model conditions. Early Monte Carlo models favored catastrophic resurfacing and ruled out equilibrium resurfacing models with very specific incremental resurfacing areas [15,16]; however, geologic data rules out catastrophic resurfacing. New Monte Carlo models test changes in resurfacing rates through time, and examine different incremental resurfacing areas [59-61]. Model results indicate that crater observations can be met through a range of surface histories over >3.5 Ga, and include ~5000-500 km^2 resurfacing areas. These models caution against evolution models that assume a short (<1Ga) recorded surface history [62-65].

Global geodynamic evolution: A possible global evolution that emerges is relatively simple at a long-wavelength time-scale, although rich histories develop locally. Crustal plateaus and rtt formed early marking an era of globally thin lithosphere and bolide-impact drive processes [34]; deformation belts likely formed late during this era, representing endogenic-driven processes. Time-transgressive evolution of the Artemis superplume marks the Artemis era that affected ~30% of the surface, and also resulted in the rise of Ishtar Terra above a complimentary downwelling. This relatively singular mantle flow pattern subsequently evolved to more localized mantle plumes–marked by coronae-dominated volcanic rises (e.g., Bell, Eistla), and downwellings forming broad lowland basins. Further gradational thickening of the lithosphere lead to an increase in localized regional endogenic-driven tectonomagmatic activity marked by corona-chasma chains, fracture zones, and large rift-dominated volcanic rises of the BAT region. During thin lithosphere time Venus experienced dominantly steady-state resurfacing driven by large bolide impact and crustal plateau formation. With time, large bolides waned, the lithosphere thickened, and craters accumulated across the surface, with the most dramatically modified in the young tectonomagmatic BAT region.

References: [1] Schaber G.G. et al (1992) *JGR* 97, 13257-302; [2] Phillips R.J. et al (1992) *JGR* 97, 15923-48; [3] Herrick R.R. et al (1997) *Venus II*, 1015-46 [4] Hauck S.A. et al (1998) *JGR* 103, 13635-42; [5] McKinnon W.B. et al (1997) *Venus II,* 969-1014; [6] Hansen V.L. & D.A. Young (2007) *GSA-SP 255*-73; [7] Izenberg N.R. et al. (1994) *GRL* 21, 289-92; [8] Basilevsky A.T. & J.W. Head (2002) *Geol.* 30, 1015-8; [9] Phillips R.J. & N.R. Izenberg (1995) *GRL* 22, 1517-20; [10] Head J.W. et al (1992) *JGR* 97, 13153-98; [11] Crumpler L.S. et al (1997) *Venus II* 697-756; [12] Herrick R.R. & V.L. Sharpton (2000) *JGR* 105, 20245-62; [13] Stofan E.R. et al (2005) *Icarus* 173, 312-21; [14] Herrick R.R. & M.E. Rumpf (2011) *JGR* 116; [15] Bullock M.A. et al (1993) *GRL* 20, 2147-50; [16] Strom R.G. et al (1994) *JGR* 99, 10899-922; [17] Basilevsky A.T. & J.W. Head (2000) *PSS* 48, 75-111; [18] Basilevsky A.T. & J.W. Head (1996) *GRL* 23, 1497; [19] Basilevsky A.T. & J.W. Head (1998) *JGR* 30, 8531-44; [20] Head, J.W. & A.T. Basilevsky (1998) *Geol*. 26, 35-8; [21] Hansen V.L. (2000) *EPSL* 527-42; [22] Bindschadler, D. L. et al (1992) *JGR* 97(E8), 13495-532; [23] Hansen V.L. et al (1999) *Geol.* 27, 1071-1074; [24] Phillips R.J. & V.L. Hansen (1994) *AREPS* 22, 597-654; [25] Ivanov M.A. & J.W. Head (1996) *JGR* 101, 14861-908; [26] Phillips R.J. & V.L. Hansen (1998) *Sci*. 279, 1492-97; [27] Ghent R.R. & I.M. Tibuleac (2002) *GRL* 29, 994-7; [28] Hansen V.L. & J.J. Willis (1996) *Icarus* 123, 296-312; [29] Hansen V.L. & J.J. Willis (1998) *Icarus* 132, 321-43; [30] Gilmore M.S. et al (1998) *JGR* 103, 16813-40; [31] Hansen V.L. (2006) *JGR* 111 [32] Bindschadler, D. L. et al (1992) *JGR* 97(E8),13,563-577; [33] Romeo I. & D.L. Turcotte (2008) *EPSL* 276, 85-97; [34] Hansen V.L. et al (2000) *JGR* 105, 4135-52; [35] Ruiz J. (2007) *PSS*, 55, 2063-70 ;[36] Bindschadler D.L. (1995) *RGP* 33, 459-67; [37] Hansen V.L. & I. Lopez (2010) *Geol*., 38, 311-4; [38] Bannister R.A. & V.L. Hansen (2010) *USGS SIM-3099;* [39] Hansen, V.L. & A. Olive (2010) *Geol.* 38, 467-70; [40] Bilotti F. & J. Suppe (1999) *Icarus* 139, 137-57; [41] Sandwell D.T. et al (1997) *Icarus* 129, 232-44; [42] Hansen V.L. & R.J. Phillips (1995) *Geol.* 23, 292-6; [43] McGill G.E. (2000) *U.S. Geol. Surv. I-2637;* [44] Solomon S.C. et al (1999) *Sci.* 87-90; [45] Anderson F.S. & S.E. Smrekar *(*1999*) JGR* 104*(*E12*),* 30743-56; [46] McGill G.E. (2004) *Icarus* 172, 603-12; [47] DeShon H.R. et al (2000) *JGR* 105, 6983-95; [48] Lopez I. & V.L. Hansen (2016) *this vol.;* [49] Hansen V.L. et al. (2015) I-2476, 1:10M-scale, in rev.; [50] Bullock M.A. & G.H. Grinspoon (2001) *Icarus* 19-37; [51] Stofan E.R. & Guest J.E. (2000) *U.S. Geol. Surv. I-2799;* [52] Smrekar S.E. et al (2010) *Sci.* 328, 605-8; [53] Shalygin E.V. et al. (2015) *GRL* 42, 4762-9; [54] Addington E.A. (2001) *Icarus* 149, 16-36; [55] Brian A.W. et al (2005) *USGS SIM-2813* [56] Hansen V.L. (2005) *GSAB* 117, 808-22 [57] Grindrod P.M. et al (2010) *GRL* 37 [58] Guest J.E. & E.R. Stofan (1999) *Icarus* 139, 55-66 [59] Bond T.M. & M.R. Warner (2006) *LPSC 37*, #1957 [60] Bjonnes E.E. et al (2012) *Icarus* 217 451-61; [61] O'Rourke J.G. et al. (2014) *GRL* 41, 8252-60; [62] Turcotte D.L. et al (1999) *Icarus* 139, 49-54; [63] Romeo I. (2013) *PSS* 87, 157-72; [64] Romeo I. & D. Turcotte (2010) *PSS* 58, 1374-80; [65] Taylor F. & D. Grinspoon (2009) *JGR* 114, E00B40.

WHISTLER-MODE WAVE OBSERVATIONS FROM VENUS EXPRESS: THE SMOKING GUN FOR LIGHTNING ON VENUS

R.A. Hart, *(UCLA, EPSS, Los Angeles, CA, USA, rhart@igpp.ucla.edu),* **C.T. Russell,** *(UCLA, EPSS, Los Angeles, CA, USA),* **T.L. Zhang,** *(Austrian Academy of Sciences, Vienna, Austria).*

Introduction:

Many observations of venusian lightning have been made over the last few decades. Lightning was seen optically by Venera 9 and also from a 60" ground telescope. The electric field detector on the Pioneer Venus Orbiter (PVO) could detect lightning, but only in darkness due to the magnetic field configuration and the requirements for whistler propagation. PVO also detected lightning with its electric antenna when it entered the Venus atmosphere. The Galileo spacecraft detected radio waves from lightning during its flyby of Venus. Most recently, Venus Express detected lightning via whistler-mode waves at extremely low frequencies (ELF) with its onboard dual fluxgate magnetometer.

Whistler-mode waves are right-hand polarized electromagnetic waves generated by lightning. They propagate with a frequency between the local electron and ion gyrofrequencies ($\Omega = qB/m$), which are ELF waves at Venus. Whistlers are transverse waves and they are guided along the direction of the local magnetic field. Detection of these waves on the dayside of Venus is less likely because the magnetic field is perpendicular to the wave's vertical motion thus hindering its ability to be guided to the spacecraft at higher altitudes. However, when the magnetic field dips into the atmosphere these waves can be detected on the dayside as well as the nightside. In this study we present a statistical analysis of these Venus Express observations and the effects on detection due to conditions within the ionosphere.

Wave Analysis:

Whistlers were identified using the dual fluxgate magnetometer onboard Venus Express. Waves are initially flagged when the transverse power exceeds the compressional power by an order of magnitude and are then confirmed as whistlers using Fourier analysis. The signals must pass three tests (**Figure 1**): the power is predominantly transverse, they are right-hand circularly polarized, and they propagate along the magnetic field. These features are characteristic of whistler-mode waves whose expected source is lightning. In total, we detected 2,237 distinct signals resulting in nearly 200 minutes of total wave activity throughout the mission.

We examined the magnetic field data in search of whistlers for 10 minutes about periapsis on each orbit throughout the Venus Express mission. Periapsis latitude increased 3° per year until 2009 when it then

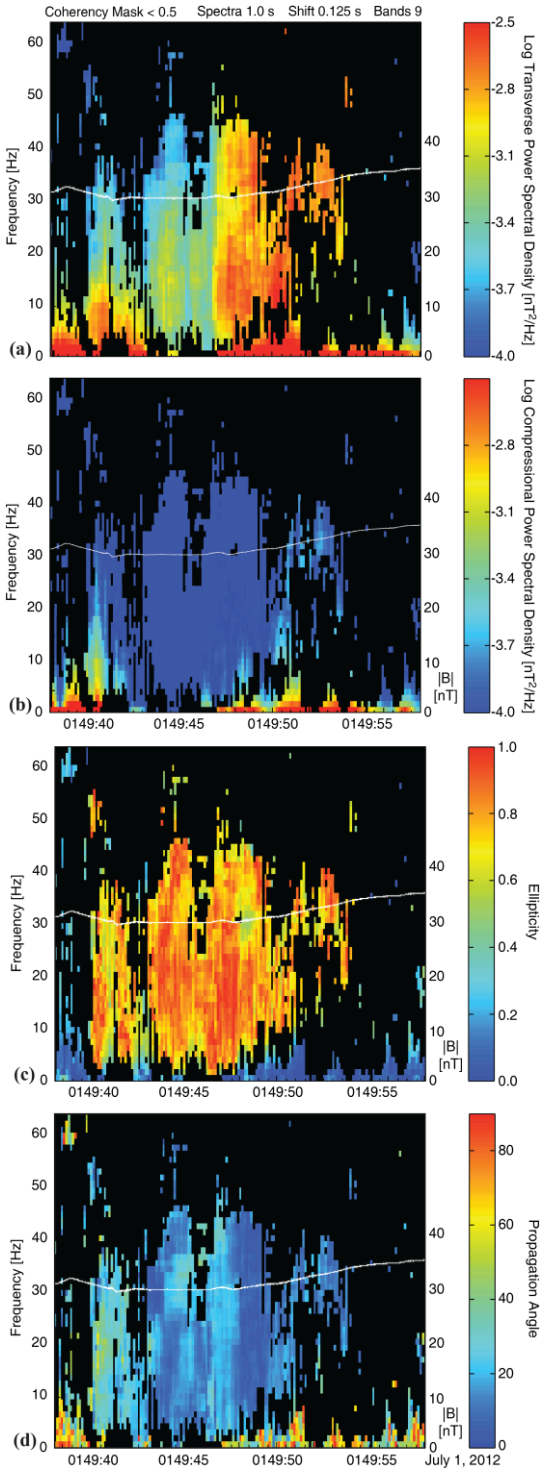

Figure 1. Dynamic spectra of (a) transverse power, (b) compressional power, (c) ellipticity, and (d) propagation angle of waves seen on 1 July 2012. White line shows magnetic field magnitude.

began to decrease until the end of the mission in 2014. The altitude of periapsis varied between 165 and 355 km as gravitational forcing lowered it and thrusters were used to raise it again (**Figure 2**). Most of the signals (75%) were detected when the spacecraft was between 200 to 350 km altitude. Within this range, ELF wave activity was observed 1-2% of the time on average.

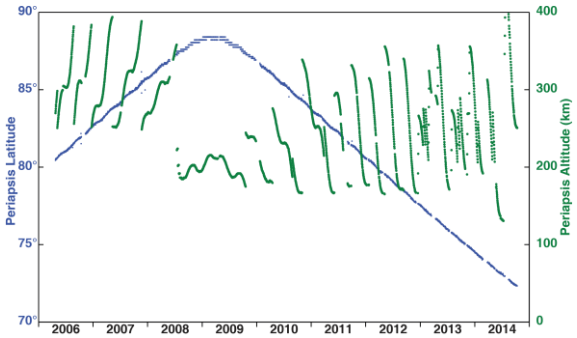

Figure 2. Variations in Venus Express periapsis.

Discussion:

Venus Express spanned the length of almost an entire solar cycle, which enabled us to compare the detection rates between the solar minimum phase and the solar maximum phase. During solar maximum the ionosphere is highly charged enable it to stave of the interplanetary magnetic field, however, during solar minimum the ionospheric electron density is lower which allows the solar wind magnetic field to sink in and magnetize the ionosphere (**Figure 3**). When there is a strong +Y-component (anti-orbital direction) to the solar wind magnetic field it creates asymmetries in the ionospheric plasma flow from the subsolar point to the poles. The flow is much slower over the northern hemisphere and creates a buildup of the field. Because all of our observations are at high northern latitudes we see a strong correlation with our detection rates and a $+B_y$ magnetic field (**Figure 4**). There was no apparent correlation with the magnetic field and our statistics during the solar maximum phase, which is due to the lack of magnetization of the ionosphere.

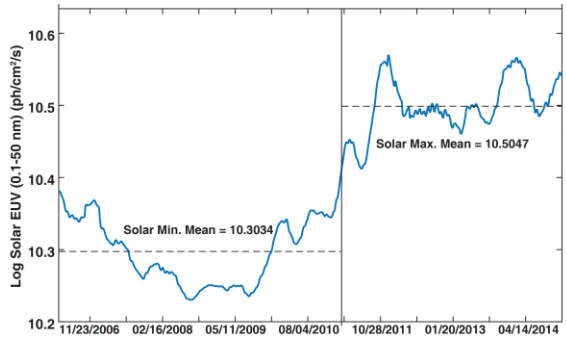

Figure 3. Solar EUV is the primary source of ionization in the Venus ionosphere.

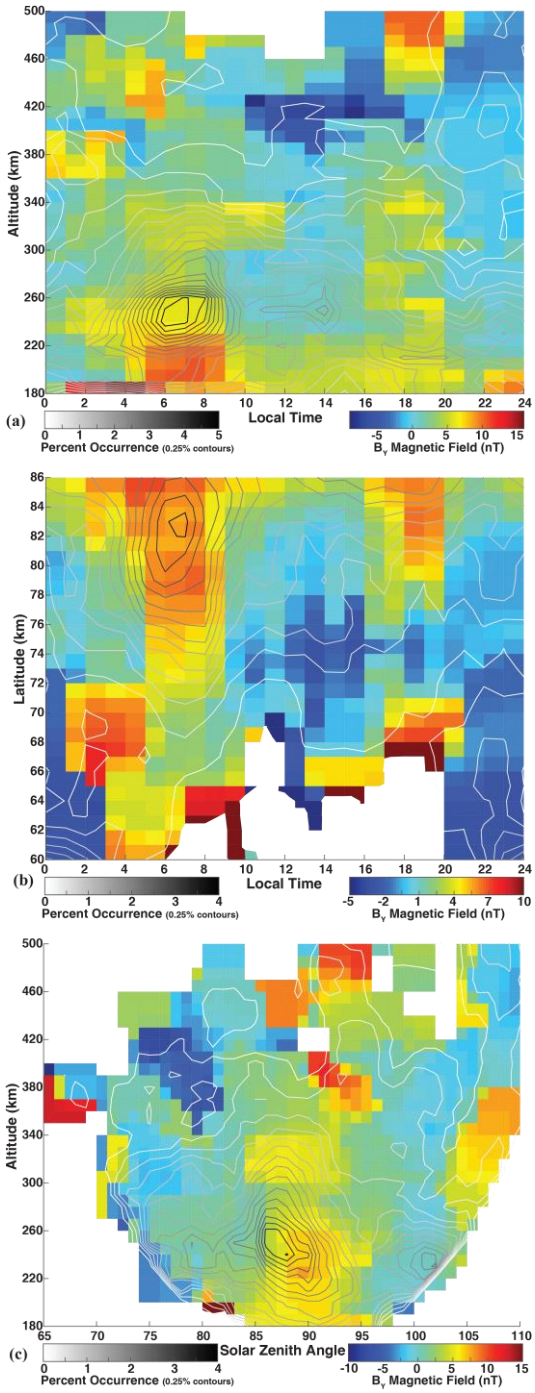

Figure 4. Contours of whistler detection statistics and B_y component of the magnetic field for the solar minimum period as defined in **Figure 3**.

References:

Russell, C.T., et al. (2013), Venus Express observations of ULF and ELF waves in the Venus ionosphere: Wave properties and sources, Icarus, 226, 1527–1537

Villarreal, M. N., et al. (2015), Characterizing the low-altitude magnetic belt at Venus: Complementary observations from the Pioneer Venus Orbiter and Venus Express, J. Geophys. Res. Space Physics, 120, 2232–2240.

GEODYNAMIC EVOLUTION OF VENUS: TESTING MODELS WITH GLOBAL STRATIGRAPHIC AND CHRONOLOGIC OBSERVATIONS.

James W. Head[1], Mikhail A. Ivanov[2], Alexander T. Basilevsky[2], E. M. Parmentier[1], [1]Earth, Environmental and Planetary Sciences, Brown University, Providence, RI 02912 USA. [2]Vernadsky Institute, RAS, Moscow, Russia (james_head@brown.edu).

Acquisition of Earth-based radar image observations [1], followed by regional image coverage (Venera 15/16) [2] and finally global image coverage by Magellan [3], together with global altimetry [4], have provided the data necessary to analyze stratigraphic relationships [5] and produce a global geological map of Venus [6]. The resulting stratigraphic column provides an outline of the major themes in the geological evolution of Venus in terms of fundamental processes such as tectonism [7] and volcanism [8]. The paucity of superposed [9] and embayed impact craters [10] and the impression that they are randomly distributed precluded the traditional counting of superposed craters on individual geological units to derive an impact crater size frequency distribution-based absolute chronology [11]. The utilization of techniques of buffered crater counting and related methods has recently provided a basis for linking the sequence of events in the geology/stratigraphy to an absolute chronology [12]. We now have an interpretative framework for the geologic history of Venus that we can use as a basis for testing models for the geological, thermal and geodynamic evolution of Venus.

The geological interpretative framework [6] shows that the geological history of Venus can be characterized by three basic consecutive phases (Fig. 1): **Phase I** represents the period prior to the formation age of the geomorphological/geological units on the surface (the pre-Fortunian Period) and occupies the majority of the history of Venus. Although some rocks comprising the oldest observed preserved unit, the tessera, could date from this era, the observed geologic record starts with Phase II. **Phase II** is comprised of two regimes, an initial *global tectonic regime* [8] which begins with the intense tectonic deformation (the Fortunian Period) interpreted to have formed the globally distributed tesserae highlands of thickened crust that comprise about 7.3% of the planet, followed by many tectonic structures in the surrounding highly deformed plains, including ridge belts, groove belts and coronae. The second regime in Phase 2, the *global volcanic regime*, [8] starts with the emplacement of volcanic plains dotted with thousands of small shield volcanoes, and is immediately followed by regional plains interpreted to have been emplaced as flood basalts in lows between the tesserae highlands, and then deformed by wrinkle ridges. The shield and regional plains comprise 61.3% of the surface of Venus. Thus, the vast majority of the observed surface geologic units on Venus (80.7%) formed over a relatively short period of time (the Fortunian and Guineverian Periods), estimated to have lasted less than several hundreds of millions of years. **Phase III** represents a distinctive change in style, an extended period of global network rifting (the Atlian Period), with rift zones often radiating from topographic rises; volcanism continues (perhaps to today [13]), but is primarily characterized by lobate lava flows associated with the rifts (the *network rifting-volcanism regime* [8]). In summary, geodynamic and thermal evolution models should be consistent with the geological record which consists of the majority of history leaving no geological/geomorphological record (Phase I), followed by Phase II, a period of intense global tectonic deformation followed immediately by global shield plains and regional plains volcanically resurfacing over 60% of the planet, followed by Phase III, relative quiescence and development of a global rifting system linking several broad rises. The last two phases occurred in less than the last ~15-20% of the history of Venus.

The advent of global image, topography and gravity data produced by Magellan led to a series of geodynamic models [14-15] that can be broadly categorized as follows (Fig. 2): *Volcanic Resurfacing Models*, in which massive flooding erases pre-existing craters and then volcanic activity essentially ceases [9], or constant very high rates of volcanic resurfacing produce a surface that erases craters as they are produced [16]. *Uniform-Evolutionary Models* explain the general geology by high rates of tectonic resurfacing followed by a rapid increase in the strength of the lower crust, leading to crustal stability and low rates of volcanic resurfacing [17], or a transition in the convective vigor of the mantle from a period of earlier rapid crustal recycling, to crustal stabilization and hot-spot volcanism [18]. In *Catastrophic-Episodic Models*, Venus periodically transitions from a global plate tectonic regime to a one-plate planet, and then back again, with the current geologic record representing an intermediate phase of the one-plate planet regime [19], or continuous vertical crustal accretion results in the buildup of a depleted mantle layer that is thermally and compositionally negatively buoyant and founders, causing global catastrophic deformation followed rapidly by global volcanism linked to the convective rise of fertile mantle; this is followed by relative quiescence until vertical crustal accretion repeats the process [20].

Comparison of these classes of models to the geologic record [6] (Fig. 2) leads us to currently favor the *catastrophic-episodic models*: for example, the depleted mantle overturn model [20] appears to account for the deformation observed in the tesserae (overturn)

and the nature of global volcanism in the shield plains followed rapidly by regional volcanism that could be due to near-global pressure-release melting of convectively rising fertile mantle, followed geologically rapidly by relative quiescence. Further modeling and model discrimination need to address several questions: 1) What is the history of long-wavelength topography and how does this provide data on thermal structure and evolution? 2) What is the composition of rocks that form the tesserae terrain? 3) Is there evidence for ancient periods of plate tectonics in the current geologic record? 4) Are the tesserae highlands due to Airy isostasy, Pratt isostasy, or thermal effects? 5) What factors dictate the scale of overturn and are they consistent with the observations? 6) What are the predictions of these models for the formation and evolution of the atmosphere and are they consistent with observations? We assess these models and questions.

References: 1) Campbell et al. 1997, *Venus II*, 503; 2) Barsukov et al. (1992) *Venus GGG*, U of A.; 3) Saunders et al. (1992) *JGR* 97, 13067; 4) Ford and Pettengill (1992) *JGR* 97, 13103; 5) Basilevsky and Head (2000) *PSS* 48, 75; 6) Ivanov and Head (2011) *PSS* 59, 1559; 7) Ivanov and Head (2013) *PSS* 84, 66; 8) Ivanov and Head (2015) *PSS* 113-114, 10; 9) Schaber et al. (1992) *JGR* 97, 13257; 10) Herrick et al. (1997) *Venus II*, 1015; 11) McKinnon et al. (1997) *Venus II*, 969; 12) Kreslavsky et al. (2015) *Icarus* 250, 438; 13) Shalygin et al. (2015) *GRL* 42, 4762; 14) Phillips et al. (1997) *Venus II*, 1163; 15) Schubert et al. (1997) *Venus II*, 1245; 16) Phillips et al. (1992) *JGR* 97, 15523; 17) Solomon (1993) *Physics Today* 46, 48; 18) Arkani-Hamed and Toksoz (1984) *PEPI* 34, 232; 19) Turcotte (1993) *JGR* 98, 17061; 20) Parmentier and Hess (1992) *GRL* 19, 2015. .

Figure 1. Stratigraphic units, sequence and timing of the geological history of Venus [6-8}

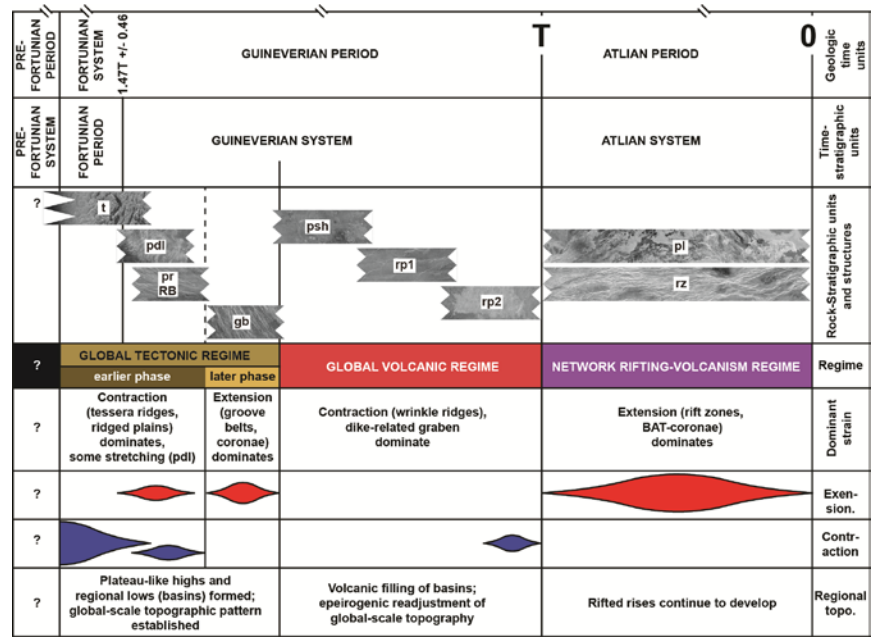

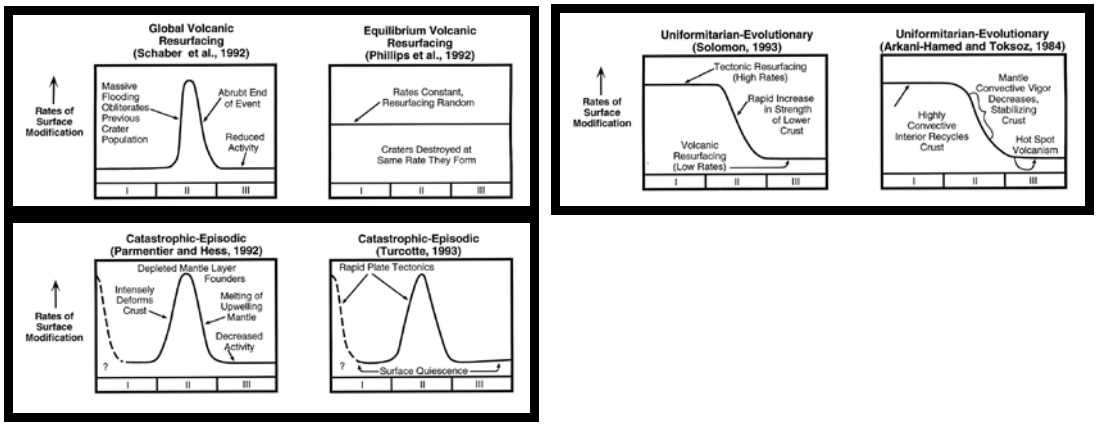

Figure 2. Synthesis of Venus geophysical/geodynamic models. Upper left: Volcanic resurfacing models. Upper right: uniform evolutionary models; Lower left: Catastrophic-Episodic models. I-III refer to the phases of geological history outlined in the text and [6].

VERITAS: HIGH-RESOLUTION IMAGING OF THE SURFACE OF VENUS TO ADDRESS CRITICAL SCIENCE QUESTIONS.

James W. Head[1], Scott Hensley[2], Suzanne E. Smrekar[2], M. Darby Dyar[3], Martha S. Gilmore[4] and the VERITAS Team. *[1]Department of Earth, Environmental and Planetary Sciences, Brown University, Providence, RI 02912 USA* (james_head@brown.edu); *[2]Jet Propulsion Laboratory,4800 Oak Grove Drive, Pasadena, CA 91109 USA* (shensley@jpl.nasa.gov; ssmrekar@jpl.nasa.gov); *[3]Mount Holyoke College, South Hadley, MA 01075 USA* (mdyar@mtholyoke.edu); [4]Earth and Environmental Sciences, Wesleyan University, Middletown, CT 06459 (mgilmore@wesleyan.edu).

The *Venus Emissivity, Radio Science, In-SAR, Topography, And Spectroscopy* (VERITAS) Mission is a Discovery mission that proposes to investigate the origin and evolution of Venus, the planet most like Earth. Its top-level goal is comparative planetology: how terrestrial planets evolve and how seemingly similar planets can evolve to significantly different outcomes. VERITAS [Smrekar et al. this conference] will accomplish this by testing specific hypotheses about current processes on Venus and assessing past history by acquiring and using new and superior global datasets. These will include images and a DEM from radar/INSAR, a multispectral map of NIR emissivity, a greatly improved gravity field, and detailed images and profiles of the atmosphere for a full Venus day.

VERITAS looks back into the history of Venus for evidence of relatively recent geologic processes and a possible Earth-like past, and helps to constrain the current atmosphere, and the climate evolution of Venus. VERITAS constrains the history of volcanism (today and over the past billion years) to determine the nature of recent tectonic and mantle convection processes and their influences on climate. VERITAS is designed to constrain the composition of surface materials and their alteration by the atmosphere, including highland areas that may preserve evidence of a water rich past, and also to assess possible recent volcanism.

To obtain data in support of these objectives, VERITAS carries a small, focused suite of instruments, with a capable telecom system, in low-altitude polar orbit. Among the instruments is the Venus Interferometric Synthetic Aperture Radar (VISAR), which produces a global digital elevation model (DEM) with 250-m horizontal and 5-m vertical resolution and SAR images of the surface at 30-m resolution [Hensley et al. this conference]. The combination of surface topography, elevation, and ~125 km resolution gravity data will provide unprecedented knowledge of the tectonic and impact cratering history of Venus, the timing and mechanisms of volcanic resurfacing, and the nature of mantle processes responsible for them. In addition the Venus Emissivity Mapper [VEM] will observe the surface in 6 spectral bands to constrain global changes in Fe mineralogy [Helbert et al., this conference]. VEM objectives include determining the composition and origin of tesserae and searching for recent and active volcanism.

VERITAS also has the capability of obtaining targeted high-resolution images at ~15 m resolution for up to about 20-25% of the planet in the primary mission. This capability offers unprecedented opportunities to address specific questions on a host of important and fundamental science question. Choices of high-resolution targets is so important that the VERITAS team is soliciting community input for both the planning stages of the mission (targets chosen prior to orbit insertion) and the operational stages of the mission (targets chosen following the initial acquisition and analysis of VERITAS image data). In this contribution we outline some of our initial ideas for high-resolution targeting, and solicit community input at and following the Venus 2016 Conference. Requests for further information and target suggestions can be addressed to james_head@brown.edu. Following is an abbreviated list illustrating the types of features and problems that we envision for high-resolution imaging targets:

Past and Future Missions:

1. Venera/VEGA Landing Site Regions: Place surface panoramas and analyses in context.
2. *Selection of Future Landing Sites*: Outline areas for future lander, rover and sample return missions.

Volcanic Activity and History:

1. Candidate Sites of Active Volcanism: Document Characteristics and possible changes. At least three major regions.
2. Volcanological Vent Characterization: Provides clear evidence for nature and effusion rates, etc.
3. Volcanological Emplacement Characterization: Data on surface roughness, flow structure, texture, channels, etc.
4. Evidence for Pyroclastic Activity: Assess proposed explosive volcanism areas and deposits; implications for magmatic volatile content.
5. Pancakes and Festoons: Viscous lavas and implications for global petrogenesis.
6. Canali characterization and stratigraphic relationships: Overbank, distal deposits, detailed structure, nested canali.

Chronology and History:

1. Characterization of globally defined units: Need specific characterization of each previously defined unit.
2. Age relationships of globally defined units: Need documentation and testing of contact relationships.
3. Impact Crater modification/embayment relationships: Have craters been modified in interiors, exteriors?
4. Layering in Impact Crater Walls: What types of layering are exposed in tesserae (e.g., Khatun Crater in Tellus) and in the plains.
5. Layering in Tellus Regio: Lava flows or sedimentary?

Tectonic Structures and Evolution:

1. Wrinkle Ridge/Ridge Belt Formation, Chronology and Stratigraphy: What are structural and embayment relationships?
2. Graben/wrinkle ridge stratigraphy: Critical relationship for regional and global lithospheric state of stress.
3. Rift Zones Tectonic/Volcanic Relationships: Stratigraphy and timing of rifting and volcanism, modification of slopes.
4. Testing Predictions of Candidate Subduction Zones:

Detailed features predicted by flexure, subduction.

Tessera Origin and Evolution:

1. Nature of Pristine Tessera: Compare "pristine" tessera and tessera "modified" by impact airfall.
2. Nature of Tessera Domains: What defines the differences in structural domains (folds, syntaxes, shear zones, etc.).
3. Tessera structural chronology: What is the sequence of structural events in tesserae (folds, faults, ribbon terrain, etc.).

Other Processes/Features:

1. Significance and rates of Eolian Resurfacing: Nature and movement of dunes and parabolas. Does impact airfall produce the indurated deposits seen at Venera lander sites?
2. Nature of Altitude-Dependent "Snowline" Boundaries: Layers, coatings, grain size?

Targeting Approach: The primary mission consists of Science Phase I, when the orbiter is in a highly elliptical orbit prior to aerobraking, and Science Phase II, when the spacecraft is in low circular orbit. VEM observes during the relatively short Science Phase I, potentially providing new sites of recent or active volcanism. In Science Phase II, the spacecraft completes 3 cycles, in which Venus makes 3 complete rotations under the spacecraft, providing 3 opportunities to observe any location with VISAR. VEM observes the surface while on the nightside of Venus [Helbert et al., this conference].

VISAR will be continuously observing the surface, expect during communications passes. Nominal mapping consists of a global DEM and 30 m resolution image data acquisition. High-resolution (15 m) image targets and repeat pass interferometry (RPI) targets will be acquired over selected, high priority targets, as described above. The number of RPI targets allows for sampling the full range of geologic environments where there is evidence for current or recent volcanic activity [1-3]. The total number of high-resolution targets can be increased through the use of optical communications and during an extended mission.

References: [1] Bondarenko et al. (2010) *GRL* 37, L23202; [2] Shalygin et al. (2015) *GRL* 42, 4762; [3] Smrekar et al. (2010) *Science* 328, 605; doi:10.1126/science.1186785

Acknowledgement: A portion of this research was conducted at the Jet Propulsion Laboratory, California Institute of Technology, under contract with the National Aeronautics and Space Administration.

.

THE VENUS EMISSIVITY MAPPER (VEM) CONCEPT. J. Helbert[1], D. Wendler[1], I. Walter[2], T. Widemann[3], E. Marcq[4], A. Maturilli[1], S. Ferrari[5,1], M. D'Amore[1] , N. Müller[6], M. D. Dyar[7], and S. Smrekar[6], [1]Institute for Planetary Research, DLR, Rutherfordstrasse 2, 12489 Berlin, Germany (joern.helbert@dlr.de), [2]Institute for Optical Sensorsystems, DLR, Rutherfordstrasse 2, 12489 Berlin, Germany,[3]LESIA,[4]LATMOS, Université Paris-Saclay, [5]Department of Earth and Environmental Sciences, University of Pavia, Via Ferrata 1 - 27100 Pavia, Italy, [6]Jet Propulsion Laboratory, California Institute of Technology, 4800 Oak Grove Dr., Pasadena CA, 91109, [7]Dept. of Astronomy, Mount Holyoke College, South Hadley, MA 01075.

Based on experience gained from using the VIRTIS instrument on Venus Express to observe the surface of Venus and the new high temperature laboratory experiments, we have developed the multi-spectral Venus Emissivity Mapper (VEM) to study the surface of Venus. VEM imposes minimal requirements on the spacecraft and mission design and can therefore be added to any future Venus mission. Ideally, the VEM instrument will be combined with a high-resolution radar mapper to provide accurate topographic information, as it will be the case for the NASA Discovery VERITAS mission [1] or the ESA EnVision M5 proposal [2].

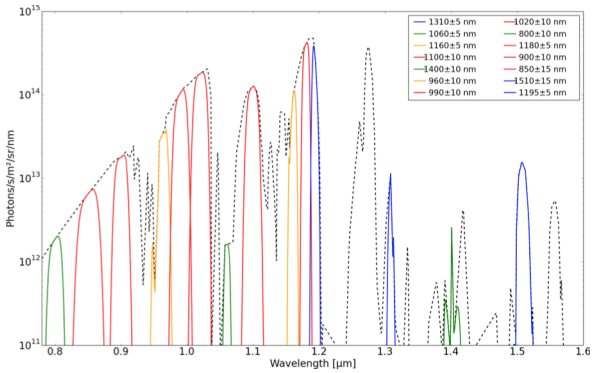

Figure 1. VEM current filter selection, the dashed envelope is a synthetic Venus night side spectrum [3] – Red are surface bands, blue bands for cloud correction, green straylight correction and yellow bands to detect water vapor [4]

The permanent cloud cover of Venus prohibits observation of the surface with traditional imaging techniques over most of the visible spectral range. Fortunately, Venus' CO_2 atmosphere is transparent in small spectral windows near 1 μm (**Figure 1**). Ground observers have successfully used these windows during the flyby of the Galileo mission at Jupiter and most recently for the VMC and VIRTIS instruments on the ESA Venus Express spacecraft. Observations have revealed compositional variations correlated with geological features, but existing data sets contain only a few channels. VEM offers an opportunity to gain significant information about surface iron-bearing mineralogy by virtue of having five different channels for surface observations.

The VEM concept: VEM is focused mainly on observing the surface, mapping in all near-IR atmospheric windows using filters with spectral characteristics optimized for the wavelengths and widths of those windows. It also observes bands necessary for correcting atmospheric effects [4]; these bands also provide valuable scientific data on cloud thickness, cloud opacity variations, and particle size distribution and H_2O abundance variations in the lowest 15 km of the atmosphere [3].

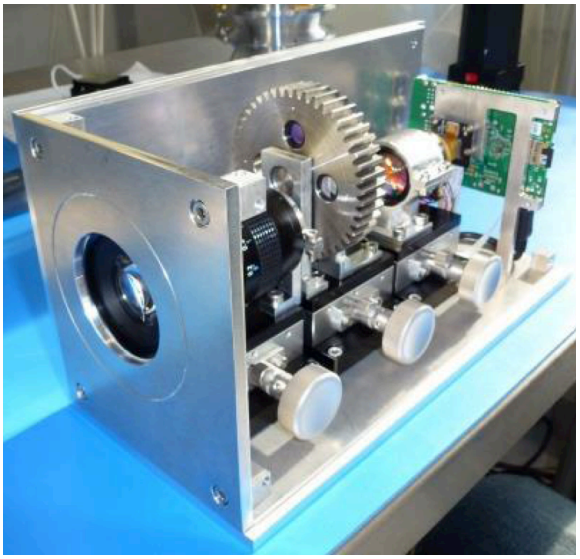

Figure 2. First VEM breadboard with telecentric and relay optics, however using filter wheel instead of filter array.

VEM is a pushbroom multispectral imaging system. A baffle protects VEM from scattered light. Telecentric optics image the scene onto the filter array. This image is relayed by a four-lens objective onto the detector. The field of view (FOV) of the optics is 30º, yielding a swath width of 113 km at an altitude of 215 km to provide comprehensive sampling of the surface emissivity and repeat coverage between tracks.

To split the light into several bands, VEM uses a multilayered dielectric-coating ultranarrow-band filter array instead of a grating to maximize the signal to the detector. The filter array is located at an intermediary focus of the optical path. We image each band onto the

17 512-pixel rows of the detector. The surface bands are spatially sandwiched between the cloud bands to provide calibration before and after each surface data acquisition.

To minimize VEM development risk, a model philosophy with a prototyping approach has been utilized. Combined with the extensive test program planned using test facilities at DLR in Berlin, this ensures that performance issues are identified early and can be mitigated without endangering the development schedule.

A first very simple breadboard [6] for VEM has been set up (**Figure 2**) and is currently used for testing with the high temperature chamber at PEL [7,8] measuring Venus analogs at typical Venus surface temperatures.

Laboratory experiments: Measuring emissivity at 1 μm at Venus analog temperatures is already very challenging for many reasons. For example, the emissivity of stainless steel used to heat samples via induction increases strongly towards shorter wavelength at high temperatures. This results in a non-negligible contribution to total radiance from our sample cups. At the same time, many natural materials have a high transparency at 1 μm. To solve both issues at the same time, we are currently limiting ourselves to slabbed samples of materials with low transparency that are heated by placing them on a stainless steel disk completely obscured by the sample.

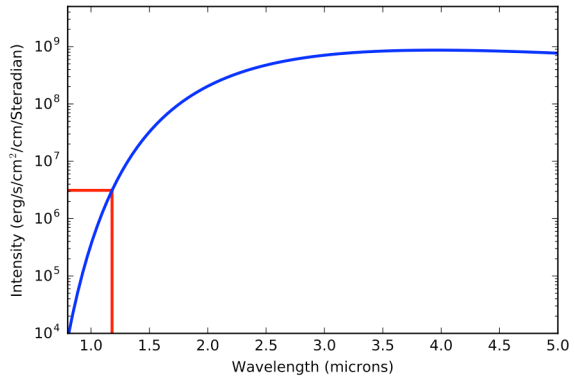

Figure 3: Blackbody curve at Venus surface temperature – within the range covered in our measurements the signal decreases by more than two orders of magnitute

Extending the measurements below 1 μm adds significant new challenges. The main challenge is the very low thermal emission due to the fact that we are on the steep flank of the Planck curve (**Figure 3**). Between 1.18 μm and 0.8 μm the signal drops by more than two orders of magnitude.

Therefore even the use of a steel disk under the slab for heating seems not to be enough. The glow of the steel scattered in the chamber becomes a non-negligible noise term that results in an apparent increase of the emissivity around 0.9 μm. We are currently testing a baffling system (**Figure 4**), which improves the situation but cannot solve it completely.

Figure 4. Current test configuration in the chamber – Sample at 450°C illuminated by the glowing steel disc.

Work on this challenge is ongoing.

Still the preliminary results [8] confirm our early measurements for basalt and extend them for the first time below 1 μm. There remains a continuum contribution from the scattered light, which has to be removed by improvements in the setup.

Conclusion: Observing the surface of Venus in the near infrared requires a dedicated instrument. VIRTIS observations have successfully demonstrated that important information can be extracted from the windows in the visible portion of the spectrum, but the design of the instrument limited its use for surface investigations. Deploying an instrument like VEM in orbit or on an aerial platform will provide new insights into the mineralogy of Venus. In combination with a high-resolution radar mapper that provides accurate topographic data as planned for the VERITAS mission or for the ESA EnVision mission proposal, this will allow a global mapping of the surface composition at a spatial scale of approximately 50 km [1,2,9]. Combining the near infrared data with radar derived geological information will allow further conclusions on the evolution of Venus to be drawn.

References: [1] Smrekar S. et al. (2016) this meeting. [2] Ghail, R. et al. (2016) this meeting. [3] Wilson C.F. et al. (2009) Icarus, 814-817 [4] Helbert J. et al. (2013) Infrared Remote Sensing Instrumentation XXI, 8867, doi: 10.1117/12.2025582. [5] Mueller N. et al. (2008) JGR, 113(E5), 1–21. [6] Wendler D. et al (2015) http://elib.dlr.de/101033/ [7] Helbert J. et al. (2013) *EPSL*, 369-370 [8] Helbert J. et al. (2016) LPSC #1947 [9] Hensley S. et al. (2016) LPSC #1947.

VERITAS: A PROPOSED NASA DISCOVERY MISSION TO VENUS WITH An X-BAND INTERFEROMETRIC MAPPING RADAR

S. Hensley, S. Smrekar, *Jet Propulsion Laboratory, California Institute of Technology, US (scott.hensley@jpl.nasa.gov@jpl.nasa.gov)*, **R. Seu, P. Lombardo**, *University of Rome La Sapienza, Roma, Italy* and **N. Mueller, J. Helbert**, *Deutsches Zentrum für Luft- und Raumfahrt, Berlin, Germany* and **The VERITAS Science Team**

Introduction: NASA has selected 5 potential Discovery class missions for additional study prior to down selection of one or two missions in early 2017 [1]. The **V**enus **E**missivity, **R**adio Science, **I**nSAR **T**opography **A**nd **S**pectroscopy (VERITAS) Mission is a proposed mission to Venus that was selected as one of these missions. It is designed to obtain high-resolution imagery and topography of the surface, using an X-band radar configured as a single pass radar interferometer (called VISAR) and a multi-spectral NIR emissivity mapping capability (called VEM).

Magellan, a NASA mission to Venus in the early 1990s, mapped nearly the entire surface of Venus with an S-band (12 cm) synthetic aperture radar and microwave radiometer and made radar altimeter measurements of the topography, [2]. Although these measurements revolutionized our understanding of the geophysical processes that have shaped the evolution of the surface of Venus, the lack of finer resolution imagery and topography of the surface than that obtained by Magellan has hindered finding the answers to key questions concerning the processes and evolution of the surface.

VERITAS Science Objectives: A deep understanding of solar system evolution is limited by a great unanswered question: How Earthlike is Venus? We know that these twin planets formed with similar bulk composition and size. Yet Venus followed a divergent evolutionary path, losing its surface water and becoming hotter than Mercury. How did this happen? The answer has profound implications for the potential for life in the universe and how terrestrial planets become habitable.

The proposed VERITAS mission is designed to probe the geologic evolution of tesserae, look for buried features in plains of Venus, resolve the chronology of resurfacing events and look for signatures of tectonic deformation, e.g., subduction. VERITAS will look for evidence of geologic processes that are currently operating on Venus including volcanism, weathering and faulting. Finding evidence of past water through mineralogical investigations or present water through volcanic outgassing has major implication for the geologic evolution of Venus.

Instrument Overview: The VISAR instrument is a single pass interferometric X-band radar with a wavelength of 3.8 cm designed to obtain both global imagery and topography measurements of the surface of Venus. Radar requirements were predicated on answering key questions about the evolution of the surface of Venus and how Venus evolved so differently than Earth [3].

Topographic mapping accuracy requirements are the driver for the VISAR design as a single pass radar interferometer. The operating frequency of X-band was dictated by two primary factors, the attenuation in the Venus and spacecraft accommodation. A best comprise between these factors was used to set the operating frequency.

The radar operates with a bandwidth of 20 MHz that results in a range resolution of 7.5 m, which projects to a ground resolution of 15 m. The radar has a 0.6m×3.9m antenna resulting in a 14.5 km swath width and an azimuth resolution of 2 m. The radar is designed to generate 15 m imagery with at least 7 looks and topographic maps with a posting of 250 m and a height accuracy of 5 m. See [3] for more details. Figure 2 shows a diagram of the instrument and the imaging geometry.

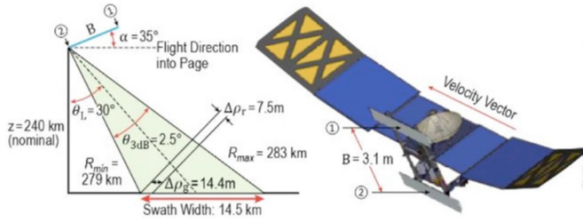

Figure 2. *VISAR flight configuration and observing geometry are optimized for InSAR DEM acquisition with baseline separation B = 3.1 m, look angle of θl=30°, range resolution of Δρr=7.5 m, range of ρ=281 km and swath width of 14.5 km at an altitude of 240 km (high end of altitude range of platform).*

Radar Operations: The VISAR radar will operate from an average altitude of 220 km and have a look angle of 30°. Data will be collected on both ascending and descending orbits for about 11 orbits before turning to Earth for 5 orbits to downlink this data. The resulting gap will be filled in during the subsequent cycle (1 cycle = 1 Venus sidereal day=243.015 days). Because the raw data volume is too large to downlink to Earth onboard processing of the raw data to interferograms reduces the data volume 1000 is done prior to downlink fold [3]. An exception to this is raw data is downlinked for targeted regions where inter-cycle repeat pass radar interferometry will be used to look for surface deformation either from volcanoes or faults [4, 5]. The

thick Venus atmosphere permits such observations as shown in [6].

VISAR Products: Planned products to be generated by the VISAR radar include:

- Global 30 m medium resolution X-band backscatter imagery of the surface at 31° incidence angle (30° look angle).
- High-resolution 15 m resolution imagery of targeted areas covering approximately 23% of the planet surface. See Figure 3 for a comparison of Magellan and VERITAS imagery for various science investigations.

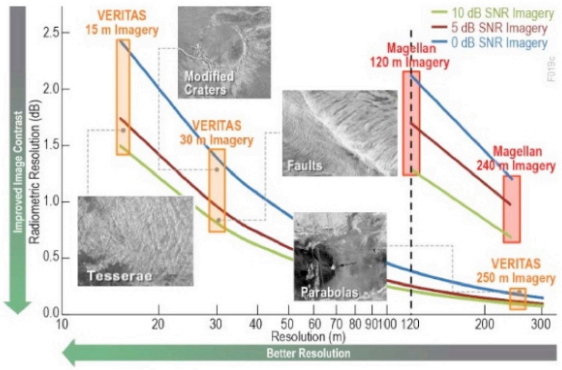

Figure 3. *Radiometric resolution of Magellan data is insufficient to look for subtle variation in backscatter in very radar dark regions, e.g., parabolas. For example, Magellan data are inadequate to observe the mechanisms removing the very dark extended impact crater ejecta deposits and unequivocally determine if they are volcanically flooded. At present it is almost always impossible to determine the stratigraphy of extended ejecta blankets relative to features such as lava flows that intersect with the ejecta. Roughly 80% of impact craters have dark floors. If they are dark due to volcanic flooding, the surface age is reduced by a factor of 2-5 [7]. VERITAS will provide the altimetry and high-resolution images needed to unambiguously resolve impact crater modification and thus the whether or not Venus catastrophically resurfaced.*

- Topographic maps with a spatial resolution of 250 m and a height accuracy of 5 m. The estimated height accuracy includes atmospheric losses, radar backscatter variations (estimated by converting S-band Magellan measurements to X-band) and the radar imaging geometry. During Phase A we will estimate performance spatially based on Magellan backscatter and topography and generate histograms of expected performance as a function of backscatter, elevation and various terrain types. Different terrain types have different combinations of slope and backscatter.
- Another new data layer for planetary sciences will be an elevation precision layer associated with the topography product made possible using radar interferometry for elevation measurements. This product will provide an estimate of the elevation precision for each elevation measurement based on the single pass interferometric correlation and mapping geometry. Thus, users will be able to see areas where elevation measurements are more or less precise and factor that into their analyses. For example, this layer can be used in generating maximal likelihood slope estimates.
- Repeat pass interferometric maps of surface deformation for approximately 12 targeted regions with dimensions of 200km×200km. Allowable numbers and target dimension are being further investigated during Step II. See [6].
- Repeat pass correlation maps, which after correcting for SNR correlation (that can be estimated from the single pass data), can be used to generate bounds on the amount of temporal and volumetric correlation. Temporal correlation can be used to infer sub wavelength (3.8 cm) scale changes on the surface.

Tie points between overlapping mapping strips will be used to improve the ephemeris and in a bundle adjustment procedure to remove residual cross-track elevation tilts due to baseline and other sensor calibration errors prior to mosaicking the strips.

One of our key science objectives will be to assess if Venus is geologically active. One means of looking for recent activity will be comparison of VISAR imagery to Magellan imagery. Differences in wavelength, incidence angle and look direction (for some imagery since Magellan alternated look direction between cycles) will complicate this assessment. To mitigate these problems we plan to look for changes in regions with distinct morphological boundaries above a particular area threshold (conservatively ~25 km^2). Additionally, DLR's airborne F-SAR radar has acquired simultaneous data at X- and S-bands over representative volcanic surfaces to provide actual X to S-band backscatter comparisons that can be used to tune change detection algorithms.

VISAR and VEM: The combination VISAR and multispectral NIR emissivity observations is integral to achieving the science objectives. VISAR will provide the resolution and accuracy of topographic measurements to decouple atmospheric from surface returns. Their combined measurements enable both mineralogy, via VEM, and geomorphology and surface chronology via a combination VISAR and VEM.

References:

[1] Brown and Cantillo, *NASA News*, 30 Sep 2015. [2] Saunders, R. et al. (1992) *JGR*., 97:13,06713,09 [2] S. Smrekar, et al., (2016) LPSC XLVII. VERITAS Mssion [3] Hensley, S. et al. (2015) Proc Asia Pacific SAR [4] Smrekar, S.E., et al. (2010) Science, 328 [5] Shalygin, E. et al. (2015) GRL, 42. [6] Hensley, S., and S. Shaffer (2010), LPSC XLI, Abstract #2369. [7] Herrick, R.R. and M.R. Rumpf (2011) *JGR 116*, E02004.

Acknowledgement: A portion of this research was conducted at the Jet Propulsion Laboratory, California Institute of Technology, under contract with the National Aeronautics and Space Administration.

INITIAL STEREO MATCHING TESTS WITH MAGELLAN OPPOSITE LOOK DATA.

R. R. Herrick, *Geophysical Institute, University of Alaska Fairbanks, Fairbanks, AK, USA (rrherrick@alaska.edu)*

Introduction:

The Magellan mission collected SAR images over 3 Venusian days, or "Cycles". During Cycle 3 stereo images with the same look direction (~20° angular separation) as Cycle 1 were collected for ~20% of the planet; our successful processing of this data [1] using an iterative cross-correlation stereo radargrammetry method generated topography with 1-2 km horizontal resolution, a great improvement over Magellan altimetry. We could produce a significant new data set if we could achieve anywhere near this level of success with the opposite-look Magellan data collected during Cycle 2; the opposite-look data covers a larger portion of the planet (~40%), and the images are more contiguous and have a higher signal-to-noise ratio. Unfortunately, the opposite-look images are much harder to work with in an automated fashion and are simply not amenable to image matching using cross-correlation. Figure 1 illustrates the problem; it shows a steep-sided volcanic dome in the Cycle 1, Cycle 2, and Cycle 3 Magellan imaging. In opposite-look data, topographic slopes produce opposing changes in image brightness (i.e., a slope is bright in one image and dark in the other), but changes in surface roughness or dielectric constant produce similar changes in both images. In terms of a cross-correlation algorithm, geologic features can thus be both correlated and anticorrelated between the two images. Here I discuss initial results attempting to develop automated methods to conduct stereo photogrammetry between opposite-look pairs. I focus on two approaches: 1) pre-processing of the SAR image pairs to enhance the roughness/material-properties (similar between images) and reduce/change the slope-caused differences; and 2) use another "similarity measure" besides cross-correlation. The methods being tried could potentially be valuable as a risk-mitigation strategy for the VERITAS mission, as the techniques being developed could be used for stereo matching between VERITAS X-band images and the Magellan images in order to produce topography, should single-pass InSAR prove unsuccessful.

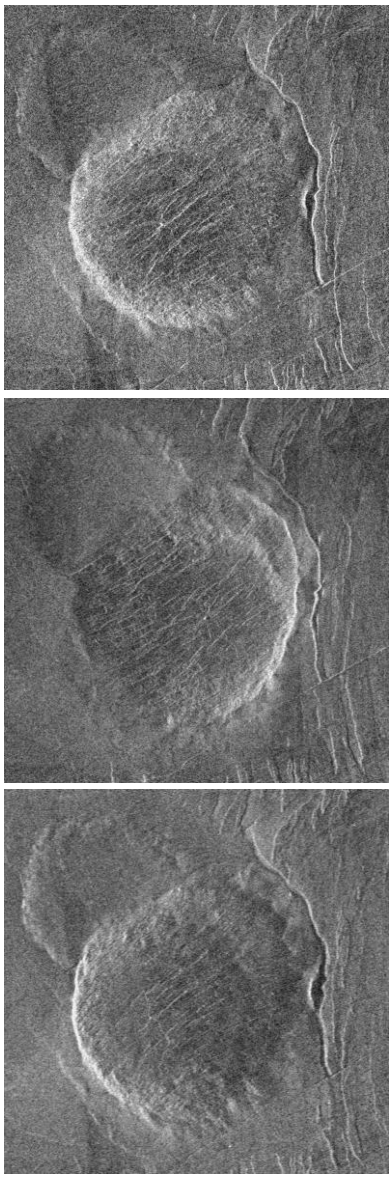

Figure 1. From top to bottom, Cycle 1, Cycle 2 ("opposite look"), and Cycle 3 ("same-side stereo") images of a steep-sided dome on Venus located at 26 S, 80 E. Image is 60 km across. Note that the pattern of fractures on top of the dome looks similar in all three images, but slopes striking North-South look very different in the Cycle 2 image.

Pre-processing of images:

We have been trying a few different approaches to pre-processing the SAR images. In general terms, variations in surface roughness, and small-scale fracturing and cracking, on low-slope terrains look similar between the left- and right-looking images, as do features oriented parallel to the look direction (i.e., perpendicular to the parallax direction). A couple of approaches we are testing are directional filtering to reduce the albedo effects of radar-facing slopes, and edge-detection algorithms that should produce a similar-albedo edge from opposite-albedo slopes. A problem, however, is that both techniques also accentuate high-frequency noise.

Mutual Information Techniques:

Mutual information techniques [e.g., 2] have the

potential to overcome the problem that slopes produce brightness variations of opposite polarity while roughness produces variations of the same polarity. The basic idea with mutual information is that images with matching patterns will have the same distribution of intensities within a histogram, even if the values within the histogram are different. In other words, mutual information relies on minimizing the mapping of pixel values from one image to another. As a thought exercise, imagine two five-colored shirts with matching patterns. We would be able to match images of the shirts with the mutual information technique, even if all of the colors were different between the two shirts. However, cross-correlation would require that the relative darks and lights be the same between the two shirts. The idea then, with opposite-look Magellan data, is that slopes striking perpendicular to the radar produce a different brightness than the rest of the image, and it should not matter to the mutual information technique whether that difference is an increase or decrease.

Status and the Remaining (Big) Problem:

While tests with both pre-processing the images and matching using mutual information produced success in small, carefully selected samples (e.g., Figure 2), after working with the data for a while it is clear that the primary problem with the opposite-look data is not the slope/roughness ambiguity, which the mutual information technique can adequately handle. It is that the parallax is simply too great between the opposite look images. All of the potential automated matching algorithms, including mutual information, rely on a similarity of the basic pattern of the image, regardless of the polarity and strength of the albedo differences. Our approach to dealing with this particular issue will be to first try a partial orthorectification of the opposite look images using the Magellan altimetry data. The large angular separation between the opposite-look images means that if one can successfully collect match points, then the vertical resolution of the data will be substantially better than the same-side stereo results.

References: [1] Herrick, R. R. et al. (2012) *EOS, 93*, 125-126. [2] Cole-Rhodes, A. A. and Varshney, P. K. (2011) in *Image Registration for Remote Sensing*, Le Moigne et al., eds., 131-149.

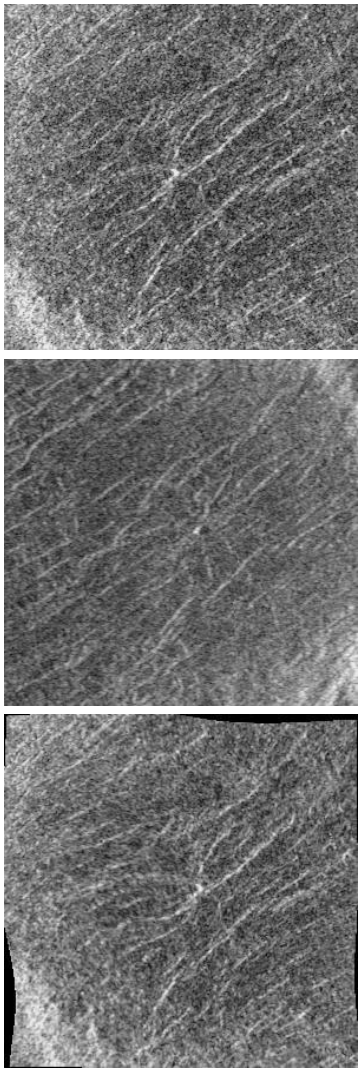

Figure 2. Top of dome in Figure 1. Top image is Cycle 1 image, middle is Cycle 2 image, and bottom is Cycle 1 warped to Cycle 2 using mutual information technique to obtain match points between the Cycle 1 and Cycle 2 images. Note that in the bottom image that the central pit is correctly moved to its corresponding location in the Cycle 2 image. Image is 22.5 km across.

Analysis of deep inversions at the Tropopause of Venus: new insights from the Radio Science Experiment (VeRa) onboard Venus Express

M. Herrmann, *Rheinisches Institut für Umweltforschung, Cologne, Germany (maren.herrmann@uni-koeln.de)*, **B. Häusler**, *Institut für Raumfahrttechnik, Universität der Bundeswehr, Munich, Germany*, **J. Oschlisniok, S. Tellmann, M. Pätzold,** *Rheinisches Institut für Umweltforschung, Cologne, Germany*, **S. Remus,** *ESTEC, Noordwijk, the Netherlands*

Abstract:

The inversion layer at the tropopause of the Venus atmosphere is a very common and prominent feature in the vertical temperature profile at higher latitudes. The inversion layer is of particular interest because it separates the stratified troposphere from the highly variable mesosphere. The altitude of the inversion layer can therefore be regarded as a likely location for the formation or presence of eddies or gravity waves [1]. The Radio Science Experiment (VeRa) onboard Venus Express [2,3] is capable to sound the Venus atmosphere from 100 km downward to 40 km [4,5] and delivered more than 800 vertical profiles of temperature, pressure and neutral number density at almost all local times and latitudes. The profiles include the tropopause which is typically located at 60 km altitude. Spatial changes of the refractive index over a short altitude range lead to multi-path effects which cannot be fully retrieved with common closed-loop recording methods. The development of a new data processing tool relying on VeRa open loop data sets provided the necessary frequency resolution to fully resolve multipath effects. The high resolution temperature profiles reveal a thin layer (only a few hundred meters thickness) which can be up to 15K colder than measured with the closed loop receiver technique.
The first occultation seasons have been analyzed and the global distribution of multipath affected profiles regarding also their dependency on local time will be shown. The new results will help finding a more consistent picture of the Venus' atmosphere for the improvement of atmospheric models.

Bibliography

[1] Tellmann, S., Häusler, B., Hinson D.P., Tyler, G.L., Andert, T.P., Bird, M.K., Imamura, T., Pätzold, M. and Remus, S.: 'Small-scale temperature fluctuations seen by the VeRa Radio Science Experiment on Venus Express'

[2] Häusler, B., Pätzold, M., Tyler, G.L., Simpson, R.A., Bird, M.K., Dehant, V., Barriot, J.-P., Eidel, W., Mattei, R., Remus, S., Selle, J., Tellmann, S. and Imamura, T.: 'Radio science investigations by VeRa onboard the Venus Express spacecraft' Planetary and Space Science 54, 2006

[3] Häusler, B., Pätzold, M., Tyler, G.L., Barriot, V.J.-P., Bird, M.K., Dehant, V., Hinson, D., Simpson, R.A., Treumann, R.A., Eidel, W., Mattei, R., Rosenblatt, P., Remus, S., Selle, J. and Tellmann, S.: , 'Venus Atmospheric, Ionospheric, Surface and Interplanetery Radio-Wave Propagation Studies with the VeRa Radio Science experiment' Eur. Space Agencys, Spec. Publ., ESA SP 1295, 2007

[4] Pätzold, M., Häusler, B., Bird, M.K., Tellmann, S., Mattei, R., Asmar, S.W., Dehant, V., Eidel, W., Imamura, T., Simpson, R.A. and Tyler, G.L.: 'The structure of Venus' middle atmosphere and ionosphere', Nature 450, 2007

[5] Tellmann, S., Pätzold, M., Häusler, B., Bird, M.K. and Tyler, G.L.: 'Structure of the Venus neutral atmosphere as observed by the Radio Science experiment VeRa on on Venus Express', Journal of Geophysical Research 114, 2009

REVIEWING VIRTIS-M MEASUREMENTS OF VENUS WINDS AT DIFFERENT ALTITUDES: GLOBAL CIRCULATION AND SOUTH POLAR VORTEX

R. Hueso, *Universidad del País Vasco (UPV/EHU), Bilbao, Spain (ricardo.hueso@ehu.eus)*, **I. Garate-Lopez**, *Universidad del País Vasco (UPV/EHU), Bilbao, Spain*, **A. Sánchez-Lavega,** *Universidad del País Vasco (UPV/EHU), Bilbao, Spain*, **J. Peralta**, *Institute of Space and Astronautical Science (ISAS), Kanagawa, Japan*, **A. García-Muñoz**, *Zentrum für Astronomie und Astrophysik, Technische Universität Berlin, Berlin, Germany,* ***G.*** **Piccioni**, INAF-*IAPS Rome Italy,* **P. Drossart**, *Observatoire de Paris, CNRS, UPMC, Univ. Paris-Diderot, Paris, France.*

Introduction:

Multi-spectral images obtained by the VIRTIS-M instrument onboard Venus Express have resulted in a treasure of observations that permit to study the atmospheric dynamics of the planet at different vertical layers over a long temporal interval. Measurements extend from the lower clouds at 45 km to the mesosphere tracing motions of oxygen airglow at around 95 km, with coverage of the cloud top at 70 km in the UV side of the visible channel. Views of the South Polar area enabled to study the dynamics of the enigmatic polar vortex. The spectral resolution of VIRTIS and its coverage of thermal radiation allow to obtain thermal maps from the upper clouds up to the mesosphere that are simultaneous to the wind measurements and allow obtaining maps of potential vorticity. Therefore, a large effort has been devoted to study the polar area and understand the vortex dynamics. In this contribution we review and combine results from previous analysis on wind motions from VIRTIS-M data.

Global dynamics of the Southern hemisphere

Several papers have been published detailing the atmospheric dynamics at different cloud layers and over different time intervals as more and more was gathered by Venus Express [1-3]. The three-dimensional structure of the winds (longitudinal, latitudinal and vertical structure from 45-70 km) was presented for an early period of data years 2006-2007) and further measurements of the lower cloud were presented covering the years 2006-2008 [2]. A later work extended results of the upper cloud with data that extended up till 2012 and producing results of an intermediate level observable in visible to near-IR wavelengths (500-900 nm) [3]. In those works indications of temporal variability were examined and considered compatible with the overall error measurements showing a global stable atmosphere with winds that do not exhibit drastic changes in time. For the upper cloud, observable in UV wavelengths, the most interesting results were the determination of the meridional circulation with a Hadley cell global motion peaking at -50º latitude, and the acceleration of the zonal and meridional winds over the local afternoon hours with motions that reach their maximum around 15-16 local time hours. The overall results for the upper cloud (best observed in UV light) agreed with overall results from the VMC camera [4]. However, there are evident differences in the interpretation and quantification of variability between the results published from both instruments and these will be reviewed in this contribution.

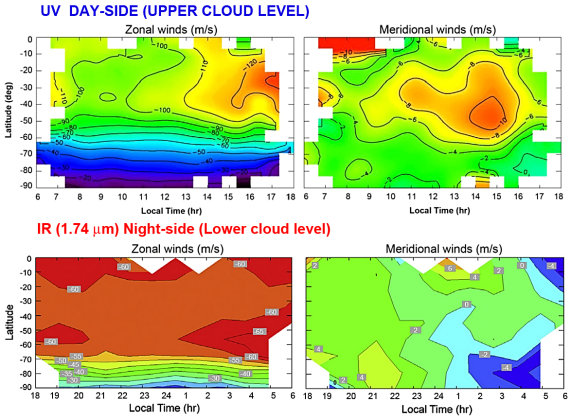

Figure 1: Zonal and meridional structure of the winds in the upper cloud level in the day-side and in the lower cloud level at night-side [2-3].

Venus South polar vortex

The elliptical orbit followed by Venus Express resulted in about 2 years of high-quality thermal infrared observations of a South Polar Vortex in Venus similar to its equivalent in the North hemisphere observed by Pioneer Venus in the 70s. The vortex is tangentially illuminated by solar light and is best observed in thermal images acquired at 3.8 and 5.1 μm sensitive to the thermal emission from the upper cloud levels [5]. The warm vortex is a vertically depressed structure with a depressed cloud top [6]. Observations at 1.74 μm establish that the vortex extends at least down to the lower cloud level (this is from the cloud top at 58-64 km to the lower cloud at 43 km) with significant changes in its morphology and motions [7, 8]. The motions do not correlate highly with the fine-scale structures observable in the infrared images.

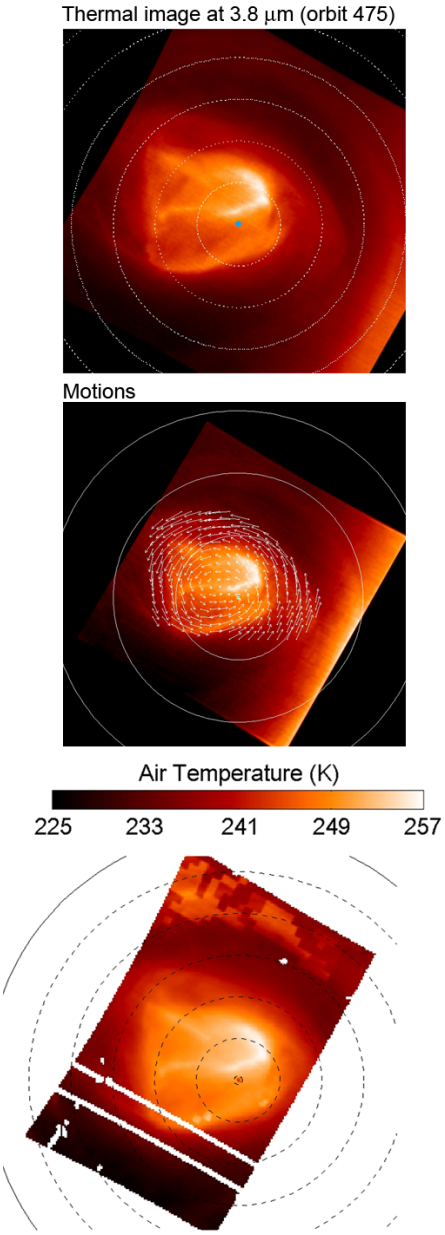

Figure 2: Example of vortex morphology in thermal infrared, motions and retrieved air temperature at cloud level.

The thermal structure of the warm vortex and the surrounding cold collar can be retrieved in high spatial resolution from VIRTIS-M spectral data in the 4.2 and 5.1 μm, but excluding the spectral region dominated by the CO 1–0 fundamental band from 4.52 to 4.80 μm region [9]. The thermal analysis shows a high correlation between 3.8, 5.1 μm images and temperature maps at the cloud top. From the motions extracted from tracking features in the images and the thermal analysis we can compute maps of potential vorticity (PV) at the cloud top that show the vortex as a small vorticity perturbation over the general state of the polar atmosphere [10]. Uncertainties in the fine-scale spatial derivatives of the wind motions do not permit to extract small scale features in these PV maps. The structure observed in many of the EPV maps at the upper cloud's level point to a weak ring of potential vorticity without any strong latitudinal gradient of PV, as should be expected in the presence of a mixing barrier. However, the thermal differences between the warm and vertically depressed vortex and the cold collar may effectively separate both regions.

References

[1] A. Sánchez-Lavega, et al., Variable winds on Venus mapped in three dimensions, Geophys. Res. Lett., 35, L13204 (2008).

[2] R. Hueso, J. Peralta, A. Sánchez-Lavega, Assessing the Long-Term Variability of Venus Winds at Cloud Level from VRTIS-Venus Express, Icarus 217, 585-598 (2012).

[3] R. Hueso, J. Peralta, I. Garate-Lopez, T. V. Bandos, A. Sánchez-Lavega, Six years of Venus winds at the upper cloud level from UV, visible and near infrared observations from VIRTIS on Venus Express, Planet. Space Sci., 113-114, 78-99 (2015).

[4] I.V. Khatuntsev, M.V. Patsaeva, D.V. Titov, N.I. Ignatiev, A.V. Turin, S.S. Limaye, W.J. Markiewicz, M. Almeida, Th. Roatsch, R. Moissl, Cloud level winds from the Venus Express Monitoring Camera imaging, Icarus 226, 140-158 (2013).

[5] G. Piccioni, et al. South-polar features on Venus similar to those near the north pole. Nature 450, 637-640 (2007).

[6] Titov, D. V. et al. Atmospheric structure and dynamics as the cause of ultraviolet markings in the clouds of Venus. Nature, 456, 620-623 (2008).

[7] I. Garate-Lopez, R. Hueso, A. Sánchez-Lavega, J. Peralta, G. Piccioni & P. Drossart, A chaotic long-lived vortex at the southern pole of Venus. Nature Geoscience, 6, 254-257 (2013).

[8] D. Luz et al. Venus's Southern Polar Vortex Reveals Precessing Circulation. Science, 332, 577-580 (2011).

[9] I. Garate-Lopez, A. García Muñoz, R. Hueso, A. Sánchez-Lavega, Three-dimensional Thermal Structure of the South Polar Vortex of Venus. Icarus, 215, 16-31 (2015).

[10] I. Garate-Lopez, R. Hueso, A. Sánchez-Lavega and A. García Muñoz, Potential vorticity of the South Polar Vortex of Venus, JGR: Planets (*submitted)*.

Ground-based observations of the periodical rotation and temporal variability of the global scale UV-feature

M. Imai , *Department of Cosmosciences, Hokkaido University, Japan. (masataka@ep.sci.hokudai.ac.jp)*,
Y. Takahashi, M. Watanabe, *Department of Cosmosciences, Hokkaido University, Japan,* **T. Kouyama**, *Information Technology Research Institute National Institute of Advanced Industrial Science and Technology.*

Introduction:

The dynamical mechanism of Venusian super-rotation remains a mystery for a long time. A planetary-scale UV feature on the cloud top level is well known as the "Y-feature," and we can understand the propagation of the planetary-scale waves from the rotation periodicity and spatial structure of this feature. The previous Pioneer Venus observations suggests that the activities of Venus's planetary waves are associated with the super-rotation, therefore, by observing the periodic variability in the Y-feature propagation, we could gain important clues for comprehending Venus' atmospheric dynamics.

Several spacecraft observations revealed the yearly variability of the mean zonal flow, however continuous dayside observations were difficult in prior spacecraft orbit nearly fixed inertial space. Since the Venus–Earth synodic periods is 584 days (> 1 Venus year; 224 days), Venus can be almost continuously observed over one Venusian year with ground-based telescope. In this study, the variability of the global scale UV-feature and the rotation periodicity are investigated.

Observations and Analysis:

We conducted ground-based Venus imaging observations, which consist of six times observation periods (OP1–OP6), at 365 nm from mid-August 2013 to the end of June 2014. Additionally, a long continuous monitoring was done from mid-April to the end of July 2015. Used telescope is the 1.6-m Pirka telescope, constructed and operated by Hokkaido University, Japan. The daily variation of the latitudinal distribution of bright and dark pattern was measured as the relative brightness from equatorial to mid-latitudinal regions in both hemispheres. This analysis technique was applied for Galileo observed images, and it was confirmed that the rotation of the prominent Y-feature was reconstructed as the periodical cycle of the bright and dark patterns, which were symmetric about the equator.

The rotation period of the Y-feature is estimated from the relative brightness variation in equatorial region using Lomb-Scargle periodgram.

Results:

Our relative measurement analysis success to show the periodical rotation of global scale UV feature. However, it was suggested that the Y-feature did not have constant form and its shape sometimes drastically change.

According to our observations, we found 3.5-day shorter or 5.2-day longer periodical component in all six observation periods with > 90% significance level, and the intensities of these components showed temporal variation like seesaw. The period changed from 5.2 days to 3.5 days at approximately nine-month. In the middle seasons of our observation periods, both shorter and longer periodical component simultaneously exist, and it is considered that the deformation of the Y-feature occurred.

Discussion:

Previously, Pioneer Venus observations found that the 4-day Kelvin wave in the Equatorial region and the 5-day Rossby wave in the mid-latitudinal regions exist. Our results suggest the dynamical state in the Venus cloud top level was changed from Rossby wave dominant to Kelvin wave dominant with a time scale of nine months. During the transition between the two dynamical states, the combination of two waves causes the drastic change of the Y-feature. We attributed the periodicity variation and the change of dominant waves to the variations in the mean zonal wind speed. The condition of the mean zonal flow in each observation period was under investigation, but the atmospheric dynamics of Venus will be further understood by the corroboration of ground-based observations with Japanese Venus Climate Orbiter AKATSUKI.

Acknowledgements:

The authors are grateful to Mr. Y. Sano, the director of the Nayoro-City observatory, and all other staffs for their support.

RENEWED OBSERVATION PLAN OF AKATSUKI

T. Imamura, *Institute of Space and Astronautical Science, Japan Aerospace Exploration Agency, Japan (imamura.takeshi@jaxa.jp)*

Introduction:

Japanese Venus orbiter Akatsuki aims to elucidate the mechanism of atmospheric circulation and cloud formation of Venus. The orbit insertion maneuver conducted in 2010 was not successful, and after the 5-years of additional interplanetary cruise, the spacecraft entered a Venus-encircling orbit in December 2015. The new orbit is much larger than the original. We are developing a long-term observation plan for this new orbit.

Observations in new orbit:

To understand the atmospheric dynamics and cloud physics of Venus, onboard science instruments sense multiple height levels of the atmosphere to visualize the three-dimensional structure and dynamics. Although the new orbit around Venus is much more elongated than the original plan, the science goals and the observation strategy are basically unchanged from the original (Nakamura et al., 2011). The pixel resolution at the Venusian surface is 70 km for UVI, IR1 and IR2 and 300 km for LIR from the apoapsis altitude of ~340,000 km, while it is 0.2-1.8 km for UVI, IR1 and IR2 and 0.87-7.8 km for LIR from the periapsis altitude of 1000-9000 km. The observation modes are roughly classified into the following groups; these observations are conducted sequentially in each orbital revolution (Fig. 1).

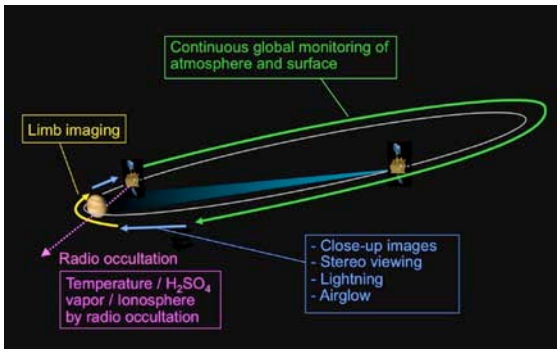

Fig. 1 Schematic of the observation sequence along the orbit

Global imaging. Global imaging is the principal mode of Akatsuki's observation. The purpose is to detect large-scale waves and the meridional circulation that may be responsible for the maintenance of the super-rotation (Giearsch, 1975; Rossow and Williams, 1979; Yamamoto and Takahashi, 2003; Takagi and Matsuda, 2007) as well as to characterize the mean-zonal wind structure. Continuous imaging enables derivation of the wind field reflecting those fluid-dynamical processes. The spatial and temporal variations of the sulfuric acid cloud layer and the minor species distributions are also major issues; the clouds are thought to be produced both through photochemistry and dynamics, and the transport of related chemical species such as SO_2 and cloud droplets at meso- to planetary scales are expected to play essential roles (Krasnopolsky and Pollack, 1994; Imamura and Hashimoto, 1998). New findings in cloud morphology are expected and should contribute to better understanding of the cloud system. Radiative energy balance of Venusian cloudy atmosphere (Lee et al., 2015) will also be studied using multi-wavelengths global images.

The observations are conducted using IR1, IR2, UVI and LIR in the portion of the orbit where the typical camera FOV of 12° exceeds the apparent Venus disk; this condition is satisfied over 96% of time in one orbital revolution except the near-periapsis region. From this portion of the orbit, cloud images will be obtained every 1-2 hours for each observation wavelength. Considering that the FOV would have exceeded the apparent Venus disk over ~60% of the orbital period in the original plan (Nakamura et al., 2011), the new orbit enables more continuous global monitoring. Another merit of the new orbit is that the observation geometry is stable over several days at the expense of the lower spatial resolution on average. By using the obtained global images, the development of the atmospheric structure is monitored, and wind vectors are derived by tracking small-scale cloud features. Monitoring of surface features on the nightside by IR1, including search for active volcanism, is also conducted mostly in this observation mode.

The camera pointing direction for this observation is not always nadir, but can be shifted to the sunlit side for dayside imaging and to the dark side for nightside imaging. The purposes of this angular offset are (1) to include the planetary limb in the image so that the pointing direction can be determined accurately from the limb position, (2) to maximize the area of the atmosphere or the surface observable with each filter, and (3) to avoid stray light when observing the nightside.

Close-up imaging. Imaging of clouds from close distances provides opportunities to unveil meso-scale structures, which should reflect small-scale convection, gravity waves, and shear instability. Such processes are expected to enhance vertical mixing of chemical species and induce vertical redistribution of momentum and energy (McGouldrick and Toon, 2007). In addition to ultraviolet wavelengths, at which Venus Express VMC also provided high-

resolution images (Titov et al., 2012), Akatsuki's simultaneous near-infrared and mid-infrared observations should provide comprehensive information on the nature of small-scale processes.

In this observation mode, a particular point on the cloud layer is continuously monitored from the distances of roughly 1000-10000 km, for the purpose of observing the temporal development of meso-scale processes and also for stereo-viewing of the cloud tops. During this observation sequence, the spacecraft attitude is controlled so that the camera FOV continuously captures roughly the same region.

Limb imaging. The vertical distribution of aerosols which extend up to ~100 km altitude is observed in limb-viewing geometry around dayside periapsis passages using UVI, IR1 (0.90 mm) and LIR. The layered distribution of aerosols seen in the limb images taken by Galileo SSI (Belton et al., 1991) and Venus Express VMC (Titov et al., 2012) suggests that unknown chemical/dynamical processes are at work in aerosol formation; extensive observations covering wider regions with multiple wavelengths would provide clues to the mechanism. When the periapsis altitude is 1000 km, the minimum distance to the tangential point is 3500 km, giving a vertical resolution of 0.7 km for UVI and IR1 and 3 km for LIR.

Eclipse observation. Lightning discharge might be closely related to cloud formation and can be an indicator of vigorous convective activity. The occurrence of lightning in the Venusian atmosphere has been the under debase in spite of various indirect observations (Russell et al., 2007).

The eclipse (umbra) region along the orbit is allocated to lightning observations by LAC. Eclipses occur mostly near the periapsis with a typical duration of 30 minutes. LAC is operated in nadir-pointing geometry and waits for lightning flashes with event trigger method. LAC can also observe airglows by continuously recording the brightness while scanning the nightside disk by the attitude maneuver or the orbital motion of the spacecraft.

Radio occultation. Radio occultation experiments (RS) using an ultra-stable oscillator (USO) are performed when the spacecraft is hidden by Venus as viewed from the tracking station (Imamura et al., 2011). Venus Express radio occultation has revealed vertical temperature profiles at various locations and localtimes (Tellmann et al., 2009); a merit of Akatsuki's observation is that the location probed by RS can be observed by the cameras a short time before the ingress or short time after the egress thanks to the equatorial orbit, enabling quasi-simultaneous observations. Since the dense Venusian atmosphere causes considerable ray bending exceeding several tens of degrees, a spacecraft steering is required to compensate for this effect while the occultation geometry changes from ingress occultation to egress occultation.

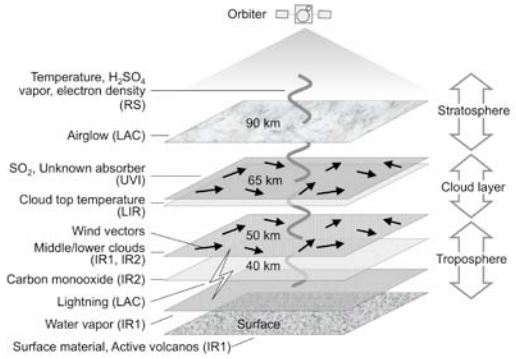

Fig. 2 Schematic of the three-dimensional observation by Akatsuki (Nakamura et al. 2011).

Bibliography:

Belton, M. J. S., et al., Imaging from Galileo of the Venus cloud deck, Science, 253, 1531–1536, 1991.

Gierasch, P. J., Meridional circulation and the maintenance of the Venus atmospheric rotation, J. Atmos. Sci., 32, 1,038–1,044, 1975.

Imamura, T. and G. L. Hashimoto, Venus cloud formation in the meridional circulation, J. Geophys. Res., 103, 31349–31366, 1998.

Imamura, T. and G. L. Hashimoto, Microphysics of Venusian clouds in rising tropical air, J. Atmos. Sci., 58, 3597–3612, 2001.

Nakamura, M. et al., Overview of Venus orbiter, Akatsuki, Earth Planets Space, 63, 443-457, doi:10.5047/eps.2011.02.009, 2011.

Krasnopolsky, V. A. and J. B. Pollack, H2O-H2SO4 system in Venus' clouds and OCS, CO, and H2SO4 profiles in Venus' troposphere, Icarus, 109, 58–78, 1994.

Lee, Y. J., et al., The radiative forcing variability caused by the changes of the upper cloud vertical structure in the Venus mesosphere, Icarus, 113, 298-308, 2015.

McGouldrick, K. and O. B. Toon, An investigation of possible causes of the holes in the condensational Venus cloud using a microphysical cloud model with a radiative-dynamical feedback, Icarus, 191, 1–24, 2007.

Rossow, W. B. and G. P. Williams, Large-scale motion in the Venus stratosphere, J. Atmos. Sci., 36, 377–389, 1979.

Russell, C. T., et al., Lightning on Venus inferred from whistler-mode waves in the ionosphere, Nature, 450, 661–662, doi:10.1038/nature05930, 2007.

Takagi, M. and Y. Matsuda, Effects of thermal tides on the Venus atmospheric superrotation, J. Geophys. Res., 112, D09112, doi:10. 1029/2006JD007901, 2007.

Tellmann, S., et al., Structure of the Venus neutral atmosphere as observed by the Radio Science experiment VeRa on Venus Express, J. Geophys. Res., 114, E00B36, doi:10.1029/2008JE003204, 2009.

Titov, D. V., et al., Morphology of the cloud tops as observed by the Venus Express Monitoring Camera, Icarus, 217, 682–701, 2012.

Yamamoto, M. and M. Takahashi, Superrotation and equatorial waves in a T21 Venus-like AGCM, Geophys. Res. Lett., 30, doi:10.
1029/2003GL016924, 2003.

GEOLOGICAL EVOLUTION OF VENUS.

M. A. Ivanov , *Vernadsky Institute, RAS, Moscow, Russia (mikhail_ivanov@brown.edu),* **J. W. Head,** *Brown University, Providence, USA,* **A. T. Basilevsky** , *Vernadsky Institute, RAS, Moscow, Russia*.

Introduction: Volcanism and large-scale tectonic deformation on Venus are related to its mantle circulation patterns and represent primary manifestations of the process of global internal heat loss [e.g., 1]. The surface of Venus displays a variety of volcanic and tectonized terrains whose morphologic characteristics are due to either emplacement of volcanic materials or superposition of tectonic structures. Here we describe the temporal distribution of tectonized terrains, their stratigraphic relationships with volcanic units, and how these outline the major episodes in the geological evolution of Venus.

Major volcanic units: Although the surface of Venus displays a variety of volcanic landforms [2-4], three major volcanic units are most important: shield plains, psh, regional plains, rp, and lobate plains, pl. Together they comprise ~96% of all volcanically dominated units and cover ~70% of the surface of Venus. *Shield plains* (psh, ~18.5% of the surface of Venus): Abundant small (2-10 km across) shield- and cone-like features (volcanic edifices [2,3,5]) characterize shield plains. Shield plains are only mildly deformed by wrinkle ridges and sparse fractures/graben. *Regional plains, lower unit* (rp1, ~33% of the surface of Venus) are composed of morphologically smooth, homogeneous, sourceless plains. Networks of wrinkle ridges deform the surface of the plains [6]. *Regional plains, upper unit* (rp2, ~9.8% of the surface of Venus) are characterized by higher radar albedo and deformed by the same families of wrinkle ridges. *Lobate plains* (~8.8% of the surface of Venus): The surface of lobate plains is occasionally disturbed by graben of rift zones. The most characteristic features of lobate plains are numerous bright and dark flow-like features. The plains are usually associated with the large dome-shaped rises (e.g., Beta, Eistla, Atla Regions, etc.).

Major tectonized units: The following five tectonized units are the most important on Venus and make up ~20% of its surface [7]. (1) *Tessera* (t, 7.3% of the surface of Venus) displays intersecting sets of contractional and extensional structures [e.g., 8]. (2) *Densely lineated plains* (pdl, 1.6%) are dissected by numerous densely packed parallel fractures. (3) *Ridged plains/Ridge belts* (pr/rb, 2.4%) are deformed by broad and long ridges that often form elevated belts. (4) *Groove belts* (gb, 8.1%) are swarms of extensional structures that completely obscure the characteristics of underlying materials at the scale of the mapping. (5) *Rift zones* (rz, 5.0%) consist of numerous parallel fissures and troughs that usually completely erase the morphology of underlying terrains.

Age relationships of volcanic and tectonic units: Clear relationships of relative age are often seen among the tectonic and volcanic units at the global scale [7]. Structures of pdl and pr/rb usually cut tessera but in some places they appear to be incorporated into the tessera structural pattern. Graben of gb cut occurrences of tessera, pdl, and pr/rb. Vast expanses of mildly deformed plains units (shield- and regional plains) embay all occurrences of t, pdl, and pr/rb and the majority of groove belts. Structures of rift zones cut the vast plains and are contemporaneous with the younger lobate plains.

Craters embayed by regional and lobate plains: The age relationships between regional plains (rp1) and lobate plains are consistently the same over the entire surface of Venus [9]. In any specific place where these units are in contact, lobate plains embay regional plains and, thus, are younger. The different morphologic characteristics of rp1 and pl and their different ages [10-12] imply that these lava units correspond to different geological epochs with apparently different styles of volcanism [9]. The main characteristic of regional plains is that the majority of their area (slightly over 80%) is concentrated only in three largest occurrences of this unit. The sizes of occurrences of lobate plains are much more evenly distributed within the observable range of areas.

The total number of craters that occur either within or on the boundaries of the areas of rp1 is 582. Out of these, 563 craters appear to be superposed on the plains and the plains embay 19 of the craters. This gives the proportion of craters embayed by regional plains as ~3%. The total number of craters on lobate plains is 79 and the plains embay 27 of them, which gives the proportion of the embayed craters in the case of lobate plains as 33%

Discussion: The majority of tectonized terrains (t through gb) are the products of tectonic resurfacing and are embayed by the vast volcanic plains and, thus, are older. There are no units with either mildly- or non-tectonized surfaces that interleave the tectonic terrains, which would be expected if the tectonic resurfacing operated only during specific phases in discrete regions. The major tectonized terrains thus define an earlier, ***tectonically dominated regime of resurfacing*** that occurred at the global-scale near the beginning of the observable geological history of Venus.

This ancient tectonic regime began with formation of the oldest unit, tessera. Both contractional (ridges) and extensional (graben) structures form tessera. There is robust evidence for the relatively old age of the ridges. This suggests that formation of tessera was due to large-scale compression that resulted in regional thickening of the crust [13,14].

The tectonic regime ended by development of pervasive groove belts that mark zones of extension. Branches of groove belts compose the tectonic components of many coronae [15] suggesting that these features are genetically related and that coronae may have punctuated the final stages of the ancient tectonic regime.

This regime was followed by emplacement of the vast volcanic plains, such as shield and regional plains,

the surfaces of which are extensively deformed by the global network of wrinkle ridges [6]. Emplacement of the plains has defined the second, ***volcanically dominated regime of resurfacing*** [16], representing a time when surface tectonic deformation related to mantle convection waned and evolved into massive, catastrophic-like, outpouring of volcanics of regional plains. The small number of embayed craters (3%) suggests that the emplacement of regional plains was geologically very rapid.

Rift zones are the stratigraphically youngest manifestations of regional-scale tectonic deformation on Venus. Rifts are spatially and temporarily associated with the youngest lava flows and often cut crests of large, but isolated, dome-shaped rises. Structures of rift zones always cut the surface of the vast plains, which means that rifts are separated in time from the ancient tectonic regime, post-date the regional plains, and represent a new phase of tectonism that was contemporaneous with the late volcanism of lobate plains. Rift zones and lobate plains define the third, ***network rifting-volcanism regime of resurfacing*** that was related to late stages of evolution of the dome-shaped rises. The much larger proportion of craters embayed by lobate plains (33%) suggests a more gradual style of emplacement of volcanic materials during this regime.

References: 1) Solomon, S.C. and J.W. Head, JGR, 87, 9236, 1982; 2) Head et al., JGR, 97, 13153, 1992; 3) Guest et al., JGR, 97, 15949, 1992; 4) Crumple and Aubele, in: Encyclopedia of Volcanoes, 727, 2000; 5) Aubele and Slyuta, EMP, 50/51, 493, 1990; 6) Bilotti, F. and J. Suppe, Icarus, 139, 137, 1999; 7) Ivanov, M.A., and J.W. Head, PSS, 59, 1559, 2011; 8) Sukhanov, A.L. In: Venus GGG, Barsukov et al., eds, 82, 1992; 9) Ivanov and Head, PSS, 84, 66, 2013; 10) Namiki and Solomon, Science, 265, 929, 1994; 11) Price et al., JGR, 101, 4657, 1996; 12) Guest and Stofan, Icarus, 139, 56, 1999; 13) Head, J.W., et al., PSS, 42, 803, 1994; 14) Bindschadler, D.L. et al., JGR, 97, 13563, 1992; 15) Stofan, E.R. et al., JGR, 97, 13347, 1992; 16) Ivanov, M.A., and J.W. Head, LPSC 43, #1037, 2012.

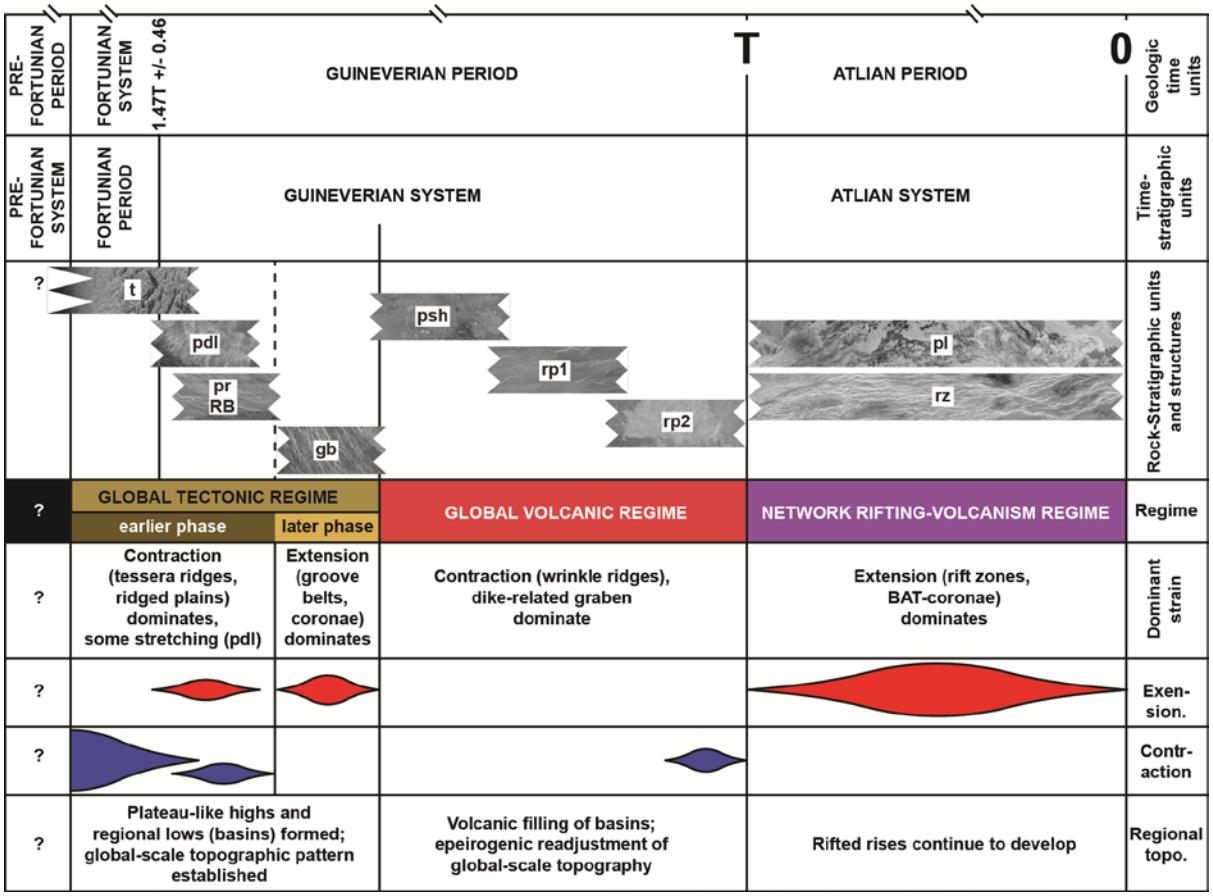

Figure 1. A global correlation chart that shows the three major regimes of resurfacing on Venus [7,9].

AKATSUKI 1μm CAMERA AWAKENS

N. Iwagami, *Univ of Tokyo (iwagami@eps.s.u-tokyo.ac.jp)*, **S. Ohtsuki**, *Senshu Univ*, **T. Sakanoi**, *Tohoku Univ*

Akatsuki 1μm camera awoke, and started to work after the successful re-try of Venus orbit insertion on 07 Dec.2015 exactly 5 years after the failer. The first image taken 2 days after at 70,000 km away is shown below representing good health of the camera. It was surprising to find almost no damaged pixel over the image although we anticipated dirty image with very many dead pixels. Probablly this is due to OFF state of the camera, and extremly low solar activity in the latest 5 years.

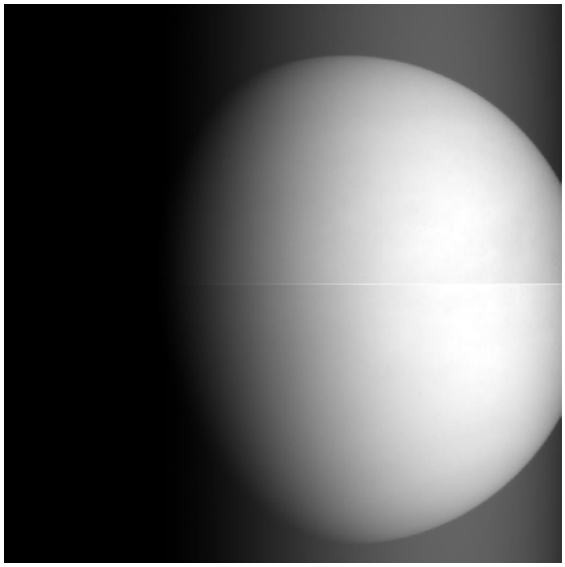

The first 0.9 μm image taken at 70,000 km away 2 days after the successful insertion.

DETECTION OF WAVES AT 60 AND 70 KM IN THE VENUS ATMOSPHERE BY GROUND-BASED IR SPECTROSCOPY

N. Iwagami, S. Kano, **M. Hosouchi**, *Univ of Tokyo (iwagami@eps.s.u-tokyo.ac.jp)*, **G-L. Hashimoto**, *Okayama Univ.*,**T. Kouyama**, *Nat. Inst. of Advanced Sci. and Tech.*, **H. Iwagami,** *Petit Vega Planetarium*, **M. Takagi**, *Kyoto-Sangyo Univ.*

Venusian atmospheric waves at 60 and 70 km are investigated by IR spectroscopy. The observation was carried out at NASA/IRTF at Mauna Kea, Hawaii in May 2014 for 10 days by using CSHELL spectrometer. As noted in Hosouchi et al. (2012), 1.7 μm CO_2 absorption structure gives information at 60 km. At first, a collaboration with VMS/VEX was planned for the 70 km information source, but cancelled. So we changed our strategy to use 5 μm radiance as another information source for 70 km. By comparing wave structures found at 60 and 70 km, it is possible to investigate the vertical structure of atmospheric waves. Such information will reveal important aspects to understand the generating mechanism for the Super Rotation. The figures below show waves found in the 1.7 μm (60 km) and 5 μm (70 km) regions. The former has an apparent period of 4.1 days and the latter 3.7 days.

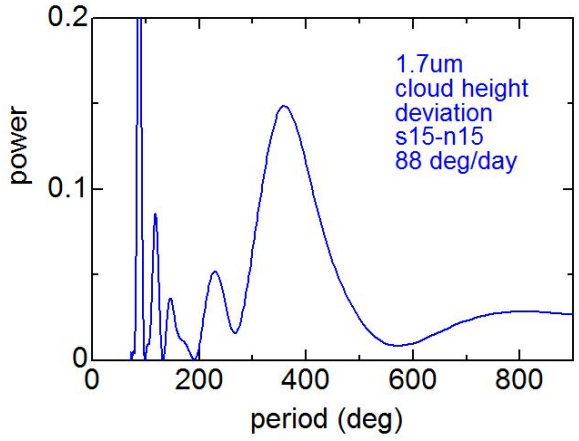

Fig.1a Power spectrum of cloud height deviation. The 88 deg/day repeating step is chosen so as to fined the wavenumber 1 peak at 360 deg

References:
Hosouchi et al, ICARUS 220, 552-560, 2012.

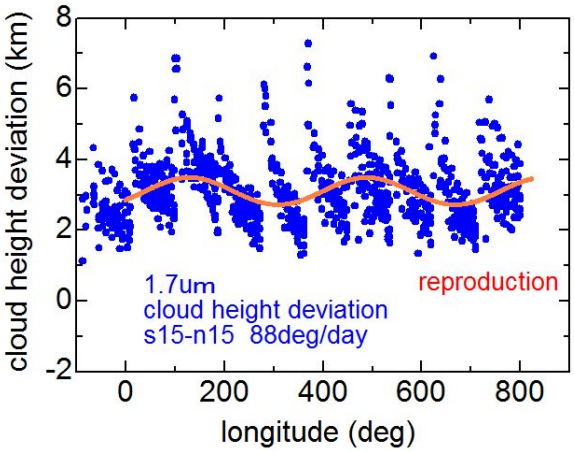

Fig.1b Cloud height deviations for 10 days with 88 deg/day repeating.

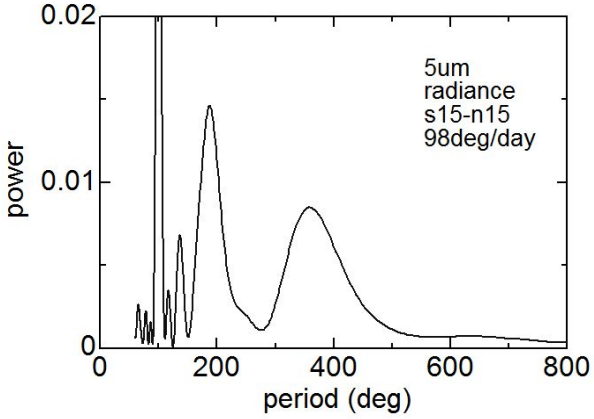

Fig.2a Power spectrum of 5 μm radiance. The 98 deg/day repeating step is chosen so as to fined the wavenumber 1 peak at 360 deg

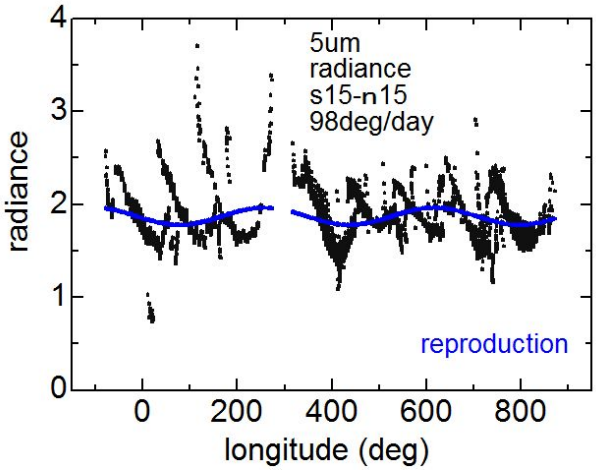

Fig.2b 5 μm radiance for 10 days with 98 deg/day repeating.

EMPIRE STRIKES BACK: VENUS EXPLORATION IN THE NEW HUMAN SPACEFLIGHT AGE.

N. R. Izenberg *(noam.izenberg@jhuapl.edu),* **R. L. McNutt, Jr.,** *Johns Hopkins University Applied Physics Laboratory, Laurel, Maryland, USA.*

Introduction:

In the highly competitive world of modern planetary exploration, opportunities for missions Venus are available, but challenging to exploit. Venus missions are detailed in the recent NASA Decadal Survey [1] and mentioned ESA's Cosmic Vision [2]. The Venera D mission – a joint effort between NASA, Russia, and others, is being explored as well. However, opportunities for Venus exploration, especially for large, high-capability missions are few and far between. A class of missions exists that provides a unique opportunity specifically for this kind of Venus science mission, and it exists on the human pathway to Mars.

Age of EMPIRE:

Venus flybys and even orbital missions, have been part of plans for human space exploration since the early days of space flight. One of the very first proposed uses of a Venus flyby for human spaceflight dates back to 1956, in a conference talk describing a one-year (and in the ensuing study extended to a 400-day) Mars-flyby, Venus-flyby mission, with a launch opportunity in 1971 [3] (Fig 1). In the ensuing decades, several NASA studies explored various Mars exploration scenarios, some of which included Venus flybys, or even dual-planet missions [4, 5, others]. The Venus flyby and rendezvous mission studies were undertaken and completed through the 1960's and early 1970's and Venus flyby components of Mars missions have surfaced on occasion throughout the decades.

Venus to Mars Today:

The current NASA plan for human exploration of Mars is expressed primarily in the Design Reference Architecture (DRA) 5.0 [6], published in 2009, and its two supplements [7, 8] published in 2009 and 2014. Venus flybys remain as valid choices in the latest plans for the human path to Mars using current and imminent technological capability such as the Space Launch System (SLS) [9].

Venus flyby scenarios currently under consideration are for "opposition" type missions to Mars (Fig. 2) in which the spacecraft swings by Venus on the outward or return leg to Mars, and mission durations at Mars are from 20 to 100 days in length [8]. The shorter Mars-stay missions, as opposed to 550-730 day stay-at Mars "conjunction" class missions occupy an enticing sweet-spot among candidate Mars rendezvous missions, combining weeks to months at Mars with shorter total mission duration and lower total mission delta-V (Fig. 3).

series of studies was termed EMPIRE (Early Manned Planetary-Interplanetary Roundtrip Expeditions), and meant to leverage Apollo-era hardware into ever more ambitious human space endeavors.

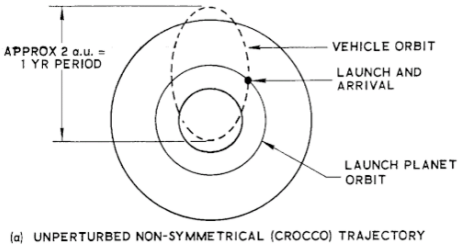

Fig. 1. First proposed manned Venus-Mars Flyby mission trajectories from [3].

Early proposals required rocket and spacecraft technology well beyond capabilities (at the time of the 1956 proposals, Atlas Mercury was the largest human mission flown by NASA), many of which proved to be completely unfeasible or unworkable over time (e.g. requiring nuclear thermal rocket engines). Similarly, long term radiation and inner solar system heat hazards could not be addressed in detail 50 years ago.

Nevertheless, a number of Human

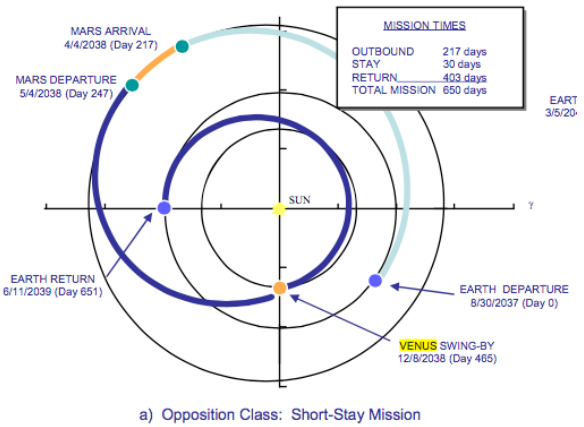

Fig. 2. Earth-Mars-Venus-Earth "Opposition Class" mission from [8]

From the very beginning, Venus flyby missions were seen not just viewed as an opportunity for getting to Mars more easily, or with possibly lower cost and risk, but also as a science opportunity. Venus flyby plans always included the "dropping off" of science payloads and science observations during the flyby. The same would be true in the modern conception of a crewed Venus flyby.

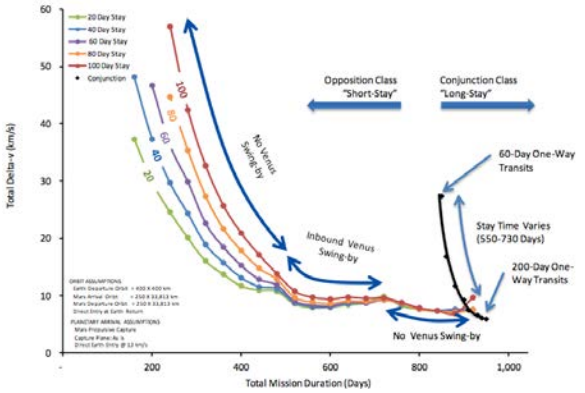

Figure 3. Example round trip ΔV as a function of total mission duration. From [4]. The "Inbound Venus Swing-by" curves delineate a "sweet spot" of mission types that minimize both mission total duration and ΔV, while creting an opportunity for dual planet science missions.

A New EMPIRE:

Most current concepts of SLS-launched missions to Mars include 4-10 rocket launches, and each SLS launch has the capability of bringing up secondary payloads (of as yet unconstrained mass). Human Mars missions that do not include a Venus flyby component still provide orbital staging opportunities for planetary missions. The DRA describes SLS secondary accommodations for multiple comsat or equivalent secondary payloads per SLS launch. These payloads could easily become opportunities for many different solar system targets, including Venus. However, on Earth-Venus-Mars-Earth (EVME) or Earth-Mars-Venus-Earth (EMVE), Venus probes in particular would be logical secondary payload choices. The flyby orbit could create enabling opportunities for one or more significant probes to be dropped during a Venus flyby trajectory, for insertion to Venus orbit or descent into the atmosphere and/or surface. The EVME mission would be most hospitable for larger Venus-destined payloads carried with the crew, since the jettisoning of Venus-bound payloads would reduce total mass for spacecraft maneuvers for the rest of the mission.

What kind of missions might be enabled by a crewed flyby a Venus? Specifically having a crew en route and during and after flyby enables several mission architectures, including, but not necessarily limited to:

- Large, potentially modular probes or constellations potentially launched in pieces and assembled by crew en route to Venus. Mission concepts includes cubesat – or larger – constellations [10], or probes launched in pieces in multiple SLS launches with final assembly en route to Venus,
- Real-Time Telemetry and human-in-the-loop probes actively guided in the Venus environment by human crew during the days or weeks around closest approach, where light-speed communication delays are minimal. These mission concepts include guide-able aerial platforms [11,12] to surface rovers [13],
- Fast sample-grab-and-return from the Venus atmosphere, rendezvousing with the departing spacecraft instead of transiting to Earth. [14]

The Opportunity:

While Venus flyby opportunities on the path of Human exploration of Mars are currently in the books, they do not have high mind-share in the human spaceflight community. Issues, technical challenges, and risks of temperature and radiation exposure in the <1 AU environment, and protection of crew and equipment are examined in the current DRA and its supplements, but Venus flybys are not at the forefront of thinking or plans.

The Venus science opportunities presented by EVME and EMVE missions are significant and unique, and in an era of renewed interest in and ambition for going to Mars, a timely – and time limited – opportunity, as Venus flyby missions.

The Venus exploration community has the opportunity at this time to voice active support not just for human crewed missions, but human exploration of Mars in particular, for the additional payload opportunities it creates. Furthermore, the Venus community has a stake in advocating for *how* we get to Mars as well. Making the case that the best path may include both planets is an idea whose time has come around again.

References:

[1] Space Studies Board, 'Vision and Voyages for Planetary Science in the Decade 2013-2022' Nat't. Acad. Press, Washington, DC, USA (2011) 410 p. [2] Bigmani G. et al. BR-247 'Cosmic Vision' ESA Pub. ESTEC, Noordwijk, Netherlands (2005) 111 p. [3] NASA Contractor Report 51709, 'EMPIRE: A Study of Early Manned Interplanetary Expeditions' , Aeronutronic Division, Ford Motor Company, 21 December 1962. [4] Dixon F. P. "The EMPIRE Dual Planet Flyby Mission," Aeronutronic Division, Philco Corporation; paper presented at the Engineering Problems of Manned Interplanetary Exploration conference, 30 September-1 October 1963. [5] Ordway F. I. III et al. "EMPIRE: Early Manned Planetary-Interplanetary Roundtrip Expeditions Part I: Aeronutronic and General Dynamics Studies," *J. Brit. Interplanetary Soc.* (1993) 179-190. [6] Drake B. G. et al. 'Human Exploration of Mars, Design Reference Architecture 5.0' IEEEAC paper #1205 (2009) 25 p. [7] Drake . B. F. Ed. 'Human Exploration of Mars Design Reference Architecture 5.0 Addendum', NASA/SP–2009–566-ADD, (2009) 406 p. [8] Drake . B. F. and Watts K. D. Eds. 'Human Exploration of Mars Design Reference Architecture 5.0 Addendum #2', NASA/SP–2009–566-ADD2, (2009) 406 p. [9] SLS Factsheet, NASA Pub. FS-2012-06-59-MSFC (2012). [10] Majid, W., et al. "A Cubesat Mission to Venus: A Low-Cost Approach to the Investigation of Venus Lightning." *AGU Fall Meeting Abstracts*. Vol. 1. 2013. [11] Lee, G., et al. "Venus Atmospheric Maneuverable Platform (VAMP) Science Vehicle Concept." *LPI Contributions* 1838 (2015): 4007. [12] Ashish, et al. "Blimplane a Conceptual Hybrid UAV for Venus Exploration." *LPI Contributions* 1838 (2015): 4034. [13] Landis, Geoffrey A., et al. "Venus Rover Design Study." *paper AIAA* 7268 (2011): 26-29. [14] Sweetser, Ted, et al. "Venus sample return missions—a range of science, a range of costs." *Acta Astronautica* 52.2 (2003): 165-172.

VENUS: OBSERVE IT WHILE IT'S HOT!

K.L. Jessup , *Southwest Research Institute, Boulder, CO, USA (jessup@boulder.swri.edu)*, **F. Mills,** Space Science Institute, Boulder, CO, USA, **S. Limaye**, *University of Wisconsin-Madison, Madison, WI, USA* **E. Marcq, J.L. Bertaux**, *LATMOS, Versailles, France*. **C. Wilson**, *Atmospheric Physics, Oxford, UK*. **T. Imamura, M. Nakamura**, *Institute of Astronautical Science Japan Aerospace Exploration Agency, Japan*

Introduction:

Venus' global-scale cloud and haze layers are composed of complexes of sulfuric acid (H_2SO_4) and water. Because the clouds play a critical role in Venus' energy balance and long-term climate evolution, accurate definition of their formation process is a high priority in Venus atmospheric studies. On a basic level it is understood that the H_2SO_4 clouds and haze form via the combination of SO_3 and H_2O, and SO_3 forms via oxidation of SO_2. Thus, sulfur-bearing and sulfur-oxidized species, such as SO_2, SO, S, OCS, H_2SO_4, are key traces of Venus' H_2SO_4 cloud/haze formation process. However, the specific pathways (which may be chemical, microphysical and/or dynamical) that balance the budget of sulfur (and oxidized sulfur) in Venus' atmosphere are ill-defined [1-3], as are the mechanisms that sustain the density of the clouds. As result, Venus' climate evolution is ill-defined, and understanding Venus' sulfur-budget is highlighted as an important Venus exploration target.

New Observation Opportunities:

The recent success of the Venus Orbit Insertion (VOI) maneuvers implemented by JAXA's *Akatsuki* spacecraft has opened up another opportunity to obtain sustained and coordinated observations of Venus' atmosphere that can be used to investigate the progression of Venus' sulfur-cycle and the formation of the H_2SO_4 clouds and haze. The primary objective of the *Akatsuki* mission is to understand Venus' atmospheric dynamics, cloud chemistry and cloud physics by observing key characteristics of Venus' atmosphere from above and below the 47-70 km cloud layer on both the day and night side. Acquisition of coordinated HST and *Akatsuki* observations of Venus' sulfur-oxide species can be used to complete *Akatsuki*'s observing objectives and as well as the atmospheric observation priorities established by VEXAG and other International Venus Exploration Organizations [4,5].

In particular, we are proposing to obtain HST spectral and imaging observations of Venus' dayside atmosphere in the 200-600 nm wavelength region. The HST images can provide high (20±2 km) spatial resolution mapping of Venus' dayside SO_2 gas absorption signature below 240 nm, the 200-400 nm cloud top brightness/ contrast, and the distribution of the unknown UV absorber as a function of local time at each latitude. The HST spectra can provide at high (50±10 km) spatial resolution, which is comparable to the expected UVI image spatial resolution at *Akatsuki* apoapsis, detailed latitude and local time detections of i) the SO_2 and SO gas absorption signatures at wavelengths < 240 nm, at high (0.27 nm) spectral resolution ii) the long-wavelength (280-330 nm) SO_2 absorption signature at high (0.27 nm) spectral resolution, and iii) the 340-400 nm spectral signature of the unknown UV absorber at medium (0.54 nm) spectral resolution. The spectral data will also provide a means to validate/accurately complete radiometric calibration of the *Akatsuki* UVI images that will be obtained at 283±6.5 and 365±7.5 nm.

The two nearest observing windows during which coordinated HST-Akatsuki observation may be obtained occur in 2017. In the first observing window, which extends through January 2017 to the first week of February 2017, Venus' p.m. quadrant is observable from the Earth. HST spectral observations obtained at this time can provide the ***first*** simultaneous measurement SO_2 and SO densities ***on Venus' p.m. quadrant*** as a function of both local time and latitude resolution without any temporal confusion. With proper planning 365 nm *Akatsuki* UVI images of Venus' partially illuminated disk can be taken near-simultaneously (within 1.5 hours) of HST/STIS *and* from the same vantage point as HST. Analysis of the 365 nm limb brightness will map the variation in the haze properties as a function of latitude along the sunlit limb, i.e. at a local Venus time of ~ noon. *This is a critical empirical constraint needed for developing models that attempt to replicate Venus' a.m. to p.m. H_2SO_4 gas and aerosol distribution asymmetries, and can ONLY be derived from observations that are centered in latitude on Venus' equator and centered in longitude on either the a.m. or p.m. terminator longitude.*

In the second observing window, which extends from mid-May 2017 to late June-2017, Venus' a.m. quadrant is observable from the Earth. Detailed spectral observation of Venus' a.m. quadrant were obtained by HST during the Venus Express mission. Photochemical and dynamical modeling [1, 6] indicates that the 70-80 km SO_2 abundance is dependent on the influx of SO_2 (or an influx of species that control the SO_2 abundance) from lower altitudes. Thus, it is currently unclear whether:

i) the species responsible for balancing out the loss and production SO_x at 70 and 80 km are directly

upwelled from lower altitudes, and if so from how low in the atmosphere, and through what process?

--or--

ii) fluctuations in the upward flux of SO_2 itself are the primary mechanism that determine the SO_2 density?

--or--

iii) the 70 to 80 km behavior is intimately linked to physical/chemical/microphysical processes occurring in the 60 to 70 km altitude region, and if so by what species/and or processes?

To segregate the import of these processes detailed empirically constrained models of the SO_2 profile over multiple altitudes at multiple times of day are needed. This need *is* the primary motivator for *new* spatially and temporally coincident pole-to-pole observations of Venus' a.m. quadrant during the Akatsuki mission when UVI images sensitive to the altitude region just below the region sampled by the short (λ < 240 nm) wavelength HST imaging and spectral observations. Additionally, in the absence of in-situ measurements, it is a high priority to obtain these observations coordinated with other ground based platforms over a range of wavelengths that have sensitivity to the lower altitude regions adjacent and below the 70-80 km cloud top region.

In each of the possible HST observing epochs details of the haze properties can be derived from analysis of limb brightness signatures captured in the 365 nm *Akatuski* images. These details can also be fed into Mie scattering models to define the impact of the aerosols on the photon (=radiation) budget as function of altitude at each local time observed. The combination of the HST derived SO_2 and SO gas observations with the radiation budget results can be fed into photochemical and microphysical models and used to investigate the impact of H_2SO_4 formation on Venus' overall sulfur budget. This has the potential to improve our overall understanding of the cloud formation process which in turn impacts modeling of Venus' long term climate evolution.

Summary:

The successful insertion of *Akatsuki* into Venus orbit on December 7, 2015 has opened up a new epoch of continuous Venus observation. This in turn provides a new opportunity to obtain coordinated observations that can capitalize, in concert, on the unique capabilities of the *Akatsuki* suite of instruments as well as other ground and space-based observing platforms, enhancing and expanding the science return of each observation.

References: [1] Jessup, et al. (2015) *Icarus*, **258**, 309-336. [2] Vandaele et al. (2016), *Space Sci. Revs.*, submitted. [3] Sandor et al. (2010), *Icarus*, **208,** 49-60. [4] VEXAG *Goals, Objectives and Investigations for Venus Exploration*, 2014. [5] Jessup et al., 2015, 13th *VEXAG meeting, Washington, D.C.*. [6] Marcq et al., 2013, *Nature GeoSci* **6**, 25-28.

ROTATION OF VENUS: PREDICTIONS & OBSERVATIONS

Ö. Karatekin, Royal Observatory of Belgium, *Brussels, Belgium (o.karatekin@observatory.be)*, **I. Holin** *Moscow, Russia*.

Introduction:

High precision rotational dynamics of Earth-like planets closely relate to their core-mantle-crust-atmosphere properties and evolution and can be characterized by the behaviour of the instantaneous spin-vector of their crust/mantle with time that includes variations. The slow rotation and dense atmosphere makes determination of Venus' spin dynamics extremely challenging. Accordingly the dynamical ellipticity and moments of inertia of Venus remain poorly known. Observations from spacecraft orbiting as well as Earth-based radar measurements have yielded different and sometimes inconsistent values for the mean rotation of Venus. Currently, Venus' rotation remains as the least known among the terrestrial planets.

Venus is a slow retrograde rotation. The rotation period of Venus and the direction of the planet's North pole was determined by NASA's Magellan orbiter using the radar images by tracking surface features [1]. The length of a day of Venus was determined to be 243.0185 Earth days. Recent observations of Venus Express with the VIRTIS instrument suggested a slightly slower spin, indicating that the rotation of the planet is not fully described by the orientation model recommended by the IAU [2]. Mueller et al [2] suggested that this discrepancy might be due to the length of day variation.

Estimates of Length-of-Day Variations

The rotations of the planets with an atmosphere (such as Earth, Mars and Titan) constantly slow down and speed up, due to the angular momentum exchange between the surface and the atmosphere, altering the length of the day (LOD). Variations on the order of millisecond over seasonal time scales have been observed for Mars and Earth, but LOD variations of Venus have not yet been measured. Despite the near-circular orbit and very small obliquity, and the resulting absence of seasons, important variations in the rotation of Venus can still exist due to the variability of the winds in the lower atmosphere over diurnal time scales. Schubert [3] suggested the possibility of having LOD variations on Venus several orders of magnitude larger than those observed for the Earth and Mars using an order of magnitude analysis based on analytical considerations. More recently, using the outputs of a GCM data, Karatekin et al. [4][5] showed that a ΔLOD around tens of seconds is plausible, indeed. This value is about the same order of magnitude as the uncertainty in the rotation period of Venus reported by Konopliv et al. [6] (~43 sec) and Davies et al. [1] (~9 sec). Cottereau et al. [7] argued that spin variation might be dominated by the tidal torque exerted by the Sun on its solid body (~2-3 minutes) rather than the effect of the atmosphere.

Measurement of Variations in Venus rotation rate by Earth-based Radar:

In spite of orbiting spacecraft missions, such as Magellan and Venus Express, the measurement of short-term variations in Venus rotation remains an open problem. The recently measured difference of ~ 6 min in the mean rotation rate [2] seems to be too large to be explained by variations. Taking into account that rotational variations of Mercury were first measured by Earth-based radar [8] using the effect of speckle displacement [9], [10], it is reasonable to analyze potentials of radar speckle tracking techniques as applied to Venus as well.

The limiting relative accuracy in the instantaneous spin rate of Venus of the Manasse-Green technique (MGT), where the baselines are not aligned to speckle displacement ([9], p. 15, 56), is $> 10^{-5}$ (for Mercury $> 10^{-4}$). But the expected variations are $< 10^{-5}$ [5], [7]. So MGT does not allow measurements of spin variations for Mercury and Venus.

The Holin [10], [11] technique (HT), where a substantially longer baseline exceeding a speckle dimension by orders of magnitude is aligned with the speckle displacement direction due to the Earth rotation, has better precision. For example, a minimum relative standard deviation characterized by the Cramer-Rao lower bound (CRLB) [12] in presence of a traditional system (electronic) noise only is for Mercury ~ 2×10^{-6} with the Goldstone / Goldstone – Green Bank (G/G-GB) radar interferometer [11], [13].

Besides system noise, CRLB is strongly dependent on the loss of signal identity that may result from a number of reasons, such as radio wave propagation in Venus atmosphere, finite speckle dimension along the radar line-of-sight, and so on. As a result, for Mercury with G/G-GB and the same level of electronic noise, the correlation coefficient $r \sim 0.5$ leads to CRLB of the order of ~ 10^{-5} only. For Venus with monochromatic G/G-GB, $r \sim 0.9$ and $r \sim 0.3$ lead to ~ 2×10^{-6} and ~ 5×10^{-6} respectively. The existing interferometer Arecibo / Green Bank – VLA (A/GB-VLA) has theoretical CRLB up to ~ 4×10^{-7} ($r \sim 0.9$), which is comparable to the level of expected variations.

It follows from the above that the situation about true values of r is important and needs clarification for both polarizations and transmitted wavelengths [13]. That would allow proper planning of the experiments. Indeed, signal-to-(electronic)noise ratio for Venus is so high, that the values $r < 1$ prevent from a rational use of the total transmission power. To avoid substantial losses in accuracy related to incoherence, a multi-frequency approach (multi-frequency HT) was developed [14]. For example, were G/G-GB multi-frequency, its CRLB in the case of $r \sim 0.5$ for Mercury would be $\sim 2.5\times10^{-6}$. Analogously for Venus, multi-frequency A/GB-VLA may reach $\sim 10^{-7}$, which should be enough to measure variations related to a Venusian atmosphere. The measurement time in all cases is within few tens of minutes.

Further improvements in the measurement accuracy can be based on multi-frequency and multi-baseline radio systems. For example, CRLB with the two antenna arrays similar to VLA and a multi-frequency radar transmitter at Arecibo is close to $\sim 2\times10^{-8}$. To reach these limits, antenna separation in receiving arrays transversely to speckle displacement should exceed a speckle dimension. Also, it is desirable to know the nature and properties of signal incoherence.

Conclusion:

If measured, LOD variations of Venus would reveal the zonal wind variability and help to model the angular momentum exchange between the planetary surface and the atmosphere. Besides the atmosphere, Venus rotation could be affected by the sun's gravitational attraction on the mantle and on the core mantle coupling. The measurements of planetary rotation could also reveal spin pole orientation, which is associated with the precession rate of the spin axis, a direct constraint on the moment of inertia of Venus. For future planetary missions, observation of LOD variations of Venus will continue to be a challenge, but an attainable goal considering the improved remote sensing capabilities.

Ground-based radar can be used to study the rotational dynamics of the terrestrial planets. High precision estimates of the instantaneous spin rate and spin-vector orientation of a rough rigid rotating planetary surface can be obtained from Earth based observations. Similar to Mercury, Earth-based radar have potentials to measure short-term variations in Venus rotation rate to $10^{-6} – 10^{-7}$ and better. Our results for Venus show that existing radar interferometers have CRLBs on the order $\sim 10^{-6}$ or better but still far from $\sim 10^{-7}$. Multi-frequency and multi-baseline systems may have CRLBs substantially better than 10^{-7} allowing measurements of the full spectrum of main variations in Venus rotation rate in spite of signal incoherence.

Bibliography:

[1] Davies M.E. et al (1992), JGR. 97(E8) [2] Mueller N. et al. (2012) Icarus 217(2), 474 [3] Schubert G. (1983), Venus, University of Arizona Press. [4] Karatekin, O., et al (2009.) BAAS 41. [5] Karatekin O. et al. (2011) Planet. Space Sci. 59, 923. [6] Konopliv, A. S. et al (1999) Icarus, 139, 3. [7] Cottereau L. et al. (2011) A & A 531, A45 [8] Margot J-L. et al. (2007) Science 316, 710 [9] Green P. E. (1968) In: Radar Astronomy (McGraw-Hill, New York), Chap. 1 [10] Holin I. V. (1988) Radiophys. Quant. Elec. 31, 371 [11] Holin I. V. (1992) Radiophys. Quant. Elec. 35, 284 [12] Carter G. C. (1987) Proc. IEEE 75, 236 [13] Holin I. V. (2010) Icarus 207, 545 [14] Holin I. V. (2014) 45th LPSC, abstract #1020.

VERTICAL PROPAGATION OF PLANETARY SCALE WAVES IN VARIABLE BACKGROUND ZONAL WINDS

T. Kouyama, *Artificial Intelligence Research Center, National Institute of Advanced Industrial Science and Technology, Tsukuba, Japan (t.kouyama@aist.go.jp),* **T. Imamura**, *Institute of Space and Astronautical Science, Department of Solar System Sciences, Sagamihara, Japan*.

Introduction:

The transport of westward momentum from the lower atmosphere to the cloud top is a key factor to maintain fast westward zonal winds, called super-rotation, in Venus atmosphere. The vertical propagation of planetary scale waves can transport momentum, resulting atmospheric acceleration or deceleration. Kelvin wave and Rossby wave have been confirmed from periodical wind speed and cloud brightness variation [cf. Del Genio and Rossow, 1990]. From a numerical calculation result, it is expected that Kelvin wave enhanced at the mid-cloud level (~60km) can propagate easily to the upper cloud level in slower background winds (~80 m/s at the equator) and accelerate atmosphere in low latitude regions, while Rossby wave can propagate in faster background winds (~100 m/s) and decelerate at mid latitudes, assuming the background zonal winds have same angular speed in all latitudes (= solid body rotation profile) [Kouyama et al., 2015]. However, since observed dayside mean zonal wind speed shows rather flat distribution in low latitudes and sometimes has mid-latitude jets (= not solid body rotation), it has been unclear the propagation of planetary scale waves in more realistic background zonal winds. Therefore in this study we focused a numerical investigation of propagation of the waves considering the observed zonal wind speed distribution.

Model and background zonal winds:

For describing the background zonal wind which has mid-latitude jets around 70 km, we used a three dimensional nonlinear primitive equation model in spherical geometry covering the Venusian atmosphere from 60 km (236 hPa) to 85 km (2.0 hPa) altitude based on Imamura, 2006. Following Kouyama et al calculations, we assume two types of the background zonal wind profile. In the fast wind profile (Model F), the wind speed increases with altitude from 60 to 70 km and decreases above 70 km at the equatorial region (Figure 1a), which is based on direct measurements (Schubert, 1983). In the slow profile (Model S), the wind speed at the equatorial region is independent of the altitude (Figure 1b). Both Models F and S have local maximum of zonal wind speed around mid-latitude at the upper cloud level. In both Models F and S the phase speeds of the imposed Kelvin and Rossby waves are assumed to be 115 m/s (period of ~3.8 d) and 77 m/s (period of ~5.8 d), respectively.

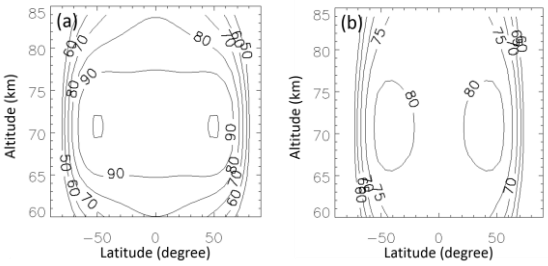

Figure 1. Background zonal wind speeds (m/s) in (a) Model F and (b) Model S.

Results:

Figure 2 shows the obtained vertical structures of the normalized amplitudes of zonal wind perturbation in Models F and S for the Kelvin and the Rossby waves. The Kelvin wave in Model F shows significant attenuation with altitude and almost disappears at 70 km altitude, while in Model S the Kelvin wave retains a significant amplitude around 70 km. On the other hand, although the amplitude of the Rossby wave in Model F is larger than that in Model S, the Rossby wave even in Model S shows a significant amplitude even above 70 km, which is clearly different from the results assuming the solid body rotation profile of the background zonal wind speed (marked with S' in Figure 2).

Imamura (2006) showed that mid-latitude jets do not influence the structure of Kelvin waves significantly but cause a poleward expansion of Rossby waves, resulting the wider discrepancy between the background zonal wind speed and the horizontal

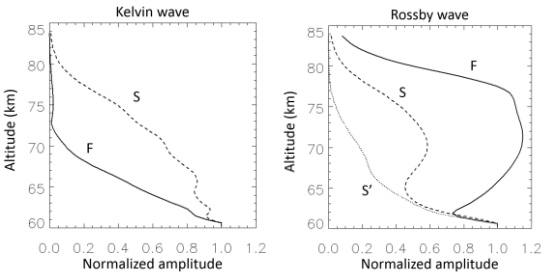

Figure 2. Vertical profiles of the amplitudes of the zonal wind disturbances at the equator region of (left) Kelvin waves and (right) Rossby waves in Models F (solid) and S (dashed). The amplitude of Rossby wave assuming the solid body rotation profile of the background winds is also plotted (dotted).

phase speed of Rossby wave in mid-latitude range, which may relax the attenuation of Rossby waves. Our results also suggest the mid-latitude jets do not affect the propagation of Kelvin waves significantly.

Conclusion:

We have investigated the vertical propagation of Kelvin and Rossby waves in the variable background winds with mid-latitude jets around the upper cloud level using a non-linear primitive equation model based on Imamura, 2006. The mid-latitude jets do not affect significantly the propagation of the Kelvin waves, while the jets may relax the attenuation of Rossby waves. If Rossby waves can propagate vertically remaining their amplitude to some extent in both faster and slower backgrounds, the time variation of domination of Rossby waves may reflect the time variation of their enhancement at the source region.

Because the propagation of waves have three dimensional structures, three dimensional observation should be useful to investigate the wave structures and evaluate atmospheric acceleration from the propagation. Venus image sets obtained from Akatsuki (Nakamura et al., 2014) and applications of the cloud-tracking method to the image sets could identify the three dimensional structures.

References:

- Del Genio, A. D. and W. B. Rossow (1990), *J. Atmos. Sci.*, 47, 293-318.
- Imamura, T. (2006), *J. Atmos. Sci.*, 63, 1623–1636.
- Kouyama et al. (2015), *Icarus*, 248, 560-568.
- Nakamura et al. (2014), *Acta Astronautica*, 93, 384-389.
- Schubert, G. (1983), *Venus I**, 681-765.

Temperature Measurements in Venus Upper Atmosphere between 2007 and 2015 from ground-based Infrared Heterodyne Spectroscopy

P. Krause, *Rhenish Institute for Environmental Research at the University of Cologne, Department for Planetary Science, Germany (pkrause@ph1.uni-koeln.de),* **M. Sornig**, **M. Herrmann**, *Rhenish Institute for Environmental Research at the University of Cologne, Department for Planetary Science, Germany,* **C. Wischnewski, G. Sonnabend, T. Stangier,** *RPG Radiometer Physics GmbH, Meckenheim, Germany,* **T. Kostiuk,** *NASA Goddard Space Flight Center, Maryland, USA,* **T. Livengood,** *NASA Goddard Space Flight Center, Maryland, USA and CRESST, University of Maryland, USA*

Introduction:

The structure of Venus atmosphere has been the target of intense studies in the past decade. Among manifold ground based observations, the recent space mission Venus Express in particular has shed light on many open questions concerning the thermal and the dynamical behavior of its atmosphere. A comprehensive understanding of this atmospheric region is still missing. Therefore, direct measurements of atmospheric parameters on various time scales and at different locations on the planet are essential for an understanding and for the validation of global circulation models.

Such observations are provided by the infrared heterodyne spectrometers THIS (University of Cologne), HIPWAC (NASA GSFC) and MILAHI (Tohoku University). These instruments fully resolve CO_2 non-LTE emission lines for Doppler-wind and temperature retrievals at a pressure level of 1µbar (~110 km) by operating around 10µm.

The Long- and short-term variability of daytime temperatures at the ~1µbar level from ground-based observing campaigns between 2007 to 2015 shall be presented. The observations yield a large quantity of temperature measurements at different positions on the planetary disk which allows to map a good part of the dayside of Venus. In addition a detailed study of the interesting but not well understood and only poorly investigated area close to the terminator will be given. Investigations on the general behavior of the temperature and differences between the morning and evening terminators are accomplished. Ongoing analysis of thermal variability and comparison to other observing methods and model calculations are in progress and will be included in the presentation if already available.

SIMULATING THE SURFACE OF VENUS ON EARTH

T. Kremic, L. Nakley, D. Vento, J. Balcerski, M. J. Kulis, N. S. Jacobson and G. C. C. Costa, *Glenn Extreme Environments Laboratory, NASA Glenn Research Center, 2100 Brookpark Road Cleveland, OH (tibor.kremic@nasa.gov)..*

Introduction: The growing interest in comparative climatology among the terrestrial planets, the explosion of planets being discovered around other stars and the exciting results of recent orbital and remote observations of Venus provide evidence for a growing case to better understand Earths sister planet. The surface of Venus is quite unlike Earth's surface conditions, and in fact is rather extreme. Science, technology, and planetary mission communities have a growing interest in the unique physicochemical properties and processes that occur under extreme temperature and pressure conditions in exotic and even hostile chemical environments such as Venus. The steadily growing catalog of exoplanets likely contains many examples of bodies with environments dramatically different than the surface of the Earth. Understanding these properties and processes will help us understand the history and present day state of inhospitable and even inaccessible regions of the Earth as well as other solar or extrasolar planets [e.g. 1, 2]. Additionally, Venus and Saturn targets are prioritized in the current Planetary Decadal Survey, with reference missions that include in-situ investigations of these challenging environments. The fact that two of the five recent Discovery mission proposals selected by NASA for further development are Venus-focused adds additional priority and even urgency to laboratory-based extreme environment investigations.

In addition to the importance of science-focused investigations, there is a current and future need for understanding the behavior of advanced technologies and materials in these extreme environments. The materials of course make up instruments and systems in missions and ultimately the success of planetary missions is dependent upon performance testing of instruments and systems in conditions that closely approximate those of the target [3, 4].

Until very recently, there was limited ability to accurately simulate Venus surface-like conditions, especially in vessels large enough to accommodate full-size instruments and components. This gap in capability is being addressed by NASA Glenn's Extreme Environment Rig, called GEER, located in Cleveland, Ohio. This large chamber allows for engineering tests of newly-developed as well as heritage instruments, while simultaneously affording opportunities for geochemical and materials-based science investigations.

GEER capabilities: This presentation provides the features and characteristics of the NASA's unique Glenn Extreme Environment Rig (GEER) and briefly mentions some of the unique contributions that may be expected based on the first few months of operations. GEER is capable of simulating the high temperature and pressure extremes up to Venus surface conditions as well as accurately reproducing the atmospheric chemical compositions of bodies in the solar system including those with acidic and hazardous elements. In the Venus configuration, GEER can reproduce conditions of the supercritical fluid expected at the surface of Venus [5]. With GEER, specific gas quantities can be very accurately injected and then controlled down to parts per million accuracy or better depending on the gas.

Currently, the amount of the chemical species present in the gas or supercritical mixture simulated in GEER can be probed by mass spectrometry. The mass spectrometry analyses are carried out by sampling gases from the GEER chamber at regular intervals for analysis with a high sensitivity quadrupole mass spectrometer which can be tuned to specific chemical species. A Raman spectrometer system has been developed and will be integrated with GEER shortly. The Raman spectrometer will be used to continuously collect the spectra of the gas or supercritical fluid mixture during the experiments and will provide complementary information based on vibrational symmetry of the chemical species present in GEER.

In addition to a summary of capabilities, the presentation provides basic operational approaches and constraints that future users may encounter. This will provide practical information for scientists, technologists and mission planners.

Operating details and some early results: In a typical simulation of an extreme environment (Fig. 1), the system is brought to very low pressures (10^{-6} Torr) at ambient temperature and is then filled with the desired gas mixture. Currently liquid water is added manually but this process is planned to be automated. All other constituents are delivered to the vessel in gas phase using high accuracy mass flow controllers at approximately 34 atm (500 psi). Heat is then applied and controlled to bring the system to the desired steady-state operating point.

Figure 1. Major GEER components.

During a test, the system is fully operated from a control room elsewhere in the building. Temperature is controlled to within 1 degree C and pressure is monitored throughout the duration of the experiment. Chemistry is monitored with mass spectrometry using the sampling process described earlier. A boost system allows the injection of high pressure gases during the experiment to change the chemistry or partial pressures or to top of the system pressure with the original mixture should small leaks occur.

At the end of the test, the system is allowed to cool and then is vented as required based on the constituents and volumes of the chemicals that are in the main vessel.

Since the GEER facility involves operations in thermochemical regimes rarely explored by other industrial or scientific apparatus, it is expected that opportunities for scientific and technical investigation and discovery will arise. In some cases this is due to inability of existing chemical models to accurately represent the observed behavior of complex systems at very high pressure and temperature. Preliminary observations of the behavior of the GEER chamber during heating and pressurization have shown a non-linear increase in pressure as temperature was increased (Fig. 2). That this behavior was observed only in the presence of a Venus-simulant atmosphere (and not when using a simple CO_2-N_2 mix) illustrates the importance and potential of using specialized laboratory facilities to probe environments that are difficult or impossible to otherwise explore.

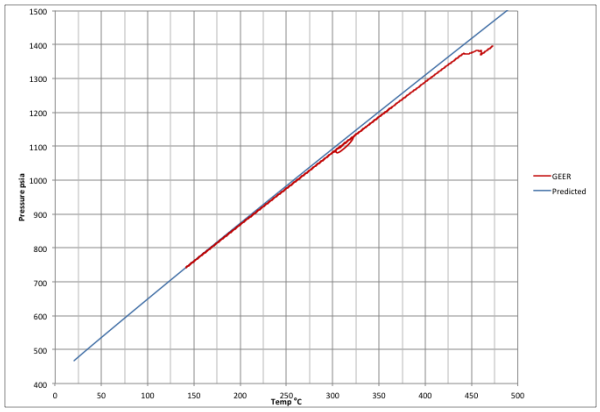

Figure 2. Temperature / Pressure Profile from GEER test.

References: [1] Venus Exploration Analysis Group (VEXAG), "Venus exploration themes" February (2014). [2] Venus Exploration Analysis Group (VEXAG), "Roadmap for Venus exploration" March (2014). [3] D. Daval et al, "Carbonation of Ca-bearing silicates, the case of wollastonite: Experimental investigations and kinetic modelling" Chemical Geology 262, 262-277 (2009). [4] Y. Kato, "Advanced high temperature gas-cooled reactor systems" Journal of Engineering for Gas Turbines and Power 132, 012902/1-012902-7 (2010). [5] B. Fegley Jr., "Venus" In: Meteorites, Comets and Planets, Chapter 2.7 Treatise on Geochemistry, Ed. A. M. Davis, Elsevier Science, 2nd ed. 127-147 (2014).

THE RESURFACING HISTORY OF VENUS: CONSTRAINTS FROM CRATER RETENTION AGES OF GEOMORPHOLOGICAL UNITS.

M. A. Kreslavsky , *University of California, Santa Cruz, CA, USA (mkreslavr@ucsc.edu),* **J. W. Head,** *Brown University, Providence, RI, USA*, **M. A. Ivanov**, *Vernadsky Institute, Moscow, Russia*.

Introduction: Because of atmospheric shielding and endogenic resurfacing, the population of impact craters on Venus (e.g., Herrick et al., 1997; Schaber and Strom, 1999) is small (about a thousand) and consists of large craters. This population has been used in numerous studies with the goal of deciphering the geologic and geodynamic history of Venus, however, the fact that the spatial crater distribution is (almost) indistinguishable from random (e.g., Phillips et al., 1992) has complicated efforts to understand this history. Despite the apparent spatial randomness, craters are not randomly distributed in respect to geological features and units (e.g., Price et al. 1996). Here we utilize the recent 1:15M-scale global geological map of Venus (Ivanov and Head, 2011) and apply rigorous statistical methods to help address this problem.

Source data: The global geologic map contains the following geomorphologic units, in general stratigraphic sequence, oldest to youngest (see Ivanov and Head, 2011 for detailed descriptions of each):

- **t**, tessera;
- **pdl**, densely lineated plains dissected by numerous subparallel narrow and short lineaments;
- **pr**, ridged plains comprising elongated belts of ridges;
- **mt**, mountain belts around Lakshmi Planum;
- **gb**, groove belts, plain material contemporaneous or predating regional plains and deformed by groove belts;
- **psh**, shield plains having numerous small volcanic edifices and locally predating regional plains;
- **rp**, regional plains deformed by wrinkle ridges;
- **sc**, shield clusters, morphologically similar to psh but occurring as small patches that postdate regional plains;
- **ps**, smooth plains of uniformly low radar brightness occurring near impact craters and at distinct volcanic centers;
- **pl**, lobate plains, fields of lava flows that typically are not deformed by tectonic structures and are associated with major volcanic centers;
- **rz**, rift zones.

For each crater from the USGS crater database (Schaber and Strom, 1999), one of us, M.A.I., registered unit(s) superposed by the crater and its continuous ejecta (that is units that predate the crater) and unit(s) that embay the crater (postdate it). This assessment is done uniformly and consistently with the Magellan radar mosaics. The results were used as source data for crater retention age inferences.

Analysis: We performed a statistical analysis of this set of observational data with a modified version of the buffered crater density approach (e.g., Fassett and Head, 2008), which rigorously and consistently takes into account the large size of craters and the fact that many craters are known to predate and/or postdate more than one unit. Mathematical justification and technical details of this approach are given by Kreslavsky et al. (2015). In this analysis we considered crater emplacement as random and resurfacing history as determined (although unknown). In this approach each unit has an effective target area for craters; this area is larger than the physical area of the exposed unit, as illustrated in Fig. 1, top plot. We obtain formal confidence intervals for the mean ages of geological units (Fig. 1, bottom plot). The ages are expressed in terms of T, the mean crater retention age of Venus, which is poorly known and is bracketed between 0.2 Ga and 1 Ga (McKinnon et al., 1997). Fig. 1 shows that there is a group of older units (t, pdl, pr, mt, gb, psh, rp) and a group of significantly younger units (sc, pl, rz), with ps occupying an intermediate position.

The formal unit ages shown in Fig. 1 are the mean unit age. The approach we use does not allow us to assess, how widely the age is scattered within each unit.

The fact that some craters are known to postdate some unit and predate another unit allowed us to estimate the mean age differences between the pairs of units at the unit boundaries. For example, 11 craters superposed on psh and embayed by rp indicate that the mean interval between local psh and rp emplacement is bracketed between $0.03T$ and $0.12T$ (90% confidence). Since the mean ages of psh and rp are not statistically distinguishable (Fig. 1), the lower boundary of $0.03T$ places an important constraint on geological history: emplacememnt of rp does not always occur immediately after emplacement of psh. To improve statistics, we considered merged units, namely a set of "old" units that stratigraphically predate the regional plains (rp) and "young" units that postdate rp. The results are shown in Fig. 2. It is seen that with the 90%-confidence, the mean intervals between the merged units are consistent with the differences between their mean ages.

We also showed that the size-frequency distributions for all units are consistent with each other, when the dependence of target area on crater size is taken into account properly (Kreslavsky and Head (2015).

Interpretation: Our observations are naturally and consistently explained in the framework of the global resurfacing scenario (e.g., Basilevsky et al., 1997; Ivanov and Head, 2013, 2015): (i) After ~*T* ago the overall resurfacing was minor, the total number of obliterated craters was minor, therefore preferential removal of small craters by resurfacing was negligible, and all size-frequency distributions are consistent with the production distribution and with each other. (ii). Intensive tectonic and volcanic resurfacing before ~*T* ago is responsible for similar mean ages of the regional plains (rp) and all pre-rp units. (iii) Formation of the post-rp units occurred slowly through the whole geological history after ~*T* ago, which produces ages close to ~0.5*T*, which is actually observed. Our results taken alone do not constrain how synchronous the intensive resurfacing was; they only indicate that its age averaged over the whole planet is close to *T*. However, other observations, namely, the absence of inverted stratigraphic sequences and the even spatial distribution of craters exclude extremely wide resurfacing age differences.

In the context of this scenario, our results provide new information on the duration of global resurfacing, at least for its latest stages that left the readable record at the surface. The presence of craters embayed by rp and older materials rejects the most radical, catastrophic version of global resurfacing (Schaber et al. 1992), under which resurfacing occurs geologically instantly. The observable "wake" of the intensive resurfacing lasted on the order of ~0.1T, tens of millions of years.

Our observations are difficult to reconcile with the non-directional or equilibrium resurfacing scenarios (e.g., Guest and Stofan, 1999).

References

Basilevsky et al., 1997. in Venus II, 1047.
Fassett, C.I., Head, J.W. 2008. Icarus 195, 61-89.
Guest, J.E., Stofan, E.R. 1999. Icarus 139, 55-66.
Herrick, R.R. et al. 1997. in Venus II, 1015-1046.
Ivanov M.A., Head, J.W. 2011, PSS 59, 1559-1600.
Ivanov M.A., Head, J.W. 2013, PSS 84, 66-92.
Ivanov M.A., Head, J.W. 2015, PSS 113, 10-32.
McKinnon, W.B. et al. 1997. in Venus II, 969-1014.
Kreslavsky, M.A. et al. 2015. Icarus 250, 438-450.
Phillips R.G. et al. 1992. JGR 97, 15923.
Price, M.H., et al. 1996. JGR 101, 4657-4672.
Schaber, G.G., Strom, R.G. 1999. LPSC 30, 1221.
Schaber, G.G. et al. 1992. JGR 97, 13257.

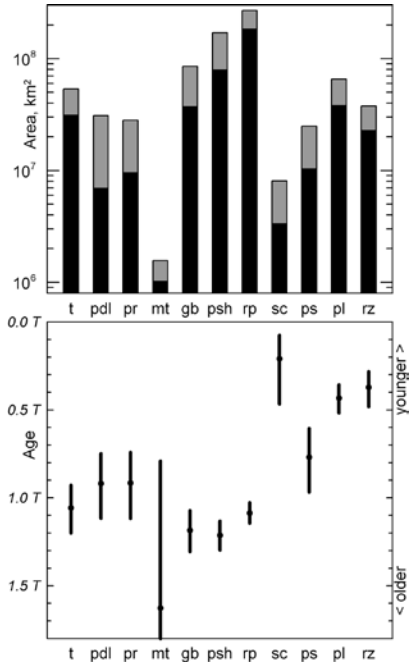

Fig. 1. Top, true areas (black bars) and effective areas (gray bars) for all units. Note the logarithmic scale of the vertical axis: due to this the length of the gray section of each bar illustrates the ratio of effective to true areas. Bottom, 90% confidence intervals for the mean age of each unit.

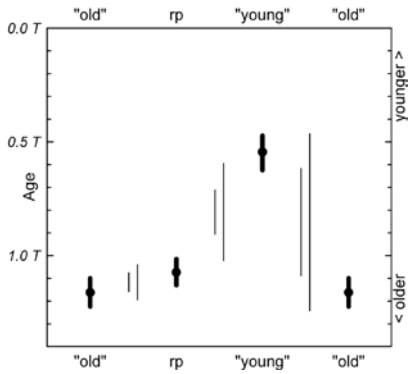

Fig. 2. Bold lines show the 90% confidence intervals for the mean age of regional plains (rp) and two merged units: "old" are merged t, pdl, pr, mt, gb, psh; "young" are merged sc, ps, pl. "Old" line is repeated twice. Pairs of thin lines show the 90% confidence intervals for the mean time difference between the pairs of (merged) units. Their vertical location is arbitrary, only their length is informative: they should be considered as freely sliding up and down.

WAVE ANALYSIS IN THE ATMOSPHERE OF VENUS BELOW 100-KM ALTITUDE, USING THE LMD VENUS GCM.

S. Lebonnois, *Laboratoire de Meteorologie Dynamique, CNRS, UPMC, Paris, France (sllmd@lmd.jussieu.fr)*, **N. Sugimoto,** *Department of Physics, Keio Univ., Yokohama, Japan*, **G. Gilli,** *Laboratoire de Meteorologie Dynamique, CNRS, UPMC, Paris, France*.

Introduction

To explain Venus's atmospheric superrotation, a mechanism of angular momentum transport (so-called GRW mechanism) was proposed by *Gierasch* (1975), completed by *Rossow and Williams* (1979). It involves balance between transport by the mean meridional circulation and transport by eddies. Current General Circulation Models (GCMs) of Venus's atmosphere that reproduce superrotation have supported that mechanism. The role of thermal tides that transport angular momentum vertically in the low latitudes was also pointed out (*Takagi and Matsuda*, 2007; *Lebonnois et al.*, 2010).

Using AFES, a high-resolution Venus GCM starting from superrotation and forced by observed heating rate profile and Newtonian cooling, *Sugimoto et al.* (2014a,b) analysed the wave activity produced in the cloud region. The large vertical zonal wind shear and latitudinal temperature gradient generate the basic state of baroclinic instability in the cloud region. At cloud-top, Rossby type waves are produced by this baroclinic activity.

In the work presented here, a new reference simulation of Venus atmospheric circulation obtained with the LMD Venus GCM (*Lebonnois et al.*, 2010) is described and the simulated wave activity is analysed.

Atmospheric structure and circulation

The LMD Venus GCM is presented in details in *Lebonnois et al.* (2010). Here, we use a new reference simulation of Venus atmospheric circulation done on a 96×96 horizontal grid, on 50 vertical levels (hybrid coordinates) up to roughly 100 km altitude (*Lebonnois et al.*, 2016). It includes topography and an upgraded planetary boundary layer scheme. Radiative transfer uses prescribed tables for solar flux (based on *Crisp*, 1986), and Net-Exchange Rate formalism for infrared wavelengths (*Eymet et al.*, 2009). Clouds are considered as uniform for the radiative transfer computations.

A fully developed superrotation is obtained both when the simulation is initialised from rest and from an atmosphere already in superrotation. Both simulations converge toward the same atmospheric situation after at least 200 Venus days (Vd) of simulation. The maximum zonal wind (up to 120 m/s) covers a region between 10^4 and 200 Pa, between 60°N and 60°S. The vertical profile of the zonal wind below 2×10^4 Pa is roughly linear with altitude, though it is approximately half the observed values. The temperature structure is in good agreement with the observations. An equator-to-pole contrast about 30 K is obtained near 60 km altitude, with a cold-collar structure visible near 3×10^3 Pa (roughly 67 km, Fig. 1) similar to the structure obtained with AFES (*Ando et al.*, 2016). The vertical profile of static stability is also in good agreement with observations.

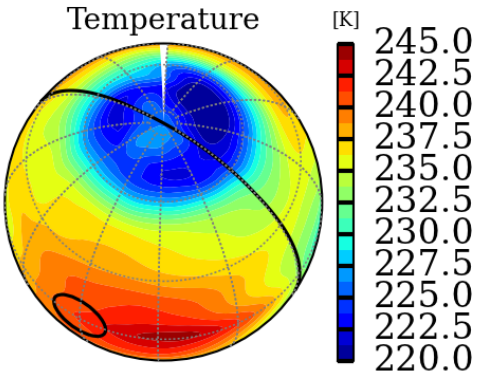

Figure 1: Temperature field at pressure p=3×10^3 Pa (∼67 km altitude) in the northern polar region. Temperature is averaged over 1/100 Vd (1.17 Ed). The black contours show the subsolar area and the terminator.

Atmospheric waves

To study the waves developing in the modeled atmospheric circulation, we use Fast Fourier Transform (FFT) to analyse frequency spectrum of temperature, zonal and meridional wind fields. To separate the different waves, we apply filters on the FFT spectra, before applying a reverse FFT. Filtering is done at these cutting frequencies: 4, 10 and 22/Vd.

In the upper cloud, the vertical angular momentum is transported by the diurnal and semi-diurnal tides. The semi-diurnal tide is dominating in the low to mid latitudes between 10^4 Pa and 10^2 Pa, while the diurnal tide dominates above 10^2 Pa, and at high latitudes. This is consistent with the analysis of previous simulations at lower resolution, discussed in *Migliorini et al.* (2012) in comparison with VIRTIS/Venus-Express dataset analysis. The amplitude of these tides (5 to 10 K in the pressure range 10^4 to 10^2 Pa) is also consistent with the observed values.

Above the cloud base (approximately 1 bar), equatorward transport of angular momentum is done by po-

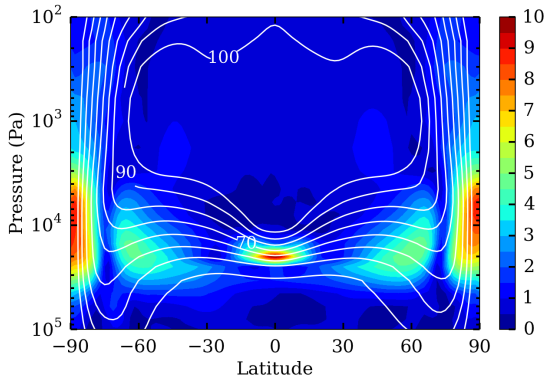

Figure 2: Amplitude of the FFT spectrum of the zonal wind, at the frequency 15.5/Vd (period around 7.3 Ed). The white contours show the mean zonal wind field (in m/s).

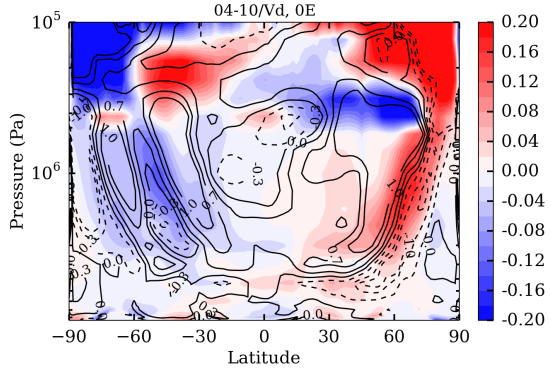

Figure 3: Instantaneous temperature (colors, in K) and meridional wind (contours, in m/s) perturbations filtered in the frequency band [04-10]/Vd, at 0° longitude.

lar barotropic and mid- to high-latitude baroclinic waves present in the cloud region, with frequencies between 5 and 20 cycles per Venus day, periods between 6 and 23 Earth days (Ed). In the middle cloud, just above the convective layer, a Kelvin type wave (period around 7.3 Ed) is present at the equator (Fig. 2), as well as a low-latitude Rossby-gravity type wave (period around 15 Ed). The waves visible at mid-latitudes in Fig. 2 have a structure similar to the baroclinic waves obtained in the AFES simulations of *Sugimoto et al.* (2014b).

Below the clouds, large-scale waves develop and play a significant role in the angular momentum balance. The dominant waves are seen at mid- to high-latitudes, with frequencies up to 30/Vd. The dominant frequency in the spectra is around 7-8/Vd. Figure 3 illustrates the meridional distribution of these waves. Meridional wind perturbations are linked to temperature perturbations: convergence is related to positive temperature perturbations, and divergence to negative. These waves are identified as gravity waves. The source region is the stable zone below the clouds (around 2-3×10^5 Pa), where these waves may be excited through the perturbations in temperature induced in this layer by the cloud-region baroclinic waves. These large-scale downward-propagating gravity waves have never been suggested before. Their role in the angular momentum budget appears to be significant in the deep atmosphere.

References

Ando, H., Sugimoto, N., Takagi, M., Kashimura, H., Imamura, T., Matsuda, Y., (2016),The puzzling Venusian polar atmospheric structure reproduced by a general circulation model, *Nature Comm.*, *In press*.

Crisp, D. (1986). Radiative forcing of the Venus mesosphere. I - Solar fluxes and heating rates. *Icarus*, *67*, 484–514.

Eymet, V., R. Fournier, J.-L. Dufresne, S. Lebonnois, F. Hourdin, and M. A. Bullock (2009), Net-exchange parameterization of the thermal infrared radiative transfer in Venus' atmosphere, *J. Geophys. Res.*, *114*, E11,008.

Gierasch, P. (1975),Meridional circulation and the maintenance of the Venus atmospheric rotation, *J. Atmos. Sci.*, *32*, 1038–1044.

Lebonnois, S., F. Hourdin, V. Eymet, A. Crespin, R. Fournier, and F. Forget (2010), Superrotation of Venus' atmosphere analysed with a full General Circulation Model, *J. Geophys. Res.*, *115*, E06,006.

Lebonnois, S., N. Sugimoto, and G. Gilli (2016), Wave analysis in the atmosphere of Venus below 100-km altitude, simulated by the LMD Venus GCM, *Icarus*, *submitted*.

Migliorini, A., Grassi, D., Montabone, L., Lebonnois, S., Drossart, P., Piccioni, G. (2012), Investigation of air temperature on the nightside of Venus derived from VIRTIS-H on board Venus-Express, *Icarus*, *217*, 640–647.

Rossow, W. B., and G. P. Williams (1979), Large-scale motion in the Venus' stratosphere, *J. Atmos. Sci.*, *36*, 377–389.

Sugimoto, N., M. Takagi, and Y. Matsuda (2014a), Baroclinic instability in the Venus atmosphere simulated by GCM, *J. Geophys. Res. Planets*, *119*, 1950–1968.

Sugimoto, N., M. Takagi, and Y. Matsuda (2014b), Waves in a Venus general circulation model, *Geophys. Res. Lett.*, *41*, 7461–7467.

Takagi, M. and Matsuda, Y. (2007). Effects of thermal tides on the Venus atmospheric superrotation, *J. Geophys. Res.*, *112*, D09112.

SENSITIVITY OF NET THERMAL FLUX TO ABUNDANCE OF TRACE GASES IN THE VENUS ATMOSPHERE BELOW THE CLOUDS

Y.J. Lee, ISAS/JAXA, Japan (leeyj@ac.jaxa.jp), **H. Sagawa**, Kyoto Sangyo University, Japan, **R. Haus**, Westfälische Wilhelms Universität Münster, Germany, **S. Stefani**, INAF-IAPS, Italy, **T. Imamura**, ISAS/JAXA, Japan, **D.V. Titov**, ESTEC/ESA, The Netherlands, **G. Piccioni**, INAF-IAPS, Italy.

Introduction

Radiative energy balance in the deep atmosphere of Venus is difficult to characterize remotely due to the dense CO_2 atmosphere and thick cloud layer. Only few in-situ experiments had measured the net flux, by Pioneer Venus small probe net flux radiometers (SNFR). Revercomb et al. (1985) simulated the net thermal flux profiles measured by the north and night probes, using 20–200 ppmv water vapour abundance below the clouds. However, this water vapour abundance is much larger than the observed abundance, 20–50 ppmv (Bezárd et al. 1990, Marcq et al. 2008, Arney et al. 2014, Haus et al. 2014). The reason for the requirement of large water vapour amount would be an insufficient gaseous opacity, especially CO_2. We use a recent gaseous opacity database, and investigate the influence of thermal opacity sources to explain the observed variability of net thermal flux profiles. Our calculations suggest that the net flux profiles measured by Pioneer Venus night and north probes are consistent with water vapour abundance of 20-50 ppmv.

Methods and Data

We used line-by-line method, combined with a 1D radiative transfer model, SHDOM (Evans 1998). We developed an atmospheric model for the 0–100 km altitude range. This model covered a broad spectral range, from 50 cm^{-1} to 8300 cm^{-1} (=1.2–200 μm). For atmospheric gases, we took into account CO_2 and N_2, and trace gases (H_2O, SO_2, OCS, CO, H_2S, HF, and HCl). CO_2 absorption line parameters were taken from HITEMP2010, and took into account sub-Lorentzian line correction factors. We carefully compared recent data and old data sets on the CO_2 collision-induced absorptions, and decided to use data in Gruszka and Borysow (1997), Baranov et al. (2004), Stefani et al. (2013), Marcq et al. (2006), and Bezárd et al. (1990). We found that Moskalenko et al. (1979)'s CO_2 collision-induced absorption data is not suitable, even though this data has been used in previous studies (Bullock and Grinspoon 2001, Takagi et al. 2010, Mendonça et al. 2015). There is considerable discrepancy with the recent data, for example, two times stronger absorption than Baranov et al.'s data in the 1100–1600 cm^{-1} range, and absorption spectrum cannot be confirmed from recent laboratory experiment measurements (Stefani et al. 2013). This laboratory experiment data have been used for our CO_2 collision-induced absorption in the 2650–3130 cm^{-1} range. We also took into account H_2O continuum in the 2000–8300 cm^{-1} range (Ptashink et al. 2011, 2012 and 2013). H_2O absorption in the 50–2000 cm^{-1} range, and those of all other gases were calculated using HITRAN2012. We used the cloud model described in Crisp et al. (1986), using 75% sulfuric acid aerosols and four different sizes. Temperature and pressure profiles were taken from VIRA. We set a standard condition of trace gases' abundances as described in Titov et al. (2007) (hereafter, STD).

Results

We firstly compare different opacities in the lower cloud layer (48–50 km), that changed by a factor of one to four, CF1.0–CF4.0. Figure 1 shows that changing cloud opacity does not strongly affect the net thermal flux below the clouds. Since the intended comparison with the measured flux profiles focuses on the altitudes below the clouds (see Fig. 3), any constant cloud factor can be used in our simulations between 1.0 and 4.0. We decide to use CF=2.8 (CF2.8) for our STD condition, as we can fit well our synthetic spectrum to an observed 2.3 μm atmospheric window spectrum, taken from VIRTIS at the low latitudinal region (Fig.1b). But note that actual 2.3 μm radiance strongly varies with latitude and local time, meaning various cloud opacities.

Secondly, we perform a sensitivity study of thermal flux to abundance of each trace gas below 52 km altitudes. SO_2, H_2O, OCS, CO, and HCl are varied within the range of observation (Bezárd et al. 1990, Marcq et al. 2006, Arney et al. 2014, Haus et al. 2014), while all other gases are fixed to the STD condition. We find most significant thermal opacity source is SO_2, when its abundance is less than 50 ppmv. This affects net thermal flux right below the clouds strongly, as shown in Fig. 2a. Such small

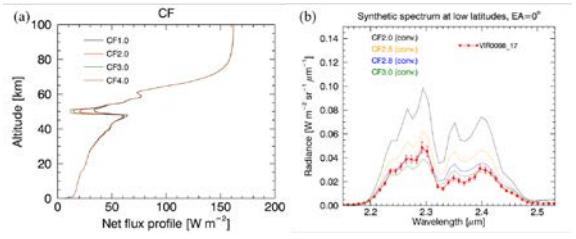

Figure 1. Effect of the lower cloud's opacity on net thermal flux (a), and a comparison between an observed radiance and synthetic spectra at the 2.3 μm atmospheric window (b). Lower cloud's opacity is varied as shown in legends (see text for details). Observed spectrum is shown with the red line of (b), taken from VIRTIS/Venus Express (Orbit number 96 and qube number 17).

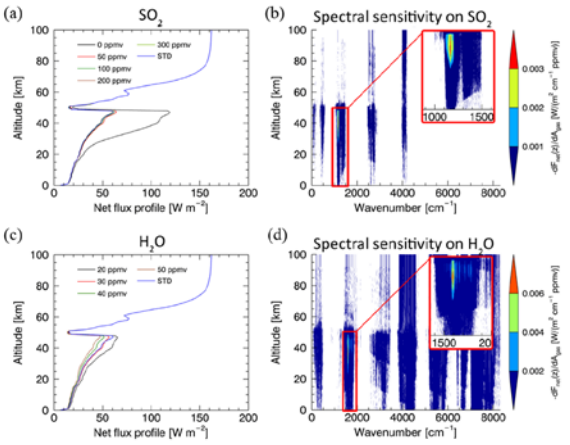

Figure 2. Sensitivity of net thermal flux on SO_2 and H_2O abundances. Integrated net flux profile is varied, depending on the SO_2 and H_2O abundances (a and c). The difference of monochromatic net flux between the minimum and maximum abundances is shown in color contours (b and d).

quantity of SO_2 would be extreme, but we find it important, as this implies that the greenhouse effect of SO_2 seems to be underestimated in a previous study (Taylor and Grinspoon 2009), which used Moskalenko et al.'s CO_2 collision-induced absorption, covering a fundamental band of SO_2 at 1151 cm^{-1} (Fig. 2b). H_2O is the second significant source as shown in Fig. 2c, when the abundance range is from 20 ppmv to 50 ppmv. Its influence is spread over a broad spectral range (Fig. 2d), implying its high potential as a greenhouse gas. OCS is the third one, when its abundance varies from 0 ppmv to 5 ppmv (not shown). Our results show that CO makes a weak influence, and HCl is negligible (not shown).

We use maximum (MAX) and minimum (MIN and MIN2) abundances of trace gases to estimate the range of net thermal flux variation below the clouds, and compare our results to the measured flux profiles. Figure 3 shows the results. MIN is perhaps extreme, due to 0 ppmv SO_2 abundance. MIN2 uses a moderate SO_2 abundance by 80 ppmv, but other gases are the same as MIN. Our results well explain the measured net flux profiles above ~35 km altitudes, using the 20–50 ppmv H_2O abundance, differently from Revercomb et al. (1985).

As we can simulate a range of net thermal flux variation as shown in Fig. 3, the observed spatial distribution of SO_2, H_2O, and OCS abundances can be interpreted as net thermal flux variations. An area having less abundances of trace gases will have stronger thermal cooling. In addition, the range of cooling rate variation at 36.5 km altitude is 0.015 K/day, from 0.014 K/day (MAX) to 0.029 K/day (MIN2) (extremely, 0.077 K/day for MIN), which is comparable to the meridional gradient of a diurnally averaged solar heating, from 0.011 K/day at equator to 0.001 K/day at a pole at the 36.1 km altitude (Tomasko et al. 1985). This implies that a careful consideration on trace gases is needed to estimate a net radiative energy balance below the clouds.

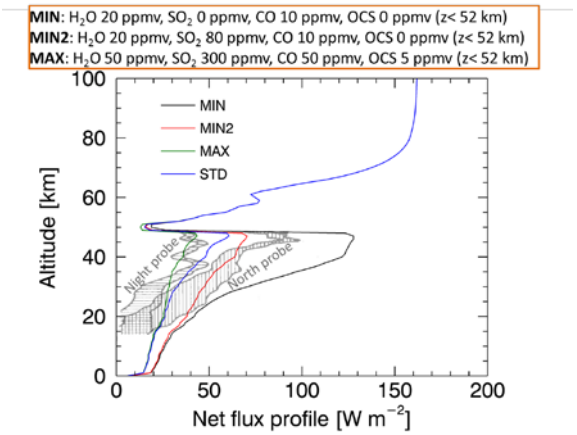

Figure 3. Comparison of net flux profiles using maximum and minimum trace gaseous abundances. The abundances of each gas are shown in the upper red box. The in-situ measurement flux profiles are marked together (grey shaded lines), taken from Revercomb et al. (1985).

Summary

We developed the atmospheric model to calculate the net thermal flux in the Venus atmosphere from surface to 100 km altitude in the 50–8300 cm^{-1} range. We carefully prepared the CO_2 absorption data, including the recent collision-induced absorption. We performed the sensitivity study of net thermal flux to abundance of trace gases, and showed that SO_2, H_2O, and OCS are important thermal opacity sources. Our model successfully explains the measured flux profiles by the north and night probes of Pioneer Venus using the observed 20–50 ppmv H_2O abundance. Too high H_2O abundance, up to 200 ppmv (Revercomb et al. 1985), is not required. Our results show the considerable influence of trace gases in the thermal energy. This implies that we need to consider trace gases carefully to calculate accurate net radiative energy balance below the clouds.

VENUS CLOUD LEVEL CONVECTION IN THE EQUATORIAL REGION

Y.J. Lee, ISAS/JAXA, Japan (leeyj@ac.jaxa.jp), **T. Imamura**, ISAS/JAXA, Japan, **K. Sugiyama**, ISAS/JAXA, Japan, **T.M. Sato**, ISAS/JAXA, Japan, **Y. Maejima**, RIKEN AICS, Japan.

Introduction

Observed UV images on Venus show cloud morphology variations near the cloud top altitudes (~70 km). A clear difference can be seen between laminar flow shaped clouds on the morning side and convective-like cells on the afternoon side of the planet in the equatorial region (Titov et al. 2012). Baker et al. (1998) suggested that deep convective motions in the low-to-middle cloud layers at the 40–60 km range can explain cellular shapes. Imamura et al. (2014) argued that this cannot be a reason, as convection in the low-to-middle cloud layers can be suppressed near sub solar regions due to a stabilizing effect by strong solar heating. The observed feature may be related to strong solar heating at local noon time (Lee et al. 2015). Also, horizontal uneven distribution of an unknown UV absorber and/or cloud top structure may trigger horizontal convection (Toigo et al. 1994). In order to examine these possibilities, we processed radiative model calculations for various cloud structures, which include the unknown UV absorber, and we employed the results into a 2D fluid dynamic model calculation. Our result suggests locally unbalanced net energy and/or horizontally uneven solar heating for possible reasons of the observed features.

Methods

We developed gaseous absorption data set of the atmosphere from surface to 100 km altitude. Gaseous absorptions of CO_2, H_2O, SO_2, OCS, CO, H_2S, HF, and HCl were included. CO_2 absorption line parameters were taken from HITEMP2010. We took into account sub-Lorentzian shape functions and CO_2 collision-induced absorptions. All other gaseous absorption line parameters were taken from HITRAN2012. The cloud aerosols were assumed to be 75% sulfuric acid with four different sizes. We compared three cloud models; 'Crcld' was taken from Crisp (1986), 'Zacld' from Zasova et al. (2007), 'ZLcld' from Lee et al. (2015). Their cloud bottom level is ~48 km and the cloud top level ~70 km, but the vertical structures are different each other. The unknown UV absorber is assumed to exist only at the upper cloud layer. Solar heating and thermal cooling were calculated over the 0.2–5 μm range and the 1.2–200 μm range, respectively, using a radiative transfer model (SHDOM, Evans 1998). Temperature and pressure profiles were taken from VIRA at low latitudes (Seiff et al. 1985), so both of thermal cooling and solar heating profiles are corresponding to those at low latitudes.

The above calculation results were employed in a 2D fluid dynamic model (CReSS, Tsuboki and Sakakibara 2007). Our model domain covered the 35–100 km altitude range with a 100 m vertical grid, but the actual valid range was from 40 km to 80 km, because of sponge layers at the bottom 5 km and the top 20 km. Horizontal distance was 100 km with a 200 m grid size. We fixed thermal cooling over all local time, but solar heating varied along local time. We assumed the length of Venusian day as an atmospheric rotation time at the 65–70 km altitudes, which is about 4 Earth days. We used a fixed heat capacity as 821 [J kg^{-1} K^{-1}], corresponding to 60 km altitude value, so this can examine a possibility of combining deep cloud level convection and cloud top level convections.

Results

We note that the equatorial region is supposed to have an upward branch of Hadley circulation. We find that our model results are affected by an assumption on the global circulation. Here, we compare four conditions. Case 1 uses different cloud structures without any assumptions on the global circulation. Case 2 assumes that the global circulation removes unbalanced net radiative energy efficiently above 60 km altitudes. Case 3 assumes an upward motion at the cloud top level. Case 4 similar to Case 2, but introduces horizontally uneven heating distribution. Cases 2-4 use one cloud model, 'Crcld'.

Case 1. Following the different vertical structures of the clouds, the thermal cooling and solar heating profiles are different for each cloud model. Our results on cloud level convection, however show that separated convective layers are present for all of three cloud models; lower convective layer near the cloud bottom (~50 km) and upper convective layer near the cloud top level (~70 km) (Fig. 1, but shown only for 'Crcld'). The result using 'Crcld' shows most clear local time variation, with opposite cycle between the upper convective layer and the lower convective layer (Fig.1). Diurnal variation is different depending on the cloud models (not shown). When we use 'ZLcld', the result shows the similar diurnal cycle for the upper convective layer as the case using 'Crcld' does. Using 'Zacld', the result shows strong convection at the upper convective layer. However, note that Case 1 does not consider the global circulation, so unbalanced radiative energy changes temperature from the initial profile. We interpret this result qualitatively.

Case 2. We assume that the global circulation would remove unbalanced net radiative energy effi-

ciently above 60 km altitude, differently from Case 1. As shown in Fig. 2a, unbalanced net energy (red lines) is removed. Under this assumption, temperature does not change with integration time. Figure 2b shows the result. This shows that the upper convective layer disappears, differently from Case 1. The lower convective layer becomes weaker than Case 1, as the cooling at the middle cloud layer is reduced.

Case 3. A fixed upward wind is assumed as shown in Fig. 3a. This causes adiabatic cooling, suppressing excessive solar heating at low latitudes, but does not remove weak cooling above the cloud top. Note that a vertical distribution of the unknown UV absorber can vary, and affect heating/cooling near the cloud top level (Lee et al. 2015). The result of convective motion is shown in Fig. 3b. The upper convective layer is reduced significantly compared to Case 1, but weakly exists. The lower convective layer is similar to Case 1.

Case 4. All conditions are the same as Case 2, but we introduce horizontally uneven solar heating above 60 km. The solar heating varies horizontally, following a sinusoidal function of 50 km cycle. This resembles no unknown UV absorber (bright UV) and more unknown UV absorber (dark UV), resulting 50% less heating and 50% more heating, respectively. Figure 4 compares vertical winds at afternoon time between Case 2 and Case 4. The result shows uneven solar heating can develop weak upward motions, at where more solar heating exist, and vice versa (Fig.4b). During night time, this structure disappears, and wave structures are enhanced.

Summary

We compared three different cloud models and a global circulation influences on convective motions at the cloud deck. Our results show that all of cloud models develop two distinct convective layers, near the cloud top and bottom levels (Case 1). The diurnal variation of the convective layers differ each other, due to different vertical radiative energy distribution. 'Crcld' and 'ZLcld', however show stronger convection near the cloud top level at local noon time. This might be qualitatively related to the observed convective-like cells at the afternoon side of Venus. The result depends on an assumed global circulation influence. Case 2 shows the disappearance of the upper convective layer. Possible other reasons of the observed convective-like cells would be related to an unbalance between the local radiative forcing and the global circulation (Case 3), and horizontally uneven solar heating distribution (Case 4).

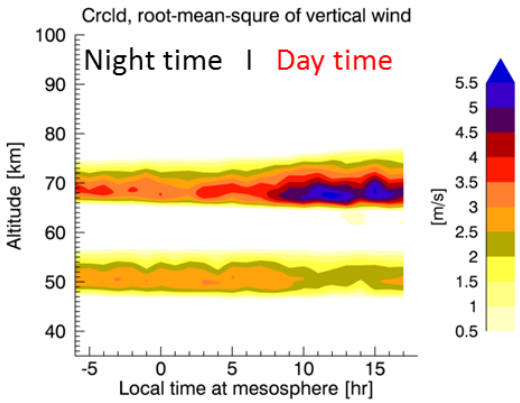

Figure 1. Diurnal variation of convective layers in the equatorial region of Venus at the 40–80 km altitude range (Case 1). Color contours show root-mean-square of vertical winds, using 'Crcld'.

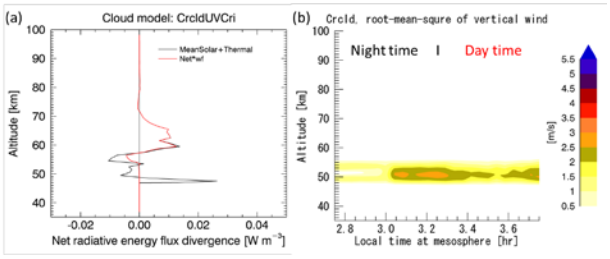

Figure 2: The condition described in Case 2, and the result in vertical winds. (a) shows diurnally averaged net radiative forcing (black solid line), and removed unbalanced net energy assuming efficient global circulation (red solid line) (see text for details). (b) shows a result of vertical winds. 'Crcld' is used for this result. The upper convective layer disappears, and the lower level convection is weakened.

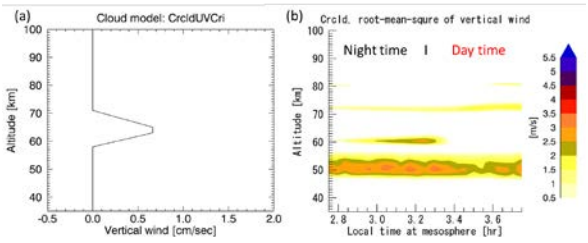

Figure 3. The assumed upward wind to cancel the excessive solar heating, described in Case 3 (a), and the result in vertical winds (b). 'Crcld' is used for this result. The upper convective layer is weakened compared to Case 1, and convective layer at 60 km is artifact.

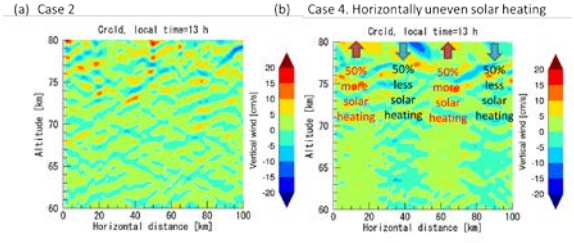

Figure 4. Snapshots of vertical wind fields at the 60-80 km altitude range at 13h local time. (a) Case 2 result. (b) Case 4 result.

THREE-DIMENSIONAL MODELLING OF VENUS PHOTOCHEMISTRY

F. Lefèvre , **A. Stolzenbach, A. Määttänen, S. Bekki,** *LATMOS, Paris, France (franck.lefevre@latmos.ipsl.fr),* **S. Lebonnois**, *LMD, Paris, France*.

We have developed a new code of the Venus atmospheric chemistry based on our photochemical model already in use for Mars (e.g., Lefèvre et al., 2004). The model provides a comprehensive description of the CO_2, sulfur, chlorine, oxygen, and hydrogen chemistries with state-of-the-art kinetics data. For Venus, the code also includes a parameterized treatment of cloud microphysics that computes the composition, number density, and sedimentation rates of sulfuric acid aerosols based on observed altitude-dependant size distributions. We have coupled this photochemical-microphysical package to the LMD general circulation model of Venus (Lebonnois et al., 2010). We will describe the results obtained with this first three-dimensional model of the Venus photochemistry. The space and time distribution of key chemical species as well as the modelled cloud characteristics will be discussed and compared to observations performed from Venus Express and from the Earth. We will place particular emphasis on sulfur species, which are subject in the GCM to three-dimensional transport and convection, condensation-evaporation-sedimentation via H_2SO_4 in the cloud layer, and photochemistry above the clouds.

References:

Lefèvre, F., et al., J. Geophys. Res., 109, doi:10.1029/2004JE002268, 2004.

Lebonnois, S., et al., J. Geophys. Res., 115, doi:10.1029/2009JE003458, 2010.

Figure legend (left):

Examples of zonally-averaged distributions of key chemical species calculated by the model. top : CO (ppmv); middle: gas-phase H_2O (ppmv); bottom : SO_2 (ppmv)

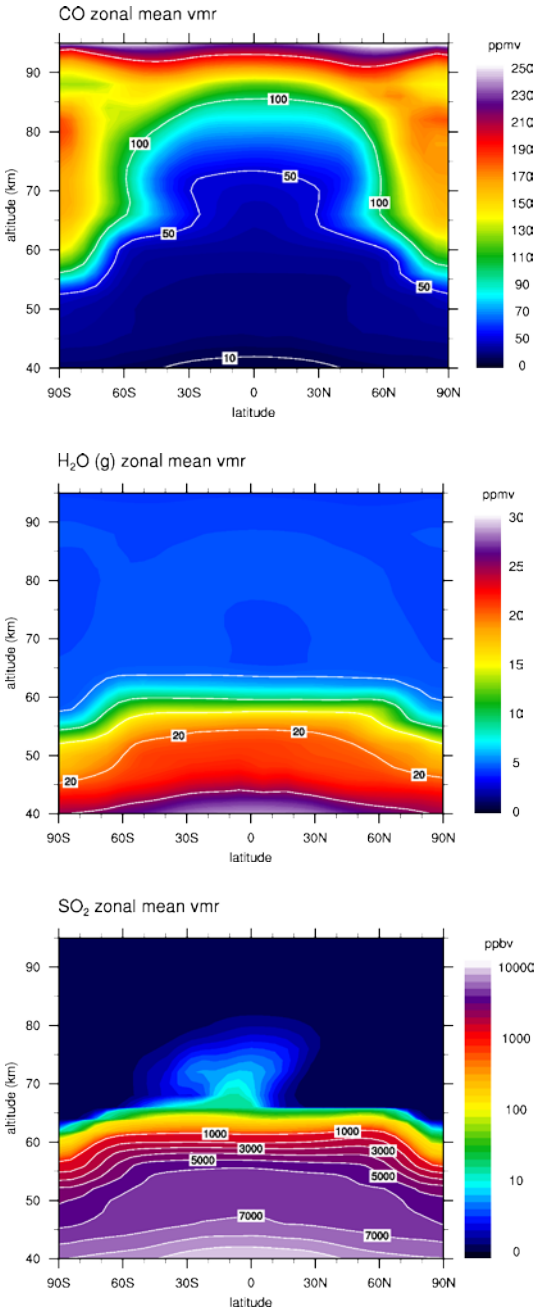

THREE-DIMENSIONAL MESOSCALE MODELING OF THE VENUSIAN CLOUD LAYER AND ASSOCIATED GRAVITY WAVES.

Maxence Lefèvre, *(maxence.lefevre@lmd.jussieu.fr)*, **Aymeric Spiga, Sébastien Lebonnois,** *Laboratoire de Météorologie Dynamique, Université Pierre et Marie Curie, Centre National de la Recherche Scientifique, Paris, France.*.

Background

Venus hosts a sulfuric acid cloud layer which properties has been investigated by Venus Express. One of the main question that remains unclear about the dynamics of the atmosphere and its interaction with the photochemistry is the characterization of the cloud convective layer which mixes momentum, heat and generates gravity waves observed too by Venus Express [13] [12]. This dynamical forcing induced by the cloud layer has been proposed as a significant contribution to the maintenance of the super-rotation [8]. However these waves develop from regional to local scales and can not be resolved by global circulation models (GCM) developed insofar.

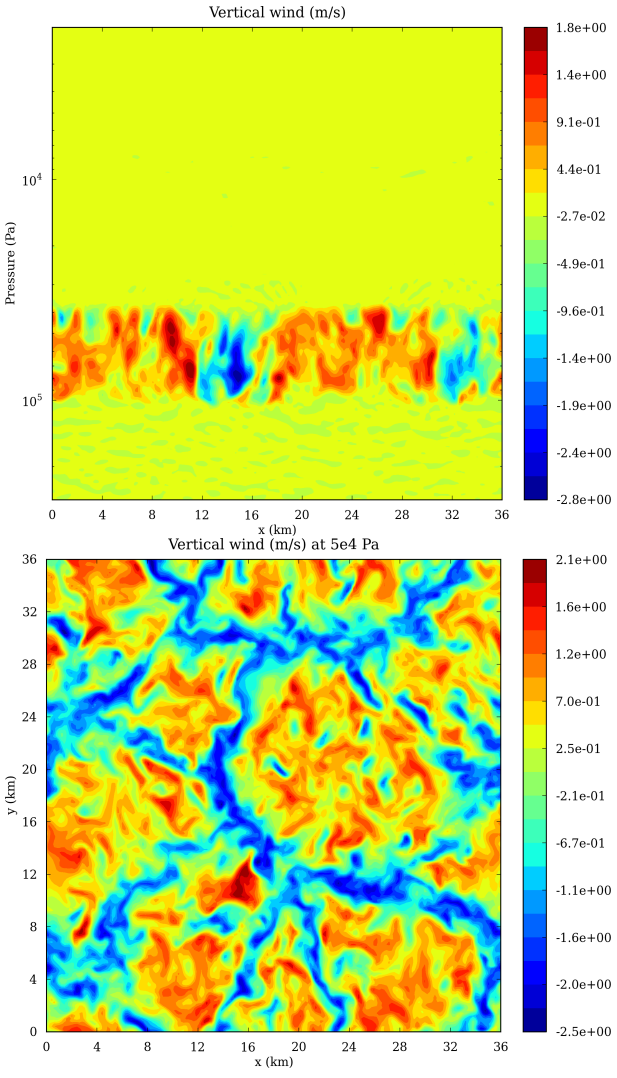

Figure 1: Convective vertical winds in the Venusian cloud layer. Top: vertical / horizontal cross-section. Bottom: horizontal cross-section at pressure level 5×10^4 Pa.

Model

Following the 2D modeling studies of Baker et al. [1, 2, 3, 4] and Imamura et al. [9], we developed at LMD a 3D Venusian mesoscale model based on the LMD Martian mesoscale model [16] which makes use of the Weather Research and Forecast terrestrial model [15]. We report a first application of this model : simulating convection in the Venusian cloud layer (and associated gravity waves) by 3D turbulent-resolving simulations (Large-Eddy Simulations, hereinafter LES). Our simulation domain is 36 km x 36 km horizontally, and ranges vertically from 40 km to 70 km. Horizontal and vertical resolution are 200 m (similar to Imamura et al 2014[9]). Our Venus LES model employs an offline radiative forcing based on heating rate by the LMD Venus GCM. We are using three distinct of heating rates, two radiative ones : a short wave (solar), a long wave (IR), and heat transfer associated with the global dynamics of the atmosphere (mainly the Hadley cell). These input files are extracted from LMDZ run which reached super-rotation [10]. To explore the sensitivity of our model we used several LMDZ runs. The runs we used all shared a common solar flux scheme based on Crisp 1986[5]. One of the simulations used [11] includes a radiative transfer based on Eymet et al (2009[6]) and a cloud model based on Zasova et al (2007[18]). The other LMDZ simulation used employs a new radiative transfer matrix and a cloud model based on Haus et al (2014[7]). By forcing our LES with thermal profiles and heating rates from these global LMDZ simulations, we are able to characterize the convection and associated gravity waves in function of latitude and local time. To show the impact of the general circulation on the convection we ran several simulations with input file from the 1D LMD Venusian physics model (i.e. without dynamics).

Results

In Fig 1, the vertical and horizontal cross-sections of the vertical wind caused by convection are presented and the Fig 2 shows the temperature perturbations induced by the gravity waves. The fields are shown at the equator at midnight. All of these figures are from simulations using input file from the LMDZ using the could model from Haus et al 2014[7].
The vertical and horizontal cross-sections of the vertical wind in Fig 1 show how the convection is organized. The convection is very active between 1.10^5 and $3.8.10^4$ Pa and it is organised in cells close to the Rayleigh-Bernard hexagonal type cell made by the ascending motion. The vertical wind values are between -4 and 2.5 m s^{-1} in the convection, values close to the ones measured by VEGA balloons (from 1 to 5 m s^{-1} , [14]) although slightly underestimated. The size of the cells is approximately of 8x8 km^2.

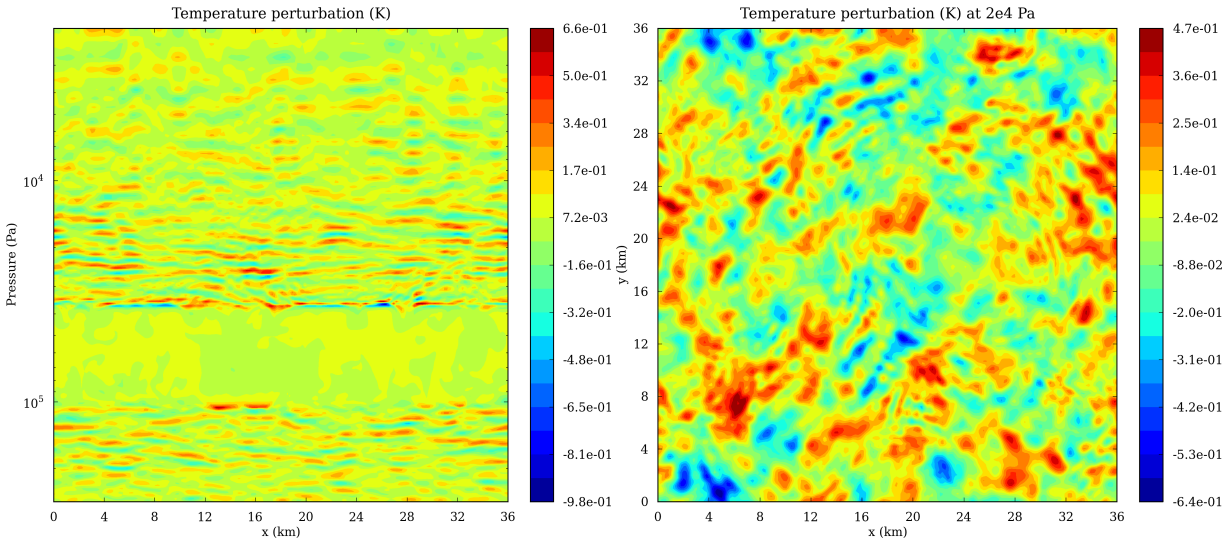

Figure 2: Convective induced gravity waves evidenced by the temperature perturbation. Top: vertical / horizontal cross-section. Bottom: horizontal cross-section above the summit of the convective layer at pressure level 2×10^4 Pa.

Each plume interacting with the stable layers (above or below) generate gravity waves with a circular wavefront which propagate both vertically and horizontally. Fig 2 presents the induced gravity waves evidenced by the temperature perturbation. The amplitude of these perturbations are about 0.5 K, closer to the summit of the convective layer it can reach 1K which is close to the VeRa observation (3 K [17]) but yet again slightly underestimated. The vertical wavelength of these waves (Fig 2 left) is around 1 km which is consistent with the VeRa observations too. Each updraft generates waves with distinct horizontal wavelength and Fig 2 the interference pattern of these waves. Further analysis shows that three different wavelengths are dominant : 1 km, 4 km and 20 km. These wavelengths are consistent with the VMC observations [13] except that we obtain circular wavefronts instead of linear ones.
We also explore the dependence of the convection on latitude and local time. We observe stronger convection on the night side and at high latitudes.
A complete analysis will be presented at the conference.

Perspectives

After analysing these results obtained with fixed heating rate profiles, we are working on a more realistic model with online radiative transfer scheme. We will also investigate the impact of the zonal and meridional shear on the convective motion. Investigating the characteristics of the gravity waves, both above and below the cloud layer is our priority, as well as their influence in maintaining the superrotation. The activity within the Planetary Boundary Layer is also a target for study with this tool.
This mesoscale model is also the first step towards a realistic gravity wave parametrization to be included in Venus GCM.

References

[1] R. D. Baker et al. *J. of Atm. Sc.*, 55:3–18, 1998.
[2] R. D. Baker et al. *J. of Geophys. Res.*, 104:3815–3832, 1999.

[3] R. D. Baker et al. *J. of Atm. Sc.*, 57:184–199, 2000.

[4] R. D. Baker et al. *J. of Atm. Sc.*, 57:200–215, 2000.

[5] D. Crisp. *Icarus*, 67:484–514, 1986.

[6] V. Eymet et al. *J. of Geophys. Res. (Planets)*, 114:E11008, 2009.

[7] R. Haus et al. *Icarus*, 232:232–248, 2014.

[8] A. Y. Hou and B. F. Farrell. *J. of Atm. Sc.*, 44:1049–1061, 1987.

[9] T. Imamura et al. *Icarus*, 228:181–188, 2014.

[10] S. Lebonnois et al. *J. of Geophys. Res. (Planets)*, 115:E06006, 2010.

[11] S. Lebonnois et al. *J. of Geophys. Res. (Planets)*, 120:1186–1200, 2015.

[12] J. Peralta et al. *J. of Geophys. Res. (Planets)*, 113:E00B18, 2008.

[13] A. Piccialli et al. *Icarus*, 227:94–111, 2014.

[14] R. Z. Sagdeev et al. *Science*, 231:1411–1414, 1986.

[15] W. C. Skamarock and J. B. Klemp. *Journal of Computational Physics*, 227:3465–3485, 2008.

[16] A. Spiga and F. Forget. *J. of Geophys. Res. (Planets)*, 114:E02009, 2009.

[17] S. Tellmann et al. *Icarus*, 221:471–480, 2012.

[18] L. V. Zasova et al. *Plan. and Sp. Sc.*, 55:1712–1728, 2007.

Trouble with Venus II – Old and New Questions.

S.S. Limaye, *Space Science and Engineering Center University of Wisconsin, Madison, Wisconsin, USA (Sanjay.Limaye@ssec.wisc.edu)*

Introduction:

Carl Sagan discussed a number of questions about Venus in a paper titled "The Trouble with Venus" (1971) published in the proceedings of the IAU Symposium No. 40 held in Marfa, Texas which largely focused on properties of the clouds (are they made of water ice?) and microwave emissions and surface temperature. Other questions he noted as clearly important and far from being solved at that time were:

- Why Venus should be rotating in a retrograde direction?
- Why Venus should be locked or almost locked in rotation at moments to inferior conjunction with the earth?
- Why (do) the clouds of Venus show a four day retrograde rotation?

He also discussed the possibility of life in the clouds. By 1971 the space missions to explore Venus were limited to Mariner 2, Venera 4, Venera 6 and Mariner 5. Since then we have obtained a huge amount of data about the planet and its atmosphere from fly-by spacecraft, orbiters, entry probes and two balloons. Yet his belief that "The question of the composition of Venus clouds is by no means solved, at least to the satisfaction of all investigators in the field at the present time. But I will be surprised if we are more than a few years from such a solution" has not yet been proven correct yet.

True, considerable advances in the knowledge of the clouds have been made. Noteworthy being the identification of sulfuric acid by Hansen and Hovenier (1974) as a candidate for the cloud particles from polarization data collected in 1930s. The identification of sulfuric acid from in-site measurements still has not been done. Neither have the important questions he raised have been answered yet despite a lot of new data, analysis and numerical modeling efforts.

Old and New Questions:

The observations and results from Pioneer, Venera 15/16, Magellan and Venus Express orbiter missions have provided significant clues about those questions supplemented by key results from the Venera and Pioneer and VeGa entry probes into the atmosphere and VeGa 1 and 2 balloons. But the same observations have also raised some new equally puzzling questions. These include the following:

- Is the atmosphere of Venus well mixed below 120 km?
- What is the impact of the lower atmospheric conditions on the supercritical state of the two primary constituents of the atmosphere?
- Is the spin rate of the solid planet changing? If so, what is the nature of the surface-atmosphere momentum exchange?
- What is the state of volcanism on Venus today?
- Are the temporal and spatial variations in sulfur dioxide abundance above cloud tops due to volcanic activity?
- What is the nature of the ultraviolet absorber(s) in the clouds?
- Why isn't the ultraviolet absorber(s) well mixed?
- What causes local, global and temporal changes in the distribution of the ultraviolet absorber(s)?
- If Venus once had liquid water on the surface, did life evolve and extant in the clouds?
- How does the solar radiation impact the cloud properties?
- Is there any impact of cosmic rays on the cloud particle nucleation in the cloud layer?
- What causes the highly dynamic changes in the atmospheric properties above 100 km?
- What processes create or maintain the atmospheric superrotation?
- Is topography necessary for superrotation?
- What is the cause of electrical activity that has been detected by Venus Express and Pioneer Venus orbiters and why is the optical detection of lightning so rare and problematic?

What measurements are needed?:

To answer some of these questions, sustained observations are needed within the atmosphere at accessible vertical levels, while some require surface and near surface observations from platforms that can survive some useful period to return valuable data. Orbiters are necessary for many concurrent observations and also for relaying the data from the in-situ platforms.

Past missions have shown that in-situ measurements can be successfully obtained below about 62 km altitude above the mean surface of Venus while limited information from accelerometers can be obtained during the entry phase from altitudes as high as 140 km. Drag measurements from orbiters through precision tracking and torque measurements (reaction wheels) have been obtained in the 160 –

130 km altitude range. The altitude range between 62-130 km is not easy to sample in-situ and measurements in this altitude range and above 130 km can only be obtained by remote sensing from orbiters and atmospheric platforms or from Earth.

Aerial Platforms. Long lived flying autonomous craft (e.g. the Venus Atmospheric Maneuverable Platform being presented at this meeting (Baines et al.) and floating platforms at different levels can address questions about the cloud properties to obtain physical and chemical properties, test for biogenic signatures, measure the atmospheric composition for temporal and spatial variations in trace species as well as primary constituents. Aerial platforms with dropsondes and risesondes can also collect meteorological data, and tracking them at high sampling rates can provide information about turbulence, small and large scale waves which will help answer questions about the maintenance of the superrotation.

Orbiters. Capable orbiters can yield global multispectral (optical to infrared) global cloud cover and aerosol distributions from nadir and limb observations, temperature and trace gas vertical profiles from remote sensing observations, solar, stellar and radio occultations. Akatsuki is demonstrating that equatorial orbit can address important science, not just polar orbits – long eccentric (e.g. Pioneer Venus, Venera orbiters and Venus Express) or short near circular like Magellan. One important capability orbiters can provide is data relay capability from the in-situ platforms on the surface and in the atmosphere to maximize their data return. Future orbiters should be equipped with such capability.

Entry Probes. Descending entry probes offer the advantage of providing a nearly vertical profile of atmospheric properties as it is carried by the ambient winds over the hour long journey to the surface in approximately one hour from an altitude of about 62 km. Precision tracking provides zonal, meridional and vertical wind speeds and on-board instruments can provide information about atmospheric composition and cloud/aerosol properties. The drawback is the time required for some of the measurements which limits the number of altitude samples that can be obtained.

Laboratory Studies. Certain questions require laboratory studies to validate the results. Thermodynamic properties of mixtures of real gases are needed to validate the results obtained from theory and from in-situ measurements. The GEER chamber at NASA/GRC is available for a variety of investigations under surface of Venus like conditions and can be useful for studying the supercritical state behavior of the two primary constituents to validate results about how well they mix.

Future Opportunities:

NASA's competed mission opportunities (Discovery and New Frontiers) offer opportunities for addressing some of these questions, but a directed mission can answer many more questions. The most recent US National Academies Decadal Survey of Planetary Science recommended a Venus Climate Mission as a flagship class mission to be launched within the decade (Visions and Voyages 2013-2022). The baseline mission studied can answer many of these missions via the balloons and dropsondes that were part of the mission architecture with an instrumented orbiter. Venera-D has been studied in Russia in the past and a NASA/IKI-Roscosmos Joint Science Definition Team is taking another look at Venera-D for implementation after 2025 which will be useful for an anticipated update of the flagship mission study by NASA in the near future. It is also possible that an international collaboration can succeed in a coordinated effort to comprehensively study Venus and its environment in answering the questions about Venus.

Acknowledgements:

This research was supported by NASA Grant-NNX09AE85G. It is a pleasure to acknowledge numerous conversations on this topic with many colleagues for their encouragement.

Bibliography:

Hansen, J.E., and J.W. Hovenier, 1974: Interpretation of the polarization of Venus. *J. Atmos. Sci.*, **31**, 1137-1160,

Sagan, C., 1971. The trouble with Venus. In Planetary Atmospheres, C. Sagan, T.C. Owen and H.J. Smith, Eds., International Astronomical Union Symposium No. 40, Marfa, Texas, US, October 26-31, 1969, D. Reidel Publishing Co.,408 pp.

National Research Council, 2013. Vision and Voyages for Planetary Science in the Decade 2013-2022. National Academies Press, Washington, DC. http://solarsystem.nasa.gov/docs/Vision_and_Voyages-FINAL.pdf

THE STRUCTURE OF THE VENUS ATMOSPHERE: INTERCOMPARISON OF VENUS EXPRESS AND GROUND BASED OBSERVATIONS OF VERTICAL TEMPERATURE AND DENSITY PROFILES

S.S. Limaye, *Space Science and Engineering Center, University of Wisconsin, Madison, Wisconsin* **, M. Pätzold)**, *RIU-Planetenforschung an der Universität zu Köln, Cologne, Germany, , USA*, **S. Bougher**, *University of Michigan, Ann Arbor, Michigan, USA*, **S. Bruinsma**, *CNES, Toulouse, France*, **S. Chamberlain**, *IASB-BIRA, Brussels, Belgium*, **R.T. Clancy**, *Space Science Institute, Boulder, Colorado, USA*, **J.-C. Gérard,** *Université de Liège, Liège, Belgium*, **G. Gilli,** *LMD, Paris, France*, **D. Grassi**, *INAF, Rome, Italy*, **R. Haus**, *University of Münster, Münster, Germany*, **M. Herrmann**, *RIU-Planetenforschung an der Universität zu Köln, Cologne, Germany*, **T. Imamura**, *ISAS/JAXA, Sagamihara, Japan*, **E. Kohler**, *University of Arkansas, Fayetteville, Arkansas, USA*, **P. Krause**, *RIU-Planetenforschung an der Universität zu Köln, Cologne, Germany*, **S. Lebonnois**, *LMD, Paris, France*, **A. Mahieux**[4,24], *IASB-BIRA, Brussels, Belgium* and *Fonds National de la Recherche Scientifique, Brussels, Belgium*, **A. Migliorini**, *INAF, Rome, Italy*, **F. Montmessin**, *LATMOS, Paris, France*, **C. Pere**, *Laboratoire Lagrange, Université Côte d'Azur, Observatoire de la Côte d'Azur, CNRS, Nice, France* and *Observatoire de Paris/CNRS/LESIA, Meudon, France*, **M. Persson**, *Oxford University, Oxford, United Kingdom*, **A. Piccialli**, *LATMOS, Paris, France* and *Observatoire de Paris/CNRS/LESIA, Meudon, France*, **M. Rengel**, *Max-Planck-Institut für Sonnensystemforschung, Göttingen, Germany* and *European Space Astronomy Centre, ESAC, ESA, Spain*, **A. Rodin**, *Space Research Institute, Moscow, Russia*, **B. Sandor**, *Space Science Institute, Boulder, Colorado, USA*, **Manuela Sornig**, *RIU-Planetenforschung an der Universität zu Köln, Cologne, Germany* and I. *Physikalisches Institut, Universität zu Köln, Köln, Germany*, **H. Svedhem**, *ESTEC, European Space Agency, Noordwijk, The Netherlands*, **S. Tellmann**, *RIU-Planetenforschung an der Universität zu Köln, Cologne, Germany*, **P. Tanga**, *Laboratoire Lagrange, Université Côte d'Azur, Observatoire de la Côte d'Azur, CNRS, Nice, France*, **A.C. Vandaele**, *IASB-BIRA, Brussels, Belgium*, **T. Widemann**, *Observatoire de Paris/CNRS/LESIA, Meudon, France* and *LESIA, UMR CNRS 8109, Paris Observatory, France* and *DYPAC, Université de Versailles-Saint-Quentin-en-Yvelines, Guyancourt, France*, **C. Wilson**, *Oxford University, Oxford, United Kingdom*, **I. Müller-Wodarg**, *Imperial College, London, United Kingdom* and **L. Zasova**, *Space Research Institute, Moscow, Russia*.

The Venus International Reference Atmosphere (VIRA) model contains tabulated values of temperature and number densities obtained by the experiments on the Venera entry probes, Pioneer Venus Orbiter and multi-probe missions in the 1980s. The instruments on the Venus Express orbiter generated a significant body of new observational data on the vertical and horizontal structure of the Venus atmosphere from 40 km to about 180 km altitude from April 2006 to November 2014. Many ground based experiments have provided data on the upper atmosphere (90-130 km) temperature structure since the publication of VIRA in 1985. The "Thermal Structure of the Venus Atmosphere" Team was supported by the International Space Studies Institute (ISSI), Bern, Switzerland, from 2013 to 2015 in order to combine and compare the ground-based observations and the VEx observations of the thermal structure as a first step towards generating an updated VIRA model. Results of this comparison are presented in five latitude bins and three local time bins by assuming hemispheric symmetry. For the first time, the intercomparison of the ground-based and VEx results provides a consistent picture of the temperature and density structure in the 40 km - 180 km altitude range. The Venus Express observations have considerably increased our knowledge of the Venus atmospheric thermal structure above ~40 km and provided new information above 100 km. There are however still observational gaps in latitude and local time above certain regions. Considerable variability in the temperatures and densities is seen above 100 km but certain features appear to be systematically present, such as a succession of warm and cool layers. Preliminary modeling studies support the existence of such layers in agreement with a global scale circulation. The intercomparison focuses on average profiles but some VEx experiments provide sufficient global coverage to identify solar thermal tidal components.

Observed temperatures in the 50 – 90 km range (approximately, 1 bar to 1 mbar levels) are broadly in agreement with VIRA temperature profiles, to within less than 10 K.. At altitudes above 90 km, Venus Express results reveal alternating warm and cold regions, with a much larger variation of temperatures. A strong solar zenith angle dependence is also found. Origin of large differences in temperatures above 90 km between different experiments are not yet understood, and may be due to sampling differences. The VEx observations will allow us to improve the empirical models (VTS3 and Keating et al. 1985) above 0.03 mbar/100 km, in particular the 100-150 km region which had pre-

viously barely been sampled observationally. The next steps needed to define the the updated VIRA model for the temperature structure of Venus atmosphere up to 150 km altitude are (1) define the grid on which this database may be provided, (2) fill what is possible with the results of the data intercomparison, and (3) fill the gaps. To do so, interpolation between the datasets using available General Circulation Models may help.

Observations with improved spatial coverage are still necessary at all altitudes, in latitude-longitude and at all local solar times for a complete description of the atmospheric thermal structure. In-situ observations in the atmosphere below 40 km are needed, especially below 12 km (only VeGa 2 sampled below 12 km).

A substantial amount of effort is needed for the update of the thermal/density structure above 90 km in tabulated form after the differences in the sampling and experimental approaches are better understood. The binned experiment data used to generate the comparison figures provided by the teams will be available from at the ISSI Team site www.issibern.ch/teams/venusatmos/ .

GEOLOGY OF THE VENUSIAN LOWLAND PLAINS: INSIGHT FROM NIOBE PLANITIA.

I. López , *Area de Geología, Universidad Rey Juan Carlos, Spain (ivan.lopez@urjc.es),* **V.L. Hansen**, *Dept. Earth & Environ. Sci., University of Minnesota, Duluth MN, USA, (vhansen@d.umn.edu).*

Introduction: We carried out 1:10M geologic mapping of Niobe Planitia (0º-57ºN/60º-180ºE, I-2467) with the aim of establish the geologic history of this region, and to test existing working models for the geodynamic evolution of Venus. The Niobe Map Area (NMA) contains a rich assemblage of basement (crustal plateaus and lowland tessera inliers) and plains materials (shield plains, volcano- and corona-related materials and large expanses of geologically undivided materials). The map area lacks large igneous rises or chasmata that commonly postdate and disrupt other volcanic plains regions of Venus.

We discuss the geology of the Niobe lowland volcanic plains based on detailed geologic and structural mapping which allows the delineation of surface units. The geologic map illustrates differences between different volcanic plains across the map area.

Methodology: Geologic analysis was carried out using: (1) NASA's Magellan full-resolution SAR data (left- and right-looking and in both normal and inverted modes) [1]; (2) Magellan altimetry; and (3) synthetic stereo images constructed using NIH-Image macros developed by Duncan Young.

Data visualization and geologic mapping was conducted using Adobe Illustrator™ with linked NASA Magellan SAR and altimetry data, MAPublisher™ to scale and place georeferenced raster datasets, and ArcGIS™ and ArcGlobe™ for compilation, analysis and final map production.

Tectonic structures: Secondary (i.e., tectonic) structures in the volcanic plains of the NMA are divided into two groups: (a) Regional structures distributed across huge expanses of the NMA; and (b) local structures that are both spatially and genetically related to individual tectonomagmatic features.

Regional contractional deformation suites.

Folds. Broad folds deform some local basal units of the volcanic plains. These folds occur in areas of deformation belts in two areas: NNW-trending folds within Lemkechen and Unelanuhi Dorsa, deforming basal materials in Akhtamar Planitia, western NMA; NNE-trending folds that deform basal materials of eastern NMA (Llorona, Vellamo and Atalanta planitiae).

Wrinkle ridges. We recognize four different suites of wrinkle ridges: (a) a regional suite; (b) local inversion structures [4]; (c) suites concentric to adjacent individual coronae; (d) wrinkle ridges that parallel adjacent tectonomagmatic features and deformation belts. The circum-Artemis trend (a), the most regionally extensive suite in the NMA, marks a suite of wrinkle ridges that extend southward to the Aphrodite map area, and define a coherent suite >13,000 km in diameter around Artemis Chasma [2]. In central NMA local N-trending wrinkle ridges show clear evidence of reactivation as inversion structures [3, 4]; that is, wrinkle ridges occur along strike with individual fractures locally buried by lava flow material. These relationships indicate that early-formed N-trending fractures were locally buried and later shortening resulting in the formation of inversion structures. In Leda Planitia wrinkle ridges define a reticulate pattern similar to that present in the basement materials and in the volcanic materials that postdate these basement materials, but the existence of reactivation has not yet been clearly established. Local wrinkle ridge suites also develop parallel to adjacent features, including concentric to adjacent coronae, and parallel to the trend of adjacent deformation belts. This geometry indicates that these suites form synchronous with, or after the formation of their adjacent 'hosts'.

Regional extensional deformation suites.

*Regional fractures***.** We identified different fracture suites of regional extent based on trend, spacing and temporal relations with volcanic materials.

Suite A. NNW-trending fractures mark the oldest fracture suite in the central part of the NMA, and in Leda Planitia this fracture trend also deforms the lower plain materials, due to reactivation of buried structures. This trend is the principal direction of ribbon structures that characterize earlier formed, underlying tessera terrain in central NMA. Examination of high-resolution SAR indicates that the NNW-fracture suite represents reactivation of local basement structures covered by thin flows or discontinuous materials from shield terrain material [5, 6]. The trend and fracture spacing of this fracture suite is constant across a great expanse of the central NMA indicating that basement structures/heterogeneity played a strong role in fracture trend [4, 7].

Suite B. NNE-trending fractures cut Leda Planitia, where the suite is best developed, and locally in central NMA. Within Leda Planitia the fractures parallel the trend of ribbon structures of Dekla Tessera (which parallel ribbon tessera fold trends to the south in northern Tellus Regio). Within Leda Planitia the fractures appear to be reactivation structures.

Artemis-radial suite. A suite of regional fractures that fans across the NMA describes a huge suite of

fractures radial to Artemis Chasma [2]. These fractures trend NE in the eastern NMA, N in central NWA, and NW in western NMA. Within central NMA N-trending fractures are the youngest recognized regional fractures at this location. Corona also decorate this fracture suite; structural elements of the corona annuli both cut and are cut by fractures of this suite, suggestive of a genetic relationship as well. Portions of the Artemis-radial suite are also locally reactivated to inversion wrinkle ridges in several locations within the NMA.

Local deformation suites.

Radial fractures. Radial fracture suites occur related to large tectonomagmatic centers. These suites can extend great distances from their foci, and therefore might be useful as local temporal markers for unit delineation (i.e., Holde Corona in Atalanta Planitia and Kurukulla Mons in Till-Hanun Planitia) [8].

In western NMA (i.e., Akhtamar Planitia) radial fracture suites connect large, otherwise isolated, tectonomagmatic centres (Hatshepsut Patera-H'uraru Corona, Uli-Ata Mons, Kaltash Corona, Kunhild Corona, Ereshkigal Corona), forming an extensive interconnected suite that in some locations is difficult to differentiate from regional fracture suites.

Concentric fractures. Concentric fracture suites occur as annuli of individual coronae in the central NMA, and appear to have formed generally synchronous with N-trending members of the Artemis-radial fracture suite. The host coronae typically lack obvious flows. The absence of flow material could result from: homogenization through weathering or a lack of coronae-sourced surface flows. Coronae located in Aphrodite Terra (ej. Kaltash and Rosmerta coronae) display annuli of concentric fractures and extensive flows that embay and postdate adjacent crustal plateaus; in these two cases flows clearly emerged from radial coronae-related fractures.

Concentric ridges. Concentric ridges mark the annuli of some coronae (e.g., Ituana and Bil Coronae). These coronae clearly source large traceable flows that bury extensive portions of the NMA [8]. Similar concentric ridges in Irnini Mons are interpreted as the result of tectonic inversion or warping of regional stress around an empty magmatic reservoir [9].

Lowland Plain Materials: The NMA includes a series of surface materials that postdate a rich assemblage of basement materials (ribbon tessera terrain and other deformed terrains). We use a geographic approximation to the description of plains although in some locations there is not a clear distinction between the different plains.

Western NMA: In the NW of the NMA, Leda Planitia is sited among different tessera blocks: Laima Tessera to the west, Dekla Tessera to the north and east and Meni Tessera to the south. It is surfaced by shield terrain that postdate basement materials, and lacks intermediate or large volcanic edifices or large near-surface magma chambers/diapirs that could form small coronae. Akhtamar Planitia, which dominates the SW of the NMA, comprises an assemblage of basal plain materials (shield terrain and undivided volcano-related materials), undivided volcanic plains and volcano- and corona-related flow units. Map relations indicate that Artemis-radial fractures predate formation of Kunhild and Ereshkigal Coronae, which are interpreted as an extinct hot-spot [10].

Central NMA: In north central NMA, Niobe, Lowana and Tilli-Hanun Planitiae are composed of basal plain materials (shield terrain and undivided shields-, volcano- and corona-related materials), undivided volcanic plains, and volcano-, shield-fields- and corona-related large flow units that locally postdate basal plains. Coronae in Niobe Planitia are preferentially circular low/calderic coronae associated with basement materials, with the exception of a cluster of coronae and volcanoes with large associated flows in Tilli-Hanun Planitia, similar to the extinct hot-spot described in Akhtamar Planitia. In south-central NMA, Sogolom Planitia is surfaced by basal plain materials and extensive corona-related flows that surround and postdate formation of adjacent ribbon-tessera terrain in Aphrodite Terra

Eastern NMA. The style of plains in eastern NMA is different. Basal materials are locally restricted to the vicinity of ribbon-tessera inliers. Atalanta and Rusalka planitiae are dominated by undivided materials with extensive flows sourced from local coronae and large volcanoes. Younger shield clusters and volcanoes with associated flows locally postdate the undivided plains. Although this regional lacks obvious extensive regional fractures trends, Artemis-radial fractures occur in W-Rusalka (consistent with fracture trends in S-Rusalka [3]. Wrinkle ridge trends display an Artemis-radial pattern (orthogonal to adjacent Artemis-concentric wrinkle ridges); these relations are consistent with the interpretation that early formed fractures were subsequently buried by local flows, and later reactivated as inversion structures [3].

References: [1] Ford J.P. et al. (1993) JPL Publ. *93-24.* [2] Hansen V.L. & A. Olive (2010) Geol., 38, 467-470. [3] DeShon H.R. et al. (2000) *J. Geophys. Res.* 105, 6983-6995. [4] Hansen V.L. (2009) U.S. Geol. Surv. SIM-3025, 1:5M map, 22pp. [5] Aubele J. (1996) LPSC XXVII, 49-50. [6] Hansen V.L. (2005) GSAB 117, 808-822. [7] Lang N.P. & Hansen V.L. (2010), *U.S. Geol. Surv.* SIM-3089, 1:5M map 15pp. [8] Ernst R.E. et al. (1995) *Earth Sci. Rev. 39,* 1-58. [8] Young D.A. & Hansen V.L. (2004) *U.S. Geol. Surv. Invest. Ser. I-2783* 1:5 M map.[9] Buczkowski D.L. (2002) *J. Struc. Geol.* 28, 2156-2168. [10] Herrick, R.R. & McGovern, P.J. (2000) *Geoph. Res. Lett. 27,* 839–842.

VEGA Balloon Dataset: PDS4 Archive Preparation.

R. D. Lorenz, *JHU Applied Physics Laboratory, Laurel, MD 20723, USA (ralph.lorenz@jhuapl.edu)*, **D. Crisp**, *Jet Propulsion Laboratory, California Institute of Technology, Pasadena, CA 91109, USA*. **L. F. Huber**, *PDS Atmospheres Node, Department of Astronomy, New Mexico State University, Las Cruces, NM 88003, USA.*

Introduction:

The two VEGA balloons launched by the Soviet Union in 1985 [fig.1] remain landmarks in planetary exploration: the first ever (and to date only) planetary balloons, and the longest-lived vehicles in the Venusian atmosphere to date. They provided unique in-situ datasets in the middle cloud layer. However, the low power direct-to-Earth radio link required severe data compression with some loss of information. The data reconstruction process has not been fully documented in the literature, and the data thereby obtained is generally available only as poorly-reproduced scatterplots in published papers. Here we report on a project to deliver the data in electronic form to the NASA PDS Atmospheres Node for community use: the dataset is intended to follow the XML-based PDS4 standard which tags elements with machine-readable identifiers to enable (for example) easier cross-referencing of comparison data. Interest in future missions has stimulated re-examination of the VEGA data, e.g. [1]

Figure 1. Flight-representative model of VEGA lander at Lavochkin Museum in Moscow. The spherical tanks at top held helium for balloon inflation. (photo: Ralph Lorenz)

Data Reconstruction:

The balloons sent back data on light level, temperature, pressure [e.g. Fig.2] and vertical winds: 12-bit values for all but the nephelometer data were transmitted directly to Earth as separate 6-bit values, with the least-significant 6 bits (LSB) transmitted on 7 successive samples (at 75s intervals), while the MSB was transmitted only once every 8 samples. While this would theoretically double the sample rate for slowly-changing quantities, in practice resulted in ambiguities because the quantities changed fast enough for the MSB to change in the 8x75s telemetry cycle time. In addition, there were a few synchronization glitches in the telemetry commutation which introduced ambiguity in the sensor to which a given value referred. These issues were resolved at the time by matching data patterns, but this process was only briefly noted in the literature at the time [2,3].

To illustrate the issue introduced by the data compression approach, consider the telemetered sequence of LSB 'ones' and MSB 'tens' : 4, 7, 2, 6, 7, 9, 3, 30, 6, 9, 2, 4, 6, 7, 1, 70, 8, 2, 1, 7, 9, 1, 3, 20, ... Do those numbers correspond to a sequence of underlying values of 14, 17, 22, 26, 27, 29, 33, 30, 36, 39, 44, 56, 67, 71, 70 .... or some other permutation, like 24, 27, 32, 26, 27, 29, 33, 30, 36,49, 54, 66, 67, 71, 70 .... The use of a dynamical model of the balloon system, together with a 'reality check' from the internal nephelometer housekeeping temperature sensor, helped resolve this ambiguity.

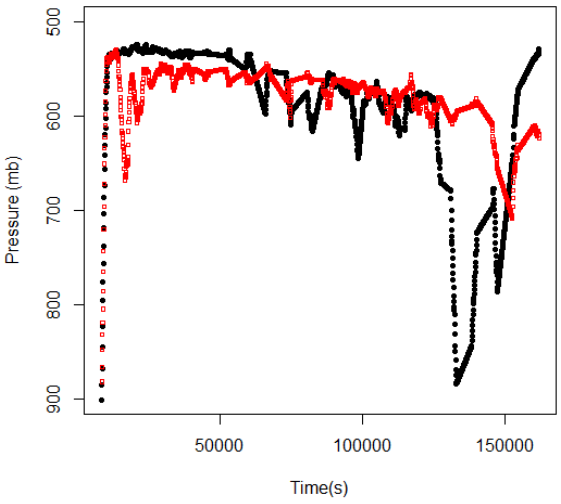

Figure 2. Example data – the pressure time series for VEGA-1 (red) and -2 (black). Note that the linear segments result from interpolation during periods when measurements were not available.

Dataset Description: The reconstructed datasets are ASCII tables of relevant parameters, together with quality flags indicating whether datapoints were measured directly and accurately, required estimation, or were interpolated.

The emerging international PDS4 standard [see https://pds.nasa.gov/pds4/about/what.shtml] is based on the eXtensible Markup Language XML. This introduces certain formal metadata elements in the data structures that tag the archive in a machine-readable way to facilitate the search for data, or for example, the identification of related datasets.

The VEGA dataset is being prepared in this format for delivery to the PDS Atmosphere Node this year.

Acknowledgement: This work is supported by NASA Planetary Missions Data Analysis Program Grant NNX13AQ13G.

References: [1] Dorrington, G. E. 2013. Preliminary Evidence for drizzle in the middle cloud layer of Venus, Advances in Space Research, 52, 505-511 [2] Linkin, V. M. et al. 1986. VEGA Balloon Dynamics and Vertical Winds in the Venus Middle Cloud Region, Science, 231, 1417-1419. [3] Ingersoll, A. P., D. Crisp, A. Grossman and the VEGA Balloon Science Team,1987. Estimates of Convective Heat Fluxes and Gravity Wave Amplitudes in the Venus Middle Cloud Layer from VEGA Balloon Measurements, Advances in Space Research, 7, 343-349

Venus' upper haze aerosol properties from SPICAV IR data

M. Luginin, *MIPT/IKI-RAS, Russia (mikhail.luginin@phystech.edu)*, **A. Fedorova** *IKI-RAS, Russia*, **D. Belyaev**, *IKI-RAS, Russia*, **F. Montmessin**, *LATMOS, France*, **V. Wilquet**, *Belgian Institute for Space Aeronomy, Belgium*, **O. Korablev**, *IKI-RAS, Russia*, **J.-L. Bertaux**, *LATMOS, France*, **A. C. Vandaele**, *Belgian Institute for Space Aeronomy, Belgium*

Introduction:

The upper haze located at 70-90 km is believed to consist of submicron aerosol particles of H_2SO_4 (Esposito et al., 1983). The distribution of particles in the upper haze is controlled by atmospheric circulation, sedimentation, and, possibly, chemistry and can also provide a source of sulfur oxides above 90 km (Zhang et al., 2012; Belyaev et al., 2012). So far, very limited information on the vertical distribution and the composition of the aerosol particles in the upper haze is available.

Data analysis of 243 orbits from the nominal mission of the Orbiter Cloud Photopolarimeter onboard Pioneer Venus resulted in an estimate of the optical properties for the haze particles (Kawabata et al., 1980). The effective radius r_{eff} was found to be 0.23±0.04 μm and the effective variance υ_{eff} to be 0.18±0.10. Sato et al. (1996) performed a more detailed analysis of the Pioneer Venus data covering 2820 days and found that the submicron haze exhibited large spatial and temporal variations.

Recently, the three channels of the SPICAV/SOIR instrument onboard the Venus Express (VEX) orbiter provided the occultation profiles in three spectral ranges: 200-300 nm, 0.65-1.7 μm, and 2.3-4.2 μm. That observations resulted in the discovery of a bimodality in size distribution in the upper haze with a small mode of radius 0.1-0.3 μm, and a large mode of radius 0.4-1.0 μm as well as the presence of detached haze layers at 75-90 km of altitude (Montmessin et al., 2008; Wilquet et al., 2009).

Observations:

SPICAV IR is based on the design of the SPICAM IR instrument flying on board the Mars Express orbiter. It is a pencil-beam spectrometer covering the spectral range of 0.65–1.7 μm based on acousto-optical tunable filter (Korablev et al., 2012). The spectrometer operates in nadir and in solar occultation modes. The field of view in solar occultation is circular and has an aperture of 0.07°. The vertical resolution varies from 1 to 25 km depending on the distance to the planet's limb. The VEX's orbit is elliptical and the distance to the surface varies from 250 to 66000 km. The pericenter is located almost above the North Pole (80°N).

Aerosol properties are determined using 10 continuum "dots" outside those intervals: 649.4, 756.6, 852.5, 982.4, 1101.1, 1159.6, 1197.3, 1273.4, 1323.0, and 1553.7 nm.

We report an analysis of aerosol measurements by the SPICAV IR spectrometer in solar occultation mode for 196 observations obtained from May 2006 till November 2014.

Method of analysis:

The solar occultation measurements are by nature self-calibrated. The reference spectrum for an occultation I_0 is obtained when observing the Sun out of the atmosphere during a sequent measurements. Inside the atmosphere solar radiance I is attenuated by extinction of aerosols and gases integrated over the line of sight L. The ratio of this flux to the reference spectrum defines a spectrum of atmospheric transmission at a target altitude: $T_\lambda(L) = I_\lambda(L)/I_0$.

Slant optical depth of aerosol is calculated from occultation techniques as $\tau_\lambda(L) = -\ln\left(T\left(L\right)\right)$, where τ_λ is the optical depth along the L.

The procedure for the retrieval of the extinction vertical profiles is identical to the one described for SPICAM solar occultations on Mars (Fedorova et al., 2009); that is by making use of the standard 'onion peeling' method. Extinction coefficient is assumed to be constant inside each atmospheric layer. This procedure was performed taking into account Rayleigh scattering of the CO_2 atmosphere.

The aerosol extinction is modeled according to the classical Mie theory. To compute light scattering by spherical particles using the Lorenz–Mie theory we applied the code of Michael Mishchenko and collaborators (Mishchenko et al., 1999). We adopted refractive indices for sulfuric acid aqueous solution with 75% H_2SO_4 concentration from Hansen and Hovenier (1974).

In our retrieval procedure we consider 2 cases for the particle size distribution.

For both cases we independently apply fitting procedure and retrieve particle radii. The spectral dependence of experimental normalized aerosol extinctions $k_{ext}(\lambda)/k_{ext}(\lambda_0)$ was fitted using a Levenberg-Marquardt algorithm, which minimizes statistically weighted χ^2 according to uncertainties of measurements. For the data analysis we choose a reference wavelength λ_0 =852.5 nm with maximal signal-to-noise ratio, this way the uncertainties of normalized extinctions are smaller.

Once a particle size distribution is retrieved, one can calculate the aerosol number density *N(z)*. In case of bimodal distribution, $N(z)$ and $\gamma N(z)$ are the number densities for the two modes.

Thereafter, aerosol scale heights were retrieved from extinction coefficient profiles and number den-

sity profiles.

Knowing aerosol scale heights, one can calculate eddy diffusion coefficient $K = V_s \frac{H H_a}{H - H_a}$, where H is the atmosphere scale height, H_a is the aerosol scale height, sedimentation velocity V_s for the case when $l > r$ equals $V_s = \frac{2}{9}\rho g \frac{r^2}{\eta}\left(1+\frac{l}{r}\right)\left(1.257+0.4e^{-1.1r/l}\right)$, ρ is sulfuric acid aqueous solution density, g – gravitational acceleration, η – dynamic viscosity, l – mean free path of a particle.

Results:

Aerosol extinction profiles

The slant optical depth and the extinction coefficient profiles were retrieved at 10 wavelengths.

In most occultations the aerosol extinction decreases smoothly from 70 to 90 km. In some instances, we observed detached haze layers at the altitudes between 70 and 90 km. The structures can be sometimes observed over consecutive orbits.

Aerosol scale heights were retrieved from each extinction coefficient profile at 10 wavelengths. A typical value of the scale height ranges from 3 to 4.5 km.

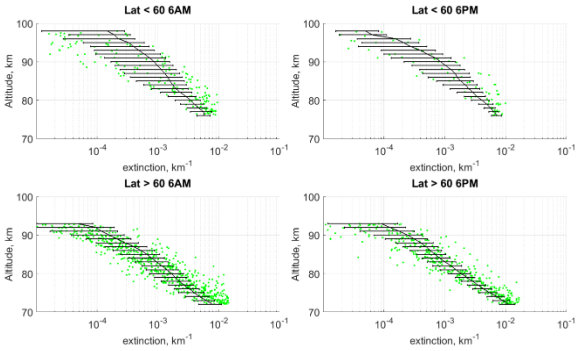

Fig. 1. Mean extinction profiles (black curve with standard dispersion) at wavelength 1197.3 nm averaged in latitude ranges 0°-60° (a, b) and 60°-90°(c, d); at the morning terminator (a, c) and at the evening one (c, d). All the individual extinction measurements are shown in green.

Extinction profiles were averaged in latitude bins 0°-60° and 60°-90° with weights of errors of individual measurements in assumption of hemispheric symmetry and at the morning and at the evening terminators. Altitudes containing detached haze layers were neglected. An example of an averaged extinction profile at wavelength 1197.3 nm is shown in Fig. 1.

Effective radii and number density profiles

To address the long-term, local time and global variations of the particles size, all retrieved effective radii were combined in 4 altitude bins: 70-75 km, 75-80 km, 80-85 km and altitudes above 85 km. All altitudes at every profile were grouped within each bin, and averaged together provided they have the same number of modes.

The variation with latitude indicates that the radius of single mode distributions is smaller at high latitudes than at low latitudes (Table 1). The variation with local time shows that the radius of the single mode is smaller in the evening than in the morning (Table 2).

Table 1
The variation with latitude of averaged effective radius. R_{eff} corresponds to the single mode case, r_{eff1} and r_{eff2} correspond to mode 1 and mode 2 of the bimodal case.

Altitude, km	Low latitudes			High latitudes		
	R_{eff}, μm	r_{eff1}, μm	r_{eff2}, μm	R_{eff}, μm	r_{eff1}, μm	r_{eff2}, μm
70 - 75	0.76±0.06	0.13±0.03	0.97±0.17	0.56±0.17	0.11±0.07	0.83±0.12
75 - 80	0.77±0.09	0.11±0.03	0.86±0.10	0.43±0.18	0.12±0.04	0.82±0.12
80 - 85	0.74±0.07	0.12±0.02	0.81±0.09	0.32±0.17	0.13±0.04	0.81±0.11
> 85	0.48±.017	0.12±0.03	0.76±0.10	0.30±0.14	0.12±0.05	0.81±0.08

Table 2
The variation with local time of averaged effective radius. R_{eff} corresponds to the single mode case, $r_{eff\,1}$ and $r_{eff\,2}$ correspond to mode 1 and mode 2 of the bimodal case.

Altitude, km	Morning			Evening		
	R_{eff}, μm	r_{eff1}, μm	r_{eff2}, μm	R_{eff}, μm	r_{eff1}, μm	r_{eff2}, μm
70 - 75	0.63±0.17	0.11±0.06	0.90±0.13	0.57±0.17	0.12±0.06	0.82±0.15
75 - 80	0.61±0.22	0.12±0.03	0.84±0.13	0.45±0.22	0.11±0.04	0.82±0.08
80 - 85	0.54±0.25	0.13±0.04	0.83±0.12	0.38±0.26	0.12±0.02	0.79±0.08
> 85	0.35±.018	0.12±0.03	0.80±0.07	0.27±0.13	0.12±0.03	0.74±0.11

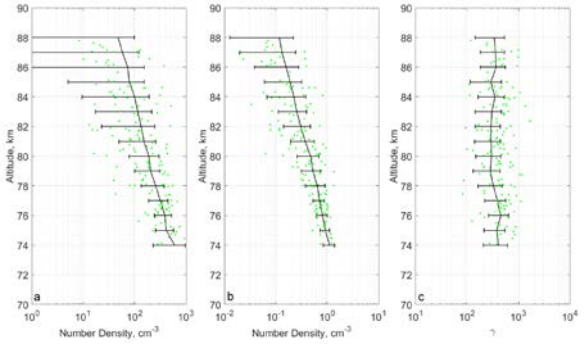

Fig. 2. Averaged profiles of the number density for mode 1 (a), mode 2 (b), and γ (c) for all orbits at bimodal case.

Altitude profiles of number densities for modes 1 and 2 are presented in Figure 2 for the whole set of orbits at bimodal case. Averaged curves for both modes decrease smoothly, from ~500 cm^{-3} at 75 km to ~50 cm^{-3} at 90 km for mode 1, and from ~1 cm^{-3} at 75 km to ~0.1 cm^{-3} at 90 km for mode 2.

Eddy diffusion coefficient was also calculated from the extinction and number density scale heights for altitudes of 75-90 km. It increases from $\sim 5 \cdot 10^4$ cm^2/s at 75 km to $\sim 10^6$ cm^2/s at 90 km and is consistent with previous results obtained by Krasnopolsky (1980) and values that were used in his models (Krasnopolsky, 2012).

Acknowledgments:
D. Belyaev and M. Luginin acknowledge support from the RFFI grant № 16-02-00633a in 2016. F. Montmessin and

J.-L. Bertaux acknowledge support from the CNES and from the CNRS. V. Wilquet and A. C. Vandaele acknowledge funding from the Belgian Federal Science Policy Office through the BRAIN program (BR/143/A2/SCOOP), from the European Space Agency (ESA – PRODEX program), as well as from the FP7 EuroVenus project (G.A. 606798). All the authors also acknowledge the support provided by ISSI, through the organization of the International Team meeting "Improved understanding of Venus clouds" (http://www.issibern.ch/teams/venusclouds/).

References:

Belyaev et al., 2012. Vertical profiling of SO_2 and SO above Venus' clouds by SPICAV/SOIR solar occultations. Icarus 217, 740–751. doi:10.1016/j.icarus.2011.09.025

Esposito et al., 1983. Venus. Univ. of Arizona, Ch. 16. The clouds and hazes on Venus, 484–564.

Fedorova et al., 2009. Solar infrared occultation observations by SPICAM experiment on Mars-Express: Simultaneous measurements of the vertical distributions of H_2O, CO_2 and aerosol. Icarus 200, 96–117. doi:10.1016/j.icarus.2008.11.006

Hansen, J. E., Hovenier, J. W., 1974. Interpretation of the Polarization of Venus. J. Atmos. Sci. 31, 1137–1160.

Kawabata et al., 1980. Cloud and haze properties from Pioneer Venus polarimetry. JGR. 85, 8129. doi:10.1029/JA085iA13p08129

Krasnopolsky, V. A., 1980. Venera 9 and 10 - Spectroscopy of scattered radiation in the atmosphere above the clouds. Kosmicheskie Issledovaniia, vol. 18, Nov.-Dec. 1980, p. 899-906. In Russian.

Krasnopolsky, V. A., 2012. A photochemical model for the Venus atmosphere at 47–112km. Icarus 218, 230–246. doi:10.1016/j.icarus.2011.11.012

Korablev et al., 2012. SPICAV IR acousto-optic spectrometer experiment on Venus Express. Planet. Space Sci. 65, 38–57. doi:10.1016/j.pss.2012.01.002

Mishchenko et al., 1999. Bidirectional reflectance of flat, optically thick particulate layers: an efficient radiative transfer solution and applications to snow and soil surfaces. J. Quant. Spectrosc. Radiat. Transf. 63, 409–432. doi:10.1016/S0022-4073(99)00028-X

Montmessin et al., 2008. Venusian Upper Haze Properties: Detection of a Multimodal Distribution at High Altitude by SPICAV/SOIR. American Geophysical Union, Fall Meeting 2008

Sato et al., 1996. Photopolarimetry Analysis of the Venus Atmosphere in Polar Regions. Icarus 124, 569–585. doi:10.1006/icar.1996.0231

Zhang et al., 2012. Sulfur chemistry in the middle atmosphere of Venus. Icarus 217, 714–739. doi:10.1016/j.icarus.2011.06.016

Wilquet et al., 2009. Preliminary characterization of the upper haze by SPICAV/SOIR solar occultation in UV to mid-IR onboard Venus Express. JGR. 114, E00B42. doi:10.1029/2008JE003186

OUR NEIGHBORING 'INDUCED MAGNETOSPHERES': BIG PICTURE SIMILARITIES AND DIFFERENCES BETWEEN VENUS AND MARS.

J. G. Luhmann, S.M. Curry, D.L. Mitchell, *SSL, University of California, Berkeley, CA, USA (jgluhman@ssl.berkeley.edu),* **Y-J. Ma, C.T. Russell**, *IGPP UCLA, Los Angeles, CA, USA,* **.C-F. Dong**, *Princeton University, Princeton, NJ, USA,* **T-L. Zhang**, *IWF, Graz, Austria,* **B.M. Jakosky**, *LASP University of Colorado, Boulder, CO, USA,* **J. Halekas**, *Unversity of Iowa, Iowa City, IA, USA,* **J.E. Connerney, Gina Dibraccio,** *Goddard Space Flight Center, Greenbelt, MD, USA.*

Abstract:

The canonical picture of an induced magnetosphere grew out of the early missions to Venus and Mars, and especially from the Pioneer Venus Orbiter (PVO) mission. Analyses of the plasma interaction with the almost purely ionospheric obstacle encountered on PVO at solar maximum at Venus allowed validations of some models and concepts that gave us a picture of a robust ionospheric current system that could largely exclude the solar wind from the obstacle interior. In this case the induced magnetospheric obstacle 'surface' was found to be located where solar wind pressure balance with ionospheric pressure was maintained as long as it was located above the nominal exobase at ~200 km altitudes. However even during this mission, observed occasional continuation into the ionosphere of the overlying draped external magnetic field hinted at much more complicated possible scenarios. In particular, this 'overpressure' situation was found to occur when solar wind (mainly dynamic) pressure exceeds the ionospheric thermal pressure at the exobase. In such an interaction, collisional inward diffusion of the external field plays a role in the plasma interaction- likely accompanied by solar wind plasma penetration. The Venus Express mission provided further support for this picture.

As the situation at Mars was evaluated in the past for comparison, it was realized by many that its weaker ionosphere might more generally produce the latter type of imperfect induced magnetosphere obstacle. The discovery of Mars' strong crustal magnetic fields on Mars Global Surveyor substantially changed that expectation. However, the nature of those crustal field features, and especially their small scales and non-uniform surface distribution, still leaves a role for induced ionospheric currents. The MAVEN observations have now shown in more detail the ways in which the planetary and induced ionospheric fields contribute to the solar wind obstacle at Mars. The interpretation of these contributions is challenging and relies on data-validated models of the solar wind interaction. We use an archive of BATS-R-US simulation results that have been shown to closely replicate the field and plasma observations around Venus and Mars to illustrate the different versions of induced magnetospheres at our neighbors in the solar system. Given the importance of ionosphere strength, we also speculate about time variations in these systems, including expectations for the upcoming possibly deep solar minimum.

LESSONS FOR THE VENUS AURORA FROM THE MAVEN MISSION?

J.G. Luhmann, C.O. Lee, Yan Li, D. Larson, R. Lillis, *SSL, University of California, Berkeley, USA (jgluhman@ssl.berkeley.edu)*, **N.M. Schneider, S. Jain, A.I.F. Stewart, B.M. Jakosky**, *LASP University of Colorado, Boulder, CO, USA*, **C.L. Gray**, *New Mexico State University, Las Cruces, NM, USA*, **Y. Futaana**, *IRF, Kiruna, Sweden*, **T-L. Zhang**, *IWF, Graz, Austria*, **C.T. Russell**, *IGPP UCLA, Los Angeles, CA, USA*, **R.A. Mewaldt**, *Caltech, Pasadena, CA, USA*, **M.L. Mays**, *Catholic University of America, Washington DC, USA*, **D. Odstrcil**, *George Mason University, Fairfax, VA, USA* .

Introduction:

When auroras in 130.4 nm emission were detected by the UVS on Pioneer Venus Orbiter (PVO) it was something of a surprise, but in hindsight should not have been considering the absence of a magnetic 'shield' around the atmosphere of Venus, and the high level of solar activity that prevailed at that time. The raster scanned UV images of these nightside emissions appeared patchy in contrast to auroral arcs seen on Earth, appearing more like the diffuse aurora. The emissions had the spectral properties associated with soft (< a few hundred eV) electron precipitation (Fox and Stewart, 1991) and also exhibited brightening in response to local solar wind pressure increases detected with the PVO plasma analyzer (Phillips et al., 1986). As the Venus ionosphere during active solar phases has a healthy source in transterminator flows from the dayside, these auroras implied only modest enhancements to nightside ion production at the time.

New Reports and their Implications:

Several decades after those initial observations, Gray et al. (2012) observed auroral green line emissions from Venus from the ground. Moreover, they were able to use newly available solar monitoring assets to associate these episodes with coronal mass ejection events observed at the Sun (Gray et al., 2014). These authors made use of the Venus Express (VEX) orbiter measurements of the solar wind plasma and magnetic field from the ASPERA-4 and MAG experiments to compare their observations of brightening with the presence of disturbed conditions. Most recently, the MAVEN spacecraft at Mars, which entered orbit in fall, 2014 and completed its prime mission this past fall, also detected a nightside diffuse auroral emission at 289 nm with the onboard ultraviolet spectrometer, IUVS (Schneider et al., Science, 2015). Moreover, with MAVEN fully instrumented with space weather particles and fields detectors, these authors were able to associate the Mars diffuse auroral emissions with the presence in the environment of solar energetic particles. They used these joint observations to calculate the altitude profile and emission intensity for various assumptions concerning the precipitating particle species and found that the observed energetic (~100 keV) electron fluxes-presumably of solar origin- could reproduce what was observed in the UV. The Mars diffuse aurora was clearly related to SEP (solar energetic particle) electron entry into the nightside atmosphere, presumably by direct access along the field lines threading the wake of this weakly magnetized planet. This makes an interesting and distinctive solar system picture of 'space weather' influences on our terrestrial planet neighbors. At Earth, solar energetic particle entry is filtered by its strong dipole field-produced magnetosphere into restricted locations such as the cusp and polar cap, where related effects are seen, including ozone destruction from the SEP protons' entry. It is therefore interesting to consider the larger picture of these energetic particle populations and their occurrence rates in the vicinity of Venus as well, and to perhaps reconsider some past observational results that may have been affected by SEPs.

The current interest in space weather throughout the solar system has led to the development of tools and models that lend insight into the causes and effects of solar energetic particle events, including their spatial distributions. While these were not available at the time of PVO, they overlap with the VEX mission for which there is some local information. Most large SEP events have their source in the shocks driven by coronal mass ejections (CMEs). However, the VEX magnetometer only records the CME disturbances that intercept Venus (as recently surveyed by Good and Forsythe, 2015), while SEP events can also occur from remote interplanetary magnetic field connections to the CME shocks. We use a heliosphere-wide SEP event model called SEPMOD (Luhmann et al., 2010) to illustrate the relationship between CME shocks and SEPs at Venus (and elsewhere), and to simulate several SEP events that should have impacted Venus during the VEX mission. While VEX does not have an energetic particle detector onboard, it has a background channel of the ASPERA-4 detector that records some signatures of SEPs impacting the spacecraft (Futaana et al., 2008). We show that some of these background signatures coincide with our simulated events

–one of which also matches one of the stronger green line auroral events reported by Gray et al. (ref). These results suggest it may be worthwhile to retrospectively examine the Venus data sets for other signatures and phenomena that may result specifically from SEP events. It is also possible to apply the model to interpret future detections of Venus aurora from Earth.

References:

Fox, J.L. and A.I.F. Stewart, J. Geophys. Res., 96, 9861-9828, 1991.

Futaana, Y. et al., Planetary and Space Sci., 56, 873-880, 2008.

Gray, C.L., N.J. Chanover, T.G. Slanger, Comparative Climatology of Terrestrial Planets (abstract), LPI contribution 1675, id8067, 2012.

Gray, C.L., N.J. Chanover, T.G. Slanger, K. Molaverdikhani, Icarus, 233, 342-347, 2014.

Luhmann, J.G., et al., Adv. Space Res., 46, 1-21, 2010.

Phillips, J.L., J.G. Luhmann, A.I.F. Stewart, Geophys. Res. Lett., 13, 1047-1050, 1986.

Schneider, N.M., et al., Science 350, doi:10.1126/science.aad0313, 2015.

Good, S.W. and R.J. Forsythe, Solar Physics, in press, 2015.

THE LATMOS VENUS CLOUD MODEL VENLA: STATUS REPORT.

A. Määttänen, *LATMOS/IPSL, UVSQ Université Paris-Saclay, UPMC Univ. Paris 06, CNRS, Guyancourt, France (anni.maattanen@latmos.ipsl.fr)***, S. Guilbon, A. Stolzenbach, S. Bekki, F. Montmessin,** *LATMOS/IPSL, UVSQ Université Paris-Saclay, UPMC Univ. Paris 06, CNRS, Guyancourt, France***.**

Introduction

The clouds of Venus and the aerosols in the Earth's stratosphere are close relatives: both are mostly composed of sulphuric acid droplets. Venus' clouds are optically thick and absorb most of the insolation arriving at Venus, letting only few percent of sunlight reach the surface and having an important climatic effect. The clouds on Venus are, based on the snapshot profile published by [6], divided in three layers that have different properties (particle size distributions, number densities, mass loads). Even though the upper cloud and upper haze can be directly studied with satellite instruments, only a handful of observations have acquired information on the properties of the lower cloud layers [6] and thus modeling is an important tool for studying the lower and middle cloud layers.

Methods

The LATMOS Venus cloud model VenLA (Venus Liquid Aerosols) is based on a terrestrial Polar Stratospheric Cloud (PSC) model [7]. The PSC model [7] is a sectional microphysical model that can describe a multimodal particle size distribution on a radius grid discretized in tens or hundreds of bins (radius intervals). In its original configuration the PCS model includes all of the microphysical processes relevant to the PSCs, including the multiple phase transitions related to the particle types including liquid and solid phases of water, sulfuric acid, nitric acid and their mixtures, and sedimentation of the particles.

The PSC model went through several modifications when becoming VenLA. The major ones include: removal of nitrous species and related cloud particle types and inclusion of the condensation nucleus particle type, addition of homogeneous and heterogeneous nucleation parameterizations, accounting for both intra-type and inter-type particle coagulation, and adding a parametrization of vertical mixing via eddy diffusion. Because of the extreme dryness of the Venus atmosphere, we also needed to add an iteration of the calculation of the weight fraction of sulfuric acid in the droplet in order to correctly account for the change in total water content.

VenLA describes the formation, growth and decay of sulfuric acid - water droplets, and when used in one-dimensional (vertical profile) version it also accounts for sedimentation and mixing of particles and vapors via eddy diffusion. Homogeneous nucleation is described with the parameterization of [14] and heterogeneous nucleation with a simple parameterization as in [3]. Condensation and evaporation are treated in two steps: simple (fast) equilibration whenever a droplet experiences a change in environmental conditions (temperature, partial pressure of water vapor) causing a change in the equilibrium composition, and (slow) condensation/evaporation during which the droplet grows/shrinks conserving the equilibrium composition [9]. We account for Brownian and gravitational coagulation (coalescence) and we use the numerical method of [4]. The coagulation kernels are calculated as in [1, 12] and the sum of the Brownian and gravitational kernels is corrected as in [10, 11]. Vertical transport (sedimentation and eddy diffusion) is treated following the method of [13] and settling velocity is calculated using [9, 1] and corrected to account for mixing. The model has undergone several updates, the latest of which focused on accounting for, in all microphysical processes, the condensation nuclei (CN) captured within the droplets. This required transforming the pure two-component solution droplet type into a "mixed" particle type that includes both volatile and CN masses.

The runs are initialized with profiles from VIRA [5] for temperature and pressure and from occultation data concerning the vapors, as in [8]. VenLA receives also as input the properties of the condensation nuclei (a lognormal size distribution defined in a given altitude range [3]). A prescribed droplet distribution can also be used as an initial state. The vapors are consumed during nucleation and condensation and replenished when the droplets evaporate or when mixing brings in vapor-rich air. In these simulations the temperature and pressure profiles are not changed and thus the simulated clouds are considered as formed in average conditions and do not reflect effects of large-scale dynamics.

Results

We will focus on finalizing the reference version of the model and reproducing the [6] in-situ observations of the cloud properties. We will present results of reference runs and sensitivity tests. We compare the results to observations on cloud droplet number densities and sizes, and to other modeling studies. One of the main sensitivity tests will be the effect of CN on the cloud properties. The nucleation pathway may prove significant in the simulations since it defines the number of

formed particles. This regulates the particle size for a constant condensible mass. In our preliminary test runs, when using only the homogeneous nucleation parameterization, we reach the observed condensed mass load, but the droplet number concentrations are too low and consequently the droplets are too large. Using heterogeneous CN activation it is much easier to attain observed number concentrations and sizes, however, the used initial CN concentration profile dictates the development of the cloud.

Summary and Conclusions

We have developed a microphysical model for Venus' sulfuric acid clouds. The VenLA cloud model and reference run and sensitivity test results will be presented, with a particular focus on the role of CN. The results will be compared with other modeling studies and observations. The VenLA model defines the baseline for a parallel project on development of a moment method scheme to be used in a global climate model (see abstract Guilbon et al., [2]).

Acknowledgements

We acknowledge the support of the French Planetology program (Programme National de Planétologie, AT-MARVEN project).

References

[1] Fuchs, N. A., 1964. Pergamon, New York.

[2] Guilbon, S., Määttänen, A., Montmessin, F., Burgalat, J., Bekki, S., 2016: Comparison of sectional and modal cloud microphysics representations for Venus: VenLA vs. MAD-VenLA. Venus International Conference abstract, 2016.

[3] James, E. P., Toon, O. B., Schubert, G., 1997. Icarus, Vol. 129, pp. 147–171.

[4] Jacobson, M. Z., Turco, R. P., Jensen, E. J., Toon, O. B., 1994. Atmos. Environ., Vol. 28, pp. 1327-1338.

[5] Kliore, A., Moroz, V., Keating, G., 1986. Pergamon, Oxford.

[6] Knollenberg, R. G., Hunten D. M., 1980. J. Geophys. Res., Vol. 85 , pp. 8039-8058.

[7] Larsen, N., 2000. DMI Sci. Rep. 00-06, Danish Meteorological Institute, DK-2001. Copenhagen, Denmark.

[8] McGouldrick, K., Toon, O. B., 2007. Icarus, Vol. 191, pp. 1-24.

[9] Pruppacher, H. R., Klett, J. D., 1997. Kluwer Academic Publishers.

[10] Sajo, E., 2008. Aerosol sci. tech., Vol. 42, pp. 134-139.

[11] Sajo, E., 2010. Aerosol sci. tech., Vol. 44, pp. 916-916.

[12] J. H. Seinfeld, S. N. Pandis 2006. Wiley.

[13] Toon, O. B., Turco, R. P., Westphal, D., Malone, R., Liu, M., 1988. J. Atmos. Sci., Vol. 45, pp. 2123-2144.

[14] Vehkamäki, H., Kulmala, M., Napari, I., Lehtinen, K. E. J., Timmreck, C., Noppel, M., and Laaksonen, A. J. Geophys. Res., Vol. 107, pp. 4622, 2002.

Ground and space based cloud-top wind velocities using CFHT/ESPaDOnS (Doppler velocimetry) and VEx/VIRTIS (cloud tracking) coordinated measurements

P. Machado (1), T. Widemann (2), J. Peralta (3), R. Gonçalves (1), J.-F. Donati (4) and D. Luz (1)
(1) Institute of Astrophysics and Space Sciences, Observatório Astronómico de Lisboa, Ed. Leste, Tapada da Ajuda, 1349-018 Lisboa, Portugal (machado@oal.ul.pt), (2) LESIA-Laboratoire d'Etudes Spatiales et d'Instrumentation en Astrophysique, Observatoire de Paris, France, (3) Institute of Space and Astronautical Science - Japan Aerospace Exploration Agency (JAXA), JAPAN, (4) Laboratoire Astrophysique de Toulouse, France

Abstract

We present wind velocity results based in the measurements of the horizontal wind field at the cloud top level of the atmosphere of Venus, near 70 km altitude in the visible range on the dayside. The purpose is to characterize the zonal and meridional wind latitudinal behaviour and profiles on hour and day timescales. The technique developed over the last decade [4,5,7,8] is based on solar lines Doppler velocity in the light scattered by cloud top particles in motion. The study has been undergone in coordination with ESA's Venus Express cloud tracking measurements. Our 2014 observations focussed on the wind field at latitudes 60°S-60°N, while VEx/VIRTIS privileged southern latitudes poleward of 45°S in search for zonal and meridional wind circulation patterns.

The 3.60-meter Canada-France-Hawaii telescope (CFHT) and the Visible Spectrograph ESPaDOnS provide a highly resolved (80.000) spectrum in the visible range (0.37-1.05 μm). ESPaDOnS and the sequential technique of visible Doppler velocimetry has proven a reference technique to measure instantaneous winds. These measurements are necessary to help validating Global Circulation Models (GCMs) [2], and to extend the temporal coverage of available datasets. The ground-based observations in the base of this project are critical in their complementarity with Venus Express data, which was recently decommissioned, and they are expected to play the same role during the ongoing Akatsuki mission.

We compared our measurements with simultaneous observations using the Visible and Infrared Thermal Imaging Spectrometer (VIRTIS) instrument from the VEx orbiter. CFHT observations included various points of the dayside hemisphere, between $+60°$N and $60°$S, by steps of $10°$, and from sub-Earth longitude $[\phi - \phi_E] = 0°$ to -50° corresponding to 7:30a - 10:50a, while VIRTIS-M UV (0.38 μm) cloud tracking measurements extended on the dayside south hemisphere between 30 and 50°S and 9:05a - 10:50a. Our analysis technique shows unambiguous characterisation of the zonal wind latitudinal, local time profile and its temporal variability. We will also present a latitudinal profile of the meridional wind measured along both hemispheres, in the mid-latitudes range. The measured meridional wind flow will be compared with a model of a 20 ms^{-1} meridional wind flow.

1. Introduction

In the Venus' lower mesosphere (65-85 km), visible observations of Doppler shifts in solar Fraunhofer lines have provided the only Doppler wind measurements near the cloud tops in recent years [4, 5, 7, 8]. The region is important since it constrains the global mesospheric circulation in which zonal winds generally decrease with height while thermospheric SS-AS winds increase [1,6]. On Venus Express, atmospheric circulation at 70 km was measured with cloud tracking by both VIRTIS-M and VMC instruments [1,3]. However, winds derived in this manner are mean velocities about time intervals or more than 30 minutes and do not reflect instantaneous wind velocity and its significant variability at shorter time scales. The main purpose of this study is therefore to provide direct and instantaneous wind velocity measurements using visible Fraunhofer lines scattered by Venus cloud tops.

2. Method and Results

With ESPaDOnS, the complete optical spectrum, from 370 to 1050 nm, is collected over 40 spectral orders in a single exposure at a resolution of about 80,000. In the single scattering approximation, the Doppler

shift measured in solar light scattered on Venus dayside is the result of two instantaneous motions: (1) a motion between the Sun and Venus upper clouds particles, which scatter incoming radiation in all directions including the observer's; this Doppler velocity is minimal near Venus sub-solar point; (2) a motion between the observer and Venus clouds, resulting from the topocentric velocity of Venus cloud particles in the observer's frame; this effect is minimal near Venus sub-terrestrial point. The measured Doppler shift is the sum of those two terms. It therefore varies with planetocentric longitude. The Doppler shift vanishes at the half phase angle meridian, where both terms cancel each other [5] and we use this meridian as "zero-Doppler-reference" to check for instrumental or calibration drifts. The Doppler velocities are modelled using two kinematical templates for the zonal wind: (1) solid rotation with v zonal = v (equator) $\times$ cos (latitude), (2) uniform retrograde velocity, v zonal = v (equator). Both models are explored within latitudinal range 60S-60N. Once the best fit is obtained, we define the acceptable domain at 2-sigma and also test alternative models, including the combination of both zonal and meridional circulations.

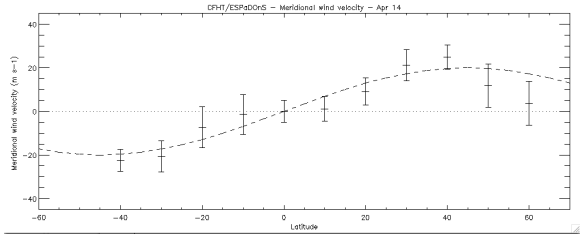

Figure 1: Meridional wind flow measured along the half phase angle meridian. We compare the measurements with a model of a 20 ms^{-1} meridional upper branch flow. Regarding the chosen referential, in both hemispheres the meridional wind is receding from equator towards the poles.

Venus Express cloud-tracking measurements using images taken with the VIRTIS instrument [1] indicate nearly constant zonal winds in the Southern hemisphere between 0 and 55 deg S, with westward zonal velocities of 105 m/s at cloud tops near 70 km, as well as a meridional, poleward component with a peak velocity of 10 $\pm$ 10 m/s. However, variability of the zonal flow, which is significant over an hour timescale, at all longitudes, is better characterized with the Doppler technique. With CFHT/ESPaDOnS measurements of Apr. 2014, velocity variations at $[\phi - \phi_E] = 0°$ and 30° lat near morning terminator are reported with an amplitude of $\pm$ 22.5 m s^{-1} relative to the mean (day-averaged) Doppler zonal velocity U = 119.5 m s^{-1}, over a period of about 2 hours, what can be indicative of local wave activity [5].

Acknowledgments - PM, DL, TW acknowledge support from the European Union Grant G.A. 606798 EuroVenus.

References

[1] Hueso, R., Peralta, J., Sànchez-Lavega, A., Icarus, Vol. 217, pp. 585-598, 2012.

[2] Lebonnois, S. et al., J. Geophys. Res., Vol. 115, E06006, 2010.

[3] Luz, D. et al., Science, Vol. 332, pp. 577-580, 2011.

[4] Machado, P., Luz, D. Widemann, T., Lellouch, E., Witasse, O, Icarus, Vol. 221, pp. 248-261, 2012.

[5] Machado, P., Widemann, T., Luz, D., Peralta, J., Icarus, Vol. 243, pp. 249-263, 2014.

[6] Sornig, M. et al., Icarus Vol. 217, pp. 863-874, 2012.

[7] Widemann, T. et al., Planetary and Space Science, Vol. 55, pp. 1741-1756, 2007.

[8] Widemann, T. et al., Planetary and Space Science, Vol. 56, pp. 1320-1334, 2008.

Cloud tracked winds at the lower cloud level using Venus' night side observations at 2.28 μm with TNG/NICS

P. Machado (1), J. Peralta (2), D. Luz (1), R. Gonçalves (1) and J. Oliveira (1)
(1) Institute of Astrophysics and Space Sciences, Observatório Astronómico de Lisboa, Ed. Leste, Tapada da Ajuda, 1349-018 Lisboa, Portugal (machado@oal.ul.pt), (2) Institute of Space and Astronautical Science - Japan Aerospace Exploration Agency (JAXA), JAPAN.

Abstract

We present results based on observations carried out with the Near Infrared Camera and Spectrograph (NICS) of the *Telescopio Nazionale Galileo* (TNG), in La Palma, on July 2012. We observed for periods of 2.5 hours starting just before dawn, for three consecutive nights. We acquired a set of images of the night side of Venus with the continuum K filter at 2.28 microns, which allows to monitor motions at the lower cloud level of the atmosphere of Venus, close to 48 km altitude. Our objective has been to measure the horizontal wind field in order to characterize the latitudinal distribution for both zonal and meridional components of the wind, to study day-to-day variability, to help constrain the effect of large scale planetary waves in the maintenance of superrotation, and mapping the cloud distribution. These observations were part of the network of ground-based observations of Venus coordinated with ESA's Venus Express orbiter for the 2012 Venus transit campaign. Ground-based observations are complementary to orbiter measurements, allowing simultaneous determination of the winds. We will present first results of cloud tracked winds from ground-based TNG observations and winds retrieved from coordinated space-based VEx/VIRTIS observations.

1. Introduction

The atmosphere of Venus is in superrotation, a state in which its averaged angular velocity is much greater than that corresponding to co-rotation with the solid globe. The circulation up to the cloud tops is characterized by an increasing zonal retrograde wind (in the East-West direction). The wind starts to build up at 10 km and amplifies with altitude, reaching a maximum at cloud tops ($\sim$ 70 km), where the atmosphere rotates about 60 times faster than the surface. Although the clouds are almost featureless in visible light, there are prominent features in UV and infra-red wavelengths. Dominant length scales are larger than 1000 km and few features are smaller than 20-30 km [6]. The cloud deck extends in altitude from 45 to 70 km, and can be divided into three main regions, centered at 48, 54 and 60 km [1]. The lowest of these is the lower cloud, where it is thought that fundamental dynamical exchanges that might also help to maintain superrotation are thought to occur [2]. The lower Venusian surface and deep atmosphere are a strong source of thermal radiation, with the gaseous CO_2 component allowing radiation to escape in windows at 1.74 and 2.28 μm. At these wavelengths radiation originates below 35 km, and unit opacity is reached at the lower cloud level, close to 48 km. Therefore, in these windows it is possible to observe the horizontal cloud structure, with thicker clouds seen silhouetted against the bright thermal background from the low atmosphere.

2. Method and results

Our objective is to provide wind measurements and a map of cloud distribution at the lower cloud level in the Venus troposphere, in order to complement Venus Express (VEX) and other ground-based observations of the cloud layer wind regime. By continuous monitoring of the horizontal cloud structure at 2.28 μm (NICS Kcont filter), it is possible to determine wind velocities using the technique of cloud tracking. We acquired a series of short exposures of the Venus disk. The best 10% of images have been selected, registered to a common coordinate system and co-added to compose a first image (A). Another series were taken at a later time, forming a second image (B). Cloud displacements in the night side of Venus, between images A and B, can be computed using both an automated technique [3] and a manual one [5]. We used a semi-automatic method, based on a phase correlation method between images [Peralta, personal communication] that increases the precision of the match be-

tween the observed cloud features (on image A) and its new location in image B. This observing strategy was similar to the one used previously by Young et al. [9] and Tavenner et al. [8] at IRTF (Fig. 1). The Venus apparent diameter at observational dates was greater than 32" allowing a high spatial precision. The 0.13" pixel scale of the the NICS narrow field camera allowed to resolve $\sim$ 3-pixel displacements. The absolute spatial resolution on the disk was $\sim$ 100 km/px at disk center, and the (0.8–1") seeing-limited resolution was $\sim$ 400 km/px. By co-adding the best images and cross-correlating regions of clouds the effective resolution was significantly better than the seeing-limited resolution. In order to correct for scattered light from the (saturated) day side crescent into the night side, a set of observations with the Br_γ filter were performed. Cloud features are invisible at this wavelength due to the high optical depth of the gaseous CO_2 component, and this technique allows for a good correction of scattered light [8].

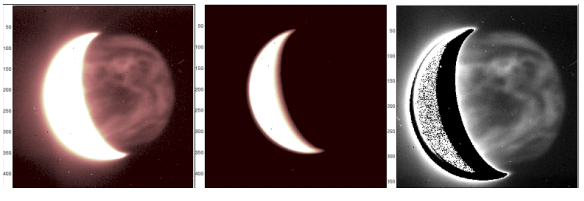

Figure 1: (From Tavenner et al., 2008 [8]): From left to right, a Continuum-K image, a Bracket-gamma, and the result of subtracting a scaled Bracket-gamma image from the one taken in Continuum-K. The black line seen in the first two images is from the IRTF SpeX slit. On these images the dark regions are clouds, the bright regions are optically thinner areas between the clouds that allow thermal emission from the lower atmosphere to escape, and the outlined crescent is the saturated day side of the planet. Images from September 14, 2007.

The completed data analysis provided the set of cloud tracked winds for the Venus lower cloud in the night side, which provides a basis for comparison with VEX-VIRTIS measurements [7].

Acknowledgements: We gratefully acknowledge the collaboration of the TNG staff at La Palma (Canary Islands, Spain). We thank the VIRTIS/Venus Express team for support with coordinated observations. We acknowledge support from Fundação para a Ciência e a Tecnologia, projects PEst-OE/FIS/UI2751/2014, POCI/CTE-AST/110702/2009 and Pessoa-PHC exchange program 2011-2013, FCT grants SFRH/BD/66473/2009 and SFRH/BPD/63036/2009 and also the Spanish MICINN for funding support through the CONSOLIDER program "ASTROMOL" CSD2009-00038 and through project AYA2011-23552.

References

[1] Esposito, L. et al., Venus III, Bougher, Hunten and Philips Eds., Sp. Sci. Ser., Arizona U. Press, pp. 415, 1997.

[2] Lebonnois, S. et al., J. Geophys. Res., Vol. 115, E06006, 2010.

[3] Luz, D., Berry, D. and Roos-Serote M., New Ast., Vol. 13, pp. 224, 2008.

[4] Luz, D. et al. Venus's Southern Polar Vortex Reveals Precessing Circulation, Science, Vol. 332, pp. 577-580, 2011.

[5] Peralta, J., Hueso, R. and Sanchez-Lavega, A., Icarus, Vol. 190, pp. 469, 2007.

[6] Rossow, W. B., Del Genio, A. D. and Eichler, T., Journal of Atmospheric Sciences, Vol. 47, pp. 2053, 1990.

[7] Sanchez-Lavega et al., Geophys. Res. Lett., Vol. 35, L13204, 2008.

[8] Tavenner, T. et al., Planetary Space Sciences, Vol. 56, pp. 1435, 2008.

[9] Young, E. et al., Bull. Am. Ast. Soc., Vol. 40, pp. 513, 2008.

COMPARISON OF THE THERMAL STRUCTURE MEASURED BY SOIR ON BOARD VENUS EXPRESS WITH A 1-D NON-LTE RADIATIVE TRANSFER MODEL.

A. Mahieux, A. C. Vandaele, V. Wilquet, *Institut Royal d'Aéronomie Spatiale de Belgique, Brussels, Belgium (arnaud.mahieux@aeronomie.be),* **J. T. Erwin, R. V. Yelle,** *Lunar and Planetary Laboratory, University of Arizona, Tucson, Arizona.*

Introduction:

SOIR was an infrared spectrometer on board Venus Express that probed the Venus terminator region from mid-2006 till end of 2014.

The measurements were taken at the morning and evening sides of the terminator, covering all latitudes from pole to pole. Its wavelength range - 2.2 to 4.3 µm - allowed a detailed chemical inventory of the Venus atmosphere [1-5], such as CO_2, CO, H_2O, HCl, HF, SO_2 and the aerosols. CO_2 was detected from 70 km up to 165 km, CO from 70 km to 140 km, and the minor species typically below 110 km down to 70 km.

Number density profiles of these species are computed from the measured spectra. Temperature profiles are obtained while computing the spectral inversion of the CO_2 spectra combined with the hydrostatic law [6].

These temperature measurements show a striking permanent temperature minimum close to the homopause (~125 km, ~100 K) and a weaker temperature maximum (100-115 km, 200-250 K). The time variability of the CO_2 density profiles spans over two orders of magnitude, and a clear trend is seen with latitude. The temperature variations are also important, of the order of 35 K for a given pressure level, but the latitude variation are small.

Radiative model:

A 1-D radiative transfer model has been developed to reproduce the SOIR terminator profiles.

This model solves the coupled, time-dependent energy balance, diffusion, and continuity equations in the vertical direction.

It accounts for heating and cooling radiative terms originating from CO_2 non local thermodynamical equilibrium (LTE), by grouping the population levels between 4 and 15 µm into 8 groups, and solving the corresponding radiative transfer equations and energy levels populations, while considering collisional de-excitation by CO_2, CO, O and N_2.

UV heating by CO_2, CO and O are also taken into account, as well as radiative cooling by minor species detected by SOIR (e.g. HCl, SO_2, and H_2O) which are found to be small in comparison to the CO_2 non LTE cooling. Aerosol cooling in the 60-110 km altitude range may be important to the thermal balance.

Discussion:

There is a good agreement between the 1D model temperature profile and the mean SOIR temperature profile, when aerosols cooling is considered in the mesosphere. Modes 1 and 2 are considered in the current study, in agreement with mean vertical profiles derived from the SOIR spectra [5].

Further we can suggest parameters that can be adjusted to improve the agreement between the model and measurements. The remaining differences can be attributed to the atmosphere dynamics at the terminator.

Future prospects:

This model will be adapted to Mars in order to study the temperature profiles derived instruments on-board the MAVEN mission and by the future instrument NOMAD on-board ExoMars.

Acknowledgments: The research program was supported by the Belgian Federal Science Policy Office and the European Space Agency (ESA – PRODEX program). The research was performed as part of the "Interuniversity Attraction Poles" programme financed by the Belgian government (Planet TOPERS). The authors also recognize the support from the FP7 EuroVenus project (G.A. 606798) as well as that of the HiResMIR International Scientific Coordination Network (GDRI). A. Mahieux would like to thank the FNRS (Belgium) for his Chargé de Recherches position and for supporting two stays at the University of Arizona.

Bibliography:

1. Bertaux, J.L., et al., A warm layer in Venus' cryosphere and high altitude measurements of HF, HCl, H2O and HDO. Nature, 2007. 450(29 November): p. 646-649, doi:10.1038/nature05974.

2. Vandaele, A.C., et al., Carbon monoxide short term variability observed on Venus with SOIR/VEX. Planet. Space Sci., 2014. (in press).

3. Mahieux, A., et al., Venus mesospheric sulfur dioxide measurement retrieved from SOIR on board Venus Express. Planet. Space Sci., 2014. (in press).
4. Mahieux, A., et al., Hydrogen Halides measurements in the Venus upper atmosphere retrieved from SOIR on board Venus Express. Planet. Space Sci., 2014. (in press).
5. Wilquet, V., et al., Optical extinction due to aerosols in the upper haze of Venus: Four years of SOIR/VEX observations from 2006 to 2010. Icarus, 2012. 217(2): p. 875-881.
6. Mahieux, A., et al., Update of the Venus density and temperature profiles at high altitude measured by SOIR on board Venus Express. Planet. Space Sci., 2014. (submitted).

BEPI COLOMBO FLY-BY's AT VENUS

V. Mangano, *INAF-IAPS, Roma, Italy (valeria.mangano@iaps.inaf.it),*
S. Orsini, A. Milillo, C. Plainaki, A. Mura, *INAF-IAPS, Roma, Italy.*

BepiColombo is a dual spacecraft mission to Mercury likely to be launched in early 2018 and carried out jointly between the European Space Agency (ESA) and the Japanese Aerospace Exploration Agency (JAXA). An extensive suite of high resolution scientific instruments, flying on the two spacecraft, allows addressing a wide range of scientific questions that will provide important clues on the origin and formation of Mercury as well as the terrestrial planets in general.

The first spacecraft, the Mercury Planetary Orbiter (MPO) comprises eleven experiments and will focus on a global characterization of Mercury through the investigation of its interior, surface, exosphere and magnetosphere. In addition, it will test Einstein's theory of general relativity. The second spacecraft, the Mercury Magnetosphere Orbiter (MMO), led by JAXA, will carry five experiments to study the environment around the planet including the planet's exosphere and magnetosphere, and their interaction processes with the solar wind.

Both spacecraft will be launched in a composite with a propulsion element, the Mercury transfer module and a sunshade cone to protect the MMO.

During the long cruise to Mercury (about 6.5 years), BepiColombo will have two fly-by's at Venus in 2019 and 2020. Due to the composite launch and cruise configuration (MCS) of both spacecraft, together with the propulsion element, not all the instruments will be able to operate during cruise.

MMO will be shielded by a sunshade cone, thus allowing instruments to detect signals only within a conical field-of-view around the composite's –Z axis. On the other hand, on the MPO only the instruments non-obstructed by the MTM or not requiring pointing. Figure 1 shows the composite spacecraft MCS and MPO configuration and axes. In general, such an instrumentation that could partially operate includes ion monitors, spectrometers and remote sensing instrumentation.

In this presentation, the opportunity of Venus fly-by's will be analyzed in terms of geometry and scientific instruments potentially involved. Possible interesting scientific cases (by instruments devoted to the investigation of interplanetary environment, like IMF, solar wind and radiation monitors) that can allow new analyses of the Venus environment are also presented, just to indicate the way these specific scientific objectives could be achieved, whenever such BepiColombo involved instrumentation will be activated in the nearby of Venus.

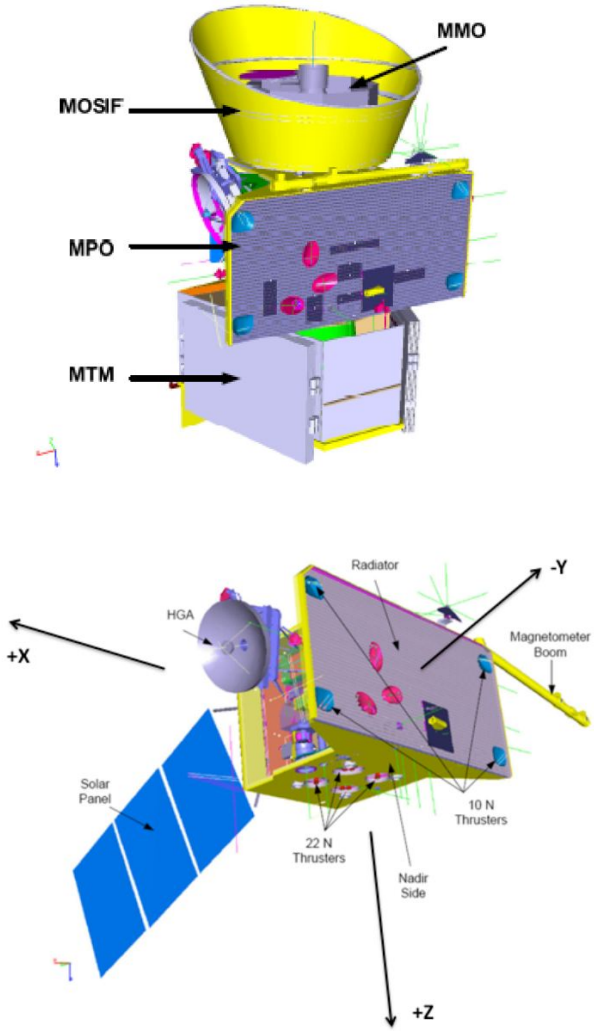

Figure 1: (top)Mercury Composite Spacecraft (MCS) with its four main components; (bottom) MPO configuration with instruments, antennas and solar panel.

A 1D RADIATIVE-CONVECTIVE MODEL OF H_2O-CO_2 ATMOSPHERES AROUND YOUNG TELLURIC PLANETS: AN UPDATE.

E. Marcq, *LATMOS / Université Paris-Saclay (emmanuel.marcq@latmos.ipsl.fr)*, **A. Salvador, A. Davaille,** *FAST, Université Paris-Saclay*, **H. Massol, É. Chassefière,** *GEOPS, Université Paris-Saclay*.

Introduction

The study of the early phases of the evolution of terrestrial planets has recently known significant progress [1,2,3,5]. It appears that their cooling phase during the magma ocean stage is first dominated by a radiative cooling stage through its atmosphere. If the planet is able to reach radiative balance during this stage, then its further evolution is dominated by the escape flux, and no large scale condensation of water occurs (Hamano-type II planets). On the other hand, if the planet is far enough from the sun, then radiative equilibrium cannot be reached until the outgoing flux has fallen below the runaway greenhouse limit, implying the condensation of most atmospheric water vapor into a global water ocean, thus sheltering most water from atmospheric escape (Hamano-type I planet). In the solar system, Earth is clearly a type-I planet, whereas Venus was most likely a type-II planet from quite early on in its history [1,2].

Recent work

Since the publication of [2], the atmospheric part of the model, first described in [3], has known significant updates and changes, namely:

- switch from a z-grid to a p-grid extending up to the mesopause at $P = 0.1\,\mathrm{Pa}$;
- correction of a bug affecting the k-correlated computation of OLR;
- including N_2 pressure as well as H_2O and CO_2;
- improvement of the numerical stability and integration scheme;
- rewriting of the FORTRAN code for easier visualization and coupling with other models through a *Python* API.

Main results

The qualitative results from [3] are still reproduced by our model, as well as the type I/type II dichotomy from [1,5]. Above a critical surface temperature T_c whose value depends on the atmospheric H_2O and CO_2 inventory, the blanketing is inefficient, leading to a cloudless atmosphere remaining hot even at higher altitudes.

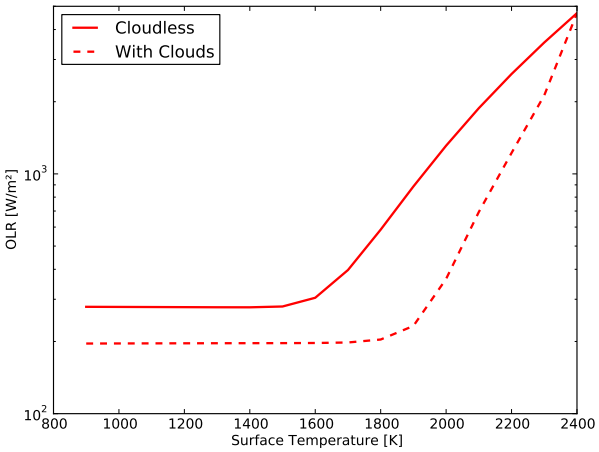

Figure 1: OLR vs. surface temperature for surface pressures of $300\,\mathrm{bar}$ of H_2O, $100\,\mathrm{bar}$ of CO_2 and $1\,\mathrm{bar}$ of N_2 with and without taking into account the radiative effect of clouds. T_c is close to $1600\,\mathrm{K}$ in the cloudless case and $1800\,\mathrm{K}$ if the blanketing effect of thick water clouds is taken into account.

OLR can reach high values and strongly increases with increasing surface temperature, leading to a rapid cooling (less than 10^5 year) of these young magma ocean planets. Very young planets thus radiate efficiently in near infrared windows and even into the visible range, making them easy to detect spectroscopically.

On the other hand, below this critical temperature, the modeled atmospheres closely resemble a typical H_2O driven runaway greenhouse atmosphere [4]: the OLR reaches an asymptot, known as *Nakajima's limit*[6] at about $280\,\mathrm{W/m^2}$ in a cloudless atmosphere (Fig. 1); optically thick water clouds form high up in the atmosphere, and the radiative mesosphere is cool enough. Such atmospheres are very close to global radiative balance, and their cooling is therefore much slower – assuming they are able to cool down at all before atmospheric escape becomes significant (type-I planets can, type-II cannot). The detectability prospect for such exoplanets is thus no better than for typical telluric planets.

Future work

Extensions and improvements of this model are still in development. By order of priority:

- adopting a 1D spherical geometry wherever possible. It is especially needed for hot and massive atmospheres around smaller telluric planets;
- including stellar radiation in the k-correlated radiative transfer code, so that we can discard the simplistic albedo parametrization currently in use;
- addressing the issue of vertical stability of the atmosphere with respect to the vertical molecular weight profile below and above the water cold trap (whenever present).

Bibliography

1 K. Hamano *et al.*, Nature (2013)

2 T. Lebrun *et al.*, JGR (2013)

3 E. Marcq, JGR (2012)

4 J. Leconte *et al.*, Nature (2015)

5 K. Hamano *et al.*, A& A (2015)

6 S. Nakajima *et al.*, JAtS (1992)

PAST AND PRESENT VOLCANISM OF VENUS

Markiewicz W.J.[1], Shalygin E.V.[1], Basilevsky A.T.[1,2,3], , Titov D.V.[4], Ignatiev N.I.,[5], Head J.W.[3], *[1] Max-Planck-Institut für Sonnensystemforschung, 37077 Göttingen, Germany; [2] Vernadsky Institute, 119991 Moscow, Russian Federation, [3] Brown University, Providence, Rhode Island 02912, USA; [4] ESA-ESTEC, 2200 AG Noordwijk, The Netherlands; [5] Space Research Institute, 117997 Moscow, Russian Federation.*

First reliable information on widespread volcanism on Venus was resulted from analysis of side-looking radar imagery taken by Venera-15-16 (e.g., Barsukov et al., 1986). Morphology of the observed volcanic landforms and results of geochemical measurements by Venera 8, 9, 10, 13, 14 and Vega 1, 2 landers (Surkov, 1997) showed the essentially basaltic character of Venusian volcanism. Results of radar survey taken by Magellan mission allowed to improve understanding of Venusian volcanism (e.g., Head et al., 1992) and to suggest stratigraphic classification of Venusian terrains and landforms, including volcanic ones (e.g., Basilevsky and Head, 1998). Then as a result of global geologic mapping of Venus the stratigraphic classification was made more reliable (Ivanov & Head, 2011, 2013). The most widespread are various volcanic plains, but volcanic edifices, mostly shield volcanoes are also not rare.

The most widespread are plains with wrinkle ridges (pwr), also called regional plains (Figure 1, left), occupying ~42% of Venus surface (Ivanov & Head, 2011). Their morphology and age relations with impact craters suggest widespread and high-yield volcanic eruptions happened during relatively short time at ~0.5-1 Ga. Shield plains (psh) (Figure 1, right) occupy 18.5% of Venusian surface and represent numerous coalescing volcanic shields typically formed before emplacement of regional plains. Younger than these are smooth plains (ps, ~2%) and lobate plains (pl, ~9%) (Figure 2), the latter form both plains *per se* and gentle-sloping shield volcanoes.

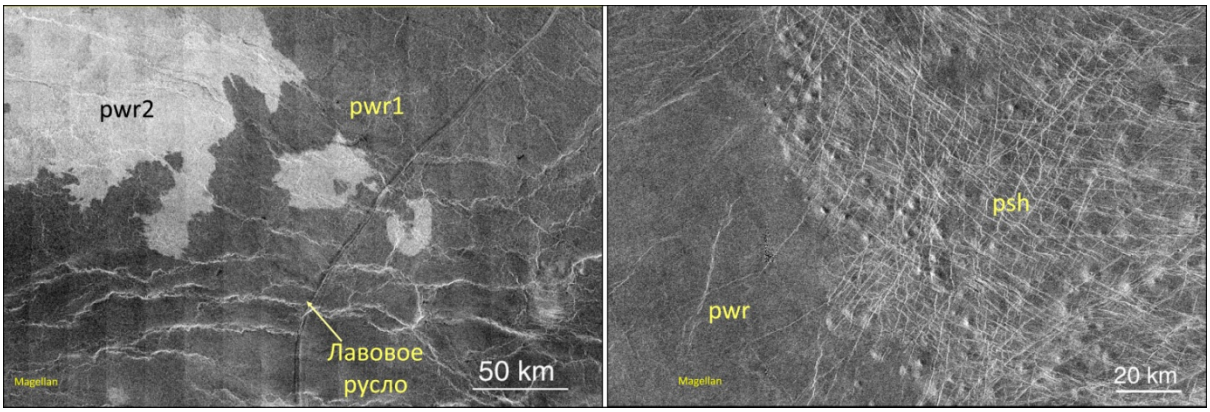

Figure 1. Left – plains with wrinkle ridges, the older (pwr1) and younger (pwr2) subunits with enigmatic channnel of Baltis Vallis; Right – shield plains (psh) embayed by plains with wrinkle ridges (pwr)

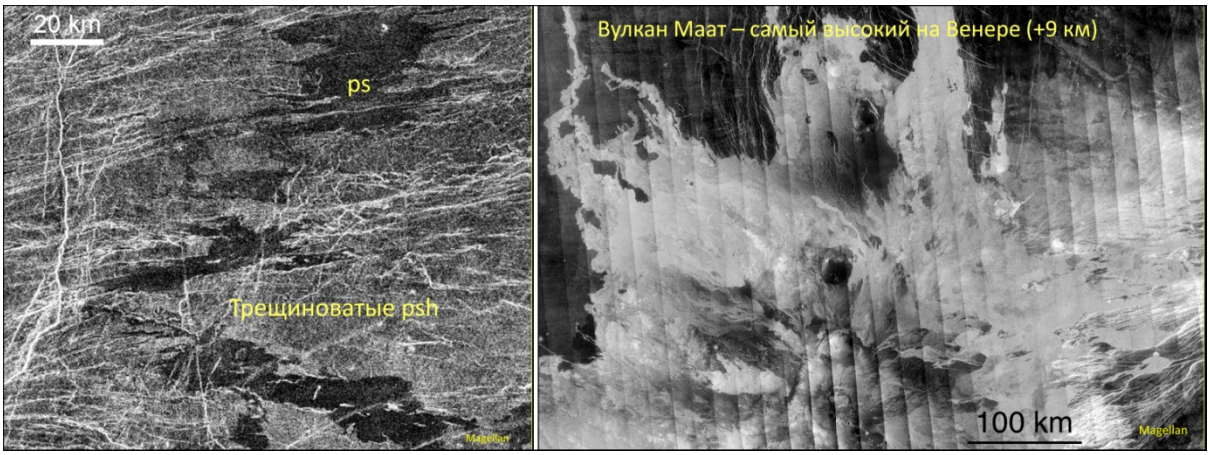

Figure 2. Left – smooth plains (ps) filling depressions within shield plains (psh); Right – lobate flows forming Maat Mons, the highest volcano on Venus. Radar-bright flows are superposed on the darker regional plains.

On Venus are also observed volcanic steep-sided domes (Pavri et al., 1992). They could be formed by eruptions of viscous, probably non-basaltic, silicic lavas, or high viscosity of these lavas may be due to presence of numerous gas bubbles. Understanding the nature of these high-viscosity lavas is one of unresolved problems of Venusian volcanism. We plan to work on this

problem through analysis of 1-micron surface emissivity data taken by Venus Monitoring Camera (VMC) onboard of Venus Express (VEX). First results gained by this approach are given in Basilevsky et al. (2012).

Another intriguing problem of Venusian volcanism is a presence or absence of now ongoing volcanic activity. Some representatives of the youngest volcanic unit (pl) based on their characteristics, in particular, age relations with dark-parabola impact craters, were dated as formed within the last few tens of million years from now, that is geologically present (e.g., Basilevsky, 1993). But issue of now ongoing volcanic activity remained unresolved. Works of Bondarenko et al. (2010) and Smrekar et al. (2010) suggested such possibility but did not reliably prove it. More reliable information was recently gained through analysis of the VEX VMC data by Shalygin et al. (2015) who showed that in one of geologically young rift zones, Ganiki Chasma, there are observed "hot" spots which appear and disappear at the days to months time scale (Figure 3).

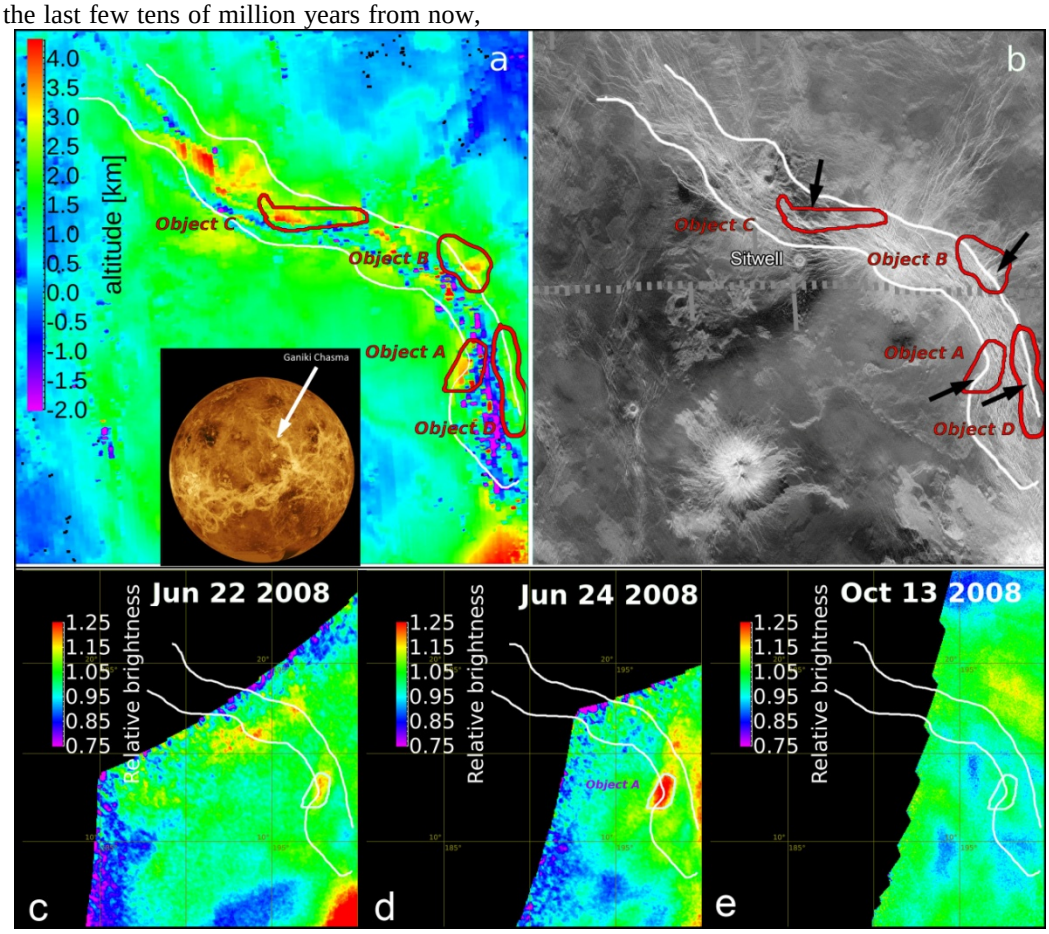

Figure 3. a) Topographic map of Ganiki Chasma area with transient spots (objects A-C), white arrow in the figure inlet shows locality of Ganiki Chasma; b) Magellan radar image of this area; c-e) Transient spot A seen/not seen during several observation sessions.

Because orbital spacecraft's view is blurred by the clouds, the areas of increased emission appear spread out over large areas of about 100 km across, but the hot regions on the surface below are probably much smaller. Indeed, for the hotspot known as 'Object A', as an option, the real hot area may only be around 1 square kilometre in size, with a temperature of 830 °C, much higher than the global average of 480°C.

So, concluding, Venus was volcanically active at least during the last 0.5-1 Ga and seems to keep being active now. Venusian volcanism is mostly basaltic one, but there is some evidence of possible non-basaltic, silicic volcanoes, which we plan to check in new analyses of the VEX VMC data. Also we plan to continue search for new pieces of evidence of now ongoing volcanic activity on this planet.

References: [1] Barsukov et al., 1986. J. Geophys. Res. 91. No B4. D378-D398. [2] Basilevsky, 1993. Geophys. Res. Lett. 20(10), 883-886. [3] Basilevsky &. Head. 1998. J. Geophys. Res., 103, 8531-8544. [4] Basilevsky et al., 2012. Icarus. 217. 434-450. [5] Bondarenko et al., 2010. Geophys. Res. Lett. 37, L23202. [6] Head et al., 1992. J. Geophys. Res., 97, 13,153-13,197. [7] Ivanov & Head, 2011. Planet. Space Sci. 59 (13). 1559-1600. [8] Ivanov & Head., 2013. Planet. Space Sci. 84. 66-92. [9] Pavri et al., B., 1992. J. Geophys. Res. 97, 13,479-13,493. [10] Shalygin et al., 2015. Geophys. Res. Lett., 10.1002/2015GL064088. [11] Smrekar et al., 2010. Science, 328 (5978), 605-608, [12] Surkov, 1997. Exploration of Terrestrial Planets from Spacecraft: Instrumentation, Investigation, Interpretation, 2nd ed., John Wiley, Hoboken, N. J. 446 p.

A 145 DAY PERIOD IN THE VENUS CONDENSATIONAL CLOUDS.

K. McGouldrick, *University of Colorado Boulder, USA (kevin.mcgouldrick@lasp.colorado.edu)***, C. C. C. Tsang,** *Southwest Research Institute, Boulder, CO, USA***.**

We have analyzed the long-term regional and global variation of emitted radiance in the several near infrared spectral windows in the Venus atmosphere that were accessible by the medium resolution, infrared channel of the Visible and Infrared Thermal Imaging Spectrometer (VIRTIS-M-IR) on the Venus Express spacecraft.

We have presented analysis of the complete VIRTIS-M-IR data set for night side emission in the near infrared spectral windows for all southern hemisphere observations made before the failure of the instrument's cooling system after orbit 921. We find no clear evidence of long-term increase or decrease in the overall radiance (hence overall cloud coverage and thickness) from analysis of just the 1.74μm and 2.30μm spectral windows that are most sensitive to the cloud variations. However, upon extending our analysis to all of the spectral windows – including those that are primarily driven by surface emission variations – we note that in almost every case (segregated by spectral window and geographic region), the overall trend of radiance is increasing over the course of the mission, suggesting a long term decrease in overall cloud coverage and thickness.

We note an unanticipated trend of increasing radiance from equator to pole in the surface-dominated windows, suggesting that selection effects that favored observations over lower elevation (hence, warmer) terrain are evident in the global (i.e., longitudinal) mean. We propose that this elevation sensitive selection effect, coupled with possible absorption by a species that can condense at temperatures similar to those near the surface of Venus might also be responsible for the variation in the limb darkening corrections with respect to latitude that were noted in previous work by others.

Our global analysis of the size parameter demonstrates an overall increase in particle size, from equator to pole, consistent with previous analysis. We also note a subtle spatial increase in the size parameter peaking at about -20° latitude; but it is difficult to state this with certainty, due to the increasing magnitude of the standard deviation of the calculated size parameter in the equatorial latitudes observed by VIRTIS-M-IR.

We observe in the VIRTIS-M-IR data that the 1.74μm and 2.30μm windows demonstrate local maxima in radiance peaking around 50° latitude, consistent with previous observations of these spectral windows, dating to the time of their discovery in the 1980's. We also measure a large amount of variability to the typical cloud coverage as at latitudes between 0° and 60°, as evidenced by the very large standard deviations about the mean in the cloud-dominated windows at those latitudes.

We find a periodic variation in the 1.74μm radiance that is most pronounced in the data from mid-latitudes ($30^\circ - 60^\circ$ latitude), binned to a seven day (circumglobal) window. A least squares frequency analysis quantifies this period that was suggested in earlier work. The oscillation has a period of approximately 145 days, and is not consistent with any known geometric or astronomical phenomena at Venus. The oscillation has an amplitude approximately twice that of the typical day-to-day variations observed; the timescale for the decay of the radiance (the increase in cloud opacity) is approximately 50 days and the timescale for the return to peak radiance is approximately 95 days. These decay and recovery timescales are consistent with response of the cloud vertical structure to the radiative-dynamical feedback; but it remains unclear why this variation would be seen only at mid-latitudes. Further modeling investigations will be necessary to elucidate the drivers of this periodicity in the clouds.

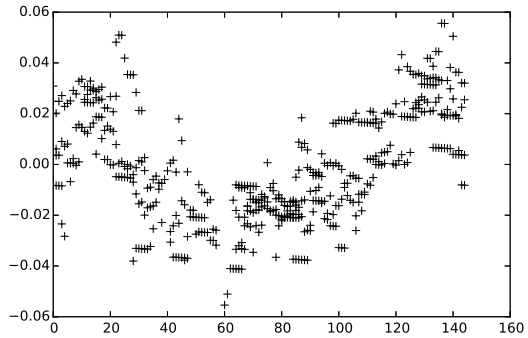

Figure 1: Periodogram for the 145 day period of the mid-latitude 1.74μm radiance. The x-axis is in units of days, the y-axis is in units of the frequency power.

Exploring Venus with a comprehensive atmospheric model

J. M. Mendonca, University of Bern, *Bern, Switzerland (joao.mendonca@csh.unibe.ch)*

Introduction: The atmospheric circulation in Venus is well known to exhibit strong super-rotation. Despite the difficulties in reproducing the physical and dynamical conditions of the Venus atmosphere in a realistic numerical approach, simulations with global circulation models are starting to unveil the mechanisms behind the formation of the strong winds. Our recent simulations with the Oxford model found that the main mechanisms driving the strong winds below and above clouds are different, and these new results will be presented and discussed. The model was able to obtain an atmospheric circulation and thermal structure above the cloud base remarkably similar to the observations. Below the cloud base the magnitude of the zonal winds obtained are weaker than the values expected from the observations, in line with what has been found by other groups as well. This difficulty is the next main challenge for all Venus general circulation models, and it has to be studied in conjunction with future observational data of the deep atmosphere. To solve this problem we are currently using a new numerical model to specifically explore the mechanisms at work to produce the observed circulation in the lower atmosphere. This new model is ideal to study physical phenomena which were missing or not well represented in previous simulations, since the fluid dynamical equations resolved in the new model are complete and coupled with flexible physical schemes.

Venus Model Results: Here we present the recent results of the Oxford Venus model, OPUS-Vr. This model includes a new radiation scheme that represents the radiative absorption and scattering by gas molecules and aerosols (Mendonca et. al, 2015), and is more complete than previous works (Lebonnois et al 2010; Yamamoto et al. 2010) because it includes explicit calculations of the solar fluxes and it is easy adaptable to different optical structures. Other new features in OPUS-Vr are the new convection and suitably adapted boundary layer schemes and a dynamical core that takes into account the dependence of the heat capacity at constant pressure with temperature.

The model is able to simulate a thermal structure and atmospheric circulation in the cloud region quantitatively similar to the one observed (Figure 1). We find that the atmospheric mechanisms forming and maintaining the strong winds in this region are a combination of zonal mean circulation, thermal tides and transient waves (Mendonca et. al., 2016). The latter are retrograde inertia-gravity waves excited by the thermal tides in the cloud region and have a key role transporting the angular momentum upgradient. These free waves transport prograde momentum mostly from the upper atmosphere to the upper cloud region. The super-rotation in the cloud region is a persistent phenomenon for the current atmospheric conditions, however, we found variability of the zonal wind distribution at jet altitudes that is significantly affected by long term oscillations (tens of Venus days) and by the presence of bi-diurnal planetary mixed Rossby-gravity waves. We also found that the magnitude of the zonal wind speed can be affected by the optical properties of the deep atmosphere near the surface. A summary of the main atmospheric phenomena found with OPUS-Vr is shown in Figure 2.

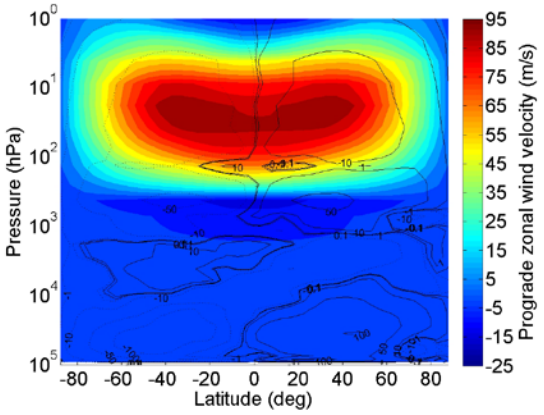

Figure 1: Zonally and time averaged (5 Venus days) zonal wind (m/s) and mass stream function (in units of 10^9 kg/s) of the reference simulation.

Lower Atmosphere: The main cause for the poor representation of the atmospheric circulation in previous numerical models below the cloud region is still unknown. I will present a new model that we have developed to explore this region of the atmosphere. The main goal is to improve the representation of the angular momentum transport, creation and destruction in the boundary layer. The possibility of physical phenomena being not resolved at the typical space resolutions used in Venus atmospheric models is also being explored by running high resolution simulations.

The new Venus model uses a new dynamical core called THOR (Mendonca et. al., 2016). THOR is part of the Exoclimes Simulation Platform (ESP), and here is applied to study Venus. The new dynamical core solves the full atmospheric fluid equations

in a rotating sphere (fully compressible – non-hydrostatic system). In summary, the main advantages of using our new dynamical scheme against other recent planetary climate models is that **1)** The atmospheric fluid flow is completely represented and no approximations are used that could compromise the physics of the problem; **2)** The model uses a specific icosahedral grid that solves the pole problem (Figure 3); **3)** The interface is user friendly and can be easily adapted to a multitude of atmospheric conditions; **4)** By using GPU computation, our code greatly improves the typical code running time. The latter is an important feature of the model since we are aiming to explore high resolution simulations. In Figure 4, we show the time and zonal average zonal winds of the "Held-Suarez" experiment used to assess the model performance for long integrations (Held & Suarez 1994).

Currently, the model is integrating for different deep Venus atmospheric conditions and the preliminary results will be presented at the conference. The results will allow us to have a better understanding on the robustness of the Venus simulations in this poorly explored region.

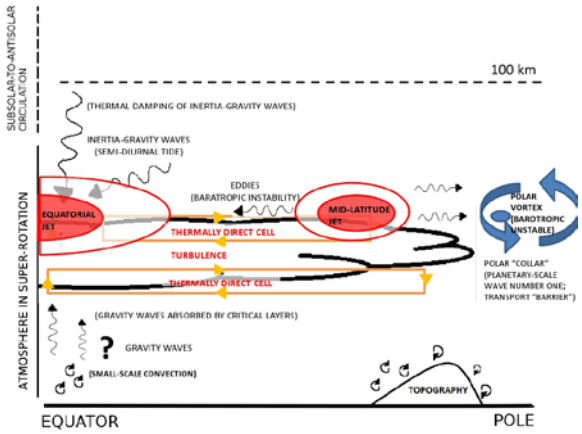

Figure 2: Sketch summarising the main mechanisms that drive the atmospheric circulation from the OPUS-Vr results. In general, the mean circulation in the cloud region is characterized by two planetary-scale Hadley cells in each hemisphere and the eddy-zonal flow interactions have a crucial role in replenishing the equatorial region with angular momentum.

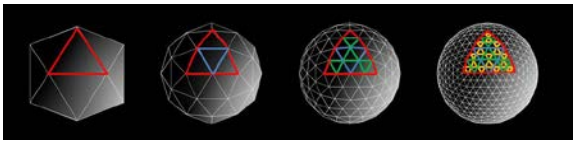

Figure 3: New model's grid.

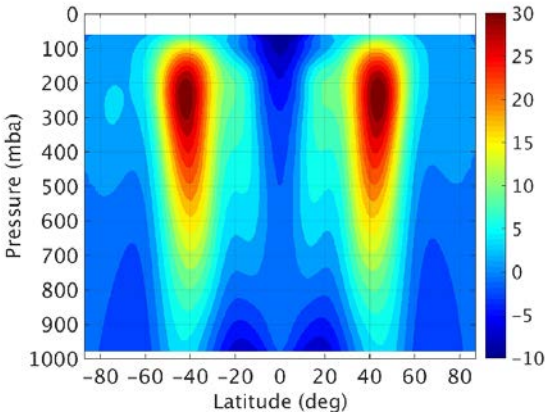

Figure 4: Zonal winds from the "Held-Suarez" experiment obtained with THOR. The model is able to closely reproduce the zonal winds for Earth-like conditions.

References:

[1] Held, I., and Suarez, M., B. Am. Meteorol. Soc, 75, 10, 1825-1830.

[2] S. Lebonnois, F. Hourdin, V. Eymet, A. Crespin, R. Fournier, and F. Forget. JGR (Planets), 115, 2010.

[3] Mendonca, J., Thesis, University of Oxford, 2013

[4] Mendonca J., Read P., Wilson C., Lee C., 2014, 105, 80-93, PlanSS.

[5] Mendonca, J., Read P., 2016, submitted.

[6] Mendonca, J., et al., 2016, in preparation.

[7] M. Yamamoto, M Takahashi, K. Ikeda, M. Takahashi, and Y. Matsuda. VEXAG International Workshop, 2010.

Rotational temperature estimation at airglow altitudes using nightside VIRTIS/Venus Express measurements

A. Migliorini , *IAPS-INAF, Rome, Italy (alessandra.migliorini@iaps.inaf.it)*, **M. Snels,** *ISAC-CNR, Rome, Italy*, **G. Piccioni, D. Grassi**, *IAPS-INAF, Rome, Italy,* **J.-C. Gérard, L. Soret,** *LPAP, Liége, Belgium*

Introduction:

The recent discovery of OH in the Venus atmosphere by Venus Express allows one to investigate the photochemistry in the upper mesosphere of the planet (Piccioni et al., 2008). The (1-0), (2-1), (3-2) and (4-3) OH transitions have been identified in the spectra acquired with the Visible and InfraRed Thermal Imaging Spectrometer (VIRTIS) on board the spacecraft. In addition the (2-0) band at 1.46 μm was also identified.

These emissions occur on average at 95 km, and have been observed so far only on the night side of the planet.

The complex structure of the OH(Δν=1) at 2.8-3.2 μm can be used to infer the rotational temperature at these altitudes, by assuming that the atmosphere is locally in a thermal equilibrium. Although this is not generally true, as demonstrated by Cosby and Slanger (2007), this assumption applies quite well at the 90-100 km altitude, where the maximum of emission occurs.

The present investigation aims to use the VIRTIS spectra to determine the temperature at the airglow altitudes. This region is indeed quite complex, and the temperature measurements at these altitudes are still controversial.

Method:

We analyzed the VIRTIS data, where the nightside of Venus was observed at limb, and showing a good signal-to-noise ratio (SNR) at the OH emission wavelengths. Data are averaged in the 90-100 km altitude range, in order to increase the SNR.
The mean spectra are compared with synthetic spectra obtained by considering the OH transitions originating from the vibrational levels ν=1-4, at 5 different rotational temperatures (T_{rot} = 150 K, 180K, 200K, 220K, and 250K). A Chi-Square test has been performed in order to determine which rotational temperature provides the best fit.

Figure 1 shows the resulting Chi-Square for three VIRTIS images. In the case of images named 383-12 and 715-02, acquired on 2007-05-09 and 2008-04-05 respectively, the minimum Chi-Square is obtained for the fit with T_{rot} = 180 K, while in the case of image 317-06 (observing date at 2007-03-04) the best fit seems to be achieved for a lower temperature, as suggested by the minimum Chi-Square shifted towards lower temperatures. This may suggest a different atmospheric temperature in the latter case. Further investigation is going on to estimate how accurately the Venus night-side temperature at about 95 km can be determined from the OH airglow emissions.

Results: Preliminary results show that, despite the limited spectral resolution of the infrared channel of VIRTIS-M, this technique is able to provide information about the Venus temperature at the airglow altitude.
Comparison with temperature estimations using $O_2(^1\Delta_g)$ observations from ground, and measurements obtained by other experiments on-board Venus Express will be also shown.

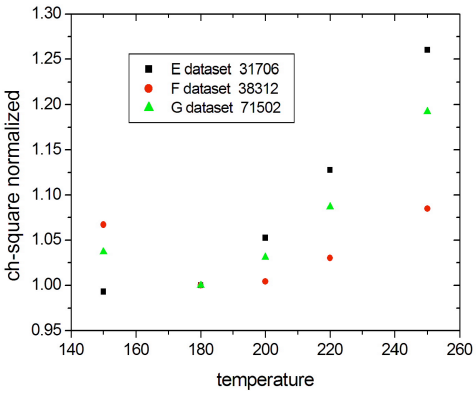

Figure 1. Chi-Square versus rotational temperatures for three VIRTIS images. The temperature at which the best fit occurs can be used to infer the Venus temperature at about 95 km height.

A dynamic and testable hypothesis to describe the evolution of the Venusian surface environment

S. Mikhail, The University of St. Andrews, The Department of Earth and Environmental Sciences, St. Andrews, UK, email: sm342@st-andrews.ac.uk; **P. H. Barry, C. J. Ballentine,** The University of Oxford, The Department of Earth Sciences, Oxford, UK; **S. P. Kelley**, The Open University, Milton Keynes, UK; **M. J. Heap**, Géophysique Expérimentale, Institut de Physique de Globe de Strasbourg, France; **C. J. Jackson,** Geophysical Laboratory, Carnegie Institution of Washington, USA

Introduction: The planet Venus is a geological enigma. Earth and Venus are almost identical in terms of size and bulk composition (e.g. bulk petrology). However, these two planets have completely dissimilar climate and geomorphology. For example, the Venusian atmosphere and surface are both dry, and Venus' proximity to the Sun combined with its massive CO_2-rich atmosphere (>90 bars) has resulted in an average surface temperature >450°C. In addition, Venus is a relatively flat planet [1-2], whereas Earth has a relatively cold, wet surface, and relatively extreme topography. We aim to address how, when, and why these two sister planets diverge into a hellish wilderness (Venus) and the archetype of habitability and geological dynamism (Earth).

Palaeoenvironmental conditions: It is possible that the surface conditions of Venus weren't always hot and dry. During the early years of the solar system the sun was less bright [3], meaning Venus could have been a habitable planet, potentially permitting liquid water. However, Venusian palaeoenvironmental conditions, and temporal information about its evolution are unknown, due to the absence of confirmed meteorites from Venus, a dearth of *in-situ* geochemical data, and the permanent cloud cover that renders optical geological investigations of the surface impossible. The only Venusian geochemical data available to geologists are major element composition and K-Th-U systematics of 3 surface rocks, and the chemical composition of the atmosphere [4-5]. Importantly, the available data include the hydrogen and argon isotope composition of the atmosphere, which we use to propose a model for the palaeoenvironmental evolution of Venus.

Input parameters: We assume Venus and Earth are made of the same chondritic material, and their similar size ($\Delta m = 1.23$) would mean they have similar internal structures (e.g. bulk mantle petrology, core/mantle volume ratio, core composition etc.), and this assumption is consistent with the geochemical observations thus far [4-5]. Their proximity to one and other (0.28 AU) dictate that the flux of exogenic material added to these planets must be on the same order. For example, the very similar $^{20}Ne/^{14}N$ ratio, and near chondritic $^{12}C/^{14}N$ ratio for Earth and Venus indicate that the process of volatile loss and addition were similar [6]. Furthermore, post-accretion exogenic addition was proportional to planetary mass (inclusive of Martian data). However, missions sent to measure the chemistry of the Venusian surface environment all provide the same puzzling result; Venus is extremely dry and Earth is wet.

Hydrogen isotope constraints on hydration: The D/H ratio of the atmosphere has been used to propose Venus once had enough water on the surface to host a global ocean (<10 to >500 meters deep; see [7-8]). The loss of this ocean can be readily explained by the hot surface temperature, meaning any water on Venus would be a gas, and the lack of a core-driven geodynamo impairs the planets ability to deflect solar wind, thus its water was lost to space. In short, photolysis of H_2O in the atmosphere was followed by loss of the non-gravitationally bound H atoms. However, the timing of the water loss is unconstrained.

Argon isotope constraints on desiccation: Of the atmospheric isotope data available, the isotopes of argon are the most dynamic. The data include the relative abundances of two primordial isotopes (^{36}Ar & ^{38}Ar), and one radiogenic daughter product, ^{40}Ar. The latter is produced from the decay of ^{40}K with a long half-life (1250 Ma). Venus and Earth appear to have very similar bulk K/U ratios [9], and show similar atmospheric $^{36}Ar/^{38}Ar$ ratios [10]. Therefore, both planets should have the same bulk ^{40}Ar production, and one would assume similar atmospheric $^{40}Ar/^{36}Ar$ ratios. However, Venus has an atmospheric $^{40}Ar/^{36}Ar$ of only 1.03 ± 0.04 compared with 298.56 and 1900 ± 300 for Earth and Mars respectively [10-11]. This is puzzling because Ar is a highly incompatible in silicates ($D < 0.001$) and a highly volatile element (boiling point −185°C). Therefore, volcanism should outgas Ar to the atmosphere [12]. The presence of subduction zones on Earth has greatly altered the $N/^{36}Ar$ geochemistry of the Earth's atmosphere relative to Venus and Mars [13]. However, this cannot explain the very low $^{40}Ar/^{36}Ar$ ratio of the Venusian atmosphere, because ^{40}Ar degassing is insensitive to fO_2 and the surface rocks on Venus have similar K-abundances to those on Earth [4]. The simplest explanation of these data is that the transfer ^{40}Ar generated in the crust and mantle to the surface is retarded on Venus, relative to Earth and Mars. In addition, the exceedingly high $^{40}Ar/^{36}Ar$ of the Martian atmosphere reflects the extreme loss of ^{36}Ar from Mars (due to its weaker gravity and lack of a magnetic field), allowing for later degassing of more radiogenic Ar to dominate the modern atmosphere. Loss of Ar is not important for the atmospher-

ic budgets of Earth or Venus, evidenced by their unfractionated $^{36}Ar/^{38}Ar$ value [6]. We argue that the low $^{40}Ar/^{36}Ar$ ratio for the Venusian atmosphere reflects: (i) a reduced volcanic flux through its history (relative to Earth), and (ii) the loss of water early in Venus' history.

Dynamic Model:

Low volcanic flux: The geology of the Venusian surface is >90% volcanic, but the frequency of volcanism is unknown [14]. The high surface temperature on Venus (>450°C) means the Venusian geotherm is therefore offset relative to Earth. Using high-temperature deformation data for basaltic rocks at confining pressures consistent with depths of up to 15 km [15-16], we find that ductile deformation prevails in the Venusian lithosphere, whereas the dominant deformation mode for the lithosphere on Mars and Earth is brittle (for the same depth). In other words, the depth of the brittle-ductile transition (BDT) is much closer to the surface on Venus than on Mars or Earth. This means plume-lithosphere interactions on Venus are unique relative to other known tectonic regimes in our solar system. Conversely, for Earth, Mars, Mercury, the Moon, and telluric asteroids like 4-Vesta, the primary mode of magma migration in the crust is through dikes propagating along faults. However, due to the fact that the majority of the Venusian crust is ductile, faulting is prohibited, which inhibits dike formation below the ductile-brittle transition (which, according to the high-temperature triaxial data, can be as shallow as 4 km below the surface). It is therefore probable that a high proportion of magmatism on Venus does not result in volcanism. Instead, the rate of plutonism will be greatly increased because sills and diapirs dominate magma transport pathways. This notion elegantly harmonizes the proposed quiescence of Venusian volcanism since the global resurfacing event 500-800 Ma with the question of how a planet can be almost volcanically dormant while it's mantle temperature must be close to the solidus of peridotite (e.g. [9]). This means the majority of ^{40}Ar produced in the bulk silicate Venus (BSV) is trapped, unless liberated by diffusive processes.

Early desiccation of Venus: The lack of ^{40}Ar transport to the atmosphere by diffusion on Venus is because the system rapidly reaches equilibrium with the intergranular medium (shutting off chemical transport and because Venus's crust lacks fluids as a mobilizing agent (shutting off mechanical transport). This is despite diffusion coefficients through minerals large enough to model efficient mobility [17]. In short, for telluric planets, mass-transfer along the grain boundary of silicates and oxides are limited to a very thin layer over time periods measured in gigayears [18]. Therefore we argue the low $^{40}Ar/^{36}Ar$ ratio in the atmosphere reflects the loss of water early in Venus' history. This was a consequence of the early cessation [19], or a total absence [20] of a core-driven geodynamo. This impaired the planets ability to deflect solar wind, thus losing water following photolysis. Following dehydration, Venus no longer possessed an efficient transport mechanism/medium to remove the excess ^{40}Ar in the BSV, resulting in the low $^{40}Ar/^{36}Ar$ ratio in the present-day atmosphere.

Testable Hypothesis: Importantly, the model presented here forms a testable hypothesis. Future determinations for the xenon isotope composition of the Venusian atmosphere will affirm, or disprove our model by applying temporal constraints to the origin and evolution of the Venusian atmosphere. This is because, as stated previously, the mobilization of noble gases from the lithosphere into the atmosphere requires fluids [21-22]. Therefore, if fluids are required to liberate ^{40}Ar from the bulk silicate Venus (BSV), then the same would be true for ^{129}Xe. The $^{129}Xe/^{130}Xe$ ratio reflects the abundance of ^{129}Xe generated by the decay of the moderately short-lived iodine isotope, ^{129}I (half-life 15.7 million years). For example, excess ^{129}Xe in Earth's mantle is taken as evidence that Earth degassed most of its initial atmosphere before the extinction of ^{129}I [23], where Earth's mantle exhibits a higher $^{129}Xe/^{130}Xe$ than the atmosphere, meaning mantle degassing of the primordial noble gases (e.g. ^{130}Xe) to the atmosphere before the extinction of ^{129}I (see [24]). Thus, if Venus retains volatiles in the BSV because of solar-driven desiccation in the absence of a geodynamo, then a combination of xenon and argon stable isotope ratios can be used to place upper and lower limits on the timing of atmosphere-formation and evolution (and lithosphere-formation). By comparing the $^{129}Xe/^{130}Xe$ ratio of the Venusian atmosphere with the $^{40}Ar/^{36}Ar$ ratio one can address if the process responsible for retarding ^{40}Ar degassing from the BSV into the atmosphere pre- or post-dates the lifetime of ^{129}I, which we argue, will provide the first temporal constraints for the desiccation of Venus.

References Cited: [1] McGill et al., 1983, in Venus; [2] Tanaka et al., 1997, in Venus II; [3] Sagan & Mullen, 1972, Science; [4] Baslievsky et al., 1985, Geol. Soc. Am. Bull; [5] Hoffman et al., 1980, JGR; [6] Halliday, 2013, GCA; [7] Donahue et al., 1982, Science; [8] Donahue et al., 1997, in Venus II; [19] Kalua, 1999, Icarus; [10] Porcelli & Pepin, 2002, TOG; [11] Mahaffy et al., 2013, Science; [12] Brooker et al., 2003, Nature; [13] Mikhail & Sverjensky, 2014, Nat. Geo; [14] Wilson, 2009, Nat. Geo; [15] Rocchi et al., 2003, JVGR; [16] Violay et al., 2012, JVGR; [17] Cassata et al., 2011, EPSL; [18] Namiki & Solomon, 1998, JVGR; [19] Nimmo, 2002, Geology; [20] Russell, 1993, JGR; [21] Ballentine & Burnard, 2002, RiMG; [22] Holland et al., 2013, Nature; [23] Ozima & Podosek, 1983, Noble Gas Geochemistry; [24] Moreira, 2013, Geochem. Perspectives.

SIMULATIONS OF TIME-OF-DAY VARIABILITY OF SO AND SO_2 ON VENUS.

F. P. Mills, *Fenner School of Environment and Society, Australian National University, Canberra, ACT, Australia (Frank.Mills@anu.edu.au), also Space Science Institute, Boulder, CO, USA*, **M. Allen,** *Jet Propulsion Laboratory and Division of Geological and Planetary Sciences, California Institute of Technology, Pasadena, CA, USA*, **K. L. Jessup,** *Southwest Research Institute, Boulder, CO, USA*, **B. J. Sandor,** *Space Science Institute, Boulder, CO, USA*, **Y. Yung,** *Division of Geological and Planetary Sciences, California Institute of Technology, Pasadena, CA, USA*.

Introduction

Sulfur dioxide (SO_2) plays many important roles in Venus' atmosphere. It is a precursor for the sulfuric acid that condenses to form Venus' global cloud layers and is likely a precursor for the unidentified UV absorber, which, along with CO_2 near the tops of the clouds, appears to be responsible for absorbing about half of the energy deposited in Venus' atmosphere. Photochemically, SO_2 on Venus is analogous in many respects to O_3 in the terrestrial stratosphere (1). Most published simulations of the chemistry in Venus' mesosphere have used one-dimensional numerical models that are intended to represent global-average or diurnal-average conditions (e.g., 2; 3; 4). Observations, however, have found significant variations of SO and SO_2 with latitude and local time throughout the mesosphere (e.g., 5; 6; 7; 8), indicating more nuanced modeling is required. Some recent simulations have examined local time variations of SO and SO_2 using analytical models (5), 1-d steady-state solar-zenith-angle-dependent numerical models (8), and 3-d general circulation models (GCMs) (9). No quantitative comparison has been made yet amongst the results from these different types of models. As an initial step towards this, we compare simulated SO, SO_2, and SO/SO_2 from global-average, analytical, and steady-state solar-zenith-angle (SZA) dependent models.

Methods

The Caltech/JPL photochemical model (10) is used for the numerical simulations. It applies a common core of atmospheric physics to all planets, drawing planet-specific information from custom databases, and converges to a steady-state solution via a finite-difference iterative algorithm. For these simulations, the 1-d continuity equation is solved simultaneously for all species over 58–110 km altitude. Vertical transport via eddy diffusion is set based on observations, as are the lower boundary conditions for HCl, CO, and OCS. Solar fluxes are based on measurements obtained by SORCE SOLSTICE and SORCE SIM on 26 December 2010 (11; 12). These are the closest match to HST observations obtained on 28 December 2010 (8).

For the global average simulation, photodissociation rates were calculated at 45° latitude and local noon then divided by two to average them over the day and night sides.

The results from the global average simulation were used to identify the reactions that account for at least 95% of the production and loss of SO, SO_2, and SO_x (= SO + SO_2) at 70-100 km altitude. Reactions that produce or destroy short-lived species but do not result in net production or loss of SO, SO_2, or SO_x were then excluded to yield simplified algebraic relations for the equilibrium abundances of SO, SO_2, and SO_x.

For the SZA-dependent simulations, the calculations are run to steady-state using the solar flux expected for a specified local time on Venus' equator.

Preliminary results

A common set of input data is being developed to facilitate comparisons amongst the differing types of models. Selected results from previous studies, using varying input data are shown in Fig. 1, which gives the SO_2 vertical profiles from global-average (14) and SZA-dependent (8) models, and in Equations 1 and 2, which give the approximate relations for the SO_2/SO ratio derived from the analytic model (5) for the day and night sides, respectively.

$$\left(\frac{[SO_2]}{[SO]}\right)_{day} \approx \frac{[O]}{J_{73}}(k_{154}[CO_2] + k_{165}\frac{[ClO]}{[O]} + k_{255}\frac{[ClCO_3]}{[O]}) \quad (1)$$

$$\left(\frac{[SO_2]}{[SO]}\right)_{night} \approx \frac{(k_{154}[CO_2] + k_{165}\frac{[ClO]}{[O]} + k_{255}\frac{[ClCO_3]}{[O]})}{k_{160}[CO_2] + k_{162}\frac{[OH]}{[O]}[CO_2] + k_{256}\frac{[ClCO_3]}{[O]}} \quad (2)$$

The SZA-dependent SO_2 profiles illustrate the upward shift with increasing SZA of the altitude at which optical depth unity is reached for the wavelengths where SO_2 strongly absorbs (8). The global-average SO_2 profiles show a much more gradual decrease in SO_2 mixing ratio with altitude due to the inclusion of sulphur species (besides SO and SO_2) that have sufficiently long

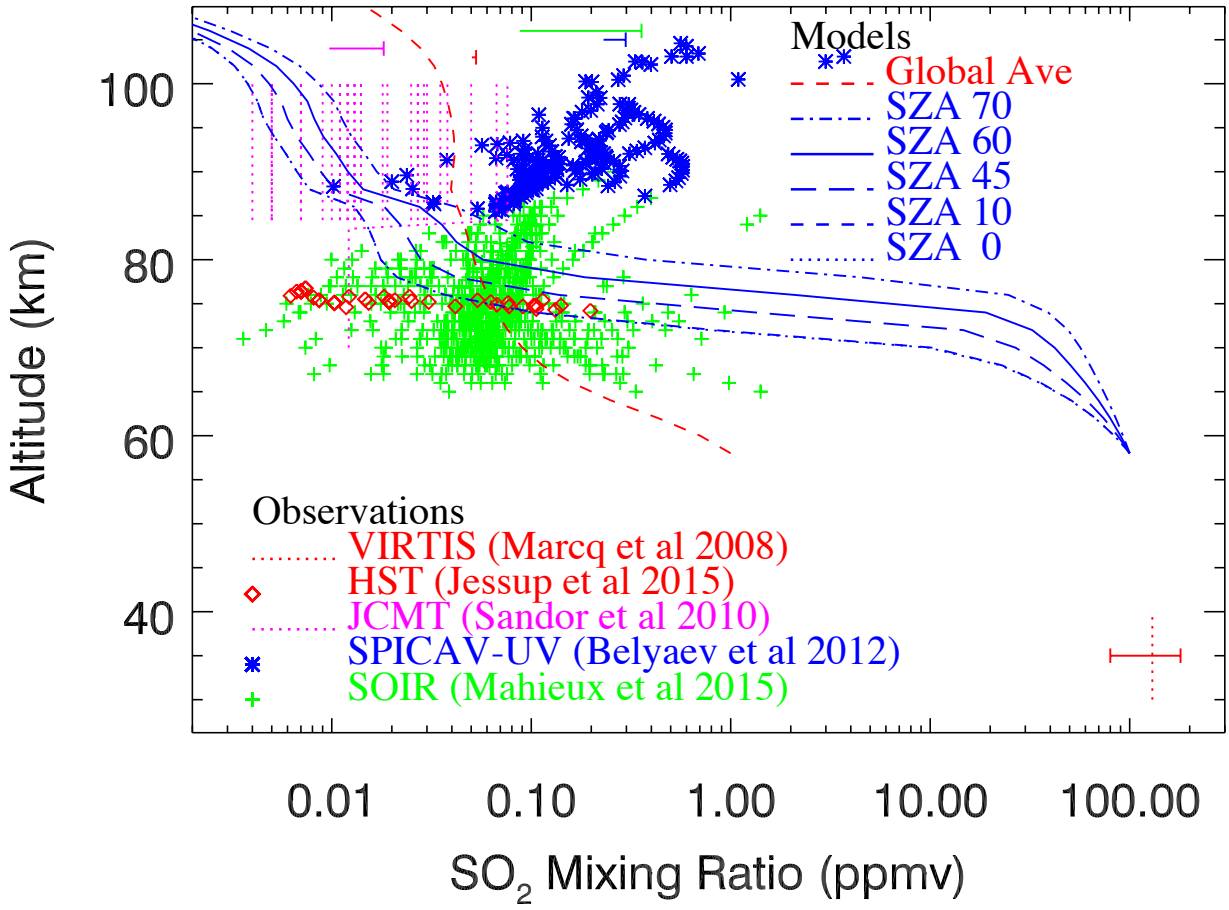

Figure 1: Observed and modeled SO_2 (after 13). Typical uncertainties on the observations are indicated by the half-error bars at the top. The global-average result is the nominal model from (14). The SZA-dependent results are updated versions of the results presented in (8).

lifetimes to be transported vertically via eddy diffusion (15). The large difference in SO_2 values in the upper cloud region (< 70 km) is due to choosing different lower boundary conditions for SO_2 in these simulations. These differences exemplify the need to compare simulations that have used common input data and photochemical schemes to isolate the effects due to the type of modeling considered.

References

[1] DeMore, W. B. and Y. L. Yung (1982). *Science* **217**, 1209–1213.

[2] Zhang, X., et al. (2012). *Icarus* **217**, 714–739.

[3] Krasnopolsky, V. A. (2012). *Icarus* **218**, 230–246.

[4] Parkinson, C. D., et al. (2015). *Planet. Space Sci.* **113–114**, 226–236.

[5] Sandor, B. J., et al. (2010). *Icarus* **208**, 49–60.

[6] Encrenaz, T., et al. (2012). *A&A* **543**, A153.

[7] Marcq, E., et al. (2013). *Nature Geoscience* **6**, 25–28.

[8] Jessup, K.-L., et al. (2015). *Icarus* **258**, 309–336.

[9] Stolzenbach, A., et al. (2014). In *EGU General Assembly 2014*, vol. 16, EGU2014–5315.

[10] Allen, M., et al. (1981). *J. Geophys. Res.* **86**, 3617–3627.

[11] Harder, J. W. et al. (2010). *Sol. Phys.* **263**, 3–24.

[12] Snow, M. et al. (2005). *Sol. Phys.* **230**, 295–324.

[13] Marcq, E., et al. (2016). Composition and chemistry of the neutral atmosphere. In preparation.

[14] Mills, F. P. and M. Allen (2007). *Plan. Sp. Sci.* **55**, 1729–1740.

[15] Vandaele, A. C., et al. (2016). Sulphur dioxide variability in the Venus atmosphere. In preparation.

LOCAL AND GLOBAL SYSTEMS ON VENUS AND EARTH: LESS ACTIVITY ON AIR-PLANET VENUS FOR CHANGE OF VOLATILES.

Y. Miura, Department of Earth Sciences, Yamaguchi University, Yamaguchi, 6753-0074, Japan. yasmiura50 @ gmail.com. **T. Tanosaki,** Kogakuin University, Hachiouji, Tokyo, 192-0015, Japan.

Introduction:

Venus and Mars of the Earth-type planets have been discussed from well-established model of "stable air-water-planet Earth" with the detailed database of Earth relatively. Present model of pre-existed "ocean-water" on two air-planets has been explained simply by disappearance of global ocean water. However, clear material evidences of present air-planets are difficult to be prepared without more global material exploration projects. The main purpose of the present paper is to elucidate new models of a) possible change of global air-planets (Venus and Mars), and b) normal air-planet with less activity (compared with water-planet Earth) based from solidified materials of three vapor, liquid and solid states (designated as VLS in this paper) during cooled processes [1-7].

Air source of carbon dioxides of two air-planets:

Two air-planets of Venus and Mars reveal carbon-dioxides-rich air globally as follows [3-7]:

1) Carbon element is combined with oxygen during high temperature to produce CO-CO_2 molecules or ions.

2) Carbon element is special one remained at extreme conditions among all volatile elements.

3) Global air system of two air-planets suggests that global air with major carbon dioxides are reformed by multiple asteroid-collision process for long periods.

4) Vapor eruption of volcanoes located near at equator might be caused tidal forces of the planetary rotations, which has to be prepared from solid interior.

Air change of carbon dioxides of air-planets:

Global air with carbon dioxides of two air-planets can be changed by artificially and naturally as follows:

1) Carbon dioxides-rich air which is stable on extreme conditions of high temperature and pressure, are difficult to change, but possible change from air state.

2) Cold air of carbon dioxides found on water-less Mars are artificially to be installed in cold water by high pressure condition if there are any fluid liquids.

3) Warm air of carbon dioxides found on global waterless-Venus is impossible to be stored on any fluid-water, if we discuss only volatiles of air and water.

4) However air of any carbon dioxides can be changed if we use other methods of other material states with extreme conditions. The detailed will be discussed in different topics of other paper [3-7].

Relation of activity ranges of material-states:

Active materials are discussed in this paper as vapor (air), liquid (fluid water) and solid (rock), called as VLS, where active air- and water-planet Earth has all three material-states found finally as crystalline molecules and rock-crystalline minerals on the surface globally. On the other hand, volatiles components of air and water are originally separated and remained as ions or plasma states on solid interior rocks of extraterrestrial celestial bodies with less activity from the primordial states except collision processes (as found in Asteroids and the Moon). More active air-planets of Venus and Mars have carbon dioxides-rich air-system after multiple collision processes of long periods, where less active celestial bodies of the Moon (Earth) and meteoroids (Asteroids) have been lost or remained volatile-components on the rocks without formation of global air system. Relation of activity ranges of materials is summarized as follows (as shown in Fig.1) [3-7]:

1) "Global water molecules (and some water ions) of volatiles" have been obtained only air- and water-planet of present "active planet" of Earth, because liquid can be remained only sandwiched by air and solid system as shown in the H_2O phase diagram.

2) "Local water molecular ions of volatiles", however, might be stored in all solid rocks of other planets (Venus and Mars etc.) with "less global activity (without global water-system)", and smaller celestial bodies of the Moon and Asteroids in the Solar System.

Main causes for activity range of materials:

Earth-type planets in the Solar System have all solidified rocks globally, because rocks are originally formed by global activity with wide collisions from all directions and with more stable material states of low temperature and pressure conditions. In order to change primordial solids with mixed volatiles and refractory elements, additional followed reactions by

higher temperature and pressure are required to form molecules and crystals under more slower reaction of the planets, where waterless-planets of Venus and Mars show unstable interior of fluid-poor reactions relatively.

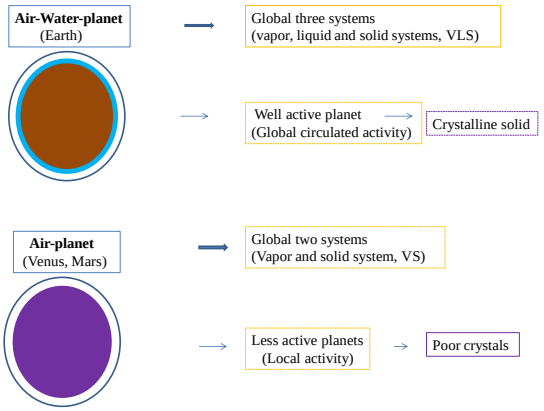

Fig1. Relation of global and local activities on air- and water-planet (Earth) with crystalline solid, and air-planets with poor crystals (Venus and Mars).

Air- and water-planet Earth with global water system after long activity, however, shows formation of "new global materials" of three VLS states under extreme conditions of high temperature and pressure caused by three "shock wave-type events" (including strong impacts, quakes and volcanisms) of local sites throughout the surface globally (cf. Fig.1) [3-7].

On the other hand, other planets and smaller celestial bodies without global water system and stable interior events, have local formation of three VLS material-states mainly local shock wave processes (mainly caused from impact collisions). Relation of main causes for activity ranges of materials is summarized as follows [3-7]:

1) At primordial period of the Solar System, all solid-rocks of celestial bodies formed by wide collisions on all directions have contained volatile elements.

2) Planet Earth has been formed by global water-system (related with giant-like impact of planetary collision), which forms global materials of three VLS states by the three shock-wave-type events.

3) Other planets and smaller celestial bodies (with less crystalline solids and without global water system) shows remained primordial and/or local developed surface with local shock impacted processes.

Solidified evidences of material-state changes:

In general, it's difficult to find direct evidences of air and liquid change from primordial planets and small celestial bodies without primordial volatiles evaporated largely. The present study in this paper, however, has main points to discuss volatiles of air and liquid VL states by remained solidified rocks with separated states of ions and/or plasma states as follows [3-7]:

1) Solidified rock texture reveals quenched processes from three VLS states during three shock-wave - related events from surface to the interiors totally.

2) Solid rock texture of clear phenocrysts and glassy to re-crystallized grandmasses after separated volatiles can be clearly found at air- and water-planet Earth with global air- and water-rocks among global three VLS states systems of air, ocean and rocks finally.

3) Solid rock texture of irregularly shaped phenocryst and glassy grandmass can be found at extra-terrestrial samples of the Moon (Apollo etc.) and meteorites from Mars (with global air system) and Asteroids (without global volatile system), which can be estimated to planet Venus.

4) It's first study on evidence for material processes of air and fluid explained by solidified rock textures of planets (including air-Venus) and small bodies [3-7].

Summary:

Present results can be summarized as follows [3-7]:

1) New model of carbon dioxides-rich air-planet Venus is discussed from air-change by extreme conditions, and remained solidified materials of vapor, liquid and solid (as VLS) states through cooling process.

2) Local water molecular ions of volatile-sources can be stored in solid rocks of air-Venus and Mars, whereas global water systems of air-planets are insufficient only from local and random shock-wave-type events of impact, quake and/or volcano for long history.

3) Fluids and air material states remained on extra-terrestrial solidified rocks can be observed by glassy grandmass of the collected Moon rocks (Apollo etc.) and fallen meteorites from Mars (with global air system) and Asteroids (without global volatile system) with local and limited compositional changes.

References:

[1] Miura Y. (1994): *Astro. Soc. Pacific Conf. Ser., 63*, 259-264. [2] Miura Y. and Fukuyama S. (1999): *J. Materials Proc. Tech.* (Elsevier), 85, 192-193. [3] Miura Y. (2011): *VEXAG*-9, #45, 51. [4] Miura Y. and Tanosaki T. (2015): *Venus Lab. Tech. WS (Virginia, USA)* #4006. [5] Miura Y. (2015) *Earth atmosphere/ionosphere (Nara, Japan)*, P.5. [6] Miura Y. (2015): *JpGU-2015(Chiba, Japan).* # PCG32-11.pp.1. [7] Miura Y. (2015): *SPS-2015 (Sendai, Japan)*, No.20. pp.2.

A CONCEPT MISSION: INSECT-SWARM OF MICROBOTS FOR VENUSIAN SURFACE EXPLORATION.

M. Nikhil, *Technical University of Berlin, Berlin, Germany (nikhil.more@campus.tu-berlin.de; nikki.august29@gmail.com)*, **S. Balaji**, Technical University of Berlin, *Berlin, Germany*.

Introduction:

Even though Venus is extremely different from Earth, it is important to explore this planet to understand the future fate of our own planet – Earth. The more understanding we have, of the planetology of Venus, easier it would turn out to predict if Earth was eventually becoming another Venus and to take actions to avoid such a fate. It has been a long unanswered question as to why the two sister planets took such different paths of evolution despite starting on similar lines while coming into existence.

Motivation:

There have been more missions involving a Fly-by maneuver or an Orbiter and fewer ones that involve a Lander. As we understand it, there are two reasons for this. Firstly, it is technically challenging to be able to land on the Venusian surface. Secondly, studying the atmosphere takes precedence because the atmosphere is considered as the primary reason for the hostile nature of the planet. Our mission proposal involves landing on the surface and studying the surface because the surface characteristics and the atmosphere work in collaboration to make the planet so hostile, even though Atmosphere might seem like a rather more aggressive perpetrator.

Studying the surface might give us better insight of the dynamics it shared with the atmosphere. Also, it might let us predict if it would be possible to have some form of permanent base-of-operation on the surface by locally nullifying the natural hostilities of the planet.

Technology Elements:

The main technology elements required for this mission are a spacecraft that would travel to Venus, a mother space probe with landing capability, and 1000 units of microbots that form an Insect-swarm by the virtue of Insect-swarm algorithms.

Material. The Venusian surface temperature of 900 Fahrenheit is the biggest challenge for survival of any man-made machinery. So, we propose the use of 'Buckytubes' material for the mother space probe as well as the microbots. Buckytubes is an entirely new class of structural materials based on pure carbon nanotubes, a variant of the so-called 'Buckyballs' but without the molecular imperfections. It is the strongest and the stiffest material possible in the universe with strength/weight ratio 600 times that of high strength steel and it will not rust or corrode to 1000 Fahrenheit. Its flexibility allows tolerance to buckling and rebounding from an elongation of about 20-30% without damage. Also, it conducts heat 3 times better than pure diamond. And even though it is being considered to make only 'structures' as of now, there is hardly any component of a spacecraft that could not eventually be made of Buckytubes.

Size Approximation. The prefix "micro" is used to refer to components, modules, and systems with size in the order of a few millimeters to a few centimeters. The term "microbot" hence refers to a robot with a size up to a few millimeters or centimeters.

Mission Scenario:

A spacecraft would be used to carry the mother space probe to Venus. It might not be necessary to have a dedicated spacecraft. The mother space probe could be carried as a piggy-back entity with any other spacecraft involved in a fly-by mission. The mother space probe would land on the surface using its landing capabilities and deploy all the units of the microbots which it carried within itself. The mother space probe also acts as the communication beacon – a link between the microbots and the earth or the relay satellite. The microbots use sensing and probing capabilities to study the surface composition and the mother space probe monitors the survivability of the microbots on Venusian surface.

Mission Details:

The mother probe would land on a 'pancake dome' because should a permanent construction ever be considered on the Venusian surface, the pancake domes would offer a favorable terrain. It would then deploy microbots out onto the Venusian surface.

The mircobots have to be specified for 5 capabilities: Structure, Power, Locomotion, Communication, and Sensors. The basic structure consists of integrated and assembled multi-chip modules. The power

source would be a stack of thin film lithium batteries. 5 to 10 stacked together would give sufficient power output. Communication would be through radio frequency as optical communication, despite being rather suitable for microbots, poses issues in this case due to the necessity of line-of-sight. Also even though RF Communication would be a problem for longer distances, it would suffice to communicate with the neighboring microbots and with the mother space probe. Locomotion would be of the crawling inchworm type. It might turn out to be a good option for surface terrain of a pancake dome on Venus if due to its relative flatness. The sensors would include miniaturized X-ray and mass-spectrometers, imagers, and analyzers for geo-chemical analysis; pressure, temperature, and dust sensors; accelerometers and gyroscopes for locomotion.

The microbots and the mother space probe will not survive against the temperatures unless made out of buckytubes material or provided with cooling mechanisms. Hence, the material is crucial. The inchworm type of crawling motion is still being analyzed for its feasibility. All the deployed microbots will crawl radially outward from the mother space probe and form a network of distributed sensors. This mission can hence analyze an area on Venusian surface at a rather lesser cost, and also serve as a mission for technology demonstration so that this technology can be utilized for exploring more areas as well as farther and larger areas on Venus and other planets too. The high cost of buckytubes material would pay itself off through the reduction in weight and increased endurance capability that it offers.

Bibliography:

[1] Bekey, Ivan. ***Advanced Space System Concepts and Technologies 2010 – 2030.***

[2] Hakan Svedhem & Oliver Witasse. ***Exploring the Venus – Answering the Big Questions with Venus Express.*** Solar System Mission Division, Directorate of Science and Robotic Exploration, ESTEC, Noordwijk, The Netherlands.

[3] P. Corradi, A. Menciassi, P. Dario. ***Space Application of Micro-Robotics: A Preliminary Investigation of Technological Challenges and Scenarios.*** Center for Research in Microengineering, Pisa, Italy.

[4] S. Dubowsky, K. Iagnemma, S. Liberatore, D. M. Lambeth, J. S. Plante, P. J. Boston. ***A Concept Mission: Microbots for Large Scale Planetary Surface and Subsurface Exploration.*** Massachusetts Institute of Technology, Cambridge, USA, and New Mexico Institute of Mining & Technology, Socorro, New Mexico.

VENUS ATMOSPHERE VARIABILITY AS ERROR SOURCE FOR SURFACE EMISSIVITY.

N. Mueller[1], C. Tsang[2], S. Smrekar[1], J. Helbert[3], and **M. D. Dyar[4]**, [1]California Institute of Technology – Jet Propulsion Laboratory, 4800 Oak Grove Drive, Pasadena, CA 91109 USA, nils.muller@jpl.nasa.gov, [2] Department of Space Studies, Southwest Research Institute, Boulder, CO 80302 USA, [3]Institute for Planetary Research, DLR, Rutherfordstrasse 2, 12489 Berlin, Germany, Dept. of Astronomy, Mount Holyoke College, South Hadley, MA 01075 USA.

Introduction: Venus surface thermal emission is observable through spectral windows in the atmosphere. It is possible to derive surface emissivity from nightside near infrared observations by correcting for the effects of the atmosphere, but many atmospheric parameters are not well known. Within limits it is possible to constrain atmospheric parameters when fitting the full near infrared spectrum observed by the VIRTIS-M IR spectrometer on Venus Express with a radiative transfer (RT) model, but uncertainties remain [1].

Here we compare the variability of surface emissivity derived from only two bands at 1.02 µm and 1.31 µm with the instrumental error budget, in order to estimate the magnitude of non-instrumental error sources. We show that emissivity precision at a given elevation is mostly limited by instrumental noise, not by unaccounted atmospheric variability.

Model: We use a radiative transfer model [2] to calculate the top of atmosphere radiance for Venus' nightside in the range of 1 to 1.4µm with parameters including a) cloud particle number density, b) lower atmosphere water vapor, c) topography, d) and surface emissivity.

a) The clouds of Venus are mostly composed of sulfuric acid/water droplets of various size that are scattering with little absorption. We assume that particle number density in the lower cloud layer is sufficient to model the impact on radiance both windows. The clouds have more variable properties such as size distribution, cloud altitude distribution, H_2SO_4 concentration, but their impact is relatively small in this wavelength range [1].

b) Water vapor in the lower atmosphere affects the 1.1 and 1.18 µm windows but has little impact on the 1.02µm window studied here. The water vapor abundance in the lower atmosphere is expected to be constant within the VIRTIS uncertainty of 1.5 % [3], and it is kept constant for this study.

c) Topography determines both surface temperature (using the adiabatic temperature lapse rate) and atmospheric column thickness and thus lower atmosphere extinction. The lower atmosphere is thought to be well-mixed thermally because convective heat transfer is much more efficient than radiative cooling and heating [4].This results in a very small horizontal temperature variation. Near-infrared observations by Galileo have been used to constrain horizontal temperature variation of the atmosphere in contact with the surface to < 2 K [5], but theoretical estimates are with 0.1 K much smaller [4]. The absorption of CO_2 at pressures and temperatures close to the surface is not well known and thus derived emissivity includes an error depending on topography. To study the variance of the atmosphere independent from this error, we limit the data to a narrow interval of surface elevation and keep the model parameter elevation constant.

d) Surface emissivity is the locally constant quantity that we wish to derive using the above simplified assumptions. Any variability in the atmospheric parameters not accounted for will manifest as variability in derived emissivity.

Instrumental precision: The VIRTIS spectra archived in the ESA Planetary Science Archive need to be processed further before they can be compared to RT model spectra. VIRTIS data show a non-linear detector response and some straylight from the bright side of the planet [6]. This is corrected for based on statistical analysis of spectra observing deep space, following [7].

The instrumental noise and uncertainty introduced by the detector response and straylight corrections are estimated from the standard deviation of the corrected radiance of spectra observing deep space (see Table 1).

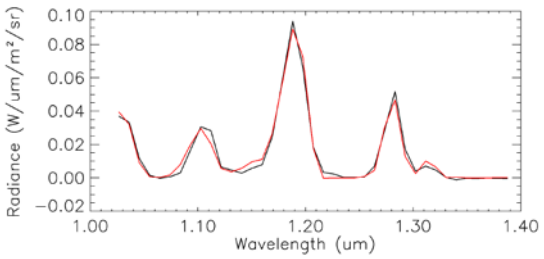

Figure 1. Corrected VIRTIS spectrum (black) fitted with a RT model spectrum (red) by shifting spectral registration and changing bandwidth.

Derived emissivity standard deviation: To have a sample with little horizontal variance, we select all VIRTIS M IR spectra with 3sec exposure from the nightside of the planet with footprints corresponding to a topography between –50m and +50m relative to the mean planetary radius and within -50° to -10° N and 260° and 280°E. Spectra are corrected for non-linear detector response, straylight and limb darkening [8].

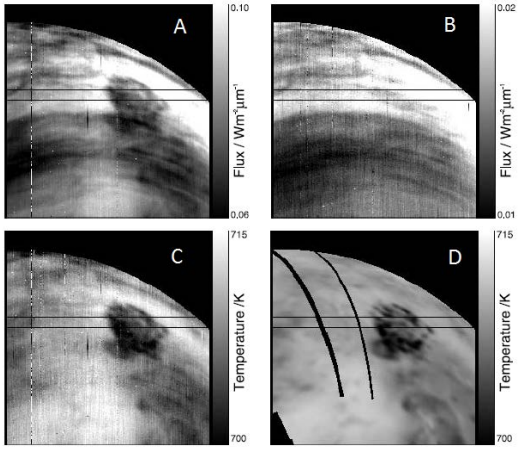

Figure 2. VIRTIS 18 sec exposure image of Alpha Regio, Venus and declouding as in [9]. Shown is (A) near infared flux at 1.02µm and (B) 1.31µm. (C) is derived surface brightness temperature. (D) is predicted brightness temperature based on Magellan altimetry.

The spectral registration of VIRTIS apparently shifted during the Venus orbit insertion maneuver [6]. Thus we fit the spectra with RT model spectra using band width and a spectrally flat offset to the original band center wavelengths as free parameters (see Fig. 1 for an example).

The new spectral registration matching RT model and data allows us the derivation of emissivity following the approach of [8], however using RT model results as lookup tables instead of data statistics. Figure 2 illustrates the process of combining two band to reduce the effect of atmospheric variability.

The standard deviation of the resulting emissivity is σ_e = 0.09. To compare this standard deviation to the instrumental precision, we derive the relevant partial derivatives of RT model radiances at the average conditions. The description and values are given in table 1. Assuming independent and normally distributed errors in the two bands, the estimated error of emissvity is then:

$$\Delta e = \sqrt{\left(\frac{de}{dI_s}\Delta I_s\right)^2 + \left(\frac{de}{dI_s}\frac{dI_s}{dI_c}\Delta I_c\right)^2} = 0.07.$$

Discussion and Conclusions: Assuming independent, normally distributed errors, the residual error, (e.g. due to atmospheric variability) is sqrt(σ_e^2 –Δe^2) = 0.05. An estimate by [1] for the 1σ error due to atmospheric variability, that cannot be accounted for by only 1.31 µm radiance, is 0.07 [1, table 3, <Atm> row], indicating that their assumptions on variability of cloud parameters are conservative. Inconsistent with our observations is a horizontal variability of surface temperature on the order of 1.5 K, which would result in an error of 0.14 [1, table 3, ΔT0 row]. Smaller trends of surface temperature with latitude [see 1] cannot be excluded and will be investigated further.

However there is no indication that our assumption of a horizontally uniform lower atmosphere is grossly incorrect, and the errors introduced by our simplified cloud model are not large and can be effectively reduced by combining several images. Even though the accuracy of the derived emissivity is difficult to verify owing to the lack of in-situ data, the precision of emissivity and thus the ability to distinguish geological units based on emissivity is mostly limited by the instrumental precision of VIRTIS, when comparing areas of the same elevation.

As discussed by [1] the main obstacle in investigating the variation of emissivity on the spatial scale of geologic features is the uncertainty and low resolution of the Magellan altimetry. Therefore high resolution and accurate altimetry such as that of the proposed VERITAS mission [10] would provide the greatest improvement to emissivity estimates.

Most of the spatial information relevant for emissivity is carried by narrow bands in the window centers. The Venus emissivity mapper (VEM) of the VERITAS proposal focusses on these bands at much improved signal to noise ratio compared to VIRTIS [11]. VEM observes wide surface swaths overlapping orbit to orbit, thus providing the repeated coverage required for statistically reducing residual errors resulting from unaccounted atmospheric variability.

References: [1]Kappel D. et al. (2015) PSS 113-114, 49–65. [2] Tsang C. et al. (2008) JQSRT, 109, 1118–1135. [3] Bezard B. et al. (2009) JGR, 114, E00B39. [4] Stone P. (1975) J. Atmos. Sci., 32, 1005-1016. [5] Hashimoto G.L. et al. (2008) JGR, 113, E00B24. [6] Cardesín Moinelo A. et al. (2010) IEEE Trans. Geosci. Remote Sens., 48, 3941. [7] Kappel D. et al. (2012) Adv. in Space Res., 50, 228–255. [8] Mueller N. et al. (2008) JGR, 113, E00B17. [9] Nunes D. et al (2013), AGU Fall meeting, #P41D-1961. [10] Smrekar S. et al. (2016), 47th LPSC, #2439. [11] Helbert J. et al. (2016), 47th LPSC.

Acknowledgement: A portion of this research was conducted at the Jet Propulsion Laboratory, California Institute of Technology, under contract with NASA.

Table 1. Values used in the calculation of predicted variability of derived emissivity.

Description	[Symbol] = unit	Value
Instrumental precision of band 0 at ~1.02 µm observing space	$[\Delta I_s]$ = mW/µm/m²/sr	1.5
Instrumental precision of band 30 at ~1.31 µm observing space	$[\Delta I_c]$ = mW/µm/m²/sr	0.5
Standard deviation of surface observing band 0 at ~1.02 µm	$[\sigma I_s]$ = mW/µm/m²/sr	4.9
Standard deviation of cloud observing band 30 ~1.31 µm	$[\sigma I_c]$ = mW/µm/m²/sr	1.4
Partial derivative of surface observing band wrt to emissivity	$[dI_s/de]$=mW/µm/m²/sr	35
Partial derivative of surface observing band wrt cloud observing band	$[dI_s/dI_c]$	3.7

Detecting Active Lava Flows from Venus Orbit

N. Mueller[1], J. Helbert[2], S. Smrekar[1]. NASA Jet Propulsion Laboratory/Caltech, Pasadena, CA, 91109, USA (nils.muller@jpl.nasa.gov)), [1]California Institute of Technology – Jet Propulsion Laboratory, 4800 Oak Grove Drive, Pasadena, CA 91109 USA, nils.muller@jpl.nasa.gov, [2]Institute for Planetary Research, DLR, Rutherfordstrasse 2, 12489 Berlin, Germany.

Abstract:

We present a model of the signatures of active lava flows observable through spectral windows from orbit and data processing methods for isolating these signatures in near-infrared images. We estimate the thermal emission of lava flows based on models for the analysis of remote observation of eruptions on Earth and Io, however adjusted to the different thermal environment of the Venus surface. We also approximate scattering in the 70 km thick atmosphere below the clouds tops [1]. The results indicate that only large and intense eruptions could have been reliably detected with VIRTIS data from the Venus Express mission.

Background:

The surface of Venus is geologically young compared to other terrestrial planetary bodies except Earth and Io. Most of the young surface has an origin in effusive volcanism. A wide range of global rates of volcanism are discussed for Venus. This is due to the fact that the cratering record of the surface - shielded from impacts by the atmosphere- does not constrain whether the volcanism occurs constantly or episodically through time. A significant constraint on the current volcanic activity would contribute much to this discussion [1].

The Venus Express (VEX) mission included the imaging instruments Venus Monitoring Camera (VMC) and Visible and Infrared Imaging Spectrometer (VIRTIS), which had the capability to observe volcanic activity. No clear signatures of active volcanism have been reported for VIRTIS M IR data, however transient bright spots in VMC images have been interpreted as most likely to be caused by eruptions [2].

Signatures of active lava flows:

Thermal emission of active flows: Lava flow thermal emission is modelled as a function of time assuming an effusion rate and flow thickness, which constrains areal growth and age of the flow surface. The flow surface cools rapidly, which greatly diminishes the contribution to thermal emission (Fig 1). Lava flows consist of cooling crust and a fraction of exposed liquid core [3]. Cooling occurs mostly by radiation and convection. On Venus surface winds are low and free convection and radiative cooling are coupled due to the IR opaque CO2 atmosphere [4], which reduces efficiency of both. Finally the model imposes a limit on the areal growth and thus thermal emission if the total heat loss from an lava flow reaches a certain fraction of the heat supplied at the vent, as it is assumed in studies of Earth and Io remote sensing data of eruptions [e.g. 5,6].

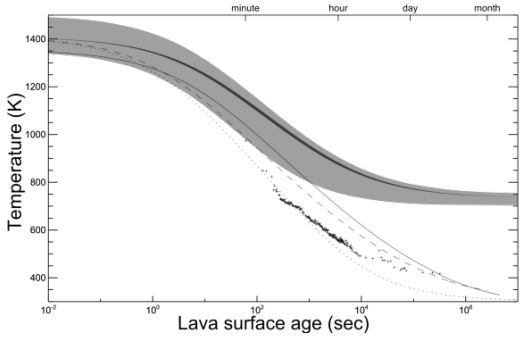

Figure 1 Lava surface temperature as function of time since eruption for Earth and Venus under various assumptions.

Atmospheric scattering: The areal extent of active flows is assumed to be small compared to the area over which its emission is scattered by the atmosphere. Thus we model them as a point source adding to the background radiance. The radiance distribution of a point source observed at the top of the atmosphere is approximately a Gaussian with a full width half maximum of 100 km [1].

Data processing:

Straylight correction: VEX VIRTIS data was acquired from above the south pole, with the bright dayside close to the field of view, resulting in some straylight offsetting the thermal emission observed in the nightside. VIRTIS data are corrected by subtracting an average straylight spectrum derived from deep space observations fitted to wavelengths with negligible emission [e.g. 7]. VMC does not use a straylight correction since the near infrared observations are only done when VEX is eclipse.

Cloud correction: The cloud opacity is variable, and the signature of an eruption needs to be distinguished from this variability in order to be unambiguously detectable. In order to reduce this variability it is possible to correct for cloud opacity if simultaneous observations at a wavelength where the emission originates below the clouds but above the surface are available [8], e.g. the 1.31 micron band of VIRTIS. VMC does not have a band for cloud correction. Their identification of anomalies relies on their fixed location at the surface, while the cloud features move together the superrotating atmosphere.

Background subtraction: The background thermal emission can be estimated based on altimetry [9], in order to distinguish eruptions from expected surface temperature variation. If longterm observations of the surface are available, it is additionally possible to account for surface emissivity. By sub-

tracting the average radiance over time, the transient excess thermal emission introduced by active lava flows is separated from the background. The VMC data cannot be processed with this approach since the variable atmospheric transmittance cannot be accounted for. The VMC background correction instead assumes that the contrast, i.e. the ratio of radiance between topographic high and low region remains constant. By dividing observed and modeled images, scaled to unity at a reference location, they provide an estimate of excess thermal emission relative to background emission.

Spatial filtering: Since the size of an eruption signature is well known to be approximately 100 km due to atmospheric scattering, it is possible to spatially filter the data. The most straightforward is a filter with high pass properties, such as subtraction of a moving average with a diameter larger than 100 km. This reduces residual atmospheric and instrumental errors.

Results and Discussion:

Using the above data processing on VIRTIS-M IR data we estimate that it would be very likely to detect active eruptions with 1 km^3 lava effused within 10 days or a sustained effusion rate of >800 m^3/sec. This corresponds to a 1GWum^{-1}sr^{-1} signature with a maximum that is ~1.2 times background emission. Under less conservative assumptions the same brightness could be achieved with 0.01 km^3 lava and effusion rates >30 m^3/sec. [10] presents historical eruption data from 1840 to 1980 for three volcanos that can be compared to these detection criterions (Fig. 2). Under optimistic assumptions some of the more intense eruptions would have been detected, if they happened in the field of view of VIRTIS.

The transient bright spots at fixed locations at Ganikki Chasma in VMC data reported by [2] have a size and intensity consistent with the above discussed ranges of effusion volumes and rates detectable by VIRTIS. On Earth these are rare events on historical timescales. Several eruptions like this per year suggest a high rate of volcanic activity.

A constraint on the global rate of volcanism, however, depends not only on the number of observed eruptions and detection capability, but also on how extensively the surface was monitored, the style of volcanism, i.e. distributions of effusion rates and volumes, and on how eruptions on Venus are distributed over space and time.

The VIRTIS data set covers much of the southern hemisphere several times with the above discussed detection capability, which is mostly limited by instrumental noise. VMC data is limited to eclipse seasons and show atmospheric noise at the level of observed anomalies. Together the two datasets from Venus Express have limited coverage and detection capability and probably do not place a strong constraint on the rate of volcanic activity.

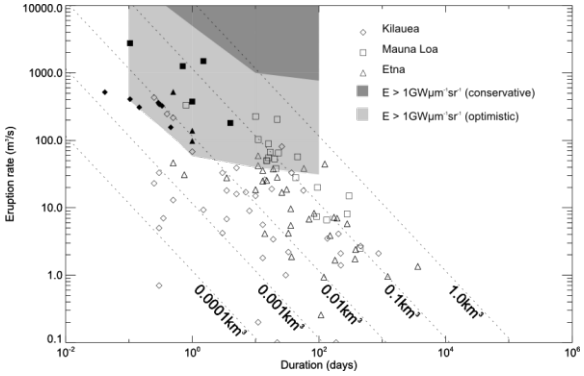

Figure 2 Historical eruption data compared to the capability of VIRTIS to detect eruptions for different assumptions.

The spacecraft Akatsuki of the Japan Aerospace Exploration Agency was recently inserted into Venus orbit, albeit at a larger apocenter distance than originally planned [11]. The infrared cameras on board are designed with the aim of detecting volcanic activity.

The proposed VERITAS mission [12] includes the Venus Emissivity Mapper (VEM) [13] designed to be capable to detecting much smaller eruptions than VIRTIS owing to higher signal to noise ratio. The imaging would begin in the initial VEX like orbit, where the greater distance results in wider coverage. The later low circular orbits will produce only 100 km wide image swaths. These swaths overlap from orbit to orbit, so that even short lived eruptions or the often most intense initial phases of eruptions [10] could be observed several times, should they coincide with the observation. This would greatly increase the reliability of any detection.

References:[1] Hashimoto and Imamura (2001). *Icarus*, 154: 239–243. [2] Shalygin et al. (2015) GRL, 42, 4762–4769. [3] Crisp and Baloga (1990): *JGR*, 95:1255–1270. [4] Snyder (2002) *JGR*, 107:5080– 5088. [5] Davies. (2003) *JGR*, 108:5106. [6] Harris,et al. (1997) *JGR*, 102:7985–8004. [7] Kappel et al. (2012) Adv. in Space Res., 50, 228–255. [8] Hashimoto and Sugita (2003). *JGR*, 108:13–18. [9] Lecacheux et al. (1993) *PSS*, 41: 543–549. [10] Wadge (1981). *Journal of Volcanology and Geothermal Research*, 11:139–168. [11] Nakamura et al. (2011) *Earth Planets Space*, **63**, 443–457. [12] Smrekar S. et al. (2016), 47th LPSC, #2439. [13] Helbert J. et al. (2016), 47th LPSC.

Acknowledgement: A portion of this research was conducted at the Jet Propulsion Laboratory, California Institute of Technology, under contract with NASA.

THE VERTICAL STRUCTURE OF VENUS' POLAR UPPER ATMOSPHERE FROM IN-SITU DENSITY MEASUREMENTS WITH VENUS EXPRESS.

I. C. F. Müller-Wodarg, *Blackett Laboratory, Imperial College, London SW7 2AZ, U.K. (ingo@imperial.ac.uk)*, **S. Bruinsma, J.-C. Marty,** *CNES/GRGS, 18 Avenue E. Belin, F-31401 Toulouse Cedex 9, France*, **P. Rosenblatt,** *Royal Observatory of Belgium, Brussels, Belgium*, **H. Svedhem,** *ESA/ESTEC, Postbus 299, 2200 AG Noordwijk, The Netherlands*.

The Venus Express Atmospheric Drag Experiment (VExADE) was approved by ESA after the launch of the spacecraft in 2005 as a means for measuring atmospheric densities above 130 km *in-situ* using 3 alternative techniques, namely (1) Precise Orbit Determination (POD), (2) Accelerometer measurements (ACC) and (3) Torque measurements (TRQ). While POD and TRQ measurements were made from 2008–2013 at altitudes 166–186 km and latitudes 80–90°N, the ACC measurements were carried out in the final phase of Venus Express during the aerobraking period from 24 June to 11 July 2014 for altitudes of 130–134 km at 75°N latitude. POD observations provided single density measurements per flyby at periapsis, while both ACC and TRQ data gave vertical density profiles for each flyby.

We find the densities to be up to a factor of 2 smaller with respect to those of the VTS3 model (Hedin et al., 1983), illustrating that the polar upper atmosphere is more collapsed than previously thought. We find considerable variability in the densities ranging from tens of percent to an order of magnitude. This variability can be separated into day-to-day changes and, for the case of ACC measurements, of small scale wave-like perturbations with horizontal wavelengths of 100–300 km. The amplitudes of these density waves are modulated at quasi 5–day periodicity, providing evidence for wave-wave coupling between gravity waves and Rossby planetary waves above the cloud top layer. Average scale heights over the range of ACC observations (130–140 km) are 2.9±0.6 km, indicating temperatures of around 114±23 K, considerably lower than those of VTS3 for the same locations and conditions (141–159 K). Temperatures, like the amplitudes of the density waves, are modulated with a quasi 5-day period.

We present a summary of the ACC and POD dataset and carry out comparisons with other Venus Express observations obtained via remote sensing. Overall the VExADE dataset shows good consistency with these remote measurements at comparable locations, providing cross-validation between them.

The VExADE dataset, despite its modest coverage, has thus provided us with an interesting set of new findings, and thereby a new understanding about the polar upper atmosphere of Venus and its variability. The mission control and navigation experience gained during aerobraking will help plan future aerobraking campaigns with other spacecraft including ExoMars.

MORPHOLOGY AND TEMPORAL VARIATION OF THE POLAR OVAL OF VENUS REVEALED BY VENUS EXPRESS/VMC VISIBLE IMAGES

K. Muto, *The University of Tokyo, Japan (k.muto@ac.jaxa.jp)*, **T. Imamura**, *Institute of Space and Astronautical Science, Japan Aerospace Exploration Agency, Japan.*

Introduction:

Venus is covered by highly-reflective thick clouds composed mostly of sulfuric acid. Because of the near-uniform distribution of the upper cloud and the absence of notable absorption, the Venus disk is almost featureless in the visible wavelength range. The polar oval is an exception; a dark oval encircles the pole in visible range as well as in ultraviolet. Characterization of the polar oval would give clues to the complicated dynamics in the polar region of Venus, because the variation of the oval shape should reflect the life cycle of the dynamical instability and the concentration of the dark material in a narrow-banded region should be a result of unrevealed transport processes. The whole shape of the oval has been unknown because the oval is visible only on the dayside and the oval extends to the nightside. In this study we reconstruct the whole shape of the oval from Venus images taken continuously by the Venus Monitoring Camera (VMC) onboard ESA's Venus Express.

Reconstruction of the oval shape:

The VMC visible (513 nm) and ultraviolet (365 nm) images downloaded from ESA's Planetary Science Archive were projected onto the longitude-latitude coordinate of Venus with a resolution of 0.125° x 0.125° using the image processing software developed for JAXA's Venus orbiter Akatsuki (Ogohara et al., 2012). To suppress large-scale brightness variations due to viewing geometry, the brightness in each longitude-latitude pixel was divided by the cosine of the incidence angle.

Before studying polar features, noises in the images were suppressed by averaging 2-4 images taken in each orbit considering the zonal advection between the images by the westward superrotation. Figure 1 shows visible channel images four successive orbits after incidence-angle correction and averaging in each orbit. The images have been shifted in longitude considering the zonal advection of 360deg/3.5days. Figure 2 shows examples of mosaic visible and ultraviolet images constructed from images obtained in four successive orbits like the ones shown in Fig. 1 on the assumption that the shape change of the polar feature during four days is not significant. We can see dipole-like or elliptical features centered at the South Pole.

The polar oval in visible wavelength is composed of a bright core and a dark border. In ultraviolet, on the other hand, only a bright core is evident and the dark border tends to diffuse into the surrounding spiral structure. The fact that the polar oval is visible both in visible and ultraviolet wavelength suggests that the absorbing material responsible for the oval has a notable absorption from visible to ultraviolet wavelengths in contrast to the "unknown absorber" which shows absorption only in ultraviolet and violet wavelengths.

The shape of the polar oval is changing over time. Figs. 2a and 2b show near elliptical shape, while Fig. 2c shows elongated dipole-like shape. The oval extends from the Pole to ~60°S in most of the cases. Sometimes the oval becomes very faint or mostly disappears.

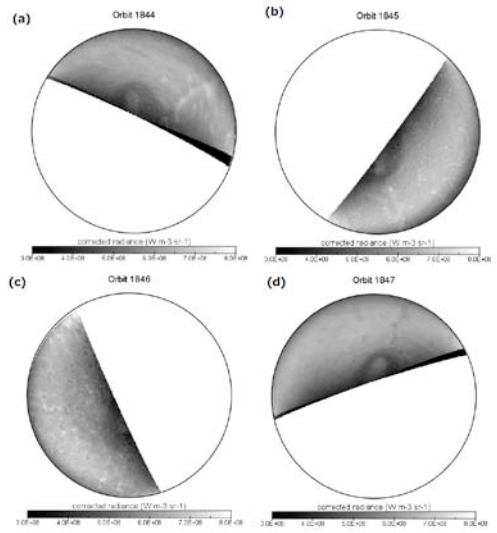

Figure 1. Images of the polar feature taken along the four successive orbits (a) 1844, (b) 1845, (c) 1846 and (d) 1847. In (b)-(d) the image were shifted eastward with respect to (a) by the angles of zonal advection in their respective elapsed times based on the superrotation period of 3.5 days.

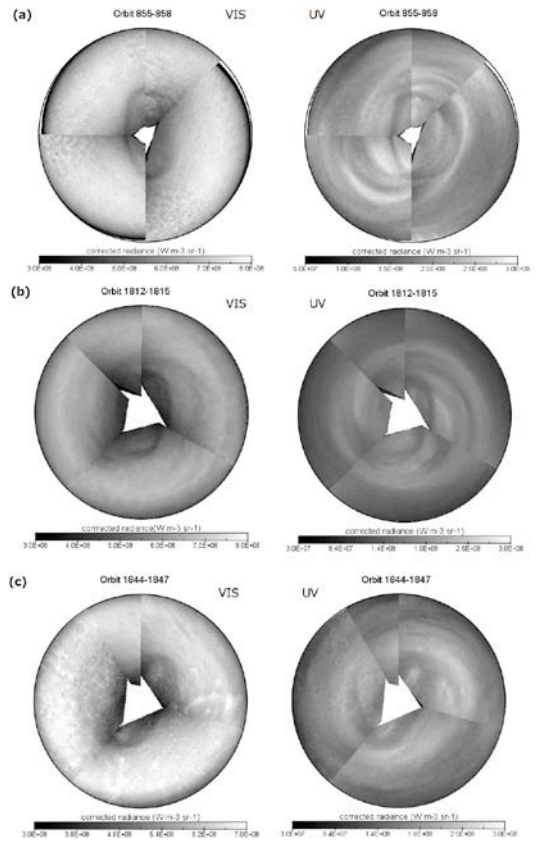

Figure 2. Mosaic images for (left) visible and (right) ultraviolet channels constructed from images taken in the four successive orbits (a) 855-858, (b) 1812-1815 and (c) 1844-1847. In each pannel the first orbit appears on the upper right, and last orbit appears on the upper left.

Temporal variation of the oval shape

To study the temporal variation of the shape of the oval, the maximum (r_{max}) and minimum (r_{min}) latitudinal distances between the inner edge of the oval and the South Pole in each image are chosen as the parameters characterizing the oval shape (Fig. 3). The ratio r_{min}/r_{max} serves as an indicator of the degree of elongating deformation. The r_{max} and r_{min} are determined by visual perception; the error in the estimation is around 1° in latitude. Since the whole shape of the oval is not visible in each single image, the r_{max} and r_{min} do not necessarily coincide with the maximum and minimum distances, respectively, from the Pole along the whole oval. However, thanks to the zonal advection with a period of ~3.5 days, the true maximum and minimum distances would be reasonably estimated by choosing the maximum r_{max} value and the minimum r_{min}, value, respectively, in the moving window with a length of four days. The original r_{max} and r_{min} are replaced with such maximum and minimum values, respectively.

Fig. 4 shows the time variation of the Lomb-Scargle periodogram (Lomb, 1976; Scargle, 1982) of r_{min}/r_{max}. The 99% significance level is shown by black lines; statistically-significant peaks are seen before Day 900 and after Day 1500. The dominant component has a period of 200-350 days before Day 800, and splits into short- and long-period components, which disappear by Day 1000. A shorter-period component with a period of ~100 days emerges around Day 1500 and continues to exist till the end of the analysis period. After Day 1500 a broader peak with periods of 150-300 days also appears. Such widely-scattered, variable periods do not seem to be explained by a Venus year (255 days), the rotation period (243 days) and a Venus day (117 days).

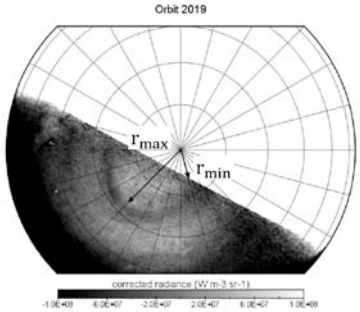

Figure 3. Oval shape parameters shown in an image taken in orbit 2019. In this example, they are detrmined as r_{max} = 26° and r_{miin} = 10°. The grid interval is 15° both in latitude and longitude.

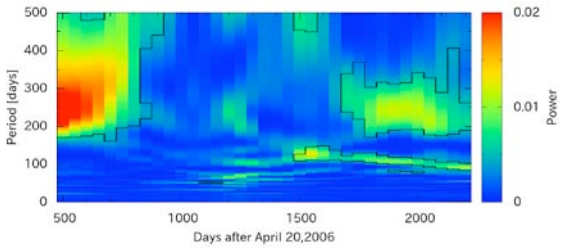

Figure 4. Time series of the Lomb-Scargle periodogram of r_{min}/r_{max}. The data length for each periodogram is 500 days. The 99% significance level is shown by black lines.

Acknowledgements:

VMC images downloaded from ESA's Planetary Science Archive were used in the analysis. We greatly appreciate the open data policy of the Venus Express project.

Akatsuki returns to Venus.

M. Nakamura, N. Ishii, T. Imamura, C. Hirose, *Institute of Space and Astronautical Science, Sagamihara, Japan (nakamura.masato@jaxa.jp, ishii.nobuaki@jaxa.jp, imamura.takeshi@jaxa.jp, hirose.chikako@jaxa.jp)*

Abstract:

ISAS successfully launched Akatsuki at 06:58:22JST on May 21st 2010, by H-IIA F17. After a half year successful cruise from the earth to Venus, the malfunction happened on the propulsion system during the Venus orbit insertion (VOI) on December 7th, 2010. The engine shut down at 158 sec during the VOI, while we planned 12 min operation. The spacecraft did not enter the Venus orbit but entered an orbit around the Sun with a period of 203 days. The orbital maneuvering engine (OME) was found to be broken and unusable, but most of the fuel still remained. ISAS's engineers decide to use the reaction control system (RSC) for orbital maneuver and three minor maneuvers in November 2011 were successfully done so that Akatsuki would meet Venus in 2015.

The Akatsuki spacecraft was rotating about the sun with a period of 199 days and was on the trajectory to meet Venus on 22nd of November, 2015 after the orbital maneuvers in November 2011. The date, November 22nd, 2015, was chosen as the shortest encounter timing with consideration of spacecraft's lifetime. Trajectory analysis done later revealed that the orbit around Venus after insertion on 22nd of November, 2015 is unstable. We decided to perform another orbital maneuver in July 2015 to let the spacecraft to meet Venus on 7th of December, 2015 with this date the orbit around Venus would be more stable.

On 7th of December, 2015, the spacecraft approached from outside of Venus orbit and captured by Venus. Fig. 1 shows the trajectory of Akatsuki with the orbit of Venus and the earth. The velocity of spacecraft about the sun was less than that of Venus after December 1, 2015, where the spacecraft's orbit was outside of Venus orbit, and Venus caught up the spacecraft from the back.

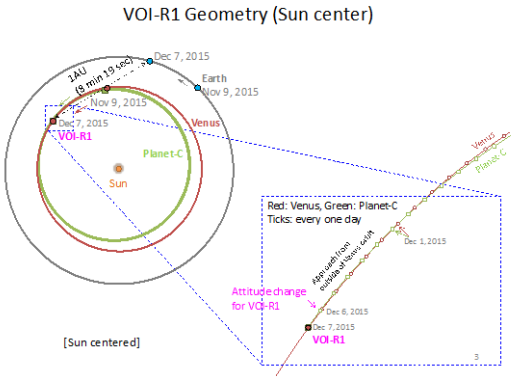

Figure 1

For the Venus orbit insertion in 2015, termed VOI-R1, four 23 Newton-class thrusters were used as opposed to 500 Newton-class OME used at the 1st VOI in 2010. VOI-R1 burn (1228 seconds) was successfully achieved from 23:51:29 on 6th of December through 00:11:57 on 7th of December (UTC, onboard time).

Akatsuki became the first satellite of a planet in Japan. After VOI-R1, the apoapsis altitude is 0.44 million km with the inclination of 3 degrees. The orbital period is 13 days and 14 hours. Fig. 2 shows the VOI-R1 geometry depicted with the Venus center coordinate. For two purposes, to decrease the apoapsis altitude and to avoid long eclipse during the orbiter, we performed a trim maneuver at the first periapsis. The apoapsis altitude is now 0.36 million km with periapsis altitude of 1,000 km - 8,000 km (varying) and the period is 10 days and 12 hours.

Akatsuki will send data over two years to us, and it means that our exploration enters the new era when Japan deliver the continuously changing planet's data to the whole world.

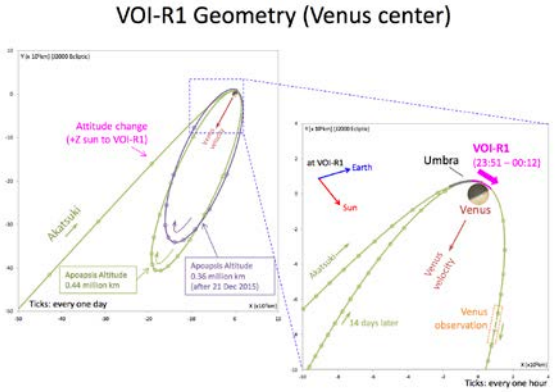

Figure 2

Cosmic ray ionization in the Venusian atmosphere

T. A. Nordheim, Jet Propulsion Laboratory, California Institute of Technology, Pasadena, USA (tom.nordheim@jpl.nasa.gov), **L. R. Dartnell**, University of Leicester, Space Research Centre, Leicester, U, **K. L. Aplin**, Department of Physics, University of Oxford, Oxford, UK, **M. Michael, S. N. Tripathi**, Department of Civil Engineering, Indian Institute of Technology, Kanpur, India. **A. J. Coates, G. H. Jones**, Mullard Space Science Laboratory, University College London, Dorking, UK & Centre for Planetary Sciences at UCL/Birkbeck, London, UK

Introduction:

The atmospheres of the terrestrial planets are constantly exposed to solar and galactic cosmic rays, the most energetic of which are capable of affecting deep atmospheric layers through nuclear and electromagnetic particle cascades. The energy deposited by these interactions is thought to be an important driver for atmospheric chemistry and may affect cloud microphysics [1][2], and in regions beneath the penetration of ultraviolet radiation, cosmic rays are the primary ionization agent. It is therefore crucial to quantify the amount of energy deposited by cosmic rays in the atmosphere by altitude.

Detailed studies have considered the propagation of cosmic rays in the atmospheres of Earth, Mars, Titan and the Giant Planets. However, previously only a few studies [1][2] have considered such interactions in the Venusian atmosphere, notably using numerical approximations to describe cosmic ray interactions. We have performed modelling of cosmic ray interactions in the Venusian atmosphere using a full 3D Monte Carlo model which explicitly simulates individual particle interactions [3]. Using these results, we have computed new cosmic ray ionization and electrical conductivity profiles for the Venusian middle and lower atmosphere. We have also investigated the effect of severe solar energetic particle events, which may produce very large enhancements in the atmospheric ionization rate at certain altitudes. Our results will be discussed within the context of atmospheric chemistry and electrical phenomena in the Venusian atmosphere.

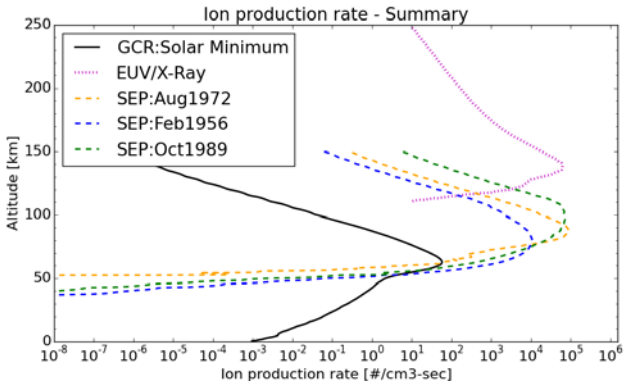

Figure 1 - Summary of cosmic ray ionization rates for galactic cosmic rays (GCR) at solar minimum and for three prototypical solar energetic particle (SEP) events. EUV/X-Ray ionization rates from Peter et al. [2014][6] are shown for comparison.

References:

[1] Aplin et al., Atmospheric electrification in the Solar System, Surv. Geophys., 27, 63-108, 2006.
[2] Michael et al., Highly charged cloud particles in the atmosphere of Venus, J. Geophys. Res., 114, E04008, 2009
[3] Dubach et al., The lower ionosphere of Venus, Planet. Space Sci., 22, 535-536, 1974.
[4] Borоucki et al., Predicted Electrical conductivity between 0 and 80 km in the Venusian atmosphere, Icarus, 51, 302-321, 1982.
[5] Nordheim et al., Ionization of the Venusian atmosphere from solar and galactic cosmic rays, Icarus, 245, 80-86, 2015.
[6] Peter et al., The dayside ionospheres of Mars and Venus: Comparing a one-dimensional photochemical model with MaRS (Mars Express) and VeRa (Venus Express) observations, Icarus, 233, 66-82, 2014.

SULFURIC ACID VAPOR IN THE ATMOSPHERE OF VENUS AS OBSERVED BY THE VENUS EXPRESS RADIO SCIENCE EXPERIMENT VERA.

J. Oschlisniok , *Rheinisches Institut für Umweltforschung, Abteilung Planetenforschung, Universität zu Köln, Köln (joschlis@uni-koeln.de)*, **M. Pätzold**, *Rheinisches Institut für Umweltforschung, Abteilung Planetenforschung, Universität zu Köln, Köln,* **B. Häusler**, *Institut für Raumfahrttechnik, Universität der Bundeswehr München, Neubiberg,* **S. Tellmann**, *Rheinisches Institut für Umweltforschung, Abteilung Planetenforschung, Universität zu Köln, Köln, M*. **K. Bird**, *Argelander – Institut für Astronomie, Bonn,* **T. Andert**, *Institut für Raumfahrttechnik, Universität der Bundeswehr München, Neubiberg.*

Introduction:

The cloud deck within Venus' atmosphere, which covers the entire planet between approx. 50 and 70 km altitude, consists mostly of liquid and gaseous sulfuric acid. The gaseous part increases strongly just below the main clouds and builds an approx. 15 km thick haze layer of H_2SO_4. This region is responsible for a strong absorption of radio waves as seen in VeRa radio science observations. The amount of the absorption, which is used to derive the abundance of gaseous sulfuric acid, depends on the signal frequency. VeRa probed the atmosphere of Venus between 2006 and 2015 with radio signals at 13 cm (S-band) and 3.6 cm (X-band) wavelengths. We present H_2SO_4 profiles derived from S-band and X-band absorption during the first occultation season in 2006. The comparison of the H_2SO_4 profiles derived from both frequency bands provides a reliable picture of the H_2SO_4 abundance. Distinct differences in the S- and X-band profiles may give a clue to increased SO_2 abundances. The derived VeRa results shall be compared with results provided by other experiments onboard Venus Express as well as with previous missions.

Comparison between VeRa and VIRA profiles from the Venus atmosphere and ionosphere

M. Pätzold, **S. Tellmann, M.K. Bird, K. Peter,** *RIU-Planetenforschung an der Universität zu Köln, Cologne, Germany*, **B. Häusler**, *Institut für Raumfahrttechnik und Weltraumnutzung, Universität der Bundeswehr München, Neububerg, Germany*

The Venus Express Radio Science experiment VeRa sounded the neutral atmosphere and ionosphere with the spacecraft's radio signals from 2006 until early 2014 in 15 occultation seasons. About 800 vertical profiles of temperature, pressure, neutral number density in the altitude range 40 km to 100 km and electron density from the base of the ionosphere at 100 km to the ionopause (located between 300 km and 600 km depending on the state of the solar wind) were obtained. The profiles have an altitude resolution of about 500 m and cover all feasible solar zenith angles and local times (Häusler et al., 2006; Pätzold et al., 2007).

The profiles from the neutral atmosphere which are neutral number density, temperature, pressure as a function of altitude, are compared with the Venus International Reference Atmosphere (VIRA) model which was compiled from the observations of the Venera missions and the Pioneer Venus orbiter mission in the 1970s and 1980s (Seiff et al., 1985; Bauer et al., 1985). VIRA is an empirical constructed model of the structure and composition of the neutral and ionized atmosphere from the surface to 1,000 km altitude. The general agreement between the VeRa and VIRA temperature profiles is quite good, in particular in the low and middle latitude range. The differences increase in the higher latitudes above 75° and 85°. These differences might be caused by differences within the data sets, e.g. differences in the local time coverage or the latitudinal coverage. The cold collar and the rotating hot polar dipoles lead to significant temporal temperature variations in the high latitudes. Atmospheric waves like gravity waves and thermal tides might also contribute to the observed differences in the mesosphere.

The VeRa electron density profiles are compared with the VIRA ionospheric database (Bauer et al., 1985), which consists primarily of *in situ* and radio sounding electron density data from the Pioneer Venus Orbiter mission. VIRA is found to be insufficient with regard to altitude coverage and resolution, structure representation, and solar cycle phase. A new Venus reference ionosphere model is needed which describes the altitude structure of the ionosphere from the base to the ionopause at high resolution, for all solar zenith angles and for solar minimum and maximum conditions.

References

Bauer, S.J., L.M. Brace, H.A. Taylor, Jr., T.K. Breus, A.J. Kliore, W.C. Knudsen, A.F. Nagy, C.T. Russell, and N.A. Savich (1985), The Venus Ionosphere, Adv. Space Res., 5(11), 233 –267.

Häusler, B., M. Pätzold, G. L. Tyler, R.A. Simpson, M.K. Bird, V. Dehant, J.-P. Barriot, W. Eidel, R. Mattei, S. Remus, J. Selle, S. Tellmann and T. Imamura, 2006. Radio science investigations by VeRa onboard the Venus Express spacecraft, Planet. Space Sci., 54**,** 1315 – 1335.

Pätzold, M., B. Häusler, M.K. Bird, S. Tellmann,R. Mattei, S.W. Asmar. V.Dehant, V., Eidel, W., Imamura, T, R.A. Simpson, G.L. Tyler, 2007. The structure of Venus' middle atmosphere and ionosphere, Nature, 450, 657-660.

Seiff, A., J. T. Schofield, A. J. Kliore, F. W. Taylor, and S. S. Limaye 1033 (1985), Models of the structure of the atmosphere of Venus from the surface to 100 kilometers altitude, Adv. Space Res., 5(11), 3 –58.

Understanding the role of rotation and temperature distribution on Venus' general circulation

M. Parisi, J. Yuval, E. Galanti, Y. Kaspi

Weizmann Institute of Science, Israel

One of the most striking features in the atmospheric circulation of Venus is the tropospheric superrotation, with wind speeds of over 100 m/s. Despite the increasing efforts in observations, both Earth-based and *in situ*, this feature in particular and the general circulation of this planet in general is not yet well understood. We have set up a 3D general circulation model (GCM) for Venus' dynamics in order to better understand fundamental mechanisms that drive atmospheric phenomena. Despite their similarities in mass and size, there are some crucial differences between Earth and Venus that make the latter extremely inhospitable, with a surface temperature of over 700 K and an atmosphere composed of 96% carbon dioxide and 92 times heavier. A unique aspect of this planet is its slow rotation rate, 2 orders of magnitude smaller than Earth's. As a result, it is expected that the Coriolis force does not play a major role in Venus' atmospheric dynamics, differently from our planet. To leading order, the circulation satisfies the cyclostrophic balance, in which the pressure gradient is compensated by the centrifugal acceleration. Our model uses a Newtonian cooling scheme to represent radiation with a longitudinally symmetric relaxation temperature derived from Pioneer Venus data. The model general circulation is shown to be in good agreement with the observations. To better understand the governing physics, we investigate the effect of varying some of its model physical parameters on Venus' circulation. By changing the rotation rate, making Venus spin faster or slower, we study whether this parameter is important in the main balance of the flow. Surprisingly, preliminary results suggest that the Coriolis acceleration may indeed play a major role in the insurgence of the superrotation in the troposphere, where the jets are up to 60 times faster than the surface rotation. In addition, we study an iterative method in order to find the diabatic heating which reproduces the measured temperature profile on Venus. Reproducing the mean temperature profile enables investigating whether this leads to a more realistic circulation. An additional capability of our method is taking into account the vertical structure of the relaxation time, which might be a key factor in the circulation.

PHOTOCHEMICAL CONTROL OF THE DISTRIBUTION OF VENUSIAN WATER & SULPHURIC ACID AEROSOLS IN THE CLOUDS AND UPPER HAZE LAYER OF VENUS, PLUS NEW INSIGHTS REGARDING SO_2

C. D. Parkinson, **S. W. Bougher,** CLaSP Department, University of Michigan, Ann Arbor, MI USA *(theshire@umich.edu*), **P. Gao, Y. L. Yung**, Caltech, Pasadena, CA, USA

Introduction and Motivation:

Recent observations of enhanced amounts of SO_2 at 100 km by Venus Express (1, 2, 3) suggest that there is a hitherto unknown source of gaseous sulphur species in the upper atmosphere of Venus, in contrast to previous expectation (4). Zhang et al. (5, 6) argue that the photolysis of H_2SO_4 vapour derived from evaporation of H_2SO_4 aerosols provides a source of SO_3, which upon photolysis yields SO_2. Other chemical schemes not involving H_2SO_4 pathways (e.g. polysulphurs (6) or those not including the influence of evaporation and condensation of sulphuric acid haze particles (7)) have been suggested, but still discovering the unknown source of gaseous sulphur species has remained elusive. Analogous to O_2 and NO airglow studies (8), SO_2 can be used as an effective atmospheric tracer, which in lieu of wind data, give important clues to the dynamics of the Venus upper atmosphere.

Numerical modeling of the chemistry and dynamics of the Venus middle atmosphere has been performed for effective data analysis and the subsequent interpretation of key tracer species recently observed by VEx. Additionally, a microphysical cloud model has been employed to determine how chemistry and dynamics can affect the aerosol creation and distribution in Venus' upper atmosphere with the view to solving the longstanding problem of the source of the unknown UV absorber and cloud banding in Venus' upper atmosphere (9,10).

Models

Photochemical Model: The Caltech/JPL KINETICS model solves the 1-D continuity equation for the chemical species used in this study (9, 10). The major photochemical pathway for SO_2 above the cloud tops has SO_2 exchanging rapidly with SO and SO_3. However, formation of H_2SO_4 followed by condensation, which sequesters SO_2 in aerosol particles and remove it from active chemistry.

VTGCM: The Venus Thermospheric General Circulation Model (VTGCM) is a 3-D finite difference hydrodynamic model of Venus' upper atmosphere (8, 11, 12, 13, 14, 15, 16, and 17). The VTGCM solves the time-dependent primitive equations for the neutral upper atmosphere. The diagnostic equations (hydrostatic and continuity) provide geopotential and vertical motion fields. Additionally, the prognostic equations are typically solved for steady-state solutions for the temperature, zonal and meridional velocities, and the mass mixing ratios of specific species.

Microphysical Cloud Model: The microphysical cloud model is the Community Aerosol and Radiation Model for Atmospheres (CARMA) v3.0 (18, 19, 20, and 21) as modified by Gao et al. (22) to simulate a 1-D column of the Venus atmosphere. Parkinson et al. (10) employed this scheme using model atmospheres from the photochemical model described in section 2.1. The microphysics simulates the nucleation of sulphuric acid onto sulphur and meteoric dust; particle growth and loss by condensation, evaporation, and coagulation; and transport by diffusion and sedimentation.

Results and Discussion

Figure 1 shows decreasing the H_2O volume mixing ratio (VMR) at the lower boundary (LB) from 35 to 18 ppm causes corresponding decreases in the H_2O higher up due its removal above the cloud tops by formation of H_2SO_4. Further lowering this value below 17 ppm, there is a sudden collapse of H_2O above ~65km. The reason is the complete sequestration of H_2O by H_2SO_4 aerosols resulting in a chemical bifurcation as its value falls below a critical value. Figure 2 shows the result of using stable vs collapsed H_2O model atmopsheres in the microphysical cloud model. The effects of the changed water profiles drastically affects the microphysics: we see changes in the periodicity of the precipitation in the equatorial region of Venus' at 54 km, and changes from a relatively stable uniform haze layer at 84 km for a water rich case, whereas there are quasi-periodic instabilities for the collapsed water case shown.

SO_x has been added to the VTGCM, making use of the key reactions of Petrass (7). Global SO_2 and SO distributions were calculated over ~70-110 km (appropriate to solar minimum conditions), in accord with the underlying VTGCM zonal and meridional winds. Figure 3 shows calculated SO_2 VMR profiles at a different local times corresponding to recent VEx measurements (23, 24). These calculated SO_2 profiles easily reproduce observations below 85-90 km; the observed inversion layer above 90 km (increasing SO_2 VMR with increasing height) is seemingly absent when only comparing their shape. However, a closer examination of our curves with the Belyaev et al. (23) results show our calculations

do match within the reported error bars. (cf. Figure 3, upper rightmost panel with all other panels).

Conclusions

We see that SO_2 and H_2O can regulate each other via formation of H_2SO_4. Small changes in the transport rates for SO_2 may result in large changes in SO_2 above the cloud tops and below a critical value H_2O could be completely sequestered by H_2SO_4 aerosols (chemical bifurcation). This could possibly explain some of the observed variability in SO_2 and H_2O on Venus. Using model atmospheres with different lower boundary VMR values for H_2O definitely affects the microphysics and exhibits particularly extreme behaviour different for chemical bifurcation cases corresponding to a collapsed water condition in the atmosphere. Large differences occur in the precipitation cycle at the equator (a factor of ~3 decrease in timescale from 15 ppm to 35 ppm lower boundary water mixing ratio values (i.e. ~2 years vs ~8 months). The upper haze layer (84 km) at all latitudes shows a large increase in 0.3-0.6 micron sized particle when comparing a 15 ppm lower boundary water mixing ratio to 35 ppm, particularly at the poles. This makes sense, since with a chemical bifurcation there is much more SO_2 present under collapsed water conditions.

The VTGCM simulated SO_2 profiles accurately reproduce observations below 85-90 km; above 90 km these profiles fall within the observation error bars reported by Belyaev et al. (23), but are very different in shape to those obtained with the 1-D photochemical model. However, closer inspection of the VTGCM SO_2 profile shapes show that these curves may actually be more consistent with Belyaev et al. (23) observations than those from the 1-D photochemical modeling (5, 6, and 7), indicating dynamics may also play a significant role in Venus' middle atmosphere.

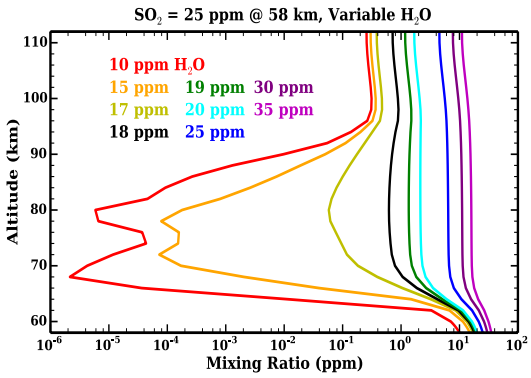

Figure 1: H_2O profiles from a lower boundary mixing ratio sensitivity study with fixed SO_2 lower boundary of 25 ppm: (Parkinson et al. (9)).

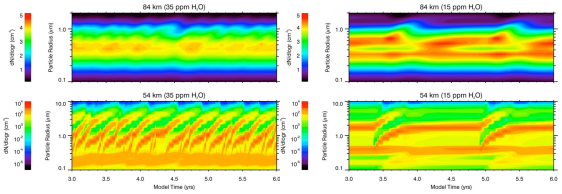

Figure 2: Aerosol size distributions as a function of time for LB VMR 35 ppm water rich (left panel) and 15 ppm water poor (right panel) scenarios. (Parkinson et al. (10)).

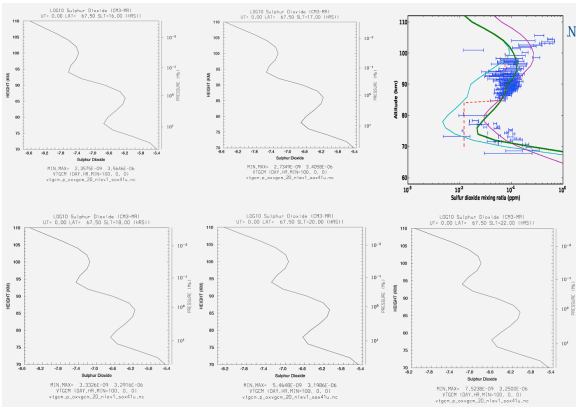

Figure 3: SO_2 distributions as a function of altitude for different local times crossing over the evening terminator. (LAT = 67.5N and LT = 16 - 22h)

References

(1) Sandor, B.J., R.T. Clancy, G.H. Moriarty-Schieven, and F.P. Mills, (2010). *Icarus,* 208. 49–60. **(2)** Mahieux, A., A. C. Vandaele, S. Robert, V. Wilquet, R. Drummond, D. Belyaev, and J. L. Bertaux, (2015). Planet. Space Sci. **(3)** Vandaele, A. C., O. Korablev, D. Belyaev, S. Chamberlain, T. Encrenaz, L. W. Esposito, K. L. Jessup, F. Lefévre, S. Limaye, A. Mahieux, E. Marcq, F. Mills, C. D. Parkinson, S. Robert, B. Sandor, A. Stolzenbach, C. F. Wilson, and V. Wilquet, (2015). Planet. Space Sci. **(4)** Yung, Y. L., and W. B. Demore, (1982), *Icarus*, *51*, 199-247. **(5)** Zhang et al., (2012). Icarus, 217. **(6)** Zhang, Xi, Mao-Chang Liang, Franck Montmessin, Jean-Loup Bertaux, Christopher Parkinson & Yuk L. Yung, (2010). *Nature Geoscience* 3, 834–837 doi:10.1038/ngeo989. **(7)** Petrass, J., Honours thesis, Australia National University, Oct 2013. **(8)** Brecht, A. S., et al. (2011). *J. Geophys. Res.,* ***116,*** E08004, doi: 10.1029/2010JE003770. **(9)** Parkinson, C. D., Y. L. Yung, L. Esposito, P. Gao, S. W. Bougher, and M. Hirtzig (2015). Planet. Space Sci., doi:10.1016/j.pss.2015.02.015. **(10)** Parkinson, C. D., P. Gao, R. Schulte, S. W. Bougher, Y. L., Yung, C. G. Bardeen, V. Wilquet, A. C. Vandaele, A. Mahieux, S. Tellmann, and M. Patzold (2015). Planet. Space Sci., doi:10.1016/j.pss.2015.01.023. **(11)** Bougher, S. W., et al. (1988). *Icarus*, ***73***, 545-573. **(12)** Bougher, S. W., et al., (1990). *J. Geophys. Res.*, ***95,*** 6271-6285. **(13)** Bougher, S. W., et al. (1997). *Venus II*, pp. 259-292, U. of Arizona Press. **(14)** Bougher, S. W., et al. (1999). *J. Geophys. Res.*, ***104***, 16591-16611. **(15)** Bougher, S. W., et al. (2008). *Space Sci. Revs.,* ***139***, 107-141, doi:10.1007/s11214-008-9401-9. **(16)** Brecht, A. S., et al. (2012). Icarus, 217(2), 759-766. **(17)** Brecht, A. S. and S. W. Bougher (2012), JGR, 117, E08002. **(18)** Turco et al. 1979, J. Atmos. Sci. 36, 699. **(19)** Toon et al. 1989, J. Geophys. Res. 94, 11359. **(20)** Bardeen et al. 2008, J. Geophys. Res. 113, D17202. **(21)** English et al. 2011, Atmos. Chem. Phys. 11, 9303 **(22)** Gao et al., (2014). Icarus, 231. **(23)** Belyaev, D., et al., (2012). Icarus 217, 740–751. **(24)** Marcq, E., et al., (2011). Icarus, 211, 58–69.

THE WINDS OF VENUS DURING MESSENGER'S FLYBY.

J. Peralta, *Institute of Space and Astronautical Science (ISAS/JAXA), Sagamihara, Japan (javier.peralta@ac.jaxa.jp),* **Y. J. Lee**, *ISAS (JAXA), Sagamihara, Japan,* **R. Hueso**, *Departamento de Física Aplicada I, UPV/EHU, Bilbao, Spain,* **R. T. Clancy**, *Space Science Institute Boulder, CO, USA,* **B. J. Sandor**, *Space Science Institute Boulder, CO, USA,* **A. Sánchez-Lavega**, *Departamento de Física Aplicada I, UPV/EHU, Bilbao, Spain,* **T. Imamura**, *ISAS (JAXA), Sagamihara, Japan,* **M. Omino**, *ISAS (JAXA), Sagamihara, Japan,* **P. Machado**, *OAL (IA), Lisboa, Portugal,* **E. Lellouch**, *LESIA, Meudon, France,* **M. Rengel**, *MPS (MPG), Germany and ESAC (ESA), Spain,* **S. Murakami**, *ISAS (JAXA), Sagamihara, Japan,* **H. Ando**, *ISAS (JAXA), Sagamihara, Japan,* **D. Peach**, *British Astronomical Association, London, UK.*

Introduction

The many space missions devoted to unveil the secrets of the planet Venus in the past decades have provided huge amounts of valuable data but still failed to properly explain why the Venus atmosphere moves at the cloud tops about 60 times faster than the solid globe, the so-called Superrotation. The crucial task of characterizing the prevailing winds has been carried out using varied techniques that include: "in situ" measurements using descending probes and balloons, remotely sensing from analysis of images acquired at different wavelengths and times to track atmospheric features, and with spectroscopy to measure the Doppler effect on the Venusian atmosphere from Earth-based observations. Despite the varied methods, these measurements are disperse, both spatially and in time, and considering the demonstrated variability of the Venus atmosphere, they have not yet been representative for a complete description of the atmospheric state at all levels and concrete moment.

It was not until the arrival of imaging spectrometers onboard spacecrafts (like NIMS on Galileo, or VIRTIS-M on Venus Express) [1,2] and a more suitable selection of filters in the CCD cameras (like VMC on Venus Express, or cameras on Akatsuki) [2,3] that it became possible to sense simultaneously different levels on Venus in both day and night sides, thus allowing to infer an instant 3D snapshot of the atmospheric circulation [4]. Moreover, during the Venus Express mission several coordinated campaigns have been successfully organized to complement the spacecraft's acquisition of data, provided the impressive development of the instrumentation and telescopes in ground based observatories, along with the revolution in the amateur community with affordable/fast cameras allowing the technique of lucky imaging.

Among these campaigns, the most complete was carried out in June 2007, when NASA's spacecraft Messenger made its second flyby of Venus towards its way to Mercury [5], at the same time that Venus Express and many ground-based observers acquired a varied set of atmospheric data. Nevertheless, most of the data was published in separate works [6,7,8,9] while the images taken by Messenger were not employed to measure the winds. In this work, we present the Venus winds obtained with the images taken by Messenger and we afford the most detailed characterization ever made of the instantaneous state of the Venus atmosphere, combining wind measurements from three different techniques and data from eight instruments on Messenger, Venus Express and diverse Earth-based telescopes.

Data and methods

The atmospheric winds can be obtained with up to three methods others than "in situ" measurements: tracking atmospheric features [4], measuring the Doppler-shift in the atmospheric spectra [9] or using the temperature of the atmosphere combined with the thermal wind equation [10]. These techniques have been repeatedly proven to provide coherent results, though only Doppler and feature tracking at cloud top have been validated with strictly simultaneous observations [11]. Since the magnitude and even the wind direction seem subject to short and long-term variations [10], the usage of time and zonally averaged profiles do not seem the most reliable approach to overcome the difficulties that General Circulation Models (GCMs) have to reproduce properly Venus circulation. For this reason, providing a complete snapshot of the Venus atmosphere at a certain moment, might prove to be an alternative valuable approach to set initial conditions and top/lower boundaries in models.

During its second flyby of Venus the 5 of June of 2007, the spacecraft Messenger compiled a varied scientific data set using several of its instruments. Concretely, the CCD camera MDIS sensed the evening side of the Venus atmosphere with very high spatial resolution images at several filters from visible to near-infrared. At the same day, the instruments VIRTIS and VMC onboard Venus Express acquired images covering other regions of the planet, while there was a complete campaign of ground-based measurements covering the moment of the event and the nearby days. In this work, we characterized the winds at several altitudes of the Venus atmosphere in both day and night using the three techniques previously described (see Table 1). Winds obtained with the Doppler technique cover altitudes 70-110 km using scattered Fraunhofer lines [9] and CO spectral-

line observations [6,7]. Feature tracking was applied on images sensing the scattered daylight at 365 nm (VMC), 433 nm and 996 nm (MDIS), while the night-side was sensed with VIRTIS using the oxygen airglow at 1.27 μm, the clouds' thermal emission at 3.8 and 5.0 μm, and the cloud opacity to surface thermal emission at 1.74 μm. Finally, the zonal component of the wind was also estimated applying the thermal wind equation for cyclostrophic regimes [10] using atmospheric temperatures derived from the CO_2 non-LTE emissions at 4.3 μm from VIRTIS-H [12], submillimeter spectral-line observations of CO [8], and the nightside spectra ranging 4.2-5.0 μm using VIRTIS cubes during Messenger flyby.

Z (km)	D/N	Instrument	Parameter
85-110	Both	HHSMT*	Winds [Doppler]
102	Night	IRAM*	
94	Day		
70	Day	UVES*	
101	Night	VEx/VIRTIS	Winds [Tracking]
70	Day	Messg/MDIS	
		VEx/VMC	
		Amateur	
65	Night	VEx/VIRTIS	
60	Day	Messg/MDIS	
45	Night	VEx/VIRTIS	
120	Day	VEx/VIRTIS*	Temperature [RT Model]
66-116	Day	JCMT*	
50-110	Night	VEx/VIRTIS	

Table 1: Summary of observations coincident with the Messenger 2nd flyby of Venus in June 2007. Instruments marked with asterisks refer to datasets from already published works, while the others were specifically calculated for this work. Acronyms Messg and VEx stand for Messenger and Venus Express, respectively.

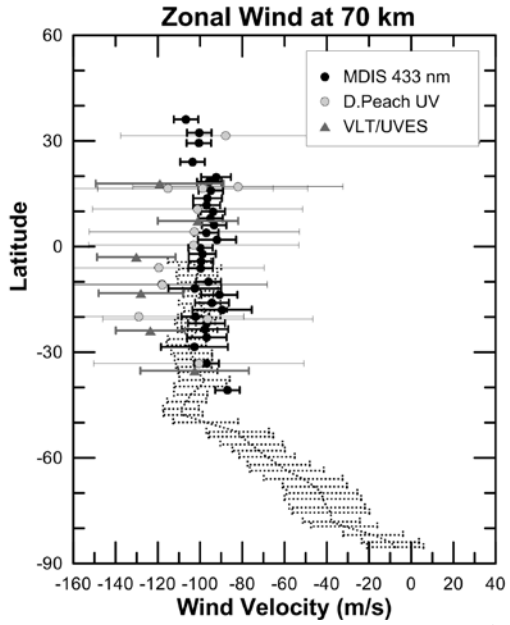

Figure 1: Zonal wind measured during the Messenger flyby. Profiles were zonally averaged in bins of 5º in latitude. Black and grey-filled circles correspond to simultaneous measurements using cloud tracking in violet images (MDIS) and ultraviolet (small telescope). Grey triangles stand for Doppler-shift in scattered Fraunhofer lines (UVES). Dashed profile corresponds to average zonal winds from VIRTIS UV images taken along the Venus Express mission [13].

Results

Figure 1 exhibits an example of winds measurements taken by different means at practically the same vertical level, in this case the cloud tops at about 70 km. Winds from cloud-tracking with ground-based images from small telescopes matches within error bars the averaged profile obtained with MDIS violet images, while the discrepancy with Doppler winds from UVES is explained in terms of slight differences in the vertical level sensed by scattered Fraunhofer lines and the strong vertical shear at the cloud tops. Zonal and meridional feature-tracked winds at day (60 and 70 km) and nigthside (45 and 101 km) were found to be consistent with previous results from Venus Express [13]. In the specific case of MDIS 996-nm images, the meridional component shows a trend opposite to cloud tops, with equatorward component instead of polewards. VIRTIS night airglow at 1.27 μm display wind components consistent with circulation towards the antisolar point.

Finally, the zonal winds obtained for same regions of latitude and local time are used to infer the corresponding vertical profile of the wind and compared with in situ profiles from Veneras, Pioneer Venus and the reference from VIRA. Dayside winds are obtained at 60, 70, 94 and 85-110 km, while the height gaps are calculated with the thermal wind equation and horizontal distribution from temperatures covering 66-116 and 120 km. Regarding nightside, winds were inferred at 45, 60, 101, 102 and 85-110 km, while gaps are calculated with temperatures covering 50-110 km. Our results are consistent with the corresponding vertical profiles measured in similar regions of latitude and local time by Venera 10 (dayside observations) and Pioneer Venus Night probe (nightside).

Bibliography

[1] Carlson et al. *Science*, 253, 1541-1548 (1991).
[2] Svedhem et al. *PSS*, 55, 1636-1652 (2007).
[3] Nakamura et al. *PSS*, 55, 1831-1842 (2007).
[4] Sánchez-Lavega. *GRL*, 35, L132042008 (2008).
[5] McNutt et al. *Acta Astron.*, 63, 68-73 (2008).
[6] Lellouch et al. *PSS*, 56, 1355-1367 (2008).
[7] Rengel et al. *PSS*, 56, 1368-1384 (2008).
[8] Clancy et al. *PSS*, 56, 1344-1354 (2008).
[9] Machado et al. *Icarus*, 221, 248-261 (2012).
[10] Piccialli et al. *Icarus*, 217, 669-681 (2012).
[11] Machado et al. *Icarus*, 243, 249-263 (2014).
[12] Peralta et al. *A&A*, 585, A53 (2016).
[13] Hueso et al. *PSS*, 113-114, 78-99 (2015).

MASS COMPOSITION ANALYSIS OF PLASMA IN THE VENUSIAN UPPER IONOSPHERE MEASURED BY ASPERA-4

M. Persson[1] *(moa.persson@irf.se)*, **Y. Futaana**[1], **H. Nilsson**[1], **G. Stenberg**[1], **S. Barabash**[1], **A. Fedorov**[2] **and M. Hamrin**[3].

[1] *Swedish Institute of Space Physics, Kiruna, Sweden*

[2] *IRAP, CNRS, Toulouse, France.*

[3] *Department of Physics, Umeå University*

Introduction:

Venus Express (VEx) orbited Venus in 2006-2014, in a highly eccentric polar orbit with a pericentre near the North Pole. During this time the Ion Mass Analyser (IMA) sensor in the Analyser of Space Plasma and Energetic Atoms (ASPERA-4) instrument measured properties such as energy and mass of the ions in the plasma environment of Venus **[**Barabash et al. 2007]**.** In this study, we develop the algorithm that can separate the mass of the ions from the data obtained from IMA. While IMA has moderate mass resolution, the separation of O+, O2+ and CO2+ is a challenging work, because the signal for each mass overlaps each other in the obtained mass spectra.

Instrumentation:

The ASPERA-4/IMA ion spectrometer measures ions with energies of 0.01–36 keV/q by separating into 96 logarithmically separated bins. IMA has a wide aperture (90˚ in the polar and 360˚ in the azimuthal directions) with a resolution of 5˚x22.5˚. The moderate mass separation capabilities provide the ability to separate mass-charge ratios of 1, 2, 4, 8, 16, 32, and >32. The time resolution to obtain the full 3-D distribution function is 192 s **[**Barabash et al. 2007]**.**

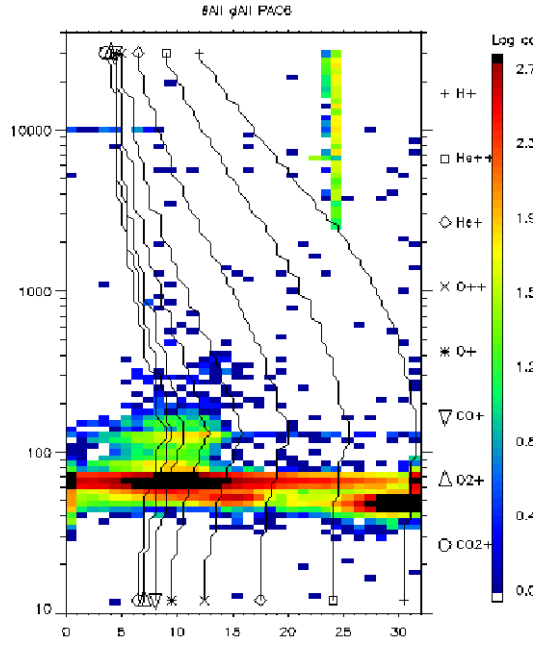

Figure 1*: VEx/IMA observations in the ionosphere. Horizontal axis is mass channel and vertical axis is the energy (eV; uncalibrated). Solid lines are mass contours. The signal at mass channels 5–15 at the energy labeled 60–70 eV is the main target of this study (O^+, O_2^+, CO_2^+).*

Data analysis:

We focus on the ionospheric data obtained from IMA, namely below 500 km. We identify the ionospheric ion population in the IMA dataset, and first produce the mass spectra (Figure 1). Calibration information gives Gaussian curves that are used to find the best fits to the obtained mass spectra to extract mass composition. Figure 2 shows the similar data analysis used for Mars Express IMA data. One can see that the sum of the three overlapping calibration curves represents the obtained data very well [Carlsson et al 2006].

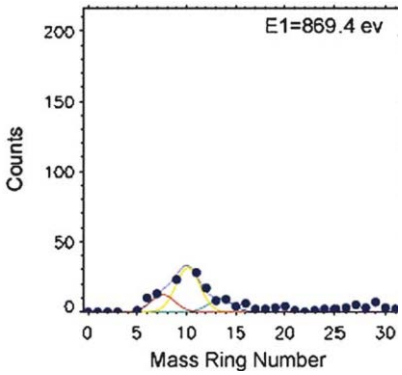

Figure 2*: An example of the mass separation using data obtained from ASPERA-3/IMA on Mars Express (Carlsson et al., 2006). Black dots represent the ion count rate measurement, and the three colored curves are the fitted components using the calibration information. The black solid curve is the sum of the three components.*

Discussion:

In this study, we can start from the identical algorithm used in Carlson et al. 2006. However, the characteristics in IMA on MEx and VEx differ. Therefore, several fitting methods are attempted, including least-square fitting or maximum likelihood, to evaluate which algorithm is the most suited.

Since the IMA data provide 4-D mass-spectra (energy, two directions, and time), the mass composition of 4-D data will be obtained in theory. However, in practice, one may need to collapse in some of the directions before fitting in order to get good count-rate statistics. The order of the collapsing is also assessed.

The optimized algorithm can be used to obtain the height profile of the ionospheric ion density composition. The mass-separated height profiles are basic characteristics of the upper ionosphere of Venus. The periods of lowered pericentre, down to altitudes below 165 km, are of particular interest for a future study. The comparison with the reported ionospheric density profile obtained form the PVO measurements [Taylor et al., 1980] are important for

further understanding of the physics of this environment.

References:

Barabash et al. (2007), The Analyser of Space Plasmas and Energetic Atoms (ASPERA-4) for the Venus Express mission, Planet. Space Sci., 55, doi: 10.1016/j.pss.2007.01.014.

Carlsson, E., et al. (2006), Mass composition of the escaping plasma at Mars, Icarus, 182, doi: 10.1016/j.icarus.2005.09.020.

Taylor, H. A., et al. (1980), Global observations of the composition and dynamics of the ionosphere of Venus: Implications for the solar wind interaction, J. Geophys. Res., 85, doi: 10.1029/JA085iA13p07765.

MAPPING THE THERMAL STRUCTURE AND MINOR SPECIES OF VENUS MESOSPHERE WITH ALMA

A. Piccialli (1), R. Moreno (1), T. Encrenaz (1), T. Fouchet (1), E. Lellouch (1), A. Moullet (2), T. Widemann (1)

(1) LESIA, Observatoire de Paris, CNRS, UPMC, Univ. Denis Diderot, F-92195 Meudon, France, (2) National Radio Astronomy Observatory (NRAO) 22903 Charlottesville, VA, USA (arianna.piccialli@obspm.fr)

Abstract:

Submillimeter observations obtained with the Atacama Large Millimeter Array (ALMA) offer the opportunity of probing Venus upper mesosphere and of monitoring minor species, winds and the thermal structure. Here, we report on vertical retrievals of CO temperatures, HDO, SO, and SO_2 obtained over the entire disk of Venus on November 14, 15, 26 and 27, 2011 during the ALMA Early Science observation cycle.

Introduction:

The mesosphere of Venus exhibits complex photochemistry cycles and dynamical processes that are still poorly understood. A strong variability, both on day-to-day as well as longer timescales, affects the thermal structure of this atmospheric region, especially near the morning and evening terminators, where large density and temperature variations were observed [1, 2, 3]. Sulfur dioxide and water vapor are key species in the photochemical cycles taking place in the troposphere and mesosphere of Venus [4, 5]. Both molecules are abundant in the lower troposphere (150 ppm and 30 ppm respectively [6, 7]). They are carried by convective transport, together with the Hadley circulation, up to about 60 km where SO_2 is photodissociated and combines with oxygen atoms to form SO_3. SO_3 reacts with H_2O to form H_2SO_4, which condenses in the clouds enshrouding the planet. Above the clouds, both SO_2 and H_2O are depleted down to about 0.1 ī 1 ppm and 1 ï 2 ppm respectively. Observations in the UV and in the IR, using Venus Express [8, 9] and ground-based high-resolution imaging spectroscopy [10, 11], have shown evidence for strong temporal variations of the SO_2 abundance on a timescale as short as a couple of hours, which are not well understood presently.

ALMA observations: Ground-based observing campaigns of Venus were organized in support of space exploration observations since the early stage of Venus Express operations in 2006 [2,12,13]. Earth-based observations provide complementary information to spacecraft data by allowing a complete view of the planetary disk at a given time and a long-term coverage, which is of particular interest after the end of Venus Express operations in January 2015.

Submillimeter observations obtained with the Atacama Large Millimeter Array (ALMA) offer the possibility to monitor the temporal evolution of sulfur species and water in the upper atmosphere of Venus. A first set of observations was obtained in November 2011 during the first ALMA cycle [14,15]. These observations targeted SO_2, SO, HDO and CO transitions around 345 GHz during four sequences of 30 minutes each. The Venusô disk was about 11ò with an illumination factor of 90%, so that mostly the dayside of the planet was mapped.

Assuming nominal night-time and dayside CO abundance profiles from [16], we applied an inversion algorithm to retrieve vertical temperature profiles as well as the abundances of minor species (HDO, SO, SO_2). We will present for the first time vertical profiles of temperature and minor species abundance in each pixel of the Venus disk for the four days of observations in order to study variations with latitude, and local time, as well as day-to-day variability.

References:

[1] Mahieux A. et al., *PSS*, 2015. [2] Clancy, R. T. et al. (2012) *Icarus*, 217, 779-793, [3] Piccialli, A. et al., *PSS*, 2015. [4] Mills F. et al. (2007), in Exploring Venus as terrestrial planet, Vol. 176, GMS, p. 73. [5] Zhang X. et al. (2012) *Icarus*, 217, 714. [6] Marcq E. et al. (2008) *JGR (Planets)*, 113. [7] Bézard B. et al. (2009) *JGR (Planets)*, 114. [8] Marcq E. et al., 2011. Icarus, 211, 58. [9] Belyaev D. A. et al., 2012. Icarus, 217, 740. [10] Encrenaz T. et al., 2013. *AAP*, 559, A65 [11] Encrenaz T. et al., 2012. *AAP*, 543, A153. [12] Rengel, M. et al. (2008) *PSS* 56, 1688ï 1695. [13] Sonnabend, G. et al. (2012) *Icarus*, 217, 856ï 862. [14] Encrenaz, T. et al. (2015) *PSS*, 2015. [15] Moullet, A. et al. (2013) *AAS-DPS meeting* #45, abstract #202.01. [16] Clancy R. T. et al. (2003) *Icarus*, 161, 1.

The VIRTIS-VEX data in NetCDF format.

Romolo Politi (romolo.politi@iaps.inaf.it), **Sergio Fonte**, **Maria Teresa Capria**, **Marco Giardino**, **Diego Turrini**, **Giuseppe Piccioni**, *INAF-IAPS, Rome, Italy*, **Pierre Drossart**, **Stephan Erard**, *LESIA-OBSPM, Meudon, France*

The legacy of Venus Express (VEX) is the biggest and most recent dataset on our twin planet. This 1 TB dataset covers about 10 years of observations with scientific objectives spanning from the surface up to the upper atmosphere of Venus. After the completion of the mission, is now important to deliver these data to the scientific community at large and make them easily accessible to those who are not familiar with the PDS format, in order to maximise the scientific return of this unique data set. To reach this goal we undertook the task of translating the VIRTIS data to NetCDF format, the most common data format in atmospheric analysis. NetCDF is a set of software libraries and self-describing, machine-independent data formats that support the creation, access, and sharing of array-oriented scientific data. We will describe in detail the structure of the data in this new format with the aim to make the VIRTIS-VEX data the touchstone for the NetCDF in this field.

Stability of Pyrite under Venusian Surface Conditions. S. T. Port[1], E. Kohler[1,2], P.I. Craig[3], and V. Chevrier[1]. [1]Arkansas Center for Space and Planetary Sciences, University of Arkansas, Fayetteville, AR, 72701; [2]Harriett G. Jenkins NASA Pre-doctoral Research Fellow; [3]Lunar and Planetary Institute, Houston, TX 77058.

Introduction: The existence of pyrite (FeS_2) on the surface of Venus has been theorized since the 1980s when sulfur was revealed to be an important component of the Venusian atmosphere [1, 2]. Utilizing data obtained from the Venera and Pioneer missions, combined with Earth-based observations, scientists have attempted to determine a geochemical sulfur cycle to explain the replenishment of atmospheric sulfur [3-5]. Past chemical equilibrium calculations illustrate that pyrite, pyrrhotite (Fe_7S_8), or anhydrite ($CaSO_4$) is the most likely sulfur bearing mineral found on the surface [4-5]. However, based on the temperature range on Venus, $CaSO_4$ is not expected to greatly affect the concentration of sulfur in the atmosphere and pyrrhotite is thought to be unstable [5]. Pyrite is sensitive to temperature and may form and decompose at different locations on Venus, thereby releasing and absorbing gaseous sulfur from the atmosphere [3]. For instance, pyrite is expected to form at low temperatures and oxidize to magnetite (Fe_3O_4) at high temperatures. This process can be observed in the pyrite-magnetite buffer [3]:

$$3FeS_2 + 16CO_{2(g)} = Fe_3O_4 + 6SO_{2(g)} + 16CO_{(g)} \quad (1)$$

Pyrite may also explain the high radar reflectivity regions found on the Venusian highlands due to pyrite's high electrical conductivity [4, 6-9].

However, thermodynamic modeling and experimentation demonstrates that pyrite would decompose into iron oxides, such as magnetite or hematite, and sulfur vapor at all Venusian conditions [10]. This is due to the predicted low sulfur vapor on the surface and because the atmosphere is expected to be quite oxidative. It was measured that pyrite in a CO_2-CO-SO_2 environment would decompose as rapidly as 1225±238 days/cm on Maxwell Montes [10].

This work intends to investigate the stability of pyrite under Venusian conditions, specifically to determine the effect of SO_2 on pyrite.

Methods: Two sets of experiments were completed in order to assess the stability of pyrite on Venus: the Lindberg tube oven experiments and the Venus simulation chamber experiments. The Lindberg tube oven experiments were conducted at the University of Arkansas in Fayetteville. In these experiments 1 gram of powdered pyrite was heated to either 380°C or 460°C under either a 100% CO_2 atmosphere or a simulated Venus atmosphere, which consists of 95.6% CO_2, 3.5% N_2, and 150 ppm of SO_2. The temperature values used in the experiments represent the conditions found on the highlands (11 km) and lowlands (0 km) of Venus, respectively.

Powdered pyrite was also studied in the Venus simulation chamber at the National Aeronautics and Space Administration Goddard Space Flight Center to observe the effects of pressure on pyrite. Similarly to the oven experiments, 1 gram of pyrite was measured and inserted into the chamber at either Venusian surface or Venusian highland temperatures and pressures (460°C & 95bar, and 380°C & 55bar, respectively). The experiments were conducted in either a 100% CO_2 atmosphere or the Venus simulated atmosphere. Each experiment ran for 18 hours then the samples were removed and weighed. The samples were analyzed using X-Ray Diffraction (XRD) to determine any changes in the composition or phase of the sample.

Results: In the Lindberg oven and CO_2 atmosphere experiments, there was partial oxidation of pyrite into hematite (Fe_2O_3) at 380°C, with complete oxidation at 460°C. However, in the Venusian atmospheric composition, pyrite was completely stable at 380°C and decomposed into pyrrhotite and sulfur at 460°C.

In the Venus chamber experiments in a CO_2 environment, pyrite was mostly stable (90%) at 380°C, however some magnetite was created (10%). In the 460°C environment the pyrite was less stable (65%) and pyrrhotite (35%) formed. In the Venusian atmosphere at 380°C, 85% of the sample was still pyrite, but solid sulfur was present as well. At 460°C, the entire sample identified as pyrite indicating stability. A summary of results are found in Table 1a&b.

Table 1a&b: An overall summary of the experiments and the results are given here. Table 1a displays the conditions and results of the oven experiments and Table 1b displays the conditions and results of the chamber experiments.

a)

	460°C, 1 bar		380°C, 1 bar	
CO_2 (100%)	Fe_2O_3	100%	FeS_2 Fe_2O_3	88% 12%
CO_2 (95.55%), N_2 (3.5%), SO_2 (150ppm)	$Fe_{0.875}S_2$ S	70% 30%	FeS_2	100%

b)

	460°C, 95 bar		380°C, 55 bar	
CO_2 (100%)	FeS_2 $Fe_{0.875}S_2$	65% 35%	FeS_2 Fe_3O_4	90% 10%
CO_2 (95.55%), N_2 (3.5%), SO_2 (150ppm)	FeS_2	100%	FeS_2 S	85% 15%

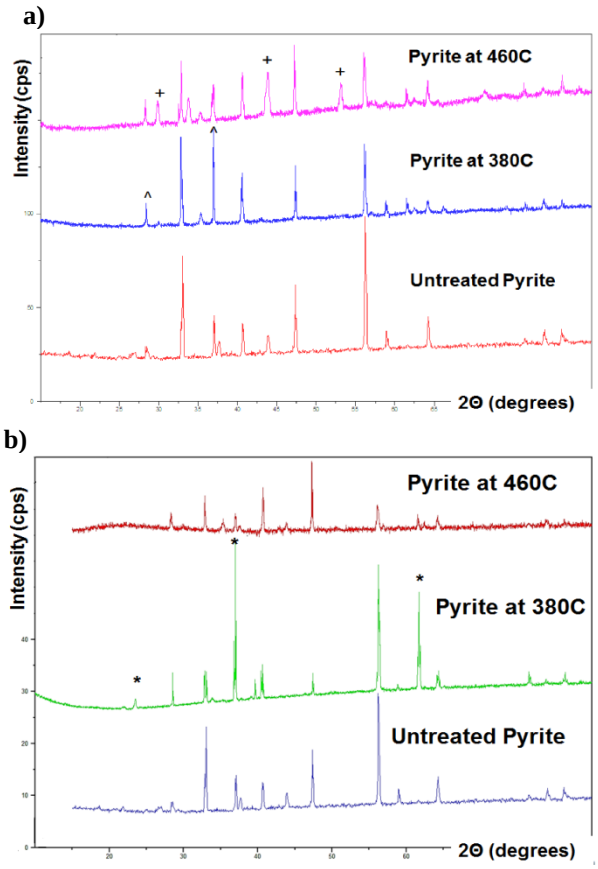

Figure 1: a) XRD results of chamber experiments of pyrite in a CO_2 atmosphere. Untreated pyrite is graphed at the bottom, followed by pyrite heated to 380°C (55bar), followed by pyrite heated to 460°C (95bar) b) XRD results of chamber experiments of pyrite in the Venus simulated atmosphere. Untreated pyrite is graphed at the bottom, followed by pyrite heated to 380°C (55bar) followed by pyrite heated to 460°C (95bar). (+) shows peaks of pyrrhotite, (^) shows peaks of magnetite, and (*) shows peaks of sulfur.

Discussion: Similar to the findings in previous thermodynamic models, pyrite was unstable and readily oxidized in a pure CO_2 environment at all pressures, with the exception of the 460°C/95 bar experiment [5, 10]. However, when the samples were placed in a mixed atmospheric environment, pyrite was found to be more stable than expected with no oxidation. The only experiments that demonstrated instability was the 460°C/1 bar and the 380°C/55 bar experiments.

The stability of pyrite in a Venus simulated atmosphere was unexpected. It appears that the SO_2 in the atmosphere prevents the oxidation of pyrite. Additionally, the identification of elemental sulfur in the 380°C and 55 bar experiment was unanticipated. Possible causes are that the sulfur was dissociated from the pyrite, or from the SO_2 in the atmosphere. If the former hypothesis is the case, then an iron byproduct would be detected. However, the absence of iron as an observable byproduct strongly supports the latter conclusion.

Conclusion: Our results show that pyrite is stable under Venusian temperature, pressure, and atmospheric conditions, but only partially stable in a 100% CO_2 atmosphere. Previous experiments did not account for pressure which may in part explain the disparity between our results. The exact source of the solid sulfur has not been determined, but it may originate from the dissociation of SO_2 gas.

Future Work: The Center for Space and Planetary Sciences at the University of Arkansas will be obtaining a Venus simulation chamber that can be connected to a gas chromatograph and will feature a sapphire window. With these new accessories, we hope to measure the atmospheric composition during the experiments. An understanding of the change in atmospheric composition will uncover more about the chemical reactions that possiblytake place on Venus.

Acknowledgments: This study was supported by Arkansas Space Grant Consortium grant #UAF2140 YR 21 and NASA Grant #NNX13AR94H.

References: [1] Prinn, R. G. (1985) *The Photochemistry of Atmospheres* (J. S. Levine, Ed.), pp. 281–336. Academic Press, New York. [2] Von Zahn et al. (1983) *Venus* pp. 299-430. Univ. of Arizona Press, Tucson. [3] Hashimoto, G. L., and Abe, Y. (2000) *Earth Planets Space*, 52, 197-202. [4] Klose, K.B., Wood J.A., and Hashimoto, A. (1992) *J. Geophys. Res*., 97, 16353-16369. [5] Fegley Jr., B. and Treiman, A.H. (1992) *AGU, Geophysical Monograph No. 66*,7-71. [6] Pettengill, G.H., et al. (1982) *Science*, 217, 640-642. [7] Pettengill, G.H., et al. (1988) *J. Geophys. Res.*, 93, 14,881-14,892. [8] Ford, P.G., and Pettengill, G.H. (1983) *Science*, 220, 1379-1381 [9] Wood, J. A. and Brett, R. (1997) *Icarus*, 128, 472-473.4. [10] Fegley Jr., B. (1997) *Icarus*, 128, 474-479.

BISMUTH TELLURIDES AND SULFIDES MIXTURES AND THEIR RELATION TO METAL FROST ON VENUS. S. T. Port[1], E. Kohler[1], and V. Chevrier[1], [1]University of Arkansas, Fayetteville, AR, 72701 (sara-port@uark.edu)

Introduction: Radar studies completed as early as the 1960s on the Venusian surface revealed unsually reflective surfaces concentrated on the highlands and mountain ranges [1-2]. These reflective regions generally manifest between 2.5 to 4.75 km above the planetary radius of 6051.0 km [3-6]. However, above this critical altitude the reflectivity rapidly decreases until it matches the same reflectivity as the surface [3].

The origin of this phenomenon is currently unknown, though it has been postulated that it occurs due to surface roughness, some unknown interaction between the atmosphere and the surface, or condensation of sulfides onto the surface [2, 7]. Modern researchers believe that the latter scenario, the metal frost model, is the most probable case [7, 8-11].

Potential candidates suggested in the literature of the metal frost model include pyrite (FeS_2), tellurium (Te), galena (PbS), bismuthinite (Bi_2S_3) and a lead bismuth sulfosalt [3-5, 7, 10]. Both bismuth sulfide and tellurium have been suggested as potential candidates in the literature and tellurobismuthite (Bi_2Te_3) is a likely product between both [9]. It is a semiconductor which would account for the high reflectivity [9]. However, preliminary experimentation completed by my colleague on Bi_2S_3 showed stability at all tested temperatures, thus demonstrating that it can not be the metal frost [9]. Te and Bi_2Te_3 were also tested and it was found that Te and Bi_2Te_3 oxidize in a CO_2 environment, but is stable in a Venus simulated atmospheric environment [9]. We propose that some formation created through a mixture of bismuth,tellurium and sulfur might provide the same emissivity as observed on Venus.

Methods: The two chosen mixtures were a 1:1 molar ratio of Bi_2S_3 and Bi_2Te_3 and a 1:3 molar ratio of Bi_2S_3 and Te, respectively. Each mixture was tested at three different temperatures representing the temperature gradient from the Venus lowlands, to the critical altitude, to the highest point on Venus, the top of Maxwell Montes. These three temperatures were 460°C (0km), 427°C (4.5km), and 380°C (11km). Each mixture was first weighed and then inserted into a CO_2 filled Lindberg tube oven for 24 hours. After completion of each experiment, each sample was weighed once more and run through an X-Ray Diffraction (XRD) which will inform us of any compositional changes that occurred to the sample during the experiments.

Results: The Bi_2S_3/Bi_2Te_3 and Bi_2S_3/Te mixtures all exhibited a color change from a dark grey after each experimental run. Samples run at 460°C were bright silver, whereas the samples heated to 380°C and 427°C only experienced a slight lightening in color. Table 1 displays the mass change for each of the experiments. The Bi_2S_3/Te mixture experienced a much greater mass change than the Bi_2S_3/Bi_2Te_3 mix.

Table 1: The change in mass of the sample from before and after the experiment.

	460°C	427°C	380°C
Bi_2S_3/Bi_2Te_3	-14mg	0mg	-5.4mg
Bi_2S_3/Te	-290mg	-85mg	-79mg

XRD analysis showed that the 380°C and 460°C heated Bi_2S_3/Bi_2Te_3 samples consisted of tetradymite (Bi_2Te_2S), Bi_2Te_3, Bi_2S_3, and tsumoite (BiTe), in order of abundance. The Bi_2S_3/Bi_2Te_3 sample heated to 427°C had the same composition as when the sample was heated to 380°C or 460°C, however there was more BiTe than Bi_2S_3. The Bi_2S_3/Te samples heated to either 380°C or 427°C identified as a mix of Bi_2Te_2S, Te, and Bi_2S_3. The Bi_2S_3/Te heated to 460°C only identified as Bi_2Te_2S and Bi_2Te_3. The final products of each experiment is summarized in Table 2.

Table 2: A list of the compounds identified by XRD in each sample for each experiment.

	460°C	427°C	380°C
Bi_2S_3/Bi_2Te_3	Bi_2Te_2S Bi_2Te_3 Bi_2S_3 BiTe	Bi_2Te_2S Bi_2Te_3 Bi_2S_3 BiTe	Bi_2Te_2S Bi_2Te_3 Bi_2S_3 BiTe
Bi_2S_3/Te	Bi_2Te_2S Bi_2Te_3	Bi_2Te_2S Bi_2S_3 Te	Bi_2Te_2S Bi_2S_3 Te

a)

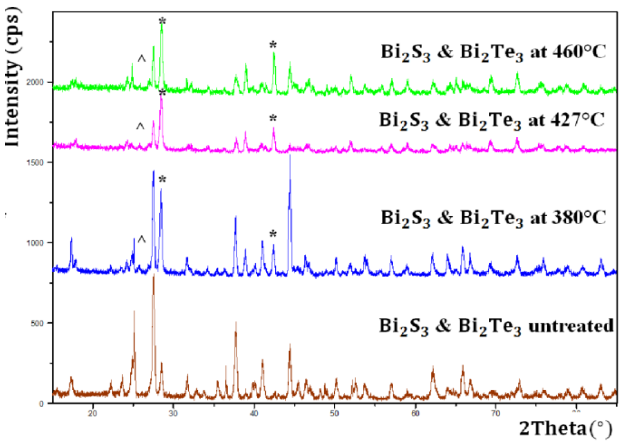

b)

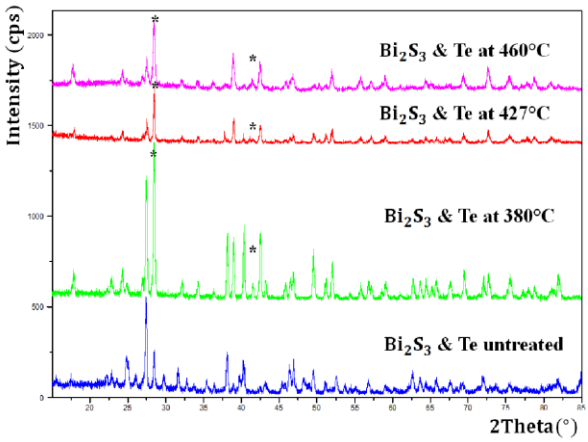

Figure 1: a) XRD patterns of the Bi_2S_3 and Bi_2Te_3 mixture experiments in a CO_2 atmosphere. Untreated mixture is found at the bottom, followed by 380°C (bottom middle), 427°C (top middle), and 460°C (top). b) XRD patterns of the Bi_2S_3 and Te mixture experiments in a CO_2 atmosphere. Untreated mixture is found at the bottom, followed by 380°C (bottom middle), 427°C (top middle), and 460°C (top)..(*) represents the formation of tetradymite and (^) represents tsumoite.

Discussion: The XRD patterns of our samples can be found in Figure 1. In Figure 1a&b the peak at 27° has a higher intensity than the peak found at 28° in the untreated sample, however as the temperature increases the intensities flip. This demonstrates the formation of Bi_2Te_2S from Bi, Te, and S because the 27° peak is representative of Bi_2Te_3 and Te, and the peak located at 28° is Bi_2Te_2S. Also, in both figures the control pattern does not exhibit a peak at 42°, but a peak does appear after heating. This peak is also representative of tetradymite. Within both figures the Bi_2S_3 signals noticeably decrease from untreated up to 460°C. Tetradymite is the most favored mineral in all experiments.

In the 460°C Bi_2S_3/Te mixture Bi_2Te_3 and Bi_2Te_2S were both created demonstrating some replacement of S with Te. However, the corresponding amount of sulfur is absent. This may be due to the vaporization of sulfur. Based on the CRC handbook, gaseous sulfur at this temperature is a definite possibility [12]. Unfortunately at this time we cannot analyze the constituents of the atmosphere in our experiments. Vaporization of sulfur would also explain the loss in mass of the sample.

Conclusion: Though the Bi_2S_3/Bi_2Te_3 and Bi_2S_3/Te mixtures do form other minerals such as Bi_2Te_2S and BiTe, both Bi_2S_3 and Bi_2Te_3 are stable at both lowland and highland conditions. However, our experiments were completed at ambient pressure and in a pure CO_2 atmospheric environment. It is possible that different results could occur if experiments are completed at Venus pressures and in a Venus simulated atmosphere. Therefore it is important to carry out multiple experiments at varying temperatures, pressures, and atmospheric conditions to try to recreate the same patterns of emissivity as seen on Venus.

Future Work: We plan to study a larger range of pressures and temperatures using the oven and to run experiments in a Venus simulated atmosphere (95.6% CO_2, 3.5% N_2, and 150 ppm of SO_2). We will be obtaining a Venus chamber in the near future that can simulate temperature and pressure conditions on Venus and will be attached to a gas chromatograph. With this new equipment we hope to measure the atmospheric composition during the experiments. An understanding of the transformation of the atmospheric composition will uncover more about the chemical reactions that can take place on Venus.

Acknowledgements: This work was funded by the NASA Solar System Workings grant #NNX15AL57G.

References: [1] Goldstein R. (1965) *J. Res. of the National Bureau of Standards* , Section D, 69, 1623-1625. [2] Ingalls, R., Brockelman, R., Evans, et al., (1968) *Lab. Tech. Report* 456. [3] Klose, K.B., Wood J.A., and Hashimoto, A. (1992) *J. Geophys. Res.* 97, 16353-16369. [4] Pettengill, G.H., Ford, P.G. and Nozette, S. (1982) *Science* 217, 640-642. [5] Shepard, M.K., Arvidson, R.E., Brackett, R.A. and Fegley Jr., B. (1994) *Geophys. Res. Letters* 21, 469-472. [6] Pettengill, G.H., Ford, P.G. and Wilt, R.J. (1992) *J. Geophys. Res.* 97, 13091-13102. [7] Schaefer, L. and Fegley Jr., B. (2004) *Geophys. Res. Letters* 21, 469-472. [8] Grieger, B., Ignatiev, N., Hoekzema, N., et al., (2004) *Bulletin American Astro. Society*, 1487. [9] Kohler, et al., (2015) LPSC XLVI, abs. #2563. [10] Pettengill, G.H., Ford, P.G. and Simpson, R.A. (1996) *Science*, 272, 1628-1631. [11] Brackett, R.A., et al., (1995) *J. Geophys. Res.*, 100, 1553- 1563. [12] Hammond, C.R. (2009) CRC Handbook of Chemsitry and Physics, 90th edition. CRC Press, Boca Raton, FL, 43, 95-104.

TITLE: Reaction of Basaltic Materials under High-Fidelity Venus Surface Conditions using the Glenn Extreme Environment Rig: First Results.

B. G. Radoman-Shaw, **R. P. Harvey,** *Case Western Reserve University, Cleveland, Ohio, USA (bgs21@case.edu)*, **N. S. Jacobson, G. C. C. Costa, L. M. Nakely,** *NASA Glenn Research Center, Cleveland, Ohio, USA.*

Introduction: Both historical and current investigations of Venus suggest that atmosphere/rock interactions play a critical role in the evolution of its atmosphere and crust. We have begun a series of systematic experiments designed to further our understanding of atmosphere-driven weathering and secondary mineralization of basaltic materials that may be occurring on Venus today. Our experiments expose representative igneous phases (mineral, glasses and rocks) to a high-fidelity simulation of Venus surface conditions using the NASA Glenn Extreme Environment Rig (GEER) located at the NASA Glenn Research Center in Cleveland, Ohio.

While recent observations of Venus' atmosphere provide fantastic new insight into the history of volatile elements for the planet (Titov et al., 2009), an important component remains enigmatic—how coupling of thermochemical processes between the atmosphere and surface materials may dramatically effect the composition and/or stability of both over time. Previous studies of possible reactions and mechanisms have often been conducted under partial surface conditions or focused on specific reactions of interest using constrained gas and mineral compositions (Fegley and Prinn, 1989; Fegley et al., 1995; Johnson and Fegley, 2002). While providing important first-order knowledge concerning Venus' climate history, these studies risk oversimplifying the reality of that planet's surface, where complex cycling of key elements (e.g. O, C, S, H) between the atmosphere and crust are probably convoluted and may involve a myriad of mineral and fluid species.

GEER is a very large (800L) vessel capable of producing a long-term, high fidelity simulation of both the physical conditions (750° K and 92 bar) and atmospheric chemistry (down to the ppb-level) associated with the Venusian surface (Fig. 1). As of this writing we have just finished the first of several planned experiments: a 42-day exposure of selected mineral, rocks and volcanic glasses. Our goal is to identify and prioritize the reactions taking place and better our understanding of their importance in Venus' climate history.

Samples: Our experiments are designed to simulate the exposure of fresh volcanic (basaltic) rock at Venus' surface, on the premise that this would be a common or even likely source of intense crust/atmosphere interactions. The materials selected for exposure to Venus surface conditions fall into three distinct groups. The first group consists of minerals that are either common in basaltic and calc-alkaline volcanic rocks or have been identified as important in prior experiments or modeling (Treiman and Bullock, 2011). The second group of materials selected for exposure is a suite of representative igneous rocks. These samples include extrusive and intrusive lithologies ranging from basaltic to felsic and from quartz-rich to feldspathoid- rich volcanic classifications.

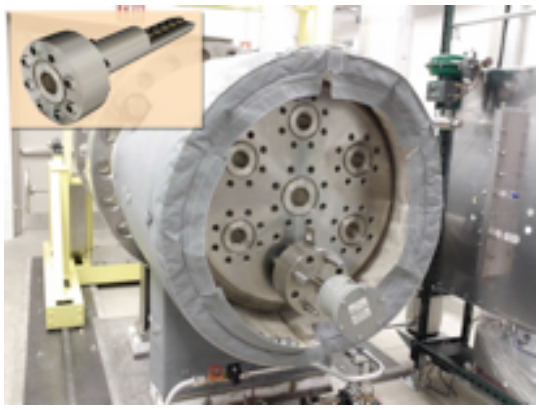

Figure 1. End view of the GEER chamber at NASA Glenn Research Center. Inset shows the rail system that attaches to one of the seven ports shown allowing exposure to high-fidelity Venus surface conditions.

The third group of phases selected for exposure consists of volcanic glasses representing quenched magmatic liquids on the surface of Venus. These allow us to explore the importance of non-crystalline materials, which make up a significant proportion of extrusive rocks on Earth and can support elemental diffusion and reactivity orders of magnitude faster than in crystalline materials. The included phases include five well-characterized USGS standard glasses ranging from basaltic to felsic compositions and several natural Hawaiian surface lava volcanic materials. These glasses are primarily mafic, under saturated basalts, containing a minor crystalline component (up to 40% olivine) and a few percent water. A third category of phases included in our experiments are 3 synthetic glasses that mimic the basalt-like elemental compositions detected by the Venera 13 and 14 and Vega 2 lander XRF instruments (Barsukov, 1992).

The materials chosen for our experiments come from a variety of sources including the National Museum of Natural History (Smithsonian Institution), the Cleveland Museum of Natural History, CWRU's in-house collections, the USGS, and the University of Hawaii. Although most have been well characterized in previous studies, we conducted our own pre-exposure analysis to verify chemical composition

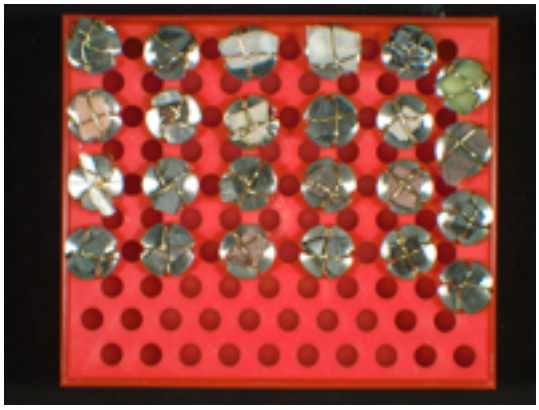

Figure 2: Overview of the mineral and rock samples for exposure.

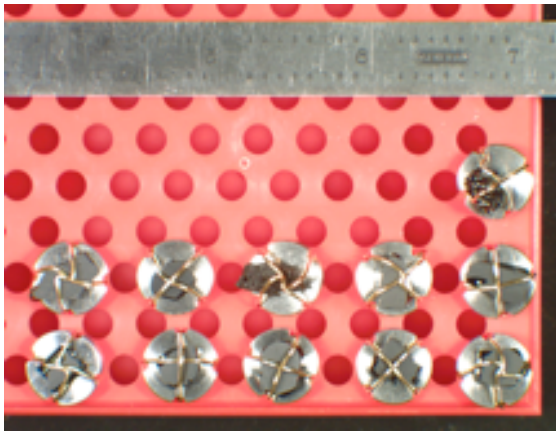

Figure 3: Overview of the glass samples for exposure. The ruler is provided for scale.

and mineralogy. We also included XRD to verify both mineralogy and crystallinity (or lack thereof). Representative optical and SEM imagery were also collected, detailing the texture of mineral surfaces, with EDS used to further identify localized phases. These analyses were done on a mounted sample, and representative samples of all materials were reserved as an unreacted standard for comparison to the exposed samples.

Experimental details:

Mounting: The recently finished experiment (a 42-day exposure) includes a total of 35 phases (14 minerals, 10 rocks, and 11 glasses). Chips of each phase were polished on two sides to provide a stable mounting surface compatible with pre- and post-analysis as well as a preferred direction for development of reaction profiles. Individual chips are approximately 1 cm with a width range between 2-4mm. Three glasses and one mineral were not polished due to their low hardness and vesicular texture. The average weight for the prepared samples is 40mg.

Individual chips were mounted on custom-made stainless steel sample holders, with gold wire attaching the chip to the mount (Figs. 2 and 3). The mount is similar in form to a standard SEM mount but made of more resistant material and with notches to allow the gold wire to grip the sample. These mounts were then loaded into a gold-coated sample tray with individual 2.5 cm-deep wells designed to collect any portion of the sample that might separate from the main chip due to exposure.

Table 1: Simulated Venus atmospheric composition loaded into GEER for the 40-day exposure.

Gas	Molar Mixing Ratio
CO_2	96.5%
N_2	3.5%
H_2O	30 ppm
SO_2	180 ppm
CO	12 ppm
OCS	51ppm
H_2S	2 ppm
HCl	0.5 ppm
HF	2.5 ppb

Conditions: The current experiment began on 20 November 2015 and ended on 7 January 2016. Sample mounts (in two trays) were loaded into GEER along a rail near the geometric center of the main chamber (a cylinder roughly 2x3 m) (Fig. 1). After purging with dry N_2 and several days of leak tests, a simulated Venus atmosphere (Table 1) was loaded into the chamber through GEER's polycontrol gas mixing system, which offers dynamic accuracy of 5 ppb ± 0.7%, thermal mass flow controllers and constant monitoring of temperature, pressure, gas composition and flow rates. To avoid sublimation loss H_2O was loaded in liquid form through a port in the gas fill lines. After a few static days allowed for mixing, internal heaters were turned on until temperatures reached our target value of 470°C and 92 bar for Venus surface conditions a few days later. In early January we turned off the heaters and did several dry nitrogen purges as we cooled down to ambient conditions; samples are now stored in a "dry box" and post-exposure analysis has begun.

Results / Discussion: A campaign of detailed "before and after" analytical electron microscopy is underway as of this writing. We hope to present a full catalog of observed reactions at the meeting.

References:

Barsukov, V. L., (1992) *in* Venus Geology Geochemistry and Geophysics, University of Arizona Press, pp.165-174.

Fegley, B. Jr. Lodders, K., Treiman, A. H., and Klingelhöfer, G., (1995) *Icarus 108*, 373-383.

Fegley, Jr., B., and Prinn, R. G., (1989) *Nature*, 337, 55-58.

Johnson, N. M., and Fegley, Jr., B., (2002) *Adv. Space. Res.* 29, 233-241.

Titov, D. V., et al., (2009) *Solar System Research*, 43:3, 185-209.

Treiman, A. H., and Bullock, M. A., (2011) *Icarus,* 217, 534-541.

Is IMF Bx component really able to impact the magnetic field structure of Venusian magnetotail?

Z. J. Rong, **Y.Wei, L. H. Chai, J. Zhong, and W. X. Wan** *Key Laboratory of Earth and Planetary Physics, Institute of Geology and Geophysics, Chinese Academy of Sciences, Beijing 100029, China (rongzhaojin@mail.iggcas.ac.cn),* **G. Stenberg, Y. Futaana, and S.Barabash**, *Swedish Institute of Space Physics, Kiruna, Sweden.*

Abstract

An earlier statistical survey suggested that the flow-aligned component of upstream interplanetary magnetic field (IMF) may play an important role in controlling the lobe-asymmetries of the Venusian magnetotail. The tail current sheet would be displaced and the magnetic field configuration would show asymmetries about current sheet. The asymmetries are expected to be more evident when the flow-aligned component becomes dominant. Here, with carefully selected cases as well as a statistical study based on Venus Express observations in the near Venus tail, we show that the lobe-asymmetries of magnetic field as well as the displacement of current sheet are common characteristics of Venusian magnetotail. However, the asymmetries and displacement of current sheet do not show a significant dependence on the flow-aligned component of the IMF. Our results suggest that the flow-aligned component of IMF cannot penetrate into the near magnetotail to impact the magnetic field structure.

LATITUDINAL AND TEMPORAL VARIABILITY OF VENUS CLOUDS AND HAZES OBSERVED BY POLARIMETRY WITH SPICAV-IR.

L. Rossi, *Faculty of Aerospace Engineering, Delft University of Technology, Delft, The Netherlands*, **E. Marcq, F. Montmessin, J.-L. Bertaux,** *LATMOS-IPSL, Guyancourt, France*, **A. Fedorova, O. Korablev,** *Space Research Institute (IKI), Moscow, Russia*, *Moscow Institute of Physics and Technology (MIPT), Dolgoprudny, Russia*, **D. Stam,** *Faculty of Aerospace Engineering, Delft University of Technology, Delft, The Netherlands*.

Introduction

The study of Venus' cloud layers is important in order to understand the structure, radiative balance and dynamics of the Venusian atmosphere. Polarization measurements have given important constraints for the determination of the constituents of the clouds and haze. From ground based observations Hansen and Hovenier[1], using a radiative transfer model including polarization, found that the main cloud layers between 50 and 70 km consist of $r \simeq 1$ µm radius spherical droplets of a H_2SO_4 -H_2O solution. In the early 1980s, Kawabata[2] used the polarization data from the OCPP instrument on the spacecraft *Pioneer Venus* to constrain the properties of the overlying haze. They found that the haze layer is composed of smaller particles with $r \simeq 0.25$ µm and similar refractive indices. Our work reproduces the method used by Hansen and Kawabata[1, 2]. We applied a radiative transfer model with polarization on the data of the SPICAV-IR instrument on-board ESA's Venus Express. Our aim is to better constrain haze and cloud particles at the top of Venus's clouds, as well as their spatial and temporal variability.

SPICAV-IR

The SPICAV-IR spectrometer on Venus Express is based on an Acousto-Optic Tunable Filter (AOTF) working in the 0.65 - 1.7 µm range, with two output beams linearly polarized in perpendicular directions, allowing us to measure the degree of linear polarization for different phase angles[4, 3]. The data give a good latitudinal and phase angle coverage. Latitudinal variations in polarization are visible in the observation data for orbits up to #2733 (Oct. 2013) with a strong increase of polarization towards the poles. At lower latitudes, polarization is quite homogeneous and we observe the glory in polarization at low phase angles, in accordance with VMC observations in photometry[5].

Cloud model

We use a radiative transfer model taking polarization into account in order to model the clouds[6, 7]. We consider a two layered model: an optically thick cloud layer of micrometric sulfuric acid particles. Above lies the haze layer of $r \simeq 0.25$µm particles with a varying column density C_h.

The glory

At low phase angle, the main feature is the glory which gives information about the main cloud particles. We retrieve the effective radius and refractive index of the particules and effective variance of the particle size distribution for a dozen glory observations. The retrieved values are in agreement with previous results: the cloud particles are spherical, with radii between 0.8 and 1.3 µm, $\nu_{eff} < 0.15$ and refractive indices between 1.39 and 1.44 at $\lambda = 1$ µm. We observe latitudinal variations with higher radii and refractive indices being observed near the equator. We also find a secular increase in the size and indices during the duration of the mission (fig 1).

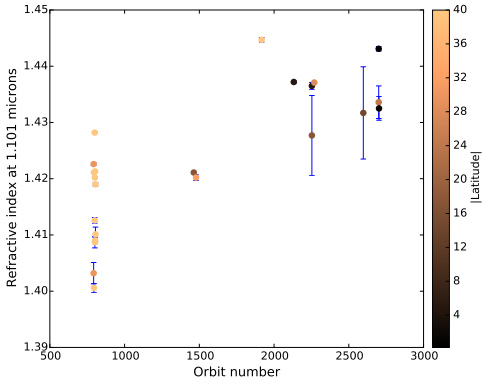

Figure 1: Retrieved refractive indices at 1.101 µm as a function of orbit number and latitude (in color). The indices increase during the mission and reach values that are higher than those expected from sulfuric acid at this wavelength (1.418 for 75% sulfuric acid and 1.425 for 95%).

The haze

At higher latitudes, the main contributor to polarization is the submicrometric haze. The modeling allows us

to measure the column density of the haze layer in the northern hemisphere. We observe that the haze column density stays relatively constant up to 50° of latitude after which C_h increases sharply towards the poles. C_h varies from 10^{-2} μm^{-2} at low latitudes up to 1 μm^{-2} at higher latitudes, in agreement with [8]. We also observe an asymmetry with respect to local time with higher column densities on the morning side than on the evening side.

Conclusion

SPICAV-IR provides global measurements of the polarization of Venus' clouds and allows us to retrieve the parameters of the cloud droplets, in agreement with previous measurements. The refractive indices and effective radii are found to be higher near the equator. Increase with mission time of these parameters is also observed, which origin remains unexplained. The haze column density is evaluated and a strong latitudinal variation is confirmed, along with a local-time variability. A coming paper (Rossi et al. 2016, in prep) will present these results in further details.

Acknowledgements This PhD thesis is funded by the LabEx *Exploration Spatiale des Environnements Plantaires* (ESEP) N^o 2011 LABX-030. We want to thank the State and the ANR for their support within the programme "Investissements d'Avenir" through the excellence initiative PSL*(ANR-10-IDEX-0001-02). We also want to thank the COST Action MP1104 "Polarization as a tool to study the solar system and beyond".

References

[1] Hansen, J. E., Hovenier, J. W., May 1974. Interpretation of the polarization of Venus. Journal of Atmospheric Sciences 31, 1137–1160.

[2] Kawabata, K., Coffeen, D., Hansen, J., Lane, W., Sato, M., Travis, L., dec 1980. Cloud and haze properties from Pioneer Venus polarimetry. J. Geophys. Res.85, 8129–8140.

[3] Korablev, O., Fedorova, A., Bertaux, J.-L., Stepanov, A., Kiselev, A., Kalinnikov, Y., Titov, A., Montmessin, F., Dubois, J., Villard, E., Sarago, V., Belyaev, D., Reberac, A., Neefs, E., may 2012. SPICAV IR acousto-optic spectrometer experiment on Venus Express. Planet. Space Sci.65, 38–57.

[4] Rossi, L., Marcq, E., Montmessin, F., Fedorova, A., Stam, D., Bertaux, J.-L., Korablev, O., 2015. Preliminary study of venus cloud layers with polarimetric data from spicav/vex. Planetary and Space Science 113114 (0), 159 – 168, sI:Exploration of Venus.

[5] Markiewicz, W., Petrova, E., Shalygina, O., Almeida, M., Titov, D., Limaye, S., Ignatiev, N., Roatsch, T., Matz, K., 2014. Glory on Venus cloud tops and the unknown UV absorber. Icarus 234, 200–203.

[6] de Rooij, W. A., van der Stap, C. C. A. H., Feb. 1984. Expansion of Mie scattering matrices in generalized spherical functions. A&A131, 237–248.

[7] de Haan, J. F., Bosma, P. B., Hovenier, J. W., Sep. 1987. The adding method for multiple scattering calculations of polarized light. A&A183, 371–391.

[8] Knibbe, W. J. J., de Haan, J. F., Hovenier, J. W., Travis, L. D., Apr. 1998. Analysis of temporal variations of the polarization of Venus observed by Pioneer Venus Orbiter. J. Geophys. Res.103, 8557–8574.

THE SUBIONOSPHERIC MAGNETIC FIELD OBSERVED BY VENUS EXPRESS: IMPLICATIONS FOR SOUNDING.

C.T. Russell, *Earth Planetary and Space Sciences, University of California, Los Angeles, CA, USA (ctrussell@igpp.ucla.edu)*, **T.L. Zhang**, *Austrian Academy of Sciences, Graz, Austria*, **M.N. Villarreal**, *Earth Planetary and Space Sciences, University of California, Los Angeles, CA, USA*, **J.G. Luhmann**, *Space Sciences Laboratory, University of California, Berkeley, CA, USA*, **P.J. Chi**, *Earth Planetary and Space Sciences, University of California, Los Angeles, CA, USA*, **S.D. Xiao**, *Austrian Academy of Sciences, Graz, Austria*, **W. Baumjohann**, *Austrian Academy of Sciences, Graz, Austria.*

Introduction:

Near the end of its life, the Venus Express spacecraft made a series of low-altitude passes as low as 130 km above the north pole of Venus. It is generally accepted since the Pioneer Venus mid-latitude surveys that Venus has no discernible intrinsic magnetic field. However, when Venus Express dipped below the ionosphere, it saw a steady weak field. This raises questions about the origin of this field and the utilization of the field to sound the planetary interior. In this paper, we examine first the observations and then discuss whether the magnetic field could be used to sound the interior electrical conductivity.

Observations:

Venus Express was inserted into a 24-hour elliptical orbit with periapsis over the north pole in Spring 2006. In late 2014, with the end of mission approaching, it was decided to use the spacecraft itself as an atmospheric probe and drop its periapsis altitude sufficiently low that aerobraking could be achieved. This exercise was successful and it also provided some interesting magnetic measurements at altitudes as low at 129.7 km. Figure 1 shows five passes for the 10 minutes surrounding lowest approach during this period. The top 5 panels show the magnetic field magnitude, and the lines mark the 140-km altitude point. The bottom panel shows the altitude versus time. Our interpretation of these data is that the spacecraft initially and finally is in the Venus ionosphere where the magnetic field is determined by the interaction of the solar wind with the ionosphere. This "induced" magnetic field produces a variable field in the ionosphere. At highest altitudes, the field is very responsive to solar wind conditions, but at low altitudes within the ionosphere, it is very slow to change as the ion-neutral coupling is strong and the time scale for convection long.

The magnetic field at about 150 km altitude can diffuse downward through the bottom of the ionosphere and enter the non-conducting ionosphere below. When that occurs, there no longer can be electric currents bounding the edges of regions of particular magnetization. Further, the speed of magnetic waves becomes the speed of light and the amplitude of waves drops as the velocity increases to preserve the Poynting vector of any electromagnetic waves.

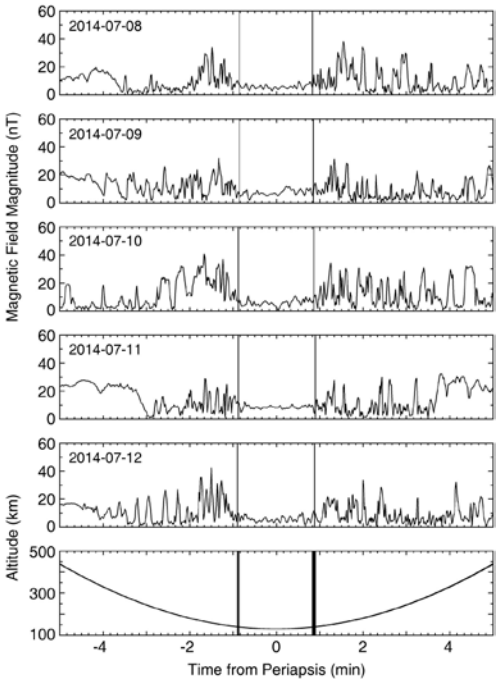

Figure 1. Magnetic field strength as a function of time from periapsis for five consecutive passes during Venus Express aerobraking period. The 10 min data interval is corresponding to an spacecraft trajectory from over 400 km altitude to periapsis around 130 km altitude and back to over 400 km altitude as shown in the lowest panel. Periapsis altitude for these orbits ranged from 129.7 to 130.7 km and solar zenith angle from 93.6° to 95.3°.

We examine this further in Figure 2 that shows 33 individual passes as a function of altitude for a total of 66 traces. Peak magnetic field in the ionosphere at 150-km altitude are as high as 40 nT, but only 10 nT at 130 km. The median magnetic field is shown by the red trace. It varies from 14 T at 150 km to 7 nT at 130 km. Moreover, it becomes much more quiet. Panel b shows the standard deviation of the magnetic from its average

value every 12 seconds. The time-varying field from 5 nT to about 1 nT and the ratio of the time-varying field to the steady field goes from about 35% down to 15%. Not only is the magnetic field weaker at low atlitudes, it is much quieter both absolutely and fractionally.

Electromagnetic Sounding: The existence of fluctuating fields at low altitudes introduces the possibility of sounding the crust electromagnetically. However, the weakness of the fluctuations means that this must be done close to the surface and not at altitudes such as from a balloon or airplane. One promising possibility was raised by Villarreal et al. (2015) that the steady state component itself could serve as the inducing field and that the spatial pattern of the induced field could be used to sound the size of the core. This is illustrated in Figure 3.

References: Villarreal M.N. et al. (2015) *JGR, 120,* 2232-2240.

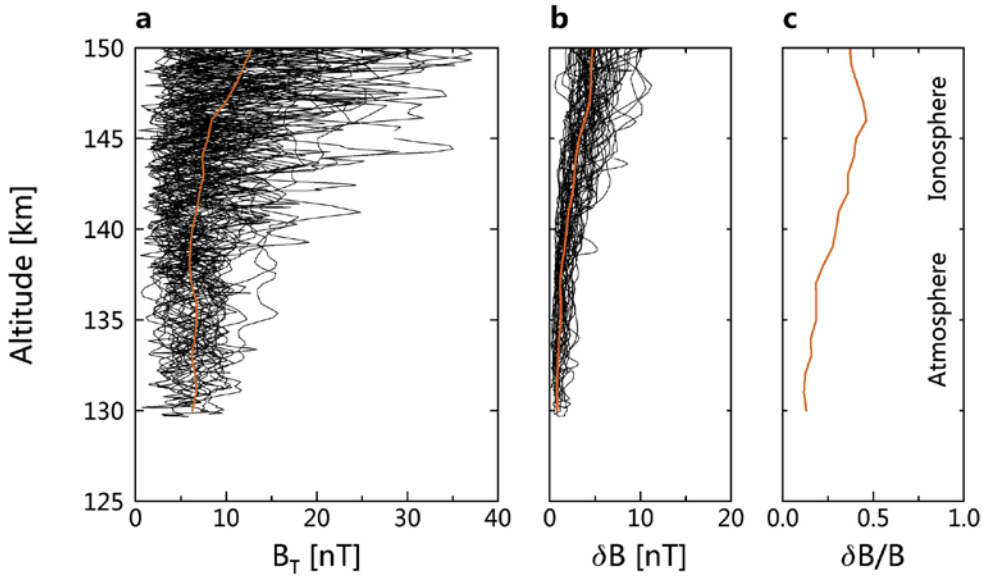

Figure 2. Altitude profiles of magnetic field strength (panel a) and fluctuation amplitude (panel b) and their ratio (panel c). Sixty-six profiles from 33 passes during June 6 to July 12, 2014, when the Venus Express periapsis altitude was below 150 km, are displayed. The field strength data shown in left panel is 1 second resolution and the magnetic field fluctuation δB is indicated as the standard deviation of the field in 12 second bin. The red lines in panels a) and b) are medians. The red line in panel c) is the ratio of these medians.

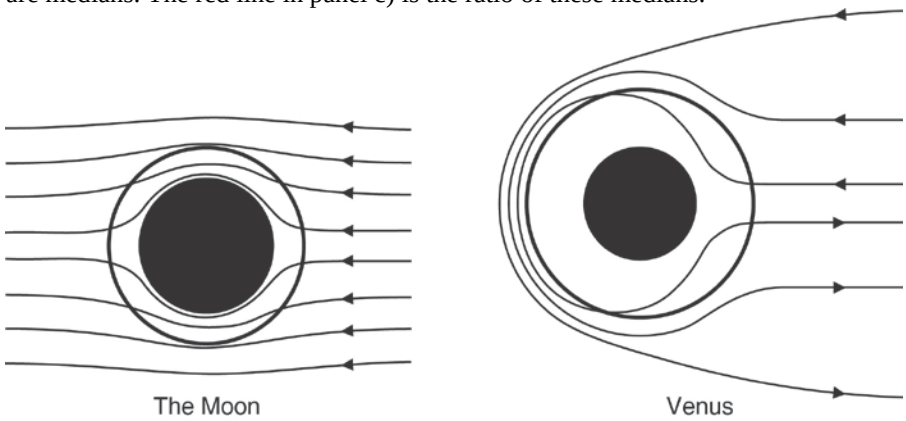

Figure 3. For sounding the highly conducting core of Venus (or Mars)), the solar wind interaction electric field that penetrates the planetary atmosphere can be used to determine the size of the core. This is analogous to the method used to first determine the size of the lunar core; illustrated on the left.

LIGHTNING OBSERVATIONS AT VENUS: A REVIEW OF THE MEASUREMENTS OVER THE LAST HALF CENTURY.

C.T. Russell, *(UCLA, EPSS, Los Angeles, CA, USA (ctrussell@igpp.ucla.edu)*, **R.A. Hart,** *(UCLA, EPSS, Los Angeles, CA, USA)*, **R.J. Strangeway,** *(UCLA, EPSS, Los Angeles, CA, USA)*,**T.L. Zhang,** *(Austrian Academy of Sciences, Graz, Austria).*

Introduction:

In the second half of the 20th century, an extensive program of Venus exploration was launched by the Soviet Union and by the United States. Both programs searched for and reported successful detections of lightning. Venera 9 found lightning flashes using the visible spectrometer (Fig. 1), and electromagnetic signals using VLF search coils on the Venera 11-14 landers (Fig. 2). The Venera 11-14 signals were interpreted to show that lightning was occurring near 50-km altitude, both near and far from the landing site. Pioneer Venus was sensitive to such signals only in the dark ionosphere and reported electric signals, possibly due to lightning in narrow-band channels at 100 and 700 Hz. The electromagnetic energy flux (Poynting vector) of these signals was almost constant with altitude, indicating that the altitude variation of the electric wave amplitude was due to index of refraction changes (Fig. 3).

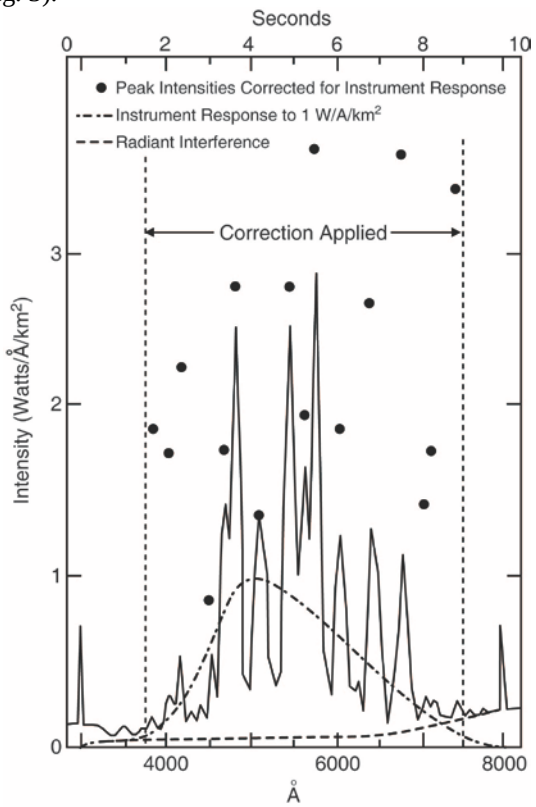

Figure 1. Venera 9 lightning flashes. (Russell, 1993)

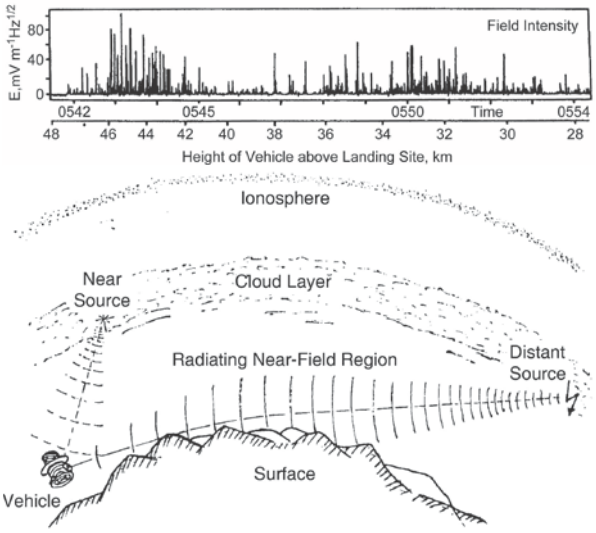

Figure 2. Signals seen onVenera 12 search coils and their interpretation. (Ksanfomaliti et al., 1983)

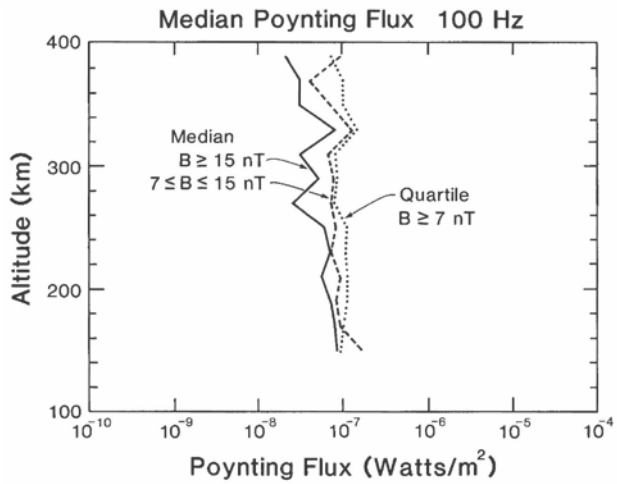

Figure 3. Median Poynting flux as a function of height. (Russell et al., 1989)

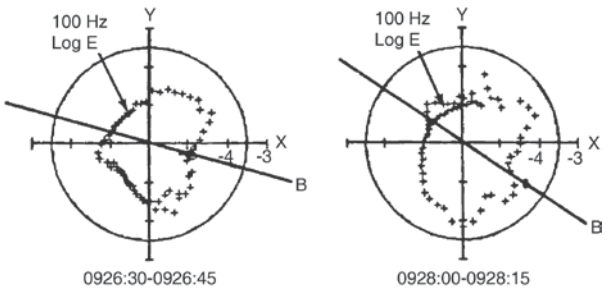

Figure 4. Wave amplitude versus rotation angle showing that the maximum signal occurred perpendicular to the magnetic field consistent with propagation parallel to the field.

The Galileo spacecraft reported radio signals above the ionospheric plasma frequency near 1 MHz that were interpreted as lightning. And lightning flashes were reported from an Earth telescope. Plots of the wave amplitude versus the direction of the magnetic field showed that the waves were transverse to the field and the velocity along the field (Figure 4).

But not all searches were successful. A search for scattered light from lightning with the PVO star sensor was not successful, and a close pass of Cassini by Venus was much quieter than the subsequent close pass by Earth.

In 2006, Venus Express was injected into orbit with low-altitude approaches over the north pole. It carried a dual magnetometer system digitized at 128 samples per second for each magnetometer. The 1-meter separation between sensors allowed the varying magnetic field fo the spacecraft to be removed, and the ambient signals to be detected. The properties of the resulting detected ELF signals showed that the waves were right-handed electron magnetic waves of the type expected to be generated by atmospheric signals propagating through the ionosphere (Fig. 5).

In this review, we summarize the properties of these waves and where and how often they are observed.

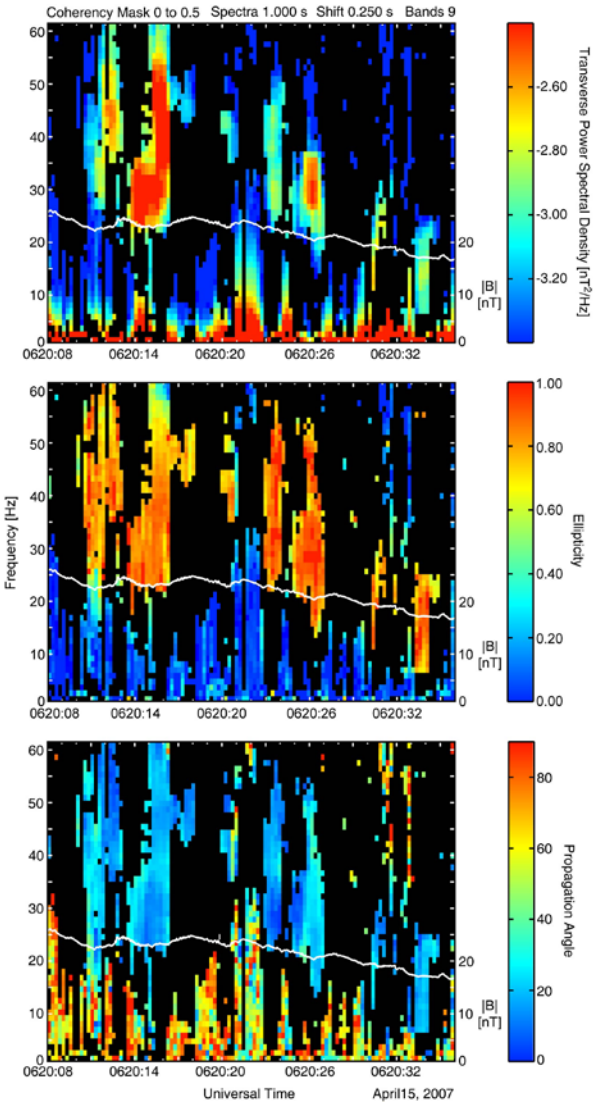

Figure 5. (Top) Transverse power of waves seen by VEX on April 15, 2007. (Middle) Ellipticity. Red is right-handed. (Bottom) Propagation angle. Blue is along the field. White line shows magnetic field magnitude. (Russell et al., 2013)

References:

Ksanfomaliti, L. V. (1983). Electrical activity of the atmosphere of Venus. I. Measurements on descending probes, *Kosmich. Issled.* 21: 279-296.

Russell, C. T., et al. (1989). VLF bursts in the night ionosphere of Venus: Estimates of the Poynting flux, *Geophys. Res. Lett.* 16(6): 579-582.

Russell, C. T. (1993). Planetary lightning, *Annu. Rev. Earth Planet. Sci.*, 21: 43-87.

Russell, C.T., H. Leinweber, T. L. Zhang, J. T. M. Daniels, R. J. Strangeway and H. Wei (2013). Electromagnetic waves observed on a flight over a Venus electrical storm, *Geophys. Res. Lett.*, 40(1): 216-220.

VENUS CLOUD MORPHOLOGY AND MOTIONS FROM LONG-TERM GROUND-BASED OBSERVATIONS (*)

A. Sánchez-Lavega, *Universidad País Vasco UPV-EHU, Bilbao, Spain (agustin.sanchez@ehu.eus)*, **R. Hueso, S. Pérez-Hoyos**, **I. Mendikoa**, **J. F. Rojas**, *Universidad País Vasco UPV-EHU, Bilbao, Spain*, **J. Peralta**, *Japan Aerospace Exploration Agency, Japan*

Introduction

Venus shows a spatially and temporally variable cloud morphology allowing to track the winds and wave motions as shown by the detailed images obtained by the different missions to the planet since 1974 (Mariner 10, Pioneer-Venus, Galileo and Venus Express) [1-6]. However, reported ground-based images of the Venus clouds are in general scarce in time. They mostly concentrate in short periods due to the intrinsic difficulties of observing the planet from the ground. Since Venus is an inner planet, its orbital position relative to the Sun and Earth (the phase angle) restricts the visibility of the illuminated part of the disk whose size varies from 64.5 arcsec (inferior conjunction, full night side) to 9.9 arcsec (superior conjunction, full dayside illuminated disk) [7]. Most important are the angular separation between the Sun and Venus in the sky, that reaches a maximum elongation ~ 48°, and its altitude above the horizon. These two angles impose serious security constraints to observe the planet from large telescopes in most observatories. Taking together, these conditions limit the observing periods to 2-3 months around elongations, when Venus reaches a size of ~ 37 arcsec and is half illuminated both for imaging of the day-side and night-side parts of the planet [7].

However, this is not typically the case for amateur astronomers or in the case of employing small telescopes whose observing limits of proximity to the Sun are not so strict. Moreover, the introduction among the amateurs of high resolution planetary imaging methods using the "lucky imaging" technique [8], allows monitoring Venus's clouds with small telescopes in the optical range (wavelengths from 0.38-1 micron) during practically its whole orbit. Therefore, long term evolution of the clouds and their motions at the two spectral ranges where they show enough contrast, i.e. ~ 0.4 μm (UV) and 0.95 μm (NIR), can be currently reached with the regular participation of well equipped observers. The Venus Amateur Observing Project (VAOP) coordinate by ESA was launched in 2007, and is one of such initiatives (http://sci.esa.int/VAOP) [9]. Here we first report an initial study of the cloud morphology and motions from 2007 to 2015 based on images from dedicated observers [10].

We complement the present study reporting on the first images of Venus obtained with our new high resolution camera *PlanetCam UPV-EHU* [11] that works simultaneously in the visible (0.38-1 μm) and the SWIR (1-1.7 μm) channels and that allows observations in the "lucky imaging" mode using short exposure times and accumulation of several thousand frames even using narrow band filters [11].

Data and methods

For the long-term study of the cloud morphology and motions we used Venus images downloaded from two public databases:

(1) ALPO Japan (http://alpo-j.asahikawa-med.ac.jp/Latest/Venus.htm)

(2) Venus Amateur Observing Project (VAOP), ESA web address (http://sci.esa.int/VAOP).

We covered the period 2007 – 2015. The selected images were obtained in two main spectral ranges UV (350-400 nm) and NIR (950-980 nm) sensitive to two altitude levels within the upper cloud layer [3]. The images are navigated using the WinJUPOS free software [12]. We use the system 2 longitude for Venus that corresponds to the approximate rotation period of the atmosphere (4 days). Thus cloud features are quasi-stationary in this system. The navigation allows determining the longitude and latitude of any feature on the disk.

On the other hand, the *PlanetCam* images were obtained in three observing runs in 2014 and 2015 using the 2.2 m telescope at Calar Alto Observatory in Spain. They were processed with our own pipeline for quality selection and re-centering of the image series to construct the final scientific image. The images are calibrated in absolute reflectivity *I/F* using standard stars.

Results

Observing Venus from Earth implies that only features between latitudes from ~ 60°N to 60°S are accessible to measurements. In Figure 1 we present an example of a full map of the Venus clouds in 2007 from UV images. The image composition from several days using system 2 longitudes (where clouds are approximately at rest) allows to make visible the major features on Venus clouds. In particular the planetary-scale Y structure is clearly seen [13].

In Figure 2 we show a wind velocity profile derived from UV images obtained in 2007 and 2012. We tracked the major cloud elements along few days (typically between 1 and 10-15 days) yielding

velocity errors (~ ± 5 m/s) at the resolution from ground (~ 500 km). These errors are smaller when compared with the error velocities obtained from individual tracer measurements on high resolution spacecraft images (~ ± 15 m/s) whose temporal separation is typically < 1 hr. However the major source of velocity error on ground-based images comes from the identification of the tracers themselves and their size and pointing.

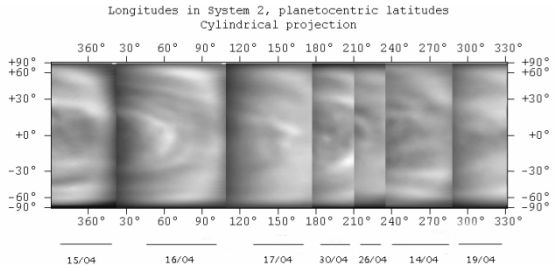

Figure 1. Cylindrical map projection of Venus composed from ground-based images in the UV obtained in April 2007.

As we can see in Figure 2 there are large differences between the plotted profiles corresponding to a large period (1974-2015) [1-6]. The ground-based profile for 2007 and 2012 fall in between the spacecraft profiles but its shape differs from the latitudinal flat behavior shown in the spacecraft data. The large differences between profiles shows the importance of doing a continuous monitoring of the winds in order to look, for example, for a relationship between speed and cloud morphology and their spatial periodicities. This should allow us to discern between atmospheric mass flow and wave displacements.

As a final result we show in Figure 3 a set of images obtained recently with *PlanetCam UPV-EHU* near simultaneously at wavelengths from 0.38 to 1.7 μm. When comparing the cloud morphology at the selected wavelengths it becomes evident that we are sensing different altitudes in the atmosphere. The images are being analyzed in terms of absolute reflectivity calibration in order to fix the sounding cloud levels in the atmosphere.

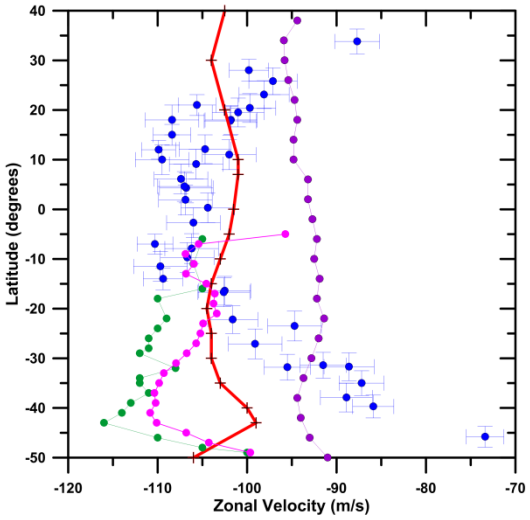

Figure 2. The zonal wind velocity profile from ground-based images in 2007 and 2012 (blue dots with error bars). For comparison we show the profiles from images from Pioneer-Venus OCPP (violet, [1]), Galileo NIMS (red, [2]) and Venus Express VIRTIS (green and magenta, [3-5]). The spacecraft wind data have a typical uncertainty of ± 15 m/s.

Future research

Ongoing research includes the reanalysis of 2007-2012 datasets and new wind measurements of the 2014-2015 observing campaigns, both for the UV and NIR spectral ranges. We want also to perform a photometric calibration and radiative transfer modeling of the *PlanetCam* images at selected wavelengths in the range 0.38-1.7 μm. In addition we are currently installing a Meade 14" (36 cm) at Calar Alto Observatory equipped with "lucky imaging" cameras and different magnifications for the optical range that will be remotely controlled from our University (~ 1,000 km away). This telescope will be dedicated to monitor the Solar System planets and Venus will be one of its main targets, allowing us to observe without the severe restrictions imposed to major telescopes, as described above. We hope these observations also serve as a support to the Japanese JAXA mission currently in orbit around Venus.

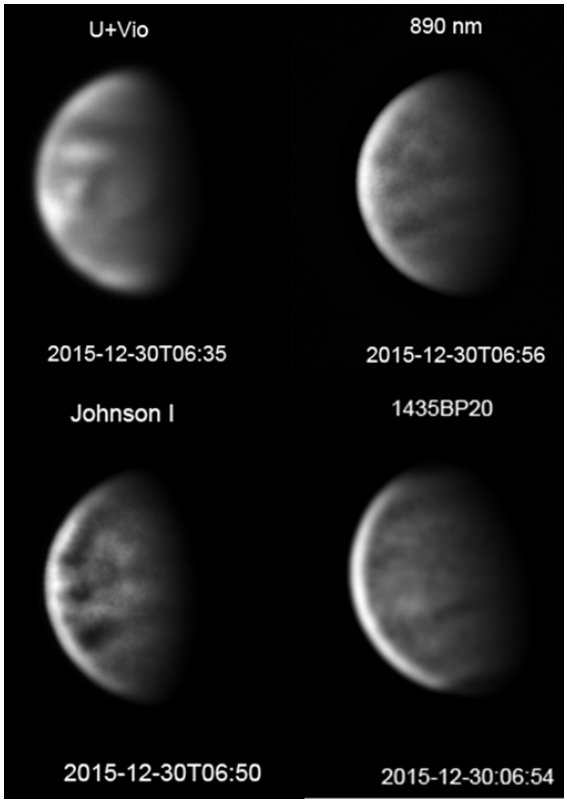

Figure 3. Images from PlanetCam UPV-EHU obtained the 30th December 2015 with the 2.2 m telescope at Calar Alto Observatory (CAHA, Spain). The wavelengths corresponding to the filter nomenclature are approximately: 380-410 nm (U+Vio), 890 nm (methane absorption band), 725-950 nm (Johnson I), 1.435 μm (CO_2 absorption band).

Acknowledgements

This work was supported by the Spanish MICIIN project AYA2012-36666 with FEDER support, Grupos Gobierno Vasco IT-765-13, UPV/EHU UFI11/55 and Infraestructura grants from G. Vasco and UPV/EHU. We thank the long observing efforts of many outstanding amateur observers that provided a large part of the observations here analyzed.

References

[1] S. S. Limaye, Venus Atmospheric Circulation: Known and Unknown, J. Geophys. Res. 112, E04S09 (2007)

[2] J. Peralta, R. Hueso, A. Sánchez-Lavega, A reanalysis of Venus winds at two cloud levels from Galileo SSI images, Icarus 190, 469-477 (2007)

[3] A. Sánchez-Lavega, et al., Variable winds on Venus mapped in three dimensions, Geophys. Res. Lett., 35, L13204 (2008)

[4] R. Hueso, J. Peralta, A. Sánchez-Lavega, Assessing the Long-Term Variability of Venus Winds at Cloud Level from VRTIS-Venus Express, Icarus 217, 585-598 (2012)

[5] R. Hueso et al.,Six years of Venus winds at the upper cloud level from UV, visible and near infrared observations from VIRTIS on Venus Express, Planet. Space Sci., 113-114, 78-99 **(**2015)

[6] I.V. Khatuntsev et al.,Cloud level winds from the Venus Express Monitoring Camera imaging, Icarus 226, 140-158 (2013)

[7] L. Colin, Basic facts about Venus, in *Venus I*, eds. D. M. Hunten, L. Colin, T. M. Donahue, V. I. Moroz, (University of Arizona Press, Tucson, 1983) pp. 10-26.

[8] O. Mousis et al., Instrumental methods for professional and amateur collaborations in planetary astronomy, Exp. Astron., 38, 91-191 (2014)

[9] G. Barentsen and D. Koschny, The Venus ground-based image Active Archive: A database of amateur observations of Venus in ultraviolet and infrared light, Planet. Space Sci., 56, 1444-14449 (2008).

[10] A. Fernández Roiz, Morfología de las nubes y medida de vientos en Venus a partir de imágenes obtenidas con telescopios en Tierra, Ms. Thesis, Universidad del País Vasco UPV-EHU (2014).

[11] I. Mendikoa et al., "PlanetCam UPV/EHU: A two channel lucky imaging camera for Solar System studies in the spectral range 0.38-1.7 μm", Publ. Astron. Soc. Pacific (in the press, 2016).

[12] Grischa Hahn, WinJUPOS, http://www.grischa-hahn.homepage.t-online.de/astro/index.htm (2016)

[13] J. Peralta et al., "Venus's major cloud feature as an equatorially-trapped wave distorted by the wind", Geophys. Res. Lett., 42, 705-711 (2015)

(*) Based in part on images retrieved from ALPO Japan and VAOP public databases

OBSERVATIONS OF VENUS MESOSPHERIC HDO WITH THE JAMES CLERK MAXWELL TELESCOPE (JCMT): IMPLICATIONS FOR H_2O TEMPORAL VARIATION.

B. J. Sandor, R. T. Clancy, *Space Science Institute, Boulder, CO, USA (sandor@spacescience.org)*.

Introduction

Sixty submm spectroscopic observations of Venus mesospheric HDO were made in the eleven year period 2005-2015 with the James Clerk Maxwell Telescope (JCMT), located on Mauna Kea, Hawaii. Observations were of the 335.3955 GHz (primarily) and 225.8967 GHz transitions. HDO is seen as an absorption feature, corresponding to spectrally resolved absorption in the (colder) Venus mesosphere (70-100 km) from the spectrally featureless blackbody continuum emission of the (hotter) deep atmosphere. HDO abundance is retrieved based upon fractional (percent) absorption at the HDO transition frequency from the blackbody continuum. Shape of the pressure-broadened absorption line supports retrieval of the HDO vertical distribution within the 70-100 km range with altitude resolution 10 to 30 km (depending upon s/n of the observation). These 2005-2015 observations extend the previously reported [1] 1998-2004 submm HDO measurements.

Discussion

The motivation for ground-based submm measurements of HDO is that HDO can be used as a proxy for water (H_2O) abundance in the Venus mesosphere, and the much larger HDO/H_2O ratio in the Venus vs terrestrial atmosphere supports significantly greater sensitivity to HDO spectroscopic transitions than to those of H_2O. For a fixed HDO/H_2O ratio in the Venus mesosphere, H_2O abundance is connected to the measured HDO by a simple scaling factor. While there is controversy regarding the best value of the Venus HDO/H_2O ratio [2, 3, 4], time variation of measured HDO in combination with any time-invariant ratio directly corresponds to time variation of total water. Any temporal variation of the HDO/H_2O ratio would be much smaller than observed variation of HDO, contributing a small, quantifiable source of uncertainty to inferrence of water abundance behavior.

The unique value of these ground-based submm observations is two-fold. First, they constitute an 18-year record of HDO (H_2O) abundances determined with a single measurement system. Second, these measurements are essentially global, owing to the coarse (14 arcsec at best) spatial resolution of the data. HDO and H_2O abundances at 70-100 km altitude have been measured at much higher spatial resolution with Venus Express (VEX) instruments [e.g. 3], data which are themselves uniquely valuable for that reason. However each VEX observation is of a spatially discrete location (local time and latitude), such that distinguishing spatial variation from any global temporal variability with VEX data alone is challenging. In contrast, each JCMT measurement characterizes global abundance at the time it was made. Ground-based observations are thus complimentary with those obtained from a Venus-orbiting platform. The one caveat to JCMT's characterization of global conditions is that the ground-based data have very little weighting poleward of 50° latitude, and none at all poleward of 70°. Whether the global context provided by JCMT is appropriate for interpretation (or comparison) with VEX measurements made within the Venus polar vortex is therefore uncertain.

Analysis to date indicates factor-of-20 temporal variation of HDO within the period 2005-2015, with a range of abundances similar to that observed in 1998-2004 [1]. For a Venus D/H ratio 157x greater than the terrestrial ratio [2] the JCMT HDO data indicate H_2O abundances ranging from 0.13±0.02 ppm to 2.6±0.3 ppm. For Venus D/H ratios 240x [3] or 95x [4] the terrestrial value, interpreted Venus water abundances would be smaller or larger (respectively), but the time variation of water is 20x for any assumed (time invariant) D/H ratio. Largest 2005-2015 HDO abundances were observed in 2010. A detailed time series analysis will be presented.

References

[1] Sandor, B. J. and R. T. Clancy. *Icarus* **117,** 129-143. 2005.
[2] Bjoraker, G. L., et al. *BAAS* **24,** p995. 1992.
[3] Fedorova, A., et al. *J. Geophys. Res.* **113,** E00822. 2008.
[4] Krasnopolsky, V. A. *Icarus* **224,** 57-65. 2013.

Mid-infrared spectroscopy of Venus obtained by Subaru/COMICS

T.M. Sato, *Institute of Space and Astronautical Science, Japan Aerospace Exploration Agency, Kanagawa, Japan (takao@stp.isas.jaxa.jp)*, **T. Satoh**, *Institute of Space and Astronautical Science, Japan Aerospace Exploration Agency, Kanagawa, Japan*, **H. Sagawa**, *Kyoto Sangyo University, Kyoto, Japan*, **A. Yamazaki**, *Institute of Space and Astronautical Science, Japan Aerospace Exploration Agency, Kanagawa, Japan*, **T. Kouyama**, *National Institute of Advanced Industrial Science and Technology, Ibaraki, Japan*, **T. Imamura**, *Institute of Space and Astronautical Science, Japan Aerospace Exploration Agency, Kanagawa, Japan*

Introduction:

Venus is completely shrouded by a curtain of dense clouds (50-70 km) with total optical thickness of 20-40 at visible wavelengths. The upper sulfuric acid (H_2SO_4) clouds reflect ~76% of the incident solar radiation back to space [1]. Approximately 50% of the solar energy absorbed by Venus is deposited at altitudes higher than 64 km mainly due to unknown UV absorber mixed in the upper clouds [2]. The resultant solar heating in the cloud layer excites thermal tides, which may play key roles in the maintenance of the atmospheric super-rotation [3]. The mid-infrared images obtained by the Cooled Mid-Infrared Camera and Spectrometer (COMICS) mounted on Subaru Telescope provided several important findings in the cloud top altitudes (~70 km), such as the possibility of the synchronization in brightness temperatures between the northern and southern hemispheres, and temporally variable small-amplitude patterns in the entire disk [4]. In this conference, we will show the mid-infrared spectra of Venus obtained by Subaru/COMICS and primitive results of atmospheric parameters retrieved from the observed spectra with an inversion technique [5].

Observations:

A ground-based spectroscopy of Venus was carried out at the solar phase angle of ~90˚, with the morning terminator in view, with Subaru/COMICS on October 29, 2007 (UT). The entire N-band (8-13 μm) spectra were obtained with a spectral resolving power of R ~ 250, which is equivalent to that of the Fourier Spectrometer onboard Venera 15 [6]. The slit, which was sufficient to capture the northern and southern limbs of Venus (angular diameter ~25 arcsec), was set to be parallel to the central meridian of Venus just off the nightside limb and Venus was scanned toward the dayside limb. The observed thermal radiation in this wavelength coverage is sensitive to altitudes ~65-70 km.

Results:

Slit-scan images were made from a total of 78 spectra. Figure 1 is a slit scan image at 8.663 μm. Polar hot spots and cold collars in both hemispheres are clearly seen and day-night asymmetry is also found from this slit-scan image, which are consistent with the characteristics of snapshots at 8.66 μm taken by imaging observations on the same date [4]. Figure 2 is examples of spectra obtained at the equatorial region and the southern cold collar indicated by circles in Figure 1. The spectra near 9.6 μm are unavailable due to the contamination of ozone (O_3) in the Earth's atmosphere even after the careful data reduction. There are two identifiable carbon dioxide (CO_2) bands (12.1 and 12.7 μm). For both bands, the spectral features appear in absorption for the equatorial region and in emission for the southern cold collar. This qualitative characteristic is consistent with our knowledge obtained from Venera 15 [6]. Such information as well as overall spectral shape is useful to retrieve atmospheric parameters, for example, cloud top temperature, cloud top altitude, and cloud scale height.

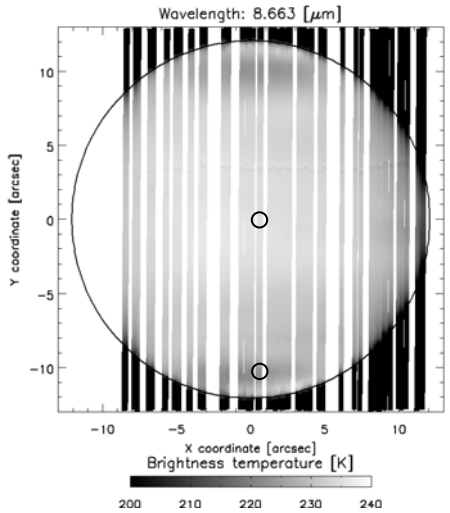

Figure 1. Slit scan image at 8.663 μm.

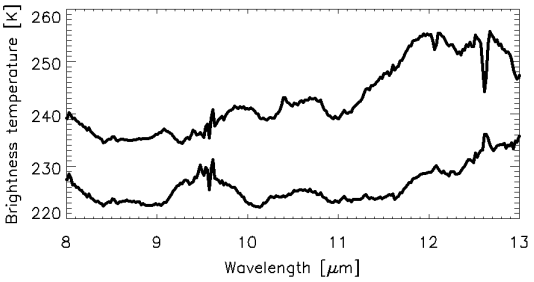

Figure 2. Examples of the spectra obtained at the equatorial region (top) and the southern cold collar (bottom) indicated by circles in Figure 1.

Summary:

We present the ground-based mid-infrared spectroscopy of Venus obtained by Subaru/COMICS. The spectral features are generally consistent with those by the measurements of Venera 15. The atmospheric parameters will be retrieved from the observed spectra with an inversion technique [5] and a radiative transfer model used in [4].

Acknowledgments:

This study is based on data collected at Subaru Telescope and obtained from the SMOKA, which is operated by the Astronomy Data Center, National Astronomical Observatory of Japan. T.M. Sato is supported by a Grant-in-Aid for the Japan Society for the Promotion of Science (JSPS) Fellows.

Bibliography:

[1] Crisp, D. and Titov, D.: The thermal balance of the Venus atmosphere, in Venus II, Univ. of Ariz. Press, 1997.

[2] Tomasko, M.G. et al.: Measurements of the flux of sunlight in the atmosphere of Venus, J. Geophys. Res., Vol. 85, pp. 8167-8186, 1980.

[3] Takagi, M., Matsuda, Y.: Effects of thermal tides on the Venus atmospheric superrotation, J. Geophys. Res., Vol. 112, D09112, doi:10.1029/2006JD007901, 2007.

[4] Sato, T.M. et al.: Cloud top structure of Venus revealed by Subaru/COMICS mid-infrared images, Icarus, Vol. 243, pp. 396-399, 2014.

[5] Smith, W.L.: Iterative solution of the radiative transfer equation for the temperature and absorbing gas profile of an atmosphere, Applied Optics, Vol. 9, pp. 1993-1999, 1970.

[6] Moroz, V.I.: Venus spacecraft infrared radiance spectra and some aspects of their interpretation, Applied Optics, Vol. 25, pp. 1710-1719, 1986.

INITIAL SCIENTIFIC RESULTS WITH IR2 ONBOARD AKATSUKI.

T. Satoh , *Institute of Space and Astronautical Science, JAXA, Japan (satoh@stp.isas.jaxa.jp)* , **IR2 Team**, *Japan*.

Introduction:

Japan's Venus Climate Orbiter, Akatsuki, successfully has become an orbiter around Venus on 7 Dec 2015, VOI-R1 (Nakamura et al., submitted to *Earth, Planets, and Space*). Three cameras, UVI, IR1, and LIR were switched on and carried out the first imaging observation soon after the VOI-R1 but IR2 needed more time than these 3 cameras, to achieve the desired cooling of the sensor (< 70 K) and optics (< 190 K). The first in-orbit image of Venus by IR2 was obtained on 11 Dec 2015 at the wavelength of 2.02 μm (**Figure 1**).

About IR2:

IR2 is designed to work in the wavlength region of 1.5 – 2.4 mm as indicated by its name, IR for infrared and 2 for 2-mm region. The available filters on IR2 are 1.65 μm (astronomical H band for the zodiacal light), 1.735 μm (window of CO_2 atmosphere for night-side observations), 2.02 μm (CO2 absorption band for day-side cloud-top altimetry), 2.26 μm (night-side), and 2.32 μm (night-side but in the CO absorption band).

With these passbands, IR2 will allow various studies of Venus atmosphere: dynamics in the middle to lower atmosphere (zonal and meridional circulations, turbulences and eddies) as tracked using the cloud features seen in 1.735 and 2.26 μm; aerosol properties and their spatial and temporal variabilities; cloud-top altimetry by analyzing intensity variations of 2.02-μm images as they are manifestations of different path lengths of reflected sunlight in the strongly-absorbing CO_2 atmosphere; transportation and chemical processes by mapping and tracking the spatially inhomogeneous CO under the main cloud deck, as visualized by differentiating the 2.26- and 2.32-μm image pair.

To best achieve these scientific themes, IR2 was carefully designed and developed (Satoh, et al., submitted to *Earth, Planets, and Space*). The most notable feature is the usage of the one-stage Stirling cycle cryo-cooler and the PtSi CSD/CCD sensor (1M pixels) both of which are manufactured by Japanese companies (the sensor by MELCO and the cryocooler by SHI).

Operation is on-going:

As of this writing, Akatsuki is still in the initial check-out phase and IR2 is under charactrization of its cooling system. As the cooler is affected by the incident heat by the sunlight to the compressor and the cold head, the responses of the system to various space craft attitudes and solar-incident conditions (sometimes hours of long umbra passage) for long and stable operations.

We expect to acquire images of Venus, both day-side and night-side, with IR2 soon after these check-outs and characterizations are done. At the conference, findings and initial results from such data will be presented.

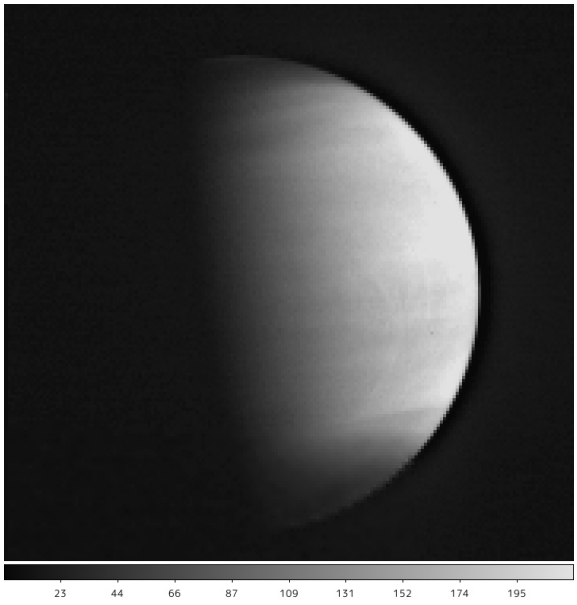

Figure 1: The first 2.02-mm image of Venus acquired with IR2 onboard Akatsuki in orbit. The distance from Venus was about 0.41 million km.

Dynamics and Circulation of the Venus Atmosphere: Expected Contributions of Akatsuki Observations.

G. Schubert, *Department of Earth, Planetary and Space Sciences, (schubert@ucla.edu), University of California, Los Angeles, CA, USA*, **S. Lebonnois,** *Laboratoire de Météorologie Dynamique, Paris, France*, **F. Lefevre, and A. Solzenbach,** *Laboratoire Atmosphères, Milieux, Observations Spatiales, Paris, France*.

New data from the Akatsuki Venus mission will help us better understand the dynamics and circulation of the planet's atmosphere. Comparison of Akatsuki observations with the characteristics of a Venus General Circulation Model (VGCM) will facilitate the interpretation of the observations and provide an assessment of the realism of the VGCM predictions. The Laboratoire de Météorologie Dynamique (LMD) VGCM will be used for this purpose.

Akatsuki will provide very good coverage of cloud-top winds and temperatures in the equatorial region, both on the dayside and nightside. This will put constraints on wave properties and activity at this level that can be compared with previous observations and results from the VGCM and other theoretical studies. Compared to Venus-Express, Akatsuki will give much better coverage of the equatorial regions.

Akatsuki will also provide winds in the lower regions of the cloud on the nightside. This data set will supplement Venus-Express data and give additional temporal coverage of long-term wind variations. The precision of wind retrievals should be better than Venus-Express for the low- to mid-latitude region, with both north and south hemispheres at the same time. The north-south wind will be of specific interest both at cloud-top and in the lower cloud to better constrain the largely unknown meridional circulation.

Monitoring of SO_2 and CO by Akatsuki will also contribute to understanding the circulation and discriminate among proposed explanations for the observed long term variations in SO_2 concentration above the clouds. The LMD VGCM includes a photochemical model that allows study of these distributions in a coupled dynamics/photochemistry analysis.

Akatsuki's images should help constrain the mixing processes going on in the upper cloud near the subsolar point. The Akatsuki observations will supply information on the sizes and shapes of the small-scale cells, their time evolution and their relation to the UV absorber and SO_2 distributions.

EXCITED NITRIC OXIDE EMISSION IN THE ATMOSPHERES OF TERRESTRIAL-LIKE PLANETS

Tom G. Slanger, *Center for Geospace Studies, SRI International, Menlo Park, California, U.S.A. (tom.slanger@sri.com)* and **Konstantinos S. Kalogerakis**, *Center for Geospace Studies, SRI International, Menlo Park, California, U.S.A.*

Abstract

Emission from electronically-excited NO has been observed from all the terrestrial planets, typically from the v′ = 0 progressions of the *C*-*X* and *A*-*X* transitions in the ultraviolet (UV), commonly referred to as the NO δ and γ bands. Figure 1 shows such an example obtained during the Venus Express (VEX) mission [*Gérard et al*., 2008]. The source is two-body recombination of N- and O-atoms, and the two band systems are not independent—NO(*A*) is fed by NO(*C*) *via* the infrared NO(*C*-*A*) 0-0 band at 1.22 μm. This latter emission has been identified by VEX in the Venus nightglow on the shoulder of the much stronger O_2 Infrared Atmospheric 0-0 band at 1.27 μm, as shown in Figure 2 [*Garcia-Muñoz et al*., 2009]. This observation lends encouragement to the idea that the 1.22-μm emission ought to be discernible in the terrestrial nightglow, thereby making it possible to carry out ground-based detection of NO. The three NO systems—*C*-*X*, *A*-*X*, *C*-*A*—are expected to have similar intensities, suggesting that the principal impediment to observing the IR emission is detector sensitivity. Figure 3 shows an example of a laboratory spectrum of the 1.22 μm emission [*Amiot and Verges*, 1982]. In addition to the NO UV bands in the nightglow, a much stronger source of these bands was found in a meteor train from Pioneer Venus data [*Huestis and Slanger*, 1993]. This feature extended for at least 1000 km, and was evidently caused by a grazing meteor. Detection of meteors by NO emission may be a useful technique.

References

Gérard, J.-C., C. Cox, A. Saglam, J.-L. Bertaux, E. Villard, and C. Nehmé, *J. Geophys. Res. Planets*, 113(E5), E00B03 (2008).

Garcia-Muñoz, A., F.P. Mills, G. Piccioni, and P. Drossart, PNAS 106(4), 985-988 (2009).

Amiot, C., and J. Verges, *Physica Scripta* 25(2), 302 (1982).

Huestis, D.L., and T.G. Slanger, *J. Geophys. Res. Planets* 98(E6), 10839-10847 (1993).

Acknowledgment

This material is based, in part, upon work supported by the U.S. National Science Foundation under awards AST-1410297 and AGS-1441896.

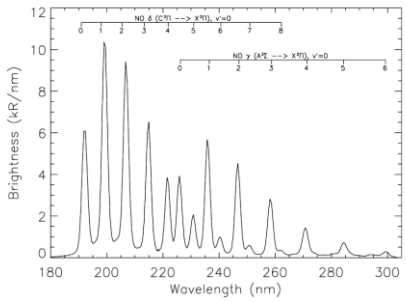

Figure 1. VEX spectrum of NO UV nightglow at 90-120 km (adapted from *Gérard et al*., 2008)

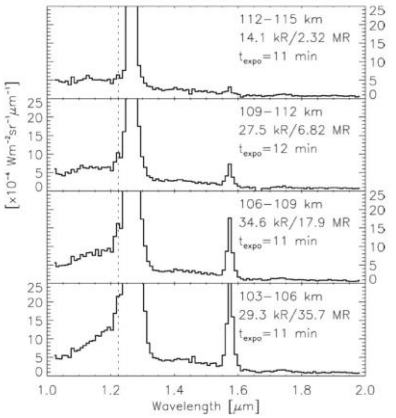

Figure 2. VEX spectrum of the NO 1.22-μm emission (adapted from *Garcia-Muñoz et al*., 2009).

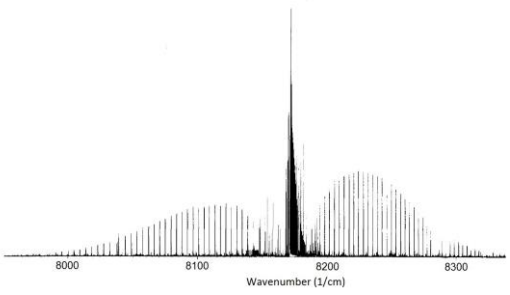

Figure 3. High-resolution laboratory spectrum of the NO 1.22-μm *C*–*A* emission (adapted from *Amiot and Verges*, 1982). The Q branch is the most prominent feature.

VERITAS (VENUS EMISSIVITY, RADIO SCIENCE, INSAR, TOPOGRAPHY AND SPECTROSCOPY): A PROPOSED DISCOVERY MISSION

S. E. Smrekar[1], S. Hensley[1], M.D. Dyar[2], J. Helbert[3], and the VERITAS Science Team, [1]Jet Propulsion Laboratory, Caltech, 4800 Oak Grove Dr., Pasadena, CA 91109, ssmrekar@jpl.nasa.gov; [2]Dept. of Astronomy, Mount Holyoke College, South Hadley, MA 01075; [3]Inst for Planetary Research, DLR, Rutherfordstrasse 2, 12489 Berlin, Germany.

Introduction: VERITAS addresses one of the most fundamental questions in planetary evolution: How Earth-like is Venus? These twin planets diverged down different evolutionary paths, yet Venus may hold lessons for past and future Earth. For example, Venus' hot lithosphere may be a good analog for early Earth, which may limit the development of plate tectonic [1]. Determining the factors that lead to the initiation of plate tectonics would inform our predictions for rocky Earth-sized exoplanets. The conditions leading to Venus' greenhouse atmosphere may also inform our understanding of Earth's future. VERITAS would answer key questions about Venus' geologic evolution, determine what processes are currently active, and search for evidence for past or present water.

Mission Overview: VERITAS accomplishes its 2.4 [Earth] year mission over the course of three Venus rotations, or cycles. The slow rotation of Venus allows data swaths to be acquired sequentially, with overlap from orbit to orbit. Most of the planet will be mapped in cycle 1, with gaps filled in cycles 2 and 3. Cycles 2 and 3 also permit (RPI) pass interferometry for change detection and repeat VEM coverage. VERITAS carries two instruments: 1) Venus Interferometric Synthetic Aperture Radar (VISAR) and 2) Venus Emissivity Mapper (VEM, plus a gravity science investigation.

Payload: The VISAR X-band [2] measurements include: 1) a global digital elevation model (DEM) with 250 m postings, 5 m height accuracy, 2) Synthetic aperture radar (SAR) imaging at 30 m horizontal resolution globally, 3) SAR imaging at 15 m resolution for targeted areas, and 4) surface deformation from RPI at 2 mm precision for targeted, potentially active areas.

VEM [3] will produce surface coverage of ~88% of the surface in six NIR bands located within five atmospheric windows and of eight atmospheric bands for calibration and water vapor measurements.

VERITAS will use Ka-band uplink and downlink to create a global gravity field with 3 mgal accuracy / 145 km resolution (130 spherical harmonic degree and order or d&o) and providing a significantly higher resolution field with much more uniform resolution than that available from Magellan.

Geologic Evolution: VERITAS answers key science questions via: 1) examining the origin of tesserae plateaus -possible continent-like features, 2) assessing the history of volcanism and how it has shaped Venus' young surface, 3) looking for evidence of prior features buried by volcanism, and 4) determining the links between interior convection and surface geology. In particular, VERITAS will examine the stratigraphy and nature of tesserae deformation features, determine the processes modifying impact craters, search for evidence of pre-existing features such as buried impact basins, and determine the origin of tectonic features such as huge arcuate troughs that have been compared to Earth's subduction zones.

Water and Surface Composition: VERITAS looks for the chemical fingerprint of past water in the form of low Fe, high Si rock in the tessera plateaus and larger tesserae inliers, and for present day volcanic outgassing of volatiles in the form of near surface water variability associated with recent or active volcanism. The thick cloud layer on Venus does not allow for classic spectroscopy methods. But the five atmospheric adsorption windows in the CO_2 atmosphere near 1 μm allow the Fe mineralogy to be investigated [3-5]. In comparison, the VIRTIS instrument mapped <50% of the surface using broader spectral windows. To date only one band at 1.02 microns has been successfully reduced over the southern hemisphere. VIRTIS was not designed with surface spectroscopy in mind, whereas VEM is optimized for this purpose [3].

VEM will address key scientific questions by providing a near global map at six spectral bands sensitive to iron mineralogy. This data set can be used to discriminate between weathered and unweathered basalt, search for recent volcanism, and distinguish between different hypotheses for surface weathering processes and products. VEM will also determine if tesserae plateaus have compositions distinct from the plains. Tessera plateaus are proposed to be equivalent to Earth's continents, which may require basalt to be melted in the presence of water to form. VEM will determine if tesserae globally are more felsic or mafic, and thus analogous to continental crust or not.

In addition to surface mineralogy, specific VEM bands are dedicated to detecting near-surface water vapor [3]. Venus Express has found the distribution of water vapor in the atmosphere to be quite uniform. Thus any new near-surface variations are highly like-

ly to indicate outgassing. Observations would be correlated with other indicators of surface change (see below) to provide convincing evidence of present day outgassing. Due to the high surface pressure on Venus, observable outgassing would require significant interior water and thus be an extremely valuable constraint on Venus' overall evolution.

Current Activity: Several studies have found evidence of current or recent volcanism on Venus. [6] used Magellan emissivity data to argue for active volcanism. [7] found bright regions interpreted as active volcanism using Venus Monitoring Camera data. Several studies [8,9] used atmospherically corrected NIR data from the VIRTIS spectrometer to identify regions with iron mineralogy different from typical plains basalt. Regions with high NIR surface emissivity have been interpreted as unweathered and thus geologically recent volcanism [10].

VERITAS uses a variety of approaches to search for present day activity, including 1) tectonic and cm-scale volcanic surface deformation, 2) chemical weathering, 3) thermal emission from recent or active volcanism, 4) topographic or surface roughness changes, and 5) comparisons to past mission data sets including Magellan radar images and Venus Express surface imaging. VERITAS has numerous means of identifying surface activity. VERITAS can compare X-band to Magellan S-band SAR imaging after accounting for look and wavelength differences. This methodology will be validated using Tandem-X X-band and S-band data acquired simultaneously in Iceland. This approach further requires that new features such as lava flows have a different radar backscatter than the pre-existing flows. VEM data at 1.02 μm will also be compared with VIRTIS data acquired at that wavelength. Again, instrument characteristics will need to be accounted for to permit accurate comparisons.

VERITAS can also detect very small changes in surface elevation using targeted RPI. Larger variations, such as new lava flows, could be seen in topography data or surface correlation of radar images. These detection methods are key to obtaining a more global view of surface activity because ~40% of the surface consists of 'featureless' plains – areas where radar backscatter does not reveal specific flows. New flows in these areas might resemble prior flows in backscatter, but could be detected based on their unweathered composition with VEM or as a different elevation or surface correlation with VISAR.

Gravity Science: The Magellan spherical harmonic gravity field was expanded to d&o 180 [11] to ~d&o d&o 100, available only over very limited equatorial regions. The average resolution is only d&o 70. These long wavelengths contain no information on elastic thickness [12]. Similarly methods such as gravity gradiometry are not viable at the average resolution [13]. VERITAS data, with an average resolution of 145 km, will enable estimation of elastic thickness (a proxy for thermal gradient) and resolution of tectonic features indicative of specific processes [13].

Targeting approach: *Imaging.* VERITAS will obtain global imaging at 30 m, and ~23% of the surface at 15m resolution. The high resolution images are limited only by downlink volume. Thus an extended mission would provide an opportunity to obtain extended, possibly global 15 m coverage. Initial targets will be proposed by science team members responsible for assuring each level 1 science objective. This list will be expanded through community input acquired via both workshops and a target suggestion website, similar to that developed for HiRISE images of Mars.

RPI Targeting. This resource is also limited only by data volume, as it requires full resolution data, and by delta-V needed to maneuver into position for the 2nd pass [x]. Thus the initial allocation is for 12 200km × 200 km targets. The exact dimension and number of possible targets will be assessed during Step II. Mission design considerations that could enhance the delta-V budget will be considered. Initial RPI targets will focus on those regions proposed to be currently or recently active based on Venus Express data. These targets will very likely expand as VERITAS discovers active regions using the methods described above.

Conclusions: VERITAS will create a rich data set of high resolution topography, imaging, spectroscopy, and gravity. These co-registered data [x] will be on par with those acquired for Mercury, Mars and the Moon that have revolutionized our understanding of these bodies. VERITAS would be an extremely value asset for future Venus missions, providing a very accurate topography plus surface composition map to optimize targeting of probe or lander missions as well as for later investigations of surface change.

References: [1] Bercovici D. and Y. Richard (2014) *Nature 408*, 513; [2] Hensley S. et al. (2016) VISAR, this meeting. [3] Helbert J. et al. (2016) VEM, this meeting. [4] Dyar M.D. et al. (2016), this meeting. [5] Mueller N. et al. (2016) this meeting. [6] Bondarenko, N.V. and J.W. Head (2004) *JGR 109*, 9004. [7] Shalygin et al. (2012) *PSS 73*, 294. [8] Helbert J. et al. (2008) *GRL 35*, L11201. [9] Mueller, N. et al. (2008) *JGR 113*, E00B17. [10] Smrekar et al. (2010) *Science 328*. [11] Konopliv A. et al. (1999) *Icarus 139*, 3. [13] Wieczorek M. (2007) *Treat. Geophy., 10*, 165. [4] Andrews-Hanna J. et al. (2016) LPSCXLVII.

Acknowledgement: A portion of this research was conducted at the Jet Propulsion Laboratory, California Institute of Technology, under contract with NASA.

A STATISTICAL MODEL OF RELATIVE SURFACE AGE ON VENUS.

S. E. Smrekar, *Jet Propulsion Laboratory, Caltech, Pasadena, USA* (ssmrekar@jpl.nasa.gov). **M. Xie and M.S. Handcock**, *Deptment of Statistics, University of California Los Angeles, CA, USA*.

Introduction:

Interpretation of the crater population on Venus is fundamental to understanding its geologic evolution. The crater population has been used to argue that Venus under goes episodic mobile lid tectonics [e.g. 1], that it has experienced voluminous volcanic outgassing events capable of inducing surface temperature changes of ±100°C [2], and that has had either directional or non-directional geologic events [3,4]. The key to interpreting Venus crater population is the interaction between volcanism, craters, and crater ejecta.

Our objective is to follow up on the work of Phillips and Izenberg [5], who used the removal of the extended ejecta, the fine grained halos and parabolas to investigate resurfacing and relative age. We use spatial point processes to examine halo and parabola removal. Rather than using Monte Carlo methods to simulate volcanism, we compare actual volcano populations and geologic units to the relative age units defined by crater density and halo removal.

Background:

Halo removal and relative age. Impact craters on Venus larger than ~10 km all have fine grained deposits termed halos and parabolas (Fig. 1). The parabolas are all carried downwind to the west by up to ~2000 km. Halos are generally somewhat larger particles with radii of several hundred km. The parabolas cover a much larger area than impact craters, thus making them a indicator of regional resurfacing.

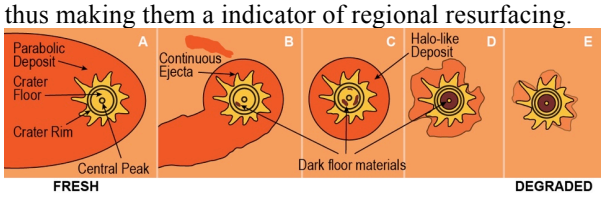

Fig. 1. Impact ejecta degrades from a full parabola, to a halo, to a degraded or absent halo.

Phillips and Izenberg [5] proposed that the combination of crater density (n) and ratio of the number of craters without halos to the total number of craters (p) could be used to infer how parabolas and halos are removed. The hypothesis is that the youngest regions are those that have experienced sufficient volcanism to both fill and thus remove craters as well as halos & parabolas, that old regions have little volcanism but that halos & parabolas are removed via aeolian or chemical weathering. This hypothesis leads to the definitions of relative age regions in Table 1. Rather than the 3 age bins considered by [5] we have 5 bins. Very young differs from young in that the halos have not yet been removed. An additional category has both high n and high p. Such a region might develop if there is little removal of halos via either volcanism or erosion.

Relative age	Crater Density (n)	Ratio of craters w/ halos to total craters (p)
Very Young	Low	High
Young	Low	Low
Intermed.	Average	Average
Old	High	Low
Unmodified	High	High

Table 1. Relative age unit definitions.

Method:

We use 60,000 evenly spaced points over the sphere as the counting centers. For the radius of the counting bins, we try 875, 1750, 4000, 6000 km to assess the relevant size of the geologic unit. The numbers of craters, halos, as well as volcanoes in each circular counting bin are recorded in order to study the relative age.

Data Sets: The data sets we use are: 1) The LPI crater database, 2) the Brown volcano database (http://www.planetary.brown.edu/planetary/databases/venus_cat.html) 3) a corona database (Ellen Stofan, pers. comm.) and 4) the geologic map of Ivanov and Head [6] to determine those craters located on plains units. Roughly 40% of the surface consists of volcanic plains regions where distinct volcanoes cannot be resolved. In this analysis coronae are grouped with volcanoes.

Results:

The density of craters versus the proportion of craters with halos (Fig. 2) forms the basis for the relative age units. Young units have n < ~1.1

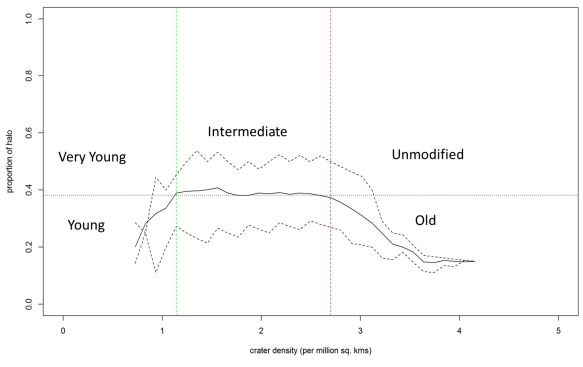

Fig. 2. Total crater density versus the ratio of craters with halos to the total number of craters for a counting region with a radius of 1750 km. Solid line is the mean value within each bin. Dashed lines are the 25th and 75th percentiles.

craters/10^6 km^2, and old units have n> ~2.7 cra-

ters/10^6 km^2. For comparison, we plot volcano density versus crater density (Fig. 3). Figure 4 shows the map distribution of these units.

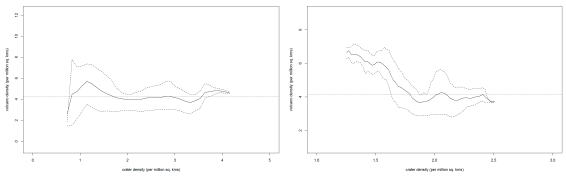

Fig. 3. Density of identified volcanoes (v) versus n.Left:counting radius 1750km; Right: counting radius 4000km.

Discussion & Preliminary Conclusions:

The density of identifiable volcanoes (v) shows is greater at low n, and is somewhat greater at high n, corroborating the hypothesis that volcanic resurfacing is operating to remove halos and craters in those regions identified as young. In 'old' regions, those with high n, volcanism may removing halos in some areas, but not craters. Chemical or aeolian weathering may also be removing halos. This will be investigated further. The role of featureless plains will also be investigated.

Note that these results are sensitive to the radius of the counting region. The shape of the curve in Fig. 2 is only seen for a radius of 1750 km. This radius corresponds to the scale of the parabola deposits. However, volcano density is seen to be larger in regions with lower crater density at all scales, and low to average in regions with high crater density. This is consistent with the role of volcanism as the primary means of lower crater density at all scales, and low to average in regions with high crater density. This is consistent with the role of volcanism as the primary means of removing both craters and their extended ejecta blankets.

Identification of relative age units provides valuable insights into Venusian geology. We note that areas with high emissivity from VIRTIS data are at least partially within young or very young units, supporting the interpretation of these regions as relative young [7]. areas could be used to aid targeting of high resolution imaging, interferometry as proposed for VERITAS [8] and planning landing sites.

References:

[1] Moresi L. and V. Solomatov (1998) *Geophys. J. Int., 133,* 669 [2] Bullock M.A. and D.H. Grinspoon (2001) *Icarus, 150*, 19. [3] Basilevsky A.T. and J.W. Head (1995) *Earth Moon Planets, 66*, 285. [4] Guest J.E. and E.R. Stofan (1999) *Icarus, 139*, 55. [5] Phillips R.J. and N.R. Izenberg (1995) *GRL, 22*, 1517. [6] Ivanov M.A. and J.W. Head (2011) *PSS, 59*, 1159. [7] Smrekar S.E. (2010) *Science, 308*, 605. [8] Smrekar S.E. et al. (2016) *LPS XCVII,* Abstract #2439.

Acknowledgement:

A portion of this research was conducted at the Jet Propulsion Laboratory, California Institute of Technology, under contract with the National Aeronautics and Space Administration.

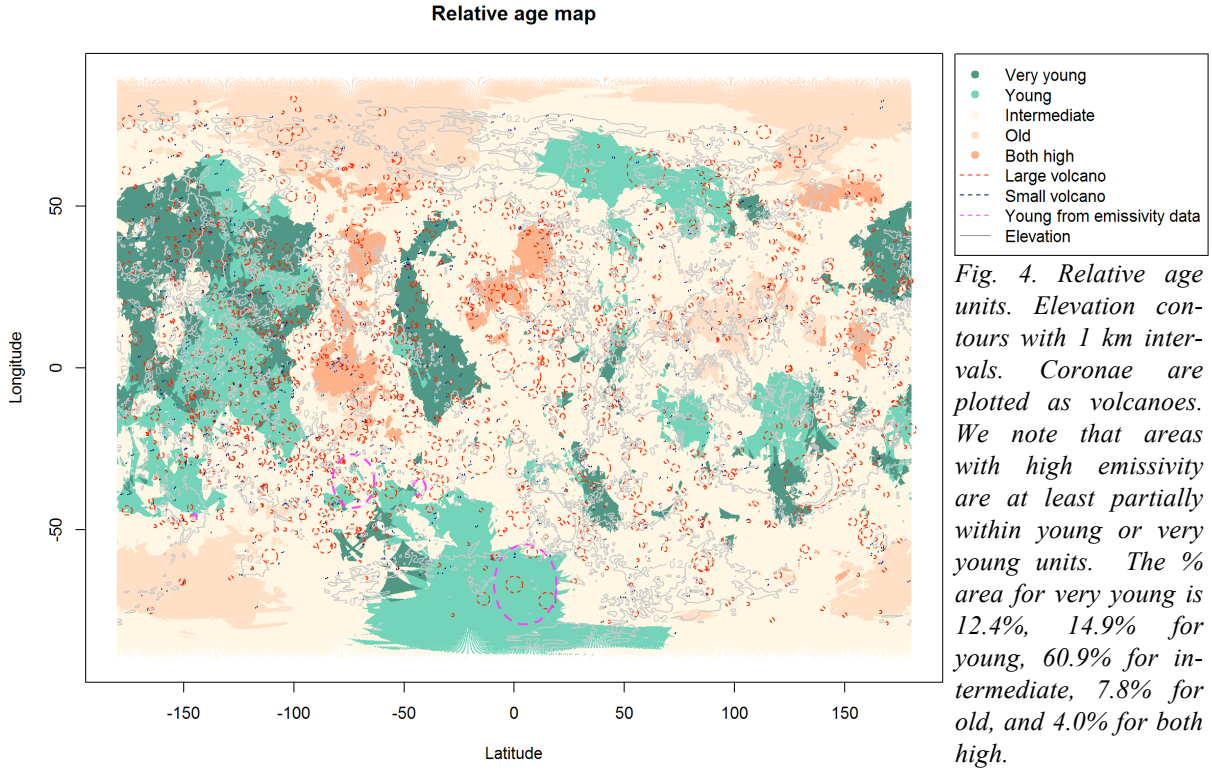

Fig. 4. Relative age units. Elevation contours with 1 km intervals. Coronae are plotted as volcanoes. We note that areas with high emissivity are at least partially within young or very young units. The % area for very young is 12.4%, 14.9% for young, 60.9% for intermediate, 7.8% for old, and 4.0% for both high.

THE $O_2(a^1\Delta)$ VENUS NIGHTGLOW INTENSITY: INTERNAL VERSUS SOLAR ACTIVITY CONTROL

L. Soret, J.-C. Gérard, *LPAP, Université de Liège, Belgium (Lauriane.soret@ulg.ac.be)*

Introduction:

The $O_2(a^1\Delta_g)$ Venus nightglow emission at 1.27 µm occurs in the atmospheric region governed by the subsolar to antisolar circulation. Several studies showed that the intensity of this emission is highly variable on a timescale of hours. Here, we study the possible correlation between the solar flux and the O_2 infrared emission using VIRTIS-VEx spectral images at 1.27 µm that has been predicted to exist by the VTGCM model calculations by Bougher and Borucki (1994).

VIRTIS data:

Using the entire VIRTIS-M-IR nadir database, Soret et al. (2014) generated seven statistical maps of the $O_2(a^1\Delta_g)$ emission, each containing 500 observations. The purpose was to analyze the location of the brightest spot of the emission and its variations over time. Here, we analyze the intensity of the emission over time. Several methods have been used by Soret et al., (2015) to do so (evolution of the emission maximum, evolution of the average intensity, …) Here we present the results of a new analysis using a masking technique to calculate the time evolution of the nightglow brightness. However, none of them follow the same trend over time.

Solar flux data:

We now focus on solar flux variations in the time of VIRTIS observations (between May 2006 and October 2008), which were collected during a deep solar minimum. We use the SOHO-CELIAS/SEM (Judge et al., 1998) EUV daily average full solar disk fluxes at 1 AU between 0.1 and 50 nm available from the Space Sciences Center of the University of Southern California. $EUV_{0.1–50}$ daily average fluxes decrease from 2.6 in May 2006 to 1.9 in October 2008 at the Earth. These values have been adapted to Venus by taking into account the distance from the Sun to the planet, but also the shift in date, considering the difference in solar longitude of the two planets. Values at Venus vary from 4.4 to 3.4, which corresponds to a decrease of 10.4% of the solar flux at Venus compared to a complete solar cycle (ranging from 13.5 to 3.9)

Comparison of VIRTIS and SEM datasets:

The linear correlation coefficient between the solar flux and the intensity peak is found to be 0.62, which expresses the global decreasing trend for both quantities. This coefficient is not higher because internal variations of the two studied variables do not occur simultaneously. More significantly, the correlation coefficient between the solar flux and the averaged intensities is found to be 0.35, meaning that no relation-ship exists between the $O_2(a^1\Delta_g)$ brightness and the solar activity.

Conclusions:

Contrary to the VTGCM calculations, we do not observe here a correlation between the $O_2(a^1\Delta_g)$ brightness and the solar flux. However, VIRTIS data were acquired during a deep solar minimum and, more importantly, during a relatively stable phase of the solar activity. A high level of variability of the $O_2(a^1\Delta_g)$ emission has been detected in the same dataset from day to day though (Hueso et al., 2008; Soret et al., 2014). It thus appears that the variability is more controlled by internal than external conditions: transport appears to play a major role in the nightglow emissions than the solar activity eventually does. This conclusion is at least valid for solar minimum conditions. A space mission with global imaging capabilities over an entire solar cycle would definitely allow determining the relative role played by solar activity and internal factors.

References:

Bougher, S.W., Borucki, W.J., 1994. Venus O_2 visible and IR nightglow: Implications for lower thermosphere dynamics and chemistry. J. Geophys. Res.: Planets(1991–2012) 99 (E2), 3759–377.

Hueso, R. et al., 2008. Morphology and dynamics of Venus oxygen airglow from Venus Express/Visible and Infrared Thermal Imaging Spectrometer observations. J. Geophys. Res. 113.

Soret, L. et al., 2014. Time variations of $O_2(a^1\Delta_g)$ nightglow spots on the Venus nightside and dynamics of the upper mesosphere. Icarus 237, 306–314.

Soret, L. and Gérard, J.-C., 2015. Is the $O_2(a^1\Delta_g)$ Venus nightglow emission controlled by solar activity? Icarus, 262, 170-172.

Experimental setup for the optical characterisation of gases at typical planetary atmospheric conditions

S.Stefani (1), G.Piccioni (1), M.Snels (2) and A.Adriani (1)
(1) IAPS-INAF via Fosso del Cavaliere 100, Rome Italy ,
(2) ISAC-CNR via Fosso del Cavaliere 100, Rome Italy
(Stefania.Stefani@iasp.inaf.it / Fax: +390645488188)

Abstract

An experimental setup employed to study the optical properties of gases at "typical" planetary conditions, in particular CO_2, the principal absorber of the Venus atmosphere, has been developed. Two dedicated gas cells have been integrated with a Fourier Transform InfraRed (FT-IR) spectrometer. The first cell, a High Pressure High Temperature (HP-HT) gas cell, is designed to sustain a pressure up to 200 bar and a temperature up to 570 K with an optical path of about 2 cm. The second cell, a Multi Pass (MP), is a cell with a variable optical path from 2.5 to 30 m, able to work with pressure up to 10 bar and temperature up to 473 K. Another cell, independent from the FT-IR, is designed to sustain a pressure up to 100 bar, presently working at ambient temperature (300 K), and makes use of the Cavity Ring Down (CRD) technique with a tunable laser, able to mimic an optical path of up to 25 km, thus suitable for weak absorptions in thin or dense atmosphere.

1. Introduction

The study of the optical properties of gases at planetary conditions are very important to interpret the remote sensing data, in particular those acquired by the VIRTIS instrument on board VENUS-EXPRESS (G. Piccioni e al Eur. Space Agency Spec. Publ., ESA SP-1295, 2007). For this purpose, we have built up an experimental apparatus which allows us to reproduce similar physical conditions found in the deep atmosphere of Venus. The experimental data obtained are used to update the database for the radiative transfer calculations in order to improve the accuracy of the composition parameters retrieval from remote sensing data analysis.

2. Experimental setup

The HP-HT gas cell, shown in figure 1, allows us to simulate in the lab similar physical conditions found in the deep atmosphere of Venus below the clouds. In this way it is possible to measure the optical properties of CO_2 from 50 down to 16 km of equivalent altitude above the Venus' surface.

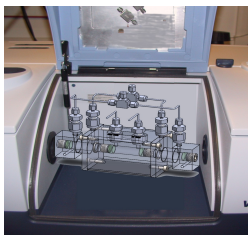

Figure 1: HP-HT gas cell coupled with the FT-R, used to acquire the CO_2 absorption coefficients

This cell, however, characterized by an optical path of 2 cm, is not sufficient to study the weak absorptions. For this reason, we use the Cavity Ring Down (CRD) technique to record precisely the loss rate of the gas and then the absorption coefficients. The cell is shown in figure 2. It is not coupled with the FT-IR but uses dedicated tunable lasers at different wavelengths, allowing to obtain very long absorption path lengths of several tens of km. Thanks to this setup, we have studied in an unprecedented way the 1.18 μm transparency window of Venus' atmosphere.

Figure 2: CRD gas cell employed to study the CO_2 loss rate @ 1.18 μm

Another cell, a Multi Pass (MP), has a variable optical path from 2.5 to 30 m, able to work with gases at a pressure up to 10 bar and temperature up to 473 K (see figure 3).

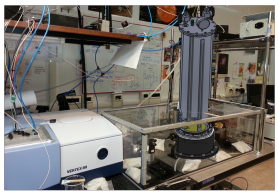

Figure 3: MP gas cell used to acquire the CO_2 CIA bands.

This is suitable to study in more details weak but important absorptions such as the Collision-Induced-Absorption (CIA), line mixing and far wings, particularly relevant for the Venus atmosphere and data interpretation.

2.1 Results and discussions

We reproduced in our HP-HT gas cell the real Venusian physical conditions for CO_2 in a grid from the VIRA profile (Seiff A. Adv. Space Ree. Vol.5, No.11, pp.3-58, 1985). For each point of the grid we measured the absorbance of the gas (JQRST, vol. 117, pp21-28, 2013). Some results are shown in figure 3.

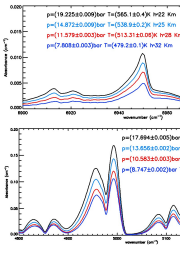

Figure 3: CO_2 absorption coefficients acquired according to the VIRA profile

Using a DFB laser to illuminate the CDR gas cell, we measured the carbon dioxide loss rate in the spectral range from 1179 to 1182 nm, varying the pressure from 1 up to 38 bar and maintaining the temperature constant at 294 K. As shown in figure 4, the attenuation due to CO_2 varies quadratically with the density (Snels M. et al., JQRST, vol. 133, pp. 464-471,2014).

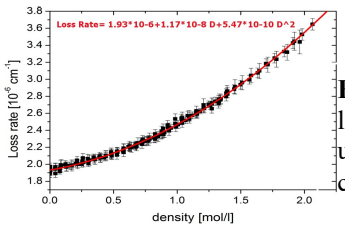

Figure 4: CO_2 loss rate measured using the CRD gas cell

Finally, using the MP gas, we have performed the relevant measurements on the Collisional Induced Absorption bands. The spectra obtained in the spectral range of interest at different pressures and room temperature, are shown in figure 5.

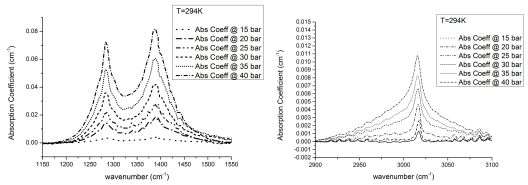

Figure 5: CIA CO_2 bands acquired at different pressures and room temperature.

3. Summary and Conclusions

The CO_2 spectra have been measured for a wide range of temperatures, pressures and for a large spectral range. All data are now available and can been downloaded from: http://exact.iaps.inaf.it. A theoretical model including line mixing effects as well as far wings corrections for the strongest absorption bands reproduces satisfactory the laboratory spectra, for all pressures and temperatures explored so far (H. Tran et al. JQRST vol. 112, 925-936, 2011). First measurements obtained using the innovative design of the Cavity Rind Down technique, have been performed on carbon dioxide in the 1180 nm transparency window of Venus. The quadratic component measured varying the pressure from 38 down to 1 bar is in good agreement with analyses performed by (Bézard B. et al. Journal of Geophysical Research (Planets) vol. 114, pp 12, 2009, Bézard B. et al. Icarus vol.216, Issue 1, pp 173–183, 2011) by using the data acquired by VIRTIS at Venus on NADIR looking geometry. For what concerns the Collisional Induced Absorption (CIA) bands, the band integrated intensity shows a quadratic dependence versus density in the spectral range [1150-1550] cm^{-1} and [2900-3100] cm^{-1} opposed to the absorption by isolated molecules, which follows Beer's law. This behavior suggests an absorption by pairs rather than by individual molecules.

4. Work in progress

In order to extend further the temperature and pressure range, and to overcome some present limitations, we designed a new heatable\coolable cell placed inside a vacuum chamber. With the new cell we plan to develop a setup valid for both FT-IR and CRD techniques, allowing us to measure the optical properties of gases with pressure from 50 down to a few bars and a temperature from -200 up to 250°C.

Acknowledgements

We acknowledge the ASI and INAF support of this research in the framework of the VENUS Express (I/050/10/02), JUICE-MAJIS (2013/056-R.O.), JUNO-JIRAM (2014/050-R.O.) and WOW 2013 contracts.

SOLAR WIND PRECIPITATION - A COMPARISON BETWEEN MARS AND VENUS.

G Stenberg Wieser (*gabriella@irf.se),* **H. Nilsson, Y. Futaana, M. Holmström**, **S. Barabash,** *Swedish Institute of Space Physics, Kiruna, Sweden*.

Introduction:

The induced magnetospheres of Venus and Mars, constitute obstacles to the solar wind flow. Induced currents are set up in the ionosphere and the interplanetary magnetic field lines drape around the planets, forming a magnetic barrier on the dayside and an elongated magnetotail on the nightside. The magnetic barrier is not impermeable; the gyro radii of typical solar wind ions are comparable in size to the thickness of the barrier and some ions gyrate down to the upper atmosphere, where they collide with the atmospheric particles and are captured. The precipitating ions transfer energy, momentum and matter from the solar wind to the upper atmosphere.

Instrumentation:

The plasma instrument packages ASPERA-3 and ASPERA-4 on the two spacecraft Mars Express and Venus Express are very similar and invite to a comparison between the two plasma environments. We used the Ion Mass Analyser (IMA) on both spacecraft to investigate the solar wind precipitation onto the upper atmospheres.

Results:

We estimate the net precipitation of solar wind ions on both planets. Models suggest that an inflow of alpha-particles from the solar wind is necessary to explain the amount of Helium observed in the atmospheres.

We compare the inflow of He^{2+} ions with the estimated escape of He^{+} and conclude that the solar wind contribution is negligible on both planets.

We also compare the characteristics of the precipitation on the two planets. We conclude that on Mars we regularly observe precipitating solar wind ions inside the induced magnetosphere boundary (IMB). The precipitation is clearly guided by the solar wind convection electric field and He^{2+} and H^{+} are seen independently of each other. On Venus precipitation of He^{2+} is only observed close to the IMB and always together with H^{+}. The precipitation events on Venus have no clear correlation with the solar wind electric field.

References:

Diéval et al., J. Geophys. Res., 2012
Diéval et al., Earth Planets Space, 2012
Stenberg et al., Grophys. Res. Lett., 2011
Stenberg et al., Planet. Space Sci., 2015
Stenberg et al., submitted to Geophys. Res. Lett., in revision 2016

ION HEATING FROM WAVE PARTICLE INTERACTION ON VENUS.

G Stenberg Wieser (*gabriella@irf.se), Swedish Institute of Space Physics, Kiruna, Sweden,* **N. Edberg, M. André,** *Swedish Institute of Space Physics, Uppsala, Sweden,* **Y. Futaana**, **S. Barabash,** *Swedish Institute of Space Physics, Kiruna, Sweden*

Introduction:

We are using Venus Express observations of oxygen ions and magnetic fields inside the bowshock of Venus to investigate if waves at the oxygen cyclotron frequency are likely to result in perpendicular ion heating in a similar way to what happens at Earth.

We also compare cases with an undisturbed solar wind with cases when the Venusian induced magnetosphere is hit by a CIR (corotation interaction region) or a CME (coronal mass ejection). The initial results suggest that there is an increased wave activity on the dayside of Venus when the planet is impacted by CIRs and CMEs.

Instrumentation:

We use the Ion Mass Analyzer (IMA), which is part of the sensor package ASPERA-4 on Venus Express, and the magnetometer, MAG on the same spacecraft.

Preliminary results:

Our initial results suggest that

1. The wave activity at a given frequency increases during CME/CIR.
2. The wave frequency at the gyrofrequency sometimes increases and sometimes stays constant.
3. The available wave energy is sufficient to accelerate O^+ ions to 1 keV.

References:

Edberg et al., (2011), Atmospheric erosion of Venus during stormy space weather, *J. Geophys. Res.*, *116*, A09308, doi:10.1029/2011JA016749

TIMELINE AND EVENTS OF THE VENUS EXPRESS MISSION.

H. Svedhem, D. Titov, *ESA/ESTEC, Noordwijk, The Netherlands (H.Svedhem@esa.int)*, **P. Martin, D. Merritt**, E*SA/ESAC, Madrid, Spain*, **A. Williams**, E*SA/ESOC, Darmstadt, Germany*, **C. Wilson**, University of Oxford, *Oxford, UK*.

Introduction:

The Venus Express mission was launched by a Soyuz-Fregat launcher from Baikonur, Kazakhstan, on 9 November 2005 and arrived at Venus and performed a Venus orbit insertion main engine burn on 11 April 2006. After a sequence of orbit control manoeuvres the operational 24 h period, highly elliptical near polar orbit was reached in May 2006. Scientific operations continued until the end of the mission in December 2014, with only short breaks during the solar conjunction periods.

Conditions characterising the mission :

A large number of parameters are defining what observations can be done during the mission and when they are best performed. In the early years of the mission the observations were in general divided in a constant ratio between the different instruments on board, taken into account the respective operational constraints. In the latter phase of the mission more campaign related observations were performed, focussing on a limited number of scientific objectives. Some of these campaigns were performed as joint observations with ground telescopes.

Parameters of importance for the scheduling and prioritisation of observations include (among others): pericentre location and altitude, solar aspect angle, pointing restrictions and data rate. Periodic orbit maintenance (pericentre rising manoeuvres) were required and at times limited the time available for observations. Specific types of observations require specific conditions like Earth occultation for Radio science, and Eclipses for solar occultation measurements and for surface observations. Such Earth occultations and Eclipses occur in seasons of variable duration, distributed in a semi regular pattern during the mission.

Unaccounted events: During the mission a number of unplanned events and equipment failures occurred. After launch during the instrument checkout it was discovered that the turnable mirror of the PFS pointing mechanism did not rotate, resulting in a non-functional instrument. Despite several latter attempts this was never solved. At the arrival at Venus it became obvious that the VMC detector had been partly burned in an irreversible way, by being excessively exposed to the Sun during the cruise to Venus. It was discovered that the S-Band signal of the communication system, which is also used for certain radio science applications, had a loss of about 15dB in the receive and transmit chain. The cryo-cooler of Virtis-M failed in 2008 and of Virtis-H in 2011, leaving only the visible-UV channel operative after this date.

A (limited) number of safe mode transitions of the spacecraft system took place, mostly related to the solid state mass memory, SSMM, primarily during the first years of the mission. This led to interruption of science operations for a number of days each time. Occasionally the Star trackers lost track and orientation was taken over by the inertial navigation system, but with pausing of science operation at these times. The likely cause for this is high energetic radiation due to solar flares.

This presentation will cover the basic timeline of the mission and the unexpected events. Possible causes and resolutions to these events will be discussed as well as the related consequences for the mission and the science at large.

SLOW ROTATING PLANETS WITH DIURNAL CYCLE: A PARAMETER STUDY OF THE ATMOSPHERIC DYNAMICS USING A SIMPLE GCM.

F. Tabataba-Vakili, *Department of Physics, Oxford, UK (fachreddin.tabataba-vakili@physics.ox.ac.uk)*, **P. L. Read,** *Department of Physics, Oxford, UK*.

Introduction

Parameter studies of slow-rotating planets aim to characterise the effect of rotation rate, friction, radiative properties, and other factors to understand the emergence and maintenance of equatorial super-rotation on bodies similar to Venus and Titan. To analyse and compare the dominant contributions to their circulation in the most general way, it is beneficial to study the properties of different circulation regimes with reference to non-dimensional parameter spaces. Recently, Mitchell et al. (2014) have studied the effect of the seasonal response of an idealised planet, finding that strong seasonal forcing can hinder the emergence of equatorial super-rotation due in part to an increased cross-equatorial momen-tum advection.

In the current work, we focus on simulations performed within a large set of parameters that aims to examine the effect of the diurnal cycle on slow rotating bodies. While such studies often do not reach into the peculiar parameter regime of Venus, they aim to shed light on the fundamental dynamical mechanisms that enable equatorial super-rotation.

Model Description and Parameters

For this study we use a hierarchy of simple GCMs with increasing temporal resolution in thermal forcing (i.e. annually averaged, seasonal cycle, diurnal cycle) using a simple 2-band, semi-gray radiation scheme for a terrestrial-style planetary atmosphere. We use the PUMA model a simplified GCM with a pseudo-spectral core developed by the University of Hamburg (Fraedrich et al., 2005).

The following non-dimensional parameters are varied:

- Thermal Rossby number: $\mathcal{R}o = R\Delta_H/(2\Omega a)^2$, where R is the universal gas constant, Δ_H is the relative equator-to-pole potential temperature difference, Ω is the planetary rotation rate, and a is the planetary radius.
- Ekman number: $Ek = (2\Omega\tau_f)^{-1}$, where τ_f is the frictional time-scale of the Rayleigh friction scheme
- Thermal relaxation number: $\mathcal{A}t = 2\Omega\tau_{atm}$, where the atmospheric thermal equilibrium timescale τ_{atm} can be approximated via $p_s c_p/(4(2-\epsilon)\sigma T^3 g)$, where a variation of the surface pressure p_s shows most promise at varying $\mathcal{A}t$.
- Seasonality parameter $\alpha = (\omega\tau_s)^{-1}$, where ω is the angular frequency of the planet's orbit and τ_s is the thermal inertia timescale of the planetary surface.
- Greenhouse Parameter: $\mathcal{G} = \tau_{sw}/\tau_{lw}$, where τ_{sw} and τ_{lw} are short- and long-wave optical depths.

Results

While in many cases the effect of adding diurnal insolation is negligible, in certain cases we find strong prograde equatorial winds when activating the diurnal cycle. Figs. 1 and 2. show one such case. In this case the parameters that vary from their Earth equivalents are the planetary rotation rate with $\Omega = \frac{1}{8}\Omega_E$ and the Greenhouse parameter with $\mathcal{G} = 1$. Figure 1 results in an atmosphere that is expected for these parameters: there is weak equatorial super-rotation in the upper atmosphere and the temperature profile is nearly constant in pressure (due to the enhanced short-wave optical thickness). When the diurnal cycle is activated (see Fig. 2) a nonlinear mechanism enhances the equatorial super-rotation with velocity values of over 100 m/s.

We aim to find the parametric dependence of this lonlinear mechanism within our parameter space and further analyse the evolution of momentum and energy transfer during spin-up and equilibrated phases.

References

K. Fraedrich, E. Kirk, U. Luksch, and F. Lunkeit. The portable university model of the atmosphere (PUMA): Storm track dynamics and low-frequency variability. *Meteorologische Zeitschrift*, 14(6):735–745, 2005.

J. L. Mitchell, G. K. Vallis, and S. F. Potter. Effects of the seasonal cycle on superrotation in planetary atmospheres. *The Astrophysical Journal*, 787(1):23, 2014.

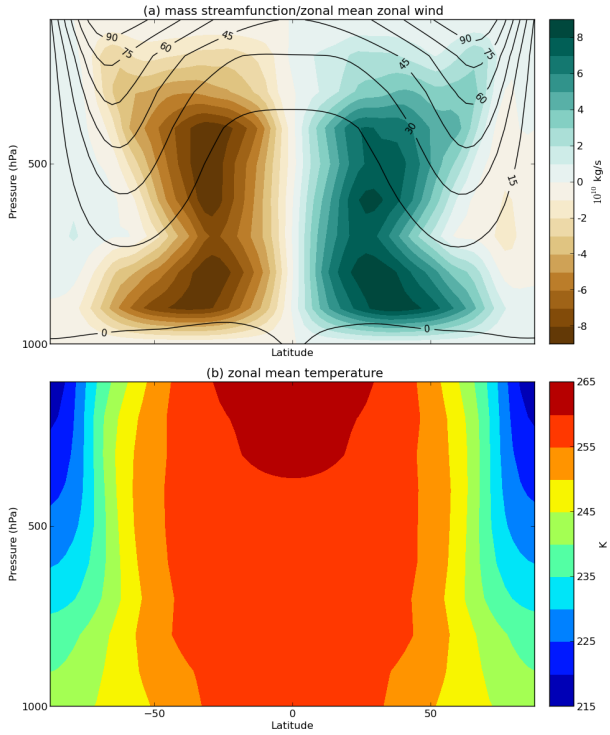

Figure 1: Simularion without diurnal cycle with $\Omega = \frac{1}{8}\Omega_E$, $\tau_s = 360$ days and $\mathcal{G} = 1$ after 10 model years. All other parameters were set to Earth equivalents. The plots show (a) the zonal-mean meridional mass streamfunction (colours) and the zonal-mean zonal wind (contours); and (b) the zonal-mean temperature.

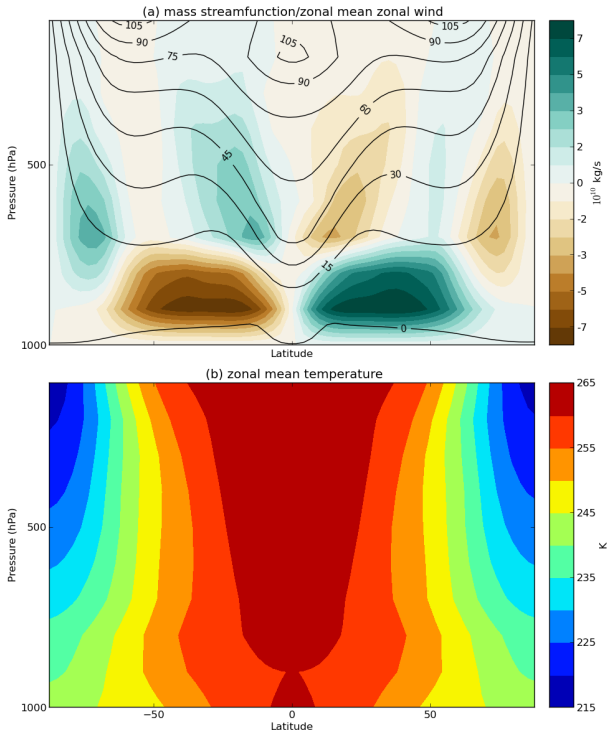

Figure 2: same as Fig. 1, but with diurnal cycle.

INITIAL RESULTS OF THE VENUSIAN CLOUD-TOP TEMPERATURE OBSERVATION BY AKATSUKI/LIR.

M. Taguchi, *Rikkyo University, Tokyo, Japan (taguchi@rikkyo.ac.jp)*, **T. Fukuhara**, *National Institute of Information and Communication Technology*, *Koganei*, *Japan*, **T. Imamura**, **M. Nakamura**, **M. Suzuki**, **T. M. Sato**, *Institute of Space and Astronautical Science, Sagamihara, Japan*, **N. Iwagami**, *University of Tokyo*, *Tokyo*, *Japan*, **M. Ueno**, *Kobe University*, *Kobe*, *Japan*, **G. L. Hashimoto**, *Okayama University*, *Okayama*, *Japan*, **T. Kouyama**, *National Institute of Advanced Industrial Science and Technology*, *Tsukuba*, *Japan*, **S. Takagi**, *Tokai University*, *Hiratsuka*, *Japan*, and **M. Sato**, *Hokkaido University*, *Sapporo, Japan*.

Introduction:

The Longwave Infrared Camera (LIR) onboard Akatsuki took Venus images just after the first challenge in Venus orbit insertion (VOI) in December 2010[1]. They showed several interesting features in the brightness temperature distribution at the cloud top, however, quality and quantity of the data were far insufficient for studies in details. Akatsuki was finally thrown into a Venus orbit at the second attempt at VOI (VOI-R1) in December 2015 after the unwilling five year cruise around the Sun. It had been confirmed before VOI-R1 that LIR as well as the other cameras onboard Akatsuki was still very good in health. Observations of Venus were started immediately after the VOI-R1 operation. More than 20 Venus images in thermal infrared have been acquired by LIR so far, and observations are continuing to accumulate Venus images day by day.

This presentation will introduce initial results of observation of Venus by LIR, and also show a perspective in future studies in the atmospheric dynamics using brightness temperature and wind distributions derived from the LIR data.

Instrumentation:

LIR is a small light-weighted thermal infrared camera using an uncooled micro-bolometer array with 320 x 240 effective pixels as an image sensor, and acquires a snapshot of thermal radiation emitted from the cloud top of Venus in the wavelength region of 8 to 12 μm[2]. The FOV of LIR is designed to fit the full Venus disk to it from the distance of 4.8 R_V from the center of Venus. Since Akatsuki is orbiting in a far elongated elliptical orbit compared to the originally planned orbit, LIR can capture the full Venus disk in most of an orbiting period. The pixel field-of-view is 0.05°, which is four times larger than those of UVI, IR1 and IR2.

LIR has an internal image accumulation function to improve noise-equivalent temperature difference (NETD). This function is called as primary accumulation, which is performed during each exposure. Image data are sent to DE, and up to 32 images can be accumulated. This is called as secondary accumulation. In the nominal observation sequences both primary and secondary accumulation numbers are set to be 32 which gives the best NETD according to the pre-launch test results, and an image acquisition sequence takes about two minutes. An image acquisition sequence without accumulation is also equipped to take an image with a very short exposure time of 1/30 sec, and used when the ground speed of spacecraft is large.

Observation:

In the first orbiting period LIR took 19 images from Dec. 7 to Dec. 11. The shortest time separation between successive images was two hours. This is chosen so that a wind vector field can be properly derived by a cloud-tracking method. From Dec. 12 to Jan. 14 observation was suspended due to important operations on spacecraft which did not allow the observations in parallel. Observation restarted on Jan. 15.

As a matter of course data amount that can be transferred from spacecraft to ground is limited by bit rate of telecommunication. In the nominal observation plan time interval of image acquisition by LIR is two hours, and it can be shortened to be one hour in a special observation period.

Initial Results:

In the first shot by LIR after VOI-R1 several amazing features which have never been seen before are identified at a glance. A huge bow-shape high temperature region extending from the northern high-latitudes across the equator to the southern high-latitudes exists around the evening terminator. The temperature in the southern polar region seems to be the highest in the snapshot. Dark filament-like streaks aligned north-south direction are found in the low latitudes. They are also identified in the UV image. Interpretation of these interesting features will be discussed in the presentation.

References:

1) Taguchi et al., 2012, Icarus, 219, 502-504, doi:10.1016/j.icarus.2012.01.024.
2) Fukuhara et al., 2011, Earth Planets Space, 63, 1009-1018, doi:10.5047/eps.2011.06.019.

THERMAL TIDE IN THE VENUS ATMOSPHERE.

M. Takagi, *Faculty of Science, Kyoto Sangyo University, Kyoto, Japan (takagi.masahiro@cc.kyoto-su.ac.jp)***, N. Sugimoto,** *Research and Education Center for Natural Sciences, Department of Physics, Keio University, Yokohama, Japan***, Y. Matsuda,** *Department of Astronomy and Earth Science, Tokyo Gakugei University, Koganei, Japan***.**

Introduction

It has been pointed out that the Venus atmospheric superrotation may be generated and maintained by the momentum transport associated with the vertical propagation of the thermal tide (Fels and Lindzen, 1974; Plumb, 1975; Newman and Leovy, 1992; Takagi and Matsuda, 2007). However, spatial distributions of winds and temperature deviations associated with the thermal tide, which may be also important to the material transport at the cloud levels, have not been fully investigated so far.

Recently, the thermal tide has been detected in observational data obtained by the VIRTIS-M onboard Venus Express (Peralta et al., 2012). The result shows that the diurnal tide is predominant in high latitudes, whose meridional wind is about 4.7 m/s. It is strongly expected that detailed wind distributions associated with the thermal tide will be obtained by the Venus Climate Orbiter "Akatsuki" in the near future. It is necessary to investigate the structure of the thermal tide theoretically and/or numerically so that the observational results can be interpreted in terms of dynamics.

In the present study, we investigate the winds and temperature distributions associated with the thermal tide by using a Venus general circulation model (GCM).

Model

The GCM used in the present study is AFES for Venus (Sugimoto et al., 2014a, b). The resolution is set to T63L120, where T and L denote the truncation number for spherical harmonics and number of vertical levels. The model atmosphere extends from the ground to 120 km. The vertical eddy diffusion coefficient is assumed to be constant, $0.15\,\mathrm{m^2 s^{-1}}$. The horizontal eddy viscosity is represented by the second-order hyper viscosity, whose damping time for the maximum wavenumber component is 0.03 Earth days. Rayleigh friction is used at the lowest layer to mimic the surface friction. In the upper atmosphere above 80 km, a sponge layer is used only for eddy components. The solar heating is based on the work of Tomasko et al. (1980). The infrared radiative process is simplified by the Newtonian cooling approximation, where the temperature is relaxed to a prescribed horizontally uniform distribution based on Venus International Reference Atmosphere (VIRA).

The initial state is assumed to be an idealized superrotating flow in solid body rotation. It is assumed that the zonal flow increases linearly with height from the ground to 70 km, and is constant above. The velocity at the equator is 100 m/s at 70 km. The initial temperature distribution is balanced with the zonal flow. It is assumed that the direction of the planetary rotation and the basic zonal flow is eastward (positive) in the present study, as in the Earth condition. The GCM is integrated for 5 Earth years. A quasi-equilibrium state is obtained after 1 Earth year at the cloud levels. Data used in the following analysis is sampled after 4 Earth years.

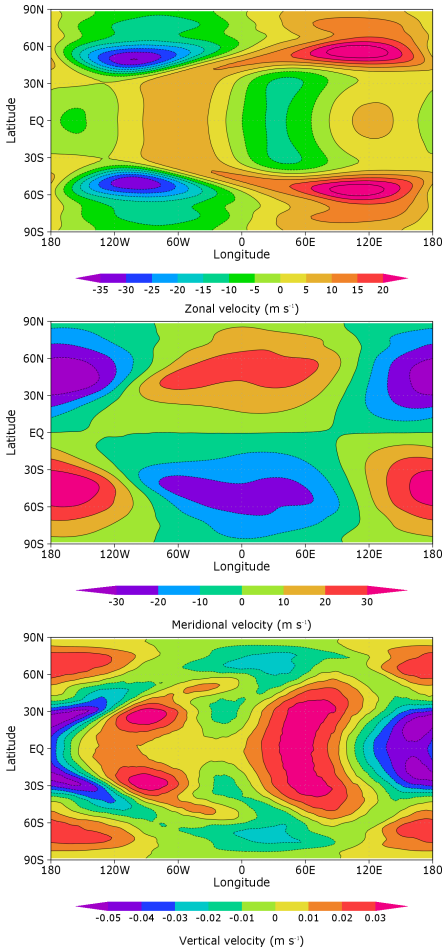

Figure 1: Wind distributions of the thermal tide: (upper) zonal, (middle) meridional, and (lower) vertical wind. The planetary rotation is eastward. The subsolar point is located at the center of the panels (0 degree longitude on the equator).

Results

Figure 1 shows horizontal distributions of the zonal, meridional and vertical winds associated with the thermal tide at 70 km. The semidiurnal tide (with a zonal wavenumber of 2) is predominant in low latitudes, as shown in the zonal and vertical wind distributions. However, in high latitudes poleward of 60 degrees, the diurnal tide is predominant in the wind distributions. The meridional wind velocity in high latitudes is about 10 m/s. This result is consistent with the work of Peralta et al. (2012). It is noted that the center of the upward wind is not located at the subsolar point. The strong upward wind is observed at early afternoon and near the morning and evening terminators. It is also interesting that Y-shape structures can be seen in the vertical wind distribution. The dayside Y-shape structure associated with the upward wind is formed mainly by the diurnal and semidiurnal components. However, in the nightside Y-shape structure with the downward wind, a tidal component with zonal wavenumber 3 is important, which may be excited by the nonlinear interaction between the diurnal and semidiurnal tides.

Figure 2 shows a zonal-vertical distribution of the vertical wind associated with the thermal tide on the equator. Above 55 km, it seems that the thermal tide (the diurnal tide) is trapped; the phase is almost unchanged in the vertical direction. This result indicates that the subsolar-antisolar (SS-AS) circulation is predominant at these levels. The vertical velocity of the SS-AS circulation is 0.04 m/s at the cloud top level, which is about 10 times as strong as that of the mean meridional circulation (not shown). It is inferred that the SS-AS circulation is quite important to the material transport at the cloud levels in the Venus atmosphere.

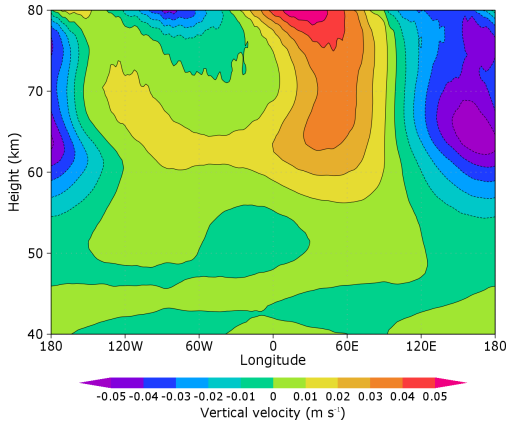

Figure 2: Zonal-vertical distribution of the vertical wind associated with the thermal tide between 40 and 80 km on the equator.

It is also noted that small scale disturbances with short periods less than 10 Earth days are strongly excited at the cloud top levels. Horizontal distributions of their vertical wind indicate that these disturbances are strongly affected by the thermal tide.

Concluding remarks

The distributions of winds and temperature deviations associated with the thermal tide have been investigated by using the Venus GCM. At the cloud levels, the diurnal and semidiurnal components are predominant. However, the component with zonal wavenumber 3 is strongly excited in the vertical wind distribution related to the Y-shape structure. The vertical wind of the diurnal tide or the SS-AS circulation is much stronger than that of the mean meridional circulation.

It is also found in our simulation result that fast traveling waves with a period of about 5 Earth days are excited in the equatorial region, which may be related to the so-called Kelvin wave. The excitation mechanism of these fast waves should be investigated in detail.

The preliminary analysis also indicates that the mean meridional circulation at 50–90 km levels is strongly affected by the thermal tide and fast traveling waves excited by the baroclinic and/or barotropic instabilities in mid- and high-latitudes. In order to elucidate the dynamical balance, the EP-flux and the residual mean meridional circulation associated with these waves are investigated in detail.

References

[1] Fels, S. B., and R. S. Lindzen (1974), The interaction of thermally excited gravity waves with mean flows, Geophys. Fluid Dyn., 6, 149191.

[2] Plumb, R. A. (1975), Momentum transport by the thermal tide in the stratosphere of Venus, Quart. J. R. Met. Soc., 101, 763-776.

[3] Newman, M., and C. Leovy (1992), Maintenance of strong rotational winds in Venus' middle atmosphere by thermal tides, Science, 257, 647650.

[4] Peralta. J., D. Luz, D.L. Berry, C.C.C. Tsang, A. Sánchez-Lavega, R. Hueso, G. Piccioni, P. Drossart (2012), Solar migrating atmospheric tides in the winds of the polar region of Venus, Icarus, 220, 958-970.

[5] Sugimoto, N., M. Takagi, and Y. Matsuda (2014), Baroclinic instability in the Venus atmosphere simulated by GCM, J. Geophys. Res. Planets, doi:10.1002/2014JE004624.

[6] Sugimoto, N., M. Takagi, and Y. Matsuda (2014), Waves in a Venus general circulation model, Geophys. Res. Lett., 41, 74617467, doi:10.1002/2014GL061807.

A plan to study the Venus' upper haze based on SOIR/Venus Express and AKATSUKI.

Seiko Takagi, *Tokai University Research and Information Center, Japan (seiko@tokai-u.jp),* **Arnaud Mahieux,** *Belgian Institute for Space Aeronomy; Fonds National de la Recherche Scientifique, Bruxelles, Belgium,* **Valérie Wilquet,** *Belgian Institute for Space Aeronomy, Bruxelles, Belgium,* **Séverine Robert,** *Belgian Institute for Space Aeronomy, Bruxelles, Belgium,* **Rachel Drummond,** *Belgian Institute for Space Aeronomy, Bruxelles, Belgium; IndoSpace Ltd., 6 Nuneham Square, Abingdon,Oxon, OX14 1EH., UK,* **Ann Carine Vandaele,** *Belgian Institute for Space Aeronomy, Bruxelles, Belgium,* **Naomoto Iwagami,** *Department of Earth and Planetary Science, the University of Tokyo*

Abstract:

The Venus cloud consists of a main cloud deck at 47 – 70 km, with thinner hazes above and below. The upper haze on Venus lies above the main cloud surrounding the planet, ranging from the top of the cloud (70 km) up to as high as 90 km.

The Solar Occultation in the InfraRed (SOIR) instrument onboard Venus Express (ESA) was designed to measure the Venusian atmospheric transmission at high altitudes (65 – 165 km) in the infrared (2.2 – 4.3 μm) with high spectral resolution. We investigated the optical properties of the Venus's haze above 90 km using the SOIR solar occultation observations. Vertical and latitudinal profiles of extinction, optical thickness, and mixing ratios of aerosols were retrieved. We find that haze extinction and optical thickness at low latitudes are two times higher than those at high latitudes. One of the noticeable results is that aerosols mixing ratio increases with altitude above 90 km at high and low latitudes. Therefore we speculate that aerosols could be produced at such high altitudes.

On December 7, 2015, AKATSUKI (JAXA) arrived at Venus after orbit insertion. Some instruments onboard AKATSUKI will observe characteristics of haze particles. In this presentation, a plan to elucidate Venus cloud including haze layer creation and maintain process in using observation data of SOIR/Venus Express and AKATSUKI will be proposed.

EXPOLARION FOR LIGHTNING IN VENUS WITH LAC ONBOARD AKATSUKI

Y. Takahashi, *Hokkaido University, Sapporo, Japan (yukihiro@mail.sci.hokudai.ac.uk)*, **M. Imai**, *Hokkaido University, Sapporo, Japan,* **M. Sato**, *Hokkaido University, Sapporo, Japan.*

Introduction:

In order to detect the signature of lightning activity in Venus, extensive investigations using data obtained with spacecraft and ground-based telescopes have been carried out. However, we don't reach consensus on the existence of lightning in that planet. Indeed there exist some strong indications of electrical discharge both in optical and radio wave measurements. But these "evidences" are sometimes not accepted in the majority of researcher community. For example, it is reported that the magnetometer on board Venus Express recorded whistler mode waves whose source could be lightning discharge occurring well below the spacecraft. On the other hand, it is also pointed out that such radio wave can be generated by a kind of plasma instability other than lightning discharge. An infrared sensor, VIRTIS of Venus Express, doesn't show the positive indication of lightning flash at this moment. LAC is the first sensor designed for the lightning detection in Venus.

Strategy:

In order to identify the optical flash caused by electrical discharge in the atmosphere of Venus, at least, with an optical intensity of 1/10 of the average lightning in the Earth, we built a high-speed optical detector, LAC (Lightning and Airglow Camera), on board Akatsuki spacecraft (Figure 1). Unique performance of LAC compared to other equipments is the high-speed sampling rate at 32 us interval for all 32 pixels of APD matrix, enabling us to distinguish the optical lightning flash from other pulsing noises. We selected OI 777 nm line, the most expected emissions in CO2 atmosphere based on the laboratory experiment. The light curve will be stored for each optical by pre-triggering with maximum length of 2 seconds.

Though, unfortunately, the first attempt of the insertion of Akatsuki into the orbit around Venus was failure in December 2010, the second one carried out in December 7 in 2015 was quite successful. We checked out the sound condition of high voltage system of LAC on January 20, 2016 for the first time after the launch. Due to some elongated orbit than that planned originally, we have umbra for ~30 min to observe the lightning flash in the night side of Venus every ~10 days after April 2016. Here we would report the instrumental status of LAC and the testing result together with future plans and strategy of LAC operation.

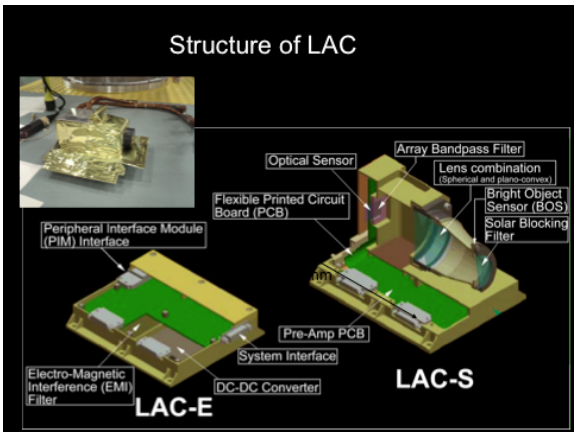

Fig.1 Structure of LAC.

VENUS MESOSPHERE AT THE TERMINATOR, STUDIED DURING THE SOLAR TRANSITS

P. Tanga[1], Th. Widemann[2], Ch. Pere[3], M. Roos-Serote[4]
[1]Laboratoire Lagrange, Université Côte d'Azur, Observatoire de la Côte d'Azur, CNRS, Nice, France
[2]LESIA, UMR CNRS 8109, Paris Observatory, France
[3]DYPAC, EA 2449, Université de Versailles-Saint-Quentin-en-Yvelines, Guyancourt,France
[4]University of Michigan, Ann Arbor, USA

Introduction: The existence of a Venusian atmosphere was first revealed during a Venus transit in front of the Sun, more than 3 centuries ago. The fascinating aspect of the planet at the beginning and end of a transit, surrounded by a thin 'aureole' of illuminated atmosphere, has been constantly reported since then, but only modern imaging devices have allowed to exploit this circumstances to remotely measure significant physical quantities.

After a first attempt with the data relative to the 2004 transit (Tanga et al. 2012a), we organized a more extensive campaign in 2012, involving observations through both space- and ground- based telescopes (Pasachoff et al. 2013).

A specific coronagraph design based on the Lyot scheme was also conceived and replicated in several copies in the attempt of improving the SNR of the aureole signal in proximity of the solar disk (Venus Twilight Experiment, Tanga et al. 2012b).

Here we report on the different data sets collected during the 2012 transit, and present conclusions based on imaging from the Solar Dynamic Observatory (SDO), from Hinode, and by the instruments of the Venus Twilight Experiment.

Our goal is to provide an updated review of the results obtained during the Venus transits of the XXI century.

Image analysis: The analysis of the aureole brightness has required the development of specific techniques, in order to extract the photometry at different latitudes and to manage the strong background gradients that are usually present close to the solar limb.

The data sets above have been analyzed, thus extracting the photometry from about 300 images.

In 2012 we have been able to trace the whole evolution of the aureole, from the faintest portion visible only close to the rotational pole of the planet, before the 1st or after the 4th contact, to the brightest illumination occurring very close to the 2nd and 3rd contact, a few arcseconds from the solar limb.

Modeling: The aureole is a refracted, extremely flattened image of a portion of the solar photosphere, having the same surface brightness if the atmosphere is totally transparent. The thickness of the refracting layer, is unresolved in remote observations.
We explored different approaches to model the variation of the aureole brightness, ranging from simple isothermal modeling to multi-layer. We implemented both direct (starting from an imposed vertical profile) and inverse modeling (iteratively determining the vertical profile).

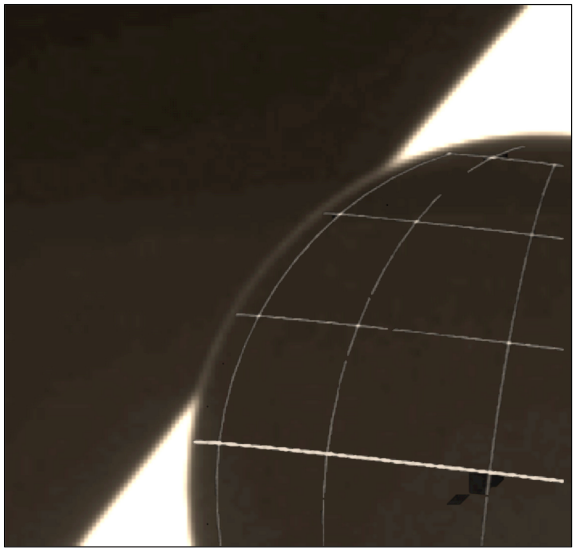

Fig. 1 - The aureole of Venus (upper left limb portion) superimposed to planetocentric coordinates during the ingress of the 2012 transit. It appears as an extremely thin line against the lower solar corona in this image obtained by the Hinode satellite at the 550 nm continuum).

Our final model results provide at the same time the vertical density profile (from which temperature can be derived), the altitude of the absorbing clouds (optical thickness τ=1) and the maximum altitude that we can probe with aureole.

Results: The various data sets available have proven to be complementary to each other, in terms of time sampling, spatial and spectral resolution.

While less accurate than the local terminator measurements obtained by SOIR on board Venus Express, aureole modeling has the advantage of being able to cover simultaneously a wide range of latitudes.

During the 2012 event only the extreme southern latitudes were not observable, due to the relative geometry of Venus at the ingress and egress of the event.

We were able to favorably compare the aureole-derived vertical profiles to those obtained by the

Venus Express/SOIR experiment (Mahieux et al. 2015), performed during the transit itself. This was done at the single latitude (+49°) sampled by SOIR during the event, however providing a suitable validation to our approach (Pere et al. 2016a).

Our inverse model, retrieving the vertical temperature profiles at all altitudes (Widemann et al. 2014, Pere et al. 2015, Pere et al. 2016b), detects a cold layer (at ~86-94 km altitude on average) whose thickness seems to be dependent on latitude (thicker towards the N pole than at the equator). The opaque layer altitude (τ=1) is also latitude dependent, being lower at high altitudes (minimum of 86 km at +82°) than at the equator (91 km).

Eventually our model shows that a relevant contribution to the aureole flux comes from deep layers where aerosol absorption cannot be neglected, allowing us to put some constraints on the aerosol dispersion scale height.

Aknowledgements - PT, TW, CP acknowledge support from the European Union Grant G.A. 606798 EuroVenus.

Bibliography

Mahieux et al. 2015, Planet. & Space Sc., 113, 347
Pasachoff et al. 2013, AAS DPS #222, id.217.01
Pere et al. 2015, EPSC2015-692
Pere et al. 2016a, A&A, in publication
Pere et al. 2016b, submitted
Tanga et al. 2012a, Icarus 218, 1, 207
Tanga et al. 2012b, AAS DPS #44, id.508.07
Widemann et al. 2014, AAS DPS #46, id.302.06

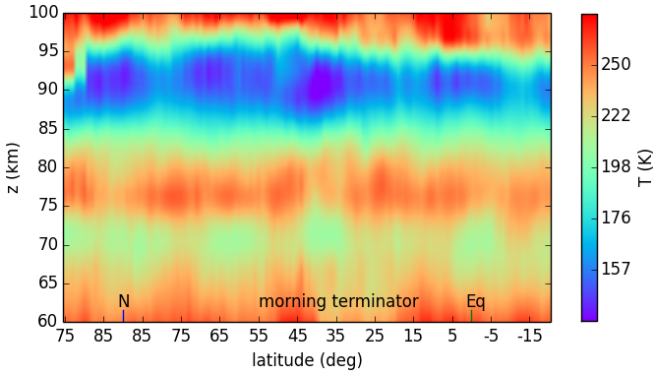

Fig. 2 – Temperature along the morning terminator, as determined during the transit of Venus on June 5-6 2012, from aureole observations (HMI - SDO data set). The presence and extension of the cold layer at ~90 km is mapped at the same time at all latitudes from the North pole to the Equator.

ZONAL WINDS IN THE VENUS ATMOSPHERE DEDUCED FROM VERA RADIO OCCULTATION MEASUREMENTS.

S. Tellmann , *Rheinisches Institut für Umweltforschung, Department of Planetary Research, University of Cologne, Cologne, Germany (silvia.tellmann@uni-koeln.de),* **B. Häusler**, *Institute of Space Technology and Space Applications, Universität der Bunudeswehr München, Neubiberg, Germany,* **M. Pätzold**, *Rheinisches Institut für Umweltforschung, Department of Planetary Research, University of Cologne, Cologne, Germany,* **M.K. Bird**, *Rheinisches Institut für Umweltforschung, Department of Planetary Research, University of Cologne, Cologne, Germany* **D.P. Hinson**, *SETI Institute, Mountain View, CA, USA,* **T. Imamura**, *Institute of Space and Astronautical Science, Japan Aerospace Exploration Agency, Kanagawa, Japan,* **G.L. Tyler**, *Department of Electrical Engineering, Stanford University, Stanford, CA, USA.*

Introduction:

Winds in the Venus atmosphere can only be determined directly by in situ measurements from entry probes or by the tracking of cloud features in the UV or infrared at the top of the cloud layers. These methods provide wind estimates from the surface of the planet to the top of the cloud layer. Above the clouds, Zonal winds can only be inferred from meridional cross sections of temperature assuming cyclostrophic balance (Newman et al., 1984; Piccialli et al., 2008, 2012).

VeRa temperature profiles from two special campaigns sensed the upper troposphere and mesosphere of Venus at almost the same position on consecutive orbits. Certain temperature characteristics seen repeatedly after a couple of orbits clearly indicate the rotation rate of the atmosphere at different altitude levels. These temperature markings can be used to deduce zonal winds at certain positions and local times in the Venus atmosphere.

The VeRa Experiment:

The Venus Express Radio Science Experiment VeRa regularly sounded the Venus neutral atmosphere and ionosphere using the spacecraft radio subsystem in the one-way radio mode at X-band (8.4 GHz) and S-band (2.3 GHz) in Earth occultation geometry. An Ultra-Stable Oscillator (USO) provided a high quality on-board frequency reference for refractivity measurements, from which electron density profiles in the ionosphere and profiles of pressure, temperature and neutral number density of the neutral atmosphere are derived [Häusler et al., 2006; Pätzold et al., 2007]. Radial profiles of neutral number density from the atmospheric-induced Doppler shift during the occultations cover the altitude range 40–90 km. These are then used to derive vertical profiles of temperature and pressure [Tellmann et al., 2009]. The VeRa data set, consisting of more than 800 atmospheric profiles, covers almost all latitudes and local times with a high vertical resolution.

During two special measurement campaigns VeRa could analyse the atmosphere in the low latitudes (20° N, -35° S) and high latitudes (65° N) during consecutive orbits at the same position and local time for a couple of days. The rotation of the atmosphere can clearly be identified in these measurements, providing valuable information about the rotation rate of the atmosphere.

Zonal Winds:

Zonal wind speeds deduced from the two special VeRa campaigns can be compared with zonal winds speeds inferred from meridional temperature cross section assuming cyclostrophic balance. Both methods reveal maximum wind speeds at the top of the clouds with decreasing velocities above and below.

The results are in general good agreement with findings from Piccialli et al., (2008, 2010, 2012), using VIRTIS measurements and VeRa measurements from the first occultation seasons.

The vertical and latitudinal structure of the temperature and zonal wind field provides valuable information about the dynamical state of the atmosphere and can be used to get insight into possible regions of baroclinic and/or barotropic instabilities. These instabilities are correlated with the generation of eddies in the Venus atmosphere.

References

Häusler, B., M. Pätzold, G. L. Tyler, R.A. Simpson, M.K. Bird, V. Dehant, J.-P. Barriot, W. Eidel, R. Mattei, S. Remus, J. Selle, S. Tellmann and T. Imamura, 2006. Radio science investigations by VeRa onboard the Venus Express spacecraft, Planet. Space Sci., 54**,** 1315 – 1335.

Newman, M., G. Schubert, A. Kliore, and I.R. Patel, 1984. Zonal winds in the middle atmosphere of Venus from Pioneer Venus Radio Radio Occultation data, J. Atm. Sci., 41, 1901 - 1913.

Pätzold, M., B. Häusler, M.K. Bird, S. Tellmann,R. Mattei, S.W. Asmar. V.Dehant, V., Eidel, W., Imamura, T, R.A. Simpson, G.L. Tyler, 2007. The structure of Venus' middle atmosphere and ionosphere, Nature, 450, 657-660.

Piccialli, A., S. Tellmann, D.V. Titov, S.S.

Limaye, I.V. Khatuntsev, M. Pätzold, and B. Häusler, 2012. Dynamical properties of the Venus mesosphere from the radio-occultation experiment VeRa onboard Venus Express, Icarus, 217, 669 - 681.

Piccialli, A., 2010. Cyclostrophic Wind in the Mesosphere of Venus from VenusExpress Observations. Ph.D. Thesis. University of Braunschweig, Germany.

Piccialli, A. et al., 2008. Cyclostrophic winds from the Visible and Infrared Thermal Imaging Spectrometer temperature sounding: A preliminary analysis. J.Geophys. Res. (Planets) 113, 147–155.

Tellmann, S., M. Pätzold, B. Häusler, M.K. Bird, and G.L. Tyler, 2009. The Structure of the Venus Neutral Atmosphere as observed by the Radio Science Experiment VeRa on Venus Express, J. Geophys. Res., doi:10.1029/2008JE003204.

CLOUDS AND AEROSOLS ON VENUS: AN OVERVIEW.

D.V. Titov, *ESA/ESTEC, Noordwijk, The Netherlands (Dmitri.titov@esa.int)*, **N.I. Ignatiev,** *Space Research Institute (IKI), Moscow, Russia*, **K. McGouldrick,** *Laboratory for Atmospheric and Space Physics, University of Colorado-Boulder, USA*, **V. Wilquet,** *Belgian Institute for Space Aeronomy, Brussels, Belgium*, **C.F. Wilson**, *Department of Physics, Oxford University, UK*.

The past decade demonstrated significant progress in understanding of the Venus cloud system. Venus Express observations revealed significant latitudinal variations and temporal changes in the global cloud top morphology. The cloud top altitude varies from ~72 km in the low and middle latitudes to ~64 km in the polar region, correlated with decrease of the aerosol scale height from 4 ± 1.6 km to 1.7 ± 2.4 km marking a vast polar depression. The UV imaging shows the middle latitudes and polar regions in unprecedented detail. The eye of the Southern polar vortex was found to be a strongly variable feature with complex morphology and dynamics.

Solar and stellar occultations give access to a vertical profiling of the light absorption by the aerosols in the upper haze. The aerosol loading in the mesosphere of Venus investigated by SPICAV experiment onboard Venus Express between 2006 and 2010 was highly variable on both short and long time scales. The extinction at a given altitude can vary with a factor of 10 for occultations separated by a few Earth days. The extinction at a given altitude is also significantly lower towards the poles (by a factor 10 at least) compared to the values around the equator, while there is apparently no correlation between the extinction and the latitude in the region comprised between ±40° around the equator.

Based on Mie theory and on the observed spectral dependence of light extinction in spectra recorded simultaneously in the UV (SPICAV-UV), in the near IR (SPICAV-IR), and in the short-and mid-wavelength IR (SPICAV-SOIR), the size distribution of aerosols in the upper haze of Venus was retrieved, assuming H_2SO_4/water composition of the droplets]. The optical model includes H_2SO_4 concentrations from 60 to 85%. A number of results are strikingly new: (1) an increase of the H_2SO_4 concentration with a decreasing altitude (from 70-75% at about 90 km to 85% at 70 km of altitude) and (2) Many SOIR/SPICAV data cannot be fitted when using size distributions found in the literature, with an effective radius below 0.3 μm and a variance of about 2. The scale height of the upper haze is found to be 6.9 ± 5.1 km.

The lower & middle cloud layers – those at 48 – 60 km altitudes – are difficult to observe, as they are hidden by upper clouds. Nevertheless, both nightside near-IR sounding and radio occultation has provided valuable insight into cloud processes in this region. Near IR sounding reveals the morphology of the lower/middle clouds 'backlit' by thermally emitted photons from the lower atmosphere. The morphology of these clouds changes on timescales of order of 24 hours. The vertically integrated cloud optical depth is twice as great in the polar collar (at 75 degrees latitude) compared to low latitudes. Spectral band ratio analysis, if interpreted strictly in terms of Mode 1/ 2 / 2'/3 particles of H_2SO_4:H_2O mixtures, suggests that the acidity of the cloud particles is higher near the polar collar and in regions of optically thick cloud. Particles in the centre of the polar vortex exhibit anomalously high band ratios so are significantly larger and/or of different composition than those at low latitudes.

Radio occultation from Venus Express confirms that the atmosphere is in convective equilibrium from 50-60 km. Sulphuric acid vapour profiles calculated from the absorption of the radio signals show an atmosphere saturated with sulphuric acid in the cloud layer. Both of these results are consistent with the understanding of convective condensational cloud at altitudes of 50-60 km.

Microphysical simulations of the aerosol populations in the atmosphere of Venus have received a boost from the recent exploration of particle properties carried out by various teams using Venus Express over the last decade or so. Numerous groups are applying separate models to the coupled problems of the Venus clouds. Quasi-periodic variability of aerosol population properties has been found in model simulations by several groups under both forced and unforced conditions. Since the clouds play such a significant role in the energy and momentum balance of the atmosphere of Venus – which then feed back into variations in the aerosols themselves – constraining the magnitude and timescales of these variations is a key to understanding the current, past, and future Venusian environment. This paper gives a summary of new observations and modelling efforts that will form the basis for a relevant chapter in the Venus III book.

MODELING PLUME INITIATED SUBDUCTION AT CORONAE ON VENUS

S. M. Tomlinson, University of California Los Angeles, USA (stomlinson@ucla.edu), **S. E. Smrekar,** Jet Propulsion Laboratory/Caltech, USA, **A. Davaille**, Laboratoire FAST, CNRS / Univ. Paris-Sud / Université Paris-Saclay, France.

Introduction: Unlike Earth, Venus lacks a global system of plate tectonics; a process directly related to heat loss and likely related to planetary habitability. This makes the factors influencing the initiation of plate tectonics an important study in rocky planet evolution. Given Venus' similiarity to Earth in size, composition, and heat production; fundamental questions include: why does Venus lack plate tectonics and how does Venus lose its heat through a single plate? Here we study plume induced subduction, a process which could be related to the early stages of plate tectonics. To do this we study subsurface density variations inferred from modeling gravity and topography data at two corona, Artemis and Quetzalpetlatl to look for similar density variations predicted by recent laboratory expirements (Fig. 1). In these expirements, one sided subduction is achieved via a mechanism similar to a concept proposed by [1]. (F1) shows the experiment in an aqueous dispersion of colloids dried from above and heated from below. The side views (1B-C) show the vertical cross-section along the green line in the top view (1A). The hot plume has been highlighted in red. Its impact under the surface skin results in three arcuate bulges (in yellow on (1A)) and three subduction zones along those bulges (in bright white on (1B-C)).

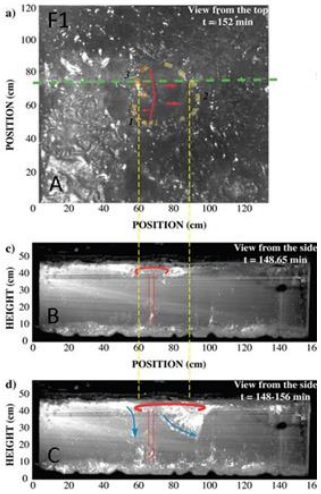

Background: Coronae are featrues unique to Venus. One possible formation mechanism consists of an upwelling mantle plume interacting with the lithosphere. Although there is no evidence of distinct plates on Venus, [2] showed many trenches occuring at some coronae are strikingly similar to terrestrial ocean-ocean subduction zones, and several studies have provided mechanisms which could link plumes to subduction zones. [1,3-4] Whether subduction is occurring on Venus despite its single plate is not well understood and could be happening via a plume induced subduction process. This form of localized subduction provides a mechanism to initially break the lithosphere, potentially allowing plate tectonics to follow.

Methods and Results: To model subduction, we calculate geoid-to-topography ratios (GTRs) for specific features at each corona and fit a profile of the Bouguer gravity data across each corona's trench using a model of a cold, dense subducting thermal lithorsphere with a low density basaltic crust.

Data analysis-GTR. The geoid anomaly decreases as the compensation depth increases, giving a larger GTR. GTRs for two of the largest coronae are shown in (Fig. 2-3). GTRs at the trenches (31.4±11.6 m/km (Artemis) and 19.5±5.6 m/km (Quetzalpetlatl)), are far greater than other regions at each coronae- consistent with a slab at depth.

Artemis Results-GTR. (Fig. 2). (2A) Regionally corrected Bouguer gravity (gravity due to topography removed from free air gravity) showing subsurface density variations for Artemis corona. Due to a topographic plateau to the north, a best fitting plane is removed from the free air gravity, topography, and geoid separately before performing the GTR and slab model analysis. Black crosses show the trench location, red markers show the profile location in (Fig. 5). (2B) shows the GTRs for regions indicated by circles in (2A): Black, red, green, and grey points show the GTRs for the entire coronae, the region of the trench, and the rifts to the north and northwest, respectively

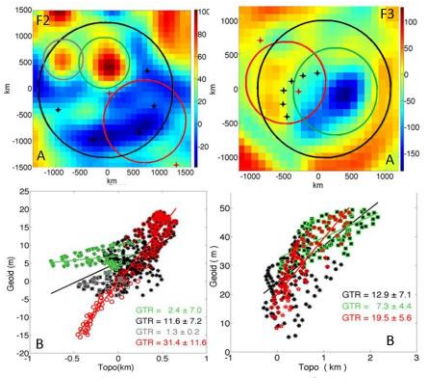

Quetzalpetlatl Results-GTR (Fig. 3). (3A) shows the Bouguer gravity for Lada Terra. Black and red crosses as in (Fig. 2). The large negative anomaly in the center is accounted for in the slab model analysis

(see Fig. 5B). (Fig. 3B) shows the GTR for circular regions in (3A). Green markers indicate Boala coronae.

Data analysis-Slab model. The subducting slab model consists of a low density crust and high density thermal lithosphere. (Fig. 4) shows a diagram of the slab model (not to scale), where only shaded region is modeled.

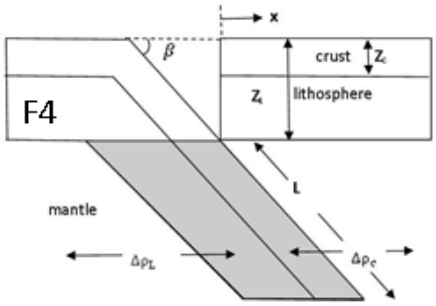

The model incorporates crustal density contrast $\Delta\rho_c$, thermal lithospheric density contrast $\Delta\rho_L$, crustal thickness, Z_C, lithospheric thickness, Z_L, plate length, L, and subduction angle, β. The crustal and mantle densities are based on Earths measurements, 2900 and 3300 kg/m^3, respectively. The thermal density contrast is estimated by $\Delta\rho_{Thermal} \cong \rho_M \alpha \Delta T/2$, where $\alpha = 2.4*10^{-5}\ K^{-1}$, is the coefficient of thermal expansion and $\Delta T/2$ is the mean temperature difference across the lithosphere; based on the surface (~460C) and estimated mantle temperatures (~1300C), giving $\Delta\rho_L \cong 32\ kg/m^3$. The other four parameters vary incrementally. β is 30, 60 or 90°, based on lab experiments (Fig. 1 & [6]). Z_C and Z_L range from 10 to 50 km and 75 to 200 km, in increments of 10 and 25 km, respectively. The plate length increases in increments of 250 km, ranging between 20-80% of the corona diameter [6]. This corresponds to 500-2000 km for Artemis and 250-1000 km for Quetzalpetlatl. The resolution of each model was lowered to match that of the data using a running average technique and then compared to the data via RMS error analysis.

Slab mode results. All prefered models have an RMS < 10 mgal, a crustal thickness of 10 km and subduction angle between 60-90° for Artemis, and 30-90° for Quetzalpetlatl. For Artemis (radius=1300km), prefered models have a lithospheric thickness and slab length between 75-100 km and 500-1500 km, respectively. For Quetzalpetlatl (radius=650km), prefered models have a lithospheric thickness and slab length between 100-150 km and 250-750 km, respectively. (Fig 5) shows the results of the slab model analysis. The origin indicates the lowest topographic point in the trench. Distance increases from the trench toward the corona center. Artemis (5A). The regional slope in gravity and topo due to the plateau to the north is removed. At Quetzalpetlatl (5B), a 30 mgal correction is added to account for the large negative anomaly in the corona center, likely due to a low density plume. Because the model anomaly goes to zero at large distance from the trench, the 30 mgal correction was chosen to align the model and data far from the site of subduction. The same models are preferred without the correction but have an RMS greater by approximately 10 mgal.

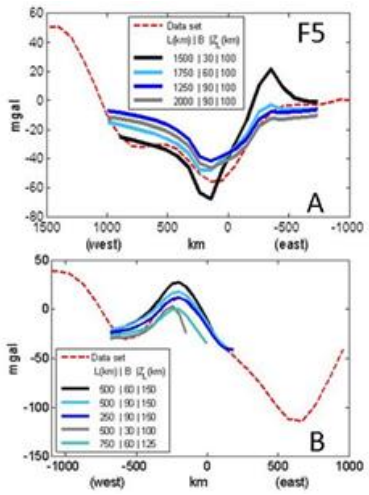

Discussion and Conclusions: The GTR uncertainties are relatively high, which could be caused by the low resolution of the gravity data relative to the size of the specific features. In both cases, the GTR of the trench region is much larger than other regions of the corona. The density anomalies at Quetzalpetlatl are consistent with a subducting slab in the presence of a hot mantle plume. This finding offers support to surface thermal emissivity data interpreted as indicating volcanism < 2.5 mya and probably much younger, 250,000 years or less. [7] At Artemis, there is strong evidence that the topography has been uplifted from below, and the negative gravitational anomaly is consistent with low density material such as a plume. Gravitational anomalies at both coronae can be fit using a dipping slab model over a large parameter space with plate lengths constrained by laboratory experiments. This suggests that Artemis and Quetzalpetlatl could be active sites of plume initiated subduction; causing local resurfacing in the corona centers. Plume-initiated subduction could lead to the development of plate tectonics, but may require cooler, stronger lithosphere to allow plates to develop [6].

References: [1] Sandwell D.T. and G. Schubert (1992) Science, 257, 766-770. [2] McKenzie D. et.al. (1992) J. Geophys. Res., 97, 13, 533-13. [3] Schubert G and D. T. Sandwell, (1995). [4] Smrekar S.E., and E.R. Stofan (1997) Science 277, 1289-1294. [5] James, P.B., M.T. Zuber, R.J. Phillips (2013) *J. Geophys. Res*, 118, 859-875. [6] Smrekar. S. E et. al. (2016) Plume Induced Subductionon Venus, submitted. [7] Smrekar S.E. et. al. (2010) Science, 328, 605-608.

Acknowledgement: A portion of this research was conducted at the Jet Propulsion Laboratory, California Institute of Technology, under contract with the National Aeronautics and Space Administration.

DETAILED STRUCTURAL AND GEOLOGICAL MAP OF A HIGH FRACTURED ZONE ON WESTERN APHRODITE TERRA AND ITS IMPLICATIONS FOR HEAT TRANSFER

D. Tovar, *Department of Earth and Environmental Sciences, University of Minnesota - Duluth, USA (tovar035@d.umn.edu)*, **V.L. Hansen**, *Department of Earth and Environmental Sciences, University of Minnesota - Duluth, USA,* **J.B. Swenson**, *Department of Earth and Environmental Sciences, University of Minnesota - Duluth, USA.*

Introduction: Venus and Earth, originated a remarkably similar distance from the Sun during early solar system formation, have similar size and density; therefore composition, internal structure, and heat budget should be similar. Plate tectonic processes play a key role in dissipating heat on Earth. According to data provided by NASA's Magellan mission, it has been broadly accepted that Venus lacks plate tectonics based on comparative hypsometry analysis; hence a fundamental question arises: how does Venus dissipate heat? Similarities in the hypsometry of Earth's oceans and Venus's surface (except for crustal plateaus and Ishtar Terra) suggest thermal isostasy is currently operative at the global scale on Earth and Venus [1]. Venus' extensive fracture zones might be conceptually correlative to Earth's divergent boundaries that might be correlated with regions of significant heat transfer. Extensive fracture zones are located in southern Aphrodite Terra, characterized by well developing as well as varied surficial expressions. Fractures may interact at depth creating a subsurface magmatic plumbing system [2]. We are developing a detailed structural analysis of a targeted portion of an Aphrodite fracture zone in order to gain insight about the architectural evolution through time and space and, ultimately, to construct thermal models to investigate possible mechanisms of heat diffusion on Venus. The map area (15S-20S/110E-124E), characterized by extreme density of fractures and pit chains, encloses over 700,000 km^2. Right-look, left-look and stereo coverage by Magellan SAR imagary offers an excellent data set, which we employ in mapping.

Map Area: The fracture zone (FZ) includes two zones characterized by E- and NW-trending lineaments; a coronae-like feature with concentric and radial lineaments marks the intersection of the main fracture trends (Fig 1). The SW part of the map area encompasses the FZ boundary. FZ is located topographically high in contrast to its surroundings. Using radar Magellan SAR and altimetry data we mapped lineaments, lineament trends and structural domains. We focus here on tectonic lineaments, which characterize the FZ.

Tectonic lineaments. They define four broad suites based on orientation and/or patterns. We map lineaments according to width; wider lineaments, which are easy to map, clearly represent pit chains with well-developed troughs; narrower lineaments appear to mark fractures, although detailed element interpretation is limited by data resolution. Wide lineaments are widely spaced, facilitating their mapping, whereas narrow lineaments are so closely spaced, i.e. at or near data resolution, as to define a penetrative fabric across the map area. The northern part of the FZ is defined by intersecting suites of penetratively-developed fractures that define scallop-like packages with ~30° of curvature over ~500 km; the eastern FZ is dominated by the corona structure.

Structural domains. Four structural domains (A-D) defined based on lineament density, represent structural facies and not material units (Fig 1). Domains A-D define regions of decreasing fracture density and, together with cross-cutting relations, provide a record of progressive evolution of the FZ architecture and, by extrapolation, the magmatic plumbing system. Domain D (lowest lineament density) occurs outside and along the boundary of the FZ. Domain D lies at the lowest elevation in the map area, and slopes away from the FZ preserving lava flow structures and canali, which clearly indicate that local tectonic lineaments served as magma conduits; pit chains leak, cut, and are buried by flows. Domain C occurs within the FZ and along the inside of the FZ; lineaments are widely spaced, yet clearly cut across domain boundaries. Domain A, with the highest fracture density, typically includes interesting suites of fractures. Domain B is transitional between A and C. Topographically, domains A-C cross topography; that is, there is no a simple relationship between topography and domain boundaries, as with domain D. The FZ preserves a record of time-transgressive lineament (suite) development, and local surface burial occurring during FZ evolution.

Observations: All of the lineaments are long narrow structures with extreme aspect ratios; lineament length scales vary from meters to hundreds of kilometers. Lineaments are characterized by varying in shape, length, width, border geometry, and floor smoothness. Pit chains vary from isolated pit craters sequence to coalescing pit. Troughs are characterized by smooth floor delimited by walls that vary from curved to straight borders; also are commonly associated to long lengths (hundreds of meter to kilometers) rather than short lengths (meters). The spatial distribution and variation of both pit chains and troughs might be interpreted as evolutionary stages of the same structure created by either a single mechanism or many mechanisms acting at depth. Cross-cutting relations indicate that the lineaments formed time transgressively and preserve a record of FZ evolution.

References: [1] Rosenblatt, P. et al. (1994) GRL,21, 465-468. [2] Le Corvec, N. et al. (2013) JGR SE, 118, 968-984.

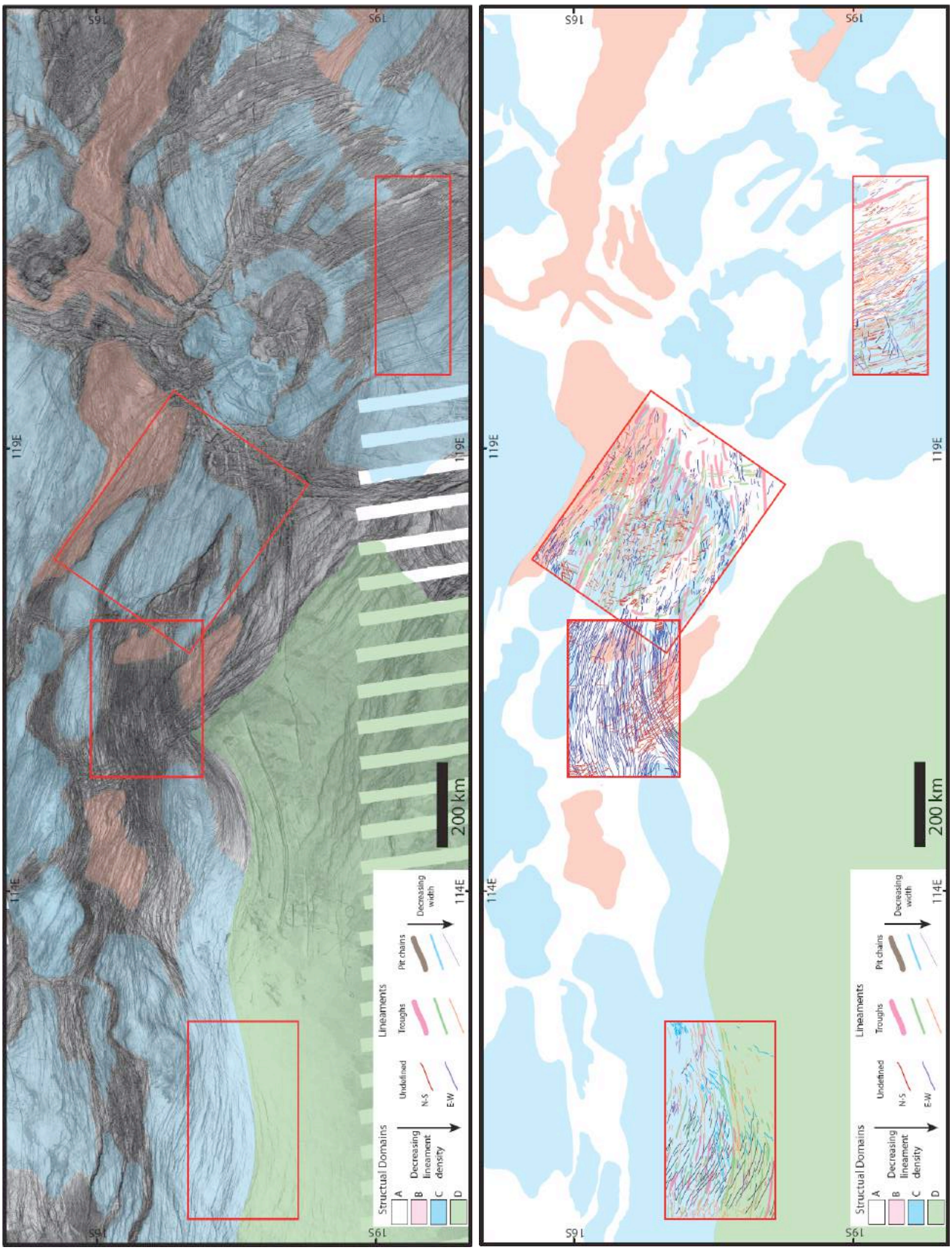

Figure 1: Mercator projection of structural domain and lineament maps of a portion of a fracture zone (15S-20S/110E-124E), southern Aphrodite Terra, Venus. Four targeted area illustrate detailed relations. Maps shown with and without SAR base.

THE HEAVY NOBLE GASES OF VENUS

M. G. Trainer, **P. R. Mahaffy, N. M. Johnson, L. S. Glaze, P. G. Conrad, W. B. Brinckerhoff,** *NASA Goddard Space Flight Center, Greenbelt, MD, USA (Melissa.trainer@nasa.gov)*, **K. Zahnle**, *NASA Ames Research Center, Moffet Field, CA,* **S. K. Atreya,** *University of Michigan, Ann Arbor, MI, USA.*

Introduction:

The exploration of Venus has the potential to inform our understanding of the origin and diversity of terrestrial planets, understand how the evolution of terrestrial planets relates to the evolution of life, and explore the processes that control climate on Earth-like planets [1]. For one, despite the gross similarities between these "twin planets", Venus and Earth present quite differently in their current states. It is unknown if this apparent divergence was intrinsic, programmed during accretion from distinct nebular reservoirs, or a consequence of either measured or catastrophic processes during planetary evolution. Even if the atmosphere of Venus is a more "recent" development, its relationship to the resurfacing of the planet's enigmatic surface is not well understood. Resolving such uncertainties directly addresses the hypothesis of a more clement, possibly water-rich era in Venus' past as well as whether Earth could become more Venus-like in the future.

Origin, evolution, and noble gases:

A key issue that remains after more than 50 years of planetary exploration is the formation and evolution of the Venus atmosphere, particularly in the context of the other terrestrial planets [2]. For instance, the discovery that Ne and Ar on Venus are nearly as abundant as they are in the most gas-rich (CI chondrite) meteorites (Figure 1) suggests differences in formation materials or evolutionary pathways for Venus and Earth. In particular, these abundances suggest: 1) chondrites have little to do with how Venus got its noble gases, or 2) Venus has suffered very little atmospheric escape compared to Earth. The first is a profound question of origins, the latter of divergent evolution. To test either hypothesis requires knowing substantially more about noble gases within the Venus atmosphere.

Previous Measurements and Current Needs:

Noble gas data for Venus' atmosphere are woefully incomplete. We will review the current state of knowledge regarding the noble gas inventory in Venus' atmosphere, based on in situ measurements over 30 years ago. Measurements of Kr from separate mission campaigns are discrepant by a factor of 15 (Figure 1), and prohibit the discrimination between solar and chondritic sources. Xenon has not been measured at Venus, but is needed to resolve uncertainties among models of the original atmospheric composition and potentially lead to a more refined understanding of the relative importance of planetary degassing on Venus, Earth, and Mars [3].

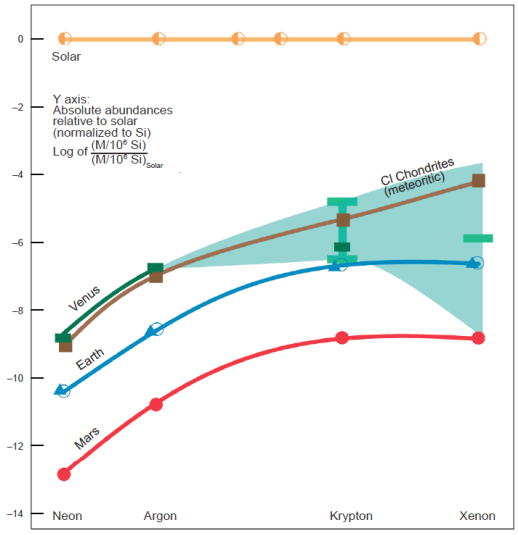

Figure 1. Noble gas abundances for Earth, Mars, Venus, chondrites, and the Sun. Missing Xe and poorly constrained Kr data for Venus are critical for understanding the history of its early atmosphere. From Baines et al. [4].

The abundance and isotopic distribution of this heavy noble gas in particular provide insight into mysteries regarding the terrestrial planets, such as the relative depletion of radiogenic ^{129}Xe on Earth and the striking mass fractionations of non-radiogenic Xe isotopes on Earth and Mars with respect to solar wind and meteorites. Venus is the missing puzzle piece needed to understand the history of the terrestrial planets, in addition to deconvolving its own story of evolution.

Future In Situ Investigations with Heritage Instrumentation and Approach:

Noble gas measurements are only possible through in situ investigations. Given the transitional nature and uncertainties regarding the location of the homopause, above which gases fractionate by mass, measurements from orbit cannot capture the representative composition of these species. Further, the low abundances of heavy noble gases in planetary atmospheres present an analytical challenge for any in situ instrument to achieve accurate measurement of both elemental and isotopic compositions. Such measurements have been demonstrated during probe descent has been demonstrated previously by the Galileo Probe Mass Spectrometer (GPMS) investigation at Jupiter [5,6]. GPMS used two enrichment cells to scrub the ingested atmosphere of H_2 and other active gases in order to enhance noble gases and their isotopes. These ground-breaking measurements

were acquired with < 10 minutes of MS time, following ~10 minutes of gas processing during which direct MS measurements of the atmosphere were made.

For a future Venus mission, improvements to the enrichment process, pumping throughput, and instrument sensitivity over GPMS and Pioneer Venus MS would result in successful measurement of noble gas targets. Such advancements have been implemented on the Mars Science Laboratory Sample Analysis at Mars (SAM) investigation [7]. SAM's wide dynamic range quadrupole MS, and the incorporation of both scrubbers and getters into the gas manifold, effectively remove chemically active gases such as CO_2, trace noble gases from sub-picomole to nanomole abundances to be measured. In particular, following enrichment of noble gases relative to the atmosphere, static mass spectrometry is utilized to maximize the signal from these low abundance, inert species. This capability has been recently demonstrated on Mars to secure *in situ* measurements of Xe and Kr [8,9]. Further, these measurements can be secured in concert with critical accurate profiles of trace gases, as planned for the Deep Atmosphere Venus Investigation of Noble gases, Chemistry, and Imaging (DAVINCI) mission concept [10]. Measurements of trace species such as SO_2, H_2S, and H_2O in the lower atmosphere will help to elucidate the sulfur cycle and gain insight into crustal oxidation and volcanism, which can speak to the probability of past surface water.

References: [1] NRC (2011) *Visions and Voyages for Planetary Science in the Decade 2013-2022*, National Academies Press, Washington, DC. [2] VEXAG (2014) *Goals, Objectives, and Investigations for Venus Exploration.* [3] Pepin, R. O. (2006) *Earth Planet. Sci. Lett. 252*, 1-14. [4] Baines K. H. et al. (2013) in *Comparative Climatology of Terrestrial Planets,* Mackwell et al., eds., 137-160. [5] Niemann et al. (1992) *Space Sci. Rev. 60,* 111-142. [6] Mahaffy et al. (2000) *JGR, 105,* 15061-15071. [7] Mahaffy P. R. et al. (2012) *Space Sci Rev 170*, 401-478. [8] Conrad et al. (2014) LPS XLV, Abstract #2366. [9] Conrad et al. (2016) submitted to *Nature Geoscience*. [10] Glaze et al. (2016) Abstract, this meeting.

Variations of Carbon Monoxide in the Venus Troposphere from Venus Express/VIRTIS in 2006 and 2007

Constantine C. C. Tsang, *Southwest Research Institute, Department of Space Studies, 1050 Walnut Street, Suite 300, Boulder, Colorado, 80302, USA (con@boulder.swri.edu)*, **Kevin McGouldrick**, *University of Colorado, Laboratory for Atmospheric and Space Physics, Discovery Drive, Boulder, Colorado, 80302, USA*

Introduction:

The understanding of spatial and temporal variations in tropospheric abundances of trace gases such as carbon monoxide (CO) is key to understanding the deep atmosphere of Venus. These gases are entrained in the global circulation, as well as being key ingredients to creating the sulfuric acid clouds. Long-term temporal variations of these species across Venus's disc would be provide key insights into the large-scale circulation and cloud forming processes in the troposphere. CO used as an atmospheric tracer provides the deepest probe into the atmosphere where circulation patterns can be studied.

Background:

The Venus Express spacecraft orbited Venus from April 2006 to December 2014. The Visible and Infrared Thermal Imaging Spectrometer (VIRTIS) is an imaging spectrometer that covers 0.3 to 5.0 µm. Nightside thermal emission at 2.35 µm is sensitive to CO (2-0 vibrational band) at 35 km above the surface, approximately 15 km below the lower cloud layer. Previous measurements prior to Venus Express, largely ground-based studies, have focused on the general equator-to-pole trend of CO, up to latitudes of ~60N/S [1, 2]. After arriving at Venus, Venus Express measured abundances of CO and other trace abundances systematically. Measurements by VIRTIS of the near-infrared nightside thermal emissions were conducted from April 2006 through October 2008, when the MIR channel ceased operations. Until now, this has lead to small-scale maps of CO being produced [3] and examination of correlations between CO and OCS [4, 5]. Longer term and more global studies have also been conducted. Band-ratio techniques were developed so that studies into CO over the large number of observations could be possible [6], and global synoptic picture of CO and other species could be conducted [7]. Further ground-based observations have confirmed some of these findings [8, 9].

Motivation:

However, global maps of CO as a function of latitude, longitude, local solar time, and solar time, using the full dataset from Venus Express have yet to be produced. Here, we produce the first full 2D maps of this kind over a number of years, to get as global a picture of CO at 35 km as possible, thereby allowing constraints to be placed on future general circulation models. This work is also being conducted in conjunction with a study of long-term variations of 1.73 µm thermal emission brightnesses, a proxy of cloud optical depth in the lower atmosphere, with the same data [10]. This will allow us to search for potential correlations between time varying features in the zonal wind at the cloud base, and the CO abundance lower down in the atmosphere.

Data and Method:

We have analyzed almost 1 year of data, from April 2006 through March 2007, which includes all observations with integration times greater than 0.3 seconds. Values of radiances and CO are averaged over 1°x1° in longitude and latitude, and 1hr local time. To be conservative, we reject pixels with incidence angles less than 100 degrees, and emission angles greater than 80 degrees. We also reject values with high cloud opacity that have 2.30 µm radiances below 0.02 W/m^2/sr/µm. This produces a dataset that includes a total of 816 individual observations, spanning 255 unique days. Following a validated method [7], we derive the CO concentration by ratioing the 2.32µm flux to the 2.29 µm flux. Maps of CO, from 20°S to 75°S, as a function of latitude, longitude, local solar time and time are created.

Results:

A map of CO in local solar time during the evening and morning hemispheres is produced. Initial results indicate the evening hemisphere shows the strongest equilibrating flow of CO from pole to equator, is at 22hr. The weakest flow seems to be at 04 hr on the morning side, where the gradient is strongest. A map of CO in longitude shows the general expected equator-pole trend. However, tentative indications show a minimum at longitudes centered around 0°.

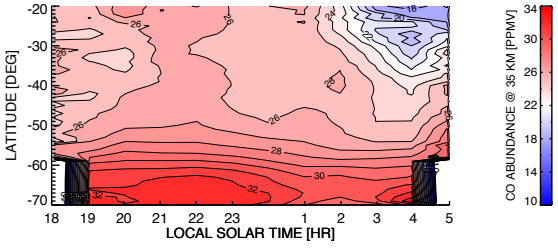

A time varying nature of CO is also discovered, where on one hand, the CO gradient is completely absent in the troposphere, and on other days, the CO gradient is incredibly strong. These results need to be

confirmed with further scrutiny of the data, not least because the data analyzed in this presentation only comprise approximately half of the total data available.

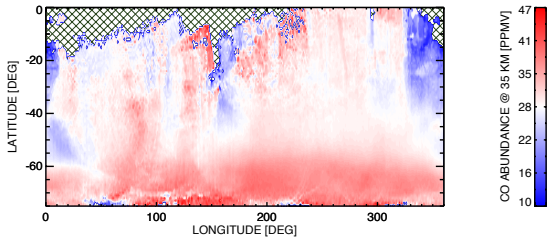

Conclusions:

We are in the mist of conducting a large-scale study of CO in the troposphere of Venus with 50% of the VIRTIS-MIR data analyzed. We confirm a correlation of CO with LST, and potential correlations of CO with certain planetocentric longitudes. Day to day variation of CO is also seen, as observed in previous works. Future work will confirm these observations, including the search for potential periodic features seen in the day-to-day data.

Acknowledgements:

This work is supported by NASA's Planetary Mission Data Analysis Program, grant number NNX14AP94G.

References:

[1] Bezard et al. (1990), Nature, 345, 508-511 [2] Collard et al. (1993), Planetary and Space Sciences, 41, 487–494 [3] Tsang et al. (2008), JGR, 113, doi:10.1029/2008JE003089.E00B08. [4] Marcq et al. (2008), JGR, 113, doi:10.1029/2008JE003074 [5] Yung et al. (2009), JGR, 114, E00B34 [6] Tsang et al. (2009), Icarus, 201,432-443 [7] Barstow et al. (2012), Icarus, 217, 542-560 [8] Cotton et al. (2012), Icarus, 217, 570-584 [9] Arney et al. (2014), JGR, 119 [10] McGouldrick and Tsang (2015), DPS-2015 Abstract #2365381

NEUTRAL COMPOSITION OF THE VENUS ATMOSPHERE MEASURED BY SPICAV/SOIR ON BOARD VENUS EXPRESS: A COMPENDIUM.

A. C. Vandaele, A. Mahieux, V. Wilquet, S. Chamberlain, B. Ristic, S. Robert, I. R. Thomas, L. Trompet, *Royal Belgian Institute for Space Aeronomy, Brussels, Belgium (a-c.vandaele@aeronomie.be),* **J.-L. Bertaux**, *LATMOS, Paris, France.*

Introduction: The Solar Occultation in the Infrared (SOIR) instrument on-board Venus Express is an infrared spectrometer covering the 2.2 - 4.3 μm spectral region. This instrument allows the detection of several key species of the Venus atmosphere, including CO_2, CO, H_2O/HDO, HCl, HF and SO_2. From the CO_2 density measurements, temperature is inferred giving information on the thermal structure of the atmosphere. Here we described the kind of data (profiles, latitudinal average, etc.) that have been obtained during the complete duration of the mission.

SOIR dataset: The Royal Belgian Institute for Space Aeronomy (BIRA-IASB) was in charge of SOIR's development and operations as well as its data pipeline.

BIRA-IASB carried out several studies on the composition of Venus mesosphere and lower thermosphere The retrieval method has been described in detail in several papers introducing the solar occultation method [1], deriving CO_2 densities [2, 3] and trace gases such as CO [4, 5], HCl and HF [6], SO_2 [7-9], H_2O and HDO [10]. Temperature and total density, and therefore structure, has been retrieved from the CO_2 observations [2, 3, 11, 12]. Density and temperature profiles of the upper atmosphere of Venus (60 km to 170 km) at the terminator have been retrieved from SOIR's spectra using different assumptions, wherein the hydrostatic equilibrium and the local thermodynamical equilibrium in the radiative transfer calculations.

The SOIR spectra give also access to information on the aerosol content in the upper haze. Light extinction due to aerosols and cloud top altitudes have been obtained [13, 14] as well as the H_2SO_4 concentration in the droplets [15].

These results allow us to produce an Atmospheric model of Venus called Venus Atmosphere from SOIR measurements at the Terminator (VAST). Data obtained by SOIR will also contribute to update the Venus International Reference Atmosphere (VIRA) [16].

Recently, the treatment of the raw data to transmittance has been optimized, and a new dataset of spectra has been produced. All raw spectra (PSA level 2) as well as calibrated spectra (PSA level 3) have been delivered to ESA's Planetary Science Archive (PDS). Consequently the re-analysis of all spectra has been undergone. We will describe in detail the new derivation of the transmittances, and the updated dataset.

Results: In the following of the paper, we will describe in detail the data derived from the SOIR instrument, their coverage in terms of latitude, local solar time and altitude. As a general comment, solar occultation observations provide information on a very important region of the atmosphere, i.e. the terminator, the limit between the day and night sides of the planet. As a consequence the observations of SOIR correspond either to 6 am or 6 pm, even if at high latitude the definition of time starts to be meaningless. This region is crucial because it is a place of large longitudinal gradients in temperature and density.

Acknowledgments: The research program was supported by the Belgian Federal Science Policy Office and the European Space Agency (ESA – PRODEX program). The research was performed as part of the "Interuniversity Attraction Poles" programme financed by the Belgian government (Planet TOPERS). The authors also recognize the support from the FP7 EuroVenus project (G.A. 606798) as well as that of the HiResMIR International Scientific Coordination Network (GDRI). A. Mahieux would like to thank the FNRS (Belgium) for his Chargé de Recherches position.

References:

1. Vandaele, A.C., et al., *Composition of the Venus mesosphere measured by SOIR on board Venus Express.* J. Geophys. Res., 2008. **113**: p. doi:10.1029/2008JE003140.
2. Mahieux, A., et al., *Update of the Venus density and temperature profiles at high altitude measured by SOIR on board Venus Express.* Planet. Space Sci., 2015. **113-114**: p. 309-320.
3. Mahieux, A., et al., *Densities and temperatures in the Venus mesosphere and lower thermosphere retrieved from SOIR on board*

Venus Express: Carbon dioxide measurements at the Venus terminator. J. Geophys. Res., 2012. **117**(E07001): p. doi:10.1029/2012JE004058.

4. Vandaele, A.C., et al., *Carbon monoxide short term variability observed on Venus with SOIR/VEX*. Planet. Space Sci., 2015. **113-114**: p. 237-255.
5. Vandaele , A.C., et al., *Carbon monoxide observed in Venus' atmosphere with SOIR/VEx*. Icarus, 2016. **(subm.)**.
6. Mahieux, A., et al., *Hydrogen Halides measurements in the Venus upper atmosphere retrieved from SOIR on board Venus Express.* Planet. Space Sci., 2015. **113-114**: p. 264-274.
7. Belyaev, D., et al., *First observations of SO2 above Venus' clouds by means of solar occultation in the infrared*. J. Geophys. Res., 2008. **113**: p. doi:10.1029/2008JE003143.
8. Belyaev, D., et al., *Vertical profiling of SO2 and SO above Venus' clouds by SPICAV/SOIR solar occultations.* Icarus, 2012. **217**(2): p. 740-751.
9. Mahieux, A., et al., *Venus mesospheric sulfur dioxide measurement retrieved from SOIR on board Venus Express.* Planet. Space Sci., 2015. **113-114**: p. 193-204.
10. Fedorova, A., et al., *HDO and H_2O vertical distributions and isotopic ratio in the Venus mesosphere by Solar Occultation at Infrared spectrometer onboard Venus Express.* J. Geophys . Res . 2008. **113**(E00B22): p. doi:10.1029/2008JE003146.
11. Mahieux, A., et al., *Densities and temperatures in the Venus mesosphere and lower thermosphere retrieved from SOIR onboard Venus Express: Retrieval technique.* J. Geophys. Res., 2010. **115**(E12014): p. 10.1029/2010JE003589.
12. Mahieux, A., et al., *Rotational temperatures of Venus upper atmosphere as measured by SOIR on board Venus Express.* Planet. Space Sci., 2015. **113-114**: p. 347-358.
13. Wilquet, V., et al., *Optical extinction due to aerosols in the upper haze of Venus: Four years of SOIR/VEX observations from 2006 to 2010.* Icarus, 2012. **217**(2): p. 875-881.
14. Wilquet, V., et al., *Preliminary characterization of the upper haze by SPICAV/SOIR solar occultation in UV to mid-IR onboard Venus Express.* J. Geophys. Res., 2009. **114**: p. E00B42.
15. Wilquet, V., et al. *SPICAV/SOIR mesospheric aerosols observations and characterization*. in *Geophysical Research Abstracts, 16, 11491*. 2014.
16. Vandaele , A.C., et al., *Contribution from SOIR/VEX to the updated Venus International Reference Atmosphere (VIRA).* Adv. Space Res., 2016. **57**: p. 443-458.

Sulfur Dioxide variability in the Venus Atmosphere

A.C. Vandaele, A. Mahieux, V. Wilquet, S. Chamberlain, *Royal Belgian Institute for Space Aeronomy, Brussels, Belgium (a-c.vandaele@aeronomie.be)*, **O. Korablev, D. Belyaev**, *IKI, Russia*, **Th. Encrenaz**, *Obs. Paris, France*, **L. Esposito**, *LASP, USA*, **K.L. Jessup**, *SwRI, USA*, **F. Montmessin, F. Lefèvre, E. Marcq, A. Stolzenbach**, *LATMOS, France*, **S. Limaye**, *U.Wisc., USA*, **F. Mills**, *ANU, Australia, and SSI, USA*, **C.D. Parkinson**, *U. Mich., USA*, **B. Sandor**, *SSI, USA*, **C. Wilson**, *Univ. Oxford, UK*

Introduction:

SO_2 is strongly related to the formation of the cloud and haze layers on Venus, which are mostly composed of complexes of sulfuric acid and water. The presence of SO_2 in the atmosphere and its variability could be proof of active on-going volcanism on Venus. The variability of the SO_2 is a topic of high intrigue. For example, consideration of SO_2 cloud-top abundances derived from the time of the Pioneer Venus (~1978) through to the end of the Venus Express Mission in 2014, suggests that long-term variations of the SO_2 abundance on the scales of several years may be cyclical in nature, with no direct relation to local time variations. Temporal changes are also observed in the super-rotation period and global cloud cover, which may indicate a strong coupling between circulation and SO_2 abundance above cloud-tops.

Recent observations of sulfur oxides (SO_2, SO, OCS, and H_2SO_4) in Venus' mesosphere also have generated controversy and great interest in the scientific community. These observations revealed unexpected spatial patterns and spatial/temporal variability that have not been satisfactorily explained by models. Particularly intriguing are the layer of enhanced gas-phase SO_2 and SO in the upper mesosphere, and variability in the maximum observed SO_2 abundance and the sign of the equator-to-pole SO_2 abundance gradient that are also not uniquely linked to local time variations. Because sulfur oxide chemistry on Venus is closely linked to the global-scale cloud and haze layers, sulfur oxide observations provide important insight into the ongoing chemical evolution of Venus' atmosphere and its dynamics.

Motivation:

Existing observations have been obtained using multiple platforms, observing techniques, and wavelengths. Each has its own unique strengths and limitations. Although there is strong agreement on some features, there are significant unresolved apparent disagreements among current observations and between observations and models. These apparent disagreements need to be analyzed and assessed carefully to synthesize a clear understanding of sulfur oxide chemistry on Venus. These investigations have been performed via 1) the comparison and validation of observations obtained between ~1978 and 2014, including observations from the Pioneer Venus, Vega, Venera-15 and Venus Express missions, as well as observations from Earth-based telescopes and the Earth-orbiting Hubble Space Telescope; and 2) modelling of the SO_2 and sulfur-oxide family photochemistry. To facilitate this work, an ISSI international team entitled 'SO_2 variability in the Venus atmosphere' was formed to enable a detailed investigation of each of the different aspects of Venus' sulfur chemistry cycle.

Data sets:

In this study, we tried to reconcile the following different observations: previous measurements performed by the Venera probes and Pioneer Venus, as well as more recent observations carried out from Earth or from space-borne instruments, both those on board Venus Express (SPICAV, SOIR, and VIRTIS) or those on the Hubble Space Telescope.

A first step was the direct comparison of SO_2 abundances obtained by these various instruments. This led to a better understanding of the limitations of each technique used to determine the SO_2 abundance, either at localized altitudes, as profiles or as integrated column values. In a next step, the SO_2 abundance was investigated in terms of spatial and temporal variability, on small/short and large/long scales, as well as relative to local time. In addition, the most recent findings from photochemical and dynamical modeling schemes designed to investigate the observed vertical and horizontal (both latitudinal and local time) gas density distributions were considered.

Results:

There are a number of trends that were determined from the detailed comparison of the observations. For example, comparison of the individual datasets indicates that dayside gas abundance detected in the 60-100 km altitude range was observed to vary by a factor of 2-5 as a function of local time; similarly, one-to-one comparison of observations made in the 60-100 km altitude range at specific lati-

tudes and local times indicates that the SO_2 gas abundance varied by a factor of 2-10 on the time scale of a few Earth days.

At the cloud tops the long-term average of the SPICAV data shows that during the VEx campaign the 70-80 km dayside SO_2 gas abundance was typically highest in the equatorial region and decreased with increasing latitude. At the same time, both the SPICAV and HST observations indicate that the latitudinal SO_2 gradient in the 70-80 km altitude region was variable, that the sign of the latitudinal gradient could change, and that the variation in the latitudinal gradient was correlated with the overall abundance of the SO_2 gas. The remaining trends associated with the variability in the altitude profiles of Venus' sulfur-oxides will be presented at conference. Likewise, a summary of the correlation and contradictions between the observed and modeled behavior as function of altitude, latitude and local time will be presented.

Summary:

The analysis undergone within the ISSI International Team has been the subject of a publication, whose main conclusions will be presented and discussed here. This presentation will summarize the results obtained from the comparison of the individual data sets, and between the observations and different models. Lessons learned regarding the dependence and variations of SO_2 with latitude, as well as with time will be presented. Lastly, these studies have highlighted areas where additional laboratory and/or observational measurements are needed. These details will also be discussed.

Acknowledgments*:*

The authors wish to thank the International Space Science Institute (ISSI) for their fruitful support. Most of the authors were members of the ISSI International Team "Sulfur Dioxide variability in the Venus atmosphere" who met during the 2013-2015 in the facilities of ISSI in Bern, Switzerland. Investigator Sandor was supported by the U.S. National Science Foundation by NASA. F.P. Mills also acknowledges partial support under NASA to Space Science Institute. The research program was supported in Belgium by the Belgian Federal Science Policy Office and the European Space Agency (PRODEX), the FNRS, the PlanetTOPERS and SCOOP projects. Some authors also recognize the support from the FP7 EuroVenus project. O. Korablev, D. Belyaev acknowledge support from Roscosmos and the Russian Academy of Science (FANO). E.Marcq, F. Montmessin, F. Lefèvre and A. Stolzenbach acknowledge support from CNES and from the Programme National de Planétologie (PNP) of CNRS/INSU. C. D. Parkinson also acknowledges support with funding in part by NASA to the University of Michigan. The HST observations were obtained through NASA/HST program 12433. Additional funding for the analysis of the HST observations was provided through funding from the NASA Early Careers Program and the NASA Planetary Atmospheres Program. The authors would additionally like to acknowledge Adriana Ocampo, NASA Headquarters, John Grunsfield, NASA Headquarters, Alan Stern, SwRI, Claus Leither, Space Telescope Science Institute, and Håkan Svedhem, Venus Express Project Scientist for their support in the acquisition of the joint HST-Venus Express Venus Observing Campaign.

DEFINITIVE MINERALOGY FOR A VENUS LANDING MISSION.

Alian Wang, *Dept. Earth and Planetary Sciences and McDonnell Center for Space Sciences, Washington University in St. Louis, MO, USA;* ***James Lambert and Steve Monacos,*** *Jet Propulsion Laboratory, Los Angeles, CA, USA;* ***Ian Hutchinson and Melissa McHugh,*** *University of Leicester, Leicester, UK.*

The key questions for a Venus lander:

A Venus landing mission is long over-due, since the success of Vega 1 and Vega 2 in 1985, and those of Venera 8, 9, 10, 11,12, 13, and 14 (1972-1981). The geochemical data from Venera and Vega landing sites suggest a basaltic crust, but rich in incompatible elements (K, Th, U), similar to alkali-rich terrestrial oceanic island [1]. Based on those data, we can make limited estimations on Venus surface mineralogy. Very different from Mars and Moon, Venus has the youngest surface built through relatively recent volcanic activities, and a dense atmosphere of high pressure and high temperature near the surface. Venus would have the most interesting atmosphere-surface interactions. These characters make ***the mineralogy of the surface of Venus to be "the single most fundamental question" faced by any Venus landing mission [2].*** The other two key questions are the chemical composition of the lower 22 km of Venus atmosphere, and the oxidation state of the surface of Venus [2, 3].

Definitive mineralogy by microbeam *in situ* Raman:

A microbeam Raman system on a Venus lander could provide finger-print spectra of silicates, carbonates, sulfates, phosphates, oxides, sulfides, hydroxides, etc. for *definitive mineral phase identifications*. In addition, the Raman peaks of minerals are very sharp and non-overlapping in most cases even in the spectra of mineral mixtures (rocks and regolith), thus the mineral ID can be made by direct inspection of raw spectra.

Furthermore, a Raman system working in visible spectral range (i.e., using 532 nm excitation) allows the laser beam and Raman photon collection through a transparent window (fused silica or sapphire). This character will enable Raman measurements to be made behind a window in a Venus lander. The Venus surface/subsurface samples could be delivered onto that winder from outside. In addition, it takes 10 s to < 1 minute to obtain a Raman spectrum (using MMRS or CIRS, to be described later), thus to get > 100 spectra in 2 hours during a landed Venus mission.

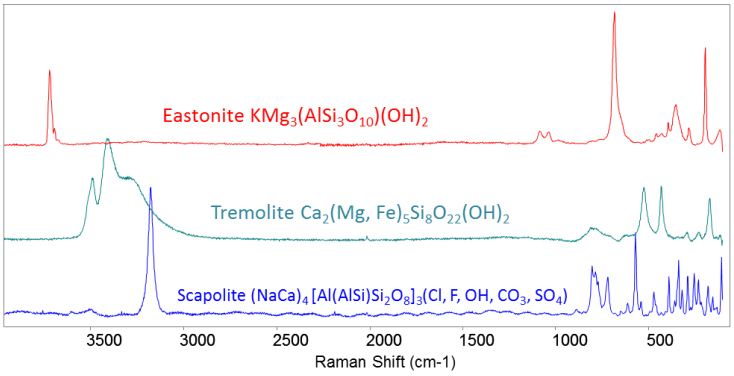

Fig. 1. Raman spectra of three hydrous silicates that may be stable at Venus surface

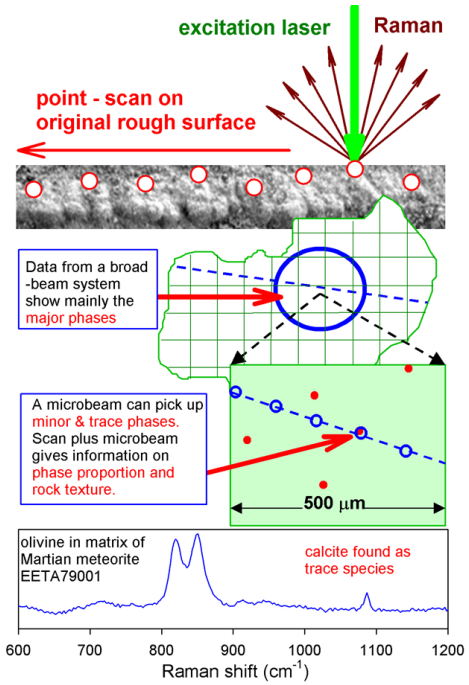

Fig. 2. The detection of a trace calcite in EETA79001 matrix by microbeam in situ Raman

Complete Mineral ID: The first-order mineral ID by Raman spectroscopy can address extremely important Venus science questions.

For example, thermodynamic equilibrium calculations predict many rock-forming hydrous silicates are unstable at Venus surface, but some Fe-free mica (eastonite, phlogopite), some alkali-amphiboles (tremolite), and chloride-bearing scapolite might be stable [3, 4]. They all have characteristic Raman spectra (Fig. 1) that distinguish them from many other silicates [5, 6].

Furthermore, it is critical to determine whether or not the minerals which can buffer CO_2, HCl, and HF are present at surface of Venus. XRF on Venera and Vega provided indirect evidence for the present of carbonates by *the mass deficits*

[2]. While using *in situ* microbeam Raman, direct ID of a trace carbonate phase (calcite) was achieved in a study of martian meteorite EETA79001 [7, Fig. 2]. Past study has demonstrated that F-, Cl-, and OH-bearing apatite can be distinguished by their Raman peaks [8].

The highly active volcanic processes and dense Venus atmosphere all make the sulfur-cycle to be a key player in Venus surface-atmosphere interaction. For which, to identify and to quantify the products of S-cycle (S_8, Fe_xS_y, H_2SO_4-H_2O, HSO_3-H_2O, and sulfate minerals) in Venus surface/ subsurface regolith bear great scientific significance, and they are all very strong Raman scatters (Fig. 3).

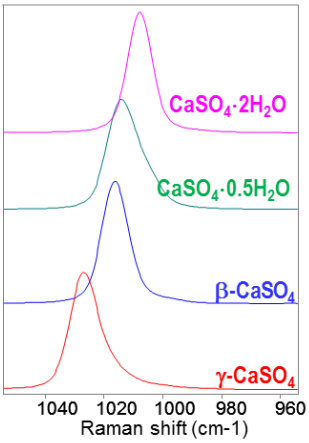

Fig 3. Variety of Ca-sulfates may exist at Venus surface.

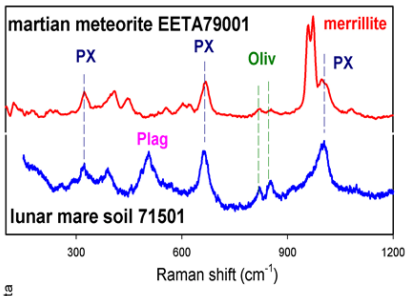

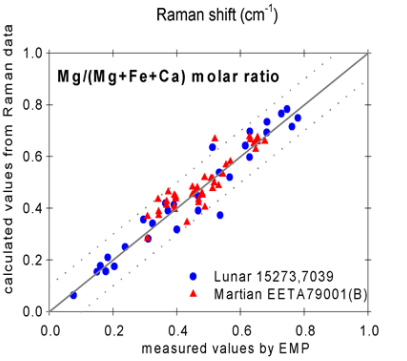

Fig. 4. Mg/(Mg+Fe+Ca) molar ratio of a pyroxene grain is derived from the accurate reading of its Raman peak positions.

For a Venus landing mission, a Raman system with very tight laser spot (microbeam Raman) is a necessity for the detection of trace minerals, in order to provide a complete mineralogy (major, minor, and trace minerals) for rocks or regolith.

Mineral Chemistry: Planetary Raman spectroscopy reveals cation speciation and cation ratio in a mineral through accurate Raman peak position readings, e.g., Mg/(Fe+Mg) in olivine [9]; Mg/(Mg+Fe+Ca) in pyroxene [10, Fig. 4]; Or-Ab-An endmembers and intermediate feldspar [11]; Fe-Ti-Cr solid-solution oxides [12]; cation speciation in carbonates [13]; and the cation speciation & hydration degrees in sulfates [14].

For a Venus landing mission, a Raman system with spectral resolution better than 10 cm^{-1} is required to provide the cation ratios within ± 0.1 uncertainty [9-14].

Rock Characterization: The intensity of a Raman peak in the Raman spectrum of a rock (or a regolith) is affected mainly by the *crystal orientation of the mineral grain* (against the incoming laser beam), which would be very hard to know during a robotic planetary mission.

Fig 5. Compositional distribution of pyroxene in martian meteorite EETA79001

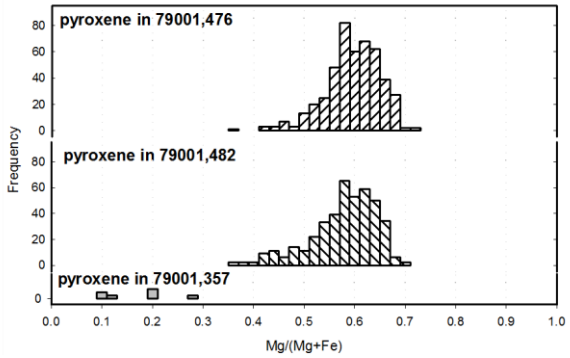

Therefore, it is *practically impossible* to extract the mineral proportions information, using the peak intensities in a Raman spectrum collected from a large sampling spot on a mineral mixture (rock or regolith). Nevertheless, the mineral proportions information can be obtained from Raman spectra collected from > 100 tiny spots on a rock (or regolith), i.e., by using a microbeam Raman system with scan capability. The proportion of a mineral in a rock (or regolith) could be counted approximately on the basis of the *occurring frequency* of its major Raman peak among > 100 Raman spectra [15]. The more sampling spots would give the higher statistical accuracy in the counts. In this way, we avoid the uncertainty in Raman peak intensity and relay only on the detection of the major Raman peak of a mineral. The difference among the Raman cross sections of minerals would be used as weighting factor in the counts.

When using a highly condensed laser beam spot (6-25 μm), it encounters single (or 2, or 3) mineral phase (s), and generates high quality Raman spectrum. A spectrum with high S/N would facilitate definitive phase ID and a high accuracy in mineral chemistry extraction. A combination of above two would provide the compositional distribution a mineral phase within a rock (e.g., pyroxene in a martian meteorite shown in Fig. 5), which can be a direct reflection of the formation history of the rock [7].

For a Venus landing mission, a Raman system with high optical throughput that can generate a good S/N spectrum in < 1 min, i.e., to accomplish a >100 spots Raman line scan in 1-2 hours, is required.

A high TRL microbeam Raman system:
Planetary Raman spectroscopy can provide rich and powerful information. However, Raman scattering is an intrinsically weak process with Raman cross sections of minerals < 10^{-13}. A Raman system for robotic planetary surface exploration requires carefully crafted optical configurations, with high Raman efficiency and robust optical-electronic-mechanic components/subsystems. Our studies of extraterrestrial materials and terrestrial field tests led to a conclusion on *the best Raman system architecture*, to satisfy the need of fine-scale, definitive, and comprehensive mineralogy for planetary surface exploration.

Fig 6. MMRS on Zoe rover in Atacama Desert (2012-2015)

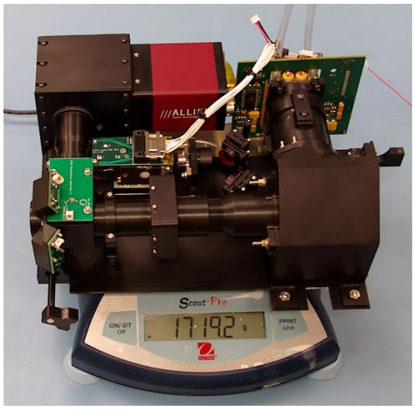
Fig 7. Current breadboard of CIRS (including a Raman spectrometer and a context imager)

MMRS & CIRS configurations use the simplest, the most mature and effective techniques, i.e. continuous wave, low power 532 nm laser, optics in visible spectral range (532-676 nm), and conventional CCD. They both satisfy the requirements mentioned in above sections, i.e., < 25 µm laser beam size, better than 10 cm^{-1} spectral resolution, line-scan capability, and especially, a f/2 optical chain to provide high Raman throughput [16, 17].

MMRS (Mars Microbeam Raman Spectrometer) development was supported by PIDDP, MIDP, ASTEP program and early MER mission development. It has a separate Raman probe connected through optical fiber to Raman spectrometer. MMRS was tested during three field seasons (2012-2015) in Atacama Desert, twice on Zoe rover (> 50 km traverse each time) and once stand-alone. These field studies [18, Fig. 6] demonstrated a solid science performance and robust engineering of MMRS (TRL 5).

CIRS (Compact Integrated Raman Spectrometer) was developed on the basis of mature MMRS technology but having an all-optics-in-one architecture (i.e., without optical fiber). CIRS was supported by MatISSE program since 2013, with a goal to reach TRL 6 [17]. Currently, a prototype of CIRS was built [Fig. 7] and preliminary tests were done. Further system optimization is in progress. The environmental tests of major optical components (and some sub-systems) were accomplished (TRL 6) or on-going.

Comparison with remote-Raman architecture: In the aspect science return, a microbeam *in situ* Raman architecture is much more advantageous than a remote-Raman in following three aspects. (1) A **25-50 µm** sampling spot [16, 17, 19] enables the detection of minor and trace minerals in a rock, while the large sampling spot (0.5-1 mm) of a remote-Raman allows only the detection of major or light-toned minerals. (2) The Raman photons throughput of a **f/2** optics is 10^2 to 10^4 times that of a f/20 to f/100 optics used by remote-Raman architecture [20]. (3) the adjustable **low power cw laser** avoids the over-heating-damaging (or the generation of LIBS) of the target minerals, when compared with the pulse laser used by remote-Raman architecture.

These are exactly the reasons that the publications by WUSTL Raman science team in past > 25 years were all based upon the use of microbeam Raman architecture, which demonstrated the wide and deep planetary applications. For the exactly same reason, before the realization of microbeam Raman architecture in 1980s, there were practically no geological applications of Raman spectroscopy, none for planetary applications.

Conclusion:
A Venus landing mission is long over-due. The mineralogy of the surface of Venus is the most important question for developing the least understanding pf Venus surface-atmosphere interaction. Microbeam in situ Raman could answer this essential question. A high TRL (5-6) microbeam Raman system on a Venus lander can provide rich information within short mission duration.

Acknowledgement: USA NASA MatISSE NNX13AM22G; UK Space Agency CREST 2 grant: ST/L005581/1.

References: [1] McLennan, 2014, 45th LPSC, abs# 1868; [2] Fegley et al., 1997, in Venus II, 591-636; [3] Fegley and Treiman, 1992, in Venus and Mars: Atmosphere, Ionosphere, and Solar Wind Interaction, 7-71; [4] Zolotov et al., 1997, Icarus, 130, 475-494; [5] Wang et al., 2015, JRS, DOI: 10.1002/jrs.4680; [6] Wang et al., 1994, Appl. Spec, 48, 959-968; [7] Wang et al., 2004, JRS, 35, 504-514; [8]. Shea et al., 1974, Arch Oral Biol. 19, 995; [9] Kuebler et al., 2006, GCA, 70, 6201-6222; [10] Wang et al., 2001, Am. Minerals, 86, 790-806; [11]

Freeman et al., 2008, Can. Minerals, 46, 1477-1500; [12] Wang et al., 2004, Am. Minerals, 89, 665-680; [13] Herman et al., 1987, Appl. Spec., 41, 437-440; [14] Wang et al., 2009, JGR, 114, doi:10.1029/2008JE003266; [15] Haskin et al., 1997, JGR, 102, 19293-19306; [16] Wang et al., 2003, JGR, doi:10.1029/2002JE001902; [17] Wang et al., 2014, Abstract #1090 for 2nd International Workshop on Instrumentation for Planetary Missions; [18] Wei et al., JRS, v10,, DOI: 10.1002/jrs.4656; [19] Rull, 2006, Spectroscopy Europe, 18, nº 1., [20] Wiens et al., 2015, AGU, P51E-05.

HIGH PRECISION GAS ISOTOPE RATIOS: LEVERAGING CURIOSITY'S SUCCESS ON MARS TO VENUS EXPLORATION

C. R. Webster, L. E. Christensen, G. J. Flesch, J. Blacksberg, D. Keymeulen, S. Forouhar, *Jet Propulsion Laboratory, Pasadena, CA (Chris.R.Webster@jpl.nasa.gov),* **P. R. Mahaffy, M. G. Trainer, P. Conrad, A. A. Pavlov, L. S. Glaze,** *NASA Goddard Space Flight Center, Greenbelt, MA,* **and S. K. Atreya,** *University of Michigan, Ann Arbor, MI.*

Mars Climate Evolution Investigated by the Sample Analysis at Mars (SAM) Instrument Suite on the Mars Curiosity Rover:

For three years, the SAM suite has been making measurements of atmospheric composition and analyzing solid samples using its Quadrupole Mass Spectrometer (QMS), Gas Chromatography (GC) columns and the Tunable Laser Spectrometer (TLS). High-impact science results have included: high precision isotope ratios in a variety of gases[1] including noble gases[2,3] that reveals the extent of atmospheric escape; detection and variability of atmospheric methane[4]; age-dating and galactic cosmic ray exposure determination[5]; the detection of organic molecules[6]; and the measurement of D/H in Hesperian mudstone[7] to assess the size and loss of ancient water reservoirs.

The measurement of isotope ratios and comparison of present-day values with the meteoric record has been critical to unlocking the time sequences of the martian planetary evolution. Recently, the measured present day value of $^{13}C/^{12}C$ in CO_2, for example, can be generated in models[8] balancing the atmospheric loss that enriches atmospheric $^{13}CO_2$ against carbonate formation that depletes it.

Venus Climate Evolution will be studied by DAVINCI Discovery Mission, with Strong Heritage from SAM-MSL:

NASA GSFC's Deep Atmosphere Venus Investigation of Noble gases, Chemistry, and Imaging (DAVINCI) mission is under consideration for the next Discovery Mission selection. DAVINCI will focus on atmospheric origin and evolution, composition and surface interaction, and surface properties, with a goal to place Venus in context with our solar system and to provide a basis for interpreting recently discovered exoplanets. Through science traceability matrices, DAVINCI has identified numerous specific requirements for measurement of gas abundances and precision isotope ratios in noble gases, C, H, N, O and S species during the descent to the surface of an atmospheric entry probe.

Capability of TLS for Measurement of Abundance and Stable Isotope Ratios of Key Gases in the Venus Atmosphere:

Atmospheric composition and precision isotope ratios will be measured by DAVINCI's Venus Mass Spectrometer (VMS) and Venus TLS (VTLS) instruments, with some planned duplication. The VTLS will have 3 channels focusing on abundances and the isotopic ratio measurements given in Table 1. The predicted spectrum for the second channel is also shown in Figure 1.

Table 1. Isotope ratios to be measured by VTLS

VTLS channel	Wave length	Gases	Isotope Ratios
1	2.78	CO_2, H_2O	$^{13}C/^{12}C$, D/H, and $^{18}O/^{17}O/^{16}O$
2	4.83	CO, OCS, CO_2	$^{34}S/^{33}S/^{32}S$, $^{13}C/^{12}C$
3	7.4	SO_2	$^{34}S/^{33}S/^{32}S$

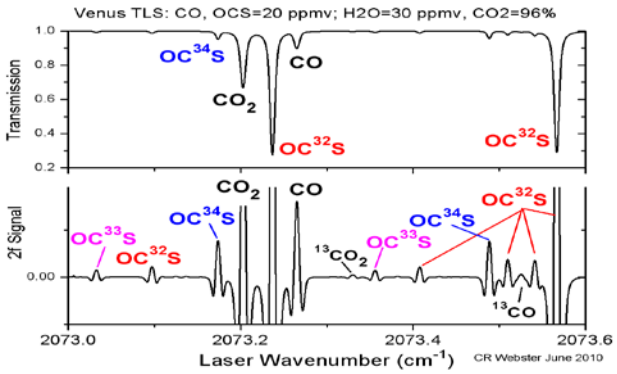

Figure 1. Example spectrum for a single VTLS channel at Venus conditions showing the rich spectral information.

We will discuss the Venus science drivers behind the measurement requirements, and the ability to meet or exceed those requirements as demonstrated by laboratory measurements of isotopic standards.

Acknowledgment. Part of the research described here was performed at the Jet Propulsion Laboratory, California Institute of Technology under contract with NASA.

References:

1. Mahaffy/Webster et al., Science 341 260-266 2013.
2. Atreya et al. (2013), GRL 40(21):5605-5609.
3. Conrad et al., AGU Dec 2015 abstract.
4. Webster et al. Science 347, 415-417 (2015).
5. Farley et al. Geochim.et Cosmochim.Acta 110, 1-12 (2013).
6. Freissinet et al. (2015) JGR Planets, submitted.
7. Mahaffy et al. Science 314, 412-414 (2015).
8. Hu et al.,Nature Comm. DOI:10.1038/ncomms10003 (2015).

Venus and Earth: Is the Divergence a (Natural) Consequence of Planetary Evolution?

M. B. Weller[1], *(matt.b.weller@rice.edu)*, **A. Lenardic**[1], [1]*Department of Earth Science, Rice University, Houston, Tx, USA.*

Introduction: A key observation is that the Earth is seemingly unique in that it exhibits plate-tectonics and a buffered climate allowing liquid water to exist at the surface over its geologic lifetime. An important aspect that has long been in consensus is that as Earth cools, plate-tectonics will eventually wane and the Earth will begin to move into stagnant-lid regime, similar to observations for current day Mars. However, while the end-state is generally agreed upon, the nature of tectonics that the early Earth, exhibited is still hotly debated [e.g., 1]. This uncertainty about the initiation, potential, and longevity of plate tectonics has been extended to extra-solar terrestrial planets and 'Super-Earths' [e.g., 2–8]. In order to understand the potential for plate-tectonics in our own Solar System, let alone extra-solar planets, the evolution of early planets, and particularly the apparent divergence in the evolution of Earth and (Earth's twin) Venus needs to be explored.

Convective Regimes, Thermal Evolution, and Bi-Stability: Planetary tectonic evolution has recently been suggested to be complex, with strong temperature induced feedbacks possible. Recent studies have shown that systems with high levels of internal heating strongly favor early immobile, stagnant-lid, or heat-pipe states [4, 9–10]. As radiogenics are depleted, the lithosphere can yield through an intermediary episodic-lid, into a mobile-lid regime. Increasing surface temperatures, operating on geologic time scales, have also been shown to cause a transition from mobile-lid convection, into and through an episodic-lid regime, before settling into stagnant-lid behavior [9, 11–13]. In contrast to the intermediary episodic-lid associated with decreasing internal heating rates and low surface temperatures, episodic regimes associated with increasing surface temperatures indicate long-lived and robust episodic activity [9].

While planets can transition between tectonic regimes overtime, the path of this evolution may be complex. Nonlinearities inherent in the convective system lead to a hysteresis of states in which multiple stable tectonic regimes are possible for the same planetary parameter values (or bi-stability) [9, 14–16]. The range in parameter space in which multiple stable solutions exists increases with increasing Rayleigh numbers or increasing viscosity contrasts [15]. Both factors are expected to increase for increasingly energetic planets. Within the bi-stability window, the tectonic regime of the system becomes a function of a planet's specific geologic and climatic history, indicating that two otherwise identical systems can exist in different states as a function of a small perturbation of the system. Taken together, these results suggest that transitions between tectonic regimes can occur at the same thermal time (e.g., temperature), but due to different evolutionary histories (e,g,, internal heating, surface temperature), these regime shifts can occur at very different temporal times.

Diverging Venus and Earth, Transitions in Tectonics: A framework of bi-stability and evolutionary pathways offer insights into the apparent Earth/Venus paradox. Early planets are highly likely to operate within a stagnant-lid regime. As radiogenics decrease, all things being held equal, it may be expected that an early stagnant-lid would yield through a transitory episodic-lid before settling into a more mature stage mobile-lid. Evidence suggests that this is perhaps the evolution of the Earth [e.g. 17–19], but evidence for early lid transitions are difficult to determine for Venus, which may currently operate within a stagnant-, or episodic-lid regime [20–22]. However, observations of Venus' surface may offer clues to if, and when, a transition may have occurred. It has been shown that ~ 80% of the surface of Venus is covered by volcanic plains, which have been suggested to have been emplaced, potentially 'catastrophically' [23, 24], within the last ~300 - ~1000 Myr [23–25]. This observation, in addition to the 92 bar Venusian atmosphere, with its strong greenhouse climate, and ~740 K surface temperature, are strongly indicative of late-stage episodic-lid transition.

It has been suggested that the transition from an early stagnant-lid for the Earth occurred ~3 Ga [26]. Assuming a nearly identical size and composition Earth and Venus, canonical models would predict a similar temporal transition for Venus. However, recent work has suggested that the bulk silicate composition of the Earth may be nonchondritic, with a 30 – 50% reduction in heat producing elements [27]. A reduction of radiogenic heat input of up to ~1/2 results in a decrease of internal temperature of up to 41%, following established internal heating scaling laws [e.g. 28 – 30]. Lower heating rates for the early Earth result in lower temperatures relative to an assumed chondiritic (heating rate) Venus. The net result is to thermally age (mature) the Earth in regime diagram space, which acts to alter transition times in absolute ages (Fig. 1). Accounting for a non-chondritic Earth, a near chondritic Venus, and a change in lid regimes for the Earth at ~ 3 Ga [26] suggest that an otherwise comparable Venus should begin to transition out of a stagnant-lid and into an episodic-lid at ~ 2.2 – 1.6 Ga, which is near the upper age limit of potential volcanic plain emplacement

ages at ~1 Ga [23, 24]. This implies that Venus potentially remained in a stagnant-lid longer than the Earth, with potentially has profound implications. Long lived stagnant-lids will tend to favor the suppression of a thermally driven core dynamo, and can also allow for a longer build up of volcanic products (e.g. CO_2) without significant volatile cycling into the interior. The longer build-up time of greenhouse gases (e.g., higher surface temperature), coupled with higher internal temperatures due to the potential of higher radiogenic abundances, in addition to increased proximity to, and increasing Solar luminosity may have allowed for Venus as we see it today.

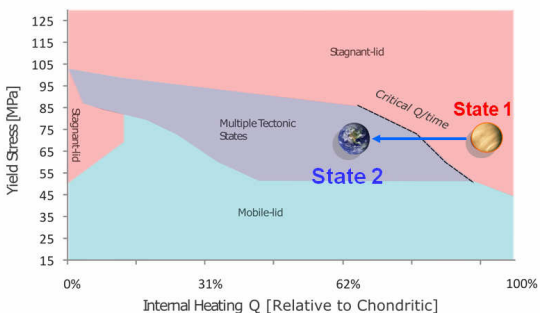

Figure 2: Regime diagram in yield stress vs, internal heating rate (s proxy for age) parameter space (from [9]). Dashed line indicates the critical internal heating rate that mobile-lids (and bi-stability) can occur. Relative positions of a chondritic Venus and non-chondritic Earth [27] at the same absolute time. Earth becomes thermally mature (cooler) relative to Venus at the same temporal time in evolution.

While both planets may have evolved along a similar initial pathway (e.g., an initial stagnant-lid), the possibility of decreased internal heating rates for the Earth allowed for Venus to remain within a stagnant-lid for a longer period of time. Over an additional ~ 1–2 Gyr, volcanic processes continually emit greenhouse gases, Solar luminosity increases (on the order of 60 K - ~40 K from closer proximity to the Sun, and ~15 K from increasing luminosity), and as a result surface temperatures may increase. As Venusian radiogenics decrease, internal temperatures drop, and Venus enters an episodic regime (similar to blue line, Fig. 2). In contrast to an early episodic transition (as may be expected for the Earth), the onset of this episodic-lid occurs in a higher surface temperature regime, which implies long-lived and extensive overturn events [9]. These overturns initiate rapid and significant pulses of melt that release large quantities of volatiles and greenhouse gases into the atmosphere. The rapid influx of greenhouse gases ensures surface temperatures increase dramatically, forcing the transitioning Venus firmly into a high surface temperature tectonic regime (episodic or stagnant-lid) [9, 11 – 13], as indicated by dashed and solid black lines in Figure 2, where on the order of ~20 K difference in surface temperatures results in stagnant or mobile-lids. These results offer insight into the Venus/Earth divergence, and may explain observables of Venus today.

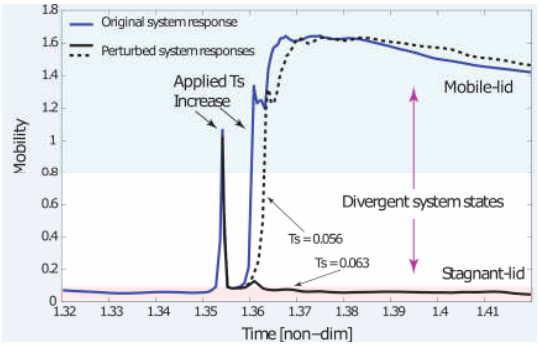

Figure 2: Numerical experiments demonstrating divergence in tectonic states near a transition to bi-stable behavior. An initial stagnant-lid (single plate) system is allowed to evolve into a mobile-lid by decreasing internal heating (from an initial high to a later intermediate stage – a proxy for system ageing, see [9] for background and discussion of numerical approaches). A surface temperature (Ts) increase is applied near a transition in tectonic behaviors (perturbed system responses). High Mobility indicates mobile-lid states (blue field), while low Mobility indicates stagnant-lid states (red field), where Mobility = Surface Vrms/ Total System Vrms (Vrms is the root mean square velocity). The dark blue line indicates the original, unperturbed system evolution. Ts is non-dimensional following the total system temperature contrast scale [0 to 1], where 1 is the core mantle boundary temperature. All cases result in long-lived stable states..

References: [1] Davies, (1993), Lithos 30, 281-289. [2] O'Neill and Lenardic (2007), GRL, 34, L19204; [3] Stein et al., (2011), GRL, 38, L21201; [4] Stein et al. (2013), EPSL, 361, 448-459; [5] Valenica et al. (2007), Astrophys. J., 670, L45 ; [6] Valenica & O'Connell (2009), EPSL., 286, 492–502; [7] van Heck and Tackley (2011), EPSL., 310, 252–261; [8] Tackley et al. (2013), Icarus, 225, 1, 50-61; [9] Weller et al. (2015), EPSL, 420, 85-94; [10] Moore & Webb, (2013) Nature; [11] Lenardic et al. (2008), EPSL, 271, 34-42; [12] Landuyt & Bercovici (2009), EPSL, 277, 29-37; [13] Foley, et al. (2012), EPSL 331, 281–290; [14] Crowley & O'Connell (2012), GJI, 188, 61–78; [15] Weller & Lenardic (2012), GRL, 39, L10202; [16] Lenardic & Crowley (2012), APJ, 755.2:132; [17] Debaille et al (2013), EPSL, 373, 83–92; [18] O'Neill & Debaille (2014), EPSL, 406, 49-58; [19] O'Neill et al. (2007), EPSL 262, 552-562 ; [20] Schubert et al. (1997), Venus II, 1245–12888 ; [21] Nimmo and McKenzie (1998), Annu. Rev. Earth Planet. Sci. 26, 23–51; [22] Moresi, L. and Solomatov, V. (1998), JGR, 133, 669-682; [23] Schaber, et al. (1992), JGR, 97, 13257–13301; [24] Strom et al. (1994) , 99, JGR 10899–10926; [25] McKinnon et al. (1997) , Venus II, 969–1014; [26] Shirey & Richardson (2011), Science, 333, 434–436. [27] Jackson & Jellinek (2013), G3, 14,8; [28] Sotin & Labrosse (1999), PEPI, 112(3– 4), 171–190; [29] Moore (2008), JGR, 113, B11407; [30] Weller et al. (in prep).

TITLE: INTERNATIONAL GROUND-BASED SUPPORT TO VENUS EXPRESS AND AKATSUKI MISSIONS, 2007-2017

Th. Widemann[1,2], C. Wilson[3], T. Imamura[4], E. Lellouch[1], H. Svedhem[5], M. Nakamura[4], the EuroVenus consortium[6]

[1]*LESIA, UMR CNRS 8109, Observatoire de Paris, Meudon, France*
[2]*DYPAC, EA 2449, Université de Versailles-Saint-Quentin, Guyancourt, France*
[3]*Oxford University, Oxford, United Kingdom*
[4]*ISAS/JAXA, Sagamihara, Japan*
[5]*ESTEC, European Space Agency, Noordwijk, The Netherlands*
[6]*European Commission Framework Program under Grant Agreement n°606798 (EuroVenus*

Introduction:

The prime objective of such multi-year coordination campaigns is to provide direct measurements at several levels in the Venus' atmosphere, in order to complement and to help interpreting the massive but sometimes indirect information obtained by the orbiting spacecraft, with a particular emphasis on mesospheric dynamics and chemistry.

The work plan for Ground-based observations of Venus is governed largely by the orbital cycles of Venus and the Earth, which constrain the observing opportunities. Since VCO/Akatsuki successfully inserted into Venus orbit on Dec. 7, 2015, a new international campaign is in preparation for the next cycle of Venus maximum elongations (East, Jan 12, 2017 ; West, June 3, 2017).

2007 Campaign:

In 2007, ESA selected a Support Investigation activity to complement the data acquisition from the Venus-Express mission [1] with ground-based observations with the following science objectives: (i) performing coordinated measurements not feasible by Venus Express, (ii) obtaining cross-validation of measurements by different techniques and record different diagnostics of similar phenomena, (iii) obtaining simultaneous measurements sampling a large range of altitudes and (iv) improving the latitudinal coverage and temporal baseline on rapidly variable phenomena. A first campaign was coordinated one year after Venus Express VOI [2] and resulted in a special issue of Planetary and Space Science (Vol. 56, August 2008).

Hubble Space Telescope:

Hubble Space Telescope Imaging Spectrograph (HST/STIS) UV observations of Venus' upper cloud tops were obtained in Dec. 2010 – Jan. 2011 in coordination with Venus Express (VEx). Thesse data were obtained simultaneously with ground-based James Clerk Maxwell Telescope sub-mm observations and 0.36 μm VEx/VMC images of Venus' cloud-tops. They allowed direct comparison and colocation of SO2 and SO gas column densities with cloud top brightness and haze particles properties [3].

Wind field:

VMC and VIRTIS-M have measure long-term behavior of wind flow regimes in Venus at different vertical levels with the use of manual or automatic cloud-tracking algorithms [4,5]. In parallel, ground-based Doppler measurements on the dayside cloud tops (Fig. 1) have shown that cloud features actually track actual atmospheric motion as evidenced by line-of-sight Doppler velocimetry of solar lines [6, 7].

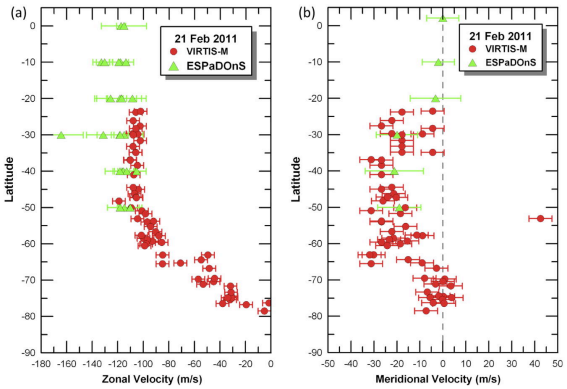

Fig. 1 - Canada–France–Hawaii telescope (CFHT) Doppler winds (green) compared to cloud-tracking wind measurements of VEx/VIRTIS-M on Feb. 21, 2011 [6].

2012 Transit of Venus:

Photometry of the thin aureole, a refracted image of the solar limb probing the terminator mesosphere during the transit, was compared to a simultaneous SOIR occultation profile obtained during the transit [8, 9, 10]. The vertical temperature profiles at all altitudes detect a cold layer at ~86-94 km altitude on average, whose thickness seems to be dependent on latitude. The opaque layer altitude (τ=1) is also latitude dependent, being lower at high altitudes (minimum of 86 km at +82°) than at the equator (91 km).

Atmospheric structure, trace gases :

Millimeter and sub-millimeter wave observations 330-360 GHz line absorptions for ^{13}CO, ^{12}CO, HDO, SO, and SO_2, bring independent coverage and monitoring of rapidly variable temperature and density measurements across the upper atmosphere of Venus [e.g. 11, 12]. Since 2012, maps of HDO and SO_2 have been obtained at 7 and 19 μm using the Texas

Echelon Cross Echelle Spectrograph (TEXES) at the Infrared Telescope Facility (IRTF). Different atmospheric levels are probed atop and within the upper cloud layer. Strong short-term spatial variations (within two hours) were observed in the SO2 maps, while no significant spatio-temporal variations were observed in the HDO maps [13,14]. From AAT, Spatially resolved measurements of H_2O, HCl, CO, OCS, SO_2, cloud opacity, and acid concentration in the IR spectral windows are also monitored [15].

Coordination with Akatsuki in 2017:

VCO/Akatsuki [14] successfully inserted into Venus orbit on Dec. 7, 2015. In general, coordinated observations will improve the latitudinal coverage and temporal baseline, while allowing cross-validation of measurements by different techniques. HST will potentially observe near maximum elongations in Dec 2016-Feb 1 2017 and May 21-June 21 2017, while requests for observing Venus will be submitted to major ground-based facilities (ALMA, JCMT, CFHT, IRTF, AAT, APO)

- Akatsuki LIR camera will observe nightside cloud-top temperature to map of global cloud-top temperature, if one assumes that the large-scale structures (e.g. associated with Y-feature) lasts this long. This can be compared to any spatial structures seen in IRTF/TeXes retrieved parameters (temperature structure, SO_2, HDO retrievals), and with wind retrievals. If wind tracking from LIR data are also available, this can also be compared with dayside wind retrievals such as those obtained with CFHT/ESPaDOnS.
- Akatsuki IR2 will observe middle/lower cloud winds through feature tracking. In principle, one could look for correlations between mean cloud opacity (as measured by mean brightness at 1.735 or 2.26 um channels) and mesospheric SO_2 and/or HDO levels observed using various techniques from the ground (IRTF, sub-mm and mm wave), balloon-borne experiments and Earth's orbit (HST) [15, 16].

Several new international science collaborative opportunities will be discussed at the meeting.

[1] Svedhem et al. 2009, JGR, 114, E00B33
[2] Lellouch et al.2008, PSS 56, 1317-1319
[3] Jessup et al. 2015, Icarus 258, 309-336
[4] Hueso et al. 2012, Icarus 217, 585-598
[5] Khatuntsev et al. 2013, Icarus 226, 140-158
[6] Machado et al. 2014, Icarus 243, 249-263
[7] Machado et al., this meeting.
[8] Wilson et al. 2012, EPSC, Madrid.
[9] Tanga et al. 2012, Icarus 218, 1, 207
[10] Tanga et al., this meeting.
[11] Clancy et al. 2012, Icarus 217, 779-793
[12] Clancy et al., this meeting.
[13] Encrenaz et al. 2013, A&A, 559, A65
[14] Encrenaz et al., this meeting.
[15] Arney et al. 2014, JGR Pl., 119, 1860-1891
[14] Nakamura et al. 2012, 39th COSPAR. p.1327
[15] Jessup et al., this meeting.
[16] Young et al., this meeting.

AEROSOLS PROPERTIES IN THE VENUS UPPER HAZE FROM SPICAV-SOIR MEASUREMENTS IN SOLAR OCCULTATION.

V. Wilquet, A.C. Vandaele, A. Mahieux, S. Robert, S. Chamberlain, *Royal Belgian Institute for Space Aeronomy, Brussels, Belgium (valerie.wilquet@aeronomie.be)*, **M. Luginin, A. Fedorova, D. Belyaev, O. Korablev,** *Space Research Institute, Moscow, Russia*, **F. Montmessin,** *LATMOS/CNRS/IPSL, Guyancourt, France*.

Introduction

SPICAV/SOIR is suit of spectrometers on-board Venus Express that was orbiting Venus for 8 years. It operates, a.o., in the solar occultation mode in the spectral ranges of 118-320 *nm* for SPICAV-UV, 0.65-1.7 μm for SPICAV-IR and 2.2-4.3 μm for the SOIR channel. Each channel has proven to be able to target the Venus upper haze at the terminator and to deliver vertical profiles of the light extinction due to aerosols over the broad spectral range covered by the instrument [1].

While the considerable number of data obtained since the arrival of VEx at Venus allows to study the geo-temporal variability of the aerosol loading [2,3], the spectral dependence of the extinction in particular orbits, directly related to the size distribution and composition of the particles, has the potential to characterize the aerosols in the mesosphere. An independent analysis of the extinction coefficients from the three channels for a limited number of observations and a recent analysis of the SPICAV-IR data [1,3] demonstrated that submicron particles consisting of concentrated sulfuric acid (75%) is not sufficient to explain the recent SPICAV/SOIR observations.

In this work we propose a global analysis of the upper haze by combining the data obtained with the three channels in one single retrieval of the particle characteristics.

Data Set

Since March 2007, the three channels can operate simultaneously in solar occultation, a self-calibrated mode of observation, allowing to estimate the particle size distribution and the concentration of sulfuric acid in the droplets from the spectral dependence of the extinction coefficients. We focus on a subset of about 120 observations, spread over six years of the mission, for which the retrieval of the extinction coefficients in the three channels is of good quality. These observations cover all latitudes but high latitude North ($60^\circ - 90^\circ$) are over-represented (75%), due to the geometry of the orbit.

The targeted altitude range depends on the latitude of the observation as the upper haze lies higher at the equator than at the poles [2,3], but it also depends on the wavelength of the measurement, typically from 70 to 95 km in the IR and from 90 to 105 km in the UV. Therefore the overlap in altitude range covered by the 3 spectrometers is limited.

Methods

A Mie-based optical model has been built for the wavelength range covered by the suit, for various uni- and bimodal log-normal size distributions and for several concentrations of H_2SO_4 comprised between 70 and 90%. For various altitudes of the extinction profiles obtained at different wavelength, the experimental values of the extinction are normalized towards the extinction at a reference wavelengths, chosen to have the smallest relative error on the retrieved extinction. The spectral dependence of the experimental normalized extinctions was fitted using a Levenberg-Marquardt algorithm, which minimizes statistically χ^2 weighted against the uncertainty of the measurements.

Results

The number of parameters to retrieve is large: 1 (uni) or 2 (bimodal) values for the effective radius and respective effective variances, as well as the ratio of the numerical densities between the two modes (bimodal only) and the sulfuric acid concentration. Therefore, a sensitivity study of these parameters on the retrieved aerosol characteristics was performed.

From this subset of data, we aim at defining a number of constraints in order to broaden the analysis to observations for which only one or two of the channels delivered valuable profiles of the extinction coefficients. Attempts to deduce the number densities profiles will also be presented. This work also confirms frequent detached layers in the upper haze at latitudes for which the vertical resolution is high. As showed in previous studies [1,3], a bimodal size distribution is often necessary to fit the experimental values.

Acknowledgments:

The research program was supported by the Belgian Federal Science Policy Office and the European Space Agency (ESA – PRODEX program). The research was performed as part of the “Interuniversity Attraction

Pole" programme financed by the Belgian government (Planet TOPERS). The authors also recognize the support from the FP7 EuroVenus project (G.A. 606798) as well as that of the BRAIN SCOOP project (Contract #: BR/143/A2/SCOOP). A. Mahieux would like to thank the FNRS (Belgium) for his Chargé de Recherches position.

References:

[1] Wilquet, V., et al., Preliminary characterization of the upper haze by SPICAV/SOIR solar occultation in UV to mid-IR onboard Venus Express. J. Geophys. Res., 2009. 114: p. E00B42.
[2] Wilquet, V., et al., Optical extinction due to aerosols in the upper haze of Venus: Four years of SOIR/VEX observations from 2006 to 2010. Icarus, 2012. 217(2): p. 875-881.
[3] Luginin, M. et al., Aerosol properties in the upper haze of Venus from SPICAV IR data, submitted.

VENUS THERMOSPHERIC DENSITIES AS REVEALED BY VENUS EXPRESS TORQUE MEASUREMENTS

C.F. Wilson, *Oxford University, Oxford, UK (wilson@atm.ox.ac.uk)*, **M. Persson**, *Swedish Institute of Space Physics, Kiruna, Sweden*. **E. Grotheer**, ESAC, Spain, **I. Müller-Wodarg**, Imperial College London, UK, **S. Damiani, M. Müller**, ESA/ESOC, Germany, **H. Svedhem**, ESA/ESTEC, Noordwijk, the Netherlands, **P. Rosenblatt**, Royal Observatory of Belgium, **S. Bruinsma**, CNES/GRGS, Toulouse.

Introduction:

Venus EXpress (VEX) orbited Venus from 2006-2014, in a highly eccentric polar orbit with a pericentre near the North Pole. During several campaigns, the pericentre altitude was lowered allowing the spacecraft to travel inside the thermosphere at altitudes as low as 165 km. During these VEX Atmospheric Drag Experiments (VExADE) campaigns, atmospheric drag was measured in two ways, using radio tracking for precise orbit determination (VExADE-POD) [Rosenblatt et al. 2012] and, secondly, using the Attitude Control System to measure the aerodynamic torque exerted on the spacecraft when orienting the solar arrays asymmetrically (VExADE-TRQ), a technique first developed for the Magellan orbiter [Tolson et al, 1995]. While the POD measurements gave a single density value per flyby (equivalent to the density at closest approach), the TRQ measurement obtained time-resolved measurements of thermospheric neutral density over an altitude range of 165 – 200 km altitude. It was not possible to use the onboard accelerometers to measure densities at these high altitudes – that was only possible in the later aerobraking campaign where pericentre altitude was lowered to 130 km altitude [Müller-Wodarg et al. 2016]. We present data from the TRQ measurements.

Data reduction

The method of calculating the densities from measured torques is described by Damiani *et al.* (2012). The measured torque exerted on the spacecraft contains not only aerodynamic torque but also gravity gradient and solar radiation pressure torques, all of which are considered when inferring thermospheric densities.

Several sources of systematic error have been considered. Damiani et al (2012) showed that almost all of the aerodynamic torques are due to forces on the solar arrays, due to their large area and large distance from the spacecraft mass, and that ignoring flow on all other faces of the spacecraft lead to uncertainties of at most 5% in the calculation of density – this simplification was therefore adopted in the present study. Following the analysis of Arona et al. (2011), we assumed an accommodation coefficient of 0.886 +/- 0.02. Including other systematic errors and the possible effects of thermospheric wind speeds, we estimate the combined systematic uncertainties to be typically < 15% at 165 – 185 km altitudes

During some passes of Venus Express we obtained thermosphere densities both from the POD and TRQ methods, allowing cross-validation of their densities. To extract a more accurate closest approach density value in the TRQ data and thereby permit cross-validation between the datasets, a Gaussian function was fit to the measured torque curve. Figure 1 shows the peak densities, simultaneously measured using the torque and POD techniques. It can be seen that the results are clearly correlated, which increases confidence in the torque technique. Densities obtained from torque measurements are typically 20% lower than those from the POD data; however, this disagreement is considered to be acceptable given the very different nature of the two methods.

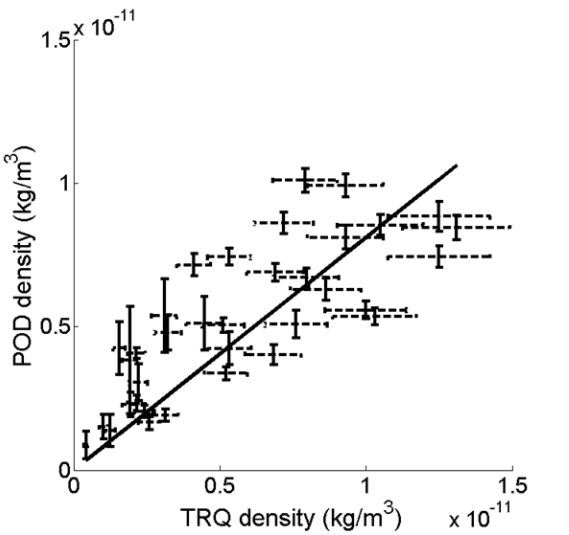

Figure 1: *Comparison between torque and tracking pericentre density values for matching orbits. Error bars include systematic and random noise. (Persson, 2015).*

Results

An example of a density profile inferred from one of the torque passes is shown in Figure 2, using data from 18 May 2011 The pericentre of this orbit was at latitude 84.8 deg N, above the dayside near the evening terminator (SZA = 85.9 deg) and the spacecraft approached pericentre travelling northwards above the dayside, crossing the terminator (defined in this case as SZA = 90°) into the nightside at 58.9 seconds after pericentre. The significant change in mass densities before and after pericentre occurs due to this passing from the dayside to the nightside, leading to a rapid collapse in density.

Data from the thermospheric density model of Hedin et al. (1983) were extracted along the spacecraft trajectory and are shown in Fig. 2 by the dotted line. It can be seen that the Hedin model also reproduces a collapse of thermospheric density from dayside to the nightside, although the gradient of this decrease ($d\rho/d(SZA)$) is smaller in the model than in the observations.

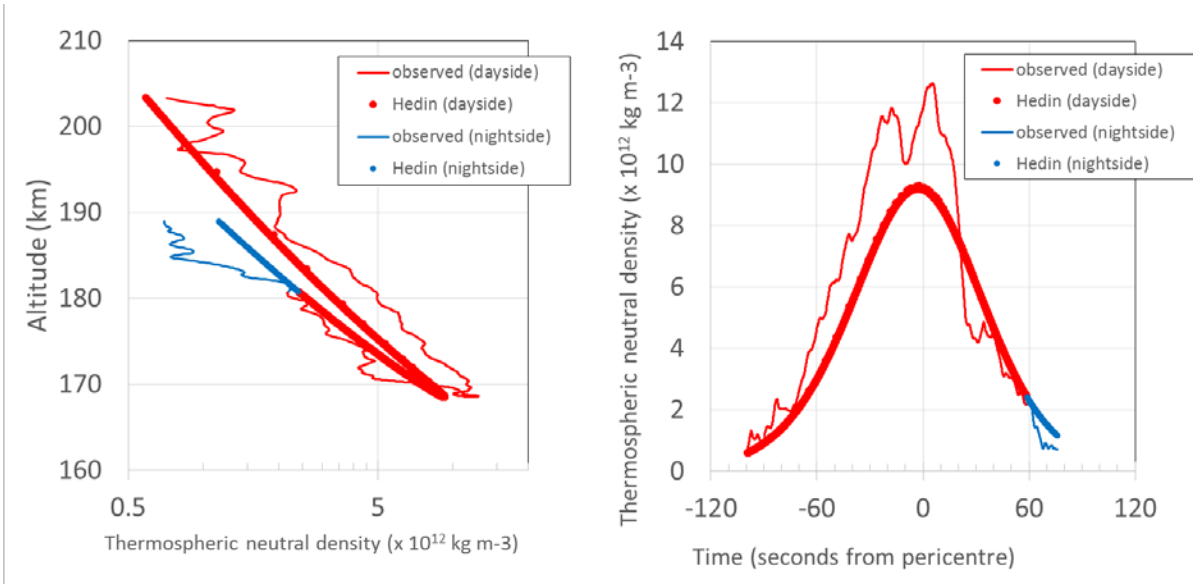

Figure 2: *Thermospheric neutral density measured by VEx torque experiment on 18 May 2011, and model densities from Hedin (1983), as a function of (a) time and (b) altitude. Red colour indicates that the spacecraft was in the dayside (SZA < 90°).*

Mean density profile

The density profile from all of the torque passes was binned by altitude and corrected for the observed horizontal density gradient with respect to solar-zenith angle (Persson 2015). The resulting vertical profiles, binned separately for morning and evening terminators, are shown in Figure 3.

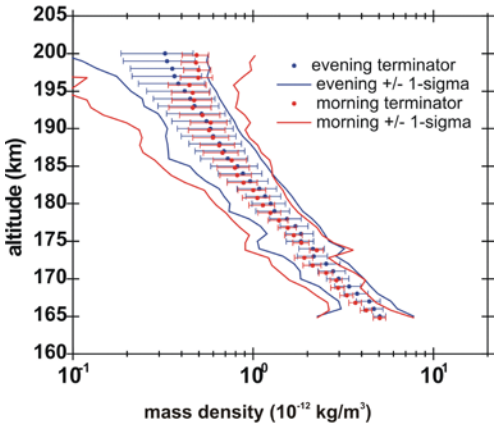

Figure 3: *Mean densities along the morning (red) and evening (blue) terminators averaged in 1 km altitude bins. Error bars show measurement errors, and solid lines show 1σ variability of measured values within each altitude bin.*

The error bars denote the measurement error as a function of altitude; the solid lines show the +/- 1 sigma dispersion of measured densities in each altitude bin, i.e. the standard deviation of mass density variability in each altitude bin. Mass densities were found to be 40 - 45% lower than those of the Hedin model, in agreement with the results from POD measurements (Rosenblatt et al., 2012). This finding, combined with the finding that the gradient $d\rho/d(SZA)$ is greater in observed data than in the Hedin model, means that observed densities at SZA > 90° in particular were much smaller than predicted by the Hedin model. We found no significant density difference between morning and evening terminators.

Wave structures

Many profiles exhibit strong oscillations in density such as those seen near pericentre in Fig. 1, with $\Delta\rho/\rho$ of up to 20%. The spacecraft is travelling nearly horizontally when passing through these structures; the horizontal wavelength is calculated to be typically in the range 100 – 400 km. This is similar in scale both to waves reported at 135 km altitude during aerobraking (Müller-Wodarg et al 2016) and waves observed near 120 km in CO_2 non-LTE emission observed by VIRTIS (Garcia et al., 2009).

References:

Arona, L et al. (2011) Venus Express solar arrays rotation experiments to measure atmospheric density. International Symposium on Spacecraft Flight Dynamics.

Damiani, S. et al. (2012), Monitoring of aerodynamic pressures for Venus Express in the upper atmosphere during drag experiments based on telemetry. International Symposium on Space Flight Dynamics.

Garcia, R. F. et al. (2009), Gravity waves in the upper atmosphere of Venus revealed by CO2 nonlocal thermodynamic equilibrium emissions, J. Geophys. Res., 114,

E00B32

Hedin, A.E. et al. (1983) Global Empirical Model of the Venus Thermosphere. J. Geophys. Res., 88, pp.73-83.

Müller-Wodarg et al. (2016), In–situ observations of waves in Venus' polar lower thermosphere with Venus Express aerobraking. Nature Physics, under review.

Persson, M. (2015), Venus Thermosphere Densities as Revealed by Venus Express Torque and Accelerometer Data, MSc thesis, IRF Sweden.

Rosenblatt, P., et al. (2012) First ever in situ observations of Venus' polar upper atmosphere density using the tracking data of the Venus Express Atmospheric Drag Experiment (VExADE). Icarus, 217, 831–838.

Tolson, R.H. et al. (1995), Magellan Windmill and Termination Experiments. International Symposium on Space Flight Dynamics.

CORRELATIONS BETWEEN TEMPERATURE STRUCTURE AND UV CONTRASTS IN THE CLOUDS OF VENUS.

C.F. Wilson[1], M. Roos-Serote[1,2], R. MacDonald[1], S. Tellmann[3], B. Häusler[4], Y.-J. Lee[5], I.V. Khatuntsev[6].
[1]AOPP, Univ. of Oxford, UK (wilson@atm.ox.ac.uk), [2]University of Michigan, USA, [3]Rheinisches Institut für Umweltforschung, Universität zu Köln, Germany, [4]Institut für Raumfahrttechnik, Universität der Bundeswehr München, Germany, [5]ISAS/JAXA, Sagamihara, Japan, [6]IKI, Moscow, Russia.

We investigate the nature of the UV contrasts exhibited by Venus clouds by examining co-located radio occultation and UV imagery data obtained from Venus Express. The images are obtained up to twelve hours away from the time of the radio occultation, so a correction scheme is developed to account for advection of clouds by winds. Also, a phase angle correction scheme is developed to compensate for the changing viewing geometry of the cloud.

We find a weak correlation between UV darkness and temperature in the 65-75 km altitudes, consistent with an explanation that UV-dark regions absorb more sunlight than UV-bright regions. The altitude region of maximum heating apparently increases with latitude, as the solar zenith angle increases, but statistical significance of this finding is low due to a small number of observations.

We find no evidence for correlations of UV brightness with static stability at any altitude. However, this may be due to the relatively low number of observations available, particularly in low-latitude regions where UV contrast formation is thought to be strongest.

The method developed here, if applied on a greater number of observations in future, shows possibilities for constraining the vertical distribution of solar UV absortion in the clouds of Venus.

Acknowledgement: Some of this work was funded from the European Union Seventh Framework Program (FP7) under grant agreement n°606798 (EuroVenus).

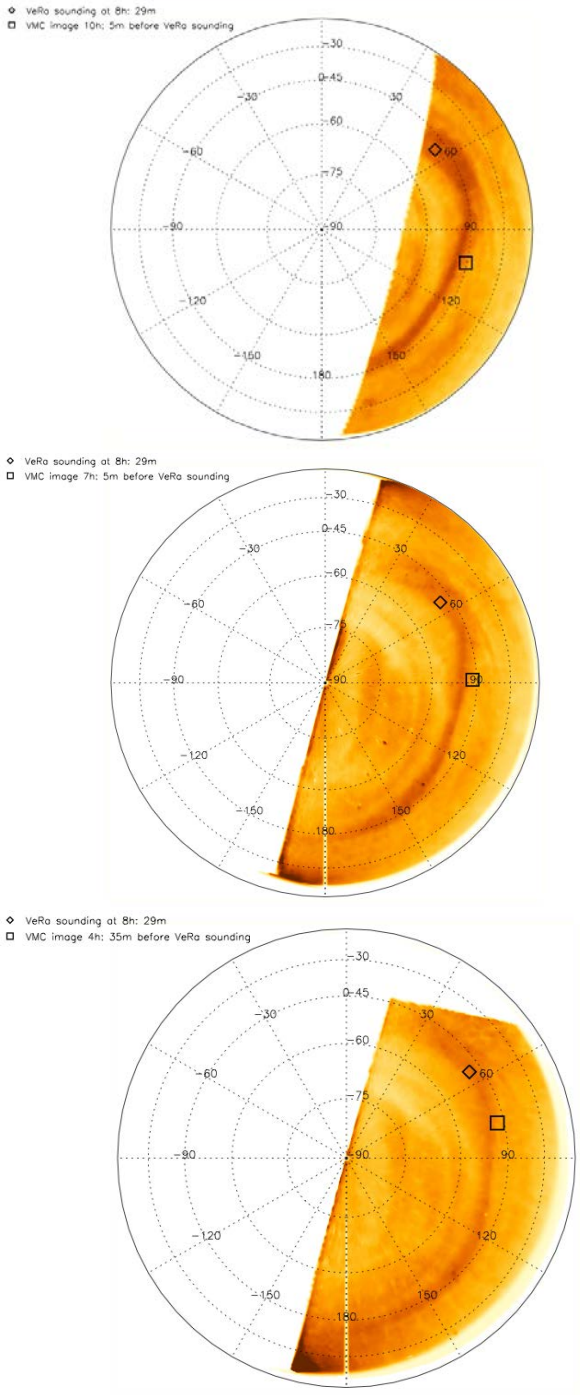

Figure: Example of VMC images showing VeRa sounded location on 25 Dec. 2013 (Orbit 2805). The three images were taken respectively 10, 7, and 4.5 hours before the VeRa sounding. In each image, the diamond indicates the actual location sounded by VeRa; the square shows the position of the sounded atmospheric region at the time the image was taken, taking into account the mean winds at this latitude and altitude.

ASCENT AND ERUPTION OF MAGMA ON VENUS: CHANGES OF STYLE WITH GEOLOGIC TIME.

L. Wilson, *Lancaster Environment Centre, Lancaster University, Lancaster, U.K. (l.wilson@lancaster.ac.uk),* **J. W. Head,** *Dept. of Earth, Environmental and Planetary Sciences, Brown University, Providence RI, U.S.A. (James_Head@brown.edu)*

Introduction: The nature of the basaltic [see review in 1] volcanic activity recorded in the surface geology of Venus has been dictated by the extreme (by Earth standards) environmental conditions combined with the variations over geologic time of the state of the crust and mantle. Here we summarize our current thinking on these issues.

Environmental factors: The massive CO_2-dominated atmosphere of Venus leads to both a high surface pressure (~4-9 MPa) and a high surface temperature (~650-730 K), both decreasing with increasing elevation [2]. Each of these leads to predictable consequences for eruptive processes and volcanic landforms.

Pressure effects. The pressure gradient in the crust on Venus is only slightly less than that in the Earth because the acceleration due to gravity is ~90% that of Earth, but the absolute pressure at the surface on Venus is so high that the exsolution of magmatic volatiles is greatly inhibited, making explosive volcanic activity less likely than on Earth and effusive activity more likely. The high pressures in the Venus atmosphere should influence the thermodynamics of the H-C-O-S-N system in such a way that CO_2 is the main constituent of the gas phase released from erupting mafic magmas there [3], with water (and SO_2) present as minor components.

We use one-component solubility functions for water and CO_2 in basalt from [4] to illustrate the relative behaviors of these species on Venus. Steady (i.e., Hawaiian-style) explosive activity requires that the volume fraction of the gas bubbles formed in a magma as the volatile is exsolved should equal or exceed a critical threshold of order 75-80%. We find that to have steady explosive activity on Venus, magmas would need to have the minimum total contents of either water (~1-2 wt%) or CO_2 (~2-4 wt%) shown in Table 1 (these values are ~10x greater than the amounts needed on Earth). To be able to contain these large amounts of volatiles, Venus magmas would need to have been generated by partial melting at depths of at least the values shown in the Table. Whatever the thickness of the Venus crust, the ~1-3 km depths implied if water were the volatile driving potential explosive activity present no problems - partial melting is likely to have taken place at greater depths so the only limitation is the presence of enough water in the Venus mantle. However, the ~30-70 km depths required for CO_2 might represent more of a challenge depending on the thermal state of the mantle. More important is the fact that the calculations of [3] imply that under Venus surface conditions no magma with a composition resembling those of typical mid-ocean ridge basalts on Earth would release more than ~ 600 ppm, i.e., 0.06 wt%, of CO_2 and ~10 ppm water These amounts are too little by factors of 30-70 to permit steady explosive volcanism, and some kind of volatile concentration process would be needed to allow such activity.

One such process is the slow rise of magma that allows gas bubbles to migrate upward through the rising melt and coalesce to form much larger bubbles that burst in the vent to drive Strombolian activity. Another is the stalling of magma beneath a chilled carapace allowing accumulations of volatiles to eventually drive a Vulcanian explosion. However, neither of these processes leads to the kind of high magma injection rate into the atmosphere that leads to wide dispersal of voluminous deposits. Few examples of explosive volcanic eruption deposits on Venus have been suggested [5-7]. The most recent proposal is a pyroclastic flow near Diana Chasma [8] covering an area of at least 5000 km^2 and having a volume of order 500 km^3. A deposit of this scale would require a protracted relatively steady eruption [9] and extreme volatile concentration [8] and an elongate fissure vent would encourage column collapse to form a flow rather than fall deposit [10].

Table 1: Minimum total volatile contents, n_{tot}, and minimum mafic magma source depths, D, to ensure steady explosive activity on Venus for 4 MPa and 9 MPa surface pressures.

Volatile	4 MPa pressure		9 MPa pressure	
Species	n_{tot} /wt%	D /km	n_{tot} /wt%	D /km
H_2O	1.07	1.05	2.26	3.03
CO_2	1.92	32.7	4.22	71.8

Temperature effects. The cooling of lava flows on Venus was modeled by [11]. Their results show that the increase in thickness with time of the chilled crust is nearly the same as on Earth in both high and low elevation areas on Venus, despite the variations in atmospheric properties, because the limiting factor is heat flow through the lava rather than heat removal by the atmosphere. Also the surface temperatures in all three cases decrease in the same way for about the first hour after eruption. However, at later times the Venus flow surfaces are hotter, and so the mean internal temperature is also greater, by about 400 K. Flows cease to advance

when the wave of cooling from their boundaries penetrates far enough into the flow body. However, analysis of flow cooling in terms of the dimensionless Grätz number [12] shows that cooling does not have to penetrate to the center of a flow to cause its advance to stop. This implies that flow cessation depends, at least in part, on the details of the cooling of the flow front material and the dynamic lateral displacement of this cooled material to form the levees between which the flow advances. Although the details of these interactions have not yet been quantified, we now anticipate that flows on Venus should advance to greater distances, possibly much greater distances, from the vent than flows on Earth for a given volume eruption rate. This must encourage the formation of long, volume-limited lava flows rather than the development of compound flow fields consisting of multiple shorter cooling-limited flows. This seems qualitatively in agreement with the presence of the major fluctus systems on Venus.

Volcanic History of Venus: The stratigraphically oldest terrains on Venus, the tesserae, appear to be formed by deformation of volcanic plains units in places [13] but pervasive deformation of tessera terrain obscures the nature of the earlier volcanic units. The oldest post-tesserae units are also very deformed volcanic plains.

Superposed on this unit are relatively undeformed plains characterized by abundant small volcanic shields [14]. These features probably represent a phase of low-effusion rate, cooling-limited flows, and are evidence for widespread shallow volcanic sources [11]. Following this, widespread radar-dark volcanic plains were emplaced globally (>70% of the surface). These plains show little evidence for abundant distributed volcanic sources; instead, source regions are not obvious, and the major features are long sinuous channels [15] many of which are similar to lunar sinuous rilles formed from high effusion rate, long duration eruptions [16]. Stratigraphic evidence suggests that these plains were initially emplaced in widespread flood events involving very high effusion rate volume limited flows, and partially through canali, which may represent picritic or komatiitic lavas formed by large degrees of partial melting [17].

After a period of compressional deformation forming wrinkle ridges, another change in style and mode of occurrence of volcanism took place, with the widespread plains units largely followed by the formation of broadly distributed centralized volcanic edifices and sources [18]. The latest activity is localized at edifices on broad volcanic rises [19], and at rifts where lithospheric thinning has permitted locally enhanced melting and volcanism [20] producing both cooling limited and volume limited flows.

Implications for the mantle: Neither plate tectonic models [21] nor monotonic thermal decay [22] readily account for the major changes in volcanic style. A depleted mantle layer overturn model [23] is consistent with many of the observations. In this scenario, a depleted mantle layer underlying a vertically accreting crust becomes unstable and overturns, causing localized crustal thickening (tessera) and extensive volcanism linked to crustal thinning and pressure-release melting of upwelling fertile mantle at a range of depths. Mantle upwelling would favor komatiitic magmas produced at deeper levels and high effusion rate fluid lavas at the surface producing long flows. In this scenario this near-surface thermal and magmatic pulse is followed geologically rapidly by stabilization, cooling and lithospheric thickening, widespread compression, and localization of volcanism to sources related to deeper mantle convection, plumes, and lithospheric thinning, marking the most recent phase of Venus volcanism. Recent analysis of Venus Express data suggest that volcanism may still be ongoing in these young rift-related areas such as Atla Regio [24].

References: [1] Filiberto, J. (2014) Icarus 231, 131. [2] Zasova, L.V. et al. (2007) Planet. Space Sci. 55, 1712. [3] Gaillard, F and Scaillet, B. (2014) Earth Planet. Sci. Lett. 403, 307. [4] Wilson, L. and Head, J.W. (1981) J. Geophys. Res. 86, 2971. [5] Guest, J.E. et al. (1992) J. Geophys. Res. Planets, 97, 15,949. [6] Campbell, B.A. (1994) Icarus, 112, 187. [7] Grosfils, E.B. et al. (2011) USGS Sci. Invest. Map 3121. [8] Ghail, R.C. and Wilson, L. (2014) Geol. Soc. London Spec. Publ. 401, doi:/10.1144/SP401.1 [9] Airey, M.W. et al., (2015) Planet. Space Sci. 113-114, 33. [10] Glaze, L.S. et al. (2011) J. Geophys. Res. 116, E01011. [11] Head, J.W. and Wilson, L. (1986) J. Geophys. Res. 91 (B9), 9407. [12] Pinkerton, H. and Wilson, L. (1994) Bull. Volcanol. 56, 108. [13] Gilmore, M. and Head, J. (1995) LPSC 26, 461. [14] Aubele, J. (1995) LPSC 26, 59; Ivanov, M.A. and Head, J.W. (2004) J. Geophys. Res. 109, E10001. [15] Baker, V. et al. (1992) J. Geophys. Res. 97, 13,421. [16] Wilson, L. and Head, J. W. (2016) Generation, Ascent and Eruption of Magma on the Moon: New Insights Into Source Depths, Magma Supply, Intrusions and Effusive/Explosive Eruptions (Part 1: Theory), *Icarus*, in press; Head, J. W. and Wilson, L. (2016) Generation, Ascent and Eruption of Magma on the Moon: New Insights Into Source Depths, Magma Supply, Intrusions and Effusive/Explosive Eruptions (Part 2: Predicted Emplacement Processes and Observations), *Icarus*, in review. [17] Head, J. et al. (1995) EOS, Trans. AGU 75, 193. [18] Basilevsky, A. et al., Resurfacing, In Venus II. [19] Keddie, S. and Head, J. (1994) Earth Moon Plan. 65, 129. [20] Magee, K. and Head, J. (1995) J. Geophys. Res. 100, 1527. [21] Turcotte, D. (1993) J. Geophys. Res. 98, 17,061. [22] Solomon, S. (1993) Phys. Today 46, 48. [23] Parmentier, E and Hess, P. (1992) Geophys. Res. Lett. 19, 2015. [24] Shalaygin, E.V. et al. (2015) Geophys. Res. Lett. 42, 4762.

Instrumentation and Initial Results of Ultraviolet Imager on AKATSUKI

A. Yamazaki, *Institute of Space and Astronautical Science, Japan Aerospace Exploration Agency, Kanagawa, Japan. (yamazaki@stp.isas.jaxa.jp),* **M. Yamada,** *Planetary Exploration Research Center, Chiba institude of Technology, Chiba, Japan*. **S. Watanabe**, *Hokkaido Information University, Hokkaido, Japan.* **T. Imamura** *Institute of Space and Astronautical Science, Japan Aerospace Exploration Agency, Kanagawa, Japan.,*

Introduction:

The beautiful UV images of the Venusian cloud top were previously performed by several Venus satellites such as Mariner 10 [Bruce et al., 1974], Pioneer Venus [Travis et al., 1979; Rossow et al., 1980], Galileo [Belton et al., 1991], Venus Express [Markiewicz et al., 2007a, 2007b; Titov et al., 2008]. These previous instruments have taken images at the wavelength around 365-nm, but what material distribution reflects the contrasting density has been unknown yet. There is the SO2 absorption band around the 283-nm wavelength, and the 283-nm images clarify the distribution of SO2.

The ultraviolet imager (UVI) on the AKATUSKI satellite takes ultraviolet images of the solar radiation scattered at the Venusian cloud top level at the both 283- and 365-nm wavelengths. There are absorption bands of SO2 and unknown absorber in these wavelength regions. UVI result into measurements of the SO2 and the unknown absorber distributions, and the sequential images lead to understand the velocity vector of the wind at the cloud top altitude.

Instrumentation:

The UVI is equipped with fast off-axial catadioptric optics, two bandpass filters and a diffuser installed in a filter wheel moving with a stepping motor, and a high-sensitive CCD devise with a UV coating. The UVI takes images of the ultraviolet solar radiation scattered from the Venusian cloud top in two wavelength ranges at the center of 283nm and 365nm.

The optics has a composite focal length of 63.3mm with an f-number of 16, and the field-of-view (FOV) of 12°. Two interference filters installed in the filter wheel select the observational wavelength of 283nm and 365nm. One diffuser also installed is used for the onboard calibration such as measurement of flat field and modification of relative sensitivity. As the detector a back illuminated type of a frame-transfer CCD with a UV sensitive coating is adopted. Its pixel size is 13μm, and the effective area is 1024 x 1024 pixels. Therefore UVI has the angular resolution of 0.012°. The output count of the CCD has the data depth of 12bit by the analog-to-digital converter. The onboard digital data processing creates make one image with the 16-bit data depth. The data size is diminished with the onboard compression to be several hundred kilo-bytes.

The nominal exposure time is 128 msec and 46 msec at the observations of the 283- and 365-nm wavelengths, respectively. CCD has no mechanical shutter, so a smear noise in transferring from the image area to the storage area degrades the signal-to-noise ratio of the signal image especially in the short exposure operation. The images have a signal-to-noise ratio of over 100 after desmearing of onboard data processing. The cooling radiator for the CCD device cools down the instrument temperature below 9°C in the observation mode to reduce the dark current. The UVI nominally take one image of the Venus cloud top level every two hours.

First Image of Venus:

UVI has taken the two UV wavelength images of Venus immediately after the operation of the Venus orbit insertion last year. The first memorial images by the AKATSUKI "satellite" of Venus were taken at the positions of ~72,000 km far from the Venus center. The solar phase angle at the sub-observer point was ~45˚ with the evening terminator. The image without any data reduction except for desmearing is very desirable for scientific analysis without damage such as radiation effect.

The UVI image at a wavelength of 283 nm presents solar radiation attenuated by SO2 absorption near the cloud top altitudes This is the first time to capture the snapshot of Venus with this wavelength. Together with the 365-nm images, the continuous UVI images will be used to derive horizontal cloud-tracked velocities near the cloud top altitudes (62—70 km) [e.g., Ogohara et al., 2012; Kouyama et al., 2013].

Summary:

The UVI imager on the AKATSUKI satellite can detect two wavelength ultraviolet radiations reflected at the cloud top, and it has also taken sequential images every two hours. The image quality is very comfortable suite to study scientific objectives before launch. We expect the interesting results from the UVI images of Venus.

Acknowledgments:

The authors are grateful to all the members of the UVI instrument team for their excellent support and effort in completing UVI, and also thank all the members of the AKATSUKI project team.